Lipids in plant development and stress responses

Dissertation

for the award of the degree
"Doctor rerum naturalium"
of the Georg-August-Universität Göttingen

within the doctoral program
"Plant Responses To Eliminate Critical Threats"
of the Georg-August University School of Science (GAUSS)

submitted by
Patricia Scholz
From Dresden, Germany

Göttingen 2022

Thesis Committee

Prof. Dr. Till Ischebeck, Green Biotechnology, Institute of Plant Biology and Biotechnology (IBBP), University of Münster

Prof. Dr. Marcel Wiermer, Biochemistry of Plant-Microbe Interactions, Institute of Biology, Freie Universität Berlin

Prof. Dr. George Haughn, Department of Botany, University of British Columbia, Vancouver, Canada

Members of the Examination Board

Referee: Prof. Dr. Till Ischebeck, Green Biotechnology, Institute of Plant Biology and Biotechnology (IBBP), University of Münster

2nd Referee: Prof. Dr. Gerhard Braus, Department of Molecular Microbiology and Genetics, Institute for Microbiology and Genetics, University of Göttingen

Further members of the Examination Board

Prof. Dr. Marcel Wiermer, Biochemistry of Plant-Microbe Interactions, Institute of Biology, Freie Universität Berlin

Prof. Dr. George Haughn, Department of Botany, University of British Columbia, Vancouver, Canada

Prof. Dr. Ivo Feussner, Department for Plant Biochemistry, Albrecht-von-Haller-Institute for Plant Sciences, University of Göttingen

Prof. Dr. Andrea Polle, Department of Forest Botany and Tree Physiology, Büsgen-Institute, University of Göttingen

Date of oral examination: 24th October 2022

All models are wrong, but some are useful.

George E. P. Box

Table of Contents

List of Abbreviations

ACP	Acyl carrier protein
c.	circa
CAS1	CYCLOARTENOL SYNTHASE 1
CB5-E	CYTOCHROME B5 ISOFORM E
cfu	Colony forming units
CLO	Caleosin
CoA	Coenzym A
CPT	Choline phosphotransferase
DAG	Diacylglycerol
dai	Days after imbibition
DGAT	Diacylglycerol acyltransferase
DGDG	Digalactosyldiacylglycerol
DGK	Diacylglycerol kinase
α-DOX1	α-Dioxygenase 1
dpi	Days post inoculation
DUF	Domain of unknown function
DW	Dry weight
EM	Electron microscopy
ER	Endoplasmic reticulum
ERD7	EARLY RESPONSIVE TO DEHYDRATION 7
FA	Fatty acid
FAD	Fatty acid desaturase
FFA	Free fatty acid
FIT	Fat storage-inducing transmembrane protein
G3P	Glycerol-3-phosphate
GPAT	Acyl-CoA:glycerol-3-phosphate-acyltransferase
HOT	Hydroxy-octadecatrienoic acid
HPL	Hydroperoxide lyase
HSD	Hydroxysteroid dehydrogenase, also known as Steroleosin
$I(1,4,5)P_3$	Inositol 1,4,5-trisphosphate
icf	Isotope correction factor
JA	Jasmonic acid
LC	Liquid chromatography
LC-MS/MS	Liquid chromatography-coupled tandem mass spectrometry
LD	Lipid droplet
LDAH	Lipid droplet-associated hydrolase
LDAP	Lipid droplet-associated protein
LDDH	Lipid droplet dehydrogenase
LDIP	LDAP-INTERACTING PROTEIN

LDNP	LIPID DROPLET-LOCALISED NTF2 FAMILY PROTEIN
LDPS	Lipid droplet-associated protein of seeds
LDS1	LIPID DROPLETS AND STOMATA 1
LIDL	Lipid droplet-associated lipase
LIME	Lipid droplet-associated methyltransferase
LOX	Lipoxygenase
LPA	Lysophosphatidic acid
LPAAT	Acyl-CoA:lysophosphatidic acid acyltransferase
LPC	Lysophosphatidylcholine
LPCAT	Acyl-CoA:lysophosphatidylcholine acyltransferase
LPEAT	Acyl-CoA:lysophosphatidylethanolamine acyltransferase
LTP	Lipid transfer protein
MAG	Monoacylglycerol
MDH	Malate dehydrogenase
MGDG	Monogalactosyldiacylglycerol
MLDP	MAJOR LIPID DROPLET PROTEIN
MS	Murashige and Skoog
MS/MS	Tandem mass spectrometry
NanoESI	Nano electrospray ionization
NPC	Nonspecific phospholipase C
OBL	Oil body lipase
OLE	Oleosin
PA	Phosphatidic acid
PAD3	PHYTOALEXIN DEFICIENT 3
PALD	PROTEIN ASSOCIATED WITH LIPID DROPLETS
PAP	Phosphatidic acid phosphatase
PC	Phosphatidylcholine
PDAT	Phospholipid:diacylglycerol acyltransferase
PDCT	Phosphatidylcholine:diacylglycerol cholinephosphotransferase
PE	Phosphatidylethanolamine
PI	Phosphatidylinositol
PI-PLC	Phosphoinositide-dependent phospholipase C
PI3P	Phosphatidylinositol 3-phosphate
PI(3,5)P$_2$	Phosphatidylinositol 3,5-bisphosphate
PI4K	Phosphatidylinositol 4-kinase
PI4P	Phosphatidylinositol 4-phosphate
PI(4,5)P$_2$	Phosphatidylinositol 4,5-bisphosphate
PIP5K	Phosphatidylinositol 4-phosphate 5-kinase
PKC	Protein kinase C
PL	Phospholipid

PLA	Phospholipase A
PLC	Phospholipase C
PLD	Phospholipase D
PS	Phosphatidylserine
Pst, Pto	*Pseudomonas syringae* pv. *tomato* DC3000
PTLD	POLLEN TUBE LIPID DROPLET PROTEIN
PUX	Plant UBX-domain containing protein
PXA1	PEROXISOMAL ABC TRANSPORTER1, also known as COMATOSE (CTS) or PEROXISOME DEFECTIVE3 (PED3)
rpm	Rounds per minute
SA	Salicylic acid
SE	Sterol ester
SG	Steryl glycoside
SDP1	SUGAR DEPENDENT 1
SDP1L	SUGAR DEPENDENT 1-LIKE
SLDP	Seed lipid droplet protein
SMT1	STEROL METHYLTRANSFERASE 1
SRP	Signal recognition particle
TAG	Triacylglycerol
TGD1	TRIGALACTOSYLDIACYLGLYCEROL 1
TGN	*trans* Golgi network
THAS1	THALIANOL SYNTHASE 1
UPLC	Ultra-performance liquid chromatography
VAP27-1	VESICLE ASSOCIATED MEMBRANE PROTEIN (VAMP) – ASSOCIATED PROTEIN 27-1

Abstract

In plant cells, lipids are important components of cellular membranes. There, they act as structure-forming and/or signal-transmitting elements. As signals, lipids are landmarks and thereby important regulators, for example of secretory processes in pollen tubes. One such signalling lipid is phosphatidic acid that can be formed by diacylglycerol kinases (DGKs), however, the role of DGKs in the secretory processes occurring in pollen tubes is so far underexplored.

One study described in this thesis sheds light on the importance of DGKs in tobacco pollen tube growth. Here, it is shown for the first time that certain DGKs are localised at the plasma membrane. The tobacco DGK NtDGK5 in particular associates to an important signalling hub in the plasma membrane shortly behind the pollen tube tip to convert diacylglycerol in phosphatidic acid. Interference with NtDGK5 function in tobacco pollen tubes caused the appearance of unusual wavy growth and misshaped tips in pollen tubes. Further transient expression assays highlighted a possible connection of NtDGK5 to the regulation of pectin secretion by other signalling lipids. In conclusion, the localisation and associated phenotypes of NtDGK5 support a role for this enzyme and its product in the fine-tuning of other signalling networks coordinating pectin secretion in tobacco pollen tube growth.

Apart from membrane lipids, more hydrophobic storage lipids can be found for example in the core of cytosolic lipid droplets (LDs). This core is delimited by a phospholipid monolayer into which proteins are embedded. These proteins convey to LDs their cellular function, so a deeper understanding of LDs requires more detailed knowledge on the composition and dynamics of the LD proteome.

In a further study, we analysed the lipidome of stressed leaves of Arabidopsis revealing that there are increased levels of the LD core component triacylglycerol in reaction to stress, including heat treatment or infection of the plants with either *Botrytis cinerea* or *Pseudomonas syringae* pv. *tomato* DC3000 *ΔavrPto/ΔavrPtoB*. Furthermore, bottom-up label-free proteomics studies enabled a thorough investigation of the dynamics of the LD proteome under stress. The results highlight especially CALEOSIN 3 as a universal stress-responsive LD protein and the α-DIOXYGENASE 1 as an LD protein that accumulated specifically in reaction to infection. In addition, proteome measurements of LD-enriched fractions from leaves in comparison to total cellular protein enabled the identification of LD-LOCALISED NTF2 FAMILY PROTEIN and CYTOCHROME B5 ISOFORM E as new LD-associated proteins.

Similar studies on LDs isolated from roots resulted in the first detailed description of the LD proteome in Arabidopsis roots. More than 20 LD proteins could be identified, which included several proposed or characterised enzymes. These studies establish leaf and root LDs as active players in cellular metabolism and stress response and open up new avenues for future LD research.

1 Introduction

1.1 Plant lipid structures and functions are diverse

Among the commonly categorised classes of biochemical molecules, lipids are probably the most diverse group. Defined by their solubility in nonpolar solvents, they comprise chemical structures ranging from very hydrophobic neutral lipids like triacylglycerols (TAGs) and sterol esters (SEs) to charged compounds like phosphoinositides.

Structurally, lipids can be divided into different groups, based on their head group and/or backbone. Glycerol as the backbone is characteristic for glycerolipids, whose hydroxyl groups in *sn-1*, *sn-2* and *sn-3* position can be esterified with the α-carboxyl group of a fatty acid (FA). In this case, TAGs are formed (Figure 1A), which represent major carbon storage compounds (Bates, 2016). TAGs carry no charge in the molecule and are thus neutral lipids. Neutral lipids can also be found among terpenes, another lipid class. In contrast to TAGs, the hydrophobicity of terpenes is not related to FAs, as terpenes derive structurally from isoprene units and are formed biochemically from the activated molecules isopentenyl pyrophosphate and dimethylallyl pyrophosphate (Hemmerlin et al., 2012). Different numbers of isoprene units can be linked in condensation reactions to give rise for example to monoterpenes (two isoprene units), sesquiterpenes (three isoprene units), diterpenes (four isoprene units) or triterpenes (six isoprene units; Hemmerlin et al., 2012). Among the triterpenes is the linear molecule squalene from which phytosterols derive (Valitova et al., 2016). As they arise from a cyclisation reaction, plant sterols have a characteristic four-ring structure carrying a side chain and a hydroxyl group at the C3-position (Figure 1B). This hydroxyl group can be conjugated i.a. to a FA thus forming SEs (Figure 1C) or a carbohydrate moiety like glucose to yield steryl glycosides (SGs, Figure 1D; Ferrer et al., 2017).
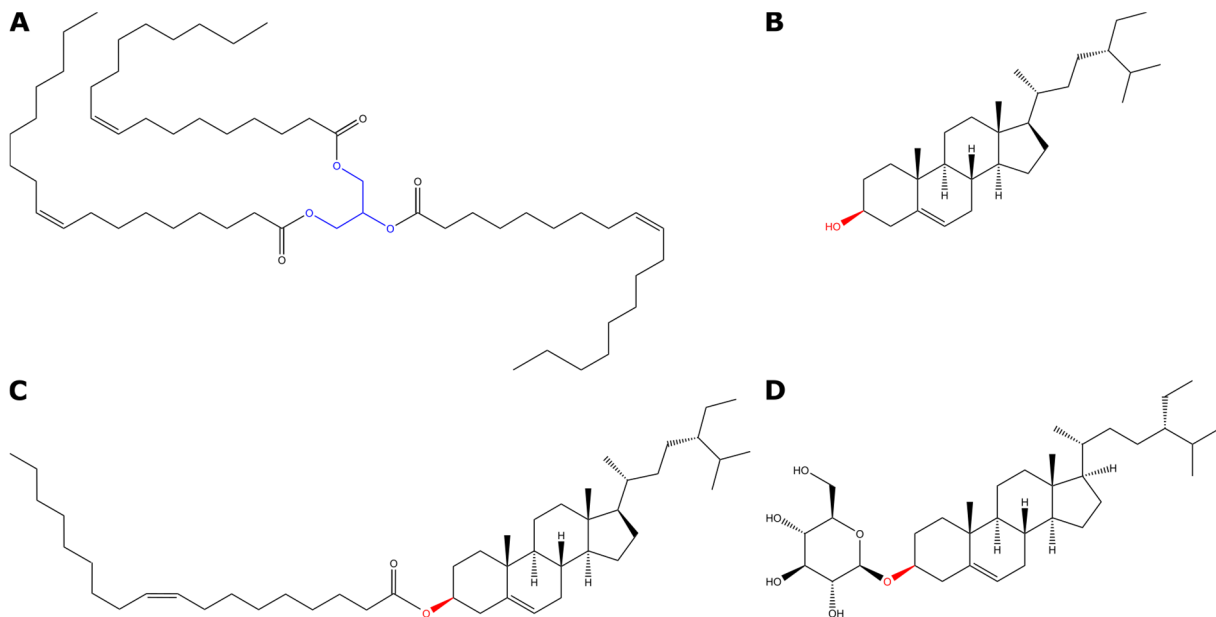
Figure 1: Structures of exemplary hydrophobic neutral lipids. In triolein as representative triacylglycerol species (A), three oleic acid molecules are esterified to a glycerol backbone (blue). Phytosterols like sitosterol have a characteristic four-ring structure (B), and a 3-hydroxyl group that can be used for conjugation to other molecules (red). If the hydroxyl group is esterified to a fatty acid, sterol esters are formed (C). However, the sterol skeleton can also be linked to a sugar like glucose, giving rise to steryl glycosides (D).

Several lipid classes contain charged residues in their structure though. For example, the hydroxyl group of glycerol in *sn-3* position can be linked to a phosphate group, which introduces negative charges and amphiphilic properties to the molecule. If the hydroxyl group in the *sn-3* position is only linked to phosphate, anionic phosphatidic acid (PA, Figure 2A) is formed. However, the phosphate can be further esterified to diverse alcohols giving rise to various head groups of phospholipids. For example, phosphatidylcholine (PC, Figure 2B) carries a choline residue linked to its phosphate group.

Finally, in addition to the so far mentioned glycerolipids and terpenes, a third lipid class, sphingolipids, can be distinguished. Sphingolipids are defined by their backbone of a long chain amino alcohol whose amino group in C2-position can be linked to FAs in an amide bond (Figure 2C). In addition, the hydroxyl group at the C1-position can be linked to different head groups of sometimes great complexity (Luttgeharm et al., 2016).
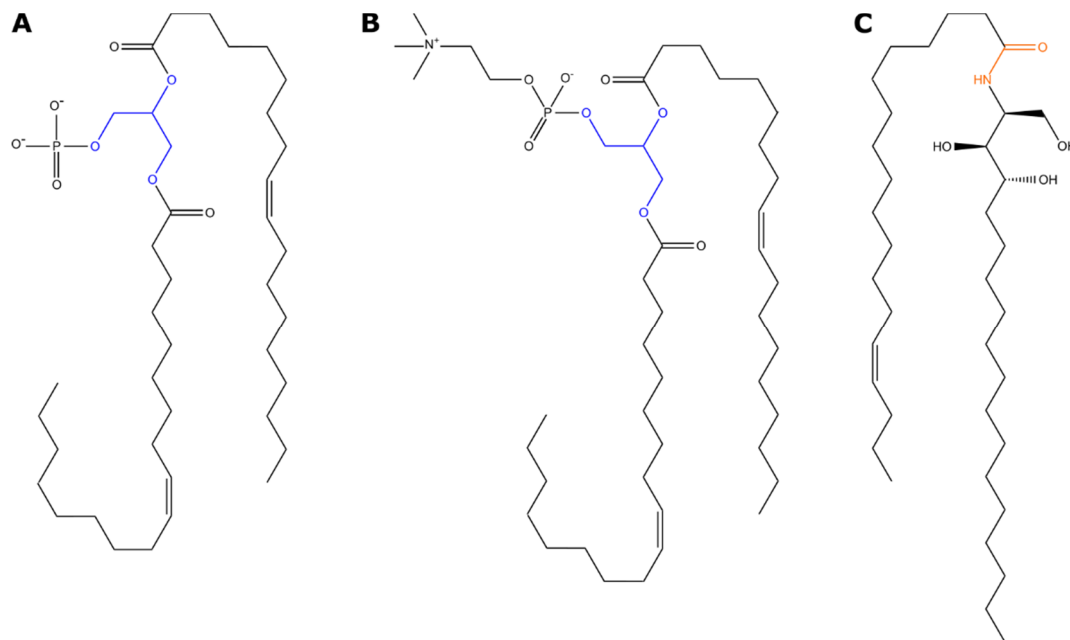
Figure 2: Structures of exemplary lipids in membranes. In phosphoglycerolipids, two acyl chains are esterified to the glycerol backbone (blue), however, a third ester bond at the *sn-3* position is formed to phosphate, yielding phosphatidic acid (A). If the phosphate group is further esterified, different phosphoglycerolipids can be formed. For example, linkage to choline gives rise to the membrane lipid phosphatidylcholine (B). Sphingolipids on the other hand are characterised by a long chain amino alcohol that contains an amino group at the C2-position. This amino group can be linked to a fatty acid by an amide bond (orange) to form ceramides (C).

The functions that lipids fulfil in plant cells are as diverse as their structures. TAG and SEs are storage compounds, providing FAs for β-oxidation and acting as energy and carbon source in germination and seedling establishment (Pinfield-Wells et al., 2005; Eastmond, 2006) but might also be important for membrane homeostasis (Ferrer et al., 2017; Ischebeck et al., 2020). Amphiphilic glycerolipids are membrane-forming: the phosphoglycerolipids PC, phosphatidylethanolamine (PE) and phosphatidylinositol (PI) are important components of non-plastidial membranes whereas glucolipids like mono- or digalactosyldiacylglycerol (MGDG, DGDG) dominate in the membranes of plastids (Ohlrogge and Browse, 1995; Hölzl and Dörmann, 2019). Sterols in membranes adjust membrane fluidity and are therefore important in adaptation to environmental conditions (Valitova et al., 2016). Among the so-called minor phospholipids, which occur only in small amounts in plant cell membranes, are important lipid signalling molecules like PA or phosphoinositides, which are phosphorylated derivatives of PI (Noack and Jaillais, 2020). In the following, two lipid contributions to plant cell organisation shall be discussed: anionic phospholipids as signals in plant membranes and storage lipids in the context of lipid droplets.

1.2 Lipid signals in plants

1.2.1 Signal transduction

All living cells have to maintain their cellular homeostasis, which requires i.a. free energy to counteract increases in entropy and ways to detect and react to internal and external signals. Intracellular signals are often exchanged between different organelles and can involve membrane contact sites (Rosado and Bayer, 2021). External stimuli can occur in a variety of forms, e.g. as electromagnetic radiation like heat or light, or as chemical compounds like plant hormones. The detection of signals requires specialised receptor proteins, which can be situated in the plasma membrane, where they are able to interact with signals outside of the cell. The presence of bacteria is for example detected due to the interaction of flagellin with the plasma membrane receptor FLAGELLIN-SENSITIVE 2 (Zipfel et al., 2004). On the other hand, there are also intracellular receptors that can localise to organelle membranes and are e.g. involved in protein quality control at the endoplasmic reticulum (ER; Strasser, 2018). Detection by a receptor forms the start of a signalling cascade, which transmits and amplifies the input signal. Due to the amplification processes, signals can be effective even at very low concentrations triggering cell wide responses with different signalling pathways.

Signal transfer is usually achieved by the modification of proteins, which in turn affect other target proteins. Protein changes in signalling cascades include, but are not limited to, phosphorylation at different target sites, ubiquitination and subsequent proteasomal degradation of target proteins, altered protein interactors, the exchange of GDP to GTP in the binding pocket of GTPases, or altered protein localisation (Krauss, 2014). Furthermore, proteins can transmit signals by producing second messengers, small molecules that diffuse from the site of synthesis/storage to their respective receptors in the vicinity. Common second messengers include soluble molecules like cyclic adenosine monophosphate or Ca^{2+} ions, gases like nitric oxide, and at least partially hydrophobic molecules that diffuse laterally in membranes like phosphoinositides or diacylglycerol (DAG; Krauss, 2014). In mammalian cells, for example, DAG acts as a signal transducer that modulates the influx of second messenger Ca^{2+} ions via protein kinase C (Colón-González and Kazanietz, 2006).

However, lipids can not only act as second messengers but can appear at different points of a signalling cascade. They can also act as the signal itself as is the case for the lipid-derived jasmonates that act as plant hormones (Wasternack and Feussner, 2018). Furthermore, lipids act as determinants of protein localisation as proteins bind to specific lipids in membranes (Lin et al., 2020; Synek et al., 2021) or change their organisation in the membrane in reaction to membrane lipid adaptations (Platre et al., 2019). Different lipid classes have different signalling functionalities and further focus in this work shall be directed on phosphoglycerolipid signals.

1.2.2 Phosphoglycerolipid signalling molecules

As mentioned previously, several lipid classes contain a phosphate moiety. In phosphoglycerolipids this phosphate is esterified to the *sn-3* position of the glycerol backbone, with PA as structurally simplest representative (Figure 2A). The phosphate is often linked to

further moieties, giving rise to the different phospholipids present in cellular membranes (Figure 3A; Li-Beisson et al., 2013). If the head group is the polyalcohol inositol it can be further phosphorylated as in phosphatidylinositol 4,5-bisphosphate (PI(4,5)P$_2$, Figure 3B). These so-called phosphoinositides are low abundant lipids, however, of huge importance as signalling molecules (König et al., 2007; Krinke et al., 2007; Noack and Jaillais, 2020) and are described in the following section.
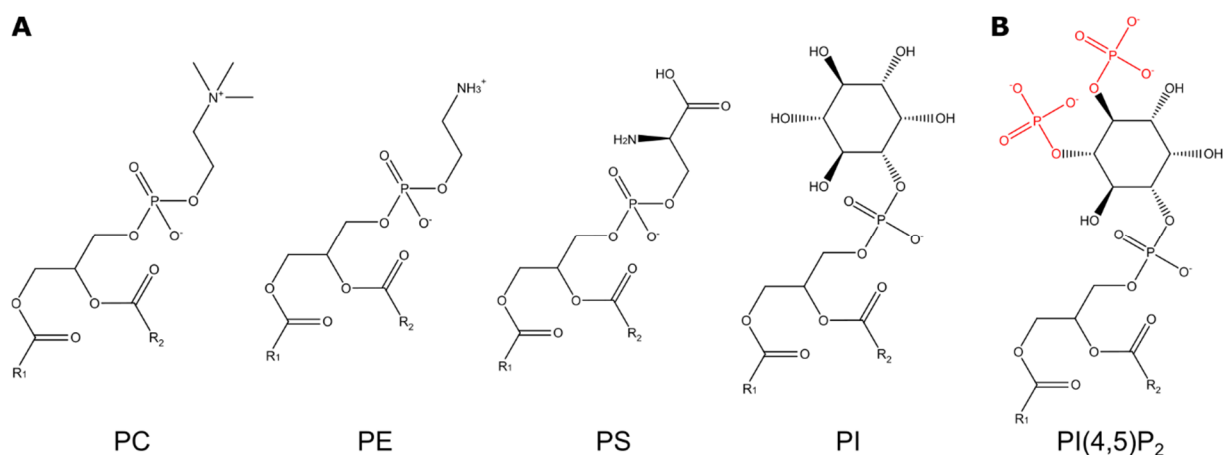
Figure 3: Different head groups of phosphoglycerolipids. In phosphoglycerolipids, the *sn-3* position is esterified to a phosphate which in turn often carries additional groups (A). Additional choline and ethanolamine moieties give rise to phosphatidylcholine (PC) or phosphatidylethanolamine (PE) that carry a positive charge at the nitrogen which overall neutralises the negative charge of the phosphate group. If the phosphate is linked to serine or inositol, phosphatidylserine (PS) or phosphatidylinositol (PI) is formed, respectively. The inositol of PI can be further phosphorylated (B, red phosphate groups) yielding phosphoinositides of which phosphatidylinositol 4,5-bisphosphate (PI(4,5)P$_2$) is a representative. In all structures, the esterified fatty acids are abbreviated as R$_1$ and R$_2$.

Phosphoinositides

The precursor molecule for the synthesis of the differently phosphorylated phosphoinositides is PI, whose synthesis takes place at the ER and shares a common pathway with the synthesis of other phospholipids. In brief, FAs are sequentially esterified to glycerol-3-phosphate to form PA (Li-Beisson et al., 2013). PI is then synthesised via the CDP-diacylglycerol pathway, whereby PA is activated with CTP to form CDP-diacylglycerol before inositol is attached in a nucleophilic substitution reaction (Löfke et al., 2008; Zhou et al., 2013b). Phosphorylation of different hydroxyl groups (at the 3', 4' or 5' carbon) of the inositol head group by specific kinases then gives rise to various phosphoinositides.

Localisation studies with fluorescent lipid probes established distinct subcellular distributions of phosphoinositides. Phosphatidylinositol 3-phosphate (PI3P) was found at late endosomes and the vacuolar membrane of Arabidopsis cells (Vermeer et al., 2006; Simon et al., 2014). PI3P at late endosomes is required for protein sorting (Pourcher et al., 2010; Gao et al., 2014) and inhibitors of the PI3P-synthesising PI 3-kinases impede vacuolar transport and autophagy (Takatsuka et al., 2004; Takáč et al., 2013). Moreover, phagophores are decorated by the PI3P kinase VPS34 as part of a complex that promotes autophagy in Arabidopsis (Marshall and Vierstra, 2018; Liu et al., 2020), underlining the importance of PI3P in this process.

Phosphatidylinositol 3,5-bisphosphate (PI(3,5)P$_2$) proved to be more challenging to study, as for this phosphoinositide the known lipid probes are less reliable. Nevertheless, PI(3,5)P$_2$ was also reported at late endosomes in root cortical cells (Hirano et al., 2017). Similar to its localisation, the physiological roles of PI(3,5)P$_2$ are obscure. In mammalian and yeast cells, PI(3,5)P$_2$ has been linked to organisation of endosomes and lysosomes or vacuoles (Hirano and Sato, 2019). In Arabidopsis, a double mutant of the PI(3,5)P$_2$-producing enzymes FAB1A and FAB1B displayed disturbed vacuole reorganisation and vacuole acidification during pollen development leading to a lethal male gametophyte phenotype (Whitley et al., 2009). However, the previously mentioned fluorescent probe could not detect PI(3,5)P$_2$ at the vacuolar membrane, so it remains unclear how it would direct alterations of the vacuole. PI(3,5)P$_2$ has also been suggested to be required for late endosomal maturation, yet again its precise signalling role is unclear (Hirano and Sato, 2019).

Phosphatidylinositol 4-phosphate (PI4P) is the most abundant phosphoinositide in plant cells (Krinke et al., 2007) and was proposed to serve functions that are associated with its downstream product PI(4,5)P$_2$ in animal cells (Marković and Jaillais, 2022). This hypothesis originated in part by the observed differences in PI4P-localisation: in animal cells, PI4P probes were reported to be dominant at the Golgi apparatus (Balla et al., 2005; Weixel et al., 2005; Simon et al., 2014) whereas they displayed a preference for the plasma membrane in plant cells (Ischebeck et al., 2010; Simon et al., 2014, 2016). However, also in plant cells, PI4P was detected at Golgi compartments (Simon et al., 2014) and PI4P-forming enzymes, namely PI 4-kinases (PI4Ks), can be found both at the *trans* Golgi network (TGN) and the plasma membrane (Preuss et al., 2006; Kang et al., 2011; Noack et al., 2022).

PI4Kβ1 has been observed at the TGN (Preuss et al., 2006; Kang et al., 2011) and shares 80% protein sequence identity with another enzyme consequently named PI4Kβ2 (Mueller-Roeber and Pical, 2002). Due to the high homology it seems likely that PI4Kβ2 is also present at the TGN and in the double mutant *pi4kβ1 pi4kβ2* the TGN was structurally altered (Kang et al., 2011). The double mutant was additionally impaired in pollen tube and root hair growth (Preuss et al., 2006; Szumlanski and Nielsen, 2009), probably as trafficking of cell wall and membrane material required in these tip-growing cells was affected. Defects in cytokinesis of the double mutant were also connected to altered vesicular trafficking (Lin et al., 2019). Finally, *pi4kβ1 pi4kβ2* was reported to accumulate the defence hormone salicylic acid (SA), although the precise connection between SA and PI4P is unclear (Sašek et al., 2014; Antignani et al., 2015).

Synthesis of PI4P at the plasma membrane is catalysed by PI 4-kinase α1 (PI4Kα1), that is targeted to the membrane via a scaffolding complex (Noack et al., 2022). There, it acts together with PA and phosphatidylserine (PS) to establish an electronegative potential (Simon et al., 2016; Platre et al., 2018). In addition to this, PI4P is able to interact with the synaptotagmins SYT1 and SYT3, thus helping to establish contact sites to the ER (Ruiz-Lopez et al., 2021). However, SYT1 is also reported to interact with PI(4,5)P$_2$ as discussed below (Lee et al., 2019), so the establishment of contact sites might require situation-dependent lipid signatures. Furthermore, PI4P at the plasma membrane also regulates exocytic trafficking processes via the exocyst complex. This complex mediates the initial contact between exocytic vesicles and their target membrane and is key component of targeted exocytosis (Zárský et

al., 2013). The recruitment of the whole complex depends on the membrane localisation of its subunit EXO70A1 (Synek et al., 2021). The initial localisation of EXO70A1 itself relies upon interaction with membrane phospholipids, most importantly PI4P. Consequently EXO70A1-localisation is largely lost, when PI4P synthesis is prevented by chemical inhibitors (Synek et al., 2021).

In addition to its own functions, PI4P is also the substrate for PI4P 5-kinases (PIP5Ks) that produce PI(4,5)P_2 by phosphorylating the hydroxyl group at the C5 of the inositol head group. In mammalian cells, PI(4,5)P_2 is a crucial signalling molecule that can be hydrolysed to inositol 1,4,5-trisphosphate (I(1,4,5)P_3) and DAG. These products of hydrolysis act as second messengers: I(1,4,5)P_3 binds to ER-localised receptors and triggers Ca^{2+}-release into the cytosol and DAG activates protein kinase C (PKC; Katan and Cockcroft, 2020). Strikingly, this does not appear to be the case in plants. Neither are there any plant receptors of I(1,4,5)P_3 known, nor were homologs of PKC found (Munnik and Testerink, 2009). Nevertheless, in Arabidopsis there are eleven isoforms of PIP5Ks which produce PI(4,5)P_2 (Gerth et al., 2017), so there must be other important functions in plants.

Initial attempts to visualise PI(4,5)P_2 in tobacco BY2 cells were complicated, as an early fluorescent probe was unable to bind PI(4,5)P_2 in the plasma membrane and instead localised to the cytosol (Van Leeuwen et al., 2007). In stable transgenic Arabidopsis plants carrying this probe, the authors did observe localisation to the tip of growing root hairs and towards the edge of the cell plate in the final stages of cytokinesis, though (Van Leeuwen et al., 2007). It thus seems as if the lipid probe used in the study was not sensitive enough to detect PI(4,5)P_2 at steady-state levels in the plasma membrane and that these levels are under non-stressed conditions very low in plant cells. They do increase after hyperosmotic stress, and fittingly the triple mutant *pip5k7 pip5k8 pip5k9* displays root growth defects after mannitol and NaCl-treatment (Pical et al., 1999; König et al., 2008; Kuroda et al., 2021). One functional role of PI(4,5)P_2 in hyperosmotic stress might be the interaction with SYT1, which mediates tethering at ER-plasma membrane contact sites and leads to enhanced connectivity between the ER and the plasma membrane (Lee et al., 2019). In addition to osmotic stress responses, studies on PIP5Ks also confirmed the importance of PI(4,5)P_2 in tip-growing cells like pollen tubes and root hairs (Ischebeck et al., 2008; Kusano et al., 2008; Sousa et al., 2008; Stenzel et al., 2008). Imaging of fluorescent lipid sensors in tobacco pollen tubes established a polarised apical plasma membrane localisation and pollen tubes showed severe growth defects when PI(4,5)P_2 levels were altered and its polar localisation was lost (Kost et al., 1999; Ischebeck et al., 2008; Sousa et al., 2008).

Different phosphoinositides can be interconverted by various kinases and phosphatases that add or remove phosphate groups at the inositol head group (Noack and Jaillais, 2020). The action of these enzymes allows reversible alterations of the respective phosphoinositide pools. However, to switch off phosphoinositide signals more definitely, phosphoinositide-dependent phospholipase C (PI-PLC) enzymes are able to cleave the inositol head group, yielding phosphorylated inositol and DAG (Pokotylo et al., 2014). DAG in turn can be phosphorylated to PA that has signalling functions itself.

Phosphatidic acid

Different from the phosphoinositides, PA is not singularly formed for signalling purposes but is also an intermediate in the *de novo* synthesis of structural membrane lipids and TAGs in the plastids or at the ER (Li-Beisson et al., 2013; Bates, 2016). PA synthesized at the plasma membrane, on the other hand, is believed to act as a signal there. This signalling PA can be formed via two pathways, either by phospholipase D (PLD) or by the concerted action of PLC and DAG kinase (DGK) enzymes (Figure 4). Disentangling the contribution of the two different pathways of signalling PA production provides a challenge that has been met in different ways: radioactive 32-P labelled phosphate is integrated faster into ATP than into structural phospholipids. Consequently, PA originating from phosphorylation of DAG with ATP as phosphate-donor is more rapidly labelled than PA originating from the action of PLDs on structural phospholipids (Arisz et al., 2009). Biochemical analysis of different time points after incubation with 32-P labelled phosphate thus allows to distinguish between the two enzyme activities, but cannot be used in live-cell imaging. There, different chemical inhibitors of DGKs and PLDs have been used (Pleskot et al., 2012). Nevertheless, to unravel the contribution of one specific enzyme to PA signalling pathways remains one of the major challenges in PA signalling research.
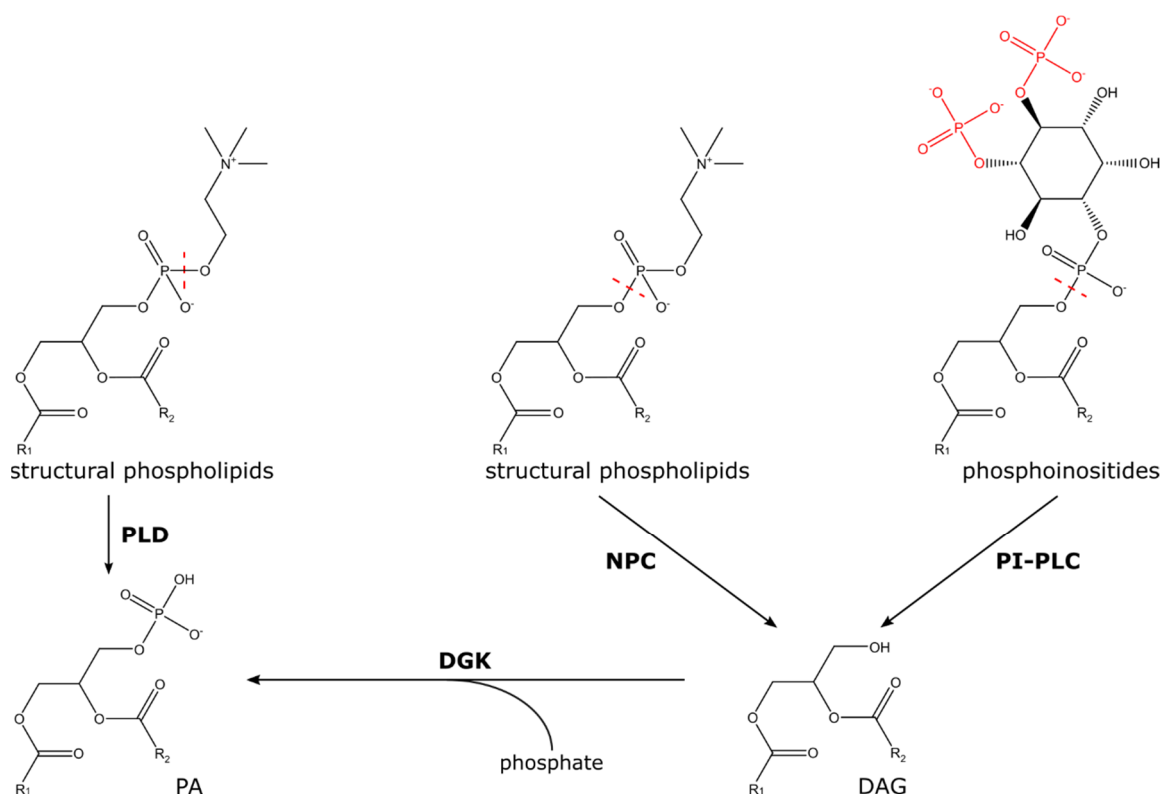
Figure 4: Different pathways of producing signalling PA. Signalling PA can be produced by the enzyme activities of either phospholipase D (PLD) or phospholipase C combined with DAG kinase (DGK). PLD acts on structural phospholipids and cleaves the bond between the phosphate group and the attached moiety (red dashed line), directly yielding PA as product. However, structural phospholipids can also be cleaved at the bond between the phosphate group and the glycerol backbone by non-specific phospholipase C (NPC), with DAG as the product. Likewise phosphoinositide-dependent phospholipase C (PI-PLC) enzymes can form DAG from phosphoinositides. Subsequent phosphorylation of DAG by DGKs then gives rise to PA. In all structures, esterified fatty acids of the glycerol backbone are abbreviated as R_1 and R_2.

Irrespective of its producing enzyme, signalling PA has been localised at the plasma membrane in Arabidopsis root and guard cells (Li et al., 2019). Although not a major contributor, it seems to assist there in the formation of the membrane potential and in the targeting of the exocyst complex (Simon et al., 2016; Platre et al., 2018; Synek et al., 2021). Instead of specific functions in optimal growth conditions, PA otherwise seems to be a stress signal that accumulates after a number of different stresses like freezing, cold stress, heat stress, salt stress, wounding, but also pathogen infection (Testerink and Munnik, 2011; Pokotylo et al., 2018; Kalachova et al., 2022). The sheer amount of – sometimes opposing – stresses triggering an increase in PA raises the question how downstream signalling remains specific to the initial PA-inducing signal. One suggested explanation attributes differences in the PA-induced responses to distinct subcellular localisation of PA-producing enzymes and isoenzymes (Pokotylo et al., 2018). Also in the plasma membrane itself, heterogeneous signalling domains might induce disparate responses (Jaillais and Ott, 2020). Another explanation could relate to the signal-transmitting proteins that bind the PA signal. PA is not in itself a homogenous molecule, as diverse acyl chains can be esterified to the *sn-1* and *sn-2* positions. In a model study, protein binding affinities to DAG varied with different combinations of esterified acyl chains (Schuhmacher et al., 2020). Similar effects could play a role in plant cells such that the PA species induced by specific stresses coordinate the respective downstream responses. In addition, the microenvironment of generated PA might influence protein binding behaviour (Pokotylo et al., 2018).

Besides its function as a stress signal, signalling PA has a role to play in tip-growing cells like root hairs and pollen tubes, although probably with different effectors (Potocký et al., 2003; Hong et al., 2009; Pleskot et al., 2012; Lin et al., 2020). In root hairs, increased root hair length was observed in Arabidopsis overexpression lines of PLDε (Hong et al., 2009). More recently it was proposed that root hair elongation requires the auxin efflux carrier PIN FORMED 2 (PIN2) and that the degradation of PIN2 is reduced by PA-dependent recruitment to the plasma membrane (Lin et al., 2020). In tobacco pollen tubes, a fluorescent PA-sensor showed a distinct plasma membrane distribution with maximum fluorescence shortly behind the pollen tube tip (Potocký et al., 2014). The very tip of growing pollen tubes was devoid of fluorescent signal (Potocký et al., 2014) and it has been suggested that the onset of PA localisation in the membrane acts as a landmark for localisation of exocyst subunits (Sekereš et al., 2017). Signalling PA in pollen tubes is produced by both the PLD- and the PLC/DGK-pathway (Potocký et al., 2003; Pleskot et al., 2012; Vaz Dias et al., 2019; Angkawijaya et al., 2020; Pejchar et al., 2020). There, PLD activity specifically has been connected to the organisation of the actin cytoskeleton (Pleskot et al., 2010, 2013), which has a very distinct structure in pollen tubes to regulate vesicle trafficking (Cai et al., 2015a; Stephan, 2017). DGK enzyme activity on the other hand has been linked to cell wall rheological properties (Vaz Dias et al., 2019) that affect extensibility during pollen tube growth (Fayant et al., 2010). Despite its structural simplicity, PA has thus complex signalling function and connects different signalling inputs and pathways into a "PA signature" that modulates subsequent signalling responses (Pokotylo et al., 2018).

1.2.3 Pollen tubes as cell biological model systems

In the study of the aforementioned lipid signalling molecules, different model systems have been used. While Arabidopsis is the most common plant model system (Koornneef and Meinke, 2010), it can provide experimental challenges due to functional enzyme redundancy, mutant lethality or reproductive defects. A recurring alternative is the study of pollen tubes, from lily, petunia or tobacco pollen (Dowd et al., 2006; Winship et al., 2016; Hemelryck et al., 2018; Pejchar et al., 2020). Among pollen tube models, Arabidopsis is also less established due to the smaller size and higher frailness of its pollen tube cell. Pollen tubes form from the vegetative cell of pollen after pollen germination to transport the sperm cells to the ovule (Borg et al., 2009), however, they can also be grown *in vitro* (Read et al., 1993; Boavida and McCormick, 2007). As pollen tubes grow they reach considerable size and growth rates of around 0.1 µm/h *in vitro*; in addition pollen tubes are easily transformed transiently (Wang and Jiang, 2011; Stephan, 2017). These properties made pollen tubes to an established model system for the processes behind its characteristic tip growth: i.a. cell polarisation, cytoskeletal organisation, endo- and exocytic processes (Kost, 2008; Chebli et al., 2013; Hepler et al., 2013; Cai et al., 2015a; Scheible and McCubbin, 2019). In terms of signalling lipids, pollen tubes proved to be an advantageous model for studying lipid signals in polarity establishment and trafficking processes, and helped to establish lipid signatures in polarised cells (Kost et al., 1999; Ischebeck et al., 2008, 2010; Potocký et al., 2014; Heilmann and Ischebeck, 2016). Interestingly, pollen tubes later turned out to be a valuable model system also in another area of plant lipid research. After seeds, pollen is the second major accumulator of neutral lipids, and in pollen tubes a high number of lipid droplets is present, which has been used i.a. for localisation studies of lipid droplet proteins (Piffanelli et al., 1998; Müller et al., 2017)

1.3 Lipid droplets – Organelles defined by neutral lipids

1.3.1 Lipid droplets are unique organelles

Eukaryotic cells are defined by compartmentalisation into different organelles. The compartmentalisation is achieved by membranes that separate the various organellar environments. In most cases, two aqueous environments are partitioned from each other, so demarcation is achieved by a phospholipid bilayer. One notable exception are lipid droplets (LDs): they consist of a hydrophobic core of neutral lipids like TAGs and SEs, hence they are delimited by a phospholipid monolayer (Tzen et al., 1993). In mammalian cells, yeast, and oil seeds of various plant species, PC was detected as the dominant phospholipid of the monolayer (Tzen et al., 1993; Bartz et al., 2007; Grillitsch et al., 2011). In addition, in mammalian and yeast cells, the phospholipid composition of LDs and total membranes was compared and a higher proportion of lysophospholipids at LDs was observed (Bartz et al., 2007; Grillitsch et al., 2011). As plant LDs are commonly small (diameter of c. 1 µm; Huang, 2018), it seems likely that the surrounding phospholipid monolayer accumulates lysophospholipids with a positive membrane curvature (Holthuis and Menon, 2014) also in plant cells. Embedded into the phospholipid monolayer are various structural and enzymatic

proteins (Kretzschmar et al., 2018, 2020; Fernández-Santos et al., 2020) that will be discussed in detail in a later section.

The core of LDs is expected to be devoid of proteins and thus metabolically inactive as the hydrophobic environment nullifies the stabilising hydrophobic effect contributing to protein structure (Pace et al., 1996; Compiani and Capriotti, 2013). Consequently, active LD processes do not happen at the "inside" of the organelle but rather at the surface, the lipid-water interface between LDs and the cytosol. The interior of LDs can be instead seen as a, at least transiently, quiescent storage area for hydrophobic compounds. All in all, LDs are thus very distinct organelles, whose roles and functions in the cellular context are yet to be fully explored.

1.3.2 Lipid droplet biogenesis takes place at the ER

The unique structure of LDs is reflected in the currently assumed model of their biogenesis, whereby LDs bud off from the ER into the cytosol (Pyc et al., 2017b; Ischebeck et al., 2020). LD biogenesis is assumed to be an evolutionary conserved process, combining a similar series of events in animals, yeast and plants, albeit the involved proteins might differ (Pyc et al., 2017b, 2021). In the current model, LD biogenesis combines the following step: synthesis of neutral lipids at the ER, formation of a neutral lipid lens between the ER leaflets, budding of the nascent LD towards the cytosol, growth and maturation of LDs (Chapman et al., 2012; Walther et al., 2017; Ischebeck et al., 2020; Nettebrock and Bohnert, 2020).

Neutral lipid synthesis at the ER

LD synthesis depends on the presence of the neutral lipids that make up the hydrophobic core and increased neutral lipid levels lead to a concomitant increase of LD number in plant cells (Zhou et al., 2013a; Fan et al., 2014; Shimada et al., 2019). Building blocks of the dominant core components TAG and SE are FAs, and glycerol or sterols, respectively. The backbone of phytosterols derives from isoprenoid precursors originating from the mevalonate pathway in the cytosol (Liao et al., 2016). Synthesis of FAs on the other hand, takes place in plastids in plant cells (Packter and Stumpf, 1975) where the fatty acid synthase complex sequentially assembles C2-units into FAs of 16-18 carbon atoms bound to the acyl carrier protein (ACP). A first desaturation at the $\Delta 9$ position of stearic acid bound to ACP also occurs in the plastids, so that FAs directly exported after synthesis are either monounsaturated or saturated (Li-Beisson et al., 2013). At the ER, acyl chains can be further elongated or desaturated: elongation by further addition of C2-units on the acyl chain of acyl-CoA and desaturation after the incorporation into the *sn-2* position of PC (Li-Beisson et al., 2013). Desaturated acyl chains in PC and other acyl chains from the cellular acyl-CoA pool can be exchanged via the concerted action of phospholipase A2 and acyl-CoA:lysophosphatidylcholine acyltransferase (LPCAT) in the Lands cycle, or the combination of forward and reverse enzymatic activity of LPCAT (Bates, 2016). Additionally, acyl chains linked to plastidial membrane lipids can be desaturated in the plastid and subsequently be exported to the ER acyl-CoA pool (Li-Beisson et al., 2013). The combined processes of FA modification and exchange between pools allow considerable acyl editing and give rise to a diverse acyl-CoA pool.

Based on the model plant Arabidopsis, the subsequent synthesis of SEs and TAGs occurs at the ER. Formation of the ester bond in SEs is catalysed by phospholipid:sterol acyltransferases (Banas et al., 2005) while the committing step of TAG synthesis is the incorporation of a third FA into DAG (Bates, 2016). In the *de novo* assembly of TAG (Figure 5), also known as the Kennedy pathway, the DAG precursor derives from the consecutive acylation of glycerol-3-phosphate via lysophosphatidic acid to PA at the ER (Chapman and Ohlrogge, 2012; Bates, 2016; Shockey et al., 2016). The resulting PA is subsequently dephosphorylated by PA phosphatases to DAG (Eastmond et al., 2010). PA and DAG can also be formed from phospholipids by PLD and PLC enzymes, respectively. However, both PLC and PLD have so far rather been studied in the context of signalling pathways, so their contribution to TAG synthesis is not clear (Pokotylo et al., 2013, 2014; Hong et al., 2016). Acylation of DAG to produce TAG can be catalysed by the activity of DIACYLGLYCEROL ACYLTRANSFERASE 1 (DGAT1) or PHOSPHOLIPID:DIACYLGLYCEROL ACYLTRANSFERASE 1 (PDAT1) (Zhang et al., 2009). Arabidopsis harbours two other DGAT enzymes, AtDGAT2 and AtDGAT3, however, they are not functionally redundant to AtDGAT1, as they are unable to compensate the loss of seed oil in a *dgat1-1* mutant with down-regulated *PDAT1* expression (Zhang et al., 2009; Hernández et al., 2012; Zhou et al., 2013a). DGAT and PDAT differ in the nature of the FA-providing substrate: DGAT1 takes acyl chains from acyl-CoA (Hobbs et al., 1999; Zou et al., 1999; Zhou et al., 2013a) whereas PDAT1 transfers acyl chains from the *sn-2* position of PC onto DAG to yield TAG and lysophosphatidylcholine (Dahlqvist et al., 2000; Zhang et al., 2009). TAG synthesis via DGAT1 and PDAT1 therefore also influences the flux through different acyl editing pathways.
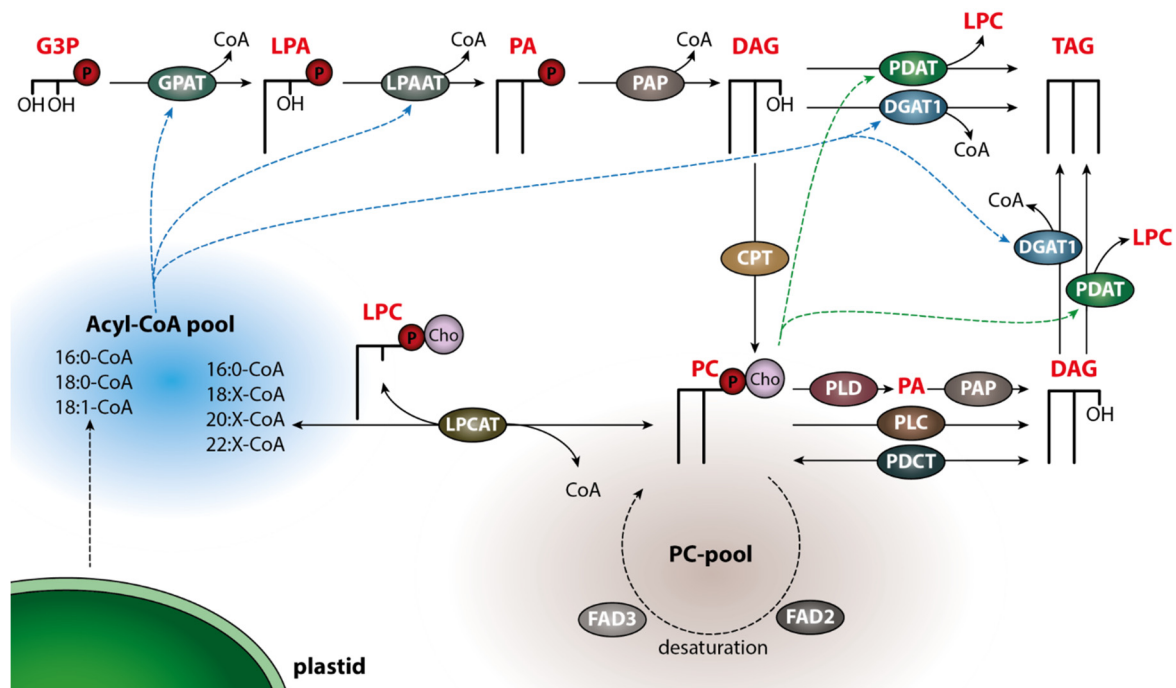
Figure 5: TAG synthesis at the ER involves different pathways. Fatty acids are synthesised in the plastid and are exported to the acyl-CoA pool in the ER. There, they can be elongated as acyl-CoAs or are incorporated at the *sn-2* position of lysophosphatidylcholine (LPC) which gives rises to phosphatidylcholine (PC). In PC, additional double bonds are introduced into the acyl chains by the activity of fatty acid desaturases (FADs). Exchange between the acyl-CoA pool and the PC-pool is mediated by acyl-CoA:lysophosphatidylcholine acyltransferase (LPCAT) and gives rise to a greater variety in the acyl-CoA pool. In a linear sequence of reactions, these acyl chains can be sequentially added to glycerol 3-phosphate (G3P) for *de novo* synthesis of TAGs. Esterification of the first acyl chain to the *sn-1* position of G3P is catalysed by glycerol 3-phosphate acyltransferase (GPAT) and yields lysophosphatidic acid (LPA). A second acylation by acyl-CoA:lysophosphatidic acid acyltransferase (LPAAT) gives rise to phosphatidic acid (PA) that is subsequently dephosphorylated by PA phosphatase (PAP). TAG is then synthesised by diacylglycerol acyltransferases (DGATs) like DGAT1 or phospholipid:diacylglycerol acyltransferases (PDATs) like PDAT1. DGAT1 and PDAT1 differ in their acyl donor, using acyl-CoA and PC respectively. The final acylation step of TAG synthesis competes with membrane lipid synthesis for the DAG substrate, as DAG is also the precursor for PC-synthesis by choline phosphotransferase (CPT). On the other hand, PC can be converted back to DAG by the action of phospholipase C (PLC) or the concerted enzyme activities of phospholipase D (PLD) and PAP. Furthermore, the head group of PC can be transferred to another DAG molecule due to the enzyme activity of phosphatidylcholine:diacylglycerol cholinephosphotransferase (PDCT), resulting in one molecule of PC and one molecule of DAG with potentially altered acyl chain composition. The combined reactions thus give rise to a huge variety of possible TAG species with several different acyl chain combinations. In the nomenclature of indicated acyl chains, the first number indicates the total number of carbon atoms and the second number denotes the number of double bonds. Figure is taken from (Ischebeck et al., 2020).

Formation of a neutral lipid lens

After neutral lipid synthesis, phase separation of neutral lipids from phospholipids takes place in part due to biophysical effects (Thiam and Forêt, 2016). TAGs and SEs can be dissolved only to a limited amount in a phospholipid bilayer (Hamilton et al., 1983; Duelund et al., 2013) and

will demix into a lipid lens between the two layers after a critical concentration is exceeded. Local differences in ER, e.g. between sheet-like and tubular structures, might favour the nucleation process at specific sites (Thiam and Forêt, 2016). However, in animal cells the number of formed LDs was not dependent on lipid concentration in oleate loading, and in yeast, the pre-assembly of LD biogenesis at specific subdomains of the ER has been reported (Kassan et al., 2013; Choudhary et al., 2020). Furthermore, TAGs are trapped in confined regions by the seipin protein already at low concentrations (Prasanna et al., 2021; Zoni et al., 2021; Renne et al., 2022). These seipin proteins are a key regulator of LD biogenesis in animals, yeast and plants (Szymanski et al., 2007; Fei et al., 2008; Bi et al., 2014; Cai et al., 2015b). Cryo-EM structures of yeast, human and, *Drosophila* seipin complexes show them as ring-shaped oligomers of ten, eleven or twelve monomers, respectively (Sui et al., 2018; Yan et al., 2018; Klug et al., 2021). The combined transmembrane regions of the seipin monomers could surround the LD-ER connection, perhaps acting as a vent for the accumulating neutral lipids. Hence, nucleation of the initial lipid lens is probably a combination of biophysical forces guided by structural proteins.

Budding of the nascent LD towards the cytosol

After initial lens formation, nascent LDs usually bulge towards the cytosol and mature LDs exclusively bud off to this side, so LDs in other localisations have been associated with defects of the involved protein machinery (Taurino et al., 2018). Nevertheless, how the budding and its directionality are achieved are still open questions. It has been reported that membrane asymmetry supports directional budding, comprising asymmetric protein insertion and differences in phospholipid density (Chorlay et al., 2019). In addition, in animal cells, fat storage-inducing (FIT) proteins were reported to be required for proper budding (Choudhary et al., 2015). While no homologs of FIT proteins are so far known in plants (Pyc et al., 2017b), the previously mentioned seipin could also play a role here (Ischebeck et al., 2020; Zoni et al., 2021). Its solved cryo-EM structures revealed large luminal regions of the seipin protein (Sui et al., 2018; Yan et al., 2018; Klug et al., 2021), which might be involved in the directionality of LD budding when assembled in the seipin complex. Furthermore, the plant-specific oleosin proteins were described to direct LD budding upon expression in tobacco BY2 cells: when transformed cells expressed a modified oleosin targeted to the ER lumen, LDs appeared to bud off into the lumen instead of the cytosol (Huang and Huang, 2017).

Maturation of LDs

The already described seipin proteins continue to regulate LD biogenesis up to LD maturation. Unlike yeast, human and *Drosophila*, the Arabidopsis genome codes for three seipins (Cai et al., 2015b), possibly creating higher versatility in complex formation. Given the functional conservation in LD biogenesis between animal, yeast and plant cells though, they likely form a similar protein complex around the LD-ER connection. There, they are important in regulating LD size: interference with seipin expression in both overexpression and knockout lines of Arabidopsis caused the appearance of aberrantly sized LDs (Cai et al., 2015b; Taurino et al., 2018).

However, seipins are part of a larger protein machinery in Arabidopsis (Figure 6), also including the VESICLE ASSOCIATED MEMBRANE PROTEIN (VAMP) – ASSOCIATED PROTEIN 27-1

(VAP27-1; Greer et al., 2020), proteins of the LD associated protein (LDAP) family and the LDAP-INTERACTING PROTEIN (LDIP; Pyc et al., 2021). VAP27-1 interacts with Arabidopsis SEIPIN 2 and SEIPIN 3, and knockout of *VAP27-1* causes the appearance of disproportionally large LDs, similar to the *seipin 2 seipin 3* double mutant (Greer et al., 2020). The precise role of this interaction is yet unclear. LDAP proteins have initially been described as LD proteins in vegetative tissues and LDIP was found to interact with LDAPs via a yeast two-hybrid screen (Gidda et al., 2016; Pyc et al., 2017a). More recently, they were proposed as part of a model combining seipins, LDAPs and LDIP in the maturation of plant LDs (Pyc et al., 2021). There, LDIP initially interacts with seipin at the ER. With increased LD size due to neutral lipid accumulation, LDAPs associate with the LD surface, the LDIP-seipin interaction is broken and instead LDIP is stabilised at the LD surface by interaction with LDAP (Coulon et al., 2020; Pyc et al., 2021).
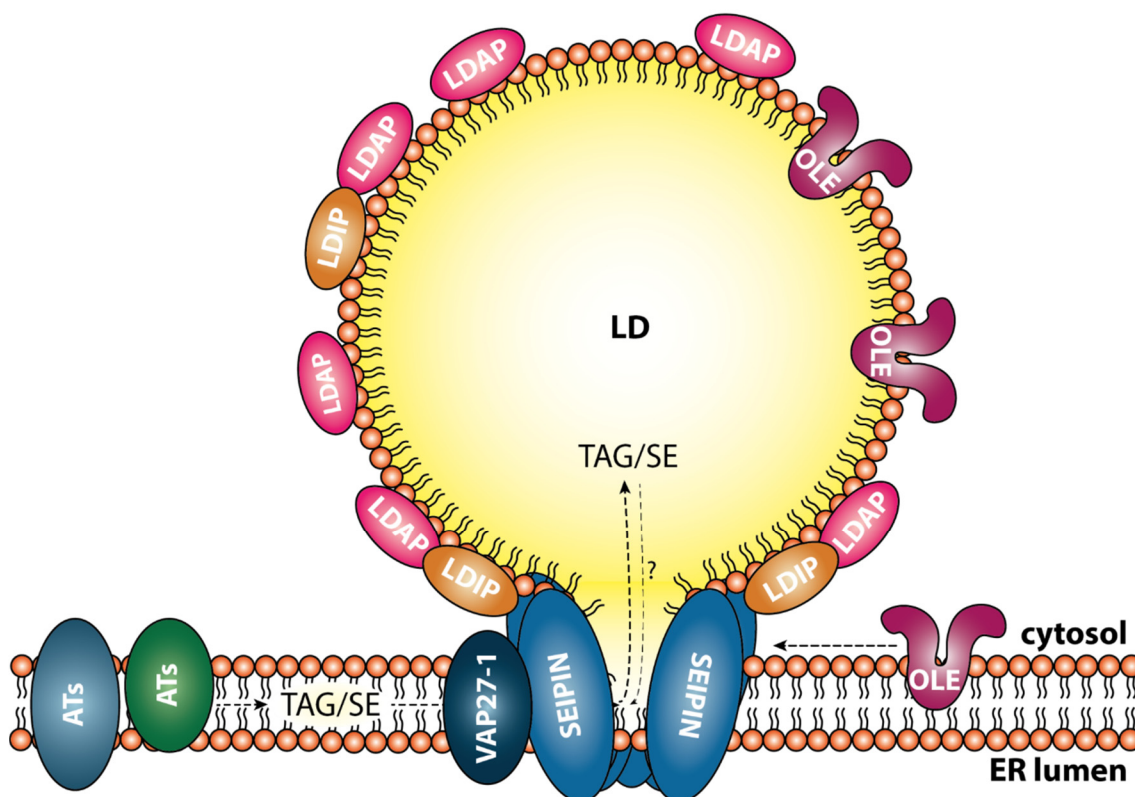
Figure 6: LD biogenesis at the ER combines various processes. LD core components like triacylglycerols (TAGs) and sterol esters (SEs) are formed by acyltransferase (AT) enzymes. These compounds are channelled into the growing LD, likely with support of seipin proteins at the ER-LD contact. There, seipin acts together with VESICLE ASSOCIATED MEMBRANE PROTEIN (VAMP) – ASSOCIATED PROTEIN 27-1 (VAP27-1), proteins of the LD associated protein (LDAP) family and the LDAP-INTERACTING PROTEIN (LDIP) to regulate the size of the forming LD. In addition, some LD coat proteins like oleosins (OLEs) target from the cytosolic leaflet of the ER to the monolayer of the LD by as of yet incompletely understood processes. Figure adapted after (Ischebeck et al., 2020).

Further proteins target to LDs from the ER (class I LD proteins) or from the cytosol (class II proteins) as the LD matures into its functional form (Kory et al., 2016). How the connection between the LD and the ER is eventually severed is not described so far. For yeast, it even has

been reported that LDs stay connected to the ER (Jacquier et al., 2011). It is not excluded that this is also the case for at least a subpopulation of plant LDs, while others lose the ER-connection and diffuse into the cytosol.

1.3.3 The lipid droplet proteome

In the phospholipid monolayer of mature LDs different proteins are embedded, which by their enzymatic or non-enzymatic properties confer specific functionalities to individual LDs. As mentioned above, two classes of LD proteins can be differentiated, although two different distinguishing features have been proposed. Kory et al. suggested differentiation into class I LD proteins that target from the ER to LDs and class II LD proteins targeting from the cytosol (Kory et al., 2016). Bersuker and Olzmann on the other hand differentiated class I LD proteins with hydrophobic hairpins and class II LD proteins with amphipathic helices (Bersuker and Olzmann, 2017). Both nomenclatures might be at least partially redundant, as ER-originating LD proteins often contain hydrophobic hairpins and LD proteins with amphipathic helices mostly target to LDs from the cytosol (Kory et al., 2016; Bersuker and Olzmann, 2017). Furthermore, proteins might contain both hydrophobic hairpins and an amphipathic helix, as was speculated for the protein PLANT UBX DOMAIN-CONTAINING PROTEIN 10 (PUX10).

The targeting of LD proteins

The best studied example of ER-originating LD proteins with a hydrophobic hairpin are the plant-specific oleosins (Hills et al., 1993; Abell et al., 1997; Beaudoin et al., 2000). Expression of a sunflower oleosin in yeast demonstrated that correct localisation to LDs was dependent on initial co-translational translocation of oleosin to the ER by the signal recognition particle (SRP) complex (Beaudoin et al., 2000). In addition, oleosins contain a highly conserved hydrophobic region with three central proline residues (Huang, 1996). This region is thought to form a hydrophobic hairpin inserting into the LD, with the proline residues (also termed "proline knot") inducing the turn of the hairpin. That these three proline residues are crucial for LD targeting was demonstrated by mutational studies: when replaced with leucine residues, the protein fails to target to LD, but is still associated to microsomal fractions (Abell et al., 1997). Oleosin thus appears to target initially to the ER via the SRP-pathway and subsequently moves into the LD monolayer mediated by its proline knot stabilised hydrophobic region. Caleosins contain a similar proline knot structure and based on sequence comparisons are thought to associated with LDs in a comparable way to oleosins (Chen et al., 1999). Finally, conserved proline residues are also found in steroleosins, although as part of a shorter "proline knob" motif different from the "proline knot" of oleosins and caleosins (Lin et al., 2002).

Another pathway for insertion into the ER before localisation to LDs has been reported for mammalian UBX DOMAIN-CONTAINING PROTEIN 8 (UBXD8). Initial UBXD8 translocation to the ER requires the peroxisome-biogenesis factors PEX19 and PEX3 that cooperate to insert UBXD8 post-translationally in ER subdomains (Schrul and Kopito, 2016). How the protein transfers from the ER to LD is less clear, however, apparently also involves PEX19 as proper localisation of UBXD8 was reliant on PEX19 farnesylation (Schrul and Kopito, 2016). Furthermore, a short hydrophobic region of around 20-30 amino acids in length was observed

as necessary and sufficient for LD targeting (Suzuki et al., 2012). Interestingly, the Arabidopsis homolog PUX10 showed a dual localisation to ER and LDs and a similar hydrophobic region was identified to be both necessary and sufficient for LD localisation (Kretzschmar et al., 2018). Thus, there is the possibility that this targeting mechanism is functionally conserved in plants.

After insertion into the ER, LD proteins need to be concentrated on the maturing LDs. The driving forces of this process are still a mystery, although multiple mechanisms have been proposed (Bersuker and Olzmann, 2017). One important difference between the ER and LDs is the contrast between a membrane bilayer and a membrane monolayer with a more hydrophobic phase beneath. The combination of monolayer and oil phase beneath is more favourable for conserved tryptophan residues in two *Drosophila* LD proteins and could drive their accumulation at LDs (Olarte et al., 2020). Other mechanisms include the selective degradation of LD proteins, when they diffuse onto the ER bilayer (Ruggiano et al., 2016) and it has also been proposed that the membrane curvature at the ER-LD connection might serve as diffusion barrier to non-LD proteins (Bersuker and Olzmann, 2017).

Comparable to the differentiation between ER and LD required of class I LD proteins, class II LD proteins need to distinguish between LDs and other cellular membranes as they target to LDs from the cytosol. They might recognise the LD monolayer due to physicochemical properties like electrostatic potential, curvature or packing defects (Bigay and Antonny, 2012). The latter means that the phospholipid monolayer does not completely cover the components beneath so that hydrophobic patches, TAGs and/or SEs in the case of LDs, are exposed. Packing defects have often been attributed as a major determinant of protein localisation to LDs, as molecular dynamics simulations showed an increased number of packing defects on the LD surface compared to bilayer membranes (Kim and Swanson, 2020; Kim et al., 2022). It is thought that amphiphilic helices of LD proteins will recognise and interact with the exposed neutral lipids (Rowe et al., 2016; Prévost et al., 2018) and amphipathic helices as LD targeting region have been described e.g. in human perilipin proteins (Rowe et al., 2016). In plants, the LDAP proteins are remote homologs of perilipins (Pyc et al., 2021), however, in localisation studies it was observed that the full length protein is required for LD targeting (Gidda et al., 2016). An amphipathic helix has been reported as required for targeting in its interacting protein LDIP though (Pyc et al., 2017a).

As further modes of protein interaction with LDs, insertion via lipid-anchors and interaction with LD scaffolding proteins have been suggested (Kory et al., 2016). An example for the second would be the interaction of the protein CELL DIVISION CYCLE 48A with PUX10 in the degradation of LD proteins (Deruyffelaere et al., 2018; Kretzschmar et al., 2018). As more and more LD proteins are discovered and their targeting mechanisms described, the research on LD targeting will surely uncover additional details how the interaction between LDs and their surface proteins shapes both players.

Identification of new plant LD proteins has been driven by proteomic screens

As documented in the previous paragraph, there are a variety of targeting mechanisms for LD proteins. Consequently, there is no conserved sequence conferring LD localisation resulting in an inability to predict new LD proteins from sequence information alone. Hence, discovery of new LD proteins has so far been powered by cell biological and proteomics studies.

In plants, the first commonly identified LD proteins were oleosins, caleosins and steroleosins present in seeds (Qu et al., 1986; Qu and Huang, 1990; Chen et al., 1999; Lin et al., 2002). In addition, in cucumber seedlings a lipoxygenase (LOX) was identified as major LD protein (Feussner and Kindl, 1992), however, LD-association of LOX appears to be species-dependent as Arabidopsis LOX1 did not localise to LDs upon transient expression in leaves (Fernández-Santos et al., 2020). Proteomic studies then provided a major breakthrough for the discovery of additional LD proteins, and by now LD proteomes of numerous algal or plant species and different plant tissues have been published (Jolivet et al., 2004; Katavic et al., 2006; Jolivet et al., 2009; Tnani et al., 2011; Horn et al., 2013; Liu et al., 2015; Thakur and Bhatla, 2016; Brocard et al., 2017; Siegler et al., 2017; Zhi et al., 2017; Kretzschmar et al., 2018; Zaaboul et al., 2018; Lupette et al., 2019; Kretzschmar et al., 2020; Hamada et al., 2020; Fernández-Santos et al., 2020; Doner et al., 2021; Veerabagu et al., 2021; Niemeyer et al., 2022).

Most of these proteomic data sets describe plant tissue enriched in LDs, like seeds (Jolivet et al., 2004; Katavic et al., 2006; Jolivet et al., 2009; Liu et al., 2015; Thakur and Bhatla, 2016; Zhi et al., 2017; Kretzschmar et al., 2018; Zaaboul et al., 2018; Kretzschmar et al., 2020; Hamada et al., 2020), pollen tubes (Kretzschmar et al., 2018), mesocarp of avocado (Horn et al., 2013) or the oil-rich tubers of yellow nutsedge (Niemeyer et al., 2022). Nevertheless, for Arabidopsis additional proteomes of senescent, drought-stressed and *Pseudomonas*-infected leaves have been described (Brocard et al., 2017; Fernández-Santos et al., 2020; Doner et al., 2021), highlighting LD proteome composition in organs that accumulate only limited amounts of oil (Kelly et al., 2013).

It needs to be considered though, that the enrichment of LDs for subsequent proteomic analysis has to balance two competing demands. On the one hand, the LD is supposed to stay as intact as possible, so that weakly associated proteins are not lost. On the other hand, contamination of other non-LD proteins should be limited. Considering the scarcity of LDs especially in leaves (Kelly et al., 2013), it seems impossible to satisfy both demands. While proteomes might thus give a good hint on the proteins present at LDs of different sources, cell biological verification is required to assign *bona fide* LD proteins. The number of high-confidence LD protein families is thus much smaller than the published proteome data suggests (Table 1, Figure 7). Additionally, some of the reported LD proteins might be specific for certain plant species, as the example of LOX shows (Feussner and Kindl, 1992; Fernández-Santos et al., 2020). Additional LD proteins have been reported due to serendipitous discovery, yet the total number of known LD proteins in plant cells is still smaller than the reported numbers of 100-150 proteins in human cell and 35-40 proteins in yeast (Olzmann and Carvalho, 2019).

Table 1: Overview of *bona fide* land plant LD proteins. Proteins or protein families were selected based on verified LD-localisation by imaging techniques. As localisation might differ between plant species, the species of original detection is indicated. Described or putative functions of the LD proteins are also listed.

Protein/Protein family	original detection in	(putative) functions
Oleosins (OLE)	Maize scutellum (Qu et al., 1986)	LD biogenesis, LD size determination
Lipoxygenase (LOX)	Cucumber cotyledons (Feussner and Kindl, 1992)	Oxylipin synthesis
Caleosin (CLO)	Sesame seeds (Chen et al., 1999)	Oxylipin synthesis, stress response
Steroleosin (HSD)	Sesame seeds (Lin et al., 2002)	Sterol metabolism
Oil body lipase (OBL)	Castor beans (Eastmond, 2004)	TAG degradation
Hydroperoxide lyase (HPL)	*Medicago truncatula* (De Domenico et al., 2007)	Oxylipin metabolism
LD associated protein (LDAP)	Avocado mesocarp (Horn et al., 2013)	LD biogenesis, abiotic stress response
α-DIOXYGENASE 1 (α-DOX1)	Arabidopsis leaves (Shimada et al., 2014)	Oxylipin synthesis, biotic stress response
LDAP INTERACTING PROTEIN (LDIP)	Y2H-screen of Arabidopsis cDNA library with LDAP as bait (Pyc et al., 2017a)	LD biogenesis
CYCLOARTENOL SYNTHASE 1 (CAS1)	Tobacco pollen tubes (Kretzschmar et al., 2018)	Sterol metabolism
STEROL METHYLTRANSFERASE 1 (SMT1)	Tobacco pollen tubes (Kretzschmar et al., 2018)	Sterol metabolism
POLLEN TUBE LD PROTEIN (PTLD)	Tobacco pollen tubes (Kretzschmar et al., 2018)	Unknown
PLANT UBX DOMAIN-CONTAINING PROTEIN 10 (PUX10)	Tobacco pollen tubes (Kretzschmar et al., 2018)	LD protein degradation
PHOSPHOLIPID:STEROL ACYLTRANSFERASE 1 (PSAT1)	Tomato (Lara et al., 2018)	Sterol metabolism
LD associated lipase (LIDL)	Arabidopsis seeds and seedlings (Kretzschmar et al., 2020)	Metabolism
LD methyltransferase (LIME)	Arabidopsis seeds and seedlings (Kretzschmar et al., 2020)	Metabolism
LD dehydrogenase (LDDH)	Arabidopsis seeds and seedlings (Kretzschmar et al., 2020)	Metabolism
LD-associated hydrolase (LDAH)	Arabidopsis seeds and seedlings (Kretzschmar et al., 2020)	Metabolism
Seed LD protein (SLDP)	Arabidopsis seeds and seedlings (Kretzschmar et al., 2020)	Membrane contact site formation
LD PROTEIN OF SEEDS (LDPS)	Arabidopsis seeds and seedlings (Kretzschmar et al., 2020)	unknown
Glycerol 3-phosphate acyltransferases (GPATs): GPAT4 and GPAT8	Infected Arabidopsis leaves (Fernández-Santos et al., 2020)	Wax synthesis
PHYTOALEXIN DEFICIENT 3 (PAD3)	Infected Arabidopsis leaves (Fernández-Santos et al., 2020)	Phytoalexin synthesis, biotic stress response

EARLY RESPONSIVE TO DEHYDRATION 7 (ERD7)	Arabidopsis leaves (Doner et al., 2021)	Stress response
PROTEIN ASSOCIATED WITH LDS (PALD)	Arabidopsis pollen (Li et al., 2022)	LD maintenance, pollen viability
LDS AND STOMATA 1 (LDS1)	Arabidopsis leaves (Ge et al., 2022)	Stomata development, LD biogenesis

The composition of the LD proteome varies not only between species but also between different developmental stages, organs and tissues of plants. For example, gene expression of oleosins in Arabidopsis is very specific to desiccating structures like seeds and in case of OLE7 and OLE8 also pollen (Klepikova et al., 2016). Consequently, they have been found in proteomic studies of LDs from tobacco pollen tubes (Kretzschmar et al., 2018) and Arabidopsis seeds and seedlings (Kretzschmar et al., 2020) but not in the LD proteome of Arabidopsis leaves (Brocard et al., 2017; Fernández-Santos et al., 2020; Doner et al., 2021). In fact, when ectopically expressed in leaves, oleosins outcompeted LDAPs at LDs, so their absence is required for normal leaf LD proteome composition (Gidda et al., 2016). In line with this, oleosins abundance decreases during seed germination (Kretzschmar et al., 2020). In general, composition of the LD proteome is altered during seed germination (Kretzschmar et al., 2020), underlining the flexibility of the LD proteome that is required to fulfil the organelle's varying function.
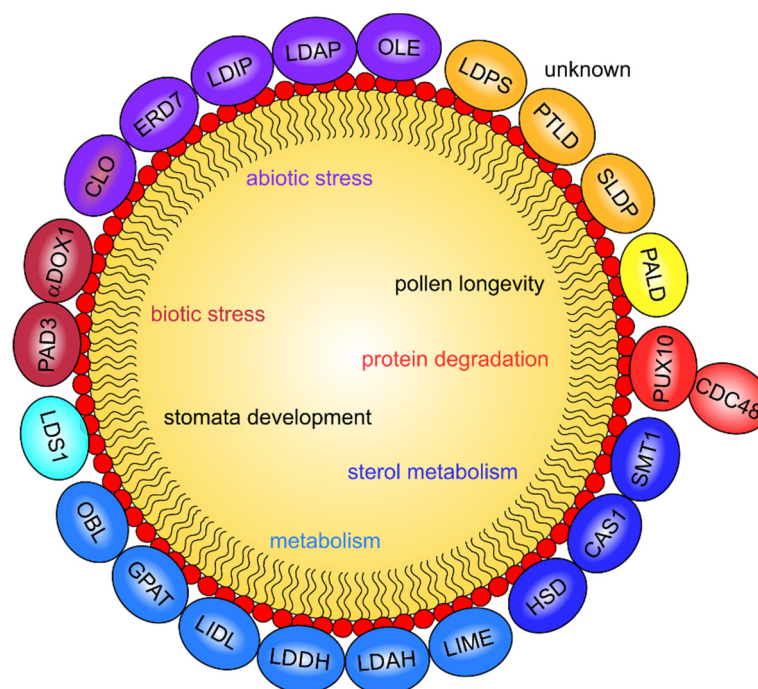
Figure 7: Overview of the known LD-associated protein families in *Arabidopsis thaliana*. Depicted are all protein families that were found at LDs in various tissues of Arabidopsis and whose localisation has been confirmed by cell biological studies. A number of these have been linked to abiotic and biotic stress functions; additionally, several proteins with (putative) functions in lipid metabolism were localised to LDs. Furthermore, individual LD proteins have been studied in the context of protein degradation, stomata development and pollen longevity. Nevertheless, there remain LD proteins with unknown functions that might further expand the physiological roles of these versatile organelles.

1.3.4 Functions of lipid droplets

Although most prominently found in seeds, it has long been argued that LDs are probably present in all types of plant cells (Murphy, 2001). This gives rise to a huge variety of possible LD functions, depending i.a. on expressed LD-related genes, plant tissues and environmental or developmental context.

LDs as storage organelles in seeds and seedlings

Due to the high LD abundance in oilseeds, initial studies focused on their role as a carbon and energy storage organelle for germination (Huang, 1992). As seeds are formed, they accumulate TAGs and SEs during seed maturation in embryonic or endosperm tissue (Baud et al., 2002; Harker et al., 2003; Baud and Lepiniec, 2010), before undergoing desiccation in late seed maturation to endure even long-term unfavourable conditions in a quiescent state (Leprince et al., 2017; Waterworth et al., 2019). In pennycress (*Thlaspi arvense*) high-oil and low-oil accessions, higher oil content was correlated with upregulated transcripts involved in LD synthesis and stability, which corroborates the role of LDs as main TAG storage sites in the seed (Johnston et al., 2022). While metabolically quiescent like the whole seed, LDs probably still need to be protected from fusing with each other. This is likely achieved due to electrostatic repulsion between the LD-covering oleosins, as oleosins are negatively charged at physiological pH (Tzen et al., 1992) and the double knockout mutants *ole1 ole2* and *ole1 ole3* in Arabidopsis displayed increased LD size in seeds (Shimada et al., 2008). Crucially, these double mutants and the respective single mutants were impaired in their germination after freezing stress (Shimada et al., 2008), so LD integrity is important for seed vigour under unfavourable conditions.

After rehydration initiates germination (Waterworth et al., 2019), TAG from LDs is metabolised providing carbon skeletons and energy for post-germinative growth. To that end, FAs need to be hydrolysed from the glycerol backbone. If hydrolysis is blocked, normal seedling establishment is only possible with an external carbon source (Eastmond, 2006). Two lipases, SUGAR-DEPENDENT 1 (SDP1) and SDP1-LIKE (SDP1L) together account for c. 95% of initial TAG lipase activity in seedlings, however, LD membranes of an *sdp1 sdp1l* double mutant retain 80-100% of DAG- and monoacylglycerol (MAG)-lipase activity (Kelly et al., 2011). SDP1 is initially localised to the peroxisomal membrane, however, upon germination it is delivered to the surface of LDs via tubular extensions of peroxisomes (Thazar-Poulot et al., 2015; Cui et al., 2016). FAs hydrolysed by SDP1 and SDP1L are imported into peroxisomes by the peroxisomal transporter PXA1 (also called COMATOSE, CTS), where they are activated to fatty acyl-CoA and then catabolised in β-oxidation (Zolman et al., 2001; Footitt et al., 2002; Fulda et al., 2004; Graham, 2008). Acetyl-CoA units derived from peroxisomal β-oxidation are subsequently converted in the glyoxylate cycle and gluconeogenesis (Graham, 2008).

SDP1 and SDP1L are both able to hydrolyse TAG and DAG with a strong substrate-preference for TAG. Therefore, FAs from MAG and to a lesser degree DAG molecules need to be hydrolysed by different lipases. TAG-, DAG- and MAG-lipase activity in Arabidopsis has been reported for OIL BODY LIPASE 1 (OBL1), and in *obl1* mutant seed extracts TAG lipase activity is strongly decreased (Müller and Ischebeck, 2018). However, no germination phenotype of the *obl1* mutant was observed, so a possible contribution to FA hydrolysis during germination

remains mysterious. If SEs play a role in providing FAs during germination is also not clear yet, as no germination defects of Arabidopsis mutants with low SE levels in seeds have been described so far (Bouvier-Navé et al., 2009). Nevertheless, the contribution of LDs to the transition from the heterotroph seed to the photoautotroph seedling is mirrored in the depletion of LDs during germination (Eastmond, 2006; Kretzschmar et al., 2018; Krawczyk et al., 2022).

LDs in pollen and pollen tube growth

Besides seeds, pollen grains are the most important sites of TAG synthesis and accumulation (Piffanelli et al., 1998; Ischebeck, 2016). Pollen without the TAG-synthesising DGAT1 and PDAT1 enzymes lacks LDs, does not mature properly and thus remains sterile (Zhang et al., 2009). Further defects were seen in Arabidopsis *pxa1* mutants that are unable to import FAs for β-oxidation, whose pollen germination and pollen tube growth are impaired (Footitt et al., 2007). In olive pollen, it has been reported that LDs enter the pollen tube from the grain, additionally lipase and phospholipase A enzyme activity as well as a LOX were localised at the LD surface (Zienkiewicz et al., 2013). In light of this observation, it is interesting to note that TAG content in germinating olive pollen did not change in the first six hours after pollen germination (Hernández et al., 2020). Hernández et al. suggest that FAs are released from TAG to fuel the initial stages of pollen germination and tube growth, however, new FA are synthesised that are subsequently esterified into new TAG species (Hernández et al., 2020). At least in tobacco pollen, *de novo* synthesis of FA has been previously described (Mellema et al., 2002), so it is possible that TAG turnover occurs and released FAs are used as energy source. Additional metabolic pathways that provide energy for pollen tube growth are likely though, and the surrounding style tissues may provide compounds for energy production (Selinski and Scheibe, 2014).

TAG levels in pollen are not comparable to seeds, as they were measured to around 1% of dry weight (% DW) in olive, 2% DW in tobacco and 4% DW in rape seed pollen (Piffanelli et al., 1997; Rotsch et al., 2017; Hernández et al., 2020). Instead, for tobacco pollen, sucrose has been reported as a transient storage compound, which accumulates in desiccated pollen and is then rapidly degraded during pollen tube growth (Rotsch et al., 2017). Also, LDs are not completely degraded during pollen germination and can be found in high numbers in growing pollen tubes (Müller et al., 2017). Therefore, additional functions for LDs have been suggested (Ischebeck, 2016). A common idea is that LDs serve as a source and sink organelle of membrane components. TAGs and SEs are relatively inert compounds that, however, can easily be converted to membrane components like sterols or membrane phospholipid precursors like DAG. LDs would thus serve as source for the vast amounts of membrane needed in the tip-growing pollen tube, while limiting the amount of cytotoxic lipid intermediates like DAG, PA or free FAs (Listenberger et al., 2003; Fan et al., 2013, 2017). In addition, LDs might be required for membrane remodelling, as acyl chain composition of the cell membrane is adjusted to different mechanical or environmental stressors. LDs would here act as a source of the required acyl chains and as a sink for the unfavourable acyl chains (Ischebeck, 2016). LDs are then needed close to sites of membrane synthesis and remodelling, i.e. in the pollen tube. It is therefore interesting to note, that Arabidopsis mutant lines disrupted in several seipin isoforms produce pollen with overlarge LDs unable to enter the

pollen tube, and have pollen transmission defects (Taurino et al., 2018). A role for LDs in the membrane homeostasis of pollen tubes was also discussed as possible reason for impaired pollen tube growth in the Arabidopsis *obl1* mutant (Müller and Ischebeck, 2018).

LDs and lipid homeostasis in leaves

Among the vegetative plant tissues, LDs have been mostly studied in leaves. LD-forming TAGs are also present in roots and stems, and similarly to leaves, their total amount is limited by SDP1 activity (Kelly et al., 2013). However, as there is scarcely any additional data on LDs in roots or stems, the following section will focus on leaves. There, LDs further need to be differentiated from plastoglobules (Lundquist et al., 2020), LD-like structures in plastids that will not be discussed in this work.

Initial studies on LDs and neutral lipids in leaves were challenged by their low amounts, especially of TAG neutral lipids. Interestingly, LDs in leaves were reported to contain more SEs than TAGs (Cai et al., 2017), nevertheless, when studying overall neutral lipids in leaves, research has so far focused on the TAG components. Lin and Oliver reported TAG isolation from thirteen different plant species, however, were also unable to detect TAGs in twelve additional species (Lin and Oliver, 2008). Regardless of this challenge, they observed trends in the TAG content of crabapple leaves that were later also of interest in Arabidopsis: firstly, they observed that TAG content increased during leaf senescence which was later correlated to increased LD numbers (Lin and Oliver, 2008; Fernández-Santos et al., 2020). Secondly, they reported diurnal changes of TAG concentration during the day. There, the report of increasing TAG content during the day stands in contrast to the results of Gidda et al. though, who reported highest number of LDs at the end of the night and a decrease of LD number during day time (Lin and Oliver, 2008; Gidda et al., 2016). This difference might be a species-dependent effect or there could be opposing trends for SEs and TAGs, which could lead to differing effects on LD numbers and TAG levels. In addition, TAG measurements of whole leaves will not distinguish between plastoglobules and LDs. Maximum number of LDs at the end of night and subsequent decrease of LD numbers during day seem to be the more probable scenario in Arabidopsis, as it was later also observed by Pyc et al. (Pyc et al., 2017a). The reasons behind this diurnal changes in LD number are not clear, albeit a role in recycling and remodelling of plant membranes during the day has been suggested (Gidda et al., 2016). This would limit LD numbers during the day, while metabolic processes during the night, possibly including the degradation of membrane lipids, could replenish LD numbers at the end of the night.

If plants are shifted from a normal day/night-cycle to extended darkness, LDs become important to avoid lipotoxic effects of free FAs (Kunz et al., 2009; Fan et al., 2017). The degradation of fatty acids by β-oxidation, or "lipid respiration" was proposed as alternative energy source, when no photosynthesis can occur (Flügge et al., 2011). However, the phenotype of mutants unable to import FAs into peroxisomes for β-oxidation show that this process needs to be tightly controlled (Kunz et al., 2009). In leaves of the peroxisomal transporter mutant *pxa1*, bleaching and necrosis phenotypes were observed and linked to an accumulation of free FAs (Kunz et al., 2009; Fan et al., 2017). Based on lipid analyses and further mutant analysis of *pxa1*, *sdp1* and a double mutant *pxa1 sdp1*, Fan et al. suggested, the following metabolic pathway under extended darkness: MGDG of the thylakoid

membrane is broken down and the resulting FAs are initially channelled into TAG synthesis at the ER. This TAG is again hydrolysed and the resulting FAs are imported into peroxisomes for β-oxidation. If the import of FAs into peroxisomes is blocked, free FAs lead to lipotoxic effects, however, lipotoxicity can be reduced when additionally the hydrolysis of LD-stored TAG is prevented (Fan et al., 2017). This highlights how free FAs are initially transferred to TAG in LDs and underlines the importance of LDs as storage organelles to prevent accumulation of lipotoxic molecules during membrane turnover. TAG was additionally observed to protect against oxidative stress implicating additional safeguarding functions of LDs (Fan et al., 2017).

The role of LDs in vegetative tissues as a transhipment point of FAs with concurrent TAG synthesis and TAG hydrolysis was also suggested in stress-responsive membrane remodelling (Figure 8). Independent of extended darkness, impaired TAG synthesis in leaves was associated with premature cell death (Fan et al., 2013), suggesting that TAG synthesis occurs continuously during normal cell function, while TAG accumulation is limited by the SDP1 lipase (Kelly et al., 2013). Furthermore, TAG accumulation has been reported as a common response to freezing, cold and heat stress as well as pathogen infection (Moellering et al., 2010; Tarazona et al., 2015; Higashi and Saito, 2019; Schieferle et al., 2021). For drought, cold and heat stress, also an increase in LD number has been observed (Gidda et al., 2016; Doner et al., 2021). Especially under heat stress, TAG accumulation has been connected to sequestering acyl chains with unsuitable characteristics for respective membrane adaptations. Heat stress increases membrane fluidity and to adapt, polyunsaturated acyl chains in membrane lipids are replaced by monounsaturated or saturated acyl chains (Niu and Xiang, 2018). The replaced acyl chains can then be sequestered into TAGs and appropriately, TAG species containing a high number of double bonds accumulated most strongly in heat stressed Arabidopsis leaves, Arabidopsis seedlings and tomato fruits (Higashi et al., 2015; Mueller et al., 2015; Almeida et al., 2021). During recovery from heat stress, TAGs in Arabidopsis leaves are again depleted, underlining their transient function (Higashi et al., 2015). Less is known about the fate of SEs. Sterols are also attributed to be important determinants of membrane structure and fluidity (Valitova et al., 2016). Hence, SEs could serve as a source of different phytosterols during membrane remodelling, which is corroborated by the measurement of decreased levels of SEs in heat-stressed Arabidopsis seedlings (Shiva et al., 2020).
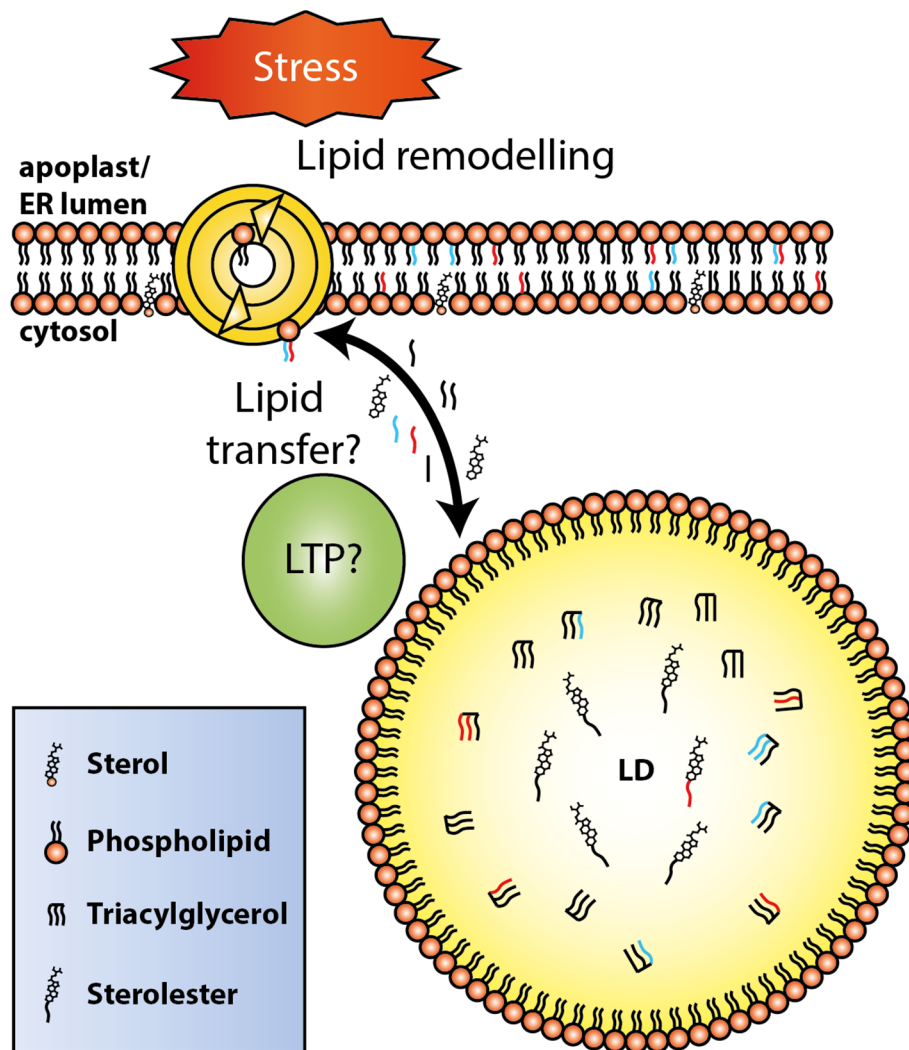
Figure 8: LDs can act as source and sink in membrane remodelling processes. Environmental stress like heat stress causes adaptation of membrane lipids, as for example polyunsaturated acyl chains are replaced by saturated or monounsaturated ones. Also, concentration of free sterols in the membrane can be altered to adjust membrane fluidity. In this case, LDs can act as both source for new membrane lipids and sink for the replaced lipid species. How lipid exchange would be mediated is unclear so far, however, an involvement of lipid transfer proteins (LTPs) might be one possibility.

The importance of LDs in abiotic stress is furthermore noticeable in Arabidopsis mutants of leaf LD coat proteins. Members of the LDAP (also SRP, small rubber particle protein homolog) protein family are the major coating proteins of LDs in leaves (Gidda et al., 2016; Kim et al., 2016). LDAP overexpression lines were observed as more drought-tolerant while knockout mutant displayed higher drought sensitivity (Kim et al., 2016). Higher drought tolerance was also seen when genes of the homologous proteins from *Taraxacum brevicorniculatum* where expressed in Arabidopsis (Laibach et al., 2018). Altogether, LDs in leaves appear to be important for their buffering capacity of FAs and other membrane lipid precursors during lipid remodelling processes. While thus at the centre of lipid homeostatic processes, they never accumulate to higher amounts (Chapman et al., 2013).

Specialised LD functions

In addition to balancing the lipidome, some special functions have been annotated to leaf LDs. Firstly, they have additional roles in guard cells. LD staining signal and TAG levels in guard cells have been described to decrease as stomata open during the dark-light transition (McLachlan et al., 2016). In *sdp1* and *pxa1* mutants with blocked TAG-degradation, stomatal opening was delayed, as was the blue-light induced cell wall acidification that occurs during the process. Cell wall acidification is connected to an H^+-ATPase, therefore the authors concluded that TAG is used as energy source in stomata to provide ATP for stomatal opening (McLachlan et al., 2016). Very recently, LDs and an LD-associated small G protein have also been reported to play a role in stomatal development (Ge et al., 2022).

Finally, TAG-stored FAs can be used as carbon source for the synthesis of oxylipins. Strongest experimental evidence for this role comes from the description of Arabidopsis plants infected with *Colletotrichum higginsianum* (Shimada et al., 2014). There, it could be shown that the LD-localised enzymes α-DIOXYGENASE 1 (α-DOX1) and CALEOSIN 3 (CLO3) act in concert to oxidize α-linolenic acid to 2-hydroxyoctadecatrienoic acid, which has antifungal properties (Shimada et al., 2014). Studies on the peroxygenase activity of CLO3 demonstrated that the enzyme can reduce hydroperoxide groups by oxidizing unsaturated FAs, yielding epoxy FAs as part of oxylipin metabolism (Blée et al., 2014; Rahman et al., 2018). Other oxylipins are synthesised by LOX, however, LD association of LOX seems to be species-dependent (Feussner and Kindl, 1992; Fernández-Santos et al., 2020). It is not excluded though, that cytosolic Arabidopsis LOX enzymes use FA derived from LDs. In *Medicago truncatula*, a further enzyme of oxylipin metabolism, a hydroperoxide lyase (HPL), was found localised to LDs (De Domenico et al., 2007). HPLs cleave products of LOX enzymes to form volatile and non-volatile aldehydes (Wasternack and Feussner, 2018). Interestingly, volatile production was linked to yet another enzyme in tomato. Tomato introgression lines with higher volatile levels were found to have higher expression levels of tomato lipase genes homologous to *AtOBL1*, which encodes an LD-associated lipase in Arabidopsis (Garbowicz et al., 2018; Ischebeck et al., 2020). Thus, different enzymes of oxylipin metabolism have been linked to LDs in various plant species and suggest LDs as additional player of its pathways. If their involvement in oxylipin synthesis follows common patterns or developed in species-specific ways rests to be determined.

1.4 Aims of this thesis

Despite a large number of research studies on lipids in plants, there are numerous questions on their overall contribution to cell homeostasis and cellular adaptation processes remaining. A large number of genes are annotated as being associated with lipid metabolism yet still await functional characterisation. In addition, the analysis of cellular functions of LDs in vegetative tissues has come into focus only recently. This work aims to contribute to a better understanding of both (i) lipid signals and (ii) the role of LDs in non-desiccating tissues.

In the first project of this thesis, the goal was to analyse the contribution of a lipid signal to tobacco pollen tube growth. Secretion and membrane trafficking are key processes of pollen tube tip growth and rely on lipid landmarks in the plasma membrane for their spatial regulation. Here, I aimed to integrate a tobacco DAG kinase into the signalling networks of growing pollen tubes. This comprised as first intention to study its localisation and enzymatic contribution to PA synthesis in pollen tubes. A second aim was to evaluate the overall impact this DAG kinase has on tobacco pollen tube growth appearance. Finally, its connection to possible downstream effectors and signalling outputs should be dissected (chapter 4).

The second part of this thesis revolves around the roles of LDs in vegetative tissues. One aim in this project was to follow the dynamics of leaf LDs in Arabidopsis plants faced with different environmental challenges. In this context, the proposed role of LDs as hub during membrane remodelling processes should be investigated from a lipid perspective. Secondly, this aim also included a more detailed study of the alterations in the leaf LD proteome following stress. Linked to the investigation of changes in the LD proteome was a second goal of identifying new LD-interacting proteins that would enlarge the molecular toolbox of LDs (chapter 5). In addition to a thorough analysis of the dynamic adjustments of LDs in leaves, a further aim was to study LDs of roots, which have received very little scientific attention so far. Here, I hoped to obtain a first overview of the LD-associated proteome in roots. Again, the identification of possible new LD-interacting proteins was an additional motivation of the proteomic study (chapter 6). Altogether, the overarching objective of this part of the thesis was the differential characterisation of vegetative LDs distinct from the storage LDs described in seeds.

2 Article I: Signalling Pinpointed to the Tip: The Complex Regulatory Network That Allows Pollen Tube Growth

The review was published online in the journal Plants in August 2020. The article can also be found online under the following DOI:

https://doi.org/10.3390/plants9091098

Author contribution:

Patricia Scholz wrote the first draft of the manuscript except for the section on the exocyst complex. She drafted initial versions of the figures. She also revised the final version of the text after input from all co-authors and reviewers.

Signalling Pinpointed to the Tip: The Complex Regulatory Network That Allows Pollen Tube Growth

Patricia Scholz *, Jannis Anstatt, Hannah Elisa Krawczyk and Till Ischebeck *

Department of Plant Biochemistry, Albrecht-von-Haller-Institute for Plant Sciences and Goettingen Center for Molecular Biosciences (GZMB), University of Goettingen, Justus-von-Liebig Weg 11, D-37077 Goettingen, Germany; jannis.anstatt@stud.uni-goettingen.de (J.A.); hannah.krawczyk@uni-goettingen.de (H.E.K.)

* Correspondence: patricia.scholz@uni-goettingen.de (P.S.); tischeb@uni-goettingen.de (T.I.);
  Tel.: +49-(0)-551-3928648 (P.S. & T.I.); Fax: +49-(0)-551-3925749 (P.S. & T.I.)

check for
updates

Abstract: Plants display a complex life cycle, alternating between haploid and diploid generations. During fertilisation, the haploid sperm cells are delivered to the female gametophyte by pollen tubes, specialised structures elongating by tip growth, which is based on an equilibrium between cell wall-reinforcing processes and turgor-driven expansion. One important factor of this equilibrium is the rate of pectin secretion mediated and regulated by factors including the exocyst complex and small G proteins. Critically important are also non-proteinaceous molecules comprising protons, calcium ions, reactive oxygen species (ROS), and signalling lipids. Among the latter, phosphatidylinositol 4,5-bisphosphate and the kinases involved in its formation have been assigned important functions. The negatively charged headgroup of this lipid serves as an interaction point at the apical plasma membrane for partners such as the exocyst complex, thereby polarising the cell and its secretion processes. Another important signalling lipid is phosphatidic acid (PA), that can either be formed by the combination of phospholipases C and diacylglycerol kinases or by phospholipases D. It further fine-tunes pollen tube growth, for example by regulating ROS formation. How the individual signalling cues are intertwined or how external guidance cues are integrated to facilitate directional growth remain open questions.

Keywords: pollen tube; phosphoinositides; small G proteins; reactive oxygen species; phosphatidic acid; lipid signalling; cell wall; secretion; exocyst complex

1. Introduction

Pollen are the male microgametophytes of seed plants, part of the short haploid phase in the life cycle of the spermatophytes. In angiosperms, the microgametophyte consists of one vegetative cell and two sperm cells formed from a generative cell, either during pollen development or later during fertilisation. After contact of the pollen grain with a compatible stigma, the vegetative cell forms a pollen tube that grows through the style to the ovule to transport the inherently non-motile sperm cells to the embryo sac [1,2]. There, the pollen tube ruptures and releases the sperm cells for double fertilisation, which concludes the gametophytic phase of the angiosperm life cycle [3–5].

Growth of the angiosperm pollen tube relies on extreme polarisation of the vegetative cell. Massive secretion of new cell wall material takes place at the very tip of the pollen tube, which exclusively extends into one direction. This extreme form of polarised cell expansion is called tip growth and occurs in plant pollen tubes as well as in plant root hairs [6,7]. The tip growth of pollen tubes reaches considerable growth rates in the range of 0.1 µm/s in vitro and 1 µm/s in vivo. Pollen tubes are thus among the fastest growing cells in the plant world [8]. The enhanced growth rate of angiosperm pollen tubes is thought to be a key factor contributing to the dominance of angiosperms in land plants

today [9]. On the other hand, it poses significant challenges to cell organisation, cell wall integrity, secretion, and signalling networks regulating the complex process of tip growth.

## 2. Pectin Is an Important Component of the Pollen Tube Cell Wall

Pollen tube tip growth is based on a delicate equilibrium between secretion of cell wall material at the pollen tube tip and turgor-driven cell expansion. The maintenance of this equilibrium and concurrent preservation of the pollen tube's shape sets special demand for the cell wall and its components. Modelling approaches demonstrated that a gradient in cell wall stiffness is required to sustain proper pollen tube shape [10–13]. This gradient changes from the more flexible apical tip towards the stiff pollen tube shank [13–15]. The cell wall component best suited to provide this gradient is pectin, a polymer characterised by its backbone containing galacturonan [12,16]. Pectin is synthesised in the Golgi apparatus and subsequently transported and secreted via secretory vesicles [17]. The apically secreted pectin is initially in an esterified state, as the carboxyl groups of the secreted galacturonan are linked to methoxy groups [16,18,19]. The esterified pectin is very flexible, allowing turgor-driven expansion. Upon cleavage of the ester bonds, pectin chains are cross-linked by Ca^{2+} ions, thus changing the rheological properties of the pectic compounds to increased stiffness [20,21]. Together with increasing abundance of cellulose and callose in the cell wall of the pollen tube shank, this leads to increased cell wall stiffness and stabilises the distal pollen tube cell wall. This results in a cell wall that resists the turgor and maintains the cylindrical shape of the pollen tube [14,22,23]. The transition from methylesterified "soft" pectin to de-esterified pectin occurs in the subapical region [14,19]. The enzymes responsible for this transition are pectin methylesterases (PMEs), that cleave the ester bonds in the secreted galacturonan monomers, enabling Ca^{2+}-crosslinking of the pectin chains [24]. Lack of PME activity frequently leads to impaired pollen tube growth, visible in decreased growth rate and pollen tube length [20,25–27]. PMEs and pectin are transported in the same secretory vesicles and are subsequently secreted at the tip of the pollen tube. Consequently, the enzymatic activity has to be controlled to prevent premature de-esterification. According to protein structure type I and type II, PMEs are distinguished that also differ in their regulation mechanism [28,29]. In type II PMEs, premature enzyme activity and de-esterification of pectin is prevented by proteinaceous pectin methylesterase inhibitors (PMEIs) that form 1:1 complexes with the enzyme [30]. For type I PMEs, it is assumed that a protein-inherent pro-region acts as an auto-inhibitor during transport, as this pro-region shows significant homology to PMEIs [28,29,31]. The activation of type I PMEs requires the cleavage of the pro-region, and mature PMEs purified from the cell wall lack this domain [31]. However, where and how this cleavage occurs is still unclear. Activation of type II PMEs on the other hand can be achieved by the removal of PMEIs from the apoplast, which is attained by the endocytic uptake of the PMEIs in the subapical region of the pollen tube [32].

3. Pectin Secretion during Pollen Tube Growth

Providing enough pectin at the apical tip to maintain the fast growth rates of pollen tubes requires abundant secretion of cell wall material. Hence, exocytic vesicles fuse at a high rate with the pollen tube plasma membrane in the tip regions, providing signalling molecules as well as cell wall and membrane material [12,33–35]. Abundant endocytic processes balance exocytosis, which serves at least two functions: Firstly, to take up regulatory molecules from the apoplast, e.g., PMEI proteins, and secondly, to internalise surplus membrane material. Due to the higher surface-to-volume ratio of the delivered secretory vesicles, more membrane lipids than required fuse with the plasma membrane. These excess phospholipids are at least partially recycled back by the budding of endocytic vesicles [32,36–38]. The exact localisation of the exo- and endo-cytic processes is a matter of debate, that shall not be discussed here but has been examined elsewhere [6,39].

The precedence of endocytic and exocytic processes in the growing region of the pollen tube, aka the tip, is mirrored in the pollen tube's subcellular structure (Figure 1). Growing angiosperm pollen tubes exhibit a pronounced zonation of the cytoplasm [33,40]. The apex of the growing tube

is packed with secretory vesicles and lacks organelles, effecting a "clear zone" in light microscopy imaging [41–43]. The concentration of vesicles is maintained by F-actin structures, most visible in the form of the "actin fringe" in the subapical region adjacent to the clear zone [41]. This subapical region is organelle-rich and forms the transition between growing tip and non-growing shank-region of the pollen tube. The shank can be divided into the proximal and the distal end, the latter of which is highly vacuolated in older pollen tubes and separated by callose plugs from the actively streaming cytoplasmic shank region [34]. The proximal shank region is organelle-rich, containing, i.a., the male germ unit of the two sperm cells and the vegetative nucleus, which is transported on microtubules maintaining a constant distance to the pollen tube tip [44]. Additionally, endoplasmic reticulum (ER) and Golgi apparatus are present, which produce the contents of the secretory vesicles accumulating at the pollen tube tip. The movement of these organelles and their vesicles towards the apex strongly relies on actin structures. Throughout the shank, strong cortical and central actin bundles serve as tracks for associated myosins and their cargos. It is speculated that the actin fringe then serves as a filter that withholds the organelles in the subapical region and allows only vesicles to pass to the apex [8,41]. The transport of membranous organelles in the pollen tube of angiosperms follows a "reverse fountain" pattern: Organelles and exocytic vesicles are transported in anterograde direction to the tip close to the cell membrane, while retrograde transport occurs along central actin cables. The typical actin structure and the "reverse fountain" streaming pattern immanently lead to the V-shape of the clear zone at the apex, also termed inverted cone [42,44].
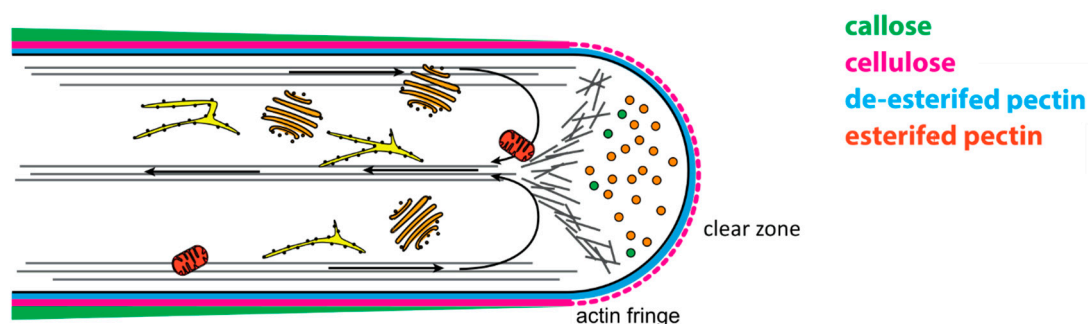
Figure 1. Tip-growing pollen tubes require a distinct subcellular organisation. The abundant secretion processes at the pollen tube tip lead to a distinct structuration in growing pollen tubes. The apex of the growing tube is packed with secretory vesicles and void of organelles leading to a V-shaped "clear zone". It is speculated that the organelles are prevented from entering that zone by the cortical actin structure of the actin fringe. Behind the actin fringe, F-actin forms strong actin bundles required for transport processes. Vesicles and organelles, like mitochondria (depicted in red), endoplasmic reticulum (yellow), and Golgi (orange) structures, are transported on cortical actin bundles towards the tip. Retrograde transport takes place on central actin cables, resulting in a "reverse fountain" pattern of cellular transport. Additional structuration can be observed in the pollen tube cell wall. Esterified pectins predominantly form the cell wall at the pollen tube tip, although the presence of cellulose has been reported in some cases. Further back, cellulose and callose are embedded in a pectin matrix of de-esterified pectin monomers crosslinked with Ca2+ ions, leading to increased stiffness of the shank cell wall.

4. Pollen Tube Growth Is Regulated by Several Interwoven Signalling Networks

The equilibrium between the cell's turgor and the secretion of pectin has to be accurately balanced to maintain proper tip growth [6], and the pollen tube must be able to redirect its growth direction in response to external guidance cues [45]. Consequently, a plethora of signalling networks and factors are involved in the regulation of pollen tube growth, including ion gradients, small GTPases, reactive oxygen species (ROS) (Figure 2), and signalling phospholipids [7,39,46–51]. A further layer of complexity is added by the cross-talk between the different signalling networks: GTPase activity

influences the pollen tube inherent calcium gradient and relies on phosphoinositides for downstream signalling, while phosphoinositides influence the regulators of GTPases [52–54]. This leads in vitro to interdependent oscillations of GTPase activity, secretion, the Ca^{2+} gradient, and the growth rate observable, e.g., in lily or tobacco pollen tubes [55–59].
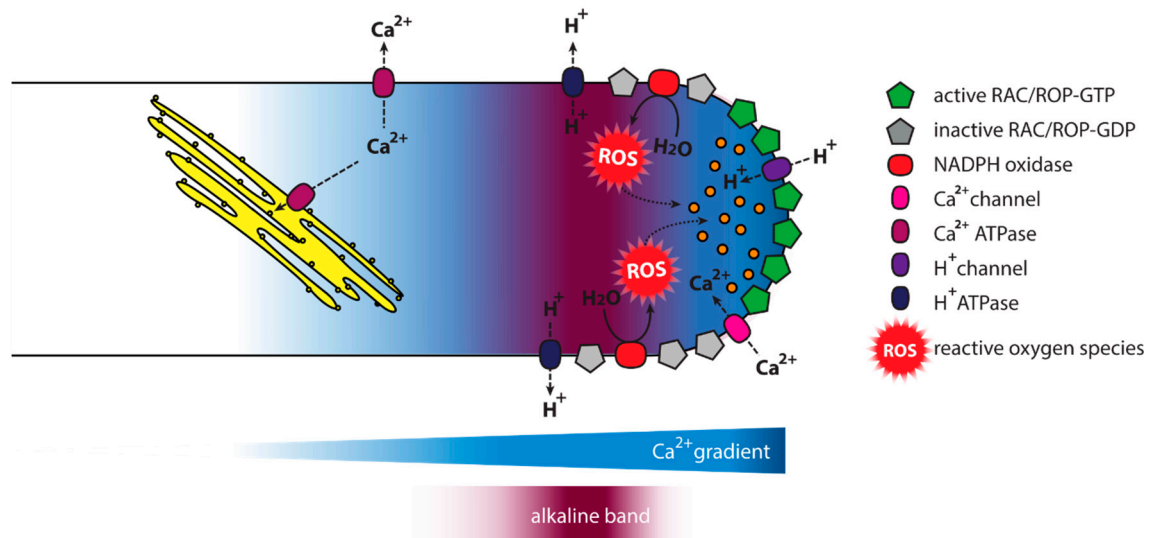
Figure 2. A complex signalling network is involved in pollen tube growth. Pollen tube growth is controlled by a variety of signalling factors, including ions, reactive oxygen species (ROS), and small Rop/Rac-GTPases cycling between active and inactive states. Furthermore, different phosphoinositides and derived lipids are involved in pollen tube growth regulation (See Figures 3 and 4).

5. Reactive Oxygen Species in Pollen Tube Growth

ROS are vital signalling molecules during fertilisation, as they control stable pollen tube growth but also induce rupture of the tube at the end of its life cycle [51,60]. First indications on the role of ROS in pollen tube growth came from studies on the tobacco NADPH oxidase (NtNOX) [61]. NOX activity is confined to the plasma membrane and accumulation of ROS at the pollen tube tip could be visualised by dihydrofluorescein diacetate or nitroblue tetrazolium staining. Furthermore, inhibition of NOX activity disturbs pollen tube growth [61,62]. ROS production was also observed in lily, pear, kiwi, *Picea meyeri*, or olive pollen tubes [63–67]. In Arabidopsis, the two respiratory burst oxidase homolog (Rboh) genes, *AtRBOHH* and *AtRBOHJ*, are expressed in pollen tubes, where their encoded proteins localise to the apical plasma membrane. AtRBOHH and AtRBOHJ are enzymatically active in a Ca^{2+}-dependent manner and pollen tube growth in the double mutant *rbohH rbohJ* is impaired [68]. Additional investigation of the *rbohH rbohJ* double mutant revealed higher amplitudes in growth rate oscillations and a tendency to burst prematurely. It was consequently proposed that AtRBOHH and AtRBOHJ serve as "speed control", to allow coordination of cell expansion and deposition of new cell wall material [69]. This model was later extended, describing AtRBOHH and AtRBOHJ as part of a cell wall integrity-controlling pathway in pollen tube growth [50,70]. There, they are proposed as downstream effectors of a complex of receptor-like kinases (RLKs) [70–72], which responds to autocrine signalling peptides of the rapid alkalinization factor (RALF) family [4,35,71]. RALF4 and RALF19 act redundantly in the maintenance of pollen tube integrity as they influence the deposition of callose and pectins in the growing pollen tubes [35]. Pollen tubes of the double mutant *ralf4 ralf19* burst prematurely, likely due to their involvement in the secretion of cell wall material [4]. RALF4/19 interact with the *Catharanthus roseus* receptor-like kinase 1-like (CrRLK1L) receptors BUDDHA'S PAPER SEAL (AtBUPS) 1/2 and ANXUR (AtANX) 1/2, of which AtANX1/2 were shown to act upstream of AtRBOHH and AtRBOHJ [70]. Furthermore, addition of RALF4 led to increased ROS production in in vitro grown pollen tubes [71]. Another member of the RALF family, RALF 34, might play an antagonistic role to

RALF4/19. RALF34 is predominantly expressed in mature ovules and its addition to pollen tubes grown in vitro induces pollen tube rupture [4]. Like RALF4/19, RALF34 is able to bind to ANX1/2 and BUPS1/2 and was proposed to outcompete RALF4/19 after the pollen tube reaches the ovule, thereby inducing pollen tube rupture [4,73]. Interestingly, pollen tube rupture and sperm release was also connected to high ROS concentrations in the filiform apparatus [60]; however, a direct connection between RALF signalling and ROS production by the female gametophyte has not been described so far.

Another described source of ROS in pollen tubes is oxidation of the polyamine spermidine catalysed by a polyamine oxidase [74,75]. Loss of polyamine oxidase activity leads to shorter pollen tubes and the tip localisation of its polyamine substrates seems to be important for physiological tip growth [75,76]. ROS signals are integrated into other signalling networks during pollen tube growth, including signalling phospholipids, small GTPases, and ion gradients [62,68,77,78]. For example, AtRBOHD triggered by abscisic acid (ABA) in stomatal closure has been shown to bind to the lipid phosphatidic acid, and phosphatidic acid increases ROS production [79]. Also, Ca^{2+} has been proposed to act both up- and down-stream of ROS signals, activating RBOH enzymes, whose ROS products could in turn trigger Ca^{2+}-influx from the apoplast in a positive feedback loop [68,80].

6. Ion Gradients in Growing Pollen Tubes

Among ions, Ca^{2+} and H^+ have been most closely linked to pollen tube growth regulation. In lily pollen tubes, a pH-zonation from the acidic tip towards an alkaline band at the base of the clear zone was described [81]. A similar pH gradient changing with growth rate oscillations was also observed in pollen tubes of tobacco and has been linked to the shank-localised, proton-exporting H^+-ATPase NtAHA [82,83]. The role of H^+ ions in the regulation of tube growth remains unclear though—initial studies on the pH gradient in *Lilium longiflorum* concluded that protons are not central to growth regulation [84]. However, later studies described a connection between pH and actin organisation during tube growth [85]. Additionally, reversible inhibition of pollen tube growth in lily using potassium cyanide (KCN) leads to a sharp decline of the pH gradient, and the alkaline band was the first ion gradient to be re-established after removal of the inhibitor [86]. A study on Arabidopsis pollen tubes connected intracellular pH changes with anion transport over the pollen tube membrane, hypothesising that protons might be part of a network reacting to γ-aminobutyric acid (GABA)-mediated signalling [87]. Further observations were made in a recent study on an Arabidopsis triple mutant lacking the three autoinhibited plasma membrane proton (H^+) ATPase (AHA) isoforms, AtAHA6, AtAHA8, and AtAHA9 [88]. *AHA6*, *AHA8*, and *AHA9* are predominantly expressed in pollen and pollen tubes and pollen of the triple mutant *aha6 aha8 aha9* shows reduced germination rates, while germinated pollen tubes grow slower and tend to stop prematurely. AHA6, AHA8, and AHA9 localised to different extents in the plasma membrane of the pollen tube shank. There, they are thought to pump protons out of the pollen tube's cytoplasm, thereby establishing a proton gradient from the tip towards the shank. Consequently, the cytoplasm of pollen tubes from the triple mutant *aha6 aha8 aha9* is more acidic and the pH gradient is strongly decreased. Further analysis of the mutant pollen tubes also revealed a decreased anion efflux from the pollen tube, a decreased membrane potential, and changes in the actin organisation, underlining the importance of proton transport across the pollen tube membrane [88].

The importance of Ca^{2+} for pollen germination and subsequent pollen tube growth has already been reported more than 50 years ago for more than 80 plant species [89]. Furthermore, the interaction between pollen tubes and the female gametophyte before double fertilisation is also accompanied by distinct Ca^{2+} dynamics in synergids, egg, and central cell [90,91]. In terms of pollen tube growth, it has been observed that growth rate oscillations and oscillations of the Ca^{2+} gradient depend on each other in vitro [92,93]. The Ca^{2+} gradient in the cytosol of growing pollen tubes is formed with peak concentrations close to the apical plasma membrane. The exact localisation of the peak Ca^{2+} concentration determines growth orientation [93,94]. Exact Ca^{2+} concentrations in the pollen tube

vary considerably between reports, depending on the methods used [95]. At the tip, values are in the range of 0.1 to 10 µM, while for the shank, values around 0.02–0.2 µM have been reported [49,95,96]. Reports agree though, that the Ca^{2+} gradient is only observable in growing pollen tubes [95]. Irrespective of the actual values, the high apical concentration of Ca^{2+} is likely established by an influx of Ca^{2+} from the apoplast, as the application of calcium chelators and calcium channel inhibitors leads to the dissipation of the Ca^{2+} gradient [97,98]. Different Ca^{2+} channels at the tip of the pollen tube are one requirement and regulation point for a Ca^{2+} gradient [99–102]. In this context, Arabinogalactan proteins in the apoplast might play a role, acting in a feedback loop that couples Ca^{2+}-influx and secretion with the physical strain at the pollen tube tip during cell wall extension [103]. Secondly, a mechanism for the efflux of Ca^{2+} in tip-neighbouring regions is required. This Ca^{2+} efflux occurs via PM- and possibly also ER-localised Ca^{2+}-ATPases, transporting the ions out of the cell or into the endomembrane system, respectively [96,104,105].

Calcium could play a direct role in secretion by triggering exocytosis, as has been shown in neurons, where a calcium influx rapidly triggers the soluble *N*-ethylmaleimide-sensitive-factor attachment receptor (SNARE)-mediated vesicle fusion of neurotransmitter-filled vesicles with the plasma membrane. The transmitting of the Ca^{2+} signal is thought to occur via the two synaptic proteins Synaptotagmin-1 and Complexin, which interact with SNARE proteins on vesicles and the presynaptic membrane in a partially assembled state [106,107]. Interestingly, Soluble NSF attachment protein 25 (SNAP-25), a protein of the SNARE complex, was in turn reported to control voltage-gated Ca^{2+} channels and Ca^{2+} concentrations in the presynaptic cell [108]. While this process serves as an example that Ca^{2+} might directly influence secretion, it is unclear if Ca^{2+} in pollen tubes would act similarly, as secretory vesicles with cell wall material are unlikely to be in a similar "clamped" state of a partially assembled SNARE complex.

Furthermore, detection of Ca^{2+} occurs via sensor proteins, like calcium-dependent protein kinases (CDPKs). CDPKs possess a regulatory Ca^{2+}-binding domain, and upon Ca^{2+}-binding, the protein kinase catalytic domain is activated, so they act as "sensor responders" [49,109]. CDPK proteins involved in pollen tube growth have been reported for Arabidopsis, maize, and petunia [110–112], and CDPK activity has been linked to the adjustment of ion fluxes across the plasma membrane [113–116]. Other Ca^{2+} sensor proteins include calmodulin, calmodulin-like proteins, and calcineurin B-proteins that act as "sensor relays" transmitting the Ca^{2+} signal via altered protein–protein interactions. Several of these sensor relays have been described in connection with tube growth, actin organisation, and regulation of K^+ transmembrane transport [117–121]. Ca^{2+}-mediated stabilisation and destabilisation of actin filaments could also play a role in establishing actin structure, as high Ca^{2+} concentrations cause disassembly of filamentous actin, acting via actin-binding proteins [122]. This regulation of actin structure connects Ca^{2+} to another signalling factor as Ca^{2+}-dependent F-actin modulation is one of two downstream pathways of the Arabidopsis Rop/Rac GTPase Rop1 [52].

7. Small GTPases Define the Pollen Tube Tip

The impact of small GTPases on tip-growing cells has been discussed in several recent reviews, therefore we will only briefly mention their basic roles and functions in pollen tube growth here [39,48,123,124]. Small monomeric GTPases (ca. 21 kDa) serve as molecular switches, cycling between an active GTP-bound state and an inactive GDP-bound state [125]. They are regulated by further proteins like guanine nucleotide exchange factors (GEFs), GTPase activating proteins (GAPs), and guanine nucleotide dissociation inhibitors (GDIs). GEFs activate small GTPases by exchanging GDP against GTP, while GAPs activate the intrinsically low GTPase activity of the monomeric GTPases [126,127]. GDIs modify subcellular localisation of small GTPases as they are able to remove the prenylated GTPases from the membrane and sequester them in the cytoplasm [128].

The superfamily of small GTPases is further divided into different GTPase families, i.a., the Rab- and the Rho-family [129]. Proteins of the Rab-GTPase family are involved in intracellular membrane

trafficking during pollen tube growth, regulating vesicle transport between Golgi apparatus and ER or from the Golgi apparatus to the plasma membrane [130,131]. In Arabidopsis, the Rab-GTPase AtRabA4d is tip-localised and regulates vesicle trafficking, and its absence causes male-specific transmission defects [132]. Arabidopsis pollen tube growth is also impaired in null mutants of AtRabD2b and AtRab2c [133]. Importantly, Rab function relies on geranylgeranylation, and mutations of the Rab geranylgeranyl transferase inhibits normal pollen and pollen tube development, similar to mutations of the Rab proteins themselves [134]. In addition to the Rab-GTPase family, GTPases of the Rop/Rac protein family are involved in tip growth of pollen tubes. Active Rop-GTPases are locally confined to the pollen tube tip, thus providing a molecular marker for polarised secretion [54,135,136]. There, they can interact indirectly with the exocyst subunit Sec3, which determines polar secretion during pollen tube growth [137–139]. Furthermore, Rop-GTPases participate in the transduction of external signals like guidance cues, the organisation of the actin cytoskeleton, and the control of vesicle fusion with the tip plasma membrane [12,52,140–143]. Lee et al. described how the activation of two antagonistic downstream pathways via the ROP-interactive CRIB-containing (RIC) proteins RIC3 and RIC4 manipulate F-actin polymerization: RIC4-mediated stabilisation of F-actin cables promotes vesicle transfer towards the tip [141]. However, RIC4-induced changes of actin structure impaired vesicle fusion at the pollen tip, which could be balanced by RIC3- and Ca^{2+}-mediated F-actin disassembly. Thus, the authors suggested that Rop-GTPase activity triggers actin polymerisation for vesicle transport to the tip via the RIC4 pathway and actin depolymerisation at the tip for vesicle fusion via the RIC3 pathway. Together, these two pathways enable the transport and secretion of cell wall material at the tip [141]. Rop-controlled cell wall deposition relying on the manipulation of F-actin structure has also been observed in other context, e.g., the shaping of xylem vessels [144].

Studies in Arabidopsis characterised AtRop1 (also named Rac11 and Arac11) as a regulator of polarised pollen tube growth whose geranylgeranyl-mediated but spatially confined localisation to the tip is required for cell polarisation [145]. A second Arabidopsis enzyme, AtRop5 (also named Rac2, Rac6, and Arac6), seems to act similarly, and induces severe depolarisation phenotypes upon transient expression in tobacco [54]. Due to its close phylogenetic relationship, AtRop3 might have a similar function in pollen tubes [146]. In tobacco, NtRac5 has been described to regulate pollen tube growth in interaction with NtRhoGAP1 and NtRhoGDI2 [147,148]. AtRop1 was also proposed to be a mediator for changes in growth direction in response to pollen tube guidance cues. In a model that describes pollen tube tip growth as a result of the exocytosis-mediated polarisation of Rop1 and the secretory cell wall extension, guidance cues were predicted to shift the localisation of Rop1 activity and thus change growth directionality [12]. In this model, Rop1 activity is proposedly modulated by the activities of RopGEFs and the RhoGAP ROP1 ENHANCER 1. RopGEFs were then proposed as integration points for guidance cues, as an increased activation of Rop1 in response to a guidance cue would cause the shift in Rop1 activity and re-direction of secretion [12]. Consequently, RopGEFs, RhoGAPs, and RhoGDIs are important modulators of pollen tube growth due to their regulation of Rop/Rac GTPases [124,136,148–150]. Thus, male transmission defects were observed when RhoGDI function was missing in Arabidopsis [149]. Additional layers of modulation are characterised, e.g., phosphorylation of RopGEFs by cytoplasmic or receptor-like kinases, which was also described as a link between external signals and change of pollen tube growth directionality [143,151,152]. Guidance cues by the female gametophyte are required for precise pollen tube growth towards the micropyle [153]. Among the guidance cues described in Arabidopsis are the cysteine-rich AtLURE1-peptides, which are secreted from the synergid cells [154]. Reception of the AtLURE1 signals at the pollen tube relies on pollen-specific receptor-like kinases (PRKs) [143]. Specifically, AtPRK6 was determined as one receptor of AtLURE1 peptides as semi-in vivo grown pollen tubes of *prk6* mutants did not react to recombinant AtLURE1.2. AtPRK6 displayed plasma membrane localisation at the pollen tube tip, and interestingly, an asymmetric accumulation of AtPRK6 towards externally applied AtLURE1 was observed, preceding the change of pollen tube growth direction. Signal transduction of AtPRK6 requires its interaction with pollen RopGEFs via a cytosolic domain: complementation

of the AtLURE1-insensitivity in *prk6* was not achieved when PRK6's cytosolic interaction domain to RopGEFs was missing [143]. Other receptor-like kinases present in Arabidopsis pollen tubes were also shown to react to AtLURE1 peptides [155]. The ectodomains of recombinant MALE DISCOVERER1 (AtMDIS1) and MDIS1-INTERACTING RECEPTOR-LIKE KINASE (AtMIK) 1/2 bind to AtLURE1.2. AtMDIS1 can directly interact with both AtMIK proteins and this interaction is enhanced by AtLURE1.2. However, unlike for AtPRK6, no connection to RopGEFs has been described, with signal transduction likely relying on transphosphorylation in the AtMDIS1–AtMIK complex [155]. It thus remains to be uncovered to which extent RhoGTPase activity is involved in pollen tube guidance and which role is played by other signalling modules.
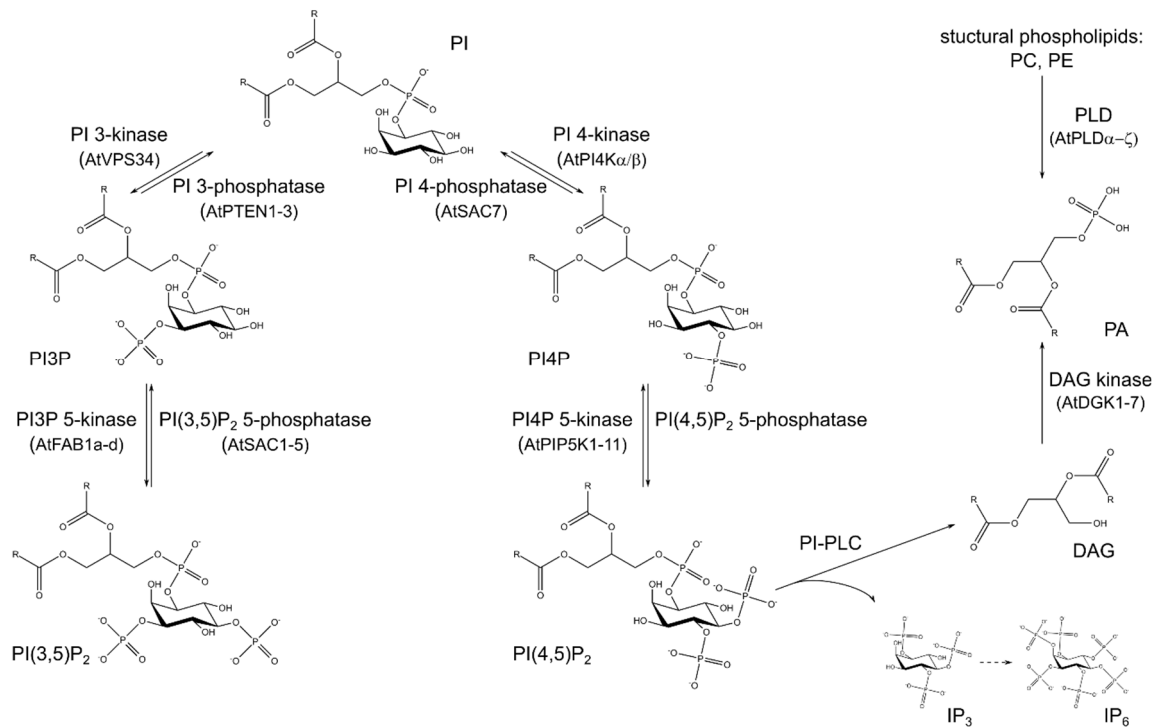

Figure 3. Signalling lipids are interconverted by a variety of enzymes. Phosphoinositides are phosphoglycerolipids carrying an inositol headgroup. Phosphorylation of different hydroxyl groups of the inositol in phosphatidylinositol (PI) gives rise to different mono- and diphosphorylated phosphoinositides. Phospholipase C-activity cleaves the bond to the *sn3*-hydroxyl group of the glycerol backbone, yielding diacylglycerol (DAG) in the process, which can be phosphorylated to phosphatidic acid (PA). Used abbreviations: DAG—diacylglycerol, IP$_3$—inositol 1,4,5-trisphosphate, IP$_6$—inositolhexakisphosphate, PA—phosphatidic acid, PI—phosphatidylinositol, PI3P—phosphatidylinositol 3-phosphate, PI4P—phosphatidylinositol 4-phosphate, PI(3,5)P$_2$—phosphatidylinositol 3,5-bisphosphate, PI(4,5)P$_2$—phosphatidylinositol 4,5-bisphosphate, PI-PLC—phosphoinositide phospholipase C, PLD—phospholipase D.

Lipid signals act together with the mentioned regulatory proteins in the regulation of Rop GTPases [53,54]. Phosphatidylinositol 4,5-bisphosphate (PI(4,5)P$_2$) acts upstream of Rop GTPase signalling by promoting plasma membrane localisation of GTP-Rop, which is part of a complex feedback loop to maintain the tip localisation of active Rop [53,136]. Due to the diverse membrane trafficking processes, the active enzyme constantly shifts to the flanks of the pollen tube tip. There, it has to be inactivated by laterally localised RhoGAP proteins [135]. RhoGDIs remove the inactive Rop GTPase from the subapical membrane and the RhoGDI/Rop-heterodimer is then transported in the cytoplasm back to the tip [147]. Tip-localised PI(4,5)P$_2$ shifts the Rop GTPase equilibrium between cytoplasm and membrane towards a membranous localisation, and RopGEFs complete

the cycling of the enzyme by exchanging GDP against GTP, activating Rop GTPase [53,136,156]. However, PI(4,5)P$_2$ was also described to act downstream of Rop GTPases. Tip-localised active AtRop5 interacts with a phosphatidylinositol 4-phosphate 5-kinase (PI4P5K), affecting the production of PI(4,5)P$_2$, which controls subsequent downstream pathways targeting the actin cytoskeleton and vesicle fusion [54].

8. Phosphoinositides and Derived Lipids form a Signalling Network

As becomes evident from the dependency of GTPase signalling on downstream signals like PI(4,5)P$_2$, the phosphoinositide signalling network (Figure 3), derived phospholipids, and the respective enzymes are crucial for normal pollen development and tube growth. The phosphatidylinositol headgroup of phosphoinositides protrudes from the plasma membrane, thus providing an anchor point for proteins with respective phosphoinositide-binding domains [7,157]. These binding domains can also be used for visualising the different lipids, as specific domains bind to the differently phosphorylated subspecies of phosphoinositides [158].
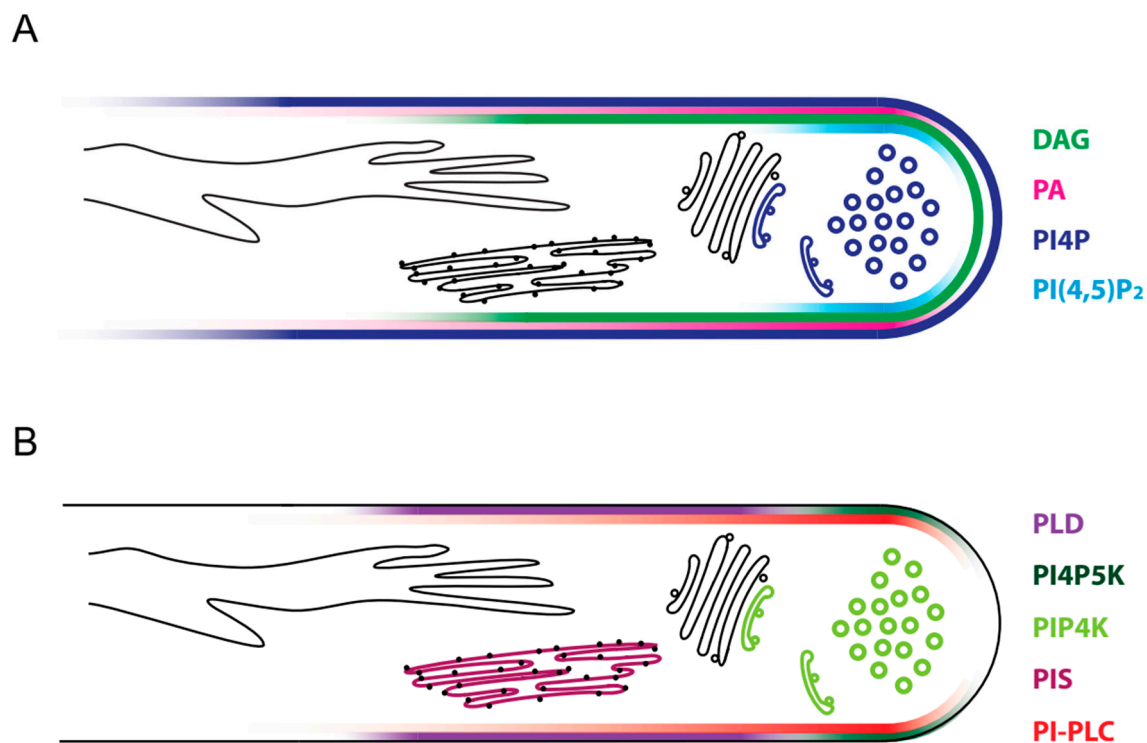
Figure 4. Several signalling lipids and the enzymes involved in their synthesis and degradation are localized at the apical plasma membrane. Several phosphoinositides and derived lipids are involved in pollen tube growth regulation. Their specific localisations in the plasma membrane are positional markers in secretory and endocytic processes and can be detected with the help of fluorescent lipid sensors (**A**). Enzymes acting on lipids of the phosphoinositide network show overlapping localisation to their products (**B**).

9. All Phosphoinositides Derive from Phosphatidylinositol

All phosphoinositides derive from phosphatidylinositol (PI) as a biochemical precursor, which is synthesised in the membrane of the ER by phosphatidylinositol synthases (PISs) from the precursors CDP-diacylglycerol (CDP-DAG) and D-*myo*-inositol (Figure 3) [159,160]. Two PIS enzymes, AtPIS1 and AtPIS2, are described in Arabidopsis [159,160]. Interestingly, the metabolic fate of PI derived from AtPIS1 or AtPIS2 seems to differ. In Arabidopsis plants overexpressing *AtPIS2*, higher levels of phosphoinositides were detected in contrast to overexpression of *AtPIS1* that caused an increase of

structural phospholipids [160]. Transient overexpression of *AtPIS1* or *AtPIS2* in tobacco pollen tubes led to wavy growth phenotypes [161]. In line with the proposed different metabolic fates of PI produced by AtPIS1 or AtPIS2, expression of *AtPIS2* led to a higher amount of affected pollen tubes. Similarly, co-expression effects of *AtPIS2* with other genes encoding for enzymes of the phosphoinositide network were far more pronounced than for *AtPIS1* [161].

The inositol of PI can carry phosphate groups in different positions, the D3-, D4-, or D5-position of the polyalcohol, giving rise to a number of different phosphoinositides. In plants, phosphatidylinositol 3-phosphate (PI3P), phosphatidylinositol 3,5-bisphosphate (PI(3,5)P$_2$), phosphatidylinositol 4-phosphate (PI4P), and phosphatidylinositol 4,5-bisphosphate (PI(4,5)P$_2$) have been characterised in different cellular functions. Of those, PI4P and PI(4,5)P$_2$ are especially important in secretory processes and pollen tube growth [7,162,163], as will be outlined in the next sections.

10. PI4P Has Regulatory Roles in the *Trans*-Golgi Network

Phosphatidylinositol 4-phosphate (PI4P) is the major monophosphorylated phosphoinositide [164,165]. Localisation studies in Arabidopsis demonstrated the presence of PI4P in the plasma membrane, recycling endosomes, early endosomes, the *trans*-Golgi network, and the Golgi complex [166]. Estimating from fluorescence intensity and affinity of the used lipid sensors, PI4P abundance seems to follow a gradient, with the highest PI4P amounts in the plasma membrane and lowest amounts in the Golgi complex [166]. In tip-growing root hairs, PI4P concentrations were highest in the plasma membrane following a tip-focused gradient [167,168]. A similar membrane localisation was observed in growing tobacco pollen tubes overexpressing a fluorescent PI4P-reporter [161] (Figure 4A).

Conversion of PI to PI4P is catalysed by phosphatidylinositol 4-kinases (PI4Ks). Among these, PI4Kβ1 and PI4Kβ2 are especially important for tip growth. In the Arabidopsis double mutant *pi4kβ1 pi4kβ2*, pollen tubes exhibit a wavy growth pattern and are shorter in length; furthermore, root hairs are also shorter and display aberrant growth morphologies. PI4Kβ1 overexpression in tobacco pollen tubes stimulates pectin secretion [161]. For AtPI4Kβ1, physical protein interaction with AtRab4Ab and AtRab4Ad was demonstrated and electron tomography imaging of Arabidopsis root cells showed that both AtRab4Ab and AtPI4Kβ1 localise to the *trans*-Golgi network (TGN) [132,169,170]. Electron tomography images of root cells further indicated that PI4Kβ1 and PI4Kβ2 might be vital for size determination of secretory vesicles at the TGN [169]. However, as the TGN integrates exocytic and endocytic vesicles, it cannot be determined if defects of PI4Kβ impair exocytic or endocytic processes. In accordance with the described TGN-localisation, transient overexpression of *AtPI4Kβ1* in tobacco pollen tubes causes alterations of the TGN morphology. In addition, in the Arabidopsis mutant *lot*, which displays defects in TGN formation in pollen grain and pollen tubes, normal PI4P membrane localisation is abolished and *lot* plants are male-sterile [161,171]. Further studies showed additional signalling functions of PI4P and AtPI4Ks in vesicle trafficking and TGN organisation during cytokinesis and lateral root formation [172,173]. Although its synthesis is particularly linked to the TGN, PI4P strongly localises to the plasma membrane at the pollen tube tip. This discrepancy raises the question of how PI4P reaches the plasma membrane. One way could be via secretion of PI4P-loaded vesicles derived from the TGN. It is however also possible that PI4P is directly synthesized at the plasma membrane. Enzymes that might be responsible are PI kinase isoforms of the α subfamily that are predicted, for example, in Arabidopsis based on sequence homology [174]. Interestingly, in yeast, two types of PI4-kinases exist, one of which localizes to the plasma membrane [175,176].

At the plasma membrane, PI4P could have a function in its own right, but can also act as a substrate for phosphatidylinositol 4-phosphate 5-kinases (PI4P5Ks) that are localised in the same plasma membrane sub-domain [7,161].

11. PI4P 5-Kinases Catalyse the Formation of PI(4,5)P$_2$ at the Pollen Tube Tip

PI4P5Ks catalyse the phosphorylation of PI4P to PI(4,5)P$_2$. Arabidopsis PI4P5Ks come in two types: AtPI4P5K10 and AtPI4P5K11 belong to type A, while AtPI4P5K1 and AtPI4P5K9 belong to type B [174].

Both types contain a C-terminal catalytic and a dimerisation domain, however, type B AtPI4P5Ks possess an additional N-terminal Membrane Occupation and Recognition Nexus (MORN)-domain unique to plants, which is involved in regulation of enzyme activity [174,177] and a linker region necessary for correct subcellular localisation [178].

According to transcriptomic studies, several Arabidopsis *PI4P5Ks* are expressed to varying degrees in the different stages of pollen development and during pollen tube growth [179,180]. For *AtPI4P5K4*, *AtPI4P5K5*, *AtPI4P5K10*, and *AtPI4P5K11*, expression in pollen and pollen tubes of Arabidopsis was also verified histochemically, using promoter-β-glucuronidase-fusion [53,181]. Furthermore, proteomic analyses detected AtPI4P5K4, AtPI4P5K5, and AtPI4P5K6 in mature pollen grains [182]. Transient expression of the respective gene in tobacco pollen tubes revealed a plasma membrane localisation of the PI4P5Ks at the subapical flanks during pollen tube growth (Figure 4B). After cessation of growth, PI4P5K localisation expanded to the extreme apex [53,181,183,184]. In parallel, $PI(4,5)P_2$ localisation has been studied using fluorescent lipid sensors similar to the previously described phosphoinositides. In accordance with the plasma membrane localisation of its biosynthetic enzymes, $PI(4,5)P_2$ is detected almost exclusively at the plasma membrane of pollen tubes but also other cells, e.g., in the root cortex [53,54,166,181]. Furthermore, plasma membrane localisation in growing pollen tube membranes is not uniform, instead, $PI(4,5)P_2$ is present in a distinct subapical domain that excludes the very tip (Figure 4A). Apical localisation of $PI(4,5)P_2$ can only be found in pollen tubes that ceded to grow [53,181,185].

Considering the tip-localisation of both PI4P5Ks and $PI(4,5)P_2$, it is not surprising that strong tip growth phenotypes are observed for several AtPI4P5K enzymes. Overexpression of type A PI4P5Ks, *AtPI4P5K10* and *AtPI4P5K11*, induces severe tip swelling and disturbance of the actin structure in tobacco pollen tubes, the overproduced $PI(4,5)P_2$ inhibits RhoGDI and thus leads to activation and depolarisation of NtRac5 [53]. For *AtPI4P5K4*, *AtPI4P5K5*, and *AtPI4P5K6*, overexpression phenotypes with excessive pectin accumulation are observed. The affected pollen tubes are often branched or stunted in growth, with the protoplast "trapped" behind the accumulated pectin at the tip [181,183,184]. Enzyme activity of PI4P5K6s from Arabidopsis and tobacco is further regulated by mitogen-activated protein (MAP) kinase (MPK)-mediated phosphorylation. MPK activity seems to diminish $PI(4,5)P_2$-production, and when *MPK* was overexpressed with *PI4P5Ks* in tobacco pollen tubes, it could reduce the aberrant pollen tube growth phenotypes [186]. The PI4P5K-produced $PI(4,5)P_2$-signal is processed, i.e., via $PI(4,5)P_2$-interacting proteins, regulating endo- and exocytosis. The Arabidopsis clathrin assembly protein EPSIN-LIKE CLATHRIN ADAPTOR PROTEIN 2 (ECA2/ PICALM5a) interacts with $PI(4,5)P_2$ in vitro and pollen tubes of the *eca2* T-DNA insertion Arabidopsis line grow shorter [187].

PI4P 5-kinases also play a role in polar tip growth and secretory processes of non-plant species [188–190]. In the nervous system, for example, PI4P is required for the normal function of several ion channels including calcium channels important for secretion [191]. However numerous other interaction partners are known, such as SNARE proteins and the proteins CAPS and Munc13 that prime vesicles for exocytosis [192]. It will be interesting to find out how conserved the role of $PI(4,5)P_2$ in secretion is across Eukaryotes. One complex that has already been shown to bind $PI(4,5)P_2$ across kingdoms [192–194] is the exocyst complex, that is crucial for secretory processes.

12. PI(4,5)P₂ Interacts with Components of the Exocyst Complex

Targeting of secretory vesicles to the correct destination is determined by tethering complexes that physically connect vesicles to the target membrane. Among them, the exocyst complex is especially important for polarised exocytosis by tethering post-Golgi vesicles to the plasma membrane. It localises to sites of maximal exocytosis in a variety of model organisms, relying on interactions with both phospholipids and small monomeric G-proteins [195–197]. The complex was originally discovered in yeast but later found to be conserved in all eukaryotes, including plants [198–200]. The exocyst complex consists of eight subunits, termed SEC3, SEC5, SEC6, SEC8, SEC10, SEC15, EXO70, and EXO84.

SEC5 is the core subunit and connects many other subunits with each other, SEC15 binds to vesicles, SEC6 interacts with SNARE proteins, and both SEC3 and EXO70 bind to PI(4,5)P$_2$ on the target membrane [137,195,197,199,201–203]. However, unlike yeast, which has only one homologue of each subunit, Arabidopsis possesses two homologues of *SEC3*, *SEC5*, and *SEC15* each, three homologues of *EXO84* and, strikingly, 23 homologues of *EXO70* in its genome [198,204].

First connections between the exocyst complex and PI(4,5)P$_2$ signalling were observed in yeast. There, the SEC3 homologue Sec3p contains a pleckstrin homology (PH) domain in its N-terminal region, which interacts with PI(4,5)P$_2$, mediating membrane binding [196,197,205]. The G-protein Rho1p can interact with the PH domain, presumably only if it is already bound to PI(4,5)P$_2$ [203]. Yeast Exo70p directly interacts with PI(4,5)P$_2$ through a polybasic region in its C-terminal domain and membrane binding of Exo70p was predicted to induce the local clustering of PI(4,5)P$_2$, potentially inducing formation of exocytic hotspots [203]. Mutation of the residues responsible for PI(4,5)P$_2$-binding leads to loss of Exo70p from the membrane, but not to secretion defects, while a combination of Exo70p and Sec3p mutations that leaves both proteins unable to bind lipids, was shown to be lethal in yeast [195,197].

Pollen tubes of Arabidopsis *sec3a*, *sec5*, *sec6*, *sec8*, *sec15a*, and *exo70C2* mutants showed male-specific transmission defects as germination and pollen tube growth were disrupted [137,199,206,207]. For the two Arabidopsis SEC3 proteins, some homology to yeast Sec3p could be observed: the N-terminal PI(4,5)P$_2$-binding PH domain is conserved, however the Rho-interaction motif is not [137,138]. The PH domain of AtSEC3A is necessary and sufficient for membrane targeting during heterologous expression in tobacco pollen tubes but dispensable during homologous expression in Arabidopsis pollen tubes [137]. Similarly, PI(4,5)P$_2$ is not required for the localisation of AtSEC3A to the germination site in Arabidopsis pollen [208]. Both studies indicate that AtSEC3A can localise to the membrane independently of PI(4,5)P$_2$, possibly relying on other exocyst components or ROP G-proteins. Indeed, the Arabidopsis adapter protein ROP Interactive Partner 1 (ICR1) was found to compensate for the missing Rho-interaction motif of AtSEC3A by connecting it to the G-protein AtROP10 [138]. Whether similar adapter proteins play a role in pollen tube growth is not yet known.

Analysis of possible functional homology of the second yeast exocyst protein with PI(4,5)P$_2$-binding ability, Exo70p, is impeded by the massive expansion of EXO70 in plants. The reason for this massive expansion is so far unclear, although different explanations have been proposed, e.g., tissue-specific expression, differences according to target sites, or specialised roles in cellular processes like autophagy, cytokinesis, or pathogen infection [209–213]. The different EXO70 isoforms might also be capable of binding different lipids [209]. Indeed, in mature trichomes, AtEXO70H4 is selectively targeted to the PA/PS-rich apical membrane domain, whereas AtEXO70A1 is selectively targeted to the PI(4,5)P$_2$-rich basal membrane domain [214]. In tobacco pollen tubes, NtEXO70A1a and NtEXO70B1 each localise to distinct parts of the plasma membrane, which both partially co-localise with PA and PI(4,5)P$_2$ [215].

Independent of lipid binding capabilities, different EXO70 family members also might have different functions in pollen tube growth. While there are discrepancies in the described gene expression, most reports agree on the expression of *AtEXO70A2*, *AtEXO70C1*, *AtEXO70C2*, *AtEXO70H3*, and *AtEXO70H5* in pollen tubes [204,207,215,216]. In most tissues of Arabidopsis, the prevalent EXO70 isoform that mediates polar exocytosis is AtEXO70A1. Although germination of *exo70A1* mutant pollen is impaired, pollen tubes appear to grow normal, so its functions are probably complemented by AtEXO70A2 [204,207]. AtEXO70C1 and AtEXO70C2 likely serve functions distinct from the main exocyst complex, since they do not interact with the core exocyst subunits. However, AtEXO70C1 and AtEXO70C2 interact with AtROH1, a member of the DUF793 protein family, which acts as a negative regulator of exocytosis [207]. Roles of AtEXO70H3 and AtEXO70H5 in pollen tubes are so far undescribed, however, other plant EXO70H proteins have been described to localise to the nucleus with possible functions independent of the core exocyst complex [209,215,217]. The tobacco NtEXO70B1 is expressed in pollen tubes and the encoded protein localises to the shank region of growing pollen

tubes, partially co-localising with NtSEC3 and the site of endocytosis. This suggests that it might function within the exocyst complex in the coordination of endocytosis [215].

In agreement with its function in yeast exocytosis, the exocyst in plant pollen tubes is widely believed to guide exocytosis during tube growth. Different exocyst subunits localise to the described sites of exocytosis in the apex and/or the subapical zone, including SEC3, SEC6, SEC8, and EXO70A [137,199,215]. Additionally, slight shifts in the localisation of AtSEC3a and AtSEC8 were shown to precede changes in the direction of pollen tube growth [137]. Nonetheless, the molecular mechanism of the exocyst complex in pollen tube growth is still unclear. Early reports in budding yeast suggested that the lipid binding Sec3p and Exo70p might bind to the membrane, marking hotspots of exocytosis, while the other exocyst subunits bind to post-Golgi vesicles. Formation of the complete exocyst complex would then serve to tether vesicles to their correct target membrane [195,218]. In Arabidopsis root epidermal cells, however, it was reported that none of the exocyst subunits depend on vesicular traffic to localise to the membrane, indicating that the exocyst complex could pre-form on the target membrane and only then bind to vesicles [219]. On the other hand, AtSEC3a was shown to decorate vesicles in the inverted cone region of pollen tubes [137].

Taken together, molecular mechanisms of the exocyst complex in pollen tube growth remain elusive. Additional research will be required to fully resolve the order and the mechanism of interaction between exocyst, vesicles, and PI(4,5)P$_2$ in the target membrane and the connections of this complex to the signalling networks important for pollen tube growth.

13. Dephosphorylation Reactions on PI4P and PI(4,5)P$_2$

The strong phenotypes resulting from the overexpression of PI 4-kinases and PI4P 5-kinases illustrate that the levels of PI4P and PI(4,5)P$_2$ must be tightly controlled. Furthermore, it seems crucial that the subdomain of the plasma membrane decorated with phosphoinositides remains clearly confined requiring the degradation of phosphoinositides diffusing out of this area. Therefore, phosphoinositides need to be degraded either by cleaving off their headgroup or by dephosphorylation. A cleavage reaction degrades the phosphoinositide "for good", yielding a lipid and a polyphosphorylated inositol as reaction products. In contrast, a dephosphorylation reaction takes a phosphoinositide one step back in the phosphorylation cascade so that it can be quickly rephosphorylated. Due to this, the dephosphorylation reactions of PI4P and PI(4,5)P$_2$ have potential for a fine-tuning of PI4P and PI(4,5)P$_2$ concentrations. However, data on respective enzyme function in pollen tubes is scarce. The phosphatase ROOT HAIR DEFECTIVE4 (RHD4/SAC7) acts on the D4-phosphate in PI4P and is required for physiological tip growth in root hairs [7,167]. The protein has been detected in mature pollen grains and transient co-expression in tobacco pollen tubes showed a partial overlap in localisation with AtRabA4d in the endosomal compartment [132,182]. AtSAC7 is part of clade II of the suppressor of actin (SAC) phosphatases together with AtSAC6 and AtSAC8 [220]. Hence, it seems likely that AtSAC6 and AtSAC8 are PI4P-phosphatases as well, especially since all three are able to complement the yeast *sac1* null mutant in a similar manner, yet there are no reports on the enzymatic activity of AtSAC6 and AtSAC8 [221]. Expression of *AtSAC6* has been reported to be pollen-exclusive, especially high during pollen maturation, and it was found in a mutant screen to be required for β-aminobutyric acid-induced sterility [221,222]. A SAC protein homologue in rice acting on PI4P and PI(4,5)P2 was linked to actin polymerisation and adjustment of cell elongation [223]. However, despite their described involvement in cell growth and tip growth in root hairs and their expression in pollen, no connection to pollen tubes has been described so far for the clade II SAC phosphatases.

The clade III protein of Arabidopsis SAC phosphatases, AtSAC9, has been proposed to act on PI(4,5)P$_2$ and inositol 1,4,5-trisphosphate and in roots of the respective mutant these two compounds accumulated [224]. The *sac9* mutant further showed a constitutively stressed phenotype, which was later connected to defects in cell wall structure and disorganised deposition of cell wall material [224,225]. Other phosphatases acting on the D5-phosphate in PI(4,5)P$_2$ have been found in the protein family of plant 5' phosphatases (5PTases) [226]. Arabidopsis possesses 15 proteins of the 5PTase family,

which can be divided into two different groups based on their protein structure. At5PTase1-11 form group I, while group II contains At5Ptase12-15 (At5PTase15, mainly labelled AtFRA3) [226,227]. Substrate specificity is mixed in those groups, as different members from both groups show in vitro substrate preferences towards soluble inositol polyphosphates or hydrophobic phosphoinositides including PI(4,5)P_2 [226]. From group I At5PTases, only *At5PTase5* is consistently expressed during different stages of the pollen life cycle, the corresponding protein was not found in mature pollen though [179,180,182]. In addition, involvement of the respective protein, variously labelled BST1, DER4, or MRH3, in the actual tip growth processes of root hairs or pollen in Arabidopsis seems to be minor [228,229]. The group II At5PTases genes *At5PTase12–14* are expressed during pollen development and tube growth according to transcriptomic data, and all three encoded proteins are detected in mature pollen [179,180,182]. These three proteins have been characterised enzymatically, which revealed in vitro substrate preference for PI(4,5)P_2 in case of At5PTase14 and inositol 1,4,5-trisphosphate in case of At5PTase12/13. However, their in vivo substrate is unclear [230]. Hence, their role in the phosphoinositide network and possible impact on pollen tube growth and regulation of cell wall secretion remains to be studied.

14. Activity of Phospholipase C Is the Main Degradation Route of Phosphoinositides

In addition to modifications of their headgroup, phospholipids can be metabolised by phospholipases like phospholipase C (PLC) and phospholipase D (PLD) [231–233]. Cleavage of phospholipids by phospholipases C (PLCs) yields diacylglycerol (DAG) and the phosphorylated headgroup as products [232,233]. PLCs acting on lipid substrates can be divided into non-specific phospholipases C (NPCs) and phosphoinositide-phospholipases C (PI-PLC). PI-PLCs specifically use phosphoinositides as a substrate, while NPCs act on structural phospholipids like phosphatidylcholine (PC) or phosphatidylethanolamine (PE) [234,235]. Influences of Arabidopsis NPCs on root growth and pollen development but not pollen tube growth have been described [236–238]. In addition, so far, no Arabidopsis PI-PLC mutant was reported to be impaired in pollen tube growth. However, studies in other model systems highlighted PI-PLC importance to counterbalance PI4P5K-activity [185,239,240]. Petunia PiPLC1 and tobacco NtPLC3 both localise to the plasma membrane in growing pollen tubes, in overlapping regions with their substrate PI(4,5)P_2, although the protein localisation tends to elongate further towards the shank [185,239]. A similar co-localisation was observed for NtPLC3 and the Arabidopsis PI4P5Ks AtPI4P5K2 and 11 after transient expression in tobacco pollen tubes [240]. For petunia PiPLC1, image time series indicated that the PLC localisation extends towards the extreme apex in phases of reduced growth and is less apical in phases of rapid growth [185]. Dominant negative expression of PLCs mutated in their active site or chemical inhibition of NtPLC3 caused a depolarisation of tip growth and swollen tube tips [185,239,240]. Additionally, PI(4,5)P_2 visualised by a lipid sensor was observed to spread further towards the shank upon PLC-inhibition [239]. The pollen tube tip phenotype of swollen tips in tobacco pollen tubes was observed upon overexpression of inactive NtPLC3 and AtPI4P5K2; however, AtPI4P5K2-induced tip swelling could be reversed by simultaneous overexpression of active NtPLC3 [240]. Taken together, PLCs seem to be important in pollen tube tip growth as the main antagonist of PI4P5Ks, regulating PI(4,5)P_2 abundance and location.

15. Inositol(poly)phosphates Are Receptors' Cofactors

On the one hand, PLC activity abolishes the PI(4,5)P_2-signal, while on the other hand, it produces two new molecules, inositol 1,4,5-trisphosphate (IP$_3$) and DAG. Cleavage of PI(4,5)P_2 to the second messengers IP$_3$ and DAG is a common signal pathway in animal cells: DAG subsequently activates protein kinase C (PKC) while an IP$_3$-receptor triggers the release of Ca^{2+} from intracellular storage [241]. However, neither for PKC nor for a canonical IP$_3$-receptor do homologues exist in the Arabidopsis genome, so PLC-dependent responses seem to be transmitted differently [242,243]. In case of IP$_3$, it was proposed that it rather acts as a precursor for higher phosphorylated inositol phosphates (IPs) and inositol pyrophosphates (IPPs) species like IP$_5$, IP$_6$, IP$_7$, or IP$_8$ [242,244,245]. A signalling role for

IPs was, for example, shown in the hormone signalling pathways of auxin and jasmonates, as the TIR1- and COI1-receptor need the cofactors IP_6 and IP_5, respectively [246–250]. Both methyl jasmonate [251] and the auxin indole acetic acid [252] have been shown to influence pollen tube growth, indicating that these hormones can be perceived by the pollen tube and regulate its growth. Interestingly, IPs are also required for targeted pollen tube growth in Arabidopsis according to studies on *ipk2α* and *ipk2β* mutants [253]. The IPK2 enzymes catalyse the reactions from IP_3 to IP_5, successive phosphorylations of the D6- and D3-position of the inositol ring. Single mutants were phenotypically inconspicuous, however, a double mutant could not be obtained, likely due to a male transmission defect, which could be traced to impaired pollen germination and pollen tube guidance [253].

16. Diacylgylcerol Kinases Have Distinct Functions in Growing Pollen Tubes

In the animal field, DAG, the second product of PLC-activity, was established to act as a second messenger and to activate protein kinase C [254,255]. However, so far, no plant orthologues of these protein kinases have been identified [256]. Consequently, a role of DAG in plant cell signalling is under debate, especially since it can be easily phosphorylated by DAG kinases (DGKs) to form PA, which makes a dissection of DAG-specific and PA-specific reactions difficult [257,258]. So far, a DAG-specific role has only been proposed to act in the development of lateral root under mild salt stress [259]. Hence, the question whether DAG has a signalling role of its own is still unanswered. In pollen tubes, DAG localises to the apex and stretches through the subapical region towards the shank, overlapping with localisation of PI-PLCs, which seem to be primary responsible for its synthesis [239]. DAG localisation also overlaps with PA-localisation, as determined by a fluorescent lipid sensor. PA shows extended localisation in the pollen tube subapical flanks, however is not present at the tube apex [260]. While part of the PA originates from PLD enzyme activity, as discussed below, PA could also be produced from PI-PLC-derived DAG by a phosphorylation reaction (Figure 2). DGKs phosphorylate the free hydroxyl group at the *sn3*-position of the glycerol in DAG, yielding PA [261]. Inhibitor studies with the PLD-inhibitor 1-butanol and the DGK-inhibitor R59022 were carried out in tobacco pollen tubes as a first attempt to study the specific effect of DGK-produced PA [262]. Changes in vacuole morphology were thus traced to DGK activity, as vacuolar strands formed aggregates that extended into the tip region. In contrast, DGK-derived PA is apparently not involved in actin organisation during pollen tube growth [262]. Arabidopsis DGKs form a seven-membered protein family, of which *AtDGK4* is exclusively expressed in pollen, and proteomic analyses detected AtDGK4 and AtDGK5 in mature pollen grains. Similarly, a tobacco DAG kinase homologous to AtDGK5 was detected during all stages of tobacco pollen development [182,262,263]. Studies on one Arabidopsis T-DNA line of *AtDGK4* reported decreased pollen tube growth rates for *dgk4* pollen [264]. Pollen tubes of *dgk4* exhibited altered cell wall properties; furthermore, the authors reported impaired membrane recycling, and additional defects in the pollen tube reaction to NO have been reported [264,265]. However, another recent study did not report significant phenotypes in the single *dgk4* mutant, only for the double mutant *dgk2 dgk4* [266]. The respective enzymes DGK2 and DGK4 are localised to the ER and are probably involved in phospholipid metabolism there [266]. DGK function and DGK-derived PA have come into the focus of pollen tube research just recently, so the distinct sensors, transmitters, and effectors of PI-PLC/DGK-derived PA are still unexplored.

17. Phospholipase D-Produced Phosphatidic Acid Regulates Pollen Tube Growth

Unlike PLCs, which give rise to DAG, PLDs cleave phospholipids between the phosphate group and the headgroup, yielding PA [231,233]. In Arabidopsis, twelve PLDs are described differing in domain structure, enzymatic properties, and substrate preferences [243,267,268]. It is interesting to note that no Arabidopsis PLD activity on phosphoinositides has been reported, implying that PLC-mediated hydrolysis is the major pathway to terminate phosphoinositide signalling [243,268]. The origin of PLD-produced PA in pollen tubes is thus likely distinct from the PA produced by the concerted activity of PI-PLC and DGK, with the PI-PLC/DGK-pathway acting on phosphoinositides rather than structural

phospholipids [235,269]. Nevertheless, PLD-activity has been demonstrated to be crucial for pollen tube growth using the PLD-inhibitor 1-butanol [270]. Subcellular analysis of tobacco pollen tubes treated with 1-butanol showed impairment of endocytosis, cell wall secretion, and actin regulation during tube growth [262]. The necessity of PA for exocytic processes has also been reported in various human cell types [271–273]. Two effects on secretion are generally discussed, firstly, that it could serve as a landmark in the plasma membrane, labelling the sites of exocytosis and recruiting proteins required for secretory processes. In this context, the anionic charge of its headgroup might help PA to interact with the positively charged domain of interacting proteins [272,274]. In line with this hypothesis, components of the tobacco exocyst complex partially colocalise with PA sensors in tobacco pollen tubes [215]. Secondly, PA influences biophysical properties of the membrane: its minimal headgroup results in a conical shape of the lipid, which in turn induces negative membrane curvature [274]. Membrane curvature is especially influential in vesicle formation so the shape of PA could be required for the endocytic recycling of vesicles at the pollen tube tip.

Several Arabidopsis PLD genes are expressed in pollen, and AtPLDα1, AtPLDα2, AtPLDβ1, and AtPLDδ are detected in mature pollen [182,262]. Despite this, no pollen tube growth phenotypes for Arabidopsis *pld* mutants have been described so far. In contrast, several tobacco PLDs are linked to pollen tube tip growth. Different *NtPLDs* were found to be expressed in pollen and germinated pollen, labelled NtPLDα2, NtPLDβ1, and NtPLDδ, and anti-sense-mediated knockdown of *NtPLDβ1* and *NtPLDδ* impaired pollen tube growth [275]. Furthermore, for NtPLDβ1, actin-binding capacity and regulation of PLD-activity by actin was demonstrated, leading to the conclusion that NtPLDβ1 is a key regulatory factor of actin organisation during pollen tube growth [275]. For NtPLDδ, a connection to ROS signalling was observed, as knockdown of NtPLDδ in tobacco pollen tubes led to a higher sensitivity towards H_2O_2. Interestingly, ROS-production by NtNOX itself is in part regulated by PLD-produced PA [62]. Recently, bioinformatic analysis of tobacco PLDδs classified five different NTPLDδs, NtPLDδ1 to 5 [276]. Overexpression of these PLDs in tobacco pollen tubes showed preferential cytosolic localisation for NtPLDδ1 and 2, plasma membrane localisation for NtPLDδ4 and 5, and an equilibrium between both compartments for NtPLDδ3. Tobacco pollen tubes overexpressing NtPLDδ3 showed the most severe phenotypes, including apical membrane invaginations. Due to the observed phenotypes, a role for NtPLDδ3 in membrane trafficking was proposed, highlighting the importance of lipid-mediated signalling for the maintenance of secretion in physiological tip growth [276].

18. Outlook

Many factors have been identified that are important for the polarisation of a pollen tube and its plasma membrane, including the channelling of secretory vesicles to the apical region by a highly specialised cytoskeleton and the regulation of exocytosis. This led to a model of a periodically oscillating system sustained and controlled by feedforward and feedback loops. In addition, external guidance cues and reacting receptors have been found. Now, the challenge emerges to understand how these external signals are integrated and transduced, so that cell wall properties are modulated that allow uneven tube extension and the pollen tube to "take a turn". Interesting questions can also be asked about the beginning and the end of pollen tube growth: How is the cell polarity originally established and how is the cell wall weakening orchestrated that ultimately leads to the bursting of the pollen tube and release of the sperm cells at the correct place? Finally, we must understand how this fragile system adapts to environmental stress to sustain pollen tube growth and why it fails in some species but not in others. This could highlight strategies for the future to prevent crop losses under weather and climate extremes.

Conflicts of Interest: The authors declare no conflict of interest.

References

1. Dehors, J.; Mareck, A.; Kiefer-Meyer, M.-C.; Menu-Bouaouiche, L.; Lehner, A.; Mollet, J.-C. Evolution of Cell Wall Polymers in Tip-Growing Land Plant Gametophytes: Composition, Distribution, Functional Aspects and Their Remodeling. *Front. Plant. Sci.* **2019**, *10*, 441. [CrossRef]

2. Johnson, M.A.; Harper, J.F.; Palanivelu, R. A Fruitful Journey: Pollen Tube Navigation from Germination to Fertilization. *Ann. Rev. Plant. Biol.* **2019**, *70*, 809–837. [CrossRef] [PubMed]

3. Amien, S.; Kliwer, I.; Márton, M.L.; Debener, T.; Geiger, D.; Becker, D.; Dresselhaus, T. Defensin-like ZmES4 mediates pollen tube burst in maize via opening of the potassium channel KZM1. *PLoS Biol.* **2010**, *8*, e1000388. [CrossRef] [PubMed]

4. Ge, Z.; Bergonci, T.; Zhao, Y.; Zou, Y.; Du, S.; Liu, M.-C.; Luo, X.; Ruan, H.; García-Valencia, L.E.; Zhong, S.; et al. Arabidopsis pollen tube integrity and sperm release are regulated by RALF-mediated signaling. *Science* **2017**, *358*, 1596–1600. [CrossRef] [PubMed]

5. Hamamura, Y.; Saito, C.; Awai, C.; Kurihara, D.; Miyawaki, A.; Nakagawa, T.; Kanaoka, M.M.; Sasaki, N.; Nakano, A.; Berger, F.; et al. Live-cell imaging reveals the dynamics of two sperm cells during double fertilization in Arabidopsis thaliana. *Curr. Biol.* **2011**, *21*, 497–502. [CrossRef] [PubMed]

6. Grebnev, G.; Ntefidou, M.; Kost, B. Secretion and Endocytosis in Pollen Tubes: Models of Tip Growth in the Spot Light. *Front. Plant. Sci.* **2017**, *8*, 154. [CrossRef] [PubMed]

7. Heilmann, I.; Ischebeck, T. Male functions and malfunctions: The impact of phosphoinositides on pollen development and pollen tube growth. *Plant. Reprod.* **2016**, *29*, 3–20. [CrossRef]

8. Stephan, O.O.H. Actin fringes of polar cell growth. *J. Exp. Bot.* **2017**, *68*, 3303–3320. [CrossRef]

9. Williams, J.H. Novelties of the flowering plant pollen tube underlie diversification of a key life history stage. *Proc. Natl. Acad. Sci. USA* **2008**, *105*, 11259–11263. [CrossRef]

10. Bidhendi, A.J.; Geitmann, A. Finite Element Modeling of Shape Changes in Plant Cells. *Plant. Physiol.* **2018**, *176*, 41–56. [CrossRef]

11. Fayant, P.; Girlanda, O.; Chebli, Y.; Aubin, C.-E.; Villemure, I.; Geitmann, A. Finite Element Model of Polar Growth in Pollen Tubes. *Plant. Cell* **2010**, *22*, 2579–2593. [CrossRef]

12. Luo, N.; Yan, A.; Liu, G.; Guo, J.; Rong, D.; Kanaoka, M.M.; Xiao, Z.; Xu, G.; Higashiyama, T.; Cui, X.; et al. Exocytosis-coordinated mechanisms for tip growth underlie pollen tube growth guidance. *Nat. Commun.* **2017**, *8*, 1687. [CrossRef]

13. Zerzour, R.; Kroeger, J.; Geitmann, A. Polar growth in pollen tubes is associated with spatially confined dynamic changes in cell mechanical properties. *Dev. Biol.* **2009**, *334*, 437–446. [CrossRef]

14. Chebli, Y.; Kaneda, M.; Zerzour, R.; Geitmann, A. The Cell Wall of the Arabidopsis Pollen Tube–Spatial Distribution, Recycling, and Network Formation of Polysaccharides. *Plant Physiol.* **2012**, *160*, 1940–1955. [CrossRef]

15. Parre, E.; Geitmann, A. Pectin and the role of the physical properties of the cell wall in pollen tube growth of Solanum chacoense. *Planta* **2005**, *220*, 582–592. [CrossRef]

16. Dardelle, F.; Lehner, A.; Ramdani, Y.; Bardor, M.; Lerouge, P.; Driouich, A.; Mollet, J.-C. Biochemical and immunocytological characterizations of Arabidopsis pollen tube cell wall. *Plant. Physiol.* **2010**, *153*, 1563–1576. [CrossRef]

17. Driouich, A.; Follet-Gueye, M.-L.; Bernard, S.; Kousar, S.; Chevalier, L.; Vicré-Gibouin, M.; Lerouxel, O. Golgi-mediated synthesis and secretion of matrix polysaccharides of the primary cell wall of higher plants. *Front. Plant. Sci.* **2012**, *3*, 79. [CrossRef]

18. Lenartowska, M.; Rodríguez-García, M.I.; Bednarska, E. Immunocytochemical localization of esterified and unesterified pectins in unpollinated and pollinated styles of Petunia hybrida Hort. *Planta* **2001**, *213*, 182–191. [CrossRef] [PubMed]

19. Li, Y.Q.; Chen, F.; Linskens, H.F.; Cresti, M. Distribution of unesterified and esterified pectins in cell walls of pollen tubes of flowering plants. *Sex. Plant. Reprod.* **1994**, *7*. [CrossRef]

20. Mollet, J.-C.; Leroux, C.; Dardelle, F.; Lehner, A. Cell Wall Composition, Biosynthesis and Remodeling during Pollen Tube Growth. *Plants* **2013**, *2*, 107–147. [CrossRef] [PubMed]

21. Mravec, J.; Kračun, S.K.; Rydahl, M.G.; Westereng, B.; Pontiggia, D.; De Lorenzo, G.; Domozych, D.S.; Willats, W.G.T. An oligogalacturonide-derived molecular probe demonstrates the dynamics of calcium-mediated pectin complexation in cell walls of tip-growing structures. *Plant. J.* **2017**, *91*, 534–546. [CrossRef] [PubMed]

22. Bidhendi, A.J.; Chebli, Y.; Geitmann, A. Fluorescence visualization of cellulose and pectin in the primary plant cell wall. *J. Microsc.* **2020**. [CrossRef] [PubMed]

23. Ferguson, C.; Teeri, T.T.; Siika-aho, M.; Read, S.M.; Bacic, A. Location of cellulose and callose in pollen tubes and grains of *Nicotiana tabacum*. *Planta* **1998**, *206*, 452–460. [CrossRef]

24. Bosch, M.; Cheung, A.Y.; Hepler, P.K. Pectin methylesterase, a regulator of pollen tube growth. *Plant. Physiol.* **2005**, *138*, 1334–1346. [CrossRef] [PubMed]

25. Jiang, L.; Yang, S.-L.; Xie, L.-F.; Puah, C.S.; Zhang, X.-Q.; Yang, W.-C.; Sundaresan, V.; Ye, D. *VANGUARD1* Encodes a Pectin Methylesterase That Enhances Pollen Tube Growth in the Arabidopsis Style and Transmitting Tract. *Plant. Cell* **2005**, *17*, 584–596. [CrossRef] [PubMed]

26. Tang, C.; Zhu, X.; Qiao, X.; Gao, H.; Li, Q.; Wang, P.; Wu, J.; Zhang, S. Characterization of the pectin methyl-esterase gene family and its function in controlling pollen tube growth in pear (*Pyrus bretschneideri*). *Genomics* **2020**, *112*, 2467–2477. [CrossRef]

27. Tian, G.-W.; Chen, M.-H.; Zaltsman, A.; Citovsky, V. Pollen-specific pectin methylesterase involved in pollen tube growth. *Dev. Biol.* **2006**, *294*, 83–91. [CrossRef]

28. Pelloux, J.; Rusterucci, C.; Mellerowicz, E. New insights into pectin methylesterase structure and function. *Trends Plant. Sci.* **2007**, *12*, 267–277. [CrossRef]

29. Wang, M.; Yuan, D.; Gao, W.; Li, Y.; Tan, J.; Zhang, X. A comparative genome analysis of PME and PMEI families reveals the evolution of pectin metabolism in plant cell walls. *PLoS ONE* **2013**, *8*, e72082. [CrossRef]

30. Wormit, A.; Usadel, B. The Multifaceted Role of Pectin Methylesterase Inhibitors (PMEIs). *Int. J. Mol. Sci.* **2018**, *19*, 2878. [CrossRef]

31. Micheli, F. Pectin methylesterases: Cell wall enzymes with important roles in plant physiology. *Trends Plant. Sci.* **2001**, *6*, 414–419. [CrossRef]

32. Röckel, N.; Wolf, S.; Kost, B.; Rausch, T.; Greiner, S. Elaborate spatial patterning of cell-wall PME and PMEI at the pollen tube tip involves PMEI endocytosis, and reflects the distribution of esterified and de-esterified pectins. *Plant. J.* **2008**, *53*, 133–143. [CrossRef] [PubMed]

33. Derksen, J.; Rutten, T.; Lichtscheidl, I.K.; de Win, A.H.N.; Pierson, E.S.; Rongen, G. Quantitative analysis of the distribution of organelles in tobacco pollen tubes: Implications for exocytosis and endocytosis. *Protoplasma* **1995**, *188*, 267–276. [CrossRef]

34. Guan, Y.; Guo, J.; Li, H.; Yang, Z. Signaling in Pollen Tube Growth: Crosstalk, Feedback, and Missing Links. *Mol. Plant.* **2013**, *6*, 1053–1064. [CrossRef] [PubMed]

35. Mecchia, M.A.; Santos-Fernandez, G.; Duss, N.N.; Somoza, S.C.; Boisson-Dernier, A.; Gagliardini, V.; Martínez-Bernardini, A.; Fabrice, T.N.; Ringli, C.; Muschietti, J.P.; et al. RALF4/19 peptides interact with LRX proteins to control pollen tube growth in Arabidopsis. *Science* **2017**, *358*, 1600–1603. [CrossRef] [PubMed]

36. Derksen, J.; Rutten, T.; Van Amstel, T.; De Win, A.; Doris, F.; Steer, M. Regulation of pollen tube growth. *Acta Bot. Neerl.* **1995**, *44*, 93–119. [CrossRef]

37. Picton, J.M.; Steer, M.W. Membrane recycling and the control of secretory activity in pollen tubes. *J. Cell. Sci.* **1983**, *63*, 303–310.

38. Steer, M.W. Plasma Membrane Turnover in Plant Cells. *J. Exp. Bot.* **1988**, *39*, 987–996. [CrossRef]

39. Guo, J.; Yang, Z. Exocytosis and endocytosis: Coordinating and fine-tuning the polar tip growth domain in pollen tubes. *J. Exp. Bot.* **2020**. [CrossRef]

40. Cole, R.A.; Fowler, J.E. Polarized growth: Maintaining focus on the tip. *Curr. Opin. Plant. Biol.* **2006**, *9*, 579–588. [CrossRef]

41. Cai, G.; Parrotta, L.; Cresti, M. Organelle trafficking, the cytoskeleton, and pollen tube growth: Organelle trafficking in pollen tubes. *J. Integr. Plant. Biol.* **2015**, *57*, 63–78. [CrossRef] [PubMed]

42. Hepler, P.K.; Winship, L.J. The pollen tube clear zone: Clues to the mechanism of polarized growth: Differential organelle movement creates a clear zone. *J. Integr. Plant. Biol.* **2015**, *57*, 79–92. [CrossRef] [PubMed]

43. Hepler, P.K.; Vidali, L.; Cheung, A.Y. Polarized Cell Growth in Higher Plants. *Ann. Rev. Cell Dev. Biol.* **2001**, *17*, 159–187. [CrossRef]

44. Chebli, Y.; Kroeger, J.; Geitmann, A. Transport Logistics in Pollen Tubes. *Mol. Plant.* **2013**, *6*, 1037–1052. [CrossRef] [PubMed]

45. Adhikari, P.B.; Liu, X.; Wu, X.; Zhu, S.; Kasahara, R.D. Fertilization in flowering plants: An odyssey of sperm cell delivery. *Plant. Mol. Biol.* **2020**. [CrossRef]

46. Ischebeck, T.; Seiler, S.; Heilmann, I. At the poles across kingdoms: Phosphoinositides and polar tip growth. *Protoplasma* **2010**, *240*, 13–31. [CrossRef]

47. Michard, E.; Simon, A.A.; Tavares, B.; Wudick, M.M.; Feijó, J.A. Signaling with Ions: The Keystone for Apical Cell Growth and Morphogenesis in Pollen Tubes. *Plant. Physiol.* **2017**, *173*, 91–111. [CrossRef]

48. Scheible, N.; McCubbin, A. Signaling in Pollen Tube Growth: Beyond the Tip of the Polarity Iceberg. *Plants (Basel)* **2019**, *8*, 156. [CrossRef]

49. Steinhorst, L.; Kudla, J. Calcium—A central regulator of pollen germination and tube growth. *Biochim. Biophys. Acta (BBA) Mol. Cell Res.* **2013**, *1833*, 1573–1581. [CrossRef]

50. Vogler, H.; Santos-Fernandez, G.; Mecchia, M.A.; Grossniklaus, U. To preserve or to destroy, that is the question: The role of the cell wall integrity pathway in pollen tube growth. *Curr. Opin. Plant. Biol.* **2019**, *52*, 131–139. [CrossRef]

51. Zhang, M.J.; Zhang, X.S.; Gao, X.-Q. ROS in the Male-Female Interactions During Pollination: Function and Regulation. *Front. Plant. Sci.* **2020**, *11*, 177. [CrossRef] [PubMed]

52. Gu, Y.; Fu, Y.; Dowd, P.; Li, S.; Vernoud, V.; Gilroy, S.; Yang, Z. A Rho family GTPase controls actin dynamics and tip growth via two counteracting downstream pathways in pollen tubes. *J. Cell Biol.* **2005**, *169*, 127–138. [CrossRef] [PubMed]

53. Ischebeck, T.; Stenzel, I.; Hempel, F.; Jin, X.; Mosblech, A.; Heilmann, I. Phosphatidylinositol-4,5-bisphosphate influences Nt-Rac5-mediated cell expansion in pollen tubes of Nicotiana tabacum: PtdIns(4,5)P2 and polar tip growth. *Plant. J.* **2011**, *65*, 453–468. [CrossRef] [PubMed]

54. Kost, B.; Lemichez, E.; Spielhofer, P.; Hong, Y.; Tolias, K.; Carpenter, C.; Chua, N.-H. Rac Homologues and Compartmentalized Phosphatidylinositol 4, 5-Bisphosphate Act in a Common Pathway to Regulate Polar Pollen Tube Growth. *J. Cell Biol.* **1999**, *145*, 317–330. [CrossRef] [PubMed]

55. Haduch-Sendecka, A.; Pietruszka, M.; Zajdel, P. Power spectrum, growth velocities and cross-correlations of longitudinal and transverse oscillations of individual Nicotiana tabacum pollen tube. *Planta* **2014**, *240*, 263–276. [CrossRef]

56. Hemelryck, M.V.; Bernal, R.; Ispolatov, Y.; Dumais, J. Lily Pollen Tubes Pulse According to a Simple Spatial Oscillator. *Sci. Rep.* **2018**, *8*, 12135. [CrossRef]

57. Hwang, J.-U.; Gu, Y.; Lee, Y.-J.; Yang, Z. Oscillatory ROP GTPase activation leads the oscillatory polarized growth of pollen tubes. *Mol. Biol. Cell* **2005**, *16*, 5385–5399. [CrossRef]

58. Qin, Y.; Dong, J. Focusing on the Focus: What Else beyond the Master Switches for Polar Cell Growth? *Mol. Plant.* **2015**, *8*, 582–594. [CrossRef]

59. Yan, A.; Xu, G.; Yang, Z.-B. Calcium participates in feedback regulation of the oscillating ROP1 Rho GTPase in pollen tubes. *Proc. Natl. Acad. Sci. USA* **2009**, *106*, 22002–22007. [CrossRef]

60. Duan, Q.; Kita, D.; Johnson, E.A.; Aggarwal, M.; Gates, L.; Wu, H.-M.; Cheung, A.Y. Reactive oxygen species mediate pollen tube rupture to release sperm for fertilization in Arabidopsis. *Nat. Commun.* **2014**, *5*, 3129. [CrossRef]

61. Potocký, M.; Jones, M.A.; Bezvoda, R.; Smirnoff, N.; Žárský, V. Reactive oxygen species produced by NADPH oxidase are involved in pollen tube growth. *New Phytol.* **2007**, *174*, 742–751. [CrossRef] [PubMed]

62. Potocký, M.; Pejchar, P.; Gutkowska, M.; Jiménez-Quesada, M.J.; Potocká, A.; de Dios Alché, J.; Kost, B.; Žárský, V. NADPH oxidase activity in pollen tubes is affected by calcium ions, signaling phospholipids and Rac/Rop GTPases. *J. Plant. Physiol.* **2012**, *169*, 1654–1663. [CrossRef]

63. Cárdenas, L.; McKenna, S.T.; Kunkel, J.G.; Hepler, P.K. NAD(P)H oscillates in pollen tubes and is correlated with tip growth. *Plant. Physiol.* **2006**, *142*, 1460–1468. [CrossRef]

64. Gao, Y.-B.; Wang, C.-L.; Wu, J.-Y.; Zhou, H.-S.; Jiang, X.-T.; Wu, J.; Zhang, S.-L. Low temperature inhibits pollen tube growth by disruption of both tip-localized reactive oxygen species and endocytosis in Pyrus bretschneideri Rehd. *Plant. Physiol. Biochem.* **2014**, *74*, 255–262. [CrossRef] [PubMed]

65. Jimenez-Quesada, M.J.; Traverso, J.A.; Potocký, M.; Žárský, V.; Alché, J.D.D. Generation of Superoxide by OeRbohH, a NADPH Oxidase Activity During Olive (Olea europaea L.) Pollen Development and Germination. *Front. Plant. Sci.* **2019**, *10*, 1149. [CrossRef] [PubMed]

66. Liu, P.; Li, R.-L.; Zhang, L.; Wang, Q.-L.; Niehaus, K.; Baluska, F.; Samaj, J.; Lin, J.-X. Lipid microdomain polarization is required for NADPH oxidase-dependent ROS signaling in Picea meyeri pollen tube tip growth. *Plant. J.* **2009**, *60*, 303–313. [CrossRef]

67. Speranza, A.; Crinelli, R.; Scoccianti, V.; Geitmann, A. Reactive oxygen species are involved in pollen tube initiation in kiwifruit. *Plant. Biol. (Stuttg)* **2012**, *14*, 64–76. [CrossRef]

68. Kaya, H.; Nakajima, R.; Iwano, M.; Kanaoka, M.M.; Kimura, S.; Takeda, S.; Kawarazaki, T.; Senzaki, E.; Hamamura, Y.; Higashiyama, T.; et al. Ca^{2+}-activated reactive oxygen species production by Arabidopsis RbohH and RbohJ is essential for proper pollen tube tip growth. *Plant. Cell* **2014**, *26*, 1069–1080. [CrossRef]

69. Lassig, R.; Gutermuth, T.; Bey, T.D.; Konrad, K.R.; Romeis, T. Pollen tube NAD(P)H oxidases act as a speed control to dampen growth rate oscillations during polarized cell growth. *Plant. J.* **2014**, *78*, 94–106. [CrossRef]

70. Boisson-Dernier, A.; Lituiev, D.S.; Nestorova, A.; Franck, C.M.; Thirugnanarajah, S.; Grossniklaus, U. ANXUR Receptor-Like Kinases Coordinate Cell Wall Integrity with Growth at the Pollen Tube Tip Via NADPH Oxidases. *PLoS Biol.* **2013**, *11*, e1001719. [CrossRef]

71. Feng, H.; Liu, C.; Fu, R.; Zhang, M.; Li, H.; Shen, L.; Wei, Q.; Sun, X.; Xu, L.; Ni, B.; et al. LORELEI-LIKE GPI-ANCHORED PROTEINS 2/3 Regulate Pollen Tube Growth as Chaperones and Coreceptors for ANXUR/BUPS Receptor Kinases in Arabidopsis. *Mol. Plant.* **2019**, *12*, 1612–1623. [CrossRef] [PubMed]

72. Zhu, L.; Chu, L.-C.; Liang, Y.; Zhang, X.-Q.; Chen, L.-Q.; Ye, D. The Arabidopsis CrRLK1L protein kinases BUPS1 and BUPS2 are required for normal growth of pollen tubes in the pistil. *Plant. J.* **2018**, *95*, 474–486. [CrossRef]

73. Ge, Z.; Cheung, A.Y.; Qu, L. Pollen tube integrity regulation in flowering plants: Insights from molecular assemblies on the pollen tube surface. *New Phytol.* **2019**, *222*, 687–693. [CrossRef] [PubMed]

74. Benkő, P.; Jee, S.; Kaszler, N.; Fehér, A.; Gémes, K. Polyamines treatment during pollen germination and pollen tube elongation in tobacco modulate reactive oxygen species and nitric oxide homeostasis. *J. Plant. Physiol.* **2020**, *244*, 153085. [CrossRef]

75. Wu, J.; Shang, Z.; Wu, J.; Jiang, X.; Moschou, P.N.; Sun, W.; Roubelakis-Angelakis, K.A.; Zhang, S. Spermidine oxidase-derived H_2O_2 regulates pollen plasma membrane hyperpolarization-activated Ca(2+) -permeable channels and pollen tube growth. *Plant. J.* **2010**, *63*, 1042–1053. [CrossRef] [PubMed]

76. Do, T.H.T.; Choi, H.; Palmgren, M.; Martinoia, E.; Hwang, J.-U.; Lee, Y. Arabidopsis ABCG28 is required for the apical accumulation of reactive oxygen species in growing pollen tubes. *Proc. Natl. Acad. Sci. USA* **2019**, *116*, 12540–12549. [CrossRef]

77. Mangano, S.; Juárez, S.P.D.; Estevez, J.M. ROS Regulation of Polar Growth in Plant Cells. *Plant. Physiol.* **2016**, *171*, 1593–1605. [CrossRef]

78. Podolyan, A.; Maksimov, N.; Breygina, M. Redox-regulation of ion homeostasis in growing lily pollen tubes. *J. Plant. Physiol.* **2019**, *243*, 153050. [CrossRef]

79. Zhang, Y.; Zhu, H.; Zhang, Q.; Li, M.; Yan, M.; Wang, R.; Wang, L.; Welti, R.; Zhang, W.; Wang, X. Phospholipase Dα1 and Phosphatidic Acid Regulate NADPH Oxidase Activity and Production of Reactive Oxygen Species in ABA-Mediated Stomatal Closure in *Arabidopsis*. *Plant. Cell* **2009**, *21*, 2357–2377. [CrossRef]

80. Wudick, M.M.; Feijó, J.A. At the intersection: Merging Ca^{2+} and ROS signaling pathways in pollen. *Mol. Plant.* **2014**, *7*, 1595–1597. [CrossRef]

81. Feijó, J.A.; Sainhas, J.; Hackett, G.R.; Kunkel, J.G.; Hepler, P.K. Growing pollen tubes possess a constitutive alkaline band in the clear zone and a growth-dependent acidic tip. *J. Cell Biol.* **1999**, *144*, 483–496. [CrossRef] [PubMed]

82. Certal, A.C.; Almeida, R.B.; Carvalho, L.M.; Wong, E.; Moreno, N.; Michard, E.; Carneiro, J.; Rodriguéz-Léon, J.; Wu, H.-M.; Cheung, A.Y.; et al. Exclusion of a Proton ATPase from the Apical Membrane Is Associated with Cell Polarity and Tip Growth in *Nicotiana tabacum* Pollen Tubes. *Plant. Cell* **2008**, *20*, 614–634. [CrossRef]

83. Michard, E.; Dias, P.; Feijó, J.A. Tobacco pollen tubes as cellular models for ion dynamics: Improved spatial and temporal resolution of extracellular flux and free cytosolic concentration of calcium and protons using pHluorin and YC3.1 CaMeleon. *Sex. Plant. Reprod.* **2008**, *21*, 169–181. [CrossRef]

84. Fricker, M.D.; White, N.S.; Obermeyer, G. pH gradients are not associated with tip growth in pollen tubes of Lilium longiflorum. *J. Cell. Sci.* **1997**, *110 Pt 15*, 1729–1740.

85. Lovy-Wheeler, A.; Kunkel, J.G.; Allwood, E.G.; Hussey, P.J.; Hepler, P.K. Oscillatory increases in alkalinity anticipate growth and may regulate actin dynamics in pollen tubes of lily. *Plant. Cell* **2006**, *18*, 2182–2193. [CrossRef] [PubMed]

86. Winship, L.J.; Rounds, C.; Hepler, P.K. Perturbation Analysis of Calcium, Alkalinity and Secretion during Growth of Lily Pollen Tubes. *Plants (Basel)* **2016**, *6*, 3. [CrossRef] [PubMed]

87. Domingos, P.; Dias, P.N.; Tavares, B.; Portes, M.T.; Wudick, M.M.; Konrad, K.R.; Gilliham, M.; Bicho, A.; Feijó, J.A. Molecular and electrophysiological characterization of anion transport in Arabidopsis thaliana pollen reveals regulatory roles for pH, Ca^{2+} and GABA. *New Phytol.* **2019**, *223*, 1353–1371. [CrossRef]

88. Hoffmann, R.D.; Portes, M.T.; Olsen, L.I.; Damineli, D.S.C.; Hayashi, M.; Nunes, C.O.; Pedersen, J.T.; Lima, P.T.; Campos, C.; Feijó, J.A.; et al. Plasma membrane H+-ATPases sustain pollen tube growth and fertilization. *Nat. Commun.* **2020**, *11*, 2395. [CrossRef]

89. Brewbaker, J.L.; Kwack, B.H. THE ESSENTIAL ROLE OF CALCIUM ION IN POLLEN GERMINATION AND POLLEN TUBE GROWTH. *Am. J. Bot.* **1963**, *50*, 859–865. [CrossRef]

90. Denninger, P.; Bleckmann, A.; Lausser, A.; Vogler, F.; Ott, T.; Ehrhardt, D.W.; Frommer, W.B.; Sprunck, S.; Dresselhaus, T.; Grossmann, G. Male–female communication triggers calcium signatures during fertilization in Arabidopsis. *Nat. Commun.* **2014**, *5*, 4645. [CrossRef]

91. Hamamura, Y.; Nishimaki, M.; Takeuchi, H.; Geitmann, A.; Kurihara, D.; Higashiyama, T. Live imaging of calcium spikes during double fertilization in Arabidopsis. *Nat. Commun.* **2014**, *5*, 4722. [CrossRef] [PubMed]

92. Holdaway-Clarke, T.L.; Feijo, J.A.; Hackett, G.R.; Kunkel, J.G.; Hepler, P.K. Pollen Tube Growth and the Intracellular Cytosolic Calcium Gradient Oscillate in Phase while Extracellular Calcium Influx Is Delayed. *Plant. Cell* **1997**, *9*, 1999–2010. [CrossRef] [PubMed]

93. Pierson, E.S.; Miller, D.D.; Callaham, D.A.; van Aken, J.; Hackett, G.; Hepler, P.K. Tip-localized calcium entry fluctuates during pollen tube growth. *Dev. Biol.* **1996**, *174*, 160–173. [CrossRef] [PubMed]

94. Malho, R.; Trewavas, A.J. Localized Apical Increases of Cytosolic Free Calcium Control Pollen Tube Orientation. *Plant. Cell* **1996**, *8*, 1935–1949. [CrossRef]

95. Zheng, R.; Su, S.; Xiao, H.; Tian, H. Calcium: A Critical Factor in Pollen Germination and Tube Elongation. *Int. J. Mol. Sci.* **2019**, *20*, 420. [CrossRef]

96. Iwano, M.; Entani, T.; Shiba, H.; Kakita, M.; Nagai, T.; Mizuno, H.; Miyawaki, A.; Shoji, T.; Kubo, K.; Isogai, A.; et al. Fine-tuning of the cytoplasmic Ca^{2+} concentration is essential for pollen tube growth. *Plant. Physiol.* **2009**, *150*, 1322–1334. [CrossRef]

97. Obermeyer, G.; Weisenseel, M.H. Calcium channel blocker and calmodulin antagonists affect the gradient of free calcium ions in lily pollen tubes. *Eur. J. Cell Biol.* **1991**, *56*, 319–327. [PubMed]

98. Pierson, E.S.; Miller, D.D.; Callaham, D.A.; Shipley, A.M.; Rivers, B.A.; Cresti, M.; Hepler, P.K. Pollen tube growth is coupled to the extracellular calcium ion flux and the intracellular calcium gradient: Effect of BAPTA-type buffers and hypertonic media. *Plant. Cell* **1994**, *6*, 1815–1828. [CrossRef]

99. Dutta, R.; Robinson, K.R. Identification and characterization of stretch-activated ion channels in pollen protoplasts. *Plant. Physiol.* **2004**, *135*, 1398–1406. [CrossRef]

100. Frietsch, S.; Wang, Y.-F.; Sladek, C.; Poulsen, L.R.; Romanowsky, S.M.; Schroeder, J.I.; Harper, J.F. A cyclic nucleotide-gated channel is essential for polarized tip growth of pollen. *Proc. Natl. Acad. Sci. USA* **2007**, *104*, 14531–14536. [CrossRef]

101. Michard, E.; Lima, P.T.; Borges, F.; Silva, A.C.; Portes, M.T.; Carvalho, J.E.; Gilliham, M.; Liu, L.-H.; Obermeyer, G.; Feijó, J.A. Glutamate receptor-like genes form Ca^{2+} channels in pollen tubes and are regulated by pistil D-serine. *Science* **2011**, *332*, 434–437. [CrossRef]

102. Wudick, M.M.; Portes, M.T.; Michard, E.; Rosas-Santiago, P.; Lizzio, M.A.; Nunes, C.O.; Campos, C.; Santa Cruz Damineli, D.; Carvalho, J.C.; Lima, P.T.; et al. CORNICHON sorting and regulation of GLR channels underlie pollen tube Ca^{2+} homeostasis. *Science* **2018**, *360*, 533–536. [CrossRef] [PubMed]

103. Lamport, D.T.A.; Tan, L.; Held, M.A.; Kieliszewski, M.J. Pollen tube growth and guidance: Occam's razor sharpened on a molecular arabinogalactan glycoprotein Rosetta Stone. *New Phytol.* **2018**, *217*, 491–500. [CrossRef] [PubMed]

104. Li, Y.; Guo, J.; Yang, Z.; Yang, D.-L. Plasma Membrane-Localized Calcium Pumps and Copines Coordinately Regulate Pollen Germination and Fertility in Arabidopsis. *Int. J. Mol. Sci.* **2018**, *19*, 1774. [CrossRef] [PubMed]

105. Schiøtt, M.; Romanowsky, S.M.; Baekgaard, L.; Jakobsen, M.K.; Palmgren, M.G.; Harper, J.F. A plant plasma membrane Ca^{2+} pump is required for normal pollen tube growth and fertilization. *Proc. Natl. Acad. Sci. USA* **2004**, *101*, 9502–9507. [CrossRef]

106. Ramakrishnan, S.; Bera, M.; Coleman, J.; Rothman, J.E.; Krishnakumar, S.S. Synergistic roles of Synaptotagmin-1 and complexin in calcium-regulated neuronal exocytosis. *Elife* **2020**, *9*. [CrossRef]

107. Zhou, Q.; Zhou, P.; Wang, A.L.; Wu, D.; Zhao, M.; Südhof, T.C.; Brunger, A.T. The primed SNARE-complexin-synaptotagmin complex for neuronal exocytosis. *Nature* **2017**, *548*, 420–425. [CrossRef] [PubMed]

108. Pozzi, D.; Corradini, I.; Matteoli, M. The Control of Neuronal Calcium Homeostasis by SNAP-25 and its Impact on Neurotransmitter Release. *Neuroscience* **2019**, *420*, 72–78. [CrossRef] [PubMed]

109. Harmon, A.C.; Gribskov, M.; Gubrium, E.; Harper, J.F. The CDPK superfamily of protein kinases: Research review. *New Phytol.* **2001**, *151*, 175–183. [CrossRef]

110. Li, J.; Li, Y.; Deng, Y.; Chen, P.; Feng, F.; Chen, W.; Zhou, X.; Wang, Y. A calcium-dependent protein kinase, ZmCPK32, specifically expressed in maize pollen to regulate pollen tube growth. *PLoS ONE* **2018**, *13*, e0195787. [CrossRef]

111. Myers, C.; Romanowsky, S.M.; Barron, Y.D.; Garg, S.; Azuse, C.L.; Curran, A.; Davis, R.M.; Hatton, J.; Harmon, A.C.; Harper, J.F. Calcium-dependent protein kinases regulate polarized tip growth in pollen tubes. *Plant. J.* **2009**, *59*, 528–539. [CrossRef] [PubMed]

112. Yoon, G.M.; Dowd, P.E.; Gilroy, S.; McCubbin, A.G. Calcium-dependent protein kinase isoforms in Petunia have distinct functions in pollen tube growth, including regulating polarity. *Plant. Cell* **2006**, *18*, 867–878. [CrossRef]

113. Gutermuth, T.; Lassig, R.; Portes, M.-T.; Maierhofer, T.; Romeis, T.; Borst, J.-W.; Hedrich, R.; Feijo, J.A.; Konrad, K.R. Pollen Tube Growth Regulation by Free Anions Depends on the Interaction between the Anion Channel SLAH3 and Calcium-Dependent Protein Kinases CPK2 and CPK20. *Plant. Cell* **2013**, *25*, 4525–4543. [CrossRef] [PubMed]

114. Zhao, L.-N.; Shen, L.-K.; Zhang, W.-Z.; Zhang, W.; Wang, Y.; Wu, W.-H. Ca^{2+}-dependent protein kinase11 and 24 modulate the activity of the inward rectifying K+ channels in Arabidopsis pollen tubes. *Plant. Cell* **2013**, *25*, 649–661. [CrossRef] [PubMed]

115. Gutermuth, T.; Herbell, S.; Lassig, R.; Brosché, M.; Romeis, T.; Feijó, J.A.; Hedrich, R.; Konrad, K.R. Tip-localized Ca^{2+} -permeable channels control pollen tube growth via kinase-dependent R- and S-type anion channel regulation. *New Phytol.* **2018**, *218*, 1089–1105. [CrossRef] [PubMed]

116. Herbell, S.; Gutermuth, T.; Konrad, K.R. An interconnection between tip-focused Ca^{2+} and anion homeostasis controls pollen tube growth. *Plant. Signal. Behav.* **2018**, *13*, e1529521. [CrossRef] [PubMed]

117. Mähs, A.; Steinhorst, L.; Han, J.-P.; Shen, L.-K.; Wang, Y.; Kudla, J. The calcineurin B-like Ca^{2+} sensors CBL1 and CBL9 function in pollen germination and pollen tube growth in Arabidopsis. *Mol. Plant.* **2013**, *6*, 1149–1162. [CrossRef] [PubMed]

118. Steinhorst, L.; Mähs, A.; Ischebeck, T.; Zhang, C.; Zhang, X.; Arendt, S.; Schültke, S.; Heilmann, I.; Kudla, J. Vacuolar CBL-CIPK12 Ca^{2+}-Sensor-Kinase Complexes Are Required for Polarized Pollen Tube Growth. *Curr. Biol.* **2015**, *25*, 1475–1482. [CrossRef]

119. Suwińska, A.; Wasąg, P.; Zakrzewski, P.; Lenartowska, M.; Lenartowski, R. Calreticulin is required for calcium homeostasis and proper pollen tube tip growth in Petunia. *Planta* **2017**, *245*, 909–926. [CrossRef]

120. Wang, S.-S.; Diao, W.-Z.; Yang, X.; Qiao, Z.; Wang, M.; Acharya, B.R.; Zhang, W. Arabidopsis thaliana CML25 mediates the Ca(2+) regulation of K(+) transmembrane trafficking during pollen germination and tube elongation. *Plant. Cell Environ.* **2015**, *38*, 2372–2386. [CrossRef]

121. Yang, X.; Wang, S.-S.; Wang, M.; Qiao, Z.; Bao, C.-C.; Zhang, W. Arabidopsis thaliana calmodulin-like protein CML24 regulates pollen tube growth by modulating the actin cytoskeleton and controlling the cytosolic Ca(2+) concentration. *Plant. Mol. Biol.* **2014**, *86*, 225–236. [CrossRef] [PubMed]

122. Qian, D.; Xiang, Y. Actin Cytoskeleton as Actor in Upstream and Downstream of Calcium Signaling in Plant Cells. *Int. J. Mol. Sci.* **2019**, *20*, 1403. [CrossRef] [PubMed]

123. Elliott, L.; Moore, I.; Kirchhelle, C. Spatio-temporal control of post-Golgi exocytic trafficking in plants. *J. Cell. Sci.* **2020**, *133*. [CrossRef] [PubMed]

124. Feiguelman, G.; Fu, Y.; Yalovsky, S. ROP GTPases Structure-Function and Signaling Pathways. *Plant. Physiol.* **2018**, *176*, 57–79. [CrossRef] [PubMed]

125. Bourne, H.R.; Sanders, D.A.; McCormick, F. The GTPase superfamily: Conserved structure and molecular mechanism. *Nature* **1991**, *349*, 117–127. [CrossRef]

126. Berken, A.; Thomas, C.; Wittinghofer, A. A new family of RhoGEFs activates the Rop molecular switch in plants. *Nature* **2005**, *436*, 1176–1180. [CrossRef]

127. Wu, G.; Li, H.; Yang, Z. Arabidopsis RopGAPs are a novel family of rho GTPase-activating proteins that require the Cdc42/Rac-interactive binding motif for rop-specific GTPase stimulation. *Plant. Physiol.* **2000**, *124*, 1625–1636. [CrossRef]

128. DerMardirossian, C.; Bokoch, G.M. GDIs: Central regulatory molecules in Rho GTPase activation. *Trends Cell Biol.* **2005**, *15*, 356–363. [CrossRef]

129. Bischoff, F.; Molendijk, A.; Rajendrakumar, C.S.V.; Palme, K. GTP-binding proteins in plants. *Cell. Mol. Life Sci. CMLS* **1999**, *55*, 233–256. [CrossRef]

130. Cheung, A.Y.; Chen, C.Y.-H.; Glaven, R.H.; de Graaf, B.H.J.; Vidali, L.; Hepler, P.K.; Wu, H. Rab2 GTPase regulates vesicle trafficking between the endoplasmic reticulum and the Golgi bodies and is important to pollen tube growth. *Plant. Cell* **2002**, *14*, 945–962. [CrossRef]

131. de Graaf, B.H.J.; Cheung, A.Y.; Andreyeva, T.; Levasseur, K.; Kieliszewski, M.; Wu, H. Rab11 GTPase-regulated membrane trafficking is crucial for tip-focused pollen tube growth in tobacco. *Plant. Cell* **2005**, *17*, 2564–2579. [CrossRef] [PubMed]

132. Szumlanski, A.L.; Nielsen, E. The Rab GTPase RabA4d regulates pollen tube tip growth in Arabidopsis thaliana. *Plant. Cell* **2009**, *21*, 526–544. [CrossRef]

133. Peng, J.; Ilarslan, H.; Wurtele, E.S.; Bassham, D.C. AtRabD2b and AtRabD2c have overlapping functions in pollen development and pollen tube growth. *BMC Plant. Biol.* **2011**, *11*, 25. [CrossRef] [PubMed]

134. Gutkowska, M.; Wnuk, M.; Nowakowska, J.; Lichocka, M.; Stronkowski, M.M.; Swiezewska, E. Rab geranylgeranyl transferase β subunit is essential for male fertility and tip growth in Arabidopsis. *J. Exp. Bot.* **2015**, *66*, 213–224. [CrossRef]

135. Klahre, U.; Kost, B. Tobacco RhoGTPase ACTIVATING PROTEIN1 spatially restricts signaling of RAC/Rop to the apex of pollen tubes. *Plant. Cell* **2006**, *18*, 3033–3046. [CrossRef] [PubMed]

136. Kost, B. Spatial control of Rho (Rac-Rop) signaling in tip-growing plant cells. *Trends Cell Biol.* **2008**, *18*, 119–127. [CrossRef]

137. Bloch, D.; Pleskot, R.; Pejchar, P.; Potocký, M.; Trpkošová, P.; Cwiklik, L.; Vukašinović, N.; Sternberg, H.; Yalovsky, S.; Žárský, V. Exocyst SEC3 and phosphoinositides define sites of exocytosis in pollen tube initiation and growth. *Plant. Physiol.* **2016**, *172*, 980–1002. [CrossRef]

138. Lavy, M.; Bloch, D.; Hazak, O.; Gutman, I.; Poraty, L.; Sorek, N.; Sternberg, H.; Yalovsky, S. A Novel ROP/RAC effector links cell polarity, root-meristem maintenance, and vesicle trafficking. *Curr. Biol.* **2007**, *17*, 947–952. [CrossRef]

139. Li, S.; Gu, Y.; Yan, A.; Lord, E.; Yang, Z.-B. RIP1 (ROP Interactive Partner 1)/ICR1 marks pollen germination sites and may act in the ROP1 pathway in the control of polarized pollen growth. *Mol. Plant.* **2008**, *1*, 1021–1035. [CrossRef]

140. Chen, C.Y.-H.; Cheung, A.Y.; Wu, H. Actin-depolymerizing factor mediates Rac/Rop GTPase-regulated pollen tube growth. *Plant. Cell* **2003**, *15*, 237–249. [CrossRef]

141. Lee, Y.J.; Szumlanski, A.; Nielsen, E.; Yang, Z. Rho-GTPase-dependent filamentous actin dynamics coordinate vesicle targeting and exocytosis during tip growth. *J. Cell Biol.* **2008**, *181*, 1155–1168. [CrossRef]

142. Stephan, O.; Cottier, S.; Fahlén, S.; Montes-Rodriguez, A.; Sun, J.; Eklund, D.M.; Klahre, U.; Kost, B. RISAP is a TGN-associated RAC5 effector regulating membrane traffic during polar cell growth in tobacco. *Plant. Cell* **2014**, *26*, 4426–4447. [CrossRef] [PubMed]

143. Takeuchi, H.; Higashiyama, T. Tip-localized receptors control pollen tube growth and LURE sensing in Arabidopsis. *Nature* **2016**, *531*, 245–248. [CrossRef] [PubMed]

144. Sugiyama, Y.; Nagashima, Y.; Wakazaki, M.; Sato, M.; Toyooka, K.; Fukuda, H.; Oda, Y. A Rho-actin signaling pathway shapes cell wall boundaries in Arabidopsis xylem vessels. *Nat. Commun.* **2019**, *10*, 468. [CrossRef] [PubMed]

145. Li, H.; Lin, Y.; Heath, R.M.; Zhu, M.X.; Yang, Z. Control of pollen tube tip growth by a Rop GTPase-dependent pathway that leads to tip-localized calcium influx. *Plant. Cell* **1999**, *11*, 1731–1742.

146. Winge, P.; Brembu, T.; Kristensen, R.; Bones, A.M. Genetic structure and evolution of RAC-GTPases in Arabidopsis thaliana. *Genetics* **2000**, *156*, 1959–1971.

147. Klahre, U.; Becker, C.; Schmitt, A.C.; Kost, B. Nt-RhoGDI2 regulates Rac/Rop signaling and polar cell growth in tobacco pollen tubes. *Plant. J.* **2006**, *46*, 1018–1031. [CrossRef]

148. Sun, J.; Eklund, D.M.; Montes-Rodriguez, A.; Kost, B. In vivo Rac/Rop localization as well as interaction with RhoGAP and RhoGDI in tobacco pollen tubes: Analysis by low-level expression of fluorescent fusion proteins and bimolecular fluorescence complementation. *Plant J.* **2015**, *84*, 83–98. [CrossRef]

149. Feng, Q.-N.; Kang, H.; Song, S.-J.; Ge, F.-R.; Zhang, Y.-L.; Li, E.; Li, S.; Zhang, Y. Arabidopsis RhoGDIs Are Critical for Cellular Homeostasis of Pollen Tubes. *Plant. Physiol.* **2016**, *170*, 841–856. [CrossRef]

150. Kim, E.-J.; Park, S.-W.; Hong, W.-J.; Silva, J.; Liang, W.; Zhang, D.; Jung, K.-H.; Kim, Y.-J. Genome-wide analysis of RopGEF gene family to identify genes contributing to pollen tube growth in rice (Oryza sativa). *BMC Plant. Biol.* **2020**, *20*, 95. [CrossRef]

151. Chang, F.; Gu, Y.; Ma, H.; Yang, Z. AtPRK2 promotes ROP1 activation via RopGEFs in the control of polarized pollen tube growth. *Mol. Plant.* **2013**, *6*, 1187–1201. [CrossRef] [PubMed]

152. Li, E.; Cui, Y.; Ge, F.-R.; Chai, S.; Zhang, W.-T.; Feng, Q.-N.; Jiang, L.; Li, S.; Zhang, Y. AGC1.5 Kinase Phosphorylates RopGEFs to Control Pollen Tube Growth. *Mol. Plant.* **2018**, *11*, 1198–1209. [CrossRef] [PubMed]

153. Higashiyama, T.; Yang, W.-C. Gametophytic Pollen Tube Guidance: Attractant Peptides, Gametic Controls, and Receptors. *Plant. Physiol.* **2017**, *173*, 112–121. [CrossRef] [PubMed]

154. Takeuchi, H.; Higashiyama, T. A Species-Specific Cluster of Defensin-Like Genes Encodes Diffusible Pollen Tube Attractants in Arabidopsis. *PLoS Biol.* **2012**, *10*, e1001449. [CrossRef] [PubMed]

155. Wang, T.; Liang, L.; Xue, Y.; Jia, P.-F.; Chen, W.; Zhang, M.-X.; Wang, Y.-C.; Li, H.-J.; Yang, W.-C. A receptor heteromer mediates the male perception of female attractants in plants. *Nature* **2016**, *531*, 241–244. [CrossRef]

156. Gu, Y.; Li, S.; Lord, E.M.; Yang, Z. Members of a novel class of Arabidopsis Rho guanine nucleotide exchange factors control Rho GTPase-dependent polar growth. *Plant. Cell* **2006**, *18*, 366–381. [CrossRef]

157. Meijer, H.J.G.; Munnik, T. PHOSPHOLIPID-BASED SIGNALING IN PLANTS. *Ann. Rev. Plant. Biol.* **2003**, *54*, 265–306. [CrossRef]

158. Noack, L.C.; Pejchar, P.; Sekereš, J.; Jaillais, Y.; Potocký, M. Transient Gene Expression as a Tool to Monitor and Manipulate the Levels of Acidic Phospholipids in Plant Cells. *Methods Mol. Biol.* **2019**, *1992*, 189–199. [CrossRef]

159. Collin, S.; Justin, A.M.; Cantrel, C.; Arondel, V.; Kader, J.C. Identification of AtPIS, a phosphatidylinositol synthase from Arabidopsis. *Eur. J. Biochem.* **1999**, *262*, 652–658. [CrossRef]

160. Löfke, C.; Ischebeck, T.; König, S.; Freitag, S.; Heilmann, I. Alternative metabolic fates of phosphatidylinositol produced by phosphatidylinositol synthase isoforms in *Arabidopsis thaliana*. *Biochem. J.* **2008**, *413*, 115–124. [CrossRef]

161. Ischebeck, T.; Vu, L.H.; Jin, X.; Stenzel, I.; Löfke, C.; Heilmann, I. Functional Cooperativity of Enzymes of Phosphoinositide Conversion According to Synergistic Effects on Pectin Secretion in Tobacco Pollen Tubes. *Mol. Plant.* **2010**, *3*, 870–881. [CrossRef] [PubMed]

162. Gerth, K.; Lin, F.; Menzel, W.; Krishnamoorthy, P.; Stenzel, I.; Heilmann, M.; Heilmann, I. Guilt by Association: A Phenotype-Based View of the Plant Phosphoinositide Network. *Ann. Rev. Plant. Biol.* **2017**, *68*, 349–374. [CrossRef] [PubMed]

163. Heilmann, I. Phosphoinositide signaling in plant development. *Development* **2016**, *143*, 2044–2055. [CrossRef] [PubMed]

164. Meijer, H.J.; Berrie, C.P.; Iurisci, C.; Divecha, N.; Musgrave, A.; Munnik, T. Identification of a new polyphosphoinositide in plants, phosphatidylinositol 5-monophosphate (PtdIns5P), and its accumulation upon osmotic stress. *Biochem. J.* **2001**, *360*, 491–498. [CrossRef]

165. Krinke, O.; Ruelland, E.; Valentová, O.; Vergnolle, C.; Renou, J.-P.; Taconnat, L.; Flemr, M.; Burketová, L.; Zachowski, A. Phosphatidylinositol 4-Kinase Activation Is an Early Response to Salicylic Acid in Arabidopsis Suspension Cells. *Plant. Physiol.* **2007**, *144*, 1347–1359. [CrossRef] [PubMed]

166. Simon, M.L.A.; Platre, M.P.; Assil, S.; van Wijk, R.; Chen, W.Y.; Chory, J.; Dreux, M.; Munnik, T.; Jaillais, Y. A multi-colour/multi-affinity marker set to visualize phosphoinositide dynamics in Arabidopsis. *Plant. J.* **2014**, *77*, 322–337. [CrossRef] [PubMed]

167. Thole, J.M.; Vermeer, J.E.M.; Zhang, Y.; Gadella, T.W.J.; Nielsen, E. *ROOT HAIR DEFECTIVE4* Encodes a Phosphatidylinositol-4-Phosphate Phosphatase Required for Proper Root Hair Development in *Arabidopsis thaliana*. *Plant. Cell* **2008**, *20*, 381–395. [CrossRef]

168. Vermeer, J.E.M.; Thole, J.M.; Goedhart, J.; Nielsen, E.; Munnik, T.; Gadella, T.W.J. Imaging phosphatidylinositol 4-phosphate dynamics in living plant cells. *Plant. J.* **2009**, *57*, 356–372. [CrossRef]

169. Kang, B.-H.; Nielsen, E.; Preuss, M.L.; Mastronarde, D.; Staehelin, L.A. Electron tomography of RabA4b- and PI-4Kβ1-labeled trans Golgi network compartments in Arabidopsis. *Traffic* **2011**, *12*, 313–329. [CrossRef]

170. Preuss, M.L.; Schmitz, A.J.; Thole, J.M.; Bonner, H.K.S.; Otegui, M.S.; Nielsen, E. A role for the RabA4b effector protein PI-4Kbeta1 in polarized expansion of root hair cells in Arabidopsis thaliana. *J. Cell Biol.* **2006**, *172*, 991–998. [CrossRef]

171. Jia, P.-F.; Xue, Y.; Li, H.-J.; Yang, W.-C. Golgi-localized LOT regulates trans-Golgi network biogenesis and pollen tube growth. *Proc. Natl. Acad. Sci. USA* **2018**, *115*, 12307–12312. [CrossRef]

172. Lin, F.; Krishnamoorthy, P.; Schubert, V.; Hause, G.; Heilmann, M.; Heilmann, I. A dual role for cell plate-associated PI4Kβ in endocytosis and phragmoplast dynamics during plant somatic cytokinesis. *Embo J.* **2019**, 38. [CrossRef] [PubMed]

173. Rubilar-Hernández, C.; Osorio-Navarro, C.; Cabello, F.; Norambuena, L. PI4KIIIβ Activity Regulates Lateral Root Formation Driven by Endocytic Trafficking to the Vacuole. *Plant. Physiol.* **2019**, *181*, 112–126. [CrossRef] [PubMed]

174. Mueller-Roeber, B.; Pical, C. Inositol phospholipid metabolism in Arabidopsis. Characterized and putative isoforms of inositol phospholipid kinase and phosphoinositide-specific phospholipase C. *Plant. Physiol.* **2002**, *130*, 22–46. [CrossRef] [PubMed]

175. Strahl, T.; Hama, H.; DeWald, D.B.; Thorner, J. Yeast phosphatidylinositol 4-kinase, Pik1, has essential roles at the Golgi and in the nucleus. *J. Cell Biol.* **2005**, *171*, 967–979. [CrossRef] [PubMed]

176. Yoshida, S.; Ohya, Y.; Goebl, M.; Nakano, A.; Anraku, Y. A novel gene, STT4, encodes a phosphatidylinositol 4-kinase in the PKC1 protein kinase pathway of Saccharomyces cerevisiae. *J. Biol. Chem.* **1994**, *269*, 1166–1172. [PubMed]

177. Im, Y.J.; Davis, A.J.; Perera, I.Y.; Johannes, E.; Allen, N.S.; Boss, W.F. The N-terminal Membrane Occupation and Recognition Nexus Domain of *Arabidopsis* Phosphatidylinositol Phosphate Kinase 1 Regulates Enzyme Activity. *J. Biol. Chem.* **2007**, *282*, 5443–5452. [CrossRef]

178. Stenzel, I.; Ischebeck, T.; Quint, M.; Heilmann, I. Variable Regions of PI4P 5-Kinases Direct PtdIns(4,5)P2 Toward Alternative Regulatory Functions in Tobacco Pollen Tubes. *Front. Plant. Sci.* **2012**, *2*. [CrossRef]

179. Honys, D.; Twell, D. Transcriptome analysis of haploid male gametophyte development in Arabidopsis. *Genome Biol.* **2004**, *5*, R85. [CrossRef]

180. Wang, Y.; Zhang, W.-Z.; Song, L.-F.; Zou, J.-J.; Su, Z.; Wu, W.-H. Transcriptome Analyses Show Changes in Gene Expression to Accompany Pollen Germination and Tube Growth in Arabidopsis. *Plant. Physiol.* **2008**, *148*, 1201–1211. [CrossRef]

181. Ischebeck, T.; Stenzel, I.; Heilmann, I. Type B Phosphatidylinositol-4-Phosphate 5-Kinases Mediate Arabidopsis and Nicotiana tabacum Pollen Tube Growth by Regulating Apical Pectin Secretion. *Plant Cell Online* **2008**, *20*, 3312–3330. [CrossRef] [PubMed]

182. Grobei, M.A.; Qeli, E.; Brunner, E.; Rehrauer, H.; Zhang, R.; Roschitzki, B.; Basler, K.; Ahrens, C.H.; Grossniklaus, U. Deterministic protein inference for shotgun proteomics data provides new insights into Arabidopsis pollen development and function. *Genome Res.* **2009**, *19*, 1786–1800. [CrossRef] [PubMed]

183. Sousa, E.; Kost, B.; Malho, R. Arabidopsis Phosphatidylinositol-4-Monophosphate 5-Kinase 4 Regulates Pollen Tube Growth and Polarity by Modulating Membrane Recycling. *Plant Cell Online* **2008**, *20*, 3050–3064. [CrossRef] [PubMed]

184. Zhao, Y.; Yan, A.; Feijó, J.A.; Furutani, M.; Takenawa, T.; Hwang, I.; Fu, Y.; Yang, Z. Phosphoinositides regulate clathrin-dependent endocytosis at the tip of pollen tubes in Arabidopsis and tobacco. *Plant. Cell* **2010**, *22*, 4031–4044. [CrossRef]

185. Dowd, P.E.; Coursol, S.; Skirpan, A.L.; Kao, T.; Gilroy, S. Petunia phospholipase c1 is involved in pollen tube growth. *Plant. Cell* **2006**, *18*, 1438–1453. [CrossRef]

186. Hempel, F.; Stenzel, I.; Heilmann, M.; Krishnamoorthy, P.; Menzel, W.; Golbik, R.; Helm, S.; Dobritzsch, D.; Baginsky, S.; Lee, J.; et al. MAPKs Influence Pollen Tube Growth by Controlling the Formation of Phosphatidylinositol 4,5-Bisphosphate in an Apical Plasma Membrane Domain. *Plant. Cell* **2017**, *29*, 3030–3050. [CrossRef]

187. Kaneda, M.; van Oostende-Triplet, C.; Chebli, Y.; Testerink, C.; Bednarek, S.Y.; Geitmann, A. Plant AP180 N-Terminal Homolog Proteins Are Involved in Clathrin-Dependent Endocytosis during Pollen Tube Growth in Arabidopsis thaliana. *Plant. Cell Physiol.* **2019**, *60*, 1316–1330. [CrossRef]

188. Kolay, S.; Basu, U.; Raghu, P. Control of diverse subcellular processes by a single multi-functional lipid phosphatidylinositol 4,5-bisphosphate [PI(4,5)P2]. *Biochem. J.* **2016**, *473*, 1681–1692. [CrossRef]

189. Mähs, A.; Ischebeck, T.; Heilig, Y.; Stenzel, I.; Hempel, F.; Seiler, S.; Heilmann, I. The essential phosphoinositide kinase MSS-4 is required for polar hyphal morphogenesis, localizing to sites of growth and cell fusion in Neurospora crassa. *PLoS ONE* **2012**, *7*, e51454. [CrossRef]

190. Raghu, P.; Joseph, A.; Krishnan, H.; Singh, P.; Saha, S. Phosphoinositides: Regulators of Nervous System Function in Health and Disease. *Front. Mol. NeuroSci.* **2019**, *12*, 208. [CrossRef]

191. Hille, B.; Dickson, E.J.; Kruse, M.; Vivas, O.; Suh, B.-C. Phosphoinositides regulate ion channels. *Biochim. Biophys. Acta* **2015**, *1851*, 844–856. [CrossRef] [PubMed]

192. Martin, T.F.J. Role of PI(4,5)P(2) in vesicle exocytosis and membrane fusion. *Subcell. Biochem.* **2012**, *59*, 111–130. [CrossRef] [PubMed]

193. Wu, B.; Guo, W. The Exocyst at a Glance. *J. Cell. Sci.* **2015**, *128*, 2957–2964. [CrossRef] [PubMed]

194. Žárský, V.; Sekereš, J.; Kubátová, Z.; Pečenková, T.; Cvrčková, F. Three subfamilies of exocyst EXO70 family subunits in land plants: Early divergence and ongoing functional specialization. *J. Exp. Bot.* **2020**, *71*, 49–62. [CrossRef] [PubMed]

195. He, B.; Xi, F.; Zhang, X.; Zhang, J.; Guo, W. Exo70 interacts with phospholipids and mediates the targeting of the exocyst to the plasma membrane. *Embo J.* **2007**, *26*, 4053–4065. [CrossRef] [PubMed]

196. Guo, W.; Tamanoi, F.; Novick, P. Spatial regulation of the exocyst complex by Rho1 GTPase. *Nat. Cell Biol.* **2001**, *3*, 353–360. [CrossRef] [PubMed]

197. Zhang, X.; Orlando, K.; He, B.; Xi, F.; Zhang, J.; Zajac, A.; Guo, W. Membrane association and functional regulation of Sec3 by phospholipids and Cdc42. *J. Cell Biol.* **2008**, *180*, 145–158. [CrossRef]

198. Elias, M.; Drdova, E.; Ziak, D.; Bavlnka, B.; Hala, M.; Cvrckova, F.; Soukupova, H.; Zarsky, V. The exocyst complex in plants. *Cell Biol. Int.* **2003**, *27*, 199–201. [CrossRef]

199. Hála, M.; Cole, R.; Synek, L.; Drdová, E.; Pecenková, T.; Nordheim, A.; Lamkemeyer, T.; Madlung, J.; Hochholdinger, F.; Fowler, J.E.; et al. An exocyst complex functions in plant cell growth in Arabidopsis and tobacco. *Plant. Cell* **2008**, *20*, 1330–1345. [CrossRef]

200. TerBush, D.R.; Maurice, T.; Roth, D.; Novick, P. The Exocyst is a multiprotein complex required for exocytosis in Saccharomyces cerevisiae. *Embo J.* **1996**, *15*, 6483–6494. [CrossRef]

201. Dubuke, M.L.; Maniatis, S.; Shaffer, S.A.; Munson, M. The Exocyst Subunit Sec6 Interacts with Assembled Exocytic SNARE Complexes. *J. Biol. Chem.* **2015**, *290*, 28245–28256. [CrossRef] [PubMed]

202. Guo, W.; Roth, D.; Walch-Solimena, C.; Novick, P. The exocyst is an effector for Sec4p, targeting secretory vesicles to sites of exocytosis. *Embo J.* **1999**, *18*, 1071–1080. [CrossRef] [PubMed]

203. Pleskot, R.; Cwiklik, L.; Jungwirth, P.; Žárský, V.; Potocký, M. Membrane targeting of the yeast exocyst complex. *Biochim. Biophys. Acta* **2015**, *1848*, 1481–1489. [CrossRef] [PubMed]

204. Synek, L.; Schlager, N.; Eliás, M.; Quentin, M.; Hauser, M.-T.; Zárský, V. AtEXO70A1, a member of a family of putative exocyst subunits specifically expanded in land plants, is important for polar growth and plant development. *Plant. J.* **2006**, *48*, 54–72. [CrossRef]

205. Yue, P.; Zhang, Y.; Mei, K.; Wang, S.; Lesigang, J.; Zhu, Y.; Dong, G.; Guo, W. Sec3 promotes the initial binary t-SNARE complex assembly and membrane fusion. *Nat. Commun.* **2017**, *8*, 14236. [CrossRef] [PubMed]

206. Cole, R.A.; Synek, L.; Zarsky, V.; Fowler, J.E. SEC8, a subunit of the putative Arabidopsis exocyst complex, facilitates pollen germination and competitive pollen tube growth. *Plant. Physiol.* **2005**, *138*, 2005–2018. [CrossRef]

207. Synek, L.; Vukašinović, N.; Kulich, I.; Hála, M.; Aldorfová, K.; Fendrych, M.; Žárský, V. EXO70C2 Is a Key Regulatory Factor for Optimal Tip Growth of Pollen. *Plant. Physiol.* **2017**, *174*, 223–240. [CrossRef]

208. Li, Y.; Tan, X.; Wang, M.; Li, B.; Zhao, Y.; Wu, C.; Rui, Q.; Wang, J.; Liu, Z.; Bao, Y. Exocyst subunit SEC3A marks the germination site and is essential for pollen germination in Arabidopsis thaliana. *Sci. Rep.* **2017**, *7*, 40279. [CrossRef]

209. Zárský, V.; Kulich, I.; Fendrych, M.; Pečenková, T. Exocyst complexes multiple functions in plant cells secretory pathways. *Curr. Opin. Plant. Biol.* **2013**, *16*, 726–733. [CrossRef]

210. Fendrych, M.; Synek, L.; Pecenková, T.; Toupalová, H.; Cole, R.; Drdová, E.; Nebesárová, J.; Sedinová, M.; Hála, M.; Fowler, J.E.; et al. The Arabidopsis exocyst complex is involved in cytokinesis and cell plate maturation. *Plant. Cell* **2010**, *22*, 3053–3065. [CrossRef]

211. Pecenková, T.; Markovic, V.; Sabol, P.; Kulich, I.; Žárský, V. Exocyst and autophagy-related membrane trafficking in plants. *J. Exp. Bot.* **2017**, *69*, 47–57. [CrossRef] [PubMed]

212. Sabol, P.; Kulich, I.; Žárský, V. RIN4 recruits the exocyst subunit EXO70B1 to the plasma membrane. *J. Exp. Bot.* **2017**, *68*, 3253–3265. [CrossRef] [PubMed]

213. Stegmann, M.; Anderson, R.G.; Ichimura, K.; Pecenkova, T.; Reuter, P.; Žárský, V.; McDowell, J.M.; Shirasu, K.; Trujillo, M. The ubiquitin ligase PUB22 targets a subunit of the exocyst complex required for PAMP-triggered responses in Arabidopsis. *Plant. Cell* **2012**, *24*, 4703–4716. [CrossRef] [PubMed]

214. Kubátová, Z.; Pejchar, P.; Potocký, M.; Sekereš, J.; Žárský, V.; Kulich, I. Arabidopsis Trichome Contains Two Plasma Membrane Domains with Different Lipid Compositions Which Attract Distinct EXO70 Subunits. *Int. J. Mol. Sci.* **2019**, *20*, 3803. [CrossRef]

215. Sekereš, J.; Pejchar, P.; Šantrůček, J.; Vukašinović, N.; Žárský, V.; Potocký, M. Analysis of Exocyst Subunit EXO70 Family Reveals Distinct Membrane Polar Domains in Tobacco Pollen Tubes. *Plant. Physiol.* **2017**, *173*, 1659–1675. [CrossRef]

216. Li, S.; van Os, G.M.A.; Ren, S.; Yu, D.; Ketelaar, T.; Emons, A.M.C.; Liu, C.-M. Expression and functional analyses of EXO70 genes in Arabidopsis implicate their roles in regulating cell type-specific exocytosis. *Plant. Physiol.* **2010**, *154*, 1819–1830. [CrossRef]

217. Pecenková, T.; Hála, M.; Kulich, I.; Kocourková, D.; Drdová, E.; Fendrych, M.; Toupalová, H.; Zársky, V. The role for the exocyst complex subunits Exo70B2 and Exo70H1 in the plant-pathogen interaction. *J. Exp. Bot.* **2011**, *62*, 2107–2116. [CrossRef]

218. Boyd, C.; Hughes, T.; Pypaert, M.; Novick, P. Vesicles carry most exocyst subunits to exocytic sites marked by the remaining two subunits, Sec3p and Exo70p. *J. Cell Biol.* **2004**, *167*, 889–901. [CrossRef]

219. Fendrych, M.; Synek, L.; Pecenková, T.; Drdová, E.J.; Sekeres, J.; de Rycke, R.; Nowack, M.K.; Zársky, V. Visualization of the exocyst complex dynamics at the plasma membrane of Arabidopsis thaliana. *Mol. Biol. Cell* **2013**, *24*, 510–520. [CrossRef]

220. Zhong, R.; Ye, Z.-H. The SAC Domain-Containing Protein Gene Family in Arabidopsis. *Plant. Physiol.* **2003**, *132*, 544–555. [CrossRef]

221. Despres, B.; Bouissonnie, F.; Wu, H.-J.; Gomord, V.; Guilleminot, J.; Grellet, F.; Berger, F.; Delseny, M.; Devic, M. Three SAC1-like genes show overlapping patterns of expression in Arabidopsis but are remarkably silent during embryo development. *Plant. J.* **2003**, *34*, 293–306. [CrossRef]

222. Ton, J.; Jakab, G.; Toquin, V.; Flors, V.; Iavicoli, A.; Maeder, M.N.; Métraux, J.-P.; Mauch-Mani, B. Dissecting the beta-aminobutyric acid-induced priming phenomenon in Arabidopsis. *Plant. Cell* **2005**, *17*, 987–999. [CrossRef] [PubMed]

223. Guo, T.; Chen, H.-C.; Lu, Z.-Q.; Diao, M.; Chen, K.; Dong, N.-Q.; Shan, J.-X.; Ye, W.-W.; Huang, S.; Lin, H.-X. A SAC Phosphoinositide Phosphatase Controls Rice Development via Hydrolyzing PI4P and PI(4,5)P2. *Plant. Physiol.* **2020**, *182*, 1346–1358. [CrossRef] [PubMed]

224. Williams, M.E.; Torabinejad, J.; Cohick, E.; Parker, K.; Drake, E.J.; Thompson, J.E.; Hortter, M.; Dewald, D.B. Mutations in the Arabidopsis phosphoinositide phosphatase gene SAC9 lead to overaccumulation of PtdIns(4,5)P2 and constitutive expression of the stress-response pathway. *Plant. Physiol.* **2005**, *138*, 686–700. [CrossRef]

225. Vollmer, A.H.; Youssef, N.N.; DeWald, D.B. Unique cell wall abnormalities in the putative phosphoinositide phosphatase mutant AtSAC9. *Planta* **2011**, *234*, 993–1005. [CrossRef] [PubMed]

226. Zhang, Z.; Li, Y.; Luo, Z.; Kong, S.; Zhao, Y.; Zhang, C.; Zhang, W.; Yuan, H.; Cheng, L. Expansion and Functional Divergence of Inositol Polyphosphate 5-Phosphatases in Angiosperms. *Genes (Basel)* **2019**, *10*, 393. [CrossRef]

227. Berdy, S.E.; Kudla, J.; Gruissem, W.; Gillaspy, G.E. Molecular characterization of At5PTase1, an inositol phosphatase capable of terminating inositol trisphosphate signaling. *Plant. Physiol.* **2001**, *126*, 801–810. [CrossRef]

228. Jones, M.A.; Raymond, M.J.; Smirnoff, N. Analysis of the root-hair morphogenesis transcriptome reveals the molecular identity of six genes with roles in root-hair development in Arabidopsis. *Plant. J.* **2006**, *45*, 83–100. [CrossRef]

229. Ringli, C.; Baumberger, N.; Keller, B. The Arabidopsis root hair mutants der2-der9 are affected at different stages of root hair development. *Plant. Cell Physiol.* **2005**, *46*, 1046–1053. [CrossRef]

230. Zhong, R.; Ye, Z.-H. Molecular and biochemical characterization of three WD-repeat-domain-containing inositol polyphosphate 5-phosphatases in Arabidopsis thaliana. *Plant. Cell Physiol.* **2004**, *45*, 1720–1728. [CrossRef]

231. Hanahan, D.J.; Chaikoff, I.L. A new phospholipide-splitting enzyme specific for the ester linkage between the nitrogenous base and the phosphoric acid grouping. *J. Biol. Chem.* **1947**, *169*, 699–705. [PubMed]

232. Irvine, R.F.; Letcher, A.J.; Dawson, R.M. Phosphatidylinositol phosphodiesterase in higher plants. *Biochem. J.* **1980**, *192*, 279–283. [CrossRef] [PubMed]

233. Wang, G.; Ryu, S.; Wang, X. Plant Phospholipases: An Overview. In *Lipases and Phospholipases*; Sandoval, G., Ed.; Humana Press: Totowa, NJ, USA, 2012; Volume 861, pp. 123–137. ISBN 978-1-61779-599-2.

234. Pokotylo, I.; Pejchar, P.; Potocký, M.; Kocourková, D.; Krčková, Z.; Ruelland, E.; Kravets, V.; Martinec, J. The plant non-specific phospholipase C gene family. Novel competitors in lipid signalling. *Prog. Lipid Res.* **2013**, *52*, 62–79. [CrossRef]

235. Pokotylo, I.; Kolesnikov, Y.; Kravets, V.; Zachowski, A.; Ruelland, E. Plant phosphoinositide-dependent phospholipases C: Variations around a canonical theme. *Biochimie* **2014**, *96*, 144–157. [CrossRef] [PubMed]

236. Ngo, A.H.; Lin, Y.-C.; Liu, Y.-C.; Gutbrod, K.; Peisker, H.; Dörmann, P.; Nakamura, Y. A pair of nonspecific phospholipases C, NPC2 and NPC6, are involved in gametophyte development and glycerolipid metabolism in Arabidopsis. *New Phytol.* **2018**, *219*, 163–175. [CrossRef]

237. Ngo, A.H.; Kanehara, K.; Nakamura, Y. Non-specific phospholipases C, NPC2 and NPC6, are required for root growth in Arabidopsis. *Plant. J.* **2019**, *100*, 825–835. [CrossRef]

238. Wimalasekera, R.; Pejchar, P.; Holk, A.; Martinec, J.; Scherer, G.F.E. Plant phosphatidylcholine-hydrolyzing phospholipases C NPC3 and NPC4 with roles in root development and brassinolide signaling in Arabidopsis thaliana. *Mol. Plant.* **2010**, *3*, 610–625. [CrossRef]

239. Helling, D.; Possart, A.; Cottier, S.; Klahre, U.; Kost, B. Pollen tube tip growth depends on plasma membrane polarization mediated by tobacco PLC3 activity and endocytic membrane recycling. *Plant. Cell* **2006**, *18*, 3519–3534. [CrossRef]

240. Stenzel, I.; Ischebeck, T.; Vu-Becker, L.H.; Riechmann, M.; Krishnamoorthy, P.; Fratini, M.; Heilmann, I. Coordinated Localization and Antagonistic Function of NtPLC3 and PI4P 5-Kinases in the Subapical Plasma Membrane of Tobacco Pollen Tubes. *Plants* **2020**, *9*, 452. [CrossRef]

241. Hokin, L.E. Receptors and phosphoinositide-generated second messengers. *Ann. Rev. Biochem.* **1985**, *54*, 205–235. [CrossRef]

242. Munnik, T.; Testerink, C. Plant phospholipid signaling: "in a nutshell". *J. Lipid Res.* **2009**, *50*, S260–S265. [CrossRef] [PubMed]

243. Hong, Y.; Zhao, J.; Guo, L.; Kim, S.-C.; Deng, X.; Wang, G.; Zhang, G.; Li, M.; Wang, X. Plant phospholipases D and C and their diverse functions in stress responses. *Prog. Lipid Res.* **2016**, *62*, 55–74. [CrossRef]

244. Lorenzo-Orts, L.; Couto, D.; Hothorn, M. Identity and functions of inorganic and inositol polyphosphates in plants. *New Phytol.* **2020**, *225*, 637–652. [CrossRef] [PubMed]

245. Tsui, M.M.; York, J.D. Roles of inositol phosphates and inositol pyrophosphates in development, cell signaling and nuclear processes. *Adv. Enzym. Regul.* **2010**, *50*, 324–337. [CrossRef] [PubMed]

246. Calderón Villalobos, L.I.A.; Lee, S.; De Oliveira, C.; Ivetac, A.; Brandt, W.; Armitage, L.; Sheard, L.B.; Tan, X.; Parry, G.; Mao, H.; et al. A combinatorial TIR1/AFB-Aux/IAA co-receptor system for differential sensing of auxin. *Nat. Chem. Biol.* **2012**, *8*, 477–485. [CrossRef] [PubMed]

247. Laha, D.; Parvin, N.; Dynowski, M.; Johnen, P.; Mao, H.; Bitters, S.T.; Zheng, N.; Schaaf, G. Inositol Polyphosphate Binding Specificity of the Jasmonate Receptor Complex. *Plant. Physiol.* **2016**, *171*, 2364–2370. [CrossRef] [PubMed]

248. Mosblech, A.; Thurow, C.; Gatz, C.; Feussner, I.; Heilmann, I. Jasmonic acid perception by COI1 involves inositol polyphosphates in Arabidopsis thaliana. *Plant. J.* **2011**, *65*, 949–957. [CrossRef]

249. Sheard, L.B.; Tan, X.; Mao, H.; Withers, J.; Ben-Nissan, G.; Hinds, T.R.; Kobayashi, Y.; Hsu, F.-F.; Sharon, M.; Browse, J.; et al. Jasmonate perception by inositol-phosphate-potentiated COI1-JAZ co-receptor. *Nature* **2010**, *468*, 400–405. [CrossRef]

250. Tan, X.; Calderon-Villalobos, L.I.A.; Sharon, M.; Zheng, C.; Robinson, C.V.; Estelle, M.; Zheng, N. Mechanism of auxin perception by the TIR1 ubiquitin ligase. *Nature* **2007**, *446*, 640–645. [CrossRef]

251. Muradoğlu, F.; Yıldız, K.; Balta, F. Methyl jasmonate influences of pollen germination and pollen tube growth of apricot (Prunus armeniaca L.). *Yüzüncü Yıl Univ. J. Agr. Sci. (Turk.)* **2010**, 183–188.

252. Gao, C.; Wang, Y.; Qu, H. Study of auxin regulation of pollen tube growth through calcium channels in Pyrus pyrifolia. *Plant. Growth Regul.* **2019**, *89*, 99–108. [CrossRef]

253. Zhan, H.; Zhong, Y.; Yang, Z.; Xia, H. Enzyme activities of Arabidopsis inositol polyphosphate kinases AtIPK2α and AtIPK2β are involved in pollen development, pollen tube guidance and embryogenesis. *Plant. J.* **2015**, *82*, 758–771. [CrossRef]

254. Nishizuka, Y. The molecular heterogeneity of protein kinase C and its implications for cellular regulation. *Nature* **1988**, *334*, 661–665. [CrossRef] [PubMed]

255. Valverde, A.M.; Sinnett-Smith, J.; Van Lint, J.; Rozengurt, E. Molecular cloning and characterization of protein kinase D: A target for diacylglycerol and phorbol esters with a distinctive catalytic domain. *Proc. Natl. Acad. Sci. USA* **1994**, *91*, 8572–8576. [CrossRef] [PubMed]

256. Islas-Flores, T.; Rahman, A.; Ullah, H.; Villanueva, M.A. The Receptor for Activated C Kinase in Plant Signaling: Tale of a Promiscuous Little Molecule. *Front. Plant. Sci.* **2015**, *6*. [CrossRef] [PubMed]

257. Arisz, S.A.; Testerink, C.; Munnik, T. Plant PA signaling via diacylglycerol kinase. *Biochim. Biophys. Acta (BBA) Mol. Cell Biol. Lipids* **2009**, *1791*, 869–875. [CrossRef] [PubMed]

258. Dong, W.; Lv, H.; Xia, G.; Wang, M. Does diacylglycerol serve as a signaling molecule in plants? *Plant. Signal. Behav.* **2012**, *7*, 472–475. [CrossRef] [PubMed]

259. Peters, C.; Kim, S.-C.; Devaiah, S.; Li, M.; Wang, X. Non-specific phospholipase C5 and diacylglycerol promote lateral root development under mild salt stress in Arabidopsis. *Plant. Cell Environ.* **2014**, *37*, 2002–2013. [CrossRef]

260. Potocký, M.; Pleskot, R.; Pejchar, P.; Vitale, N.; Kost, B.; Žárský, V. Live-cell imaging of phosphatidic acid dynamics in pollen tubes visualized by Spo20p-derived biosensor. *New Phytol.* **2014**, *203*, 483–494. [CrossRef]

261. Wissing, J.; Heim, S.; Wagner, K.G. Diacylglycerol kinase from suspension cultured plant cells: Purification and properties. *Plant. Physiol.* **1989**, *90*, 1546–1551. [CrossRef]

262. Pleskot, R.; Pejchar, P.; Bezvoda, R.; Lichtscheidl, I.; Wolters-Arts, M.; Marc, J.; Žárský, V.; Potocký, M. Turnover of Phosphatidic Acid through Distinct Signaling Pathways Affects Multiple Aspects of Pollen Tube Growth in Tobacco. *Front. Plant. Sci.* **2012**, *3*, 54. [CrossRef]

263. Ischebeck, T.; Valledor, L.; Lyon, D.; Gingl, S.; Nagler, M.; Meijón, M.; Egelhofer, V.; Weckwerth, W. Comprehensive cell-specific protein analysis in early and late pollen development from diploid microsporocytes to pollen tube growth. *Mol. Cell Proteom.* **2014**, *13*, 295–310. [CrossRef] [PubMed]

264. Vaz Dias, F.; Serrazina, S.; Vitorino, M.; Marchese, D.; Heilmann, I.; Godinho, M.; Rodrigues, M.; Malhó, R. A role for diacylglycerol kinase 4 in signalling crosstalk during Arabidopsis pollen tube growth. *New Phytol.* **2019**. [CrossRef] [PubMed]

265. Wong, A.; Donaldson, L.; Portes, M.T.; Eppinger, J.; Feijó, J.; Gehring, C. The Arabidopsis Diacylglycerol Kinase 4 is involved in nitric oxide-dependent pollen tube guidance and fertilization. *Development* **2020**. [CrossRef]

266. Angkawijaya, A.E.; Nguyen, V.C.; Gunawan, F.; Nakamura, Y. A Pair of Arabidopsis Diacylglycerol Kinases Essential for Gametogenesis and ER Phospholipid Metabolism in Leaves and Flowers. *Plant. Cell* **2020**. [CrossRef] [PubMed]

267. Eliáš, M.; Potocký, M.; Cvrčková, F.; Žárský, V. Molecular diversity of phospholipase D in angiosperms. *BMC Genom.* **2002**, *3*, 2. [CrossRef] [PubMed]

268. Li, J.; Wang, X. Phospholipase D and phosphatidic acid in plant immunity. *Plant. Sci.* **2019**, *279*, 45–50. [CrossRef] [PubMed]

269. Testerink, C.; Munnik, T. Phosphatidic acid: A multifunctional stress signaling lipid in plants. *Trends Plant. Sci.* **2005**, *10*, 368–375. [CrossRef] [PubMed]

270. Potocký, M.; Eliás, M.; Profotová, B.; Novotná, Z.; Valentová, O.; Zárský, V. Phosphatidic acid produced by phospholipase D is required for tobacco pollen tube growth. *Planta* **2003**, *217*, 122–130. [CrossRef]

271. Baneux, C.; Tanguy, E.; Thahouly, T.; Vitale, A.; Chasserot-Golaz, S.; Bader, M.-F.; Gasman, S.; Vitale, N. Phosphatidic acid metabolism regulates neuroendocrine secretion but is not under the direct control of lipins. *Iubmb Life* **2020**, *72*, 533–543. [CrossRef]

272. Tanguy, E.; Wang, Q.; Vitale, N. Role of Phospholipase D-Derived Phosphatidic Acid in Regulated Exocytosis and Neurological Disease. *Handb Exp Pharm.* **2020**, *259*, 115–130. [CrossRef]

273. Wang, H.; Zhang, C.; Xiao, H. Mechanism of membrane fusion: Protein-protein interaction and beyond. *Int. J. Physiol. Pathophysiol. Pharm.* **2019**, *11*, 250–257.

274. Noack, L.C.; Jaillais, Y. Functions of Anionic Lipids in Plants. *Ann. Rev. Plant. Biol.* **2020**, *71*, 71–102. [CrossRef] [PubMed]

275. Pleskot, R.; Potocký, M.; Pejchar, P.; Linek, J.; Bezvoda, R.; Martinec, J.; Valentová, O.; Novotná, Z.; Žárský, V. Mutual regulation of plant phospholipase D and the actin cytoskeleton: Reciprocal regulation of plant PLD and actin. *Plant. J.* **2010**, *62*, 494–507. [CrossRef]

276. Pejchar, P.; Sekereš, J.; Novotný, O.; Žárský, V.; Potocký, M. Functional analysis of phospholipase Dδ family in tobacco pollen tubes. *Plant. J.* **2020**. [CrossRef] [PubMed]

3 Article II: Finding new friends and revisiting old ones – how plant lipid droplets connect with other subcellular structures

This review was published online in the journal New Phytologist in July 2022. The online version of the article can be found under the following DOI:

https://doi.org/10.1111/nph.18390

Author contribution:

Patricia Scholz wrote the first draft except for the section on LD-peroxisome connections and revised the final version of the text. She designed figures 2 and 3 before their final editing by the journal.

New
Phytologist

TANSLEY INSIGHTS

Tansley insight

Finding new friends and revisiting old ones – how plant lipid droplets connect with other subcellular structures

Author for correspondence:
Till Ischebeck
Email: till.ischebeck@uni-muenster.de

Patricia Scholz[1] (iD), **Kent D. Chapman**[2] (iD), **Robert T. Mullen**[3] (iD) and **Till Ischebeck**[4] (iD)

[1]Department of Plant Biochemistry, Albrecht-von-Haller-Institute for Plant Sciences and Göttingen Center for Molecular Biosciences (GZMB), University of Göttingen, 37077 Göttingen, Germany; [2]Bio-Discovery Institute and Department of Biological Sciences, University of North Texas, Denton, TX 76203, USA; [3]Department of Molecular and Cellular Biology, University of Guelph, Guelph, ON N1G 2W1, Canada; [4]Institute of Plant Biology and Biotechnology (IBBP), Green Biotechnology, University of Münster, 48143 Münster, Germany

Contents

Summary

The number of described contact sites between different subcellular compartments and structures in eukaryotic cells has increased dramatically in recent years and, as such, has substantially reinforced the well-known premise that these kinds of connections are essential for overall cellular organization and the proper functioning of cellular metabolic and signaling pathways. Here, we discuss contact sites involving plant lipid droplets (LDs), including LD-endoplasmic reticulum (ER) connections that mediate the biogenesis of new LDs at the ER, LD-peroxisome connections, that facilitate the degradation of LD-stored triacylglycerols (TAGs), and the more recently discovered LD-plasma membrane connections, which involve at least three novel proteins, but have a yet unknown physiological function(s).

I. Lipid droplet functions and composition

Cytosolic lipid droplets (henceforth referred to as LDs) are subcellular structures that occur in essentially all eukaryotic species and in most of their cells. While traditionally considered to be just subcellular storage depots for neutral lipids, such as triacylglycerols (TAGs) and sterol esters (SEs), the described functions of plant LDs have expanded in recent years to include roles as both a source and sink for various hydrophobic compounds and their building blocks (Ischebeck *et al.*, 2020). Hence, plant LDs are now known to be important for fueling a wide range of developmental processes, such

as seed germination, and also for membrane remodeling during abiotic stress (de Vries & Ischebeck, 2020; Krawczyk *et al.*, 2022a). In addition, LDs support plant defenses through the production of volatiles (Garbowicz *et al.*, 2018) and phytoalexins (Shimada *et al.*, 2014; Fernandez-Santos *et al.*, 2020), and based on their reported proteomes, LDs likely have numerous other functions that remain to be elucidated (Ischebeck *et al.*, 2020).

Structurally, LDs are relatively simple, in that their core consists of TAG, SE and/or other hydrophobic substances that are partitioned from the aqueous cytosol by a phospholipid monolayer (Pyc *et al.*, 2017). Furthermore, various proteins are integrated into

the LD monolayer, some of which are thought to extend into the hydrophobic core (Huang, 2018), while others appear to be attached directly to the LD surface (Gidda et al., 2016) or through protein–protein interactions (Krawczyk et al., 2022b). Notably, in the last few years, many new LD proteins have been discovered that are directly involved in LD biogenesis, function, and/or breakdown (Horn et al., 2013; Pyc et al., 2017, 2021; Fernandez-Santos et al., 2020; Kretzschmar et al., 2020). Some of these proteins have been also implicated in mediating the physical connections that exist between LDs and other subcellular structures (Greer et al., 2020; Pyc et al., 2021; Krawczyk et al., 2022b). These connections are defined as membrane contact sites (MCSs) if the following conditions are fulfilled: (1) a connection of organelles mediated by tethering proteins, (2) no fusion of the organelles, (3) the fulfillment of a specific function(s) by the MCS, and (4) the presence of a defined proteome at the MCS (Scorrano et al., 2019). Here we focus on the connections of plant LDs with the endoplasmic reticulum (ER) and peroxisomes that are most thoroughly explored (Fig. 1a,b), and also highlight the recently-discovered MCS between LDs and the plasma membrane (Fig. 1c).

II. Lipid droplet-endoplasmic reticulum connections in plant cells

Lipid droplet formation is thought to be initiated by the synthesis of hydrophobic compounds (e.g., TAGs) at the ER, which are sequestered between the two leaflets of the ER membrane. The synthesized TAGs then aggregate into a 'lens-like' structure within the bilayer, based on biophysical processes as described by molecular dynamics simulations (Zoni et al., 2021). Simulation studies have also indicated that the protein seipin helps to accumulate and trap these 'TAG lenses' thereby defining the site of LD formation. Seipin is a membrane protein conserved across eukaryotes. It is organized in ring-shape complexes in the ER bilayer as a 10-mer in yeast (Klug et al., 2021), and an 11-mer in human (Yan et al., 2018). A single ring of seipin subunits is believed to surround the monolayer connection between the forming LD and the ER membrane, probably acting as a vent for the stream of ER-synthesized TAGs and other storage lipids entering into the growing LD (Fig. 2). In this way, the LD remains connected to the ER during formation and the LD monolayer is continuous with the outer leaflet of the ER membrane. The seipin ring might further prevent fusion of two nascent LDs at their connection sites to the ER. In Arabidopsis, there are three seipin isoforms encoded by three discrete genes (Cai et al., 2015). While the precise oligomeric nature of the Arabidopsis seipin complex is not yet known, structural homology modeling studies have indicated that the three seipin isoforms can adopt a similar three-dimensional (3D) structure as their human and yeast counterparts (Chapman et al., 2019). Ectopic expression of individual Arabidopsis seipins in plant cells influences the overall number and sizes of LDs, while loss of function of all three isoforms disrupts normal LD formation at the ER surface (Taurino et al., 2017).

In Arabidopsis, LIPID DROPLET-ASSOCIATED PROTEIN 1, 2 and 3 (LDAP 1, 2 and 3) and their interaction partner LDAP-INTERACTING PROTEIN (LDIP) also bind to nascent LDs
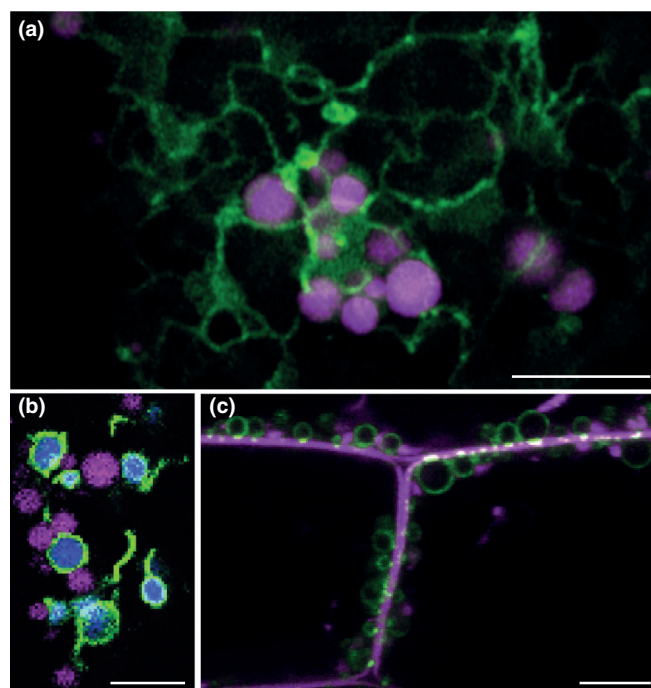
Fig. 1 Lipid droplets (LDs) form various contact sites in plant cells. (a) Contact sites of LDs with the endoplasmic reticulum (ER). Micrograph of a transiently-transformed *Nicotiana benthamiana* leaf cell expressing the ER marker protein KARYOGAMY2-CFP-HDEL (green) and stained with the neutral lipid-specific dye BODIPY 493/503, serving as a marker for LDs (magenta). Note the cell was also co-transformed with untagged *LD-ASSOCIATED PROTEIN1* and *LEAFY COTYLEDON2* in order to facilitate a proliferation of LDs. Image kindly provided by Payton Whitehead. (b) Contact sites of LDs with peroxisomes. Micrograph of an Arabidopsis seedling hypocotyl cell stably-coexpressing mCherry appended to a type 1 peroxisomal targeting signal, serving as a marker for the peroxisomal matrix (blue), and green fluorescent protein (GFP)-tagged SUGAR-DEPENDENT 1, which localizes to the peroxisomal boundary membrane, including membrane extensions called peroxules (green). LDs in the same cell were stained with the neutral-lipid specific dye Nile red (magenta). Image kindly provided by Dr Thierry Gaude; reproduced from Thazar-Poulot et al. (2015). (c) LD contact sites with the plasma membrane (PM). Micrograph of Arabidopsis seedling hypocotyl cells showing LDs surrounded by the stably-expressed LIPID DROPLET PLASMA MEMBRANE ADAPTOR fused to eGFP (green), which is especially enriched at contact sites with the plasma membrane (white). The plasma membrane was stained with FM4-64 (magenta). Image reproduced from Krawczyk et al. (2022b). Bars, 5 μm.

(Coulon et al., 2020; Pyc et al., 2021). LDIP additionally interacts with at least SEIPIN1 and SEIPIN2 and appears to function with them at the LD-ER junction (Pyc et al., 2021). Hidden Markov model searches revealed that the LDAPs and LDIP have homology with the human perilipin proteins (Box 1), and lipid droplet assembly factor 1 (LDAF1), respectively (Pyc et al., 2021). While perilipin proteins are generally considered LD surface-associated proteins with numerous functions (Itabe et al., 2017), LDAF1 forms an oligomeric complex in a 1 : 1 stoichiometry with seipin proteins during LD initiation in mammalian cells, and might additionally coat the nascent LD (Chung et al., 2019), a model that could also be considered analogous for the SEIPIN–LDIP complex. By extension, this comparison might be interpreted as a functional conservation between plants and other eukaryotes in the
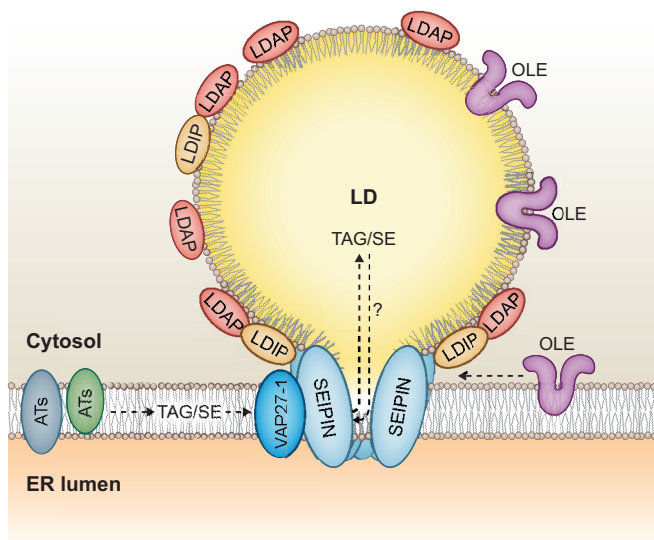
Fig. 2 Lipid droplet (LD)-endoplasmic reticulum (ER) contact sites are required for LD biogenesis. Triacylglycerols (TAGs) and sterol esters (SEs) are synthesized at the ER by different acyltransferases (ATs) and are channeled within the membrane into the growing, nascent LD at the ER-LD contact site. Seipin proteins are proposed to form a ring-shaped oligomer surrounding the ER-LD junction, regulating TAG/SE filling and LD growth. In addition, vesicle-associated membrane protein (VAMP)-associated protein 27-1 (VAP27-1) is considered part of the tether at the ER-LD contact site, interacting with seipin. LD-associated proteins (LDAP) and LDAP-interacting protein (LDIP) target from the cytosol to the nascent LD surface where they serve as an LD 'coat', and LDIP also interacts with the seipin complex at the LD-ER junction. Other LD coat proteins, such as oleosins (OLEs), are initially inserted in the ER membrane and then traffic to the LD surface via the ER-LD junction. However, the precise mechanism by which these proteins pass through the seipin complex remains to be determined. It is also not clear, if TAGs and SEs can be channeled back to the ER to be further metabolized by ER-bound lipases and/or ATs. Figure based on Ischebeck *et al.* (2020).

Box 1 Lipid droplets contact sites in yeast and animals.

In nonplant systems, many connections between lipid droplets (LDs) and other subcellular structures have been described (Valm *et al.*, 2017; Bohnert, 2020; Liao *et al.*, 2022). Association between LDs and lysosomes or the lysosome-like vacuole in yeast has been functionally connected to lipophagy (van Zutphen *et al.*, 2014; Schroeder *et al.*, 2015). However, some of the described LD contacts have different and sometimes tissue-dependent functions. For example, LD-mitochondria connections have been suggested to serve in the transfer of substrates for beta-oxidation (Bohnert, 2020) or for fatty acid activation for triacylglycerol (TAG) synthesis (Benador *et al.*, 2018). In several cases, discrete proteins have been found that are required to form the membrane contact sites (MCSs) at these connections. For instance, the human LD proteins perilipin 1 (PLIN1) and PLIN5 serve as potential tethering factors between LDs and mitochondria (Wang *et al.*, 2011; Boutant *et al.*, 2017), while in humans MOSPD2 (motile sperm domain-containing protein 2), which is a member of the ER-anchored vesicle-associated membrane protein (VAMP)-associated protein (VAP) family, forms a connection between the endoplasmic reticulum (ER) and LDs via a cytoplasmic-facing amphipathic helix that has affinity for lipid packing at the surface of the LDs (Zouiouich *et al.*, 2022). Also in humans, the mitoguardin 2 (MIGA2) protein facilitates a three-way connection between LDs, ER, and mitochondria for lipogenesis in adipocytes (Freyre *et al.*, 2019). In *Drosophila*, the protein Snazarus mediates a connection between the ER, plasma membrane and LDs in fat body cells (Ugrankar *et al.*, 2019). However, MIGA2 and Snazarus have no obvious homologs in plants, suggesting that other proteins might serve parallel roles in plant cells. By contrast, the proteins involved in the connection of LDs to the ER required for the proper formation of LDs are relatively well conserved among plants and other eukaryotic organisms.

components of the LD-ER connection complex. See Box 1 for additional information on LD connections with ER and other subcellular structures in nonplant systems.

Another component at the LD-ER connection in Arabidopsis is the VESICLE-ASSOCIATED MEMBRANE PROTEIN (VAMP)-ASSOCIATED PROTEIN 27-1 (VAP27-1). VAP27-1 has been previously described in the formation of ER–plasma membrane MCSs, where it interacts with the protein NET-WORKED 3C (Wang *et al.*, 2014). Besides this contact site, VAP27-1 localizes to the ER and LDs and physically interacts with the N-terminus of SEIPIN2 and SEIPIN3 (Greer *et al.*, 2020). As such, VAP27-1 appears to be an additional part of the tether complex at the LD-ER junction in plant cells that likely stabilizes the LD at the ER surface during biogenesis. VAP27-1 has well conserved homologs in yeast and animals and several of these VAP family proteins in other eukaryotes are known to participate in MCSs, and to facilitate lipid exchange between subcellular membranes. Interestingly, Arabidopsis cells with genetic disruptions in SEIPINs, the LDAPs, LDIP, or VAP27-1 can still form LDs. However, these LDs are often relatively large in size (Cai *et al.*, 2015; Greer *et al.*, 2020; Pyc *et al.*, 2021), and in the case of the *seipin* triple mutants, are sometimes found inside the ER lumen or the nucleoplasm instead of the cytoplasm (Taurino *et al.*, 2017). It is not clear if additive effects

would be observed in higher-order mutants or if single mutations in either gene locus are sufficient to lead to the same LD phenotype (i.e. gene locus heterogeneity).

The connection of LDs to the ER is not only important during the initiation of LD synthesis, but also during LD growth and maturation (Chapman *et al.*, 2019). It is furthermore believed that many of the proteins that associate with the LD surface are synthesized at the ER and inserted first into the ER membrane before reaching the LD (Ischebeck *et al.*, 2020). The best investigated example of this group of proteins are the oleosins, which are the most abundant LD protein family in seeds (Huang, 2018). It remains to be determined though, how these proteins traffic past the seipin ring complex in the ER membrane in order to populate the nascent, growing LD. Similarly, it is also not known if LDs completely detach from the ER at some point or if they always stay connected to the ER through a membrane continuum, as suggested in yeast (Jacquier *et al.*, 2011). Possibly involved in the former detachment process might be dynamins, which play a role in pinching off endocytotic vesicles and during fission of peroxisomes, mitochondria and plastids. Interestingly two dynamins were found as potential interaction partners of both seipin and LDIP in co-immunoprecipitation assays (Pyc *et al.*, 2021).

Another important open question is how many functions the LD-ER connection sites have. One function is clearly for LD synthesis and the deposition of hydrophobic compounds into the

growing LD, but depending upon the cell or tissue type, or the nature of the hydrophobic metabolite, this LD formation may have multiple functions. One such function is to store compounds for subsequent developmental stages, as during embryo and male gametophyte development. However, TAG accumulates and LD numbers increase also during abiotic stress. Here, it is speculated that the free fatty acids derived from stress-induced membrane lipid breakdown and remodeling are channeled into TAG to prevent lipotoxicity, making LDs an effective sink (de Vries & Ischebeck, 2020). SEs, however, decrease during heat stress in tobacco pollen tubes possibly to increase the amount of free sterols and sterol glycosides (Krawczyk *et al.*, 2022a), which could sustain membrane integrity by counteracting heat-increased membranes fluidity (Dufourc, 2008). In this regard, LDs could act as both a sink and source at the same time. LDs could also serve as a source during heat stress recovery, where TAG decreases again, as shown for leaves (Mueller *et al.*, 2015). Finally, it is possible that the building blocks of TAG could be directly used for membrane synthesis (Müller & Ischebeck, 2018; de Vries & Ischebeck, 2020), although it is not clear which lipases and/or acyltransferases would be involved in this process and if an LD-ER connection is required.

III. Lipid droplet-peroxisome connections in plant cells

Lipid droplets in oilseeds are the source of stored TAGs that are mobilized for carbon and energy during post-germinative seedling growth. The utilization of TAGs requires hydrolysis to free fatty acids by the lipase SUGAR-DEPENDENT 1 (SDP1; Eastmond, 2006) at the LD surface, and the uptake and oxidation of these fatty acids by the beta-oxidation and glyoxylate cycle pathways in the peroxisome matrix (Zienkiewicz & Zienkiewicz, 2020). Intimate connections observed by transmission electron microscopy between LDs and peroxisomes have been reported for decades (e.g. Gruber *et al.*, 1970 and recently reviewed in Esnay *et al.*, 2020), and purported functional connections have been described (Reumann & Bartel, 2016). SDP1 is localized in the peroxisomal boundary membrane, and upon seed germination, the membrane forms extensions called peroxules that surround the LD (Thazar-Poulot *et al.*, 2015). These peroxule extensions are dependent on a heteromeric protein complex called a 'retromer' complex, which is an evolutionarily-conserved multi-protein complex that mediates changes in membrane curvature. This relocalization of SDP1 in peroxules that wrap around LDs is believed to constitute an MCS that thereby facilitates the exchange of fatty acids to the peroxisomes for oxidation. Mutants disrupted in peroxule formation, fatty acid uptake, or beta-oxidation all show dramatic alterations in peroxisome morphology associated with interrupted lipid breakdown (Hayashi *et al.*, 2001; Thazar-Poulot *et al.*, 2015; Cui *et al.*, 2016). Although an MCS for peroxisomes and LDs has not been identified *per se*, nor have any tethering proteins that mediate their connection been discovered, it is possible that this connection involves VAP proteins at the ER (or the LD) and the peroxisomal membrane-bound acyl-CoA transporter, PEROXISOMAL TRANSPORTER PROTEIN1 (PXA1) (Esnay *et al.*, 2020). Certainly, the

connection between LDs and peroxisomes is an area poised for future research breakthroughs.

IV. Lipid doplet-plasma membrane connections in plant cells

During seed germination and seedling establishment of Arabidopsis, LDs are generally closely associated with the plasma membrane (Kretzschmar *et al.*, 2018). While the reason for this could be that they are simply appressed to the plasma membrane due to the large central vacuole, recent studies have shown that three proteins are specifically involved in the formation of this association (Krawczyk *et al.*, 2022b). Two of these proteins involved in LD-plasma membrane connections in Arabidopsis are the closely related SEED LIPID DROPLET PROTEIN 1 and 2 (SLDP1 and 2), which bind to LDs via a hydrophobic region near their N-termini and can also directly interact with the LIPID DROPLET PLASMA MEMBRANE ADAPTOR (LIPA) protein localized at the plasma membrane, thereby forming an MCS (Fig. 3). Consequently, if either SLDPs or LIPA are disrupted, LDs no longer align at the plasma membrane but instead cluster within the cell. Conversely, if one of the SLDPs is coexpressed with
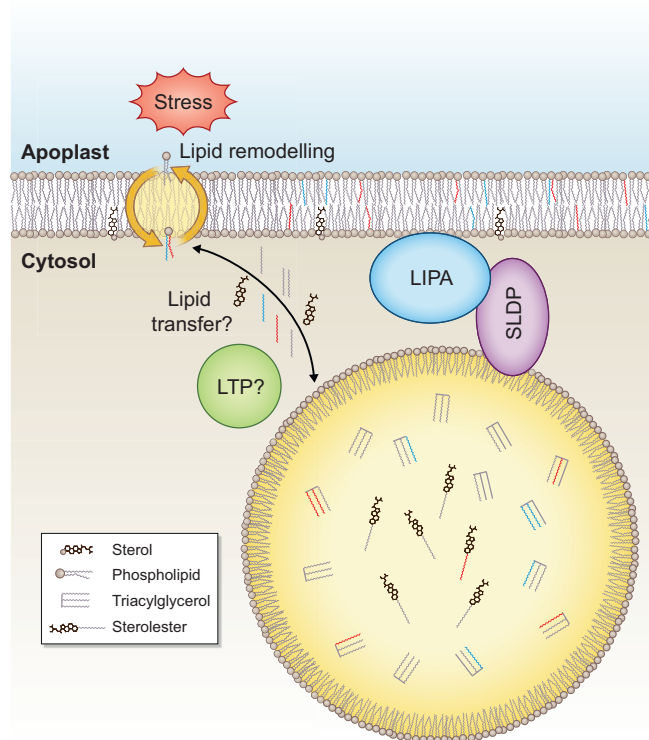
Fig. 3 Lipid droplets (LDs) can be tethered to the plasma membrane (PM). In germinating seedlings, the LD-bound seed lipid droplet proteins (SLDPs) and the PM-localized lipid droplet plasma membrane adaptor (LIPA) form a tether that anchors LDs to the PM. While the physiological role of this contact site is as of yet unclear, one possibility is that it is involved in stress-induced lipid remodeling of the PM. LDs provide a reservoir for various esterified fatty acids that could be used as a source for the adjustment of membrane phospholipids. In this model, the transport of fatty acids and/or sterol backbones would occur between the PM and LDs, possibly mediated by lipid-transfer proteins (LTPs).

LIPA in tobacco pollen tubes, wherein LDs normally move swiftly throughout the cell via the cytoplasmic streaming, they are instead immobilized at the plasma membrane.

The identification of this unique LD-plasma MCS raises questions about its cellular and physiological function. Given that TAG breakdown is not affected nor is seedling establishment strongly perturbed in *sldp* and *lipa* mutants, one can speculate that this MCS might be important under sub-optimal and/or fluctuating conditions. Membranes adapt under changing environmental conditions, and membrane lipid remodeling is often observed in plant cells under abiotic stress. The plasma membrane is the barrier between the internal and external cellular environment, and it contains a unique lipidome. Thus, it may also be that LDs provide a reservoir for lipid remodeling of the plasma membrane under stress that is important to preserve membrane function and cellular integrity. Indeed, the close proximity of the LDs might support this remodeling of the plasma membrane via the supply of lipids, including free fatty acids released from storage lipid breakdown, such as TAG, or by providing free sterols derived from SEs or other lipids. This support role might be especially important during early seedling establishment, where SLDP expression is high, as this developmental stage appears to be especially vulnerable to abiotic stress such as drought stress, since seedlings lack an established root system and can take up less water. However, the function of the SLDP–LIPA complex might not be limited to seedlings. For example, SLDP1 and LIPA expression increases during desiccation in leaf veins (Klepikova *et al.*, 2016), and a homolog of SLDP was also found in the oil-rich tubers of yellow nutsedge, which harbor a proteome similar to seeds (Niemeyer *et al.*, 2020).

V. Conclusions

Lipid droplets have been identified as key hubs for intracellular lipid metabolism and storage. Because of this, it is essential that LDs are connected to the metabolism of other subcellular compartments. For the ER and the plasma membrane, proteins are known that form junctions and contact sites. For other organelles such as vacuoles and peroxisomes, interactions and connections are described but the proteins that facilitate these contacts remain to be clearly identified. Finally, contacts of LDs to the outer membranes of mitochondria and plastids are likely, and these could play a role during lipid remodeling of these organelles as especially plastidial lipids are degraded under stress. Future goals will be to identify all contacts and proteins that form and/or make use of them. Following a better developed inventory of LD interactions with subcellular membranes, it will be possible to elucidate the functions of these contacts sites, including how they might facilitate lipid transfer between compartments. The resulting insights might form the basis for biotechnological applications, where LDs could be used as selected locations for the synthesis and storage of valuable hydrophobic compounds.

Acknowledgements

ORCID

Kent D. Chapman https://orcid.org/0000-0003-0489-3072
Till Ischebeck https://orcid.org/0000-0003-0737-3822
Robert T. Mullen https://orcid.org/0000-0002-6915-7407
Patricia Scholz https://orcid.org/0000-0003-0761-9175

Data availability

Data sharing is not applicable to this article as no new data were created or analyzed in this study.

References

Benador IY, Veliova M, Mahdaviani K, Petcherski A, Wikstrom JD, Assali EA, Acin-Perez R, Shum M, Oliveira MF, Cinti S *et al.* 2018. Mitochondria bound to lipid droplets have unique bioenergetics, composition, and dynamics that support lipid droplet expansion. *Cell Metabolism* **27**: 869–885.

Bohnert M. 2020. Tethering fat: tethers in lipid droplet contact sites. *Contact* **3**: 2515256420908142.

Boutant M, Kulkarni SS, Joffraud M, Ratajczak J, Valera-Alberni M, Combe R, Zorzano A, Canto C. 2017. Mfn2 is critical for brown adipose tissue thermogenic function. *EMBO Journal* **36**: 1543–1558.

Cai Y, Goodman JM, Pyc M, Mullen RT, Dyer JM, Chapman KD. 2015. Arabidopsis SEIPIN proteins modulate triacylglycerol accumulation and influence lipid droplet proliferation. *Plant Cell* **27**: 2616–2636.

Chapman KD, Aziz M, Dyer JM, Mullen RT. 2019. Mechanisms of lipid droplet biogenesis. *Biochemical Journal* **476**: 1929–1942.

Chung J, Wu X, Lambert TJ, Lai ZW, Walther TC, Farese RV Jr. 2019. LDAF1 and seipin form a lipid droplet assembly complex. *Developmental Cell* **51**: 551–563.e7.

Coulon D, Brocard L, Tuphile K, Bréhélin C. 2020. Arabidopsis LDIP protein locates at a confined area within the lipid droplet surface and favors lipid droplet formation. *Biochimie* **169**: 29–40.

Cui S, Hayashi Y, Otomo M, Mano S, Oikawa K, Hayashi M, Nishimura M. 2016. Sucrose production mediated by lipid metabolism suppresses the physical interaction of peroxisomes and oil bodies during germination of *Arabidopsis thaliana*. *Journal of Biological Chemistry* **291**: 19734–19745.

Dufourc EJ. 2008. Sterols and membrane dynamics. *Journal of Chemical Biology* **1**: 63–77.

Eastmond PJ. 2006. SUGAR-DEPENDENT1 encodes a patatin domain triacylglycerol lipase that initiates storage oil breakdown in germinating *Arabidopsis* seeds. *Plant Cell* **18**: 665–675.

Esnay N, Dyer JM, Mullen RT, Chapman KD. 2020. Lipid droplet–peroxisome connections in plants. *Contact* **3**: 2515256420908765.

Fernandez-Santos R, Izquierdo Y, Lopez A, Muniz L, Martinez M, Cascon T, Hamberg M, Castresana C. 2020. Protein profiles of lipid droplets during the hypersensitive defense response of arabidopsis against Pseudomonas infection. *Plant and Cell Physiology* **61**: 1144–1157.

Freyre CAC, Rauher PC, Ejsing CS, Klemm RW. 2019. MIGA2 links mitochondria, the ER, and lipid droplets and promotes de novo lipogenesis in adipocytes. *Molecular Cell* 76: 811–825.

Garbowicz K, Liu Z, Alseekh S, Tieman D, Taylor M, Kuhalskaya A, Ofner I, Zamir D, Klee HJ, Fernie AR et al. 2018. Quantitative trait loci analysis identifies a prominent gene involved in the production of fatty-acid-derived flavor volatiles in tomato. *Molecular Plant* 11: 1147–1165.

Gidda SK, Park S, Pyc M, Yurchenko O, Cai Y, Wu P, Andrews DW, Chapman KD, Dyer JM, Mullen RT. 2016. Lipid droplet-associated proteins (LDAPs) are required for the dynamic regulation of neutral lipid compartmentation in plant cells. *Plant Physiology* 170: 2052–2071.

Greer MS, Cai Y, Gidda SK, Esnay N, Kretzschmar FK, Seay D, McClinchie E, Ischebeck T, Mullen RT, Dyer JM et al. 2020. SEIPIN Isoforms interact with the membrane-tethering protein VAP27-1 for lipid droplet formation. *Plant Cell* 32: 2932–2950.

Gruber PJ, Trelease RN, Becker WM, Newcomb EH. 1970. A correlative ultrastructural and enzymatic study of cotyledonary microbodies following germination of fat storing seeds. *Planta* 93: 262–288.

Hayashi Y, Hayashi M, Hayashi H, Hara-Nishimura I, Nishimura M. 2001. Direct interaction between glyoxysomes and lipid bodies in cotyledons of the *Arabidopsis thaliana ped1* mutant. *Protoplasma* 218: 83–94.

Horn PJ, James CN, Gidda SK, Kilaru A, Dyer JM, Mullen RT, Ohlrogge JB, Chapman KD. 2013. Identification of a new class of lipid droplet-associated proteins in plants. *Plant Physiology* 162: 1926–1936.

Huang AHC. 2018. Plant lipid droplets and their associated proteins: potential for rapid advances. *Plant Physiology* 176: 1894–1918.

Ischebeck T, Krawczyk HE, Mullen RT, Dyer JM, Chapman KD. 2020. Lipid droplets in plants and algae: distribution, formation, turnover and function. *Seminars in Cell & Developmental Biology* 108: 82–93.

Itabe H, Yamaguchi T, Nimura S, Sasabe N. 2017. Perilipins: a diversity of intracellular lipid droplet proteins. *Lipid in Health and Disease* 16: 83.

Jacquier N, Choudhary V, Mari M, Toulmay A, Reggiori F, Schneiter R. 2011. Lipid droplets are functionally connected to the endoplasmic reticulum in *Saccharomyces cerevisiae*. *Journal of Cell Science* 124: 2424–2437.

Klepikova AV, Kasianov AS, Gerasimov ES, Logacheva MD, Penin AA. 2016. A high resolution map of the *Arabidopsis thaliana* developmental transcriptome based on RNA-seq profiling. *The Plant Journal* 88: 1058–1070.

Klug YA, Deme JC, Corey RA, Renne MF, Stansfeld PJ, Lea SM, Carvalho P. 2021. Mechanism of lipid droplet formation by the yeast Sei1/Ldb16 Seipin complex. *Nature Communications* 12: 5892.

Krawczyk HE, Rotsch AH, Herrfurth C, Scholz P, Shomroni O, Salinas-Riester G, Feussner I, Ischebeck T. 2022a. Heat stress leads to rapid lipid remodelling and transcriptional adaptations in *Nicotiana tabacum* pollen tubes. *Plant Physiology* 189: 490–515.

Krawczyk HE, Sun S, Doner NM, Yan Q, Lim MSS, Scholz P, Niemeyer PW, Schmitt K, Valerius O, Pleskot R et al. 2022b. SEED LIPID DROPLET PROTEIN1, SEED LIPID DROPLET PROTEIN2 and LIPID DROPLET PLASMA MEMBRANE ADAPTOR mediate lipid droplet-plasma membrane tethering. *Plant Cell* 34: 2424–2448.

Kretzschmar FK, Doner N, Krawczyk HE, Scholz P, Schmitt K, Valerius O, Braus G, Mullen RT, Ischebeck T. 2020. Identification of low-abundance lipid droplet proteins in seeds and seedlings. *Plant Physiology* 182: 1236–1245.

Kretzschmar FK, Mengel LF, Müller A, Schmitt K, Blersch KF, Valerius O, Braus G, Ischebeck T. 2018. PUX10 is a lipid droplet-localized scaffold protein that interacts with CDC48 and is involved in the degradation of lipid droplet proteins. *Plant Cell* 30: 2137–2160.

Liao PC, Yang EJ, Borgman T, Boldogh IR, Sing CN, Swayne TC, Pon LA. 2022. Touch and go: membrane contact sites between lipid droplets and other organelles. *Frontiers in Cell and Developmental Biology* 10: 852021.

Mueller SP, Krause DM, Mueller MJ, Fekete A. 2015. Accumulation of extra-chloroplastic triacylglycerols in *Arabidopsis* seedlings during heat acclimation. *Journal of Experimental Botany* 66: 4517–4526.

Müller AO, Ischebeck T. 2018. Characterization of the enzymatic activity and physiological function of the lipid droplet-associated triacylglycerol lipase AtOBL1. *New Phytologist* 217: 1062–1076.

Niemeyer PW, Schmitt K, Valerius O, Braus GH, de Vries J, Carlsson AS, Hofvander P, Ischebeck T. 2020. Co-option of a seed-like proteome by oil-rich tubers. *bioRxiv*. doi: 10.1101/2020.12.15.422834.

Pyc M, Cai Y, Gidda SK, Yurchenko O, Park S, Kretzschmar FK, Ischebeck T, Valerius O, Braus GH, Chapman KD et al. 2017. Arabidopsis lipid drop-associated protein (LDAP) – interacting protein (LDIP) influences lipid droplet size and neutral lipid homeostasis in both leaves and seeds. *The Plant Journal* 92: 1182–1201.

Pyc M, Gidda SK, Seay D, Esnay N, Kretzschmar FK, Cai Y, Doner NM, Greer MS, Hull JJ, Coulon D et al. 2021. LDIP cooperates with SEIPIN and LDAP to facilitate lipid droplet biogenesis in Arabidopsis. *Plant Cell* 33: 3076–3103.

Reumann S, Bartel B. 2016. Plant peroxisomes: recent discoveries in functional complexity, organelle homeostasis, and morphological dynamics. *Current Opinion in Plant Biology* 34: 17–26.

Schroeder B, Schulze RJ, Weller SG, Sletten AC, Casey CA, McNiven MA. 2015. The small GTPase Rab7 as a central regulator of hepatocellular lipophagy. *Hepatology* 61: 1896–1907.

Scorrano L, De Matteis MA, Emr S, Giordano F, Hajnoczky G, Kornmann B, Lackner LL, Levine TP, Pellegrini L, Reinisch K et al. 2019. Coming together to define membrane contact sites. *Nature Communications* 10: 1287.

Shimada TL, Takano Y, Shimada T, Fujiwara M, Fukao Y, Mori M, Okazaki Y, Saito K, Sasaki R, Aoki K et al. 2014. Leaf oil body functions as a subcellular factory for the production of a phytoalexin in Arabidopsis. *Plant Physiology* 164: 105–118.

Taurino M, Costantini S, De Domenico S, Stefanelli F, Ruano G, Delgadillo MO, Sanchez-Serrano JJ, Sanmartín M, Santino A, Rojo E. 2017. SEIPIN proteins mediate lipid droplet biogenesis to promote pollen transmission and reduce seed dormancy. *Plant Physiology* 176: 1531–1546.

Thazar-Poulot N, Miquel M, Fobis-Loisy I, Gaude T. 2015. Peroxisome extensions deliver the Arabidopsis SDP1 lipase to oil bodies. *Proceedings of the National Academy of Sciences, USA* 112: 4158–4163.

Ugrankar R, Bowerman J, Hariri H, Chandra M, Chen K, Bossanyi MF, Datta S, Rogers S, Eckert KM, Vale G et al. 2019. *Drosophila* Snazarus regulates a lipid droplet population at plasma membrane-droplet contacts in adipocytes. *Developmental Cell* 50: 557–572.

Valm AM, Cohen S, Legant WR, Melunis J, Hershberg U, Wait E, Cohen AR, Davidson MW, Betzig E, Lippincott-Schwartz J. 2017. Applying systems-level spectral imaging and analysis to reveal the organelle interactome. *Nature* 546: 162–167.

de Vries J, Ischebeck T. 2020. Ties between stress and lipid droplets pre-date seeds. *Trends in Plant Science* 25: 1203–1214.

Wang H, Sreenivasan U, Hu H, Saladino A, Polster BM, Lund LM, Gong DW, Stanley WC, Sztalryd C. 2011. Perilipin 5, a lipid droplet-associated protein, provides physical and metabolic linkage to mitochondria. *Journal of Lipid Research* 52: 2159–2168.

Wang P, Hawkins TJ, Richardson C, Cummins I, Deeks MJ, Sparkes I, Hawes C, Hussey PJ. 2014. The plant cytoskeleton, NET3C, and VAP27 mediate the link between the plasma membrane and endoplasmic reticulum. *Current Biology* 24: 1397–1405.

Yan R, Qian H, Lukmantara I, Gao M, Du X, Yan N, Yang H. 2018. Human SEIPIN binds anionic phospholipids. *Developmental Cell* 47: 248–256 e244.

Zienkiewicz K, Zienkiewicz A. 2020. Degradation of lipid droplets in plants and algae-right time, many paths, one goal. *Frontiers in Plant Science* 11: 579019.

Zoni V, Khaddaj R, Lukmantara I, Shinoda W, Yang H, Schneiter R, Vanni S. 2021. Seipin accumulates and traps diacylglycerols and triglycerides in its ring-like structure. *Proceedings of the National Academy of Sciences, USA* 118: e2017205118.

Zouiouich M, Di Mattia T, Martinet A, Eichler J, Wendling C, Tomishige N, Grandgirard E, Fuggetta N, Fromental-Ramain C, Mizzon G et al. 2022. MOSPD2 is an endoplasmic reticulum-lipid droplet tether functioning in LD homeostasis. *The Journal of Cell Biology* 221: e202110044.

van Zutphen T, Todde V, de Boer R, Kreim M, Hofbauer HF, Wolinski H, Veenhuis M, van der Klei IJ, Kohlwein SD. 2014. Lipid droplet autophagy in the yeast *Saccharomyces cerevisiae*. *Molecular Biology of the Cell* 25: 290–301.

4 Article III: DIACYLGLYCEROL KINASE 5 regulates polar tip growth of tobacco pollen tubes

The article was published in the journal New Phytologist and was published online in January 2022. The supplemental materials can be found online together with the full article:

https://doi.org/10.1111/nph.17930

Author contribution:

Patricia Scholz cloned the expression vector, performed recombinant protein expression and purification of NtDGK5 and its mutated variant NtDGK5 G118A. She carried out the radioactive enzyme assays whose results are shown in figures 3, S7. She did the pollen tube transformation and confocal microscopy for localisation and FRAP studies of NtDGK5 variants as presented in figure 4. She performed interactions assays of NtDGK5 variants with anionic lipids. To that end, she used purified recombinant protein or did *in vitro* translation of NtDGK5 and NtDGK5 G118A. She assayed lipid interaction in protein-lipid overlay assays and co-sedimentation assays of large unilamellar vesicles as depicted in figures 5, S4. Furthermore, she carried out pollen tube transformation, fluorescence and confocal microscopy for pollen tube phenotype analysis, investigation of lipid sensor behaviour and studies of pectin secretion shown in the figures 6, 8, 10, S8 and S11b. She performed assays of Arabidopsis *in vivo* pollen tube growth that are presented in figure S9. In terms of data analysis, she processed all the data obtained in the studies of enzyme activity, NtDGK5 localisation, pollen tube phenotypes, lipid sensor behaviour, pectin secretion and Arabidopsis *in vivo* pollen tube growth assays. She carried out the statistical analysis presented in the figures.

Patricia Scholz wrote the introduction, material and methods of experimental procedures performed by her, the results except for the sections on phylogenetic analysis and molecular dynamics simulations, and half of the discussion. She revised the final version of the manuscript. She designed the figures 3-10, S4, S7-S10.

New Phytologist

DIACYLGLYCEROL KINASE 5 regulates polar tip growth of tobacco pollen tubes

Patricia Scholz[1]* iD, Přemysl Pejchar[2]* iD, Max Fernkorn[1], Eliška Škrabálková[2,3], Roman Pleskot[2] iD, Katharina Blersch[1,4] iD, Teun Munnik[5] iD, Martin Potocký[2] iD and Till Ischebeck[1,4] iD

[1]Department of Plant Biochemistry, Albrecht-von-Haller-Institute for Plant Sciences and Göttingen Center for Molecular Biosciences (GZMB), University of Göttingen, Göttingen 37077, Germany; [2]Institute of Experimental Botany of the Czech Academy of Sciences, Prague 16502, Czech Republic; [3]Department of Experimental Plant Biology, Charles University, Prague 12844, Czech Republic; [4]Green Biotechnology, Institute of Plant Biology and Biotechnology (IBBP), University of Münster, Münster 48143, Germany; [5]Plant Cell Biology, Swammerdam Institute for Life Sciences, University of Amsterdam, Amsterdam 1000 BE, the Netherlands

Authors for correspondence:
Till Ischebeck
Email: till.ischebeck@uni-muenster.de

Přemysl Pejchar
Email: pejchar@ueb.cas.cz

Summary

• Pollen tubes require a tightly regulated pectin secretion machinery to sustain the cell wall plasticity required for polar tip growth. Involved in this regulation at the apical plasma membrane are proteins and signaling molecules, including phosphoinositides and phosphatidic acid (PA). However, the contribution of diacylglycerol kinases (DGKs) is not clear.

• We transiently expressed tobacco DGKs in pollen tubes to identify a plasma membrane (PM)-localized isoform, and then to study its effect on pollen tube growth, pectin secretion and lipid signaling. In order to potentially downregulate DGK5 function, we overexpressed an inactive variant.

• Only one of eight DGKs displayed a confined localization at the apical PM. We could demonstrate its enzymatic activity and that a kinase-dead variant was inactive. Overexpression of either variant led to differential perturbations including misregulation of pectin secretion. One mode of regulation could be that DGK5-formed PA regulates phosphatidylinositol 4-phosphate 5-kinases, as overexpression of the inactive DGK5 variant not only led to a reduction of PA but also of phosphatidylinositol 4,5-bisphosphate levels and suppressed related growth phenotypes.

• We conclude that DGK5 is an additional player of polar tip growth that regulates pectin secretion probably in a common pathway with PI4P 5-kinases.

Introduction

In flowering plants, male sperm cells are nonmotile and depend on a vegetative cell to form a pollen tube for delivery to the female embryophyte (Johnson *et al.*, 2019). Growth of pollen tubes occurs by unidirectional tip expansion, whose mechanical demands are reflected in the pollen tube's cell wall composition (Fayant *et al.*, 2010; Grebnev *et al.*, 2017). The cell wall at the shank of the pollen tube provides a rigid scaffold for the pollen tube preventing lateral extension while the higher flexibility at the pollen tube tip enables turgor-driven expansion (Fayant *et al.*, 2010; Chebli *et al.*, 2012). This cell wall at the tip is composed mainly of pectin that is continuously secreted together with modifying enzymes during pollen tube growth (Bosch *et al.*, 2005; Röckel *et al.*, 2008; Chebli *et al.*, 2012). Secretion of pectin has to be tightly controlled: if the cell wall is too rigid, the turgor will not be enough to drive further expansion and tube growth will be aborted (Bosch *et al.*, 2005; Zerzour *et al.*, 2009). On the other

hand, lack of secreted pectin will lead to thinning of the tip cell wall and finally bursting of pollen tubes (Zerzour *et al.*, 2009; Kroeger *et al.*, 2011). Consequently, pectin deposition is subject to a plethora of signaling factors including phosphoinositides and derived lipids (Heilmann & Ischebeck, 2016; Scholz *et al.*, 2020).

So far, the strongest connection between pectin secretion and signaling phospholipids has been described for phosphatidylinositol 4,5-bisphosphate (PI(4,5)P_2; Ischebeck *et al.*, 2008), which is enriched at the apical plasma membrane (PM) of pollen tubes (Kost *et al.*, 1999). PI(4,5)P_2 is formed by phosphatidylinositol 4-phosphate 5-kinases (PIP5Ks) that catalyze the phosphorylation of phosphatidylinositol 4-phosphate. Interference with their normal enzyme function in Arabidopsis has been reported to impair tube growth (Ischebeck *et al.*, 2008, 2011; Sousa *et al.*, 2008; Zhao *et al.*, 2010). Overexpression of *AtPIP5K4* or *AtPIP5K5* in tobacco (*Nicotiana tabacum*) pollen tubes leads to enhanced pectin accumulation at the tip (Ischebeck *et al.*, 2008).

Decreased activity of phosphoinositide-specific phospholipase C (PLC) can also result in increased PI(4,5)P_2 levels and defects

---

*These authors contributed equally to this work.

in pollen tube growth (Dowd *et al.*, 2006). Overexpression of an inactive variant of petunia *PLC1* in petunia pollen tubes caused the $PI(4,5)P_2$ localization to be more spread out rather than tip-localized. Furthermore, this overexpression led to pollen tube growth arrest (Dowd *et al.*, 2006). This indicates that PLC activity is a major route to degrade $PI(4,5)P_2$ and to switch off downstream signaling. However, the lipid product of PLC hydrolysis, diacylglycerol (DAG), might in turn serve as substrate for another signaling phospholipid, phosphatidic acid (PA; Munnik, 2001; Testerink & Munnik, 2005, 2011).

In animals, DAG is a signaling lipid in its own right, modulating members of the protein kinase C family (Nishizuka, 1988). By contrast, a signaling function of DAG in plant cells is still under debate, especially since homologs of protein kinase C and other typical DAG targets are missing from plants (Munnik & Testerink, 2009; Vermeer *et al.*, 2017). Instead, PA has been implicated in many signaling pathways, especially in the reaction to abiotic and biotic stresses, where it is rapidly synthesized within seconds/minutes (Munnik, 2001; Testerink & Munnik, 2005, 2011; Yao & Xue, 2018; Kim & Wang, 2020; Noack & Jaillais, 2020). In tobacco pollen tubes, PA was localized to the subapical PM, partially overlapping with $PI(4,5)P_2$ and DAG biosensors (Potocký *et al.*, 2014).

The reaction to form PA from DAG is a critical step to generate signaling PA, and is catalyzed by diacylglycerol kinases (DGKs) (Wissing *et al.*, 1989; Arisz *et al.*, 2009). There is another pathway that generates signaling PA, which is by cleavage of structural phospholipids by phospholipase D (PLD) (Hanahan & Chaikoff, 1947). The functions of PLD and PLD-derived PA have been more studied than the physiological role of DGKs (Hong *et al.*, 2016; Li & Wang, 2019). Nevertheless, different studies indicate a role for the PLC/DGK pathway in plant stress responses (Arisz *et al.*, 2009, 2013). In suspension-cultured plant cells, the majority of initial PA synthesis in response to cold shock and cryptogein elicitation was traced back to PLC/DGK activities in Arabidopsis (Ruelland *et al.*, 2002) and tobacco, respectively (Cacas *et al.*, 2017). The same was true for cold-treated Arabidopsis seedlings (Arisz *et al.*, 2013). Arabidopsis contains seven *DGKs* (Arisz *et al.*, 2009) of which *AtDGK2* was induced upon cold stress and wounding (Gómez-Merino *et al.*, 2004). Single Arabidopsis DGK-knockout (KO) mutants (i.e. *dgk2*, *dgk3* and *dgk5*) were described to be more freezing-tolerant (Tan *et al.*, 2018). Despite these studies on DGKs in stress signaling, their potential role in plant development has just recently come into focus.

The involvement of PA in pollen tube growth has been studied, albeit produced by PLD activity (Potocký *et al.*, 2003, 2014), and connected to the organization of the actin cytoskeleton (Pleskot *et al.*, 2010, 2012, 2013). There are limited reports on the impact of pollen tube-expressed AtDGK4 (Honys & Twell, 2004; Arisz *et al.*, 2009) on pollen tube growth. Some studies reported impaired pollen fitness and tube growth for *dgk4* (Vaz Dias *et al.*, 2019; Wong *et al.*, 2020), while another found reduced germination rates and effects on pollen development and pollen tube growth if DGK2 was also affected (Angkawijaya *et al.*, 2020). Interestingly, the localization of AtDGK4 in pollen

tubes was reported to be cytosolic (Vaz Dias *et al.*, 2019), despite the fact that both substrate (DAG) and product (PA) are membrane-localized. However, in another study, localization was described to be at the endoplasmic reticulum (ER) in transiently transformed *Nicotiana benthamiana* leaves and Arabidopsis protoplasts (Angkawijaya *et al.*, 2020). DGKs localized at the PM of pollen tubes remain to be identified.

Materials and Methods

Details of methods for phylogenetic and gene expression analysis, molecular dynamics simulation, molecular cloning, immunodetection, details of fluorescence recovery after photobleaching (FRAP) experiments and quantitative analysis of micrographs are provided in the Supporting Information (Methods S1–S7).

Heterologous protein expression and purification

pGEX-6P-1 constructs were transformed and proteins expressed as GST-tag fusions in *Escherichia coli* BL21 star (DE3) cells (Thermo Fisher Scientific, Waltham, MA, USA) at 16°C for 3 d after induction with 1 mM isopropyl β-D-1-thiogalactopyranoside. The original pGEX-6P-1 vector was expressed and used as a control. Cell pellets of 500 ml cultures were resuspended in lysis buffer (1× phosphate-buffered saline (PBS), pH 7.4, lysozyme, 1 mM phenylmethylsulfonyl fluoride (PMSF)) and cells were disrupted by ultrasonication. Protein purification was performed by GST-affinity chromatography with GSTrap™ Fast Flow columns (Cytiva, Chalfont St Giles, UK), using 1× PBS pH 7.4, 5 mM EDTA for washing and 50 mM Tris-HCl pH 8.0, 20 mM reduced glutathione for elution. Purified proteins were stored at −80°C in storage buffer (50 mM Tris-HCl pH 7.4, 100 mM NaCl, 10 mM $MgCl_2$, 10% glycerol) until further use for enzyme activity assays and the protein-lipid overlay assays.

Analysis of DGK activity

Diacylglycerol kinase activity was assayed by measuring the incorporation of ^{32}P-phosphate from $[\gamma\text{-}^{32}P]$-ATP into DAG to produce PA. For enzyme assays, 50 ng of protein was mixed with 200 µl of assay buffer with or without 500 µM 1,2-dioleyl-*sn*-glycerol (DOG) as substrate, prepared in liposomes (Julkowska *et al.*, 2013). Liposomes contained DOG, 1,2-dioleyl-phosphatidylcholine (DOPC) and 1,2-dioleyl-phosphatidylethanolamine (DOPE; all Sigma-Aldrich) in a molar ratio of 1 : 2 : 2 or DOPC and DOPE in a molar ratio of 3 : 2 without DAG. Liposome suspensions were pelleted by centrifugation at 100 000 *g* for 35 min at room temperature and the liposome pellet was subsequently resuspended in assay buffer (50 mM Tris-HCl pH 7.4, 10 mM $MgCl_2$, 1 mM EGTA, 1 mM ditiothreitol (DTT), 1 mM Na_3VO_4, 500 µM ATP containing *c.* 2.5 µCi $[\gamma\text{-}^{32}P]$-ATP). Reactions were started by the addition of protein, and incubated for 30 min at 25°C while gently shaking. Reactions were stopped by adding 750 µl chloroform : methanol (1 : 2, v/v) and the lipids extracted as described previously (Munnik & Laxalt, 2013; Munnik & Zarza, 2013). In brief, two phases were established by adding 750 µl chloroform and 200 µl 0.9% NaCl.

The organic lower phase was washed once with chloroform : methanol : 1 M HCl (3 : 48 : 47, v/v), dried under a stream of nitrogen, dissolved in chloroform and spotted on a thin layer chromatography (TLC) plate (Silica gel 60; Merck KGaA, Darmstadt, Germany). TLC plates were developed using a running system of chloroform : methanol : NH_4OH : water (45 : 45 : 4 : 11, v/v). A photostimulable phosphor plate (Fujifilm, Tokio, Japan) was exposed to the TLC plate for 3 d. The nonradioactive standard PA was detected by iodine staining. Phosphoimager screens were read using the FLA 3000 scanner (Fujifilm) with BASREADER 3.14 software (Elysia-raytest, Straubenhardt, Germany) and quantified with AIDA IMAGE data analyzer 3.24 (Elysia-raytest).

Lipid-binding assays

GST-NtDGK5 and GST-NtDGK5[G118A] were used to establish protein–lipid interactions on membrane lipid strips (Echelon Biosciences, Salt Lake City, UT, USA) by a protein–lipid overlay assay. Briefly, lipid strips were incubated for 1 h with 2–2.5 µg ml^{-1} of GST-tagged protein in a solution of 4% BSA in 1× PBS. Subsequently, successful protein–lipid interactions were analysed by immunodetection of the GST-tag.

For protein–lipid overlay assays with *in vitro* translated protein, the TNT® SP6 High-Yield Wheat Germ Protein Expression System (Promega) was used according to the manufacturer's instructions. Respective proteins of NtDGK5, NtDGK5[G118A], NtDGK6 and NtDGK8 carried an N-terminal HA-tag for later detection. To remove membrane-bound proteins of the *in vitro* system, samples were centrifuged at 72 000 *g* and 4°C for 20 min and the supernatant was incubated with membrane lipid strips (Echelon Biosciences) preblocked for 30 min with 4% BSA in 1× PBS.

The vesicle cosedimentation assay was adapted from Julkowska *et al.* (2013). Control liposomes were prepared from 80% DOPC and 20% DOPE, and PA-containing liposomes consisted of 60% DOPC, 20% DOPE and 20% DOPA. Each sample contained 400 nmol of total lipids. Liposomes were prepared as described in Julkowska *et al.* (2013) and diluted in modified 1× binding buffer (400 mM KCl, 25 mM Tris-HCl pH 7.5, 1 mM DTT, 0.5 mM EDTA). Subsequently, liposomes were incubated with the supernatant of *in vitro* protein reactions, prepared as described above. Protein was incubated with liposomes for 45 min at room temperature. Liposomes and bound protein were then pelleted by centrifugation at 72 000 *g* for 30 min. Total nonbound protein in the supernatant fraction was precipitated by acetone precipitation; the pellet of liposomes and liposome-interacting proteins was washed once with 1× binding buffer. Finally, both protein fractions were dissolved in Laemmli sample buffer and used for subsequent Western blot analysis (Methods S6).

Plant lines, plant growth conditions and Arabidopsis *in vivo* pollen tube assay

Arabidopsis and tobacco plants were grown as previously described (Rotsch *et al.*, 2017; Müller & Ischebeck, 2018). The Arabidopsis plant lines named here as *dgk4*, *dgk6* and *ms1* have

already been described (Wilson *et al.*, 2001; Angkawijaya *et al.*, 2020). Plant line *dgk5* was obtained as SAIL_1212-E10 from the SAIL collection (Sessions *et al.*, 2002) and the double mutant *dgk5 dgk6* was generated by crossing.

In vivo pollen tube assays of Arabidopsis *dgk* mutant lines were carried out after Mori *et al.* (2006) and Müller & Ischebeck (2018); however, instead of wild-type pistils, pistils of *ms1* plants were pollinated with pollen of *dgk* strains.

Pollen transformation

Pollen grains were transformed by particle bombardment and pollen tubes were grown as described by Müller *et al.* (2017) or based on previous protocols (Read *et al.*, 1993; Kost *et al.*, 1998). FRAP analysis and spinning disk imaging was performed 6–8 h after transformation, and microscopic imaging for phenotype and cell wall analysis was carried out 14 h after transformation. For pectin staining of pollen tube cell walls, 10 µM propidium iodide was added to the pollen tubes just before imaging.

For cotransformation, plasmids were mixed during gold precipitation before particle bombardment. For cotransformation with *AtPIP5K5* or markers for endomembrane compartments, plasmids were mixed at a ratio of 1 : 1; for cotransformation of lipid-binding domains, NtDGK5 and NtDGK5[G118A] were used at *c.* 10 : 1 ratio and the fluorescent tag control at a ratio of *c.* 3 : 1.

Epifluorescence and confocal microcopy

Epifluorescence microscopy of transformed tobacco pollen tubes was done with an Olympus BX51 by using an UPlanSApo ×10/0.40 objective (Olympus, Tokio, Japan). For mVenus-tagged constructs, the filter cube U-MWIB was used. Images were taken with an ORCA flash 4.0 V2 Digital Camera using the software HOKAWO 2.10 (Hamamatsu Photonics, Hamamatsu, Japan).

Confocal imaging of pectin stained by propidium iodide was performed with a Zeiss LSM510 confocal microscope using a Plan-Neofluar ×40/1.30 oil immersion objective (Carl Zeiss, Oberkochen, Germany). Fluorescence of propidium iodide was observed after excitation with 561 nm and detected at 689–721 nm using the HFT 405/488/561 major beam splitter.

Fluorescence recovery after photobleaching analyses were carried out with a Zeiss LSM880 equipped with C-Apochromat ×40/1.2 water immersion objective (Carl Zeiss). For mVenus imaging, optimal singletrack acquisition parameters were used (mVenus fluorescence was excited by a 514 nm laser, and the emission at 520–590 nm was recorded using a GaAsP detector).

Spinning disk confocal microscopy was carried out on the Nikon Ti-E platform with Yokogawa CSU-X1 spinning disk and sCMOS camera Andor Zyla, using a Plan Apo VC ×60/1.20 water immersion objective (Nikon, Tokio, Japan). Fluorescence of mVenus/yellow fluorescence protein (YFP) and mCherry/red fluorescence protein (RFP)-tagged proteins were excited with the respective 488 and 561 nm laser lines (laser box Agilent MLC400, Agilent Technologies, Inc., Santa Clara, CA, USA) and detected with the filter cubes Semrock brightline Em 542/27 and Semrock brightline Em 607/36.

Results

DGKs diverged into three conserved clades during early plant evolution

To describe the DGK family in tobacco, we searched the tobacco proteome and genome drafts available at NCBI and solgenomics.net, using BLAST searches with Arabidopsis DGK1, DGK4 and DGK5 as queries. Additionally, the draft genomes of *Nicotiana sylvestris* and *Nicotiana tomentosiformis* were analyzed. We found 16 genes coding for putative DGKs in the tobacco genome (Figs 1a, S1). These could be further divided into eight pairs of almost identical paralogs, reflecting that *N. tabacum* originated as a hybrid of *N. sylvestris* and *N. tomentosiformis*. To classify tobacco DGKs unambiguously and better understand the evolution of plant *DGK* genes, we significantly expanded our initial analysis (Pleskot *et al.*, 2012) and performed an exhaustive genome-wide search and reconstruction of DGK phylogeny in Viridiplantae. We analyzed genomes of representative angiosperm, gymnosperm, lycophyte, bryophyte, charophyte and chlorophyte species. This yielded a dataset of 95 DGK isoforms from 20 species (Table S1; Notes S1). Phylogenetic analysis of plant DGKs performed with two independent algorithms showed a deep evolutionary split dividing DGK isoforms into three distinct clades (Fig. S1). All clade I

genes harbor a transmembrane domain followed by two C1 domains, implicated in lipid binding (Colongonzalez & Kazanietz, 2006), in addition to DGK catalytic and accessory domains, which constitute clades II and III (Fig. 1b; Table S2). In tobacco, six *NtDGKs* are grouped in clade I, four in clade II and six in clade III (Fig. 1a,b; Table S2). Clade I can be subdivided into two subclades (containing NtDGK1-2 and NtDGK3, respectively) that probably split in early angiosperms. On the other hand, multiple DGK paralogs in clades II and III probably originated through recent gene or genome duplication events, and no apparent orthology could be assigned beyond Solanaceae (Fig. S1).

To estimate whether there is a trend in the expression pattern of DGK isoforms in the three clades, we first analyzed tobacco *DGK* expression in pollen by remapping tobacco pollen raw RNA sequencing (RNA-seq) data (Conze *et al.*, 2017) on the reference genome sequence. Publicly available pollen, leaf and root RNA-seq data from selected angiosperm species were also collected and mapped onto the phylogenetic tree (see Methods S3 for details). Our data suggest that a similar expression pattern is retained within the two subclades of clade I, with one subclade exhibiting lower expression in the pollen compared to the sporophytic tissues, while the opposite pattern could be seen for the second subclade. Conversely, no trend is apparent for clade II genes (Fig. S1).
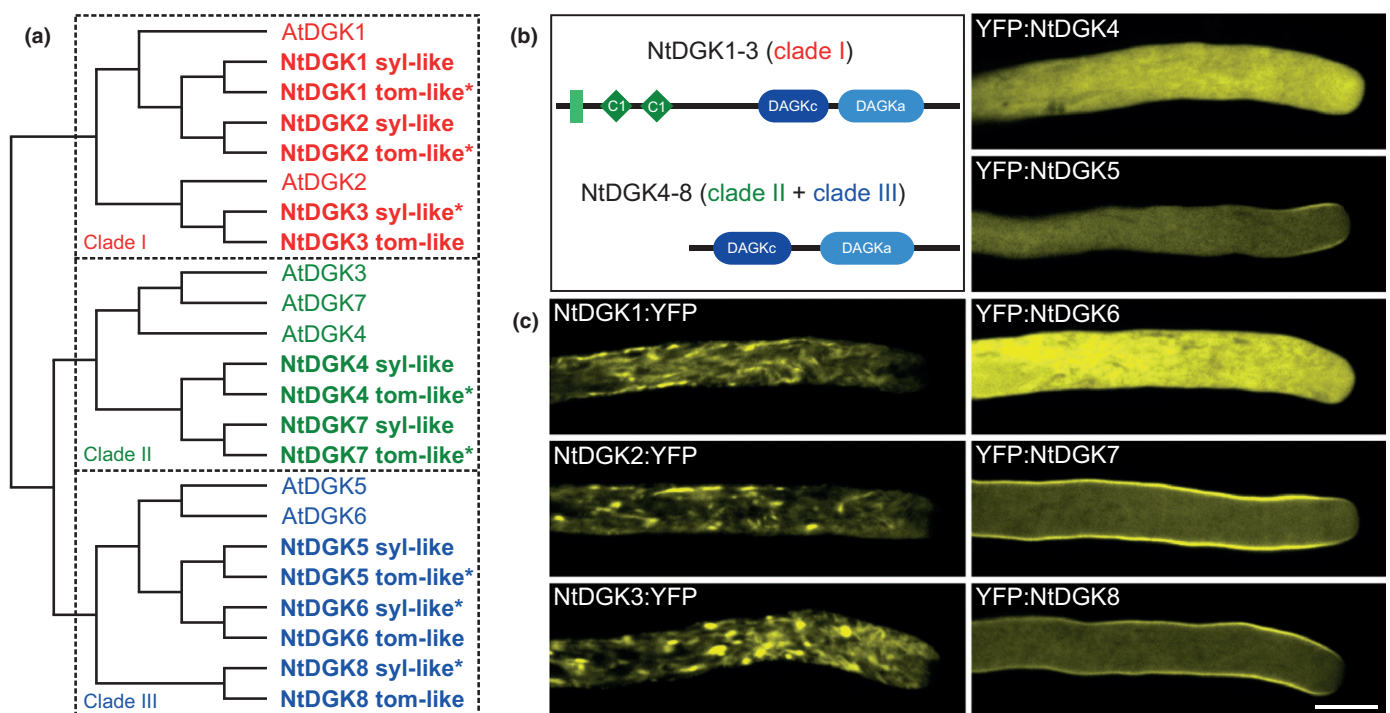
Fig. 1 Tobacco diacylglycerol kinase isoforms show distinct localization patterns in pollen tubes. (a) Phylogeny of Arabidopsis and *Nicotiana tabacum* diacylglycerol kinase (DGK) isoforms and their distribution into three clades as extracted from a full phylogenetic tree (see Supporting Information Fig. S1). Syl-like and tom-like denote NtDGK sequences derived from ancestors of *Nicotiana sylvestris* and *Nicotiana tomentosiformis*, respectively. An asterisk denotes isoforms cloned in this study. At, *Arabidopsis thaliana*; Nt, *Nicotiana tabacum*. (b) Schematic representation of the domain structure of tobacco isoforms. The green rectangle denotes the transmembrane domain. C1, diacylglycerol/phorbol esters binding domain; DAGKa, DGK accessory domain; DAGKc, DGK catalytic domain. (c) Localization of YFP-tagged NtDGK1–8 in actively growing pollen tubes. Pollen was transiently transformed with 1 µg DNA and analyzed 6–8 h after transformation. Bar, 10 µm.

NtDGK5 specifically localized to the subapical PM of growing pollen tubes

Phosphatidic acid is an important second messenger and enriched in the subapical PM of tobacco pollen tubes (Potocký *et al.*, 2014; Pejchar *et al.*, 2020). To identify which of the DGK isoforms are localized at the PM and could generate PA near the pollen tube tip, we cloned eight DGK coding sequences (one of each pair, Fig. 1a; for the list of primers see Table S3) and fused them C- or N-terminally with YFP. As the isoforms DGK1–3 are predicted to have a transmembrane region close to the N-terminus with the very N-terminus facing the noncytosolic side, we chose a C-terminal tag for these isoforms.

When transiently expressed in growing tobacco pollen tubes, DGK isoforms 1–3 from clade I did not localize to the PM but rather to endomembrane compartments (Fig. 1c). To further analyze the localization, pollen tubes were cotransformed with NtDGK1-3:YFP and the ER marker AtbCH-SP:CFP:HDEL; NtDGK1:YFP was also cotransformed with the Golgi marker CFP:StGnT$_{1-70}$ and CFP:AtVHA-a1 (Stephan *et al.*, 2014) as a marker for the trans-Goli network (TGN). Colocalization was observed only with the ER marker (Fig. S2). Clade II isoforms 4 and 7 displayed strikingly different localization, with NtDGK4 being purely cytosolic and NtDGK7 localizing homogeneously along the PM with no obvious enrichment. Among clade III isoforms, NtDGK6 was present in the cytoplasm and NtDGK8 was localized to an extended PM region. Finally, the localization of NtDGK5 was restricted to the PM region close to the pollen tube apex (Figs 1c, S3a,b).

Next, we tested whether observed localization differences within clade III isoforms were correlated with structural features and membrane-binding properties. Therefore, we constructed 3D homology models of NtDGK5, NtDGK6 and NtDGK8 and we mapped the electrostatic potential onto the solvent-excluded surface of the respective NtDGK protein (Fig. S3c–e; Methods S2).

As the plant PM is highly negatively charged, the presence of positively charged regions (caused by cationic amino acids: Lys, Arg and His) on the protein surface could be seen as a proxy for the electrostatic interaction and its strength. Indeed, we observed clear differences in the positive charge distribution among the different NtDGK isoforms of clade III correlating well with their localization in tobacco pollen tubes (Fig. S3). Furthermore, we tested the binding properties of clade III isoforms to membrane lipids by protein–lipid overlay assays. In line with previous results, NtDGK6 showed only limited binding to the plant PM lipids. By contrast, NtDGK5 and NtDGK8 displayed a similar tendency to bind to anionic phospholipids such as PA, PI4P and PI(4,5)P$_2$ (Fig. S4).

Molecular dynamics simulations predict a direct interaction between NtDGK5 and PM

As the membrane-bound DGK isoforms of clade III have no prominent membrane-binding domain, we wondered how these members could interact with the PM. To analyze this, coarse-grained molecular dynamics (CG-MD) simulations were used. This computational approach is highly accurate in describing the membrane-bound state of peripheral membrane proteins (Yamamoto *et al.*, 2020). The simulated system consisted of an NtDGK5 molecule, ions, water and a complex lipid bilayer with negatively charged phospholipids (Fig. 2a), similar to a PM of plants (Im *et al.*, 2007; König *et al.*, 2008; Furt *et al.*, 2010). We performed 10 1 μs runs of CG-MD simulations. In all replicas, we observed that NtDGK5 quickly interacted with the lipid bilayer, and remained stably bound to the membrane through the remaining simulation time (Figs 2b, S5a). Detailed inspection of different CG-MD replicas revealed distinct membrane-binding modes of NtDGK5. To further analyze and categorize these binding modes, we monitored the distance between conserved glycine G118 located in the catalytic domain, which is
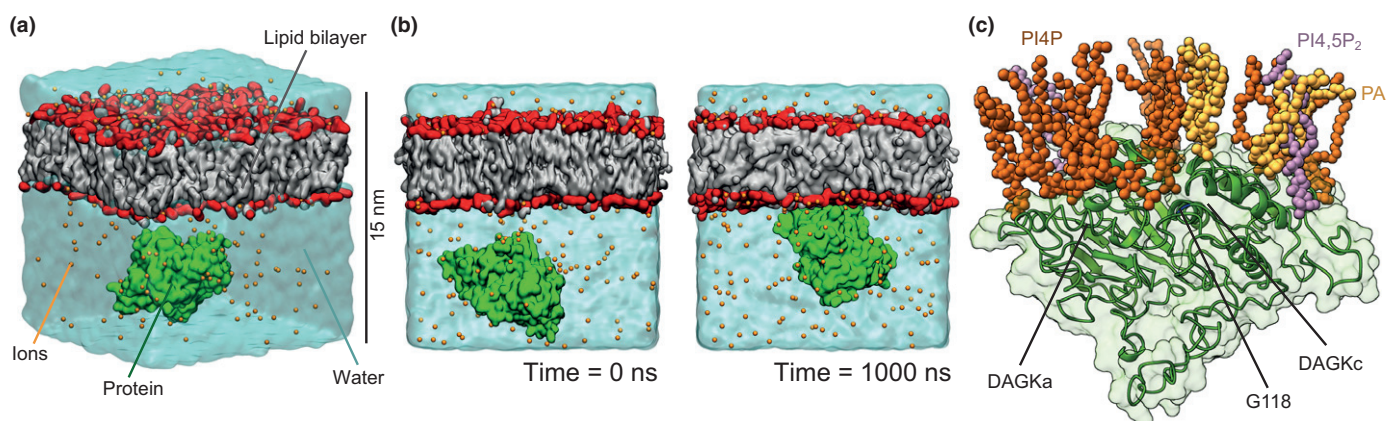
Fig. 2 Molecular dynamics simulation indicates mechanistic details of the NtDGK5–membrane interaction. (a) Simulated system composed of NtDGK5, the complex lipid bilayer, ions and water molecules. (b) Snapshots from the coarse-grained molecular dynamics simulation. Left, initial configuration (time = 0 ns). Right, the membrane-bound protein (time = 1000 ns). (c) NtDGK5 together with negatively charged lipids 0.8 nm from the protein. Both catalytic and accessory domains contribute to binding. The protein is displayed in the ribbon representation with its transparent solvent-excluded surface. Negatively charged phospholipids are shown in the van der Waals representation, PA in yellow, PI4P in orange and PI(4,5)P$_2$ in purple. DAGKa, DGK accessory domain; DAGKc, DGK catalytic domain; PA, phosphatidic acid; PI4P, phosphatidylinositol 4-phosphate; PI(4,5)P$_2$, phosphatidylinositol 4,5-bisphosphate.

important for enzymatic activity (Franks *et al.*, 2017), and the lipid bilayer. This allowed us to distinguish between a 'productive mode' of membrane binding, where G118 is close to the lipid bilayer, and 'nonproductive modes', where the catalytic site is away from the membrane (Fig. S5b). In the productive mode, both catalytic and accessory domains of NtDGK5 contributed to the interaction with the negatively charged phospholipids. All replicas of the productive mode of binding displayed the same distribution of amino acid residues involved in membrane binding (Figs 2c, S5c). Contrary to the productive mode of binding, nonproductive modes differed substantially in contact distribution, indicating random association (Fig. S5c). Together, our computational analysis predicts that NtDGK5 interacts directly with the lipid bilayer through the catalytic and accessory domains.

NtDGK5 is a DAG kinase whose activity is disrupted by a single G118A amino acid exchange

While different Arabidopsis DAG kinases have been shown to harbor DAG-kinase activity (Gómez-Merino *et al.*, 2004, 2005), NtDGK5 was previously not biochemically investigated. To confirm its putative DGK activity, we expressed and purified GST-tagged NtDGK5 in *E. coli*. Similarly, we generated a potentially kinase-dead mutant by replacing the conserved glycine 118 in the catalytic domain with an alanine (G118A). The methyl group introduced by the mutation probably interferes with ADP/ATP binding: the structural model NtDGK5 and NtDGK5^{G118A} with a superimposed ADP molecule suggested a sterical clash between A118 in NtDGK5^{G118A} and the α-phosphate group of ADP (Fig. S6). We therefore hypothesized that NtDGK5^{G118A} will be unable to complete the phosphorylation reaction. This variant might then act in a dominant negative manner *in vivo*, based on observations from a mammalian homolog carrying the corresponding substitution (Sanjuán *et al.*, 2001).

Purified GST-NtDGK5, GST-NtDGK5^{G118A} or GST-tag alone were subsequently used for enzyme activity assays, providing DAG and [γ-^{32}P]-ATP as substrates (Fig. 3a). Following the reaction, lipids were extracted and separated by TLC, and radioactive PA was quantified by phosphoimaging (Figs 3b,c, S7). Enzyme reactions with NtDGK5 led to a 30-fold increase of PA levels compared to reactions with GST only, while the NtDGK5^{G118A} lost *c.* 95% of its activity, exhibiting only a twofold increase compared to GST. These results indicate that NtDGK5 functions as a DAG kinase, and that this activity is almost completely disrupted in the mutated variant.

PM localization of NtDGK5 and NtDGK5^{G118A} differs

Next, we investigated if the PM association of NtDGK5 was affected by the amino acid exchange. Therefore, the localization of N-terminal fusions of mVenus to NtDGK5 and NtDGK5^{G118A} was compared. Interestingly, when overexpressed in tobacco pollen tubes, the mutated variant showed a more pronounced PM localization compared to wild-type NtDGK5 based on quantification of the fluorescent signal length measured from
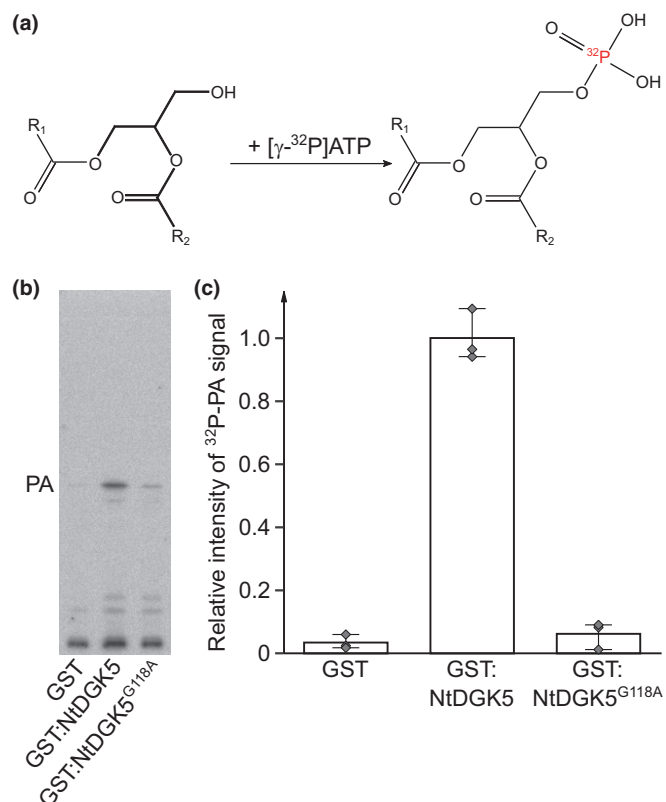
Fig. 3 NtDGK5 is a DAG-kinase that loses activity from the G118A mutation. NtDGK5 variants were expressed in *Escherichia coli* and purified protein was used for enzyme assays. Purified GST-tag alone served as a negative control. (a) For the assays, DAG and radioactively labelled [γ-^{32}P] ATP were supplied as substrates resulting in ^{32}P-labeled phosphatidic acid (PA) as a potential product. Lipid products were extracted and separated via TLC and detected with a phosphoimager. (b) Identification of the radioactive product as PA was achieved by comigration of a commercial nonradioactive standard. (c) Intensity of the radioactive signal was quantified for three reactions per construct and normalized to the average signal for enzyme assays with NtDGK5. For each protein, three independent values were obtained and are displayed as gray dots. Error bars show the 95% confidence interval around the mean.

the pollen tube tip (Fig. 4a–c). For further analysis, we calculated the PM index (PMI), the ratio between the fluorescence intensities at the PM and in the cytoplasm (Fig. 4d,e). This ratio decreased for both NtDGK5 and NtDGK5^{G118A} in strongly overexpressing pollen tubes with high fluorescence values, indicating a limited binding capacity at the PM (Fig. 4d). In strong overexpressors, PMI values converge towards 1 for NtDGK5 and NtDGK5^{G118A}, but NtDGK5^{G118A} displayed a more pronounced PM localization than NtDGK5 in low-expressing pollen tubes (Fig. 4a,b,d).

To check for possible differences in protein mobility that could explain the observed localization pattern, we performed FRAP experiments. In pollen tubes overexpressing either *mVenus:NtDGK5* or *mVenus:NtDGK5^{G118A}*, a region in the subapical membrane was bleached, and replacement of the fluorescent signal for both mVenus:NtDGK5 and mVenus:NtDGK5^{G118A} was followed for *c.* 30 s. The resulting FRAP curves were fitted with a single exponential fit, which allowed
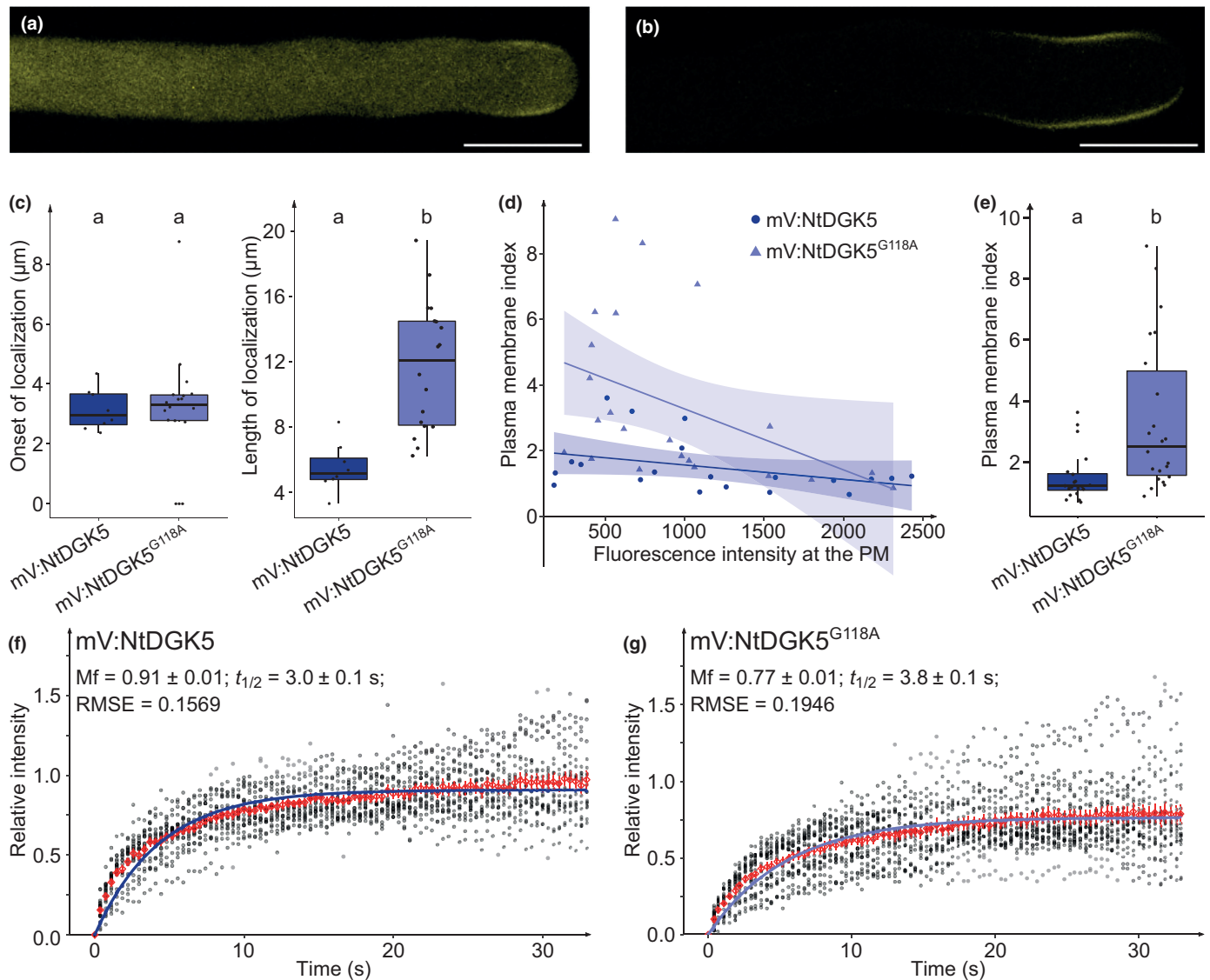
Fig. 4 NtDGK5 and NtDGK5^{G118A} differ in protein localization and mobility. NtDGK5 variants carrying an N-terminal mVenus-tag were transiently expressed in tobacco pollen tubes and transformed pollen tubes were imaged by spinning disk (a, b) or laser scanning (c–g) confocal microscopy after 6 h of growth. Both NtDGK5 (a) and NtDGK5^{G118A} (b) localized to the plasma membrane. However, NtDGK5^{G118A} localization was more pronounced with less cytosolic background. (c) The onset of plasma membrane localization relative to the tip and the total length of localization was determined. (d) Furthermore, the ratio between the fluorescence intensity at the plasma membrane and in the cytosol (plasma membrane index, PMI) was calculated. For low expression values, a more pronounced membrane localization of NtDGK5^{G118A} was observed. With increasing fluorescence intensities, the PMI decreases and reaches comparable values for NtDGK5 and NtDGK5^{G118A} at high fluorescence. Overall, PMI values of NtDGK5^{G118A} differ significantly from PMI values of NtDGK5 (e). (f, g) Protein mobility was analyzed by fluorescence recovery after photobleaching. Relative intensities of single pollen tubes at the different time points are shown in gray, while average values ± SEM are displayed in red. An exponential fit was applied to the data and is shown as blue curves. Fluorescence recovery of both NtDGK5 (f) and NtDGK5^{G118A} (g) have halftimes ($t_{1/2}$) below 4 s, but NtDGK5 recovers to higher fluorescence values than NtDGK5^{G118A}. Accordingly, the mobile fraction as estimated from the fitted curve amounted to 91% for NtDGK5 and 77% for NtDGK5^{G118A}. Boxplots in (c, e) display the first quartile, median and third quartile values and whiskers extend to the extreme data points inside of 1.5 × interquartile range. Single data points are shown as black circles. Statistical analysis was done by Kruskal–Wallis and Kruskal–Wallis *post-hoc* tests. Different letters indicate significant differences at $P < 0.05$. In the display of (d) a linear model was fitted to the single data points and is shown with the standard error shaded. $n = 8$ pollen tubes for NtDGK5 and $n = 18$ pollen tubes for NtDGK5^{G118A} in (c); $n = 20$ pollen tubes for NtDGK5 and $n = 22$ pollen tubes for NtDGK5^{G118A} in (d–g). Regression curves in (f, g) were calculated using the model $f(t) = Mf \times (1 - \exp(-t/\tau))$ with Mf = mobile fraction, τ = time constant, t = time and $f(t)$ = relative intensity. Halftime ($t_{1/2}$) was calculated as $t_{1/2} = \ln(2) \times \tau$. Bar, 10 µm.

estimates of the mobile fraction of the enzyme and the halftime of its interaction with the PM (Fig. 4f,g; Methods S7). Membrane fluorescence was recovered with a halftime of 3.0 s for NtDGK5, while recovery of fluorescence for NtDGK5^{G118A} took

slightly longer, with a halftime of 3.8 s. The mobile fraction of the respective enzymes differed more strongly: for NtDGK5, membrane fluorescence after bleaching reached 91% of the original values. Fluorescence recovery of NtDGK5^{G118A}

amounted to 77% of prebleach intensities. The mutation in NtDGK5[G118A] thus seems to induce an increased association to the PM, impeding dissociation of the enzymes to the cytoplasm. For further study of the changes induced by the G118A mutation, we evaluated the lipid binding behavior of NtDGK5 and NtDGK5[G118A] by a protein–lipid overlay assay (Fig. 5a). No qualitative changes were observed, as both protein variants were able to bind to the anionic phospholipids PA, PI4P and PI(4,5)P₂. In addition, binding ability to cardiolipin, sulfatide and phosphatidylinositol 3,4,5-trisphosphate was observed, although these lipids have so far not been detected in the plant PM (Furt *et al.*, 2011). To support these findings, we additionally tested lipid binding of NtDGK5 and NtDGK5[G118A] to large unilamellar vesicles (LUVs) by a vesicle cosedimentation assay. LUVs were constituted either from phosphatidylcholine (PC) and phosphatidylethanolamine (PE) as control or PC, PE and PA, which we chose as proxy for anionic phospholipids. Both NtDGK5 and NtDGK5[G118A] showed increased propensity to bind to LUVs containing PA, but no increase of LUV binding was observed for NtDGK5[G118A] compared to NtDGK5 (Fig. 5b,c).

Overexpression of NtDGK5 or NtDGK5[G118A] induce distinct aberrant growth phenotypes in tobacco pollen tubes

As a DAG kinase, NtDGK5 could be potentially involved in the conversion of signaling phospholipids that regulate pollen tube growth (Scholz *et al.*, 2020). We therefore checked for phenotypes in pollen tubes with altered NtDGK5 levels. To that end,

we overexpressed either *NtDGK5* or *NtDGK5[G118A]* carrying an N-terminal mVenus-tag in tobacco pollen tubes. Fourteen hours after transformation, growth phenotypes were analyzed to investigate potential effects of *mVenus:NtDGK* overexpression.

Overexpression of the two enzyme variants caused distinct phenotypes (Fig. 6; Videos S1–S3). Both *mVenus:NtDGK5* and *mVenus:NtDGK5[G118A]* induced a wavy growth pattern (mV: NtDGK5[G118A] at a much higher frequency), which is rarely observed when expressing the mVenus-tag alone (Fig. 6a–d). Together with the wavy growth pattern, *mVenus:NtDGK5[G118A]*-expressing pollen tubes often displayed swollen tips (Fig. 6c,d). *mVenus:NtDGK5[G118A]* expression also strongly increased the occurrence of short pollen tubes less than 500 µm long (Fig. 6d), an effect that was not observed for mVenus:NtDGK5.

Overall, overexpression of both *mVenus:NtDGK5* variants disturbs pollen tube growth, though differences between active and suppressed enzymes are observed. A comparison with other NtDGKs and AtDGK5 shows that the described wavy tip growth is quite specific for NtDGK5, while also NtDGK4 and NtDGK7, and the Arabidopsis DGK5 induce stunted growth (Fig. S8a–c). On the other hand, PM localization of YFP: AtDGK5 close to the pollen tube apex resembles YFP:NtDGK5 in growing tobacco pollen tubes (Fig. S8d). We also assayed *in vivo* pollen tube growth of the Arabidopsis mutants *dgk4*, *dgk5*, *dgk6* and *dgk5 dgk6* in two independent experiments. However, despite some variations, the results did not show consistent alterations of pollen tube length (Fig. S9).

Overexpression of active NtDGK5 increases pectin deposition

In previous studies on signaling lipids and their converting enzymes in pollen tube growth, connections to the deposition of cell wall components have been described (Ischebeck *et al.*, 2008). Altered cell wall deposition could also offer a possible explanation for the observed phenotypes. Consequently, we investigated the distribution of pectin, the main cell wall component of the pollen tube tip, in nontransformed cells and cells expressing mVenus-tagged *NtDGK5* or *NtDGK5[G118A]*. Pectin was stained with propidium iodide and cross-sections of the cell wall were imaged by confocal microscopy (for methodology see also Fig. S10). Initial inspection of microscopic images indicated more intense pectin staining in pollen tubes overexpressing *NtDGK5* (Fig. 7a–d). We therefore quantified propidium iodide staining of transformed pollen tubes normalized to respective neighboring nontransformed pollen tubes. Pectin accumulation was analyzed in the subapical region *c.* 20 µm behind the tip, as this pectin was probably deposited during growth and not after cessation of growth. NtDGK5 induced an increase of staining intensity in contrast to NtDGK5[G118A] and the mVenus control (Fig. 7e).

NtDGK5[G118A] expression influences PA and PI(4,5)P₂ signal intensity in the PM

Taking into account the localization of various lipid markers (Helling *et al.*, 2006; Potocký *et al.*, 2014; Pejchar *et al.*, 2020)
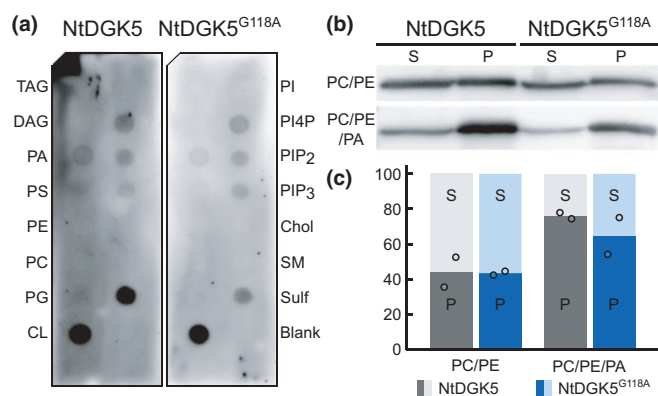
Fig. 5 NtDGK5 and NtDGK[G118A] bind to anionic phospholipids. (a) Protein–lipid overlay assays with purified recombinant GST-tagged NtDGK5 and NtDGK5[G118A] proteins. (b) Cosedimentation of LUVs with *in vitro* translated HA-tagged NtDGK5 or NtDGK5[G118A]. LUVs were prepared from PC and PE, or PC, PE and PA. After sedimentation, NtDGK5 variants were detected via Western blot in supernatants (S) and LUV-containing pellets (P). (c) Quantification of Western blot intensities. Means of fraction ratios for NtDGK5 (gray) and NtDGK5[G118A] (blue) are shown. Individual data points from two independent experiments are indicated by circles. Chol, cholesterol; CL, cardiolipin; DAG, diacylglycerol; DGK, diacylglycerol kinase; Nt, *Nicotiana tabacum*; PA, phosphatidic acid; PC, phosphatidylcholine; PE, phosphatidylethanolamine; PG, phosphatidylglycerol; PI, phosphatidylinositol; PI4P, phosphatidylinositol 4-phosphate; PIP₂, phosphatidylinositol 4,5-bisphosphate; PIP₃, phosphatidylinositol 3,4,5-trisphosphate; PS, phosphatidylserine; SM, sphingomyelin; Sulf, 3-sulfogalactosylceramide; TAG, triacylglycerol.
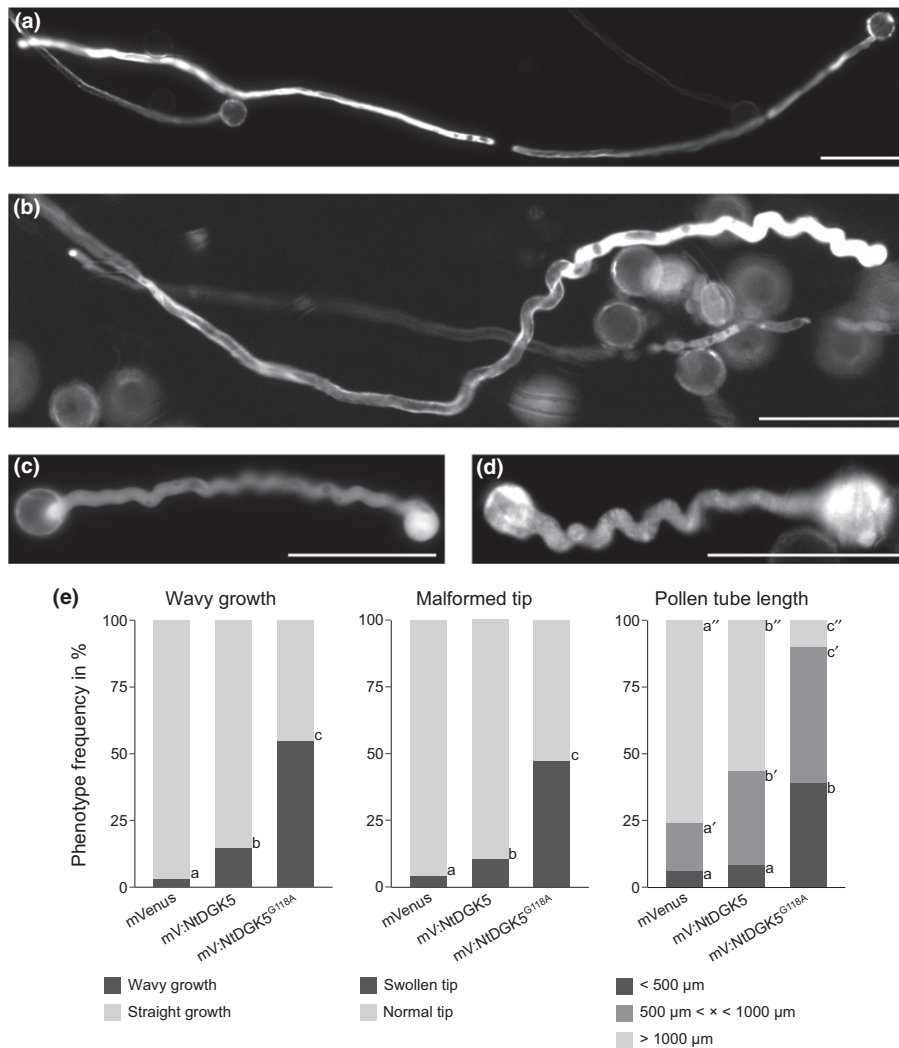
Fig. 6 NtDGK5 and NtDGK5^{G118A} overexpression induce differential growth phenotypes. Tobacco pollen tubes were transformed with NtDGK5 and NtDGK5^{G118A} linked to a fluorescent N-terminal mVenus-tag (mV) by biolistic transformation. Transformation with the fluorescent tag alone served as the control treatment (a). Growth phenotypes were analyzed by epifluorescence microscopy 14 h after transformation. Overexpression of both *mVenus: NtDGK5* (b) and *mVenus:NtDGK5^{G118A}* (c, d) induced a wavy growth phenotype. Overexpression of *NtDGK5^{G118A}* often caused the additional phenotypes of a circular swollen tip and reduced growth length (c, d). The frequency of these phenotypes was quantified (e). Statistical analysis was done using Chi square test with Holm–Bonferroni correction for multiple comparisons. Different letters indicate significant differences at $P < 0.05$. $n = 376$ (mVenus), 479 (mVenus:NtDGK5) and 321 (mVenus:NtDGK5^{G118A}) pollen tubes for wavy growth and malformed tip phenotypes; $n = 334$ (mVenus), 252 (mVenus:NtDGK5) and 204 (mVenus:NtDGK5^{G118A}) for pollen tube length analysis. Bar, 100 μm.

and NtDGK5 in tobacco pollen tubes, we next tested whether there is an overlap in their distribution. To this end, we transiently cotransformed tobacco pollen tubes with mVenus: NtDGK5 and mRFP-tagged genetically encoded lipid marker for DAG (mRFP:2xCys1), PA (mRFP:2xSpo20p-PABD) or PI(4,5)P$_2$ (mRFP:2xPH$_{PLC\delta1}$), and followed their localization. In growing pollen tubes with low levels of transgene expression, membrane mVenus:NtDGK5 was fully included within the range of mRFP:2xCys1 and mRFP:2xPH$_{PLC\delta1}$ signals. Similarly, the distribution of NtDGK5 overlaps with mRFP:2xSpo20p-PABD in the pollen tube subapex, although the area of the mVenus: NtDGK5 signal close to the tip is devoid of mRFP:2xSpo20p-PABD (Fig. S11).

Overexpression of PA-synthesizing enzymes can lead to an increase of PA in the PM of pollen tubes, detectable by an increased PMI of mRFP:2xSpo20p-PABD PA biosensor (Pejchar *et al.*, 2020). In light of these hypotheses, we coexpressed *mVenus:NtDGK5* or *mVenus:NtDGK5^{G118A}* together with the PA biosensor and used a ratiometric approach for quantification of the mRFP:2xSpo20p-PABD signal (Fig. 8a–c). Confirming visual microscopic observations, calculated PMI did not increase upon overexpression of *NtDGK5* compared to expression of free mVenus. However, overexpression of the inactive *NtDGK5^{G118A}* led to a significant decrease of the median PMI to *c.* 70% that of the control (Fig. 8d).

Previously, we found that overexpression of PI4P 5-kinases also led to increased pectin deposition (Ischebeck *et al.*, 2008), and pollen PI4P 5-kinases might be regulated by PA (Kost *et al.*, 1999; Im *et al.*, 2007). Hence, we also assayed PI(4,5)P$_2$ using a similar ratiometric approach with the PI(4,5)P$_2$ biosensor,
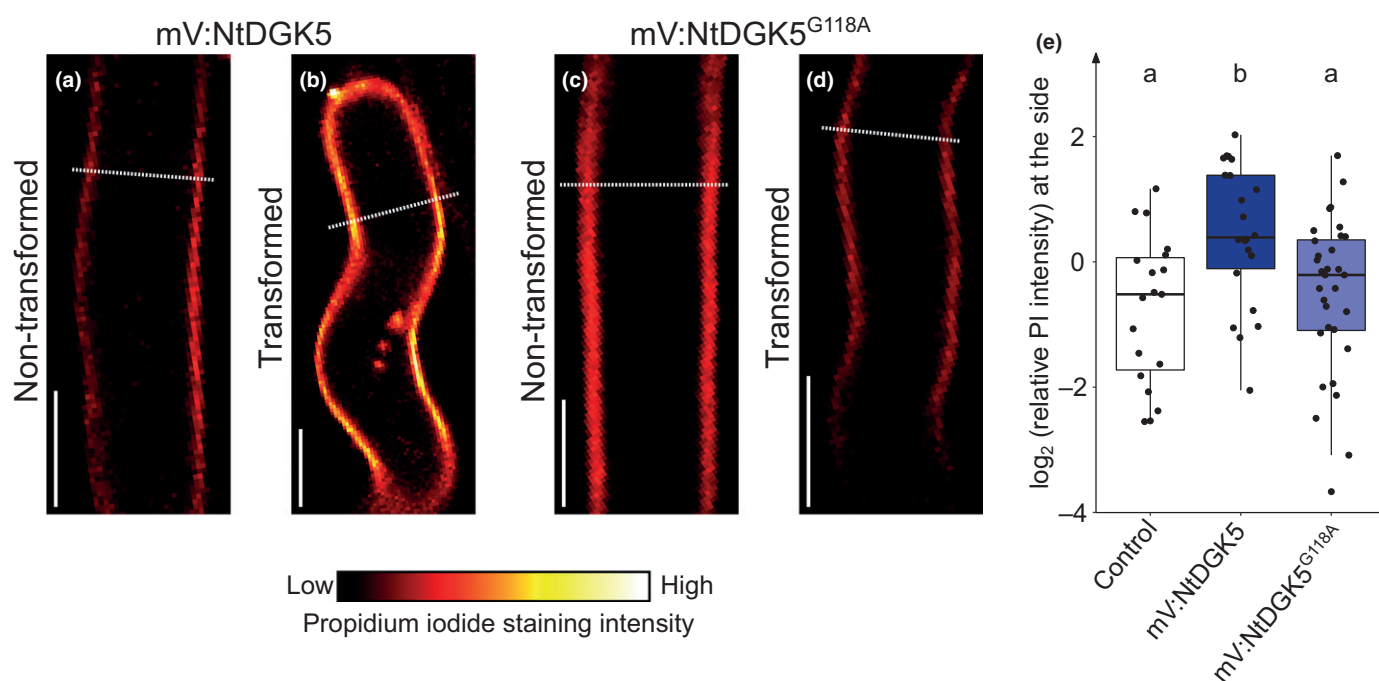
Fig. 7 Overexpression of NtDGK5 increases pectin deposition. Tobacco pollen was transformed with N-terminally mVenus-labelled (mV) NtDGK5 (b) or NtDGK5^{G118A} (d). Transformation with mVenus alone served as a control. Sixteen hours after transformation, pollen tubes were stained with propidium iodide (PI) and imaged by confocal microscopy. Staining intensity values were integrated across the cell wall *c.* 20 μm behind the tip (a–d). To balance local fluctuation of staining intensity, intensity values were also obtained across the tip and the side of neighboring nontransformed pollen tubes (a, c). Subsequently, the ratio of staining intensity between transformed and nontransformed pollen tubes was calculated. Results are displayed as boxplots showing the first quartile, median and third quartile values and whiskers extending to the extreme data points inside of 1.5 × interquartile range. Single data points are shown as black circles (e). Pollen tubes overexpressing NtDGK5 displayed a significant increase of PI intensity *c.* 20 μm behind the tip. Statistical analysis in (e) was calculated using the Kruskal–Wallis test and the Kruskal–Wallis *post-hoc* test. Different letters indicate significant differences at $P < 0.05$. $n = 19$, 22 and 32 pollen tubes for mVenus, mVenus:NtDGK5 and mVenus:NtDGK5^{G118A} in (e). Bar, 10 μm.

mRFP:2xPH$_{PLCδ1}$ (Fig. 8e–h). Overexpression of *NtDGK5* slightly reduced the median PMI of the biosensor to 72% of the control. Overexpression of *NtDGK5^{G118A}* caused an even stronger decrease of the median PMI to 27% of control values, as the PMI in many cases came down close to 1.

NtDGK5 or NtDGK5^{G118A} and AtPIP5K5 reciprocally influence pollen tube phenotypes

Based on the observed connection between PI(4,5)P$_2$ levels and overexpression of *NtDGK5* and *NtDGK5^{G118A}*, we decided to analyze the effects of NtDGK5 variants on pollen tubes with disturbed PI(4,5)P$_2$ metabolism. To increase PI(4,5)P$_2$ levels, we overexpressed the enzyme *AtPIP5K5* in tobacco pollen tubes (Ischebeck *et al.*, 2008). On a phenotype level, *mVenus:AtPIP5K5* expression causes the appearance of branched pollen tubes or pollen tubes with stunted growth (Fig. 9a,b), probably caused by pectin accumulation at the tip (Ischebeck *et al.*, 2008). mVenus-tagged *NtDGK5* and *NtDGK5^{G118A}* were then coexpressed with *mVenus:AtPIP5K5* or free mVenus as a control, and respective characteristic phenotypes were analyzed, including wavy growth and tip swelling for NtDGK5 variants, or pollen tube branching for AtPIP5K5. Pollen tube lengths were also evaluated (Fig. 9c,d).

In agreement with previous results, a wavy growth pattern was observed for NtDGK5 and NtDGK5^{G118A} in combination with the mVenus control. Interestingly, AtPIP5K5 was able to suppress this growth pattern in combination with NtDGK5, but not in combination with NtDGK5^{G118A}. By contrast, combining NtDGK5^{G118A} with AtPIP5K5 led to a strong decrease in the frequency of swollen pollen tube tips in comparison with expression of *NtDGK5^{G118A}* with the mVenus control. Vice versa, AtPIP5K5-induced branching was strongly reduced by coexpression of *NtDGK5* or *NtDGK5^{G118A}*.

Concerning pollen tube length, both NtDGK5^{G118A} and AtPIP5K5 caused a decrease in average tube length of 39% and 36%, respectively (Fig. 9d). This was also represented by an increasing frequency of pollen tubes shorter than 500 or 1000 μm (Fig. 9c). Expression of *NtDGK5* with the mVenus control did not alter pollen tube length. However, the comparison of AtPIP5K5 effects on pollen tube length with or without NtDGK5 displayed an increased abundance of short pollen tubes and an additional drop in average length induced by NtDGK5. Strikingly, the combination of AtPIP5K5 with NtDGK5^{G118A} did not equal their negative effects on pollen tube length. Instead, the length distribution shifted towards an increased frequency of pollen tubes longer than 1000 μm. Compared to the control, pollen tube length decreased by 16%, which is a lower reduction than either AtPIP5K5 or NtDGK5^{G118A} induced alone.
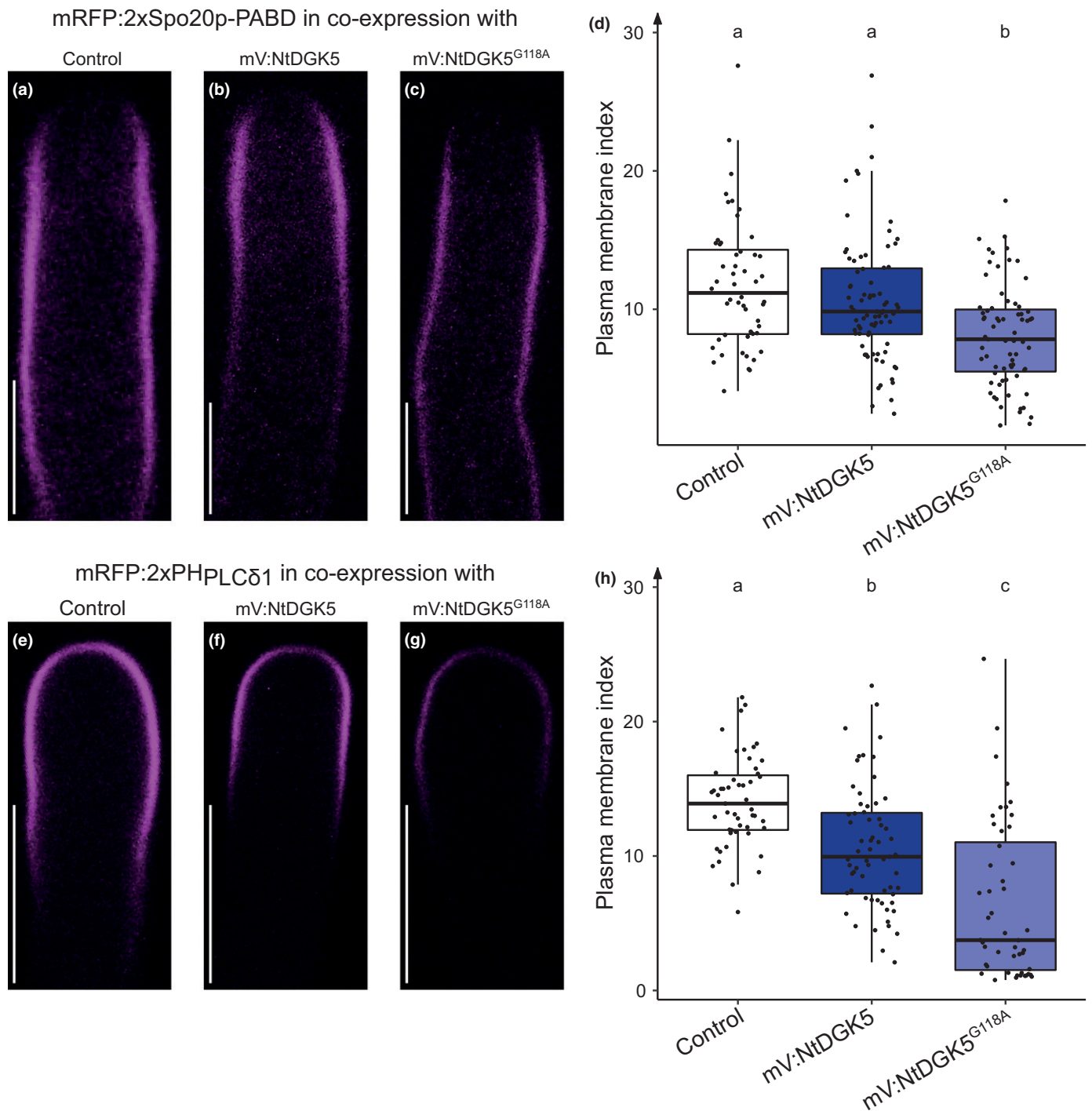
Fig. 8 NtDGK5^{G118A} overexpression reduces the plasma membrane affinity of lipid sensors for phosphatidic acid (PA) and PI(4,5)P$_2$. NtDGK5, NtDGK5^{G118A} tagged to fluorescent N-terminal mVenus (mV) and mVenus alone as a control were transiently coexpressed in tobacco pollen tubes together with the lipid sensors mRFP:2xSpo20p-PABD (a–c) or mRFP:2xPH$_{PLCδ1}$ (e–g) for PA and PI(4,5)P$_2$, respectively. For RFP-labeled lipid sensors the plasma membrane index (PMI) was calculated, dividing the fluorescence intensity at the plasma membrane by the fluorescence intensity in the cytosol. In the case of 2xSpo20p-PABD, plasma membrane localization decreased upon overexpression of NtDGK5^{G118A}, but was not significantly altered by NtDGK5 (d). By contrast, both NtDGK5 and NtDGK5^{G118A} caused a significant decrease of plasma membrane localization of mRFP:2xPH$_{PLCδ1}$. Loss of mRFP:2xPH$_{PLCδ1}$ membrane localization was more severe for overexpression of NtDGK5^{G118A} compared to NtDGK5 (h). In (d, h), boxplots display the first quartile, median and third quartile values and whiskers extend to the extreme data points inside of 1.5 × interquartile range. Single data points are shown as black circles. $n = 52$ (mVenus), 79 (mVenus:NtDGK5) and 71 (mVenus:NtDGK5^{G118A}) pollen tubes for the PA sensor (d); $n = 51$ (mVenus), 63 (mVenus:NtDGK5) and 48 (mVenus:NtDGK5^{G118A}) pollen tubes for the PI(4,5)P$_2$ sensor (h). Statistical analysis was done by one-way ANOVA with Tukey's *post-hoc* test. Different letters indicate significant differences at $P < 0.05$. Bar, 10 μm.

(a)

(b)

(c)

Wavy growth

Swollen tip

Branching pollen tubes

Pollen tube length

Straight growth
Wavy growth

Normal tip
Swollen tip

No branching
Branched pollen tubes

> 1000 µm
500 < × < 1000 µm
< 500 µm

(d)

Pollen tube length (µm)

mVenus +
mVenus

mVenus +
mV:NtDGK5

mVenus +
mV:NtDGK5^{G118A}

mV:AtPIP5K5 +
mVenus

mV:AtPIP5K5 +
mV:NtDGK5

mV:AtPIP5K5 +
mV:NtDGK5^{G118A}
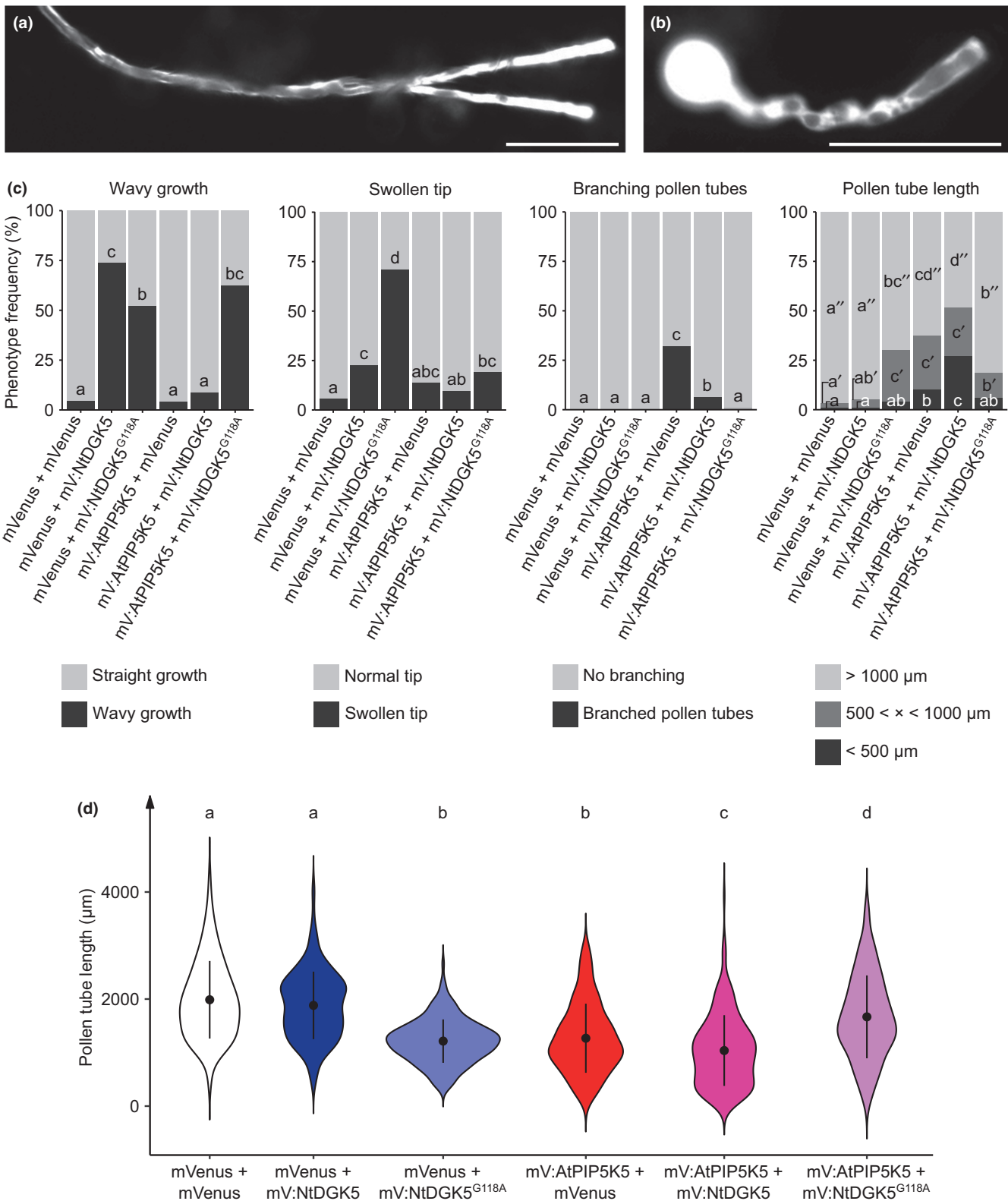
NtDGK5 and NtDGK5^{G118A} interfere with AtPIP5K5-induced apical pectin accumulation

Length measurements and phenotypic analysis of pollen tubes coexpressing mVenus-tagged *NtDGK5* variants with *mVenus:AtPIP5K5* showed that NtDGK5^{G118A} partially counteracts pollen tube phenotypes resulting from the *AtPIP5K5* overexpression-induced increase of PI(4,5)P$_2$ levels. As PI(4,5)P$_2$-induced phenotypes have been traced to excessive apical pectin secretion, we then analyzed the impact of NtDGK5 variants on

Fig. 9 NtDGK5^{G118A} can counteract AtPIP5K5-related growth phenotypes. N-terminally mVenus-labelled (mV) *NtDGK5* and *NtDGK5*^{G118A} were expressed in combination with the Arabidopsis PI4P 5-kinase *mVenus:AtPIP5K5* or *mVenus* as a control. Phenotypes of transformed pollen tubes were imaged after 14 h of growth by epifluorescence microscopy. Overexpression of *AtPIP5K5* causes the distinct phenotypes of branched (a) or severely stunted pollen tubes (b). (c) Both the NtDGK5-specific phenotypes of wavy growth and swollen tip and the AtPIP5K5-specific phenotype of branching were quantified in addition to phenotype effects on pollen tube length. (d) Pollen tube length was measured and differences between treatments were statistically analyzed. Average pollen tube length ± SD is represented by black dots with a vertical line. For phenotypic analysis in (c, d), *n* = 201 (control), 204 (mVenus + mVenus:NtDGK5), 209 (mVenus + mVenus:NtDGK5^{G118A}), 200 (mVenus:AtPIP5K5 + mVenus), 222 (mVenus:AtPIP5K5 + mVenus: NtDGK5) and 196 (mVenus:AtPIP5K5 + mVenus:NtDGK5^{G118A}) pollen tubes were analyzed. Statistical analysis was done using a Chi square test with Holm–Bonferroni correction for multiple comparisons in (c) and using one-way ANOVA with Tukey's *post-hoc* test in (d). Different letters indicate significant differences at *P* < 0.05. Bar, 100 μm.

pollen tubes where pectin secretion was increased by the expression of *AtPIP5K5*. We again used the propidium iodide staining approach to analyze pectin accumulation at the pollen tube tip.

In line with previous studies, *AtPIP5K5* overexpression caused a massive increase of pectin accumulation at the pollen tube tip (Fig. 10a,b). Since expression levels of *AtPIP5K5* and subsequent PI(4,5)P$_2$ concentrations vary considerably, the effects were highly variable. In some pollen tubes, pectin accumulation was

scarcely changed, whereas in extreme cases the pectin staining intensity of transformed pollen tubes was more than 100-fold higher than in untransformed control pollen tubes. Overall, an increased pectin secretion at the tip was observed, as the ratiometric median calculated as log$_2$-change was altered from −0.08 to 4.28 (Fig. 10g). The pectin staining intensity was similarly broadly distributed in pollen tubes coexpressing *AtPIP5K5* either with *NtDGK5* or *NtDGK5*^{G118A} (Fig. 10c–f). Nevertheless, in
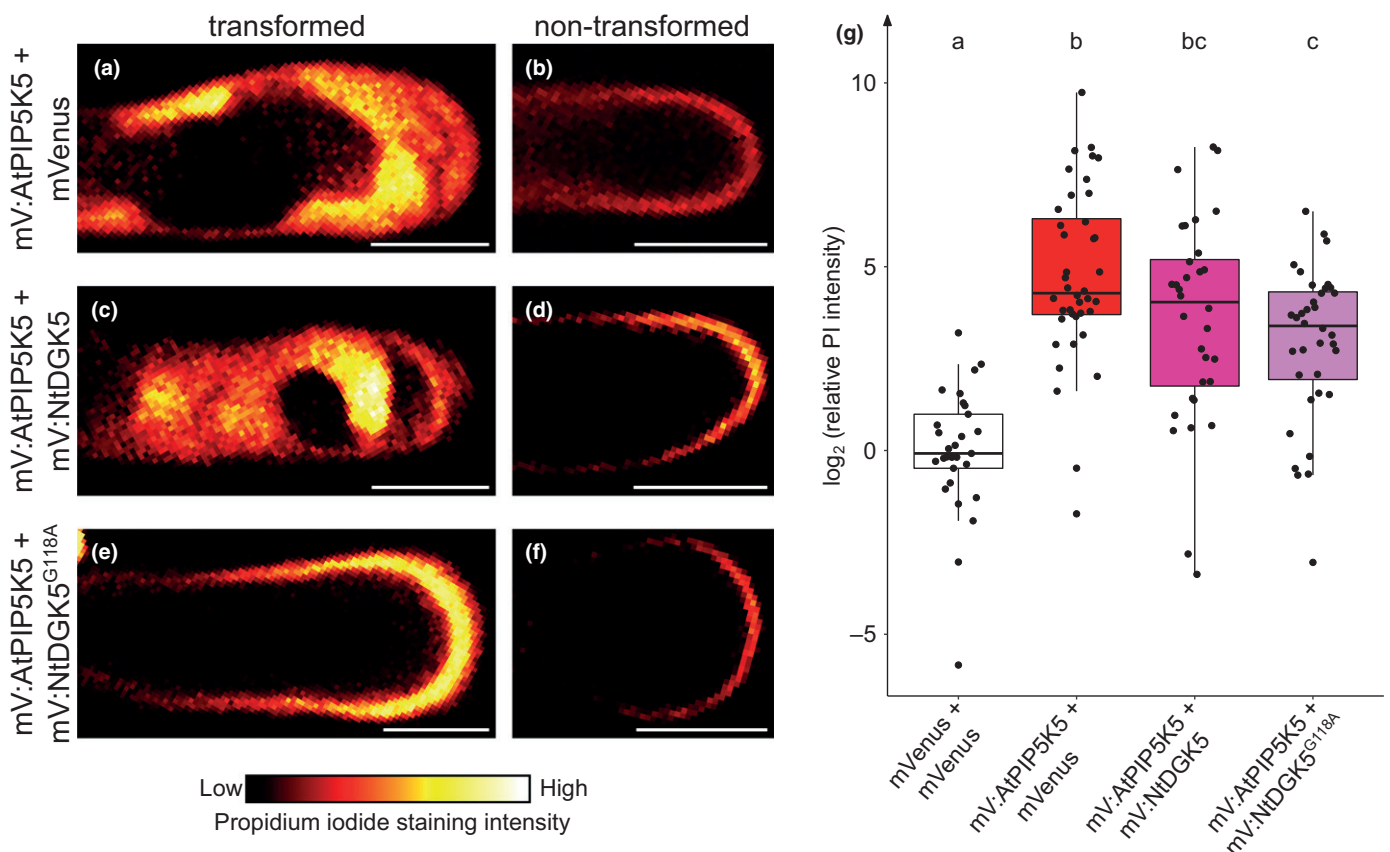
Fig. 10 NtDGK5^{G118A} can counteract AtPIP5K5-induced pectin accumulation. Tobacco pollen was transformed to overexpress fluorescently mVenus-labeled *AtPIP5K5* in combination with *mVenus* (a), *mVenus:NtDGK5* (c) or *mVenus:NtDGK5*^{G118A} (e). Expression of fluorescent tag alone served as a negative control. After 14 h of pollen tube growth, pectin was stained with propidium iodide and imaged by confocal microscopy. Staining intensity of pectin at the tip was integrated across the cell wall and normalized to the staining intensity at the tip of a neighboring nontransformed pollen tube (b, d, f). Results are shown as boxplots in (g) highlighting the first quartile, median and third quartile values and whiskers extending to the extreme data points inside of 1.5 × interquartile range. Single data points are shown as black circles. *mVenus:AtPIP5K5* overexpression caused a strong shift towards pectin accumulation in the population of transformed pollen tubes. This shift was significantly reduced in pollen tubes overexpressing *mVenus:AtPIP5K5* in combination with *mVenus:NtDGK5*^{G118A} (g). For statistical analysis of (g), *n* = 29 (control), 40 (mVenus:AtPIP5K5 + mVenus), 32 (mVenus: AtPIP5K5 + mVenus:NtDGK5) and 36 (mVenus:AtPIP5K5 + mVenus:NtDGK5^{G118A}) pollen tubes were analyzed. Significant differences were calculated with the Kruskal–Wallis test and Kruskal–Wallis *post-hoc* test. Different letters indicate significant differences at *P* < 0.05. Bar, 10 μm.

both populations of pollen tubes, median values of normalized staining intensity decreased compared to coexpression of *AtPIP5K5* and mVenus, to a $\log_2$-change of 4.04 or 3.39, respectively (Fig. 10g).

In conclusion, while the interplay of PA and phosphoinositides remains to be studied in depth, our data indicate that expression of *NtDGK5^{G118A}* leads to reduced PI(4,5)P$_2$ levels and thereby counteracts AtPIP5K5-derived phenotypes, especially the reduction in pollen tube length.

Discussion

NtDGK5 has limited binding capacity to the subapical pollen tube PM

NtDGK5 sequence analysis did not indicate transmembrane helices or covalent attachment of lipid anchors. Furthermore, considerable cytoplasmic fluorescence and short FRAP times (Fig. 4a,f) suggest that NtDGK5 is a soluble protein transiently recruited by one or several binding partners for peripheral membrane association, similar to other lipid-converting enzymes (Ischebeck *et al.*, 2008; Pejchar *et al.*, 2020; Noack *et al.*, 2021). As saturation effects were observed for the membrane association of NtDGK5 (Fig. 4d), a limited number of such binding partners can be assumed. One possible mediator of membrane binding of peripheral membrane proteins are lipid-binding domains that recognize specific lipids at the PM (Noack & Jaillais, 2020; de Jong & Munnik, 2021). For example, PLCs from tobacco and petunia localized in the apical PM of pollen tubes depend for this targeting on their C2 domains (Dowd *et al.*, 2006; Helling *et al.*, 2006) described to bind anionic lipids in a Ca^{2+}-dependent manner (Corbalan-Garcia & Gómez-Fernández, 2014). For the apical PM targeting of AtPIP5K6, on the other hand, not the presumably lipid binding MORN (membrane occupation and recognition nexus) repeat domain is important, but a variable linker domain that might confer protein–protein interactions (Stenzel *et al.*, 2012).

In comparison to some mammalian DGKs (Franks *et al.*, 2017), but also AtDGK1 and 2 (Arisz *et al.*, 2009) and NtDGK1–3 (Fig. 1b), NtDGK5 does not harbor any conserved domains implicated in lipid binding. It is still conceivable, however, that it is recruited to the PM by binding its substrate DAG enriched in the apical PM of pollen tubes (Helling *et al.*, 2006). However, the membrane association of NtDGK5 was confined to a smaller region than has been observed with a biosensor for DAG (Fig. S10). Hence, the exact localization of NtDGK5 is probably mediated, at least in part, by factors other than substrate availability. Indeed, our MD simulations and lipid-binding assays show a direct interaction between NtDGK5 and anionic phospholipids that are enriched at the plant PM (Simon *et al.*, 2016; Platre & Jaillais, 2017; Platre *et al.*, 2018). Still the question remains why the membrane-binding region *in planta* of DGK5 is so confined, especially given that other DGK isoforms and the G118A variant of DGK5 that harbors a similarly charged surface, bind to a much larger area of the PM (Figs 1, 4, S3).

Limited binding capacity for DGKs at the PM might contribute to a possible dominant negative effect of NtDGK5^{G118A}

Mutated protein variants that mediate dominant-negative effects have been proven to be valuable tools to investigate pollen tube signaling (Cheung *et al.*, 2002; Dowd *et al.*, 2006; Klahre *et al.*, 2006; Chang *et al.*, 2009). These dominant-negative effects can derive from mutated protein variants that outcompete the naturally occurring variants for crucial binding partners/regulators. Such an explanation is also possible here. Alteration of the glycine-rich loop in NtDGK5^{G118A} did not interfere with the protein's membrane association. By contrast, the association with the PM was even stronger and covered a longer stretch (Fig. 4c). Our FRAP experiments also suggested that a subpopulation of NtDGK5^{G118A} remains more strongly attached to the PM (Fig. 4g). In this way, NtDGK5^{G118A} might block the DAG substrate and possible physiological binding partners of the endogenous NtDGK5 and closely related paralogs, leading to a dominant-negative effect upon overexpression in pollen tubes and subsequent growth perturbations, as well as explain the reduced binding of the PA biosensor at the PM (Figs 6, 8). An alternative is that NtDGK5, and to a stronger degree NtDGK5^{G118A} due to its enhanced PM recruitment, induces phenotypic changes by masking PA that we found to be bound by both variants. While the active variant could partially counter this effect by generating PA, the inactive variant cannot, thereby reducing the amount of free PA in the region. Previous inhibition of DGK activity in tobacco pollen tubes with the DGK inhibitor R59022 was partially shown to decrease PA levels at the PM, but did not induce the wavy growth effects on pollen tube growth as was observed for the overexpression of NtDGK5^{G118A} (Pleskot *et al.*, 2012; Potocký *et al.*, 2014). This might be explained due to its less specific inhibition also affecting ER-localized DGKs. Disturbance of these DGKs' role in phospholipid synthesis and ER lipid composition might hamper pollen tube growth differentially from NtDGK5. While PA produced at the PM might contribute directly to polar tip growth by regulating secretory processes, DGKs at the ER might be involved in the synthesis of phosphatidylinositol and phosphatidylglycerol (Angkawijaya *et al.*, 2020). On the other hand, PA synthesized at the ER (e.g. by Arabidopsis DGK2 or DGK4; Angkawijaya *et al.*, 2020) could also be transported to the PM via the secretory pathway thereby contributing to PA signaling in the tip region. Either way, R59022-related effects might be too strong, covering subtler effects induced by NtDGK5^{G118A}.

Cell wall plasticity shapes the pollen tube

Plant cells are shaped by turgor pressure and cell wall plasticity (Ivakov & Persson, 2013). While the apical cell wall of pollen tubes is somewhat more simple than most cell walls (e.g. lacking cellulose), its plasticity can still be regulated by targeted pectin secretion and pectin-modifying enzymes (Scholz *et al.*, 2020). This allows not only balance between giving too much resistance against elongation and bursting, but also enables uniform tubular

growth. Such growth requires an uneven cell wall plasticity in the very tip region of the pollen tube, maintained by continuous targeted secretion of pectin and its modifiers orchestrated by a combination of feed-forward and feed-back regulations. Many studies have highlighted that this dynamic equilibrium can be disturbed by overexpression of various signaling proteins (Scheible & McCubbin, 2019; Scholz *et al.*, 2020). Overexpression of *AtPIP5K4* and *5*, for example, leads to a premature growth arrest, accompanied by massive pectin deposition and membrane invaginations (Ischebeck *et al.*, 2008). A similar phenotype was observed after overexpression of PLDs (Pejchar *et al.*, 2020). Furthermore, studies of the Arabidopsis mutant *dgk4* reported differences in cell wall properties of pollen tubes as determined by atomic force microscopy (Vaz Dias *et al.*, 2019). Here we show that overexpression of NtDGK5 also leads to increased pectin deposition and shorter pollen tubes (Figs 6, 7). The increased deposition could first lead to thicker cell walls and finally terminate tube elongation when the cell wall resistance becomes greater than the turgor pressure.

In addition, the tip-swelling phenotype observed upon overexpression of the NtDGK5^{G118A} variant might be explained by effects on cell wall deposition. Here, even though no effect on cell wall thickness was measured in our assay, subtle changes in pectin secretion could lead to wall thinning in certain regions, perturbing the plasticity in a way that leads to tip-swelling and ultimately growth arrest rather than regular, continuous tip growth.

More difficult to explain is the wavy growth pattern observed with its periodic nature. Pollen tube growth as an oscillating process has long been described and observed with regard to, inter alia, growth speed, Ca^{2+} concentrations and wall thickness (Feijó *et al.*, 2001; Zonia *et al.*, 2006). Experimental observations have mainly been described along the longitudinal axis of the growth direction; however, Haduch-Sendecka *et al.* (2014) also reported transverse oscillations in the width of tobacco pollen tubes that are correlated to longitudinal growth speed oscillations in tobacco pollen tubes. The observed wavy growth is therefore possibly the result of a slight asymmetry in the regulating networks that control transverse oscillations as PA levels might be increased or decreased depending on which DGK variant was used. This might result in an asymmetric pectin deposition causing one side of the pollen tube to expand more strongly, resulting in a turning of growth direction. A correction by internal feed-back loops in combination with the transverse oscillations could possibly result in the wavy shape.

NtDGK5 might influence pectin secretion as part of a larger regulatory network

As we propose that the phenotypes observed are caused by alterations in the secretion of pectin and possibly also pectin-modifying enzymes, the question arises of how DGK-produced PA could regulate such secretory processes. Generally, PA could have a direct effect on pectin secretion or an indirect effect by regulating other signaling proteins. PA has, for example, been linked to the regulation of PIP5K activity: *in vitro* experiments demonstrated an activation of Arabidopsis AtPIP5K1 via its N-terminal MORN domain by PA, which is a conserved domain in Arabidopsis AtPIP5K1–AtPIP5K9 (Im *et al.*, 2007).

Phosphatidic acid and PI(4,5)P$_2$ could then influence the rate of secretion in pollen tubes in several ways, including by the availability of secretory vesicles in the apical region, the rate of tethering of these vesicles to the PM as well as the actual rate of fusion events.

Important for the tethering of secretory vesicles to the PM is foremost the exocyst complex (TerBush *et al.*, 1996; Elias *et al.*, 2003). This complex consists of eight protein subunits and is recruited to the PM by anionic phospholipids including PA and PI(4,5)P$_2$ (Bloch *et al.*, 2016; Synek *et al.*, 2021). In addition, Sekereš *et al.* (2017) analyzed the localization of different members of the tobacco EXO70 protein family in tobacco pollen tubes and described localization to distinct membrane domains for NtEXO70A1a and NtEXO70B. The apical localization of NtEXO70A1a appeared to be limited by the presence of PA in the membrane: the onset of NtEXO70A1a coincided with the onset of the PA sensor mRFP:2xSpo20p-PABD.

Vesicle fusion could also be regulated by PA directly, or through a potential connection to PI(4,5)P$_2$ synthesis. In the animal field, PA was described to promote exocytosis through its cone shape, and for yeast interactions of PA with different SNARE proteins were described to influence membrane fusion events (Zhukovsky *et al.*, 2019). Regarding a potential regulation of vesicle fusion by PI(4,5)P$_2$, mechanistic knowledge in the plant system is very limited. However, PI(4,5)P$_2$ is established as a key player in the neuron system by regulating the activity of ion channels that influence secretion (Hille *et al.*, 2015). Furthermore, several proteins directly involved in fusion bind PI(4,5)P$_2$, including SNARE proteins and the proteins CAPS and Munc13 that prime vesicles for exocytosis (Martin, 2012).

Author contributions

PS, PP, RP, TM, MP and TI designed the research; PS, PP, MF, EŠ, RP, MP, KB and TI performed research; PS, PP, EŠ, RP, MP and TI analyzed the data; PS, PP, RP, TM, MP and TI wrote the paper with the help of all authors.

ORCID

Katharina Blersch (iD) https://orcid.org/0000-0001-7020-5587
Till Ischebeck (iD) https://orcid.org/0000-0003-0737-3822
Teun Munnik (iD) https://orcid.org/0000-0002-4919-4913
Přemysl Pejchar (iD) https://orcid.org/0000-0003-0488-7465
Roman Pleskot (iD) https://orcid.org/0000-0003-0436-9748
Martin Potocký (iD) https://orcid.org/0000-0002-3699-7549
Patricia Scholz (iD) https://orcid.org/0000-0003-0761-9175

Data availability

Data are available in the article supporting material.

References

Angkawijaya AE, Nguyen VC, Gunawan F, Nakamura Y. 2020. A pair of Arabidopsis diacylglycerol kinases essential for gametogenesis and endoplasmic reticulum phospholipid metabolism in leaves and flowers. *Plant Cell* **32**: 2602–2620.

Arisz SA, Testerink C, Munnik T. 2009. Plant PA signaling via diacylglycerol kinase. *Biochimica et Biophysica Acta (BBA) – Molecular and Cell Biology of Lipids* **1791**: 869–875.

Arisz SA, van Wijk R, Roels W, Zhu J-K, Haring MA, Munnik T. 2013. Rapid phosphatidic acid accumulation in response to low temperature stress in Arabidopsis is generated through diacylglycerol kinase. *Frontiers in Plant Science* **4**: 1.

Bloch D, Pleskot R, Pejchar P, Potocký M, Trpkošová P, Cwiklik L, Vukašinović N, Sternberg H, Yalovsky S, Žárský V. 2016. Exocyst SEC3 and phosphoinositides define sites of exocytosis in pollen tube initiation and growth. *Plant Physiology* **172**: 980–1002.

Bosch M, Cheung AY, Hepler PK. 2005. Pectin methylesterase, a regulator of pollen tube growth. *Plant Physiology* **138**: 1334–1346.

Cacas J-L, Gerbeau-Pissot P, Fromentin J, Cantrel C, Thomas D, Jeannette E, Kalachova T, Mongrand S, Simon-Plas F, Ruelland E. 2017. Diacylglycerol kinases activate tobacco NADPH oxidase-dependent oxidative burst in response to cryptogein: control of RBOHD activity by DGK. *Plant, Cell & Environment* **40**: 585–598.

Chang L-C, Guo C-L, Lin Y-S, Fu H, Wang C-S, Jauh G-Y. 2009. Pollen-specific SKP1-like proteins are components of functional scf complexes and essential for lily pollen tube elongation. *Plant & Cell Physiology* **50**: 1558–1572.

Chebli Y, Kaneda M, Zerzour R, Geitmann A. 2012. The cell wall of the Arabidopsis pollen tube-spatial distribution, recycling, and network formation of polysaccharides. *Plant Physiology* **160**: 1940–1955.

Cheung AY, Chen CY-h, Glaven RH, de Graaf BHJ, Vidali L, Hepler PK, Wu H. 2002. Rab2 GTPase regulates vesicle trafficking between the endoplasmic reticulum and the Golgi bodies and is important to pollen tube growth. *Plant Cell* **14**: 945–962.

Colongonzalez F, Kazanietz M. 2006. C1 domains exposed: from diacylglycerol binding to protein–protein interactions. *Biochimica et Biophysica Acta (BBA) – Molecular and Cell Biology of Lipids* **1761**: 827–837.

Conze LL, Berlin S, Le Bail A, Kost B. 2017. Transcriptome profiling of tobacco (*Nicotiana tabacum*) pollen and pollen tubes. *BMC Genomics* **18**: 581.

Corbalan-Garcia S, Gómez-Fernández JC. 2014. Signaling through C2 domains: more than one lipid target. *Biochimica et Biophysica Acta (BBA) – Biomembranes* **1838**: 1536–1547.

Dowd PE, Coursol S, Skirpan AL, Kao T, Gilroy S. 2006. Petunia phospholipase c1 is involved in pollen tube growth. *Plant Cell* **18**: 1438–1453.

Elias M, Drdova E, Ziak D, Bavlnka B, Hala M, Cvrckova F, Soukupova H, Zarsky V. 2003. The exocyst complex in plants. *Cell Biology International* **27**: 199–201.

Fayant P, Girlanda O, Chebli Y, Aubin C-E, Villemure I, Geitmann A. 2010. Finite element model of polar growth in pollen tubes. *Plant Cell* **22**: 2579–2593.

Feijó JA, Sainhas J, Holdaway-Clarke T, Cordeiro MS, Kunkel JG, Hepler PK. 2001. Cellular oscillations and the regulation of growth: the pollen tube paradigm. *BioEssays* **23**: 86–94.

Franks CE, Campbell ST, Purow BW, Harris TE, Hsu K-L. 2017. The ligand binding landscape of diacylglycerol kinases. *Cell Chemical Biology* **24**: 870–880.e5.

Furt F, König S, Bessoule J-J, Sargueil F, Zallot R, Stanislas T, Noirot E, Lherminier J, Simon-Plas F, Heilmann I et al. 2010. Polyphosphoinositides are enriched in plant membrane rafts and form microdomains in the plasma membrane. *Plant Physiology* **152**: 2173–2187.

Furt F, Simon-Plas F, Mongrand S. 2011. Lipids of the plant plasma membrane. In: Murphy AS, Schulz B, Peer W, eds. *The plant plasma membrane*. Berlin, Heidelberg, Germany: Springer Berlin Heidelberg, 3–30.

Gómez-Merino FC, Arana-Ceballos FA, Trejo-Téllez LI, Skirycz A, Brearley CA, Dörmann P, Mueller-Roeber B. 2005. Arabidopsis AtDGK7, the smallest member of plant diacylglycerol kinases (DGKs), displays unique biochemical features and saturates at low substrate concentration: the DGK inhibitor R59022 differentially affects AtDGK2 and AtDGK7 activity *in vitro* and alters plant growth and development. *Journal of Biological Chemistry* **280**: 34888–34899.

Gómez-Merino FC, Brearley CA, Ornatowska M, Abdel-Haliem MEF, Zanor M-I, Mueller-Roeber B. 2004. AtDGK2, a novel diacylglycerol kinase from *Arabidopsis thaliana*, phosphorylates 1-stearoyl-2-arachidonoyl-*sn*-glycerol and 1,2-dioleoyl-*sn*-glycerol and exhibits cold-inducible gene expression. *Journal of Biological Chemistry* **279**: 8230–8241.

Grebnev G, Ntefidou M, Kost B. 2017. Secretion and endocytosis in pollen tubes: models of tip growth in the spot light. *Frontiers in Plant Science* **8**: 154.

Haduch-Sendecka A, Pietruszka M, Zajdel P. 2014. Power spectrum, growth velocities and cross-correlations of longitudinal and transverse oscillations of individual *Nicotiana tabacum* pollen tube. *Planta* **240**: 263–276.

Hanahan DJ, Chaikoff IL. 1947. A new phospholipide-splitting enzyme specific for the ester linkage between the nitrogenous base and the phosphoric acid grouping. *Journal of Biological Chemistry* **169**: 699–705.

Heilmann I, Ischebeck T. 2016. Male functions and malfunctions: the impact of phosphoinositides on pollen development and pollen tube growth. *Plant Reproduction* **29**: 3–20.

Helling D, Possart A, Cottier S, Klahre U, Kost B. 2006. Pollen tube tip growth depends on plasma membrane polarization mediated by tobacco PLC3 activity and endocytic membrane recycling. *Plant Cell* **18**: 3519–3534.

Hille B, Dickson EJ, Kruse M, Vivas O, Suh B-C. 2015. Phosphoinositides regulate ion channels. *Biochimica et Biophysica Acta (BBA) – Molecular and Cell Biology of Lipids* **1851**: 844–856.

Hong Y, Zhao J, Guo L, Kim S-C, Deng X, Wang G, Zhang G, Li M, Wang X. 2016. Plant phospholipases D and C and their diverse functions in stress responses. *Progress in Lipid Research* **62**: 55–74.

Honys D, Twell D. 2004. Transcriptome analysis of haploid male gametophyte development in Arabidopsis. *Genome Biology* **5**: R85.

Im YJ, Davis AJ, Perera IY, Johannes E, Allen NS, Boss WF. 2007. The N-terminal membrane occupation and recognition nexus domain of Arabidopsis phosphatidylinositol phosphate kinase 1 regulates enzyme activity. *Journal of Biological Chemistry* **282**: 5443–5452.

Ischebeck T, Stenzel I, Heilmann I. 2008. Type B phosphatidylinositol-4-phosphate 5-kinases mediate Arabidopsis and *Nicotiana tabacum* pollen tube growth by regulating apical pectin secretion. *Plant Cell* **20**: 3312–3330.

Ischebeck T, Stenzel I, Hempel F, Jin X, Mosblech A, Heilmann I. 2011. Phosphatidylinositol-4,5-bisphosphate influences Nt-Rac5-mediated cell expansion in pollen tubes of *Nicotiana tabacum*. *The Plant Journal* **65**: 453–468.

Ivakov A, Persson S. 2013. Plant cell shape: modulators and measurements. *Frontiers in Plant Science* **4**: 439.

Johnson MA, Harper JF, Palanivelu R. 2019. A fruitful journey: pollen tube navigation from germination to fertilization. *Annual Review of Plant Biology* **70**: 809–837.

de Jong F, Munnik T. 2021. Attracted to membranes: lipid-binding domains in plants. *Plant Physiology* **185**: 707–723.

Julkowska MM, Rankenberg JM, Testerink C. 2013. Liposome-binding assays to assess specificity and affinity of phospholipid–protein interactions. In:

Munnik T, Heilmann I, eds. *Methods in molecular biology*. Plant lipid signaling protocols. Totowa, NJ, USA: Humana Press, 261–271.

Kim S-C, Wang X. 2020. Phosphatidic acid: an emerging versatile class of cellular mediators. *Essays in Biochemistry* **64**: 533–546.

Klahre U, Becker C, Schmitt AC, Kost B. 2006. Nt-RhoGDI2 regulates Rac/Rop signaling and polar cell growth in tobacco pollen tubes. *The Plant Journal* **46**: 1018–1031.

König S, Hoffmann M, Mosblech A, Heilmann I. 2008. Determination of content and fatty acid composition of unlabeled phosphoinositide species by thin-layer chromatography and gas chromatography. *Analytical Biochemistry* **378**: 197–201.

Kost B, Lemichez E, Spielhofer P, Hong Y, Tolias K, Carpenter C, Chua N-H. 1999. Rac homologues and compartmentalized phosphatidylinositol 4, 5-bisphosphate act in a common pathway to regulate polar pollen tube growth. *The Journal of Cell Biology* **145**: 317–330.

Kost B, Spielhofer P, Chua N-H. 1998. A GFP-mouse talin fusion protein labels plant actin filaments *in vivo* and visualizes the actin cytoskeleton in growing pollen tubes. *The Plant Journal* **16**: 393–401.

Kroeger JH, Zerzour R, Geitmann A. 2011. Regulator or driving force? The role of turgor pressure in oscillatory plant cell growth. *PLoS ONE* **6**: e18549.

Li J, Wang X. 2019. Phospholipase D and phosphatidic acid in plant immunity. *Plant Science* **279**: 45–50.

Martin TFJ. 2012. Role of PI(4,5)P$_2$ in vesicle exocytosis and membrane fusion. *Subcellular Biochemistry* **59**: 111–130.

Mori T, Kuroiwa H, Higashiyama T, Kuroiwa T. 2006. GENERATIVE CELL SPECIFIC 1 is essential for angiosperm fertilization. *Nature Cell Biology* **8**: 64–71.

Müller AO, Blersch KF, Gippert AL, Ischebeck T. 2017. Tobacco pollen tubes – a fast and easy tool for studying lipid droplet association of plant proteins. *The Plant Journal* **89**: 1055–1064.

Müller AO, Ischebeck T. 2018. Characterization of the enzymatic activity and physiological function of the lipid droplet-associated triacylglycerol lipase AtOBL1. *New Phytologist* **217**: 1062–1076.

Munnik T. 2001. Phosphatidic acid: an emerging plant lipid second messenger. *Trends in Plant Science* **6**: 227–233.

Munnik T, Laxalt AM. 2013. Measuring PLD activity *in vivo*. In: Munnik T, Heilmann I, eds. *Methods in molecular biology. Plant lipid signaling protocols*. Totowa, NJ, USA: Humana Press, 219–231.

Munnik T, Testerink C. 2009. Plant phospholipid signaling: 'in a nutshell'. *Journal of Lipid Research* **50**: S260–S265.

Munnik T, Zarza X. 2013. Analyzing plant signaling phospholipids through 32Pi-labeling and TLC. *Methods in Molecular Biology* **1009**: 3–15.

Nishizuka Y. 1988. The molecular heterogeneity of protein kinase C and its implications for cellular regulation. *Nature* **334**: 661–665.

Noack LC, Bayle V, Armengot L, Rozier F, Mamode-Cassim A, Stevens FD, Caillaud MC, Munnik T, Mongrand S, Pleskot R et al. 2021. A nanodomain-anchored scaffolding complex is required for the function and localization of phosphatidylinositol 4-kinase alpha in plants. *Plant Cell* koab135. doi: 10.1093/plcell/koab135.

Noack LC, Jaillais Y. 2020. Functions of anionic lipids in plants. *Annual Review of Plant Biology* **71**: 71–102.

Pejchar P, Sekereš J, Novotný O, Žárský V, Potocký M. 2020. Functional analysis of phospholipase Dδ family in tobacco pollen tubes. *The Plant Journal* **103**: 212–226.

Platre MP, Jaillais Y. 2017. Anionic lipids and the maintenance of membrane electrostatics in eukaryotes. *Plant Signaling & Behavior* **12**: e1282022.

Platre MP, Noack LC, Doumane M, Bayle V, Simon MLA, Maneta-Peyret L, Fouillen L, Stanislas T, Armengot L, Pejchar P et al. 2018. A combinatorial lipid code shapes the electrostatic landscape of plant endomembranes. *Developmental Cell* **45**: 465–480.

Pleskot R, Li J, Žárský V, Potocký M, Staiger CJ. 2013. Regulation of cytoskeletal dynamics by phospholipase D and phosphatidic acid. *Trends in Plant Science* **18**: 496–504.

Pleskot R, Pejchar P, Bezvoda R, Lichtscheidl I, Wolters-Arts M, Marc J, Žárský V, Potocký M. 2012. Turnover of phosphatidic acid through distinct signaling pathways affects multiple aspects of pollen tube growth in tobacco. *Frontiers in Plant Science* **3**: 54.

Pleskot R, Potocký M, Pejchar P, Linek J, Bezvoda R, Martinec J, Valentová O, Novotná Z, Žárský V. 2010. Mutual regulation of plant phospholipase D and the actin cytoskeleton: reciprocal regulation of plant PLD and actin. *The Plant Journal* **62**: 494–507.

Potocký M, Eliáš M, Profotová B, Novotná Z, Valentová O, Žárský V. 2003. Phosphatidic acid produced by phospholipase D is required for tobacco pollen tube growth. *Planta* **217**: 122–130.

Potocký M, Pleskot R, Pejchar P, Vitale N, Kost B, Žárský V. 2014. Live-cell imaging of phosphatidic acid dynamics in pollen tubes visualized by Spo20p-derived biosensor. *New Phytologist* **203**: 483–494.

Read SM, Clarke AE, Bacic A. 1993. Stimulation of growth of cultured *Nicotiana tabacum* W 38 pollen tubes by poly(ethylene glycol) and Cu$_{(II)}$ salts. *Protoplasma* **177**: 1–14.

Röckel N, Wolf S, Kost B, Rausch T, Greiner S. 2008. Elaborate spatial patterning of cell-wall PME and PMEI at the pollen tube tip involves PMEI endocytosis, and reflects the distribution of esterified and de-esterified pectins. *The Plant Journal* **53**: 133–143.

Rotsch AH, Kopka J, Feussner I, Ischebeck T. 2017. Central metabolite and sterol profiling divides tobacco male gametophyte development and pollen tube growth into eight metabolic phases. *The Plant Journal* **92**: 129–146.

Ruelland E, Cantrel C, Gawer M, Kader J-C, Zachowski A. 2002. Activation of phospholipases C and D is an early response to a cold exposure in Arabidopsis suspension cells. *Plant Physiology* **130**: 999–1007.

Sanjuán MA, Jones DR, Izquierdo M, Mérida I. 2001. Role of diacylglycerol kinase α in the attenuation of receptor signaling. *The Journal of Cell Biology* **153**: 207–220.

Scheible N, McCubbin A. 2019. Signaling in pollen tube growth: beyond the tip of the polarity iceberg. *Plants* **8**: 156.

Scholz P, Anstatt J, Krawczyk HE, Ischebeck T. 2020. Signalling pinpointed to the tip: the complex regulatory network that allows pollen tube growth. *Plants* **9**: 1098.

Sekereš J, Pejchar P, Šantrůček J, Vukašinović N, Žárský V, Potocký M. 2017. Analysis of exocyst subunit EXO70 family reveals distinct membrane polar domains in tobacco pollen tubes. *Plant Physiology* **173**: 1659–1675.

Sessions A, Burke E, Presting G, Aux G, McElver J, Patton D, Dietrich B, Ho P, Bacwaden J, Ko C et al. 2002. A high-throughput Arabidopsis reverse genetics system. *Plant Cell* **14**: 2985–2994.

Simon MLA, Platre MP, Marquès-Bueno MM, Armengot L, Stanislas T, Bayle V, Caillaud M-C, Jaillais Y. 2016. A PtdIns(4)P-driven electrostatic field controls cell membrane identity and signalling in plants. *Nature Plants* **2**: 16089.

Sousa E, Kost B, Malhó R. 2008. Arabidopsis phosphatidylinositol-4-monophosphate 5-kinase 4 regulates pollen tube growth and polarity by modulating membrane recycling. *Plant Cell* **20**: 3050–3064.

Stenzel I, Ischebeck T, Quint M, Heilmann I. 2012. Variable regions of PI4P 5-kinases direct PtdIns(4,5)P$_2$ toward alternative regulatory functions in tobacco pollen tubes. *Frontiers in Plant Science* **2**: 114.

Stephan O, Cottier S, Fahlén S, Montes-Rodriguez A, Sun J, Eklund DM, Klahre U, Kost B. 2014. RISAP is a TGN-associated RAC5 effector regulating membrane traffic during polar cell growth in tobacco. *Plant Cell* **26**: 4426–4447.

Synek L, Pleskot R, Sekereš J, Serrano N, Vukašinović N, Ortmannová J, Klejchová M, Pejchar P, Batystová K, Gutkowska M et al. 2021. Plasma membrane phospholipid signature recruits the plant exocyst complex via the EXO70A1 subunit. *Proceedings of the National Academy of Sciences, USA* **118**: e2105287118.

Tan W-J, Yang Y-C, Zhou Y, Huang L-P, Xu L, Chen Q-F, Yu L-J, Xiao S. 2018. DIACYLGLYCEROL ACYLTRANSFERASE and DIACYLGLYCEROL KINASE modulate triacylglycerol and phosphatidic acid production in the plant response to freezing stress. *Plant Physiology* **177**: 1303–1318.

TerBush DR, Maurice T, Roth D, Novick P. 1996. The exocyst is a multiprotein complex required for exocytosis in *Saccharomyces cerevisiae*. *EMBO Journal* **15**: 6483–6494.

Testerink C, Munnik T. 2005. Phosphatidic acid: a multifunctional stress signaling lipid in plants. *Trends in Plant Science* **10**: 368–375.

Testerink C, Munnik T. 2011. Molecular, cellular, and physiological responses to phosphatidic acid formation in plants. *Journal of Experimental Botany* **62**: 2349–2361.

Vaz Dias F, Serrazina S, Vitorino M, Marchese D, Heilmann I, Godinho M, Rodrigues M, Malhó R. 2019. A role for diacylglycerol kinase 4 in signalling crosstalk during Arabidopsis pollen tube growth. *New Phytologist* 222: 1434–1446.

Vermeer JEM, van Wijk R, Goedhart J, Geldner N, Chory J, Gadella TWJ, Munnik T. 2017. *In vivo* imaging of diacylglycerol at the cytoplasmic leaflet of plant membranes. *Plant & Cell Physiology* 58: 1196–1207.

Wilson ZA, Morroll SM, Dawson J, Swarup R, Tighe PJ. 2001. The Arabidopsis MALE STERILITY1 (MS1) gene is a transcriptional regulator of male gametogenesis, with homology to the PHD-finger family of transcription factors. *The Plant Journal* 28: 27–39.

Wissing J, Heim S, Wagner KG. 1989. Diacylglycerol kinase from suspension cultured plant cells: purification and properties. *Plant Physiology* 90: 1546–1551.

Wong A, Donaldson L, Portes MT, Eppinger J, Feijó J, Gehring C. 2020. The Arabidopsis diacylglycerol kinase 4 is involved in nitric oxide-dependent pollen tube guidance and fertilization. *Development* 147: dev183715.

Yamamoto E, Domański J, Naughton FB, Best RB, Kalli AC, Stansfeld PJ, Sansom MSP. 2020. Multiple lipid binding sites determine the affinity of PH domains for phosphoinositide-containing membranes. *Science Advances* 6: eaay5736.

Yao H-Y, Xue H-W. 2018. Phosphatidic acid plays key roles regulating plant development and stress responses. *Journal of Integrative Plant Biology* 60: 851–863.

Zerzour R, Kroeger J, Geitmann A. 2009. Polar growth in pollen tubes is associated with spatially confined dynamic changes in cell mechanical properties. *Developmental Biology* 334: 437–446.

Zhao Y, Yan A, Feijó JA, Furutani M, Takenawa T, Hwang I, Fu Y, Yang Z. 2010. Phosphoinositides regulate clathrin-dependent endocytosis at the tip of pollen tubes in Arabidopsis and tobacco. *Plant Cell* 22: 4031–4044.

Zhukovsky MA, Filograna A, Luini A, Corda D, Valente C. 2019. Phosphatidic acid in membrane rearrangements. *FEBS Letters* 593: 2428–2451.

Zonia L, Müller M, Munnik T. 2006. Hydrodynamics and cell volume oscillations in the pollen tube apical region are integral components of the biomechanics of *Nicotiana tabacum* pollen tube growth. *Cell Biochemistry and Biophysics* 46: 209–232.

Supporting Information

Additional Supporting Information may be found online in the Supporting Information section at the end of the article.

Fig. S1 Phylogenetic and transcriptomic analysis of canonical plant diacylglycerol kinases from 20 diverse species.

Fig. S2 Coexpression of clade I NtDGKs with markers for endomembrane compartments.

Fig. S3 Tobacco diacylglycerol kinase isoforms of clade III differ in their charge distribution and plasma membrane localization patterns in pollen tubes.

Fig. S4 Lipid binding properties of clade III NtDGKs.

Fig. S5 Molecular dynamics simulations reveal several membrane binding modes.

Fig. S6 G118A mutation of NtDGK5 probably interferes with ADP/ATP binding.

Fig. S7 Enzyme assays show diacylglycerol kinase activity.

Fig. S8 AtDGK5 and NtDGK isoforms show differences in induced overexpression phenotypes of tobacco pollen tubes.

Fig. S9 *In vivo* assays of Arabidopsis pollen tube growth did not show drastic alterations of pollen tube length in different *dgk* mutants.

Fig. S10 Quantitative analysis of pectin staining by propidium iodide.

Fig. S11 NtDGK5 coexpression with lipid markers in growing pollen tubes.

Methods S1 Phylogenetic analysis of diacylglycerol kinase in Viridiplantae.

Methods S2 Prediction of diacylglycerol kinase domains and protein structure.

Methods S3 Diacylglycerol kinase gene expression analyses.

Methods S4 Molecular dynamics simulation.

Methods S5 Molecular cloning of diacylglycerol kinase constructs.

Methods S6 Immunodetection of lipid strips and Western blot analysis.

Methods S7 Quantitative analyses of micrographs.

Notes S1 Sequences of diacylglycerol kinases used for the phylogenetic analysis.

Table S1 Number of DGK isoforms in each clade based on DGK phylogeny in Viridiplantae.

Table S2 Tobacco DGK isoforms, their accesion numbers and predicted domain structure.

Table S3 List of primers used in this study.

Video S1 Examples of pollen tube growth phenotypes in tobacco overexpressing NtDGK5.

Video S2 Examples of pollen tube swelling tip phenotypes in tobacco overexpressing NtDGK5^{G118A}.

Video S3 Examples of pollen tube arrested growth phenotypes in tobacco overexpressing NtDGK5^{G118A}.

Please note: Wiley Blackwell are not responsible for the content or functionality of any Supporting Information supplied by the authors. Any queries (other than missing material) should be directed to the *New Phytologist* Central Office.

5 Manuscript I: Adaptations of the leaf proteome and lipid droplets in response to pathogen infection and heat stress

The manuscript is being prepared for submission. Supplemental figures and supplemental tables are attached to the main text. Supplemental datasets containing processed proteomics and lipidomics data are available as additionally uploaded files and are included on a data drive in the printed version of this thesis. Supplemental datasets will be available online after publication.

Author contribution:

Patricia Scholz performed stress treatments, extraction of neutral lipids from Arabidopsis leaves, and preparation of total protein and LD-enriched fraction of Arabidopsis leaves. She planned and performed lipidomics and proteomics analysis with the exception of LC-MS/MS measurements. She processed the data and carried out statistical analysis. She cloned the expression vectors of candidate proteins presented in figures 7 and S9. She carried out infection assays and analysed the results.

Patricia Scholz wrote the first draft of the manuscript, designed the figures and assembled the supplemental data.

Adaptations of the leaf proteome and lipid droplets in response to pathogen infection and heat stress

Patricia Scholz [1], Nathan M. Doner [2], Cornelia Herrfurth [1,3], Magdiel Sheng Satha Lim [4], Katharina Blersch [4], Kerstin Schmitt [5,6], Oliver Valerius [5,6], John Shanklin [7], Ivo Feussner [1,3,6], Gerhard H. Braus [5,6], Robert T. Mullen[2], Till Ischebeck [4,6,*]

1 Department of Plant Biochemistry, Albrecht-von-Haller-Institute for Plant Sciences, University of Göttingen, Göttingen 37077, Germany

2 Department of Molecular and Cellular Biology, University of Guelph, Guelph, ON N1G 2W1, Canada

3 Service Unit for Metabolomics and Lipidomics, Göttingen Center for Molecular Biosciences (GZMB), University of Göttingen, Göttingen 37077, Germany

4 Institute of Plant Biology and Biotechnology (IBBP), University of Münster, Green Biotechnology, Münster 48143, Germany

5 Institute for Microbiology and Genetics and Service Unit LCMS Protein Analytics, Department for Molecular Microbiology and Genetics, University of Göttingen, Göttingen 37077, Germany

6 Göttingen Center for Molecular Biosciences (GZMB), University of Göttingen, Göttingen 37077, Germany

7 Department of Biology, Brookhaven National Laboratory, Upton, NY 11973, USA

*Author for correspondence: Till Ischebeck, Email: till.ischebeck@uni-muenster.de

Abstract

Plants must cope with a variety of different stressors during their life cycle and their adaptations to these environmental influences involves all cellular organelles. Among them, comparatively little is known about the contribution of cytosolic lipid droplets (LDs) and their core of neutral lipids and associated surface proteins to the rewiring of cellular processes in response to stress. Here, we analysed the changes that occur in the neutral lipid lipidome and proteome of Arabidopsis leaves after pathogen infections with *Botrytis cinerea* and *Pseudomonas syringae*, and heat stress. Analyses were carried out in wild type plants and an oil-rich double mutant that allowed an allied study of the LD proteome in challenged leaves. Using liquid chromatography-tandem mass spectrometry-based methods, we show that a hyperaccumulation of the primary LD core component triacylglycerol is a general response to stress and that acyl chains are remodelled during cellular adaptation. Likewise, comparative analysis of the LD protein composition in stress-treated leaves highlighted the remodelling of the LD proteome as part of the general stress response. We further identified two new LD-associated proteins whose localisation to LDs in leaves was confirmed by confocal microscopy of fluorescent protein fusions. These and other results highlight LDs as dynamic contributors to the cellular adaptation processes that underlie how plants respond to environmental stress.

Introduction

Plants naturally encounter a plethora of abiotic and biotic threats during their life cycle. Consequently, plant cells have to be highly adaptive at the transcriptomic, proteomic and metabolic level, which requires the interplay of different signalling pathways and organelles (Kumar et al., 2016; Zhu, 2016; Crawford et al., 2018). This is highlighted by the retrograde signalling between mitochondria or chloroplasts and the nucleus (Ng et al., 2014; Berkowitz et al., 2016; Leister et al., 2017), or the synthesis of the plant stress-responsive jasmonates whose biosynthetic pathways are distributed across chloroplasts, peroxisomes, and the cytosol (Bell et al., 1995; Staswick and Tiryaki, 2004; Theodoulou et al., 2005). Another pertinent example of this cellular interplay is lipid remodelling, where fatty acid (FA) synthesis and lipid turnover in the plastids, and lipid turnover in the endomembrane system act together to modify cellular membrane composition in response to stress. More specifically, acyl chains removed from the membrane lipid pool appear to be transferred into triacylglycerols (TAGs) stored in cytosolic lipid droplets (LDs). In heat-stressed seedlings for example, cytosolic TAGs with a high degree of unsaturation accumulate and the respective polyunsaturated acyl chains originate, at least in part, from chloroplasts (Mueller et al., 2015; Mueller et al., 2017). Similarly, in tobacco pollen tubes, heat stress leads to an increase in the proportion of saturated acyl chains in the membrane lipids phosphatidylcholine (PC) and phosphatidylethanolamine (PE), at the expense of mono- and polyunsaturated acyl chains, while total TAG levels increase (Krawczyk et al., 2022a). Similar effects have been observed in heat-stressed leaves of Arabidopsis (Higashi et al., 2015) and accumulation of TAG is linked to a number of stresses, e.g., freezing stress (Moellering et al., 2010), drought and cold treatment (Tarazona et al., 2015) or pathogen infection (Schieferle et al., 2021), which implies LDs are important organelles in the plant stress response.

LDs are cytosolic structures that consist of a hydrophobic core of neutral lipids, primarily TAGs and sterol esters (SEs), delimited by a monolayer of phospholipids. Embedded into and/or associated with the surface of the monolayer are various proteins that convey to the LDs different functions depending on the cellular context (Brocard et al., 2017; Ischebeck et al., 2020; Kretzschmar et al., 2020). Most studies on LDs have been carried out with tissues/organs where they are highly abundant, including seeds, seedlings and pollen (Vance and Huang, 1987; Tzen et al., 1993; Chen et al., 1999; Lin et al., 2002; Hsieh and Huang, 2004; Kretzschmar et al., 2020). Indeed, the best described LD proteomes are those in seeds, where LDs-stored neutral lipids can be up to 40% of the dry weight (Baud et al., 2002), and where members of the oleosin (OLE), caleosin (CLO) and steroleosin (also called hydroxysteroid dehydrogenase [HSD]) protein families dominate (Jolivet et al., 2004; Katavic et al., 2006; Jolivet et al., 2009; Kretzschmar et al., 2018; Kretzschmar et al., 2020).

LDs function in seeds predominantly as storage organelles and oleosins are considered to function primarily in preventing LDs coalescence (Cummins et al., 1993; Murphy, 1993). However, during seedling establishment, the stored neutral lipids must be metabolized in order to support seedling growth (Germain et al., 2001; Eastmond, 2006) and LD function(s) changes. Concomitantly, the LD proteome undergoes a transformation as the seed LD proteins are degraded and other LD proteins confer new functionalities to the LDs (Deruyffelaere et al., 2018; Kretzschmar et al., 2018; Kretzschmar et al., 2020). Among the latter, the LD-associated

protein (LDAP) family, the LDAP-INTERACTING PROTEIN (LDIP), and seipin proteins, which are actually endoplasmic reticulum (ER) membrane proteins that are situated at ER-LD junctions, are crucial for LD biogenesis (Cai et al., 2015; Taurino et al., 2018; Pyc et al., 2021). Additional LD proteins that function in seedlings have been also described, including those with enzyme activities involved in the synthesis or breakdown of primary and secondary metabolites (Corey et al., 1993; Diener et al., 2000; Shimada et al., 2014; Müller and Ischebeck, 2018).

Environmental changes also influence LD-related processes. For example, in Arabidopsis leaves, the expression of genes related to TAG degradation and synthesis correlated strongly with altered temperature conditions (Szymanski et al., 2014). Furthermore, in cold-stressed wheat plants, an upregulation in the expression of genes coding for homologs to DIACYLGLYCEROL ACYL-TRANSFERASE 1, oleosins, caleosins and steroleosins has been reported (Li et al., 2015). LD abundance in Arabidopsis leaves increases in reaction to drought, cold or heat stress (Gidda et al., 2016; Doner et al., 2021). Correspondingly, Arabidopsis plants that over-accumulate LDs, such as in Arabidopsis transgenic lines overexpressing the genes coding for LDAPs (Gidda et al., 2016), are also more drought-tolerant (Kim et al., 2016). This further suggests that LDs play a role in stress tolerance. Loss-of-function Arabidopsis mutants of the caleosins CLO3 and CLO4 also hint at a role of these proteins and LDs in drought responses. That is, the *clo4* mutant was more drought-tolerant (Kim et al., 2011), while the *clo3* mutant was more susceptible to drought (Aubert et al., 2010). While the precise role of these two caleosins in drought responses remains unclear, a connection to ABA-signalling has been suggested in both cases (Aubert et al., 2010; Kim et al., 2011).

On the other hand, a role of CLO3 in the biotic stress response has been attributed to its peroxygenase function (Shimada et al., 2014). After infection of Arabidopsis leaves with the fungal pathogen *Colletotrichum higginsianum*, CLO3 and α-DIOXYGENASE 1 (α-DOX1) accumulate at LDs in the perilesional area of the infection. There, they are likely to act in tandem to convert α-linolenic acid, as stored in the neutral lipids of LDs, into 2-hydroxy-octadecatrienoic acid (2-HOT), which then acts to impair fungal spread (Shimada et al., 2014). Overall, CLO3 is probably the best characterised LD protein in non-seed tissues with different studies focusing on its enzymatic activity, ABA-signalling and stress responses (Partridge and Murphy, 2009; Aubert et al., 2010; Blée et al., 2014).

Despite the growing knowledge on selected proteins and their roles at LDs in vegetative plant organs, the relatively low abundance of LDs in these tissues has generally been a technical challenge for lipidomic or proteomic studies. Nevertheless, successful studies have been carried out on the leaf LD proteome of senescing and drought-stress leaves, as well as leaves infected with *Pseudomonas syringae* pv. *tomato* (*Pto*) DC3000 *avrRpm1* (Brocard et al., 2017; Fernández-Santos et al., 2020; Doner et al., 2021), which have resulted in the identification of several novel LD proteins. Among them was the protein EARLY RESPONSIVE TO DEHYDRATION 7 (ERD7), which has been implicated in the Arabidopsis cold stress response (Barajas-Lopez et al., 2021; Doner et al., 2021). Additionally, two glycerol-3-phosphate 2-acyltransferase (GPAT) proteins, GPAT4 and GPAT8, were identified that catalyse the transfer of an acyl chain from acyl-CoA to glycerol 3-phosphate to produce lysophosphatidic acids (Jayawardhane et al., 2018). Further, the enzyme PHYTOALEXIN DEFICIENT 3, which reduces dihydrocamalexic acid

to camalexin (Zhou et al., 1999; Schuhegger et al., 2006), was observed to co-localise to LDs, but only after infection with *Pto* DC3000 *avrRpm1* (Fernández-Santos et al., 2020).

Despite these advances, it remains unclear what the dynamics of the LD proteome are during the plant stress response. Leaves are constantly exposed to a vast array of environmental conditions, so it seems likely that the composition of leaf LDs is highly flexible in order to react to these external signals. Here, we assessed the changes that leaf LDs undergo when subjected to biotic and abiotic stresses. Arabidopsis plants were infected with two different pathogens and exposed to heat stress and subsequently their leaf proteome and neutral lipid lipidome were analysed. Comparisons with control treatments allowed us to observe the alterations induced by the three different treatments. In addition, proteomic analysis of LD-enriched fractions isolated from leaves subjected to the various treatments enabled us to survey specifically the dynamics of the LD proteome and, in doing so, identify two novel proteins that localised to LDs.

Results

Lipidomics of heat stress and pathogen infected plants reveals differential changes in neutral lipid classes

Among the first indications for the involvement of LDs in the stress response of leaves were reports on TAG accumulation and elevated numbers of LDs induced by abiotic and biotic stresses (Gidda et al., 2016; Higashi and Saito, 2019; Doner et al., 2021; Schieferle et al., 2021). To confirm these previous observations and determine if neutral lipid levels were also increased by our treatments, we analysed changes in the neutral lipid lipidome, i.e., TAGs and SEs, in infected or heat-stressed plants (Suppl. Datasets S1, S2). Notably, we included SEs in this analysis, since they also form LDs in leaves (Shimada et al., 2019), but, compared to TAG, relatively less is known in terms of their changes, if any, upon stress. To compare and contrast the plant response to an abiotic stressor, a fungal pathogen, and a bacterial pathogen, we submitted Arabidopsis Col-0 plants to heat stress (consisting of 24 hours at 37°C) or spray-infected them with either *Botrytis cinerea* or *Pseudomonas syringae* pv. *tomato* DC3000 *ΔavrPto/ΔavrPtoB* (hereafter: *Pseudomonas*). Subsequently, neutral lipids from stressed and control-treated plants were extracted and lipidomic analysis of TAGs and SEs carried out.

Overall, the abundance of SEs was different in infected or heat-stressed plants, whereby they decreased in heat-stressed plants and a trend towards elevated SE levels was observed after *Pseudomonas* and *B. cinerea* infection (Figure 1A). Lipid remodelling in reaction to stress often includes the exchange of acyl chains, which is most prominently described for heat stress (Higashi and Saito, 2019). Therefore, we calculated the average number of double bonds in the acyl chains of SEs.
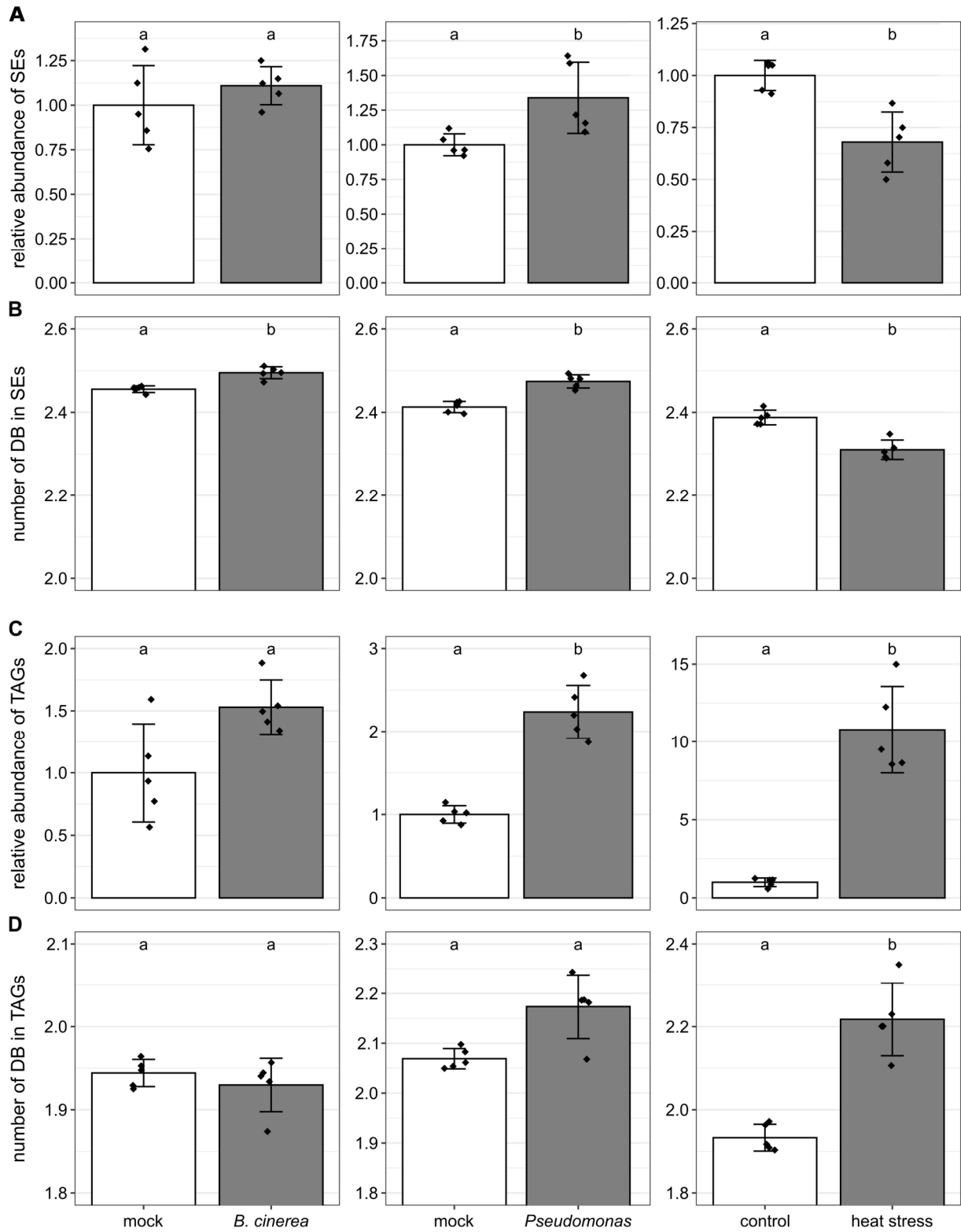
Figure 1: Changes in total abundance and saturation of neutral lipids in leaves after different stress treatments. Arabidopsis plants were infected with *Botrytis cinerea* (*B. cinerea*), *Pseudomonas syringae* pv. *tomato* DC3000 *ΔavrPto/ΔavrPtoB* (*Pseudomonas*), or kept for 24 hours at 37 °C (heat stress). After stress treatments, leaves were harvested and sterol esters (SEs) and triacylglycerols (TAGs) analysed by UPLC-nanoESI-MS/MS. Signal intensities were quantified and normalised to an internal standard. Values of all detected SE and TAG species were then added up and for each stress treatment the combined sum was normalised to the respective value of the control treatment (A, C). Furthermore, the saturation numbers i.e. the average number of double bonds (DB) in the acyl chains of SEs and TAGs were calculated for all treatments (B, D). Statistical comparisons of treatments to their respective control were calculated with the Wilcoxon-Mann-Whitney-Test, using Holm-Bonferroni correction for multiple comparisons. Values are shown as mean ± standard deviation. Different letters indicate significant differences with $p < 0.05$. n = 5 biological replicates for all treatments.

Values between two and three were observed, as polyunsaturated acyl chains dominated among the detected SE species (Figure 1B). The saturation number in SEs slightly, but significantly, increased after infection, although decreased in reaction to heat treatment. The most dominant sterol species in all conditions were sitosterol, campesterol and stigmasterol that amounted to 80%, 10% and 7%, respectively. Alterations upon treatment were most visible in sitosteryl esters, whose proportion decreased slightly after infection and increased after heat treatment (Suppl. Figure S1, Suppl. Dataset S3).

All three treatments caused an increase in TAG abundance (Figure 1C). Heat led to a relative 10-fold increase of TAG levels, whereas infection with *B. cinerea* and *Pseudomonas* resulted in a 1.5-fold and a 2-fold increase, respectively. Interestingly, the detected MS/MS signals of all TAG species together in the mock-treated plants of both infection experiments is approximately two times higher than in the non-treated control plants of the heat stress dataset. This suggests that the conditions of the mock-spray infection itself are an environmental stressor to influence TAG synthesis. Nevertheless, heat stress caused TAG levels to increase to an abundance that was not detected in either pathogen infection (Suppl. Figure S2). Similar to SEs, we calculated the saturation numbers of acyl chains in TAG, which reached values of approximately 2 (Figure 1D). Hence, polyunsaturated acyl chains also dominated among TAGs, especially the 18:2 and 18:3 species (Suppl. Dataset S2). Saturation numbers, i.e., the number of double bonds in TAGs, increased after infection with *Pseudomonas* and after heat treatment, hinting that polyunsaturated acyl chains may be channelled into TAGs in reaction to these stresses (Figure 1D). This is also supported by the increase in the TAG species 54:9, which doubled its relative proportion in the TAG pool upon heat treatment (Suppl. Figure S3, Suppl. Dataset S4). Similar changes could be seen for the TAG species 54:8, while the two TAG species 52:5 and 52:6, which contain acyl chain with 16 carbon atoms, were depleted. Changes in TAG species composition after pathogen infection were less pronounced and differed somewhat. After *Pseudomonas* infection, the fraction of both 54:8 and 54:9 increased, while after exposure to *B. cinerea* the relative amounts of 54:8 decreased and the proportion of TAG species with at least one acyl chain with 16 carbons increased.

For later proteomic studies, we used the double mutant *tgd1-1 sdp1-4* that has increased TAG levels stored in LDs (Fan et al., 2014) thereby making it easier to isolate LDs. TGD1 was originally identified as a transporter that helps to import membrane lipid precursors from the ER into plastids (Xu et al., 2003) and the *tgd1-1* mutant was later also described to accumulate TAGs in cytosolic LDs (Xu et al., 2005). SDP1, on the other hand, is a lipase that initiates storage lipid breakdown during germination (Eastmond, 2006) and also hydrolyses TAG in vegetative tissues, limiting its accumulation (Kelly et al., 2013). Disruption of SDP1 function in the *tgd1-1* background increases TAG levels from 0.6% of leaf dry weight in the *tgd1-1* mutant and even less in the wild type to approximately 8% in the *tgd1-1 sdp1-4* double mutant. Concomitantly, there were more and larger LDs in the leaves of *tgd1-1 sdp1-4* (Fan et al., 2014).
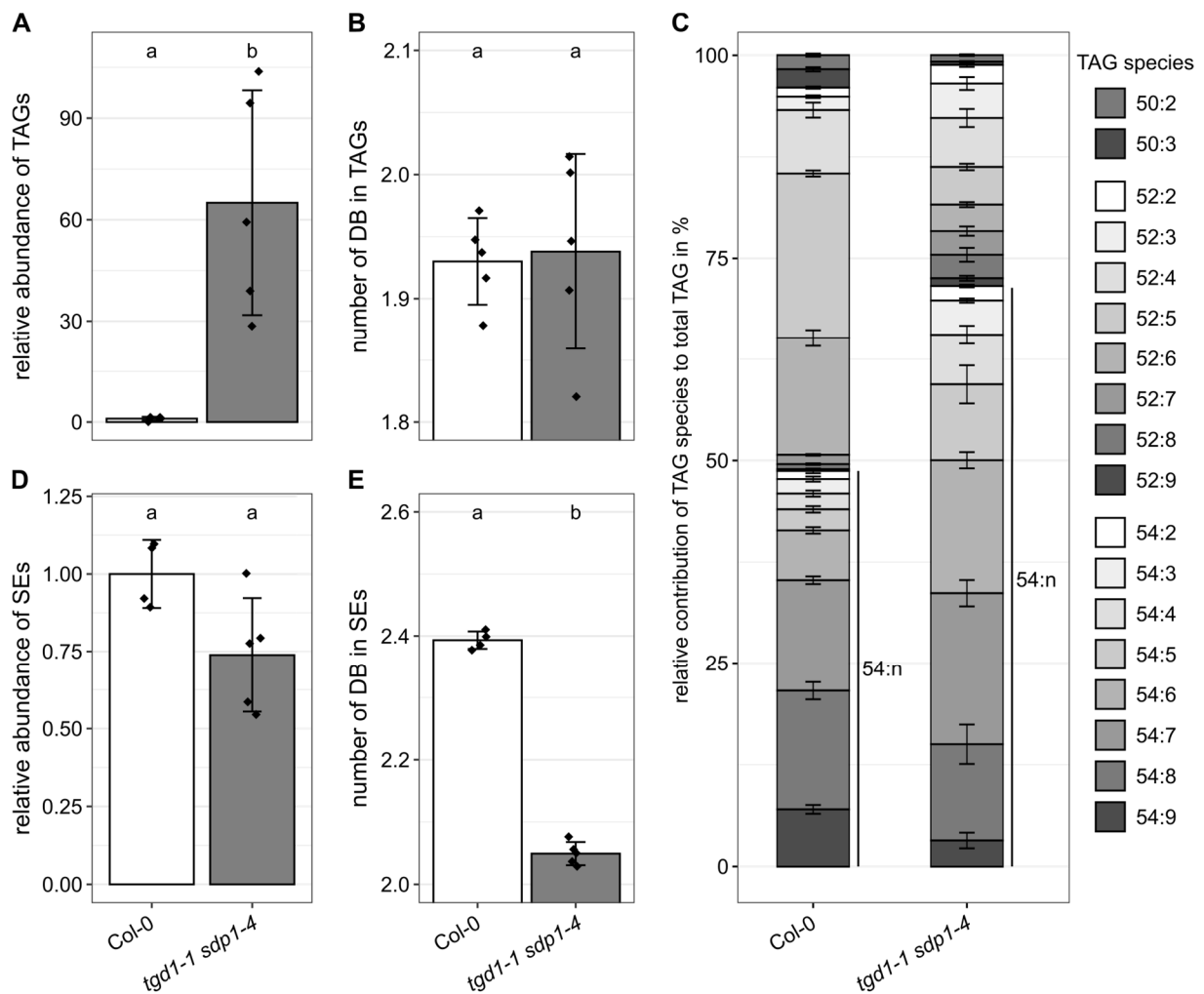
Figure 2: Neutral lipid profile of the oil-rich mutant *tgd1-1 sdp1-4*. Triacylglycerols (TAGs) and sterol esters (SEs) were determined in leaves of Arabidopsis Col-0 and *tgd1-1 sdp1-4*. Signal intensities were quantified, corrected against the internal standard and all species of TAGs and SEs were added up to obtain respective overall signal intensities. The combined sum was then normalised to TAG (A) and SE (D) values in Col-0. The average number of double bonds (DB) in the acyl chains of both TAGs and SEs was calculated and is shown in (B) and (E), respectively. Furthermore, TAG species composition was analysed and relative proportions are shown in (C). Stacked bar plots follow TAG species composition from top to bottom as indicated to the right of the plot, i.e. with the 50:2 TAG species at the top and the 54:9 TAG species at the bottom. The percentage of TAG species with 54 carbon atoms is indicated by the "54:n"-labelled lines to the right of the bars. Statistical analysis in (A), (B), (D) and (E) was done using the Wilcoxon-Mann-Whitney-Test with Holm-Bonferroni correction. Values are shown as mean ± standard deviation. Different letters indicate significant differences with $p < 0.05$. n ≥ 4 biological replicates for both lines.

We could confirm the increase of TAG levels in leaves of the *tgd1-1 sdp1-4* double mutant (Figure 2A). However, unlike in the previous characterisation of *tgd1-1 sdp1-4,* we did not observe increased desaturation levels of the acyl chains (Figure 2B). Based on the distribution of TAG species, there are increased levels of acyl chains with 18 carbons: the proportion of TAGs with 54 carbons increased from 50% to 70%. Interestingly though, the relative proportions of 54:8 and 54:9 TAG species decreased (Figure 2C). In contrast to TAGs, SE levels were depleted in *tgd1-1 sdp1-4*, to 75% of wild type levels (Figure 2D). Regarding the composition of SE components, we observed a decreased average number of double bonds in the SE acyl chains (Figure 2E). However, there were no significant differences between the wild type and the double mutant in terms of sterol species (Suppl. Figure S4).

The leaf proteome changes in response to biotic and heat stress

In addition to changes in storage lipids, it is likely that the cellular proteome, including the LD proteome, undergoes changes during stress. To test this premise, we extracted the total proteome from wild type and *tgd1-1 sdp1-4* leaves subject to either heat stress or pathogen (*B. cinerea* and *Pseudomonas*) infection, or from the respective control treatments. Furthermore, LD-enriched fractions were isolated from leaves from the wild type and the double mutant line under all conditions. For all samples, peptides were analysed by liquid chromatography-tandem mass spectrometry (LC-MS/MS) and MS raw data was processed with the MaxQuant software (Cox and Mann, 2008) to identify and quantify the original proteins. Two algorithms were used for quantification: the intensity-based absolute quantification (iBAQ) and the label-free quantification (LFQ) algorithm (Cox and Mann, 2008; Schwanhäusser et al., 2011; Cox et al., 2014). Protein quantification values were then normalised as per mille of the total combined intensity in each sample, resulting in relative iBAQ (riBAQ) and relative LFQ (rLFQ) values (Suppl. Dataset S5). rLFQ values were used for comparisons of samples with similar protein compositions, i.e., total extract (TE) samples of different conditions or genotypes. riBAQ values were used for calculations of enrichment factors, when sample composition differed strongly between LD-enriched fractions and TE fractions. Overall, this dataset allowed us to compare (i) the effects of the different stresses on the total proteome in the wild type and double mutant line, (ii) differences between the wild type and the double mutant, (iii) protein abundancies in total cellular fractions and LD fractions to identify previously unknown LD-associated proteins (iv) changes of the LD proteome under stress in the double mutant.

Based on rLFQ values, we compared changes of protein abundance in Col-0 leaves and calculated statistical significance of changes between the different treatments and their respective controls (Suppl. Datasets S6-S8). The results were visualised as volcano plots and proteins whose abundance was changed at least 1.5-fold between conditions with $p < 0.05$ were selected for further analysis (Figure 3). Initially, we checked if the stress treatments had been successful in altering the abundance of proteins previously described to be connected with the individual stresses. For instance, for *B. cinerea* infection, the phospholipase PLA2A was only detected after infection in our proteomic dataset (Suppl. Dataset S5), which is consistent with a previous study that showed its accumulation after infection and dependent on jasmonic acid (JA) signalling (La Camera et al., 2005).
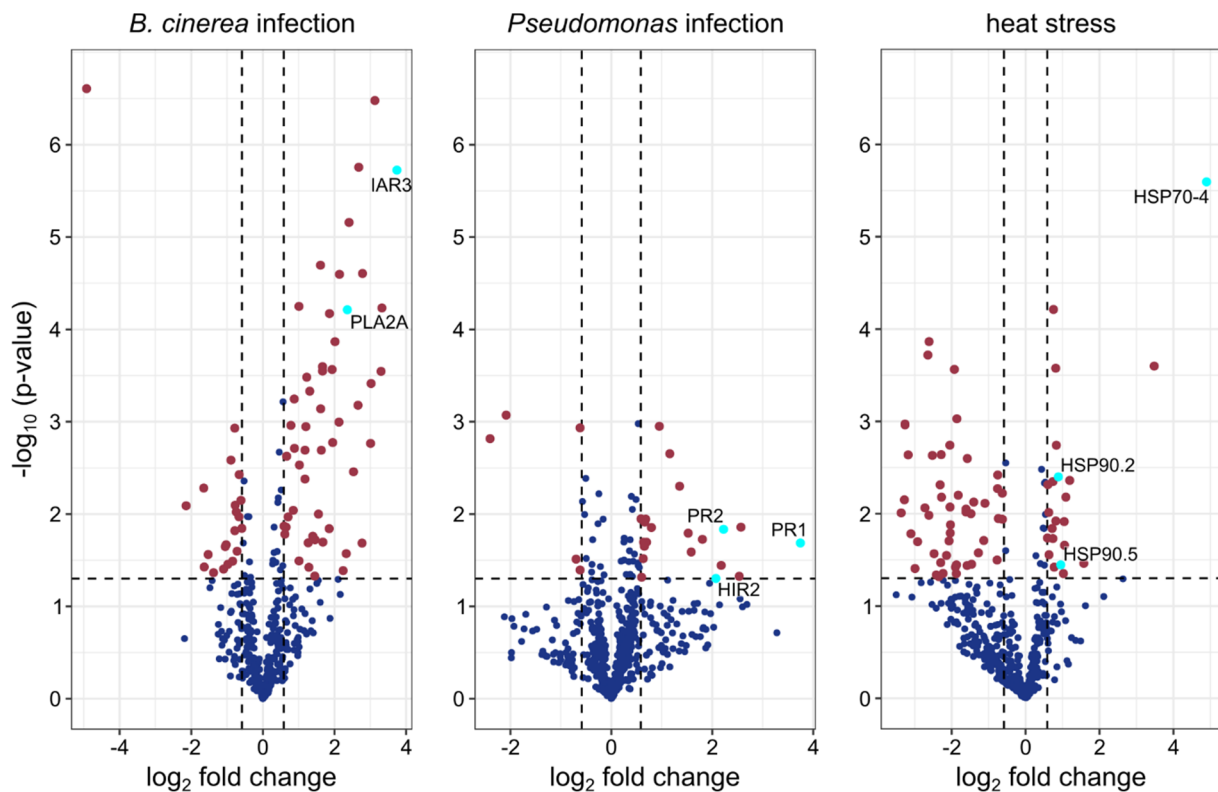
Figure 3: Alterations of total cellular proteins of Arabidopsis leaves subjected to different stress treatments. Arabidopsis plants were infected with *Botrytis cinerea* (*B. cinerea*), *Pseudomonas syringae* pv. *tomato* DC3000 *ΔavrPto/ΔavrPtoB* (*Pseudomonas*) or heat stressed for 24 hours at 37 °C. Subsequently, total protein fractions of leaves were prepared and the proteome analysed by liquid chromatography tandem mass spectrometry (LC-MS/MS). Protein abundance was quantified in MaxQuant with the LFQ algorithm. Protein abundances of individual proteins were normalised to the respective values of the control treatment and the resulting ratio was $\log_2$-transformed. Statistical significance of the $\log_2$ fold change was calculated by Student's t-test in the software Perseus 1.6.2.2. The constructed volcano plots indicate proteins that are significantly enriched (upper right) or depleted (upper left) in reaction to the individual stress treatments. For each infection, only proteins detected in all replicates of either mock-treated or infected plants were included in the analysis. For heat stress, proteins present in at least four replicates of either heat-stressed or control plants were analysed. Vertical lines indicate 1.5-fold enrichment or depletion, while the horizontal line indicates a significance of p = 0.05. Proteins further mentioned in the text are labeled and highlighted in cyan. n ≥ 3 biological replicates for each individual treatment.

JA and its bioactive form JA-isoleucine (JA-Ile) accumulate in reaction to *B. cinerea* infection (Aubert et al., 2015) and another protein that we only detected upon treatment with *B. cinerea* is the enzyme IAA-ALANINE RESISTANT 3 (IAR3; Suppl. Dataset S5), which acts on JA-Ile (Widemann et al., 2013). Interestingly, IAR3 hydrolyses the amide bond of JA-Ile thus reducing the bioactive signalling form and PLA2A was described to negatively influence plant resistance to *B. cinerea* (La Camera et al., 2005; Widemann et al., 2013). Both proteins' accumulation might therefore be a result of fungal interference rather than of plant defence reactions. Infection with *Pseudomonas* led to an expected increased protein abundance of proteins strongly connected to plant defence reactions. Among the most increased proteins after *Pseudomonas* infection were the two pathogenesis-related (PR) proteins PR1 and PR2 (Suppl. Dataset S7), both of which are known to be upregulated as part of systemic acquired resistance to pathogen infection (Uknes et al., 1993; Fu and Dong, 2013). A third PR-protein, PR5, also more than doubled in abundance (Suppl. Dataset S7). Another defence-related protein that increased upon *Pseudomonas* treatment was HYPERSENSITIVE INDUCED REACTION 2 (HIR2; Suppl. Dataset S7), which organises immune receptors at the plasma membrane into nanoclusters (Qi et al., 2011; Qi and Katagiri, 2012). Finally, in response to heat treatment, the heat shock protein HSP70-4 showed the most pronounced increase in protein abundance (Figure 3), consistent with its role in thermotolerance against long term heat stress (Wang et al., 2021). Further heat shock proteins like HSP90.2 and HSP90.5 also increased in abundance (Figure 3, Suppl. Dataset S8), indicating that the plants were able to sense and respond to the applied temperature conditions.

In order to determine if whole clusters of interacting and/or functionally-related proteins are changed under stress, we employed the web tool at the STRING v11.5 database to assess the differentially abundant proteins for each treatment with at least a 1.5 fold change and *p* < 0.05. Proteins with decreased or increased abundance were evaluated separately and only interactions of high confidence were analysed. In plants stressed with *B. cinerea* and heat, chloroplastic and photosynthetic proteins dominated amongst proteins with decreased abundance (Suppl. Figure S5), although it is unclear if this is a direct effect or indirectly observed due to altered behaviour in protein isolation. Among the proteins with decreased abundance after *B. cinerea* infection were different members of photosystem I, II and the light-harvesting complexes (Suppl. Figure S5A). Similarly, after heat treatment, proteins of photosystem II were among the decreased proteins and additionally proteins of the chloroplastic electron transport chain and subunits of RuBisCO (Suppl. Figure S5B).

The upregulated proteins of the different treatments did not form as extensive clusters as the downregulated ones (Suppl. Figure S5). Among the most extensive interaction networks was the one formed by heat shock proteins and chaperone proteins upon heat stress with the functional role of assisting protein folding (Suppl. Figure S5E). Other protein clusters mostly contained two or three proteins, nevertheless, also in these small clusters or individual proteins there were interesting trends to observe especially regarding metabolic adjustments in reaction to the applied stress treatments. For example, heat treatment induced the accumulation of two catalases, CAT2 and CAT3, likely to counteract heat-induced oxidative stress (Suppl. Figure S5E; Ono et al., 2021) and both infections caused the accumulation of glutathione S-transferase proteins (Suppl. Figures S5D, S5F). More specific for *B. cinerea*, metabolic adaptation included the upregulation of proteins involved in the biosynthesis of

tryptophan and the detoxification of cyanide as for example TRYPTOPHAN SYNTHASE ALPHA CHAIN, TRYPTOPHAN SYNTHASE BETA-SUBUNIT 1, ß-CYANOALANINE SYNTHASE C1 and NITRILASE 4 (Yamaguchi et al., 2000; Piotrowski et al., 2001).

The *tgd1-1 sdp1-4* double mutant displays alterations in the leaf proteome separate of lipid metabolism

When we examined the changes in the proteome of the oil-rich double mutant *tgd1-1 sdp1-4* after the different stress treatments, we observed some common trends with the wild type. This included for example a decrease in plastidial and photosynthetic proteins after in reaction to stress and also the treatment-dependent accumulation of proteins described in the previous section (Suppl. Datasets S9-S11). However, when proteins were selected with the same criteria as for the wild type, less than 50% of proteins were shared amongst the up- or downregulated proteins of each treatment. As these differences pointed to underlying changes in the proteome of the double mutant, we decided to compare the proteome of *tgd1-1 sdp1-4* to the wild type under non-stressed conditions (Figure 4A, Suppl. Dataset S12). Using the same selection criteria as for the analysis of treatment-induced changes (enrichment or depletion of at least 1.5-fold, $p < 0.05$), 253 proteins were selected for further analysis.

When analysed with the STRING webtool, two protein interaction networks among the downregulated proteins were most striking (Suppl. Figure S6). Several components of the light harvesting complexes (i.a. LHCA3, LHCB3) and the photosynthetic electron transfer chain (i.a. PSBA, PSBE, PETA, PETD, PSAE-2) were decreased in the double mutant. The same was true for several ribosomal proteins of both cytosolic and plastidial ribosomes. Among the upregulated proteins in the double mutant, enzymes of various metabolic pathways could be found, e.g. four glutamine synthetases (GLN1;1, GLN1;2, GLN1;3, GS2) and three proteins of the glycine cleavage system (GLDT, GLDP1, GDC-H1). The glycine cleavage system (also called glycine decarboxylase) and the glutamine synthetase GS2 are part of the photorespiration pathway and in PGLP1 and GGAT1 further enzymes of photorespiration display increased abundance in *tgd1-1 sdp1-4* (Bauwe et al., 2010).

After comparing the double mutant to the wild type proteome under non-stressed condition, we analysed the differences between both lines for different treatments and looked for common proteins that were changed between *tgd1-1 sdp1-4* and the wild type across different experiments. Taking all treatments together, there are seven datasets for the comparison of the wild type and *tgd1-1 sdp1-4*: one dataset of non-stressed plants, and three datasets each for the different stresses and their respective control or mock treatments. In these combined datasets, two proteins were found to accumulate in the double mutant in all but one condition. Firstly, the glutathione S-transferase GSTF7, which also increased in abundance after infection with *B. cinerea* or *Pseudomonas* (Suppl. Datasets S6, S7). Secondly, the PR protein PR2 that was previously seen to accumulate after *Pseudomonas* infection (Figure 3). PR2 forms together with PR1 and PR5 part of the response to salicylic acid (SA) such that their gene expression is used as readout for systemic acquired resistance (Uknes et al., 1993; Bowling et al., 1994; Fu and Dong, 2013).
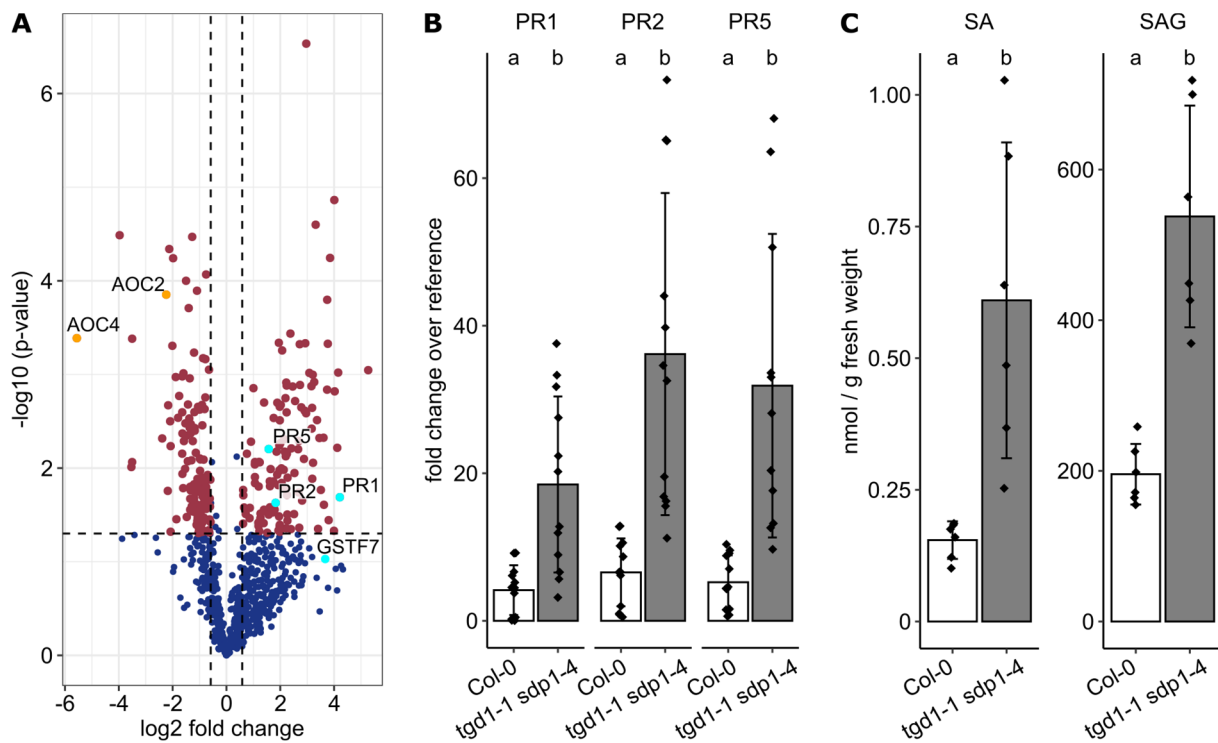
Figure 4: Differences in the proteome of Arabidopsis Col-0 compared to the double mutant *tgd1-1 sdp1-4*. The proteome of Col-0 and *tgd1-1 sdp1-4* in total protein fractions of non-stressed plants was determined. Changes in protein abundance are visualised in a volcano plot, displaying proteins accumulating (upper right) or depleted (upper left) in the double mutant (A). Proteins were only included in the analysis if they were present in all replicate samples. Vertical lines indicate 1.5-fold enrichment or depletion, and the horizontal line indicates a *p*-value of 0.05. Proteins further discussed in the text are marked: the glutathione S-transferase GSTF7 and the PR proteins PR1, PR2 and PR5 accumulate in the mutant (cyan dots), while the allene oxide cyclases AOC2 and AOC4 are depleted (orange dots). *PR* gene expression was further analysed in leaves of Col-0 or *tgd1-1 sdp1-4* and expression levels were calculated relative to the reference gene *AT3G01150* (B). Leaves of both plant lines were also analysed by UPLC-nanoESI-MS/MS for their salicylic acid (SA) and SA glucoside (SAG) content (C). P-values in (A) were calculated by Student's t-test in the Perseus 1.6.2.2 software. Values are shown as mean ± standard deviation in (B) and (C). Statistical analysis in (B) and (C) was carried out with the Wilcoxon-Mann-Whitney-Test, using Holm-Bonferroni correction for multiple comparisons. Statistical differences with *p* < 0.05 are indicated by different letters. n = 3 biological replicates in (A), n = 6 biological replicates in (B) and (C) and for (B), two independent technical replicates of each biological replicate were measured.

Interestingly, PR1 and PR5 are also significantly enriched in non-treated leaves of *tgd1-1 sdp1-4* compared to the wild type and we observed higher protein abundance of PR1, PR2 and PR5 in the double mutant after various treatments (Suppl. Figure S7).The accumulation of these PR proteins seemed to indicate higher basal levels of SA, which reciprocally influences other phytohormone levels. Most prominently, an antagonistic relationship between SA and JA has been described in Arabidopsis that allows a fine tuning of the plant defence response (Spoel et al., 2003; Pieterse et al., 2012). It is therefore interesting to note that two allene oxide cyclase proteins, AOC2 and AOC4, which catalyse the cyclisation step in the biosynthesis of JA, were found to be less abundant in *tgd1-1 sdp1-4* under non-stressed conditions (Figure 4A).

Following up on this possible changes in SA-related signalling, we tested the gene expression of *PR1*, *PR2* and *PR5* in non-stressed leaves of Col-0 and *tgd1-1 sdp1-4* by qPCR and observed increased transcript levels (Figure 4B). Finally, we also measured phytohormone levels in leaves. In line with the observed changes of *PR* gene expression and protein abundance, the base level of SA in non-stressed plants is increased in *tgd1-1 sdp1-4* (Figure 4C). Furthermore, the amount of its glycosylated derivative salicylic acid glucoside (SAG) was increased (Figure 4C). Due to the low amount of JA and JA-derivatives in non-stressed plants, we were not able to determine if their basal concentrations were also affected.

Survey of proteins enriched at leaf LDs reveals new LD proteins

An important aim of this work was to identify proteins so far unknown to localise to LDs in leaves, since our understanding of LD biology in general hinges on the understanding of its associated proteins and their functions. We therefore obtained an enriched LD fraction from leaves of *tgd1-1 sdp1-4* plants and investigated the proteome using quantitative label-free proteomics. First, to evaluate the success of LD enrichment, we combined the riBAQ values of known LD proteins and proteins observed to localise to LDs in this study (Gidda et al., 2016; Brocard et al., 2017; Pyc et al., 2017; Kretzschmar et al., 2018; Fernández-Santos et al., 2020; Kretzschmar et al., 2020; Doner et al., 2021; Ge et al., 2022; Li et al., 2022). This combined abundance of known LD proteins in LD-enriched fractions revealed a strong enrichment (Figure 5), as expected. We then tested which other organelles might co-enrich with LDs. Using the plant proteome data base (PPDB), the abundance of all proteins with an assigned unique subcellular localisation in the PPDB was combined for their respective organelles. The summed protein abundance for different organelles was compared between TE and LD-enriched fractions by calculating the ratio between the two fractions and converting it to $\log_2$-fold change values (Figure 5). The ER and plastoglobuli proteomes were most prominently enriched, which is likely a reflection of LD biogenesis at the ER and the similarities in the density of cytosolic LDs and chloroplastic plastoglobuli. In contrast, the combined abundance of known peroxisomal proteins was strongly depleted in the LD-enriched fractions (Figure 5), despite their related functional roles in fatty acid catabolism and the well-known physical interactions (Scholz et al., 2022). All other subcellular structures were either not strongly enriched or significantly depleted in the LD-enriched fractions (Figure 5).
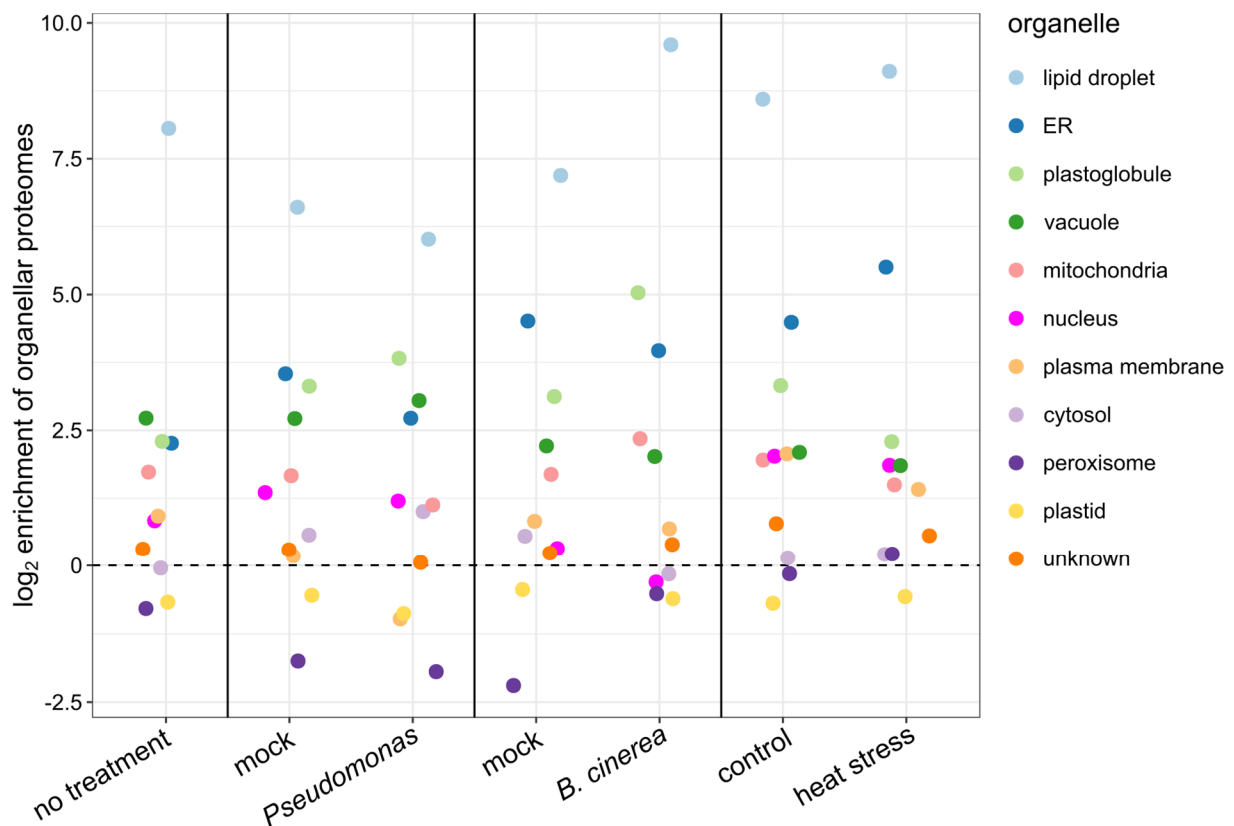
Figure 5: Enrichment of different organelle proteomes in the LD-enriched fraction. Arabidopsis *tgd1-1 sdp1-4* was subjected to the indicated treatments. Subsequently, LDs were enriched from leaves and the proteomes of this LD-enriched fraction and corresponding total protein fractions were determined by LC-MS/MS. To analyse enrichments of different subcellular organelles, proteins were assigned to their subcellular localisation according to the Plant Proteome Database and previous reports of plant LD proteins. Only proteins identified by at least two peptides and present in all replicates of the respective treatments were used for this analysis. Furthermore, assignment to organelles was only done for proteins with a unique localisation, all other proteins were designated as "unknown". The combined protein abundance of all marker proteins of the different organelles in the LD-fraction was then normalised to the respective combined protein abundances in total extract samples and the resulting enrichment ratio was log2-transformed. Organelles that contained less than five marker proteins in the LD-fraction were excluded from the analysis. The log2-value 0, equivalent to the same amounts of marker proteins in LD-enriched and total protein samples, is indicated by the horizontal dashed line. Calculations were done for each treatment individually and different experiments are separated by vertical lines. In each treatment, n ≥ 3 biological replicates.
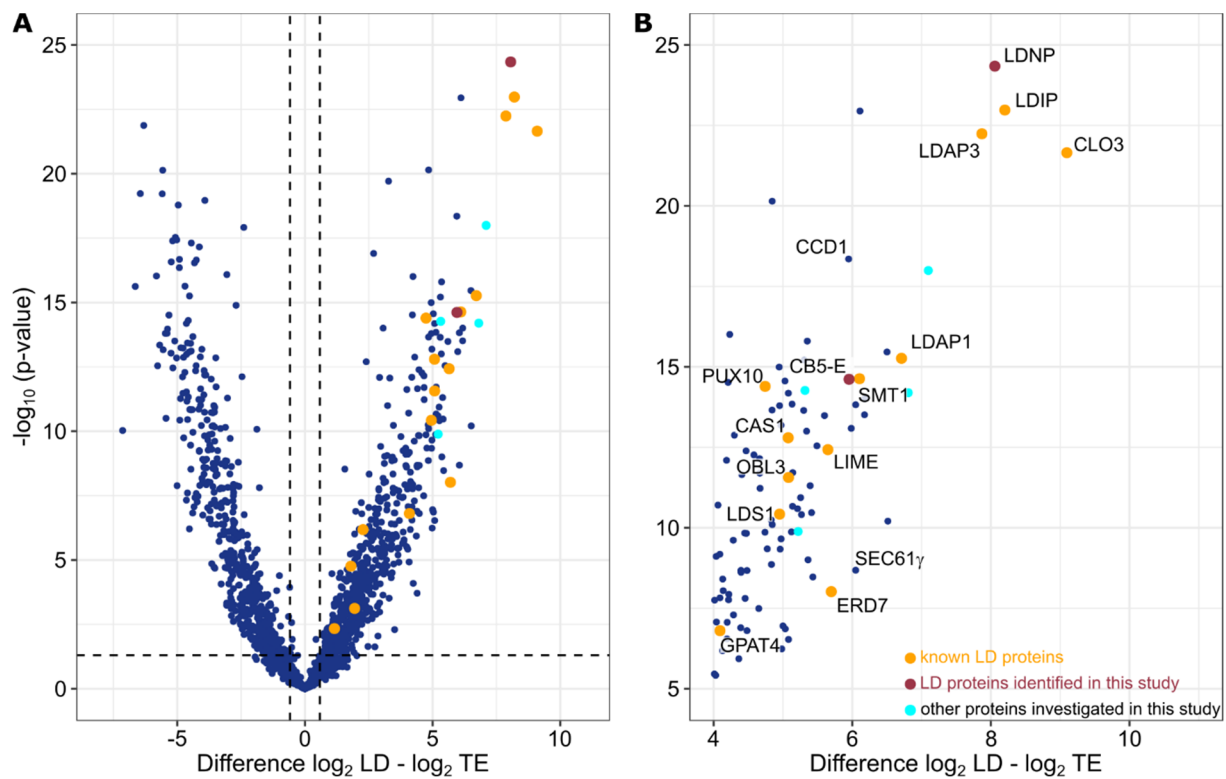
Figure 6: Enrichment analysis of proteins in the LD-enriched fractions prepared from Arabidopsis leaves. LDs were enriched from leaves of Arabidopsis *tgd1-1 sdp1-4* plants that were either untreated or subjected to different stresses. Subsequently, the proteome of the LD-enriched fractions and the corresponding total leaf protein extract was measured. Of the detected proteins a volcano plot was created, plotting the enrichment of each protein in the LD-fraction against its respectively calculated *p*-value (A). Treatments were combined, however, proteins were only included in the analysis if they were identified by at least two peptides and were present in at least three replicates. Proteins significantly enriched in the LD-fraction cluster in the upper right corner and this section of the volcano plot is depicted enlarged in (B). Previously known LD proteins are marked in orange; proteins investigated in this study that did or did not localise to LDs are highlighted in red and cyan, respectively. Known and new LD proteins are labelled, in addition the two proteins CCD1 and SEC61γ are indicated. *P*-values were calculated by Student's t-test in the Perseus 1.6.2.2 software. Vertical lines indicate 1.5-fold enrichment or depletion, while the horizontal line indicates a significance of *p* = 0.05.

In order to identify potential new LD proteins, we then calculated enrichment factors and the statistical significance of the enrichment for individual proteins (Suppl. Dataset S13). By combining all datasets from the different treatments, we were able to identify proteins that consistently showed a higher accumulation in the LD-enriched fractions (Figure 6). In total, 553 proteins significantly accumulated in LD-enriched fractions. Among those were several previously known LD proteins, most prominently CLO3, LDAP3, and LDIP. Other proteins with high enrichment values included the carotenoid cleavage dioxygenase CCD1, which has a tobacco homolog that was also found enriched in the LD proteome of tobacco pollen tubes, but did not localise to LDs when ectopically expressed in pollen tubes (Kretzschmar et al., 2018); and SEC61γ, a subunit of the SEC61 translocon previously described at ER-LD contact sites (Kretzschmar et al., 2020). In addition to the three known LD proteins, CLO3, LDAP3 and LDIP, the highest enrichment in the LD-fraction was observed for a protein (accession number AT5G04830) that has been annotated as nuclear transport factor 2 (NTF2) family member, but has not been functionally characterized. Additional proteins to study further were selected based on their enrichment value, predicted transmembrane regions, and/or possible LD-related functions. Among these were two cytochrome b_5 proteins, CB5-D and CB5-E that were both highly enriched in the LD fraction and might serve in electron transfer during possible lipid oxidation reactions at LDs.

Of the selected candidates, we analysed subcellular localisation by transient expression in *Nicotiana benthamiana* leaves, which is a well-established model plant cell system for protein localization, including LD proteins (Kretzschmar et al., 2020; Doner et al., 2021; Krawczyk et al., 2022b). Candidates were expressed with an N- or C-terminal mCherry fluorescent tag and subcellular localisation was analysed by confocal laser-scanning microscopy. To assess possible LD co-localisation, LDs were stained with the neutral lipid-specific stain Bodipy 493/503 (Listenberger and Brown, 2007). As shown in Figure 7, LD localisation was observed for two of the candidate proteins examined. The first one, which was the previously mentioned NTF2 protein family member, we termed LD-LOCALISED NTF2 FAMILY PROTEIN (LDNP), and the second one was CB5-E. Notably, we observed two different localisations for CB5-E, depending on the position of the appended mCherry moiety. That is, C-terminal mCherry-tagged CB5-E localised to reticular structures, consistent with the ER (Figure 7C), while the N-terminal mCherry-tagged CB5-E displayed both an ER localization and LD localisation, with a clear LD preference in some cells (Figure 7D). Bioinformatic tools predict a single transmembrane structure near the C-terminus of CB5-E (Suppl. Figure S8), which might be less accessible with a C-terminal-appended mCherry, therefore resulting in the observed differences in CB5-E localisation. None of the other candidate proteins examined readily localized to BODIPY-stained LDs (Suppl. Figure S9), although some displayed reticular, ER-like fluorescence patterns, which may be notable given the role of the ER in LD biogenesis.

The leaf LD proteome responds to environmental stresses

Looking at the overall LD proteome in leaves of *tgd1-1 sdp1-4* without stress treatment, CLO3 and LDAP3 were the most abundant proteins (Table 1). When their respective riBAQ values are normalised to the summed riBAQ values of all known LD proteins, they combine to around 80% of total LD protein riBAQ abundance.
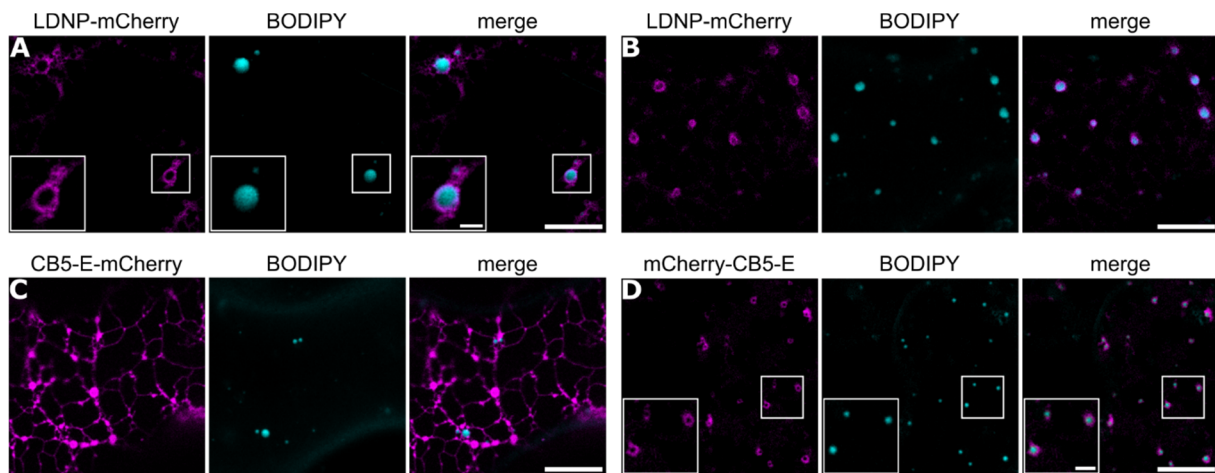
Figure 7: Two proteins were observed to associate with LDs upon transient expression in *Nicotiana benthamiana* leaves. Subcellular localisation studies were carried out by transient expression in *N. benthamiana* leaves. Candidate proteins were fused to a mCherry-tag (magenta channel) and LDs were stained with BODIPY 493/503 (cyan channel). Depicted are localisation studies of LD-LOCALISED NTF2 FAMILY PROTEIN (LDNP) and CYTOCHROME B5 ISOFORM E (CB5-E). LDNP-mCherry localisation was observed when the protein was expressed alone (A) or in co-expression with the LD-inducing DIACYLGLYCEROL ACYLTRANSFERASE 2 enzyme from mouse (B). CB5-E carrying a C-terminal mCherry-tag did not co-localise to LDs (C), however, with an N-terminal mCherry-tag association to LDs was observed (D). Boxes highlight regions of the cell shown with higher magnification in the insets. Bars = 10 μm (2 μm in insets).

Additional proteins detected in leaves without treatment included other members of the LDAP protein family, LDAP1 and LDAP2, their interacting protein LDIP, and the protein ERD7 (Gidda et al., 2016; Pyc et al., 2017; Doner et al., 2021). Several other proteins connected to neutral lipid metabolism (i.e., GPAT4, STEROL METHYLTRANSFERASE 1 [SMT1], CYCLOARTENOL SYNTHASE 1 [CAS1], OIL BODY LIPASE 3 [OBL3], LD-ASSOCIATED LIPASE 2 [LIDL2]), protein degradation (PLANT UBX DOMAIN CONTAINING PROTEIN [PUX10]) or specialised metabolism (α-DOX1, LD-associated methyltransferase [LIME]) were also found, albeit in comparatively small amounts. In addition, LDNP and CB5-E described above were found in LD-enriched fractions of non-treated leaves. GPAT8 could not be detected in non-treated leaves, however, small amounts of the protein were found in the LD proteome of the leaves from the control treatment to heat stress (Table 1).

We did not observe any additional LD proteins specific to the different stress treatments, however, we were able to follow the changes in the LD proteome composition in response to the individual stresses (Figure 8). Overall, the combined protein abundance of LD proteins in the LD-enriched fraction tended to increase after a stress, especially after infections (Figure 8A), which is consistent with the observed trend towards increased TAG levels in our lipidomics measurements (Figure 1). Increased protein abundance was not evenly distributed on all LD proteins, so that the relative proportions of detected LD proteins in the known LD proteome changed (Figure 8B, Table 1). The dominance of CLO3 and LDAP3 in the proteome was consistently observed for all treatments, as they always combined to >60% in abundance of known LD proteins. They differ, however, in their response to the applied stress treatments, i.e., the proportion of CLO3 increased after all three treatments in contrast to LDAP3 whose relative contribution either decreased or did not change. We next calculated for each protein the ratio of its abundance after stress treatment divided by its abundance in the respective controls (Figure 8C). Fitting to the observed trends in relative composition, abundance of CLO3 more than doubled in case of infection with both *B. cinerea* and *Pseudomonas*. Similarly, heat treatment also caused an upregulation of CLO3. LDAP3 did not change as much and was depleted after *Pseudomonas*-infection, consequently its proportion in the LD proteome of infected leaves was decreased. Among the low-abundant leaf LD proteins, α-DOX1 strongly accumulated at LDs after both pathogen treatments, which fits to the described functional interaction between CLO3 and α-DOX1 (Shimada et al., 2014). Interestingly, α-DOX1 did not increase in reaction to heat treatment, pointing to a more specific role in defence against pathogens. For CB5-E we could also observe an accumulation specifically after pathogen infection, although on a smaller scale than for α-DOX1. Most other proteins fluctuate in abundance but show no clear trend with the possible exception of PUX10 that was depleted after all of our treatments.

Pathogen susceptibility is not strongly altered in mutants of genes coding for LD proteins

As CLO3 and α-DOX1 reacted most strongly to pathogen infection, we tested respective T-DNA mutants for potentially altered resistance phenotypes. α-DOX1 has a homolog, α-DOX2, which shares 61% identity on the protein level and also has enzymatic activity to produce hydroxylated fatty acids but differs in expression pattern and has so far not been described as LD-localised (Bannenberg et al., 2009).
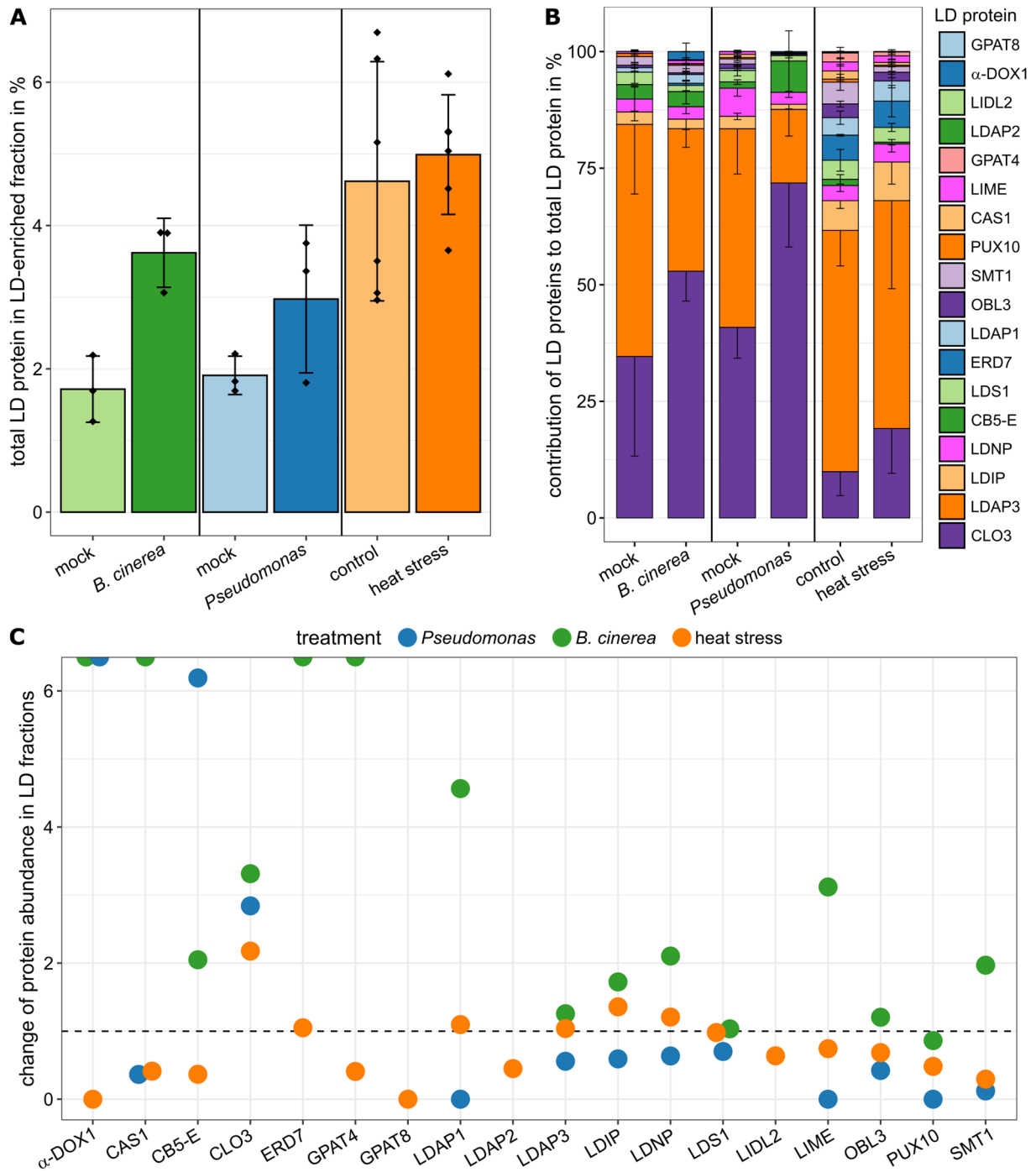
Figure 8: Changes in the known LD proteome of leaves after stress treatments. The protein abundance (riBAQ values) of known LD proteins in the LD-enriched fraction isolated from Arabidopsis leaves was followed in reaction to fungal infection with *Botrytis cinerea* (*B. cinerea*), bacterial infection with *Pto* DC3000 *ΔavrPto/ΔavrPtoB* (*Pseudomonas*) or heat stress for 24 hours at 37°C. The total LD protein abundance was calculated by summing up riBAQ values of all LD proteins for each treatment individually (A). In addition, for each treatment the relative contribution of all detected LD proteins to the total LD protein abundance was calculated (B). Stacked bar plots show the relative proportion of individual LD proteins in the order displayed in the legend, i.e. percentage of GPAT8 at the top and percentage of CLO3 at the bottom. The changes in abundance of individual proteins was followed by calculating the ratio of their riBAQ values in LD fractions of stressed plants relative to their riBAQ values in respective control treatments (C). Values above and below 1 indicate enrichment or depletion upon individual stresses, respectively. The horizontal line highlights ratios of 1. Proteins were only included if they were identified by at least two peptides and were detected in at least three replicates. n ≥ 3 replicates per treatment.
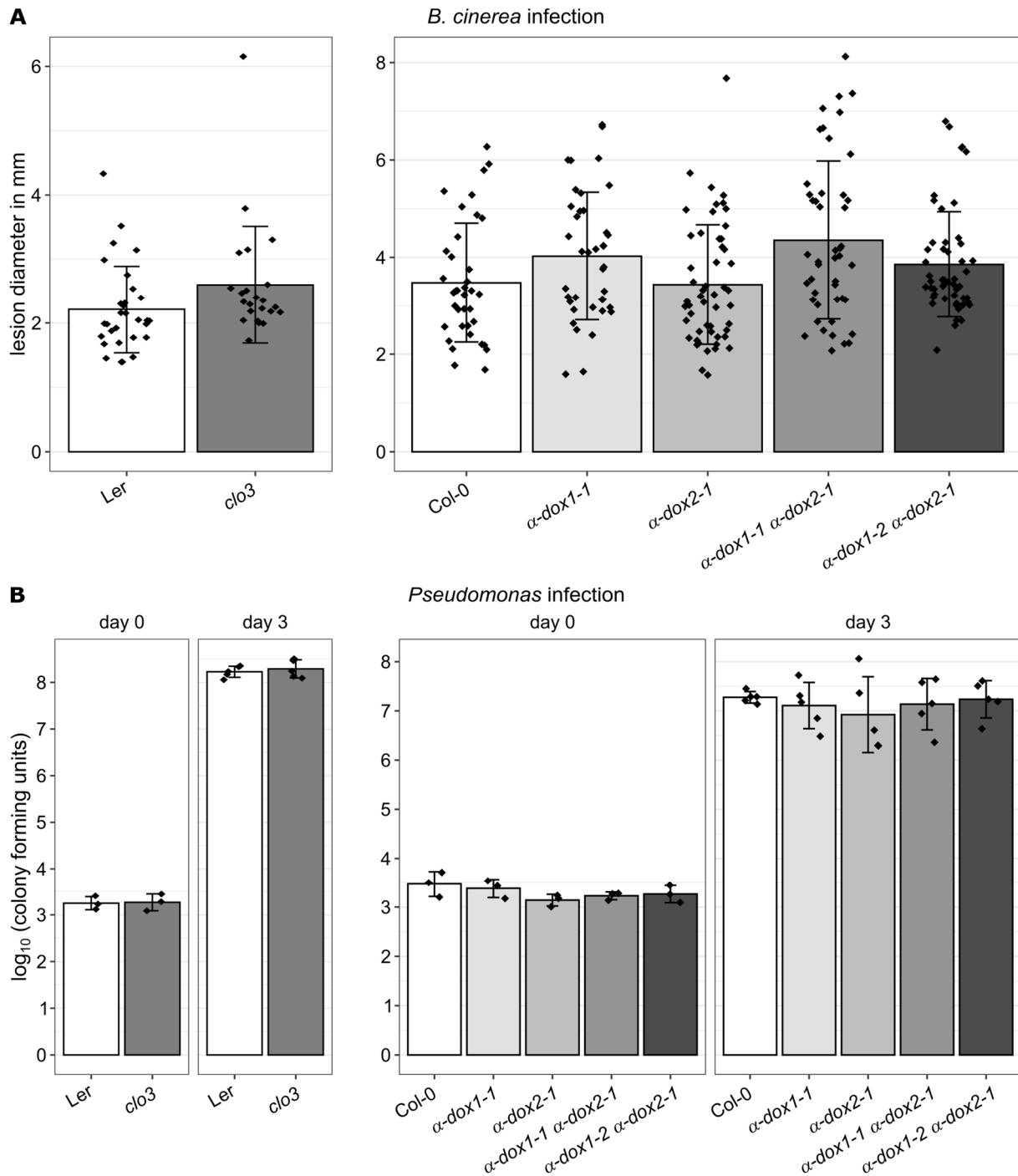
Figure 9: T-DNA mutants of *CLO3* and *α-DOX1* showed no alterations of pathogen susceptibility. The indicated mutant plants were analysed for susceptibility towards the fungal pathogens *Botrytis cinerea* (A) and the bacterial pathogen *Pseudomonas syringae* pv. *tomato* DC3000 (*Pseudomonas*, B). For *B. cinerea* assays, droplets of spores suspensions were applied to the leaves and diameters of necrotic lesions were measured three days after infection. *Pseudomonas* infection was performed by syringe inoculation. Immediately after infiltration, samples were harvested (day 0), subsequent samples were harvested three days after infection (day 3) and colony forming units were determined. Two double mutants of *α-dox1 α-dox2* were analysed that contained independent T-DNA insertions into *α-DOX1*. Statistical analysis was performed using the Wilcoxon-Mann-Whitney-Test for results of *clo3* and Kruskal-Wallis test for *α-dox* lines, however, no significant differences were observed. n ≥ 23 leaves in (A); in (B), n = 3 and 5 biological replicates per line for day 0 and day 3 samples, respectively.

Despite this difference in localisation, we decided to analyse response to pathogen infection in double mutants *α-dox1 α-dox2* to rule out enzymatic compensation of α-DOX1 function and additionally included one set of single mutants (*α-dox1-1* and *α-dox2-1*) to potentially narrow down effects of α-DOX1.

In *B. cinerea* infection, we observed a trend towards slightly larger lesions in a *clo3* mutant in the Ler ecotype background, however, the difference was not statistically significant (Figure 9A, Suppl. Figure S10). Similarly, lesion size of different *α-dox* mutants did increase but the effect was not consistently observed across experiments. The differential impact of α-DOX1 and α-DOX2 was also difficult to distinguish, as lesion size between *α-dox1* and *α-dox2* differed in one experiment but not in another (Figure 9A, Suppl. Figure S10A).

For *Pseudomonas* infection experiments, we initially used wild type *Pseudomonas syringae* pv. *tomato* DC3000 (hereafter: *Pto* DC3000), even though the lipidomics and proteomics studies were carried out with *Pseudomonas syringae* pv. *tomato* DC3000 *ΔavrPto/ΔavrPtoB* that is modified so it lost the effector proteins AvrPto and AvrPtoB (Lin and Martin, 2005). This way, we hoped to examine the importance of CLO3 and α-DOX1 independent of the additional variability of different *Pseudomonas* strains. However, we did not detect altered resistance neither for *clo3* nor for the *α-dox* mutants (Figure 9B). Infection with *Pto* DC3000 was carried out by infiltration of leaves which might circumvent defence effects of CLO3 and α-DOX1 in the stomata of leaves where bacterial entry has to be prevented. Thus, plants were spray-infected in an additional experiment, still *α-dox* mutants were not affected and *clo3* showed even a slightly decreased susceptibility (Suppl. Figure S10B).

Discussion

Biotic and abiotic stresses alter neutral lipid homeostasis in Arabidopsis leaves

Here, we studied the responses of leaf LDs to environmental challenges on lipid and protein level. Towards that end, we initially measured the levels of neutral lipids of Arabidopsis wild type leaves either spray-infected with *Pseudomonas* or *B. cinerea*, or heat-stressed for 24 hours at 37°C. All three treatments led to an increase in TAG levels, which fits with previous observations (Higashi et al., 2015; Schieferle et al., 2021). Higher temperatures lead to increased membrane fluidity so that membrane lipids are usually remodelled and acyl chains with three double bonds are replaced by less unsaturated acyl chains (Falcone et al., 2004). TAG accumulation in seedlings after a heat shock of 45°C for 90 minutes was strongly dependent on phospholipid:diacylglycerol acyltransferase (PDAT) enzyme activity (Mueller et al., 2017), which transfers acyl chains from PC to diacylglycerol (Dahlqvist et al., 2000). It thus seems likely that excess acyl chains originating from membrane lipids are channelled into TAGs to adapt biophysical membrane properties without a build-up of cytotoxic free FAs (Fan et al., 2013). This is reflected in the increase of 54:8 and 54:9-TAG species after heat stress that we and others observed (Higashi et al., 2015; Mueller et al., 2015; Mueller et al., 2017).

Unlike lipidomic changes after heat stress, which are comparatively well studied, less is known about the impact of pathogen infection. Infection of leaves with the avirulent *Pseudomonas* strain *Pseudomonas syringae* pv. *tomato* DC3000 *avrRpm1* causes an increase in TAG levels

(Schieferle et al., 2021) and leads to increased numbers of leaf LDs (Fernández-Santos et al., 2020) within one day after infection. Using another avirulent *Pseudomonas* strain (*Pseudomonas syringae* pv. *tomato* DC3000 *ΔavrPto/ΔavrPtoB*) and measuring neutral lipids after symptom development, we observed a similar trend to increased TAG levels, which was mainly driven by the TAG species 54:8 and 54:9 (Suppl. Datasets S2, S4). Fungal infection of Arabidopsis with *B. cinerea* in leaves (Figure 1) and *Verticillium longisporum* in roots (Schieferle et al., 2021) are also accompanied by a trend towards increased TAG levels. Interestingly, in case of *V. longisporum*, TAG accumulation is a systemic effect probably initiated by the infected roots. It thus seems to be the case that increased TAG levels are a general plant response to infection, however, the reasons for that are not clear yet. One possible explanation might again relate to membrane remodelling to form membrane domains as signalling hubs for immune receptor signalling, as has been reported for the HIR-proteins (Qi et al., 2011; Qi and Katagiri, 2012). Also, the receptor of bacterial flagellin, FLS2, was reported to be organised in distinct membrane clusters that become less mobile after receptor activation (Felix et al., 1999; Zipfel et al., 2004; Bücherl et al., 2017). The contribution of lipids to the establishment of these clusters is only just coming into focus (Platre et al., 2019), however, if the formation of membrane domains in immune signalling also involves adjustment of membrane lipids, TAGs might serve again as sink for excess acyl chains.

On the other hand, LDs could act as signalling hubs on their own, or their formation is induced by the pathogen rather than as plant response. For animal LDs, it has been reported that antimicrobial proteins accumulate at LDs after infection (Bosch et al., 2020) and eicosanoids specifically synthesised from LD-derived arachidonic acid could mediate immune signalling (Roingeard and Melo, 2017; Vallochi et al., 2018). A comparable plant reaction would be the synthesis of 2-HOT (Shimada et al., 2014). In this context, the accumulation of TAGs might serve as a plant response to increase LD number for expanded synthesis of antimicrobial compounds. Nevertheless, higher TAG levels could also be induced by the pathogens to obtain the plant lipids as carbon and energy source as has been reported from animal cells. There, infecting bacteria and protozoan parasites were observed to recruit LDs from the host cell for their own metabolism (Roingeard and Melo, 2017; Vallochi et al., 2018) and similar processes in plant cells cannot be ruled out.

The cellular proteome is readjusted to adapt to stress

In addition to analysing the changes in the lipidome after fungal infection, bacterial infection or heat stress, we then determined the proteome in leaves of accordingly treated plants. Proteins were quantified by label-free bottom-up proteomics and protein abundancies were compared between stress treatment and the respective mock or control treatment. Subsets of proteins were selected that showed enrichment or depletion after the applied stresses and subsequently, these subsets were analysed for the occurrence of specific protein clusters that hint at overall cellular changes in reaction to the specific stresses (Suppl. Figure S5). A common theme was the reduction in protein levels of photosynthesis-related proteins. This is not surprising given that chlorophyll fluorescence imaging studies have shown reduced quantum efficiency in response to infection (Bonfig et al., 2006; Pavicic et al., 2021) or heat stress (Kim and Portis, 2005; Salvucci, 2007). In addition, heat stress is especially linked to decreases in RuBisCO activity (Kobza and Edwards, 1987; Kim and Portis, 2005; Salvucci, 2007), consistent

with our observation of RuBisCO subunits among the depleted proteins (Suppl. Figure S5). Furthermore, for infection, several transcriptomics studies have shown that reduced gene expression of photosynthetic genes is a general response to a plethora of pathogens, possibly to allow for the upregulation of defence response pathways (Bilgin et al., 2010; Jiang et al., 2017).

Proteins that accumulated after treatment were more diverse between the treatments, conferring specificity to the plant's reaction. In the proteome of heat-stressed plants this resulted in an accumulation of heat shock proteins (HSPs; Figure 3), presumably to help protect normal protein function in the stressed cells. HSPs for example prevent the formation of protein aggregates and assist protein folding and protein transport across membranes (Lin et al., 2001; Rosenzweig et al., 2019). Additionally, several chloroplast chaperonin protein subunits were upregulated in response to heat stress, including CPN60A1 and CPN60B1 of chaperonin 60, which interacts in the assembly of RuBisCO (Hemmingsen et al., 1988; Ishikawa et al., 2003).

In the proteome of leaves after infection, proteins acting in metabolic pathways were more prominent than in leaves of heat-stressed plants (Figure 3, Suppl. Figure 5). One conspicuous change after both infections was the presence of glutathione S-transferases (GSTs) among the upregulated proteins (Suppl. Figure S5). Different GSTs were previously reported to change in abundance in a 2D-proteomics study of Arabidopsis infected with *Alternaria brassicicola* (Mukherjee et al., 2010). GSTs thus may form part of a general defence responses, although the functional role of various GST proteins are likely different. GSTF6, for example, has been implicated in the biosynthesis of camalexin (Su et al., 2011), a phytoalexine with antifungal properties against some *B. cinerea* strains (Kliebenstein et al., 2005). GSTF2, on the other hand, was suggested to bind small molecules, including antimicrobial compounds like camalexin, and to transport them within the cell to their site of action (Dixon et al., 2010; Ahmad et al., 2017). Further metabolic pathways that seemed to become important after *B. cinerea* infection were tryptophan biosynthesis and cyanide detoxification. Both might be connected to synthesis of camalexin, as it derives from tryptophan and in camalexin biosynthesis cyanide is released (Böttcher et al., 2009). Although cyanide is therefore produced endogenously in plant metabolism, it is also a cytotoxic metabolite and plants have a limited capacity for its detoxification (O'Leary et al., 2014). Hence, interference with cyanide metabolism towards elevated cyanide levels and cell death might also serve the necrotrophic life style of *B. cinerea* (Veloso and van Kan, 2018), so cyanide detoxification seems especially important in interaction with this necrotrophic pathogen. Altogether, a rewiring of metabolism towards antimicrobial compounds is a common feature against pathogen infection and the selectivity of altered metabolic pathways conveys the distinct responses towards specific pathogens.

Effects of the *tgd1-1 sdp1-4* mutations are not limited to lipid metabolism

We used the Arabidopsis double mutant *tgd1-1 sdp1-4* as a tool for LD isolation, however, we also compared it to the wild type it in our lipidomic and proteomic analyses. The original characterisation of the double mutant had highlighted its strong increase in TAG levels in leaves (Fan et al., 2014) and we confirmed this increase in our lipidomics measurements (Figure 2). Interestingly, the other important neutral lipid class in LDs, SEs, was depleted in

tgd1-1 sdp1-4 (Figure 2). As of yet, it is unclear if SEs and TAGs in plant cells are both present in mixed-compound LDs or form distinct LD subpopulations, as has been reported for LDs in some animal cells (Khor et al., 2014). Molecular dynamic simulations usually are modelled with only TAGs as core components (Bacle et al., 2017; Kim and Swanson, 2020; Kim et al., 2022) so the biophysical properties of possible mixed LDs are unclear. Consequently, it is difficult to estimate if increased TAG levels would directly interfere with SE accumulation, e.g., altering properties of mixed-compound LDs and/or by preoccupying the LD biogenesis machinery.

Besides the proteome of LD-enriched fractions we also analysed total protein fractions from leaves of *tgd1-1 sdp1-4*, which we compared to total protein fractions from Arabidopsis wild type. This comparison revealed decreased amounts of photosynthesis proteins, most notably of light harvesting complexes and proteins of the electron transfer chain (Suppl. Figure S6). As photosynthesis takes place in the chloroplasts, it seems possible that this effect is related to the loss of the plastid transporter TGD1. TGD1 is involved in the import of membrane lipid precursors into plastids and its loss in the *tgd1-1* mutant leads to a moderate reduction of thylakoid galactolipids and an altered FA profile of these galactolipids (Xu et al., 2003). Thylakoid lipids contribute to the organisation of thylakoids *in planta* (Demé et al., 2014) and although changes in their fatty acid profile have been mostly connected to temperature adaptation (Murakami et al., 2000; Kim and Portis, 2005; Hall et al., 2014) it seems reasonable to speculate that the changes of thylakoid membrane lipids impacts thylakoid assembly and thus photosynthesis. Another change we observed was the upregulation of the defence-related proteins PR1, PR2 and PR5 and the concomitant increase in SA levels in *tgd1-1 sdp1-4* (Figure 4). Neither TGD1 nor SDP1 have been linked to SA synthesis in Arabidopsis (Rekhter et al., 2019), however, previous studies reported that a knock-out of the stearoyl-ACP desaturase FAB2/SSI2 resulted in activated *PR* gene expression (Kachroo et al., 2001; Yang et al., 2016) and traced SA-accumulation in an *ssi2* mutant to decreased amounts of oleic acid (18:1Δ9; Kachroo et al., 2007). In our lipidomics measurements, we observed changes in the relative contribution of different FA species to TAGs, however, we rather measured a relative increase of 18:1 in total TAGs.

On the other hand, it has been reported that interference with plastid lipid metabolism impacts endogenous levels of jasmonates (Lin et al., 2016). There, knock-out of a gene encoding a chloroplast outer envelope protein that synthesises digalactosyldiacylglycerol caused the concomitant increase of JA and JA-Ile (Lin et al., 2016). Assuming that the *tgd1* mutation might similarly affect phytohormones that derive from plastids, the observed differing levels of SA in *tgd1-1 sdp1-4* could then also be a secondary effect of an altered crosstalk between phytohormones. In this context, it is interesting to note that reduced growth is a phenotype of both *tgd1-1* and *tgd1-1 sdp1-4* (Xu et al., 2005; Fan et al., 2014). Given the differences in TAG accumulation between the single and the double mutant (Fan et al., 2014), reduced growth is probably not caused by the hyperaccumulation of TAGs, instead, autoimmune reactions might contribute to this growth difference. If that is the case, connections between autoimmunity and mutations designed to increase TAG levels should be taken into account in any future biotechnological approaches aimed at the hyperaccumulation of TAG in vegetative tissues.

In the context of the proteome at LDs, it is notable that we detected LDAP3 as the most abundant protein of the LDAP family (Figure 8, Table 1). In previous proteomic studies of senescent or drought-stressed leaves of Arabidopsis Col-0, LDAP1 was the major LDAP protein (Brocard et al., 2017; Doner et al., 2021). One possible explanation could be differences of the LD-cytosol interface between the smaller leaf LDs in Col-0 and the larger LDs of *tgd1-1 sdp1-4* in terms of packing defects or exposed TAGs (Kim and Swanson, 2020) that would favour binding of different LDAP proteins. However, an alteration towards LDAP3 instead of LDAP1 as dominant LDAP protein likely requires a change in the expression pattern of their respective genes and it is unclear how that is triggered in the double mutant. Apart from the differences between LDAP1 and LDAP3, the composition of the LD proteome is overall quite similar to previously-published LD proteomes in senescent and drought-stressed Col-0 leaves (Brocard et al., 2017; Doner et al., 2021). Also, in these other proteomic studies, CLO3 was a dominant LD protein and, along with the LDAP proteins, comprised up to more than 90% of the LD proteome. Other less abundant LD proteins were also found, including LDIP and α-DOX1, with relative contributions to the total LD proteome that did not exceed 2% (Brocard et al., 2017; Doner et al., 2021) and thus similar to our observations in *tgd1-1 sdp1-4* (Table 1).

Observed LD-localisation of LDNP and CB5-E yields new questions about plant LD functionality

We identified two new proteins with the ability to localise to LDs in plant leaves, CB5-E and LDNP (Figure 7). Reanalysing previously published proteomic datasets, both proteins are also enriched in LD-fractions from seedlings and drought-stressed leaves, but neither were investigated further (Kretzschmar et al., 2018; Kretzschmar et al., 2020; Doner et al., 2021). CB5-E is comparatively well-characterised and was originally described as cytochrome b_5 protein able to accept electrons from the NADH-dependent cytochrome b_5 reductase CBR (Fukuchi-Mizutani et al., 1999). CB5-E is part of a five-member protein family in Arabidopsis that separates into two clades, one containing CB5-A and the other containing the other four members CB5-B-E (Maggio et al., 2007; Nagano et al., 2009). Notably, CB5-D was also enriched in our LD-enriched proteomic fractions (Suppl. Figure S9, Suppl. Dataset S13). Arabidopsis CBR and CB5 proteins are involved in desaturation reactions (Kumar et al., 2006; Kumar et al., 2012) and in microsomal fractions of castor bean, desaturation and hydroxylation reactions in the synthesis of ricinoleic acid were dependent on cytochrome b_5 proteins (Smith et al., 1992). CB5-D has also been previously localised to the ER (Maggio et al., 2007). Therefore, it was commonly assumed that the CB5 isoforms B-E all localise to the ER and serve as electron transport proteins in redox reactions. We could indeed observe ER localisation for CB5-D and CB5-E, however, CB5-E also localized predominantly to LDs in some cells (Figure 7, Suppl. Figure S9). This raises the question if particularly CB5-E could be involved in additional redox reactions on FAs from LDs.

In comparison to CB5-E, much less is known about LDNP. Expression of *LDNP* did not show specific tissue or developmental preferences (Klepikova et al., 2016) and it is annotated as nuclear transport factor 2 (NTF2) family protein, but, to our knowledge, has not been further studied. NTF2 proteins in general are well-established to mediate the transport of the small GTPase Ran into the nucleus, which is required for nuclear import (Yoneda et al., 1999; Zhao et al., 2006). However, LDNP was not initially identified as Arabidopsis NTF2 homolog (Zhao

et al., 2006), and was likely classified as NTF2 family protein based on it being predicted to contain a shared protein structural fold, which is thought to form a cone-like shape with internal cavity (Eberhardt et al., 2013). In addition to the NTF2 proteins, this same protein fold structure is also found in several other enzymatic and non-enzymatic proteins (Eberhardt et al., 2013), so it remains to be determined if LDNP serves some metabolic, transfer or other functions at plant LDs.

Changes in the LD proteome establish LDs as an additional player in stress responses

We analysed the LD proteome in leaves of the *tgd1-1 sdp1-4* double mutant after different stresses and comparison to the respective mock or control treatments enabled us also to observe the dynamics in the composition of the leaf LD proteome. When analysing these changes, it has to be taken into account that there are significant differences in the overall proteome of leaf total protein fractions between the double mutant and the wild type. The observed alterations of the LD proteome of *tgd1-1 sdp1-4* therefore might not be completely the same at leaf LDs in Col-0. Nevertheless, shared upregulated proteins between the wild type and the double mutant demonstrate that our treatments induced similar pathways in both Arabidopsis lines, hence it seems likely that our stress treatments will induce analogous reactions in the LD proteome of both the double mutant and the wild type. One example is the increased protein abundances of CLO3 and α-DOX1 that fit well with their previously described roles in pathogen defence in wild type Arabidopsis plants (Shimada et al., 2014).

CLO3 and α-DOX1 were among the strongest responding LD proteins to pathogen treatment and the protein abundance of CLO3 additionally increased after heat stress (Figure 8). This is in line with reported transcriptome changes of leaves infected with *B. cinerea* and seedlings subjected to heat, salinity and osmotic stress, i.e., *CLO3* expression was induced by all treatments, whereas *α-DOX1* expression was reported as increased for infection and osmotic but not heat treatment (Sham et al., 2015). When tested for pathogen susceptibility, however, we did not observe any significant changes in T-DNA mutants of both genes, albeit there was a slight increase of *B. cinerea*-induced lesion in *clo3* (Figure 9). This differs from results reported for another T-DNA mutant of *CLO3* where strong visual differences in lesion size of *B. cinerea* infection were observed (Sham et al., 2015). The difference might be related to the different ecotypes of the mutants, given that natural variation of *B. cinerea* susceptibility has been described for various Arabidopsis ecotypes (Denby et al., 2004).

On the other hand, α-DOX1 and CLO3 have been described to produce 2-HOT, which has no reported activity against bacterial pathogens (Prost et al., 2005). A lack in antibacterial properties of 2-HOT would be an explanation for the similar susceptibilities of *clo3* and the *α-dox* mutants towards *Pto* DC3000 in comparison to their respective wild types. While CLO3 and α-DOX1 thus may not be major contributors in the plant defence reaction against the tested pathogens, their strong reaction in the proteome of LDs implies that they form part of the general plant immune response.

How LDs are integrated in plant stress response remains an interesting question. The initial report on the involvement of CLO3 and α-DOX1 in 2-HOT synthesis also mentioned that they preferentially localise to LDs in the perilesional leaf area (CLO3) and infected, as well as perilesional leaf area (α-DOX1; Shimada et al., 2014). This raises the possibility that

environmental stresses cause or drive the formation of LD subpopulations, producing antimicrobial compounds close to the infection site or supporting TAG remodelling at specific cellular membranes. Furthermore, environmental signals might alter the interaction of LDs with other organelles, e.g. prompting the formation of membrane contact sites for lipid remodelling. A first such contact site of LDs with the plasma membrane has been recently described (Krawczyk et al., 2022b) and although the physiological relevance is unclear as of yet, the interaction of LDs in plant membrane contact sites especially in reaction to stress are an exciting avenue of future LD research.

Experimental Procedures

Plant lines and growth conditions and stress treatments

Lipidomic and proteomic experiments were carried out with Arabidopsis Col-0 and the oil-rich *tgd1-1 sdp1-4* double mutant line (Fan et al., 2014). Plant infection assays were performed on Arabidopsis insertion lines of *α-dox1*, *α-dox2*, *α-dox1 α-dox2* and *clo3* (also known as *rd20*). The Arabidopsis insertions lines for *α-dox1-1* (SALK_005633, AT3G01420) and *α-dox2-1* (SALK_029547, AT1G73680) and the double mutant *α-dox1-1 α-dox2-1* are described in (Bannenberg et al., 2009; Yang et al., 2022). A further double mutant *α-dox1-2 α-dox2-1* (SALK_042813, AT3G01420; SALK_029547, AT1G73680) was obtained by crossing. A *clo3* (FLAG_237F07, AT2G33380) line in the Ler background was obtained from Claire Bréhélin (Université de Bordeaux, Bordeaux, France; Blée et al., 2014).

Seeds of Arabidopsis lines were surface-sterilised with 6% (w/v) sodium hypochlorite and 0.1% (v/v) Triton X-100 and germinated on half-strength MS medium containing 0.8% (w/v) agar. After ten days seedlings were transferred to soil (Einheitserde SPECIAL Vermehrung, Patzer Erden, Sinntal-Altengronau, Germany) and grown under short-day condition (8 h light/16 h darkness) at 22°C in the light and 18°C in the darkness as described previously (Guzha et al., 2022). For lipidomic or proteomic analyses, plants were grown seven weeks before stress treatment was applied and samples were prepared as described below. Pathogen infection assays were carried out on six-week-old plants.

Pseudomonas syringae and *Botrytis cinerea* strains

For plant infections and further proteomic and lipidomic analysis of LDs, the *Pseudomonas* strain *Pseudomonas syringae* pv. *tomato* (*Pto*) DC3000 *ΔavrPto ΔavrPtoB* and the *Botrytis cinerea* strain B05.10 (in the following *B. cinerea*) were used. In plant infection assays of Arabidopsis mutant lines, additionally the *Pseudomonas* strain *Pseudomonas syringae* pv. *tomato* DC3000 was used.

Spores of *B. cinerea* were cultured on potato dextrose agar (PDA; Merck KGaA, Darmstadt, Germany) for ten days before conidiospores were harvested by washing them off with ¼ potato dextrose broth (PDB; Merck KGaA, Darmstadt, Germany) and filtering through Miracloth (Merck KGaA, Darmstadt, Germany). Spores were counted with a counting chamber (Fuchs-Rosenthal) and stocks in 15% (v/v) glycerol were stored at -80°C.

Pathogen treatment for proteomic analysis and subsequent LD-enrichment

For omics-samples of infection treatments, both pathogens were used in spray infections. Infection with *Pto* DC3000 *ΔavrPto ΔavrPtoB* was adapted from (Yao et al., 2013). In brief, *Pto* DC3000 *ΔavrPto ΔavrPtoB* was cultured in NYG-medium (0.5% peptone, 0.3% yeast extract, 2% glycerol; Merck KGaA, Darmstadt, Germany) with appropriate antibiotics (50 µg/ml Rifampicin, 50 µg/ml Kanamycin; Duchefa Biochemie, Haarlem, The Netherlands) over night and harvested by centrifugation (1500 x g, 20 min, room temperature) at the day of infection. Bacteria were washed once with 10 mM $MgCl_2$ and then resuspended in 10 mM $MgCl_2$ + 0.02% Silwet. Bacterial density was adjusted to an OD_{600} of 1 and the bacterial suspension sprayed onto well-watered plants until all leaves were evenly wet. Control plant were sprayed with 10 mM $MgCl_2$ + 0.02% Silwet. Plant were covered with plastic hoods to keep them at high humidity.

B. cinerea spores from glycerol stocks were diluted to a concentration of 5 x 10^4 spores/ml in ¼ PDB (Merck KGaA, Darmstadt, Germany) and pre-germinated for 4 hours at room temperature. Plants were sprayed until sprayed droplets ran off the leaves and subsequently kept at humid conditions. Mock-treated plants were treated analogously with ¼ PDB.

Plants were observed until they developed first symptoms to ensure infections were effective and plant proteome alterations had occurred. LD-enrichment was thus carried out 4-5 days after infection by ultracentrifugation adapting previous protocols (Kretzschmar et al., 2018). In addition to the pathogen- and mock-treated plants, one proteomic dataset was obtained from plants that were not treated at all.

For LD enrichment, leaves were ground in grinding buffer (50 mM Tris-HCl pH 7.5, 10 mM KCl, 0.4 M sucrose, 200 µM proteinase inhibitor PMSF; Carl Roth GmbH + Co. KG, Karlsruhe, Germany) with sea sand as abrasive agent. Grinding buffer, mortar and pestle were precooled to 0 °C and samples were kept between 0 – 4 °C during processing. To remove sand and cellular debris, samples were centrifuged for 1 minute at 100 x g. An aliquot was taken as total protein extract sample and proteins were precipitated in 96% ethanol at -20°C. Subsequently, samples were centrifuged at 100,000 x g for 35 min in a swing-out rotor. LDs were collected as fat pad from the top of the sample and washed in grinding buffer. After washing, the fat pad was collected and proteins were precipitated with 96% ethanol at -20°C.

Heat stress treatment for proteomic analysis and subsequent LD-enrichment

For heat stress, plants were kept at 37°C for 24 hours while control plants were kept at normal temperatures. LDs were enriched directly after heat stress. To that end, leaves were ground with grinding buffer (10 mM sodium phosphate buffer pH 7.5, 150 mM NaCl, 0.6 M sucrose, 25 mM Lomant reagent, 10 mM *N*-ethylmaleimide, 200 µM proteinase inhibitor PMSF; Carl Roth GmbH + Co. KG, Karlsruhe, Germany and Merck KGaA, Darmstadt, Germany). Sea sand was used as abrasive agent and together with cellular debris removed after grinding by centrifugation for 1 minute at 100 x g. Total protein extract samples were precipitated from the supernatant at -20°C with 96% ethanol in 10x excess. LDs were enriched by two ultracentrifugation steps at 100,000 x g for 60 min in a swing-out rotor. After the first ultracentrifugation, LDs were collected as fat pad and resuspended in washing buffer (10 mM sodium phosphate buffer pH 7.5, 150 mM NaCl, 0.4 M sucrose, 200 µM proteinase inhibitor

PMSF, 0.1% [v/v] Tween 20; Carl Roth GmbH + Co. KG, Karlsruhe, Germany). The LD suspension was overlaid with overlay buffer (10 mM sodium phosphate buffer pH 7.5, 150 mM NaCl, 0.2 M sucrose, 200 µM proteinase inhibitor PMSF, 0.1% [v/v] Tween 20; Carl Roth GmbH + Co. KG, Karlsruhe, Germany). After the second ultracentrifugation, LDs were collected as floating fat pad and proteins precipitated at -20°C with 96% ethanol. Before protein precipitation, samples were kept at 0 − 4°C throughout LD enrichment; buffers, mortar and pestle were precooled to the same temperature.

Proteomic sample preparation and LC-MS/MS analysis of peptides

Proteins were defatted and washed with 80% ethanol and the dissolved in 6 M urea and 5% (w/v) SDS. Determination of protein concentration, in-gel tryptic-digest and peptide desalting was carried out as described previously (Shevchenko et al., 2006; Rappsilber et al., 2007; Kretzschmar et al., 2018). Dried peptides were reconstituted in 20 µl sample buffer (2% acetonitrile, 0.1% formic acid) and subjected to LC-MS/MS analysis. To that end, 1 to 3 µl of each sample were subjected to reverse phase liquid chromatography for peptide separation using an RSLCnano Ultimate 3000 system (Thermo Fisher Scientific). Peptides were loaded on an Acclaim PepMap 100 pre-column (100 µm x 2 cm, C18, 5 µm, 100 Å; Thermo Fisher Scientific) with 0.07% trifluoroacetic acid at a flow rate of 20 µL/min for 3 min. Analytical separation of peptides was accomplished on an Acclaim PepMap RSLC column (75 µm x 50 cm, C18, 2 µm, 100 Å; Thermo Fisher Scientific) at a flow rate of 300 nL/min. The solvent composition followed a gradual change within 94 min: from 96 % solvent A (0.1 % formic acid) and 4 % solvent B (80 % acetonitrile, 0.1 % formic acid) to 10 % solvent B within 2 minutes, to 30 % solvent B within the next 58 min, to 45% solvent B within the following 22 min, and to 90 % solvent B within the last 12 min of the gradient. All solvents and acids had Optima grade for LC-MS (Thermo Fisher Scientific). Eluting peptides were on-line ionized by nano-electrospray (nESI) using the Nanospray Flex Ion Source (Thermo Fisher Scientific) at 1.5 kV (liquid junction) and transferred to the mass spectrometer. For mass spectrometry, either an Orbitrap Velos Pro hybrid mass spectrometer or a Q Exactive HF mass spectrometer (both Thermo Fisher Scientific) were used. On the Orbitrap Velos Pro hybrid mass spectrometer, full scans were recorded within a mass range of 300 to 1850 m/z at a resolution of 30,000 with the Orbitrap-FT analyser. Full scans were followed by data-dependent top 10 CID fragmentation (dynamic exclusion enabled) within the ion trap Velos Pro analyser. For the Q Exactive HF mass spectrometer, full scans were recorded in a mass range of 300 to 1650 m/z at a resolution of 30,000 and followed by data-dependent top 10 HCD fragmentation at a resolution of 15,000 (dynamic exclusion enabled). LC-MS method programming and data acquisition was performed with the XCalibur 4.0 software (Thermo Fisher Scientific).

Computational processing of MS/MS data

MS/MS raw data were processed in the MaxQuant software (version 1.6.2.17) for feature detection, peptide identification and protein group assembly (Cox and Mann, 2008). Mostly, default settings were used with additional settings as specified in Supplemental Table S1. The TAIR10 protein database was used as reference for identification. For quantification, label free quantification was calculated according to the iBAQ and LFQ algorithms (Cox and Mann, 2008; Schwanhäusser et al., 2011; Cox et al., 2014). Further data analysis was done in Perseus 1.6.2.2 (Tyanova et al., 2016), Excel (Microsoft Office) and RStudio 4.0.1 (RStudio Team (2021).

RStudio: Integrated Development Environment for R. RStudio, PBC, Boston, MA. http://www.rstudio.com/).

Protein localisation was annotated based on the Plant Proteome Database (Sun et al., 2009) as of 14th June 2022. LD localisation was assigned based on previous studies (Kretzschmar et al., 2018; Fernández-Santos et al., 2020; Kretzschmar et al., 2020; Doner et al., 2021; Ge et al., 2022; Li et al., 2022). Volcano plots were calculated in Perseus. rLFQ and riBAQ values of proteins were log2-transformed and missing values were imputed from normal distribution (parameters: width 0.3, down shift 2.5, separately for each sample). For the comparison of different treatments, plant lines or isolated fraction, p-values were calculated by two-sided t-tests. For plotting, transformed and imputed rLFQ or riBAQ values, and calculated p-values were exported and plotted in RStudio 4.0.1.

Identification of candidate proteins for LD localisation was done using web tools. Potential membrane-spanning regions were predicted using the TMHMM - 2.0 server, which predicts transmembrane helices based on hidden Markov models (Krogh et al., 2001).

Lipidomic sample preparation and measurements

Infection with *Pto* DC3000 *ΔavrPto ΔavrPtoB* and *B. cinerea*, and heat stress treatment was carried out as for proteomic samples. Samples were also harvested after the same incubation times and flash-frozen in liquid nitrogen. Extraction and analysed of neutral lipids was adapted from (Herrfurth et al., 2021). In brief, leaf material was homogenised with a ball mill and 500 mg of each sample were extracted by monophasic extraction with propan-2-ol : hexane : water (60:26:14, v/v/v) at 60°C. Tripentadecanoin was added as internal standard. After extraction, samples were centrifuged (2500 x g, 10 min) and the supernatant evaporated to dryness under nitrogen stream. Extracted lipids were reconstituted in tetrahydrofuran : methanol : water (7:2:1, v/v/v). UPLC-nanoESI-MS/MS analysis was carried out as described in (Herrfurth et al., 2021) with the parameters listed in Supplemental Table S2. Peak integration was performed with the MultiQuant software (Sciex of Danaher Corporation, Washington, D.C., USA). Quantitative analysis of integrated peak values was done in RStudio 4.0.1.

***PR* gene expression analysis via qRT-PCR**

Leaves of wild type and *tgd1-1 sdp1-4* plants were frozen in liquid nitrogen and ground to fine powder with a ball mill (Retsch GmbH, Haan, Germany). RNA was extracted from 100 mg of ground leaf material per biological replicate and line. RNA isolation was done using the Spectrum Plant Total RNA Kit (Sigma-Aldrich) and subsequently treated with DNaseI (Thermo Fisher Scientific, Waltham, MA, USA) according to manufacturer's instructions. For cDNA synthesis, 0.5 µg RNA was reverse transcribed (Maxima Reverse Transcriptase; Thermo Fisher Scientific). The reaction product was diluted 1:10 in double-distilled water before qPCR. For each qPCR sample, 4 µl of the diluted cDNA was used together with Takyon No Rox SYBR MasterMix dTTP Blue (Eurogentec, Seraing, Belgium). *AT3G01150* was chosen as reference gene (Czechowski et al., 2005), used primers for all genes of interest and the reference gene are listed in Supplemental Table S3. The following PCR program was used for amplification: 95°C for 1 min 20 s (95°C for 20 s, 58°C for 20 s, 72°C for 40 s) × 39, 72°C 4 min. Amplicons

were tested by melt curve analysis. PCR amplification and melt curve analysis were carried out in an iQ5 qPCR cycler (BioRad Laboratories, Hercules, CA, USA).

Analysis of phytohormone levels

Phytohormones were extracted by biphasic extraction with MTBE based on (Matyash et al., 2008). After extraction, phytohormones were reversed phase-separated using an ACQUITY UPLC system (Waters Corp.) and analysed by nanoelectrospray ionization (nanoESI; TriVersa Nanomate, Advion BioSciences) coupled with an AB Sciex 4000 QTRAP tandem mass spectrometer (AB Sciex) employed in scheduled multiple reaction monitoring modes (Herrfurth and Feussner, 2020) with the following modifications. For quantification, 10 ng D4-SA (C/D/N Isotopes Inc., Pointe-Claire, Canada) were added at the beginning of the extraction procedure. For SA and SAG analysis, the following mass transitions were included: 137/93 [declustering potential (DP) -25 V, entrance potential (EP) -6 V, collision energy (CE) -20 V] for SA, 141/97 (DP -25 V, EP -6 V, CE -22 V) for D4-SA, and 299/137 (DP -30 V, EP -4 V, CE -18 V) for SAG.

Molecular cloning and candidate localisation studies in *Nicotiana benthamiana* leaves

Open reading frames of candidate genes were amplified from cDNA prepared from leaf RNA that had been extracted using the Spectrum Plant Total RNA Kit (Merck KGaA, Darmstadt, Germany). Constructs were amplified with the Phusion High-Fidelity DNA Polymerase (Thermo Fisher Scientific, Waltham, MA, USA) following manufacturer's instruction and using primers listed in Supplemental Table S4. Gateway cloning into the plant binary vectors pMDC32-ChC and pMDC32-ChN was carried out as described in (Müller et al., 2017). Vector construction of pMDC32-ChC and pMDC32-ChN has been described previously in (Kretzschmar et al., 2020) and (Doner et al., 2021), respectively. Localisation of candidates was analysed in leaves of *N. benthamiana* that were transiently transformed by infiltration with *Agrobacterium tumefaciens* harbouring candidate expression vectors. Plant growth, leaf infiltration and confocal laser scanning microscopy imaging was performed as previously described (Gidda et al., 2016; Kretzschmar et al., 2020).

Plant infection assays

Pseudomonas plant infection of T-DNA mutants from genes of the LD-proteins CLO3 and α-DOX1 was done with *Pto* DC3000 according to (Yao et al., 2013), except that bacterial suspensions were prepared in 10 mM $MgCl_2$ instead of water. Three days after infection, leaf discs were harvested, homogenised in 10 mM $MgCl_2$ + 0.001% Silwet and plated on NYG plates in appropriate dilutions that enabled the counting of single colonies.

For *B. cinerea* drop infections, spores were prepared in a concentration of 5×10^4 spores/ml in ¼ PDB (Merck KGaA, Darmstadt, Germany) and pre-germinated for 4 hours at room temperature. 6 µl-droplets of the spore suspension were placed on the adaxial surface of the leaf besides the middle vein and plants were kept under high humidity conditions after infection. After three days, lesion size diameters were measured with a MarCal 16ER digital calliper (Mahr GmbH, Göttingen, Germany).

Accession numbers

AT3G01420 (α-DOX1); AT1G73680 (α-DOX2); AT2G07050 (CAS); AT5G53560 (CB5-E); AT2G33380 (CLO3); AT2G17840 (ERD7); AT1G01610 (GPAT4); AT4G00400 (GPAT8); AT1G67360 (LDAP1); AT2G47780 (LDAP2); AT3G05500 (LDAP3); AT5G16550 (LDIP); AT5G04830 (LDNP); AT1G43890 (LDS1); AT1G73920 (LIDL2); AT4G33110 (LIME1); AT4G33120 (LIME2); AT1G45201 (OBL3); AT4G10790 (PUX10); AT5G13710 (SMT1)

Supplemental Data

Supplemental Figure S1: Relative composition of sterol species in sterol esters of Arabidopsis leaves after different stress treatments.

Supplemental Figure S2: Total TAG signal intensities in Col-0 leaves after different stress treatments.

Supplemental Figure S3: Relative TAG species composition of leaves after various stress treatments.

Supplemental Figure S4: Relative composition of sterol species in leaf sterol esters of Arabidopsis Col-0 and *tgd1-1 sdp1-4*.

Supplemental Figure S5: STRING networks of differentially accumulating proteins in Arabidopsis Col-0 leaves after different stresses.

Supplemental Figure S6: STRING networks of differentially accumulating proteins in leaf total protein extracts of Arabidopsis Col-0 and *tgd1-1 sdp1-4*.

Supplemental Figure S7: Protein abundance of three pathogenesis-related proteins in Arabidopsis leaves of Col-0 *and tgd1-1 sdp1-4* after different treatments.

Supplemental Figure S8: Prediction of the membrane interacting region in CB5-E.

Supplemental Figure S9: Additional subcellular localisation studies of candidate proteins in *Nicotiana benthamiana* leaves.

Supplemental Figure 10: Additional independent experiments testing pathogen susceptibility of T-DNA mutants of *CLO3* and *α-DOX1*.

Supplemental Table S1: Metadata file for LC-MS/MS data processing with MaxQuant.

Supplemental Table S2: Parameters for lipid analysis by UPLC-nanoESI-MS/MS.

Supplemental Table S3: Primers used for gene expression analysis via qPCR

Supplemental Table S4: Primers used for Gateway cloning and sequencing

Supplemental Dataset S1: Arabidopsis leaf neutral lipids - Absolute peak areas.

Supplemental Dataset S2: Arabidopsis leaf neutral lipids - normalised icf-corrected peak areas.

Supplemental Dataset S3: Relative contribution of sterol esters with a common sterol moiety to total sterol ester signal intensity.

Supplemental Dataset S4: Relative proportions of individual TAG species.

Supplemental Dataset S5: Proteins found in Arabidopsis leaves - normalised rLFQ and riBAQ values.

Supplemental Dataset S6: Comparison of protein abundance in Arabidopsis Col-0 leaves after infection with *Botrytis cinerea* to mock-treated plants.

Supplemental Dataset S7: Comparison of protein abundance in Arabidopsis Col-0 leaves in reaction to infection with *Pseudomonas syringae* pv. *tomato* DC3000 *ΔavrPto ΔavrPtoB*.

Supplemental Dataset S8: Comparison of protein abundance in Arabidopsis Col-0 leaves after heat stress.

Supplemental Dataset S9: Comparison of protein abundance in Arabidopsis *tgd1-1 sdp1-4* leaves after infection with *Botrytis cinerea* to mock-treated plants.

Supplemental Dataset S10: Comparison of protein abundance in Arabidopsis *tgd1-1 sdp1-4* leaves in reaction to infection with *Pseudomonas syringae* pv. *tomato* DC3000 *ΔavrPto ΔavrPtoB*.

Supplemental Dataset S11: Comparison of protein abundance in Arabidopsis *tgd1-1 sdp1-4* leaves after heat stress.

Supplemental Dataset S12: Comparison of proteins in non-stressed leaves of Arabidopsis Col-0 and *tgd1-1 sdp1-4*.

Supplemental Dataset S13: Comparison of proteins in LD-enriched fractions to total protein fractions of Arabidopsis *tgd1-1 sdp1-4* leaves.

Author contribution

P.S., J.S., R.T.M. and T.I. designed the work, P.S., N.M.D., C.H., M.S.S.L., K.B., K.S., O.V., performed research, P.S., N.M.D., K.S., I.F., G.H.B. and T.I. analysed data and P.S. and T.I. wrote the manuscript.

Acknowledgements

Tables

Table 1: Composition of LD proteome in LD-enriched fractions of leaves from Arabidopsis *tgd1-1 sdp1-4*. LDs were isolated from Arabidopsis leaves *of tgd1-1 sdp1-4* in non-stressed conditions and after different stresses. Stress treatments of leaves included infection with *Botrytis cinerea* (*B. cinerea*) or *Pseudomonas syringae* pv. *tomato* DC3000 *ΔavrPto ΔavrPtoB* (*Pseudomonas*), or heat stress for 24 hours at 37°C. For each stress, a mock or control treatment was performed. The relative contribution of individual LD proteins to the total LD protein abundance (riBAQ values) was calculated for each treatment separately. * denotes proteins that could not be identified unequivocally.

Gene symbol	AGI code	Protein name	% of LD proteins						
			No treatment	Mock (*B. cinerea*)	*B. cinerea*	Mock (*Pseudomonas*)	*Pseudomonas*	control	Heat stress
α-DOX1	AT3G01420	α-DIOXYGENASE 1	0.044	0	1.864	0	0.296	0.003	0
CAS1	AT2G07050	CYCLOARTENOL SYNTHASE 1	0.455	0	0.071	0.654	0.153	1.540	0.587
CB5-E	AT5G53560	CYTOCHROME B5 ISOFORM E	2.216	3.109	3.022	1.340	5.322	1.148	0.389
CLO3	AT2G33380	CALEOSIN 3	41.633	33.859	53.205	40.516	73.881	9.051	18.235
ERD7	AT2G17840	EARLY RESPONSIVE TO DEHYDRATION 7	1.463	0	0.490	0.030	0.058	5.378	5.226
GPAT4	AT1G01610	GLYCEROL-3-PHOSPHATE ACYLTRANSFERASE 4	0.218	0	0.063	0	0	2.003	0.756
GPAT8	AT4G00400	GLYCEROL-3-PHOSPHATE ACYLTRANSFERASE 8	0	0	0	0	0	0.109	0
LDAP1	AT1G67360	LD ASSOCIATED PROTEIN 1	1.071	0.889	1.924	0.402	0	4.171	4.232
LDAP2	AT2G47780	LD ASSOCIATED PROTEIN 2	0.166	0	0.077	0	0	0.154	0.064
LDAP3	AT3G05500	LD ASSOCIATED PROTEIN 3	41.577	50.700	30.210	43.158	15.446	53.114	51.045
LDIP	AT5G16550	LDAP - INTERACTING PROTEIN	4.056	2.635	2.154	2.613	0.994	6.115	7.684
LDNP	AT5G04830	LD-LOCALISED NTF2 FAMILY PROTEIN	3.135	2.641	2.634	6.021	2.456	3.332	3.723
LDS1	AT1G43890	LIPID DROPLETS AND STOMATA 1	1.803	2.555	1.253	2.356	1.061	3.536	3.208
LIDL2	AT1G73920	LD-ASSOCIATED LIPASE 2	0.109	0	0	0	0	0.061	0.036
LIME1/2*	AT4G33110/ AT4G33120*	LD-ASSOCIATED METHYLTRANSFERASE 1/2	0.432	0.473	0.699	0.609	0	1.963	1.350
OBL3	AT1G45201	OIL BODY LIPASE 3	0.618	0.592	0.338	0.922	0.250	3.025	1.918
PUX10	AT4G10790	PLANT UBX DOMAIN CONTAINING PROTEIN 10	0.479	0.728	0.297	0.307	0	0.580	0.259
SMT1	AT5G13710	STEROL METHYLTRANSFERASE 1	0.525	1.818	1.698	1.073	0.084	4.716	1.286

References

Ahmad L, Rylott EL, Bruce NC, Edwards R, Grogan G (2017) Structural evidence for Arabidopsis glutathione transferase AtGSTF2 functioning as a transporter of small organic ligands. FEBS Open Bio **7**: 122–132

Aubert Y, Vile D, Pervent M, Aldon D, Ranty B, Simonneau T, Vavasseur A, Galaud J-P (2010) RD20, a Stress-Inducible Caleosin, Participates in Stomatal Control, Transpiration and Drought Tolerance in Arabidopsis thaliana. Plant Cell Physiol **51**: 1975–1987

Aubert Y, Widemann E, Miesch L, Pinot F, Heitz T (2015) CYP94-mediated jasmonoyl-isoleucine hormone oxidation shapes jasmonate profiles and attenuates defence responses to Botrytis cinerea infection. J Exp Bot **66**: 3879–3892

Bacle A, Gautier R, Jackson CL, Fuchs PFJ, Vanni S (2017) Interdigitation between Triglycerides and Lipids Modulates Surface Properties of Lipid Droplets. Biophys J **112**: 1417–1430

Bannenberg G, Martínez M, Rodríguez MJ, López MA, Ponce de León I, Hamberg M, Castresana C (2009) Functional analysis of alpha-DOX2, an active alpha-dioxygenase critical for normal development in tomato plants. Plant Physiol **151**: 1421–1432

Barajas-Lopez J de D, Tiwari A, Zarza X, Shaw MW, Pascual J, Punkkinen M, Bakowska JC, Munnik T, Fujii H (2021) EARLY RESPONSE TO DEHYDRATION 7 Remodels Cell Membrane Lipid Composition during Cold Stress in Arabidopsis. Plant Cell Physiol **62**: 80–91

Baud S, Boutin J-P, Miquel M, Lepiniec L, Rochat C (2002) An integrated overview of seed development in Arabidopsis thaliana ecotype WS. Plant Physiol Biochem **40**: 151–160

Bauwe H, Hagemann M, Fernie AR (2010) Photorespiration: players, partners and origin. Trends Plant Sci **15**: 330–336

Bell E, Creelman RA, Mullet JE (1995) A chloroplast lipoxygenase is required for wound-induced jasmonic acid accumulation in Arabidopsis. Proc Natl Acad Sci U S A **92**: 8675–8679

Berkowitz O, De Clercq I, Van Breusegem F, Whelan J (2016) Interaction between hormonal and mitochondrial signalling during growth, development and in plant defence responses. Plant Cell Environ **39**: 1127–1139

Bilgin DD, Zavala JA, Zhu J, Clough SJ, Ort DR, DeLucia EH (2010) Biotic stress globally downregulates photosynthesis genes. Plant Cell Environ **33**: 1597–1613

Blée E, Boachon B, Burcklen M, Le Guédard M, Hanano A, Heintz D, Ehlting J, Herrfurth C, Feussner I, Bessoule J-J (2014) The Reductase Activity of the Arabidopsis Caleosin RESPONSIVE TO DESSICATION20 Mediates Gibberellin-Dependent Flowering Time, Abscisic Acid Sensitivity, and Tolerance to Oxidative Stress. Plant Physiol **166**: 109–124

Bonfig KB, Schreiber U, Gabler A, Roitsch T, Berger S (2006) Infection with virulent and avirulent P. syringae strains differentially affects photosynthesis and sink metabolism in Arabidopsis leaves. Planta **225**: 1–12

Bosch M, Sánchez-Álvarez M, Fajardo A, Kapetanovic R, Steiner B, Dutra F, Moreira L, López JA, Campo R, Marí M, et al (2020) Mammalian lipid droplets are innate immune hubs integrating cell metabolism and host defense. Science **370**: eaay8085

Böttcher C, Westphal L, Schmotz C, Prade E, Scheel D, Glawischnig E (2009) The Multifunctional Enzyme CYP71B15 (PHYTOALEXIN DEFICIENT3) Converts Cysteine-Indole-3-Acetonitrile to Camalexin in the Indole-3-Acetonitrile Metabolic Network of *Arabidopsis thaliana*. Plant Cell **21**: 1830–1845

Bowling SA, Guo A, Cao H, Gordon AS, Klessig DF, Dong X (1994) A mutation in Arabidopsis that leads to constitutive expression of systemic acquired resistance. Plant Cell **6**: 1845–1857

Brocard L, Immel F, Coulon D, Esnay N, Tuphile K, Pascal S, Claverol S, Fouillen L, Bessoule J-J, Bréhélin C (2017) Proteomic Analysis of Lipid Droplets from Arabidopsis Aging Leaves Brings New Insight into Their Biogenesis and Functions. Front Plant Sci **8**: 894

Bücherl CA, Jarsch IK, Schudoma C, Segonzac C, Mbengue M, Robatzek S, MacLean D, Ott T, Zipfel C (2017) Plant immune and growth receptors share common signalling components but localise to distinct plasma membrane nanodomains. eLife **6**: e25114

Cai Y, Goodman JM, Pyc M, Mullen RT, Dyer JM, Chapman KD (2015) Arabidopsis SEIPIN Proteins Modulate Triacylglycerol Accumulation and Influence Lipid Droplet Proliferation. Plant Cell **27**: 2616–2636

Chen JCF, Tsai CCY, Tzen JTC (1999) Cloning and Secondary Structure Analysis of Caleosin, a Unique Calcium-Binding Protein in Oil Bodies of Plant Seeds. Plant Cell Physiol **40**: 1079–1086

Corey EJ, Matsuda SP, Bartel B (1993) Isolation of an Arabidopsis thaliana gene encoding cycloartenol synthase by functional expression in a yeast mutant lacking lanosterol synthase by the use of a chromatographic screen. Proc Natl Acad Sci U S A **90**: 11628–11632

Cox J, Hein MY, Luber CA, Paron I, Nagaraj N, Mann M (2014) Accurate Proteome-wide Label-free Quantification by Delayed Normalization and Maximal Peptide Ratio Extraction, Termed MaxLFQ. Mol Cell Proteomics **13**: 2513–2526

Cox J, Mann M (2008) MaxQuant enables high peptide identification rates, individualized p.p.b.-range mass accuracies and proteome-wide protein quantification. Nat Biotechnol **26**: 1367–1372

Crawford T, Lehotai N, Strand Å (2018) The role of retrograde signals during plant stress responses. J Exp Bot **69**: 2783–2795

Cummins I, Hills MJ, Ross JHE, Hobbs DH, Watson MD, Murphy DJ (1993) Differential, temporal and spatial expression of genes involved in storage oil and oleosin accumulation in developing rapeseed embryos: implications for the role of oleosins and the mechanisms of oil-body formation. Plant Mol Biol **23**: 1015–1027

Czechowski T, Stitt M, Altmann T, Udvardi MK, Scheible W-R (2005) Genome-Wide Identification and Testing of Superior Reference Genes for Transcript Normalization in Arabidopsis. Plant Physiol **139**: 5–17

Dahlqvist A, Stahl U, Lenman M, Banas A, Lee M, Sandager L, Ronne H, Stymne S (2000) Phospholipid:diacylglycerol acyltransferase: an enzyme that catalyzes the acyl-CoA-independent formation of triacylglycerol in yeast and plants. Proc Natl Acad Sci U S A **97**: 6487–6492

Demé B, Cataye C, Block MA, Maréchal E, Jouhet J (2014) Contribution of galactoglycerolipids to the 3-dimensional architecture of thylakoids. FASEB J **28**: 3373–3383

Denby KJ, Kumar P, Kliebenstein DJ (2004) Identification of *Botrytis cinerea* susceptibility loci in *Arabidopsis thaliana*. Plant J **38**: 473–486

Deruyffelaere C, Purkrtova Z, Bouchez I, Collet B, Cacas J-L, Chardot T, Gallois J-L, D'Andrea S (2018) PUX10 Is a CDC48A Adaptor Protein That Regulates the Extraction of Ubiquitinated Oleosins from Seed Lipid Droplets in Arabidopsis. Plant Cell **30**: 2116–2136

Diener AC, Li H, Zhou W, Whoriskey WJ, Nes WD, Fink GR (2000) Sterol methyltransferase 1 controls the level of cholesterol in plants. Plant Cell **12**: 853–870

Dixon DP, Skipsey M, Edwards R (2010) Roles for glutathione transferases in plant secondary metabolism. Phytochemistry **71**: 338–350

Doner NM, Seay D, Mehling M, Sun S, Gidda SK, Schmitt K, Braus GH, Ischebeck T, Chapman KD, Dyer JM, et al (2021) Arabidopsis thaliana EARLY RESPONSIVE TO DEHYDRATION 7 Localizes to Lipid Droplets via Its Senescence Domain. Front Plant Sci **12**: 658961

Eastmond PJ (2006) SUGAR-DEPENDENT1 Encodes a Patatin Domain Triacylglycerol Lipase That Initiates Storage Oil Breakdown in Germinating Arabidopsis Seeds. Plant Cell **18**: 665–675

Eberhardt RY, Chang Y, Bateman A, Murzin AG, Axelrod HL, Hwang WC, Aravind L (2013) Filling out the structural map of the NTF2-like superfamily. BMC Bioinformatics **14**: 327

Falcone DL, Ogas JP, Somerville CR (2004) Regulation of membrane fatty acid composition by temperature in mutants of Arabidopsis with alterations in membrane lipid composition. BMC Plant Biol **4**: 17

Fan J, Yan C, Roston R, Shanklin J, Xu C (2014) Arabidopsis lipins, PDAT1 acyltransferase, and SDP1 triacylglycerol lipase synergistically direct fatty acids toward β-oxidation, thereby maintaining membrane lipid homeostasis. Plant Cell **26**: 4119–4134

Fan J, Yan C, Xu C (2013) Phospholipid:diacylglycerol acyltransferase-mediated triacylglycerol biosynthesis is crucial for protection against fatty acid-induced cell death in growing tissues of Arabidopsis. Plant J **76**: 930–942

Felix G, Duran JD, Volko S, Boller T (1999) Plants have a sensitive perception system for the most conserved domain of bacterial flagellin. Plant J **18**: 265–276

Fernández-Santos R, Izquierdo Y, López A, Muñiz L, Martínez M, Cascón T, Hamberg M, Castresana C (2020) Protein Profiles of Lipid Droplets during the Hypersensitive Defense Response of Arabidopsis against Pseudomonas Infection. Plant Cell Physiol **61**: 1144–1157

Fu ZQ, Dong X (2013) Systemic Acquired Resistance: Turning Local Infection into Global Defense. Annu Rev Plant Biol **64**: 839–863

Fukuchi-Mizutani M, Mizutani M, Tanaka Y, Kusumi T, Ohta D (1999) Microsomal Electron Transfer in Higher Plants: Cloning and Heterologous Expression of NADH-Cytochrome *b* 5Reductase from Arabidopsis. Plant Physiol **119**: 353–362

Ge S, Zhang R-X, Wang Y-F, Sun P, Chu J, Li J, Sun P, Wang J, Hetherington AM, Liang Y-K (2022) The Arabidopsis Rab protein RABC1 affects stomatal development by regulating lipid droplet dynamics. Plant Cell **34**: 4274–4292

Germain V, Rylott EL, Larson TR, Sherson SM, Bechtold N, Carde J-P, Bryce JH, Graham IA, Smith SM (2001) Requirement for 3-ketoacyl-CoA thiolase-2 in peroxisome development, fatty acid β-oxidation and breakdown of triacylglycerol in lipid bodies of Arabidopsis seedlings. Plant J **28**: 1–12

Gidda SK, Park S, Pyc M, Yurchenko O, Cai Y, Wu P, Andrews DW, Chapman KD, Dyer JM, Mullen RT (2016) Lipid Droplet-Associated Proteins (LDAPs) Are Required for the Dynamic Regulation of Neutral Lipid Compartmentation in Plant Cells. Plant Physiol **170**: 2052–2071

Guzha A, McGee R, Scholz P, Hartken D, Lüdke D, Bauer K, Wenig M, Zienkiewicz K, Herrfurth C, Feussner I, et al (2022) Cell wall-localized BETA-XYLOSIDASE4 contributes to immunity of Arabidopsis against *Botrytis cinerea*. Plant Physiol **189**: 1794–1813

Hall TD, Chastain DR, Horn PJ, Chapman KD, Choinski JS (2014) Changes during leaf expansion of ΦPSII temperature optima in Gossypium hirsutum are associated with the degree of fatty acid lipid saturation. J Plant Physiol **171**: 411–420

Hemmingsen SM, Woolford C, van der Vies SM, Tilly K, Dennis DT, Georgopoulos CP, Hendrix RW, Ellis RJ (1988) Homologous plant and bacterial proteins chaperone oligomeric protein assembly. Nature **333**: 330–334

Herrfurth C, Feussner I (2020) Quantitative Jasmonate Profiling Using a High-Throughput UPLC-NanoESI-MS/MS Method. Methods Mol Biol **2085**: 169–187

Herrfurth C, Liu Y-T, Feussner I (2021) Targeted Analysis of the Plant Lipidome by UPLC-NanoESI-MS/MS. Methods Mol Biol **2295**: 135–155

Higashi Y, Okazaki Y, Myouga F, Shinozaki K, Saito K (2015) Landscape of the lipidome and transcriptome under heat stress in Arabidopsis thaliana. Sci Rep **5**: 1–11

Higashi Y, Saito K (2019) Lipidomic studies of membrane glycerolipids in plant leaves under heat stress. Prog Lipid Res **75**: 100990

Hsieh K, Huang AHC (2004) Endoplasmic Reticulum, Oleosins, and Oils in Seeds and Tapetum Cells. Plant Physiol **136**: 3427–3434

Ischebeck T, Krawczyk HE, Mullen RT, Dyer JM, Chapman KD (2020) Lipid droplets in plants and algae: Distribution, formation, turnover and function. Semin Cell Dev Biol **108**: 82–93

Ishikawa A, Tanaka H, Nakai M, Asahi T (2003) Deletion of a Chaperonin 60β Gene Leads to Cell Death in the Arabidopsis lesion initiation 1 Mutant. Plant Cell Physiol **44**: 255–261

Jayawardhane KN, Singer SD, Weselake RJ, Chen G (2018) Plant sn-Glycerol-3-Phosphate Acyltransferases: Biocatalysts Involved in the Biosynthesis of Intracellular and Extracellular Lipids. Lipids **53**: 469–480

Jiang Z, He F, Zhang Z (2017) Large-scale transcriptome analysis reveals arabidopsis metabolic pathways are frequently influenced by different pathogens. Plant Mol Biol **94**: 453–467

Jolivet P, Boulard C, Bellamy A, Larré C, Barre M, Rogniaux H, d'Andréa S, Chardot T, Nesi N (2009) Protein composition of oil bodies from mature Brassica napus seeds. Proteomics **9**: 3268–3284

Jolivet P, Roux E, D'Andrea S, Davanture M, Negroni L, Zivy M, Chardot T (2004) Protein composition of oil bodies in Arabidopsis thaliana ecotype WS. Plant Physiol Biochem **42**: 501–509

Kachroo A, Shanklin J, Whittle E, Lapchyk L, Hildebrand D, Kachroo P (2007) The Arabidopsis stearoyl-acyl carrier protein-desaturase family and the contribution of leaf isoforms to oleic acid synthesis. Plant Mol Biol **63**: 257–271

Kachroo P, Shanklin J, Shah J, Whittle EJ, Klessig DF (2001) A fatty acid desaturase modulates the activation of defense signaling pathways in plants. Proc Natl Acad Sci U S A **98**: 9448–9453

Katavic V, Agrawal GK, Hajduch M, Harris SL, Thelen JJ (2006) Protein and lipid composition analysis of oil bodies from two Brassica napus cultivars. Proteomics **6**: 4586–4598

Khor VK, Ahrends R, Lin Y, Shen W-J, Adams CM, Roseman AN, Cortez Y, Teruel MN, Azhar S, Kraemer FB (2014) The Proteome of Cholesteryl-Ester-Enriched Versus Triacylglycerol-Enriched Lipid Droplets. PLoS One **9**: e105047

Kim EY, Park KY, Seo YS, Kim WT (2016) Arabidopsis Small Rubber Particle Protein Homolog SRPs Play Dual Roles as Positive Factors for Tissue Growth and Development and in Drought Stress Responses. Plant Physiol **170**: 2494–2510

Kim K, Portis AR (2005) Temperature Dependence of Photosynthesis in Arabidopsis Plants with Modifications in Rubisco Activase and Membrane Fluidity. Plant Cell Physiol **46**: 522–530

Kim S, Swanson JMJ (2020) The Surface and Hydration Properties of Lipid Droplets. Biophys J **119**: 1958–1969

Kim S, Swanson JMJ, Voth GA (2022) Computational Studies of Lipid Droplets. J Phys Chem B **126**: 2145–2154

Kim YY, Jung KW, Yoo KS, Jeung JU, Shin JS (2011) A Stress-Responsive Caleosin-Like Protein, AtCLO4, Acts as a Negative Regulator of ABA Responses in Arabidopsis. Plant Cell Physiol **52**: 874–884

Klepikova AV, Kasianov AS, Gerasimov ES, Logacheva MD, Penin AA (2016) A high resolution map of the Arabidopsis thaliana developmental transcriptome based on RNA-seq profiling. Plant J **88**: 1058–1070

Kliebenstein DJ, Rowe HC, Denby KJ (2005) Secondary metabolites influence Arabidopsis/Botrytis interactions: variation in host production and pathogen sensitivity. Plant J **44**: 25–36

Kobza J, Edwards GE (1987) Influences of Leaf Temperature on Photosynthetic Carbon Metabolism in Wheat. Plant Physiol **83**: 69–74

Krawczyk HE, Rotsch AH, Herrfurth C, Scholz P, Shomroni O, Salinas-Riester G, Feussner I, Ischebeck T (2022a) Heat stress leads to rapid lipid remodeling and transcriptional adaptations in Nicotiana tabacum pollen tubes. Plant Physiol **189**: 490–515

Krawczyk HE, Sun S, Doner NM, Yan Q, Lim MSS, Scholz P, Niemeyer PW, Schmitt K, Valerius O, Pleskot R, et al (2022b) SEED LIPID DROPLET PROTEIN1, SEED LIPID DROPLET PROTEIN2, and LIPID DROPLET PLASMA MEMBRANE ADAPTOR mediate lipid droplet-plasma membrane tethering. Plant Cell **34**: 2424–2448

Kretzschmar FK, Doner NM, Krawczyk HE, Scholz P, Schmitt K, Valerius O, Braus GH, Mullen RT, Ischebeck T (2020) Identification of Low-Abundance Lipid Droplet Proteins in Seeds and Seedlings. Plant Physiol **182**: 1326–1345

Kretzschmar FK, Mengel LA, Müller AO, Schmitt K, Blersch KF, Valerius O, Braus GH, Ischebeck T (2018) PUX10 Is a Lipid Droplet-Localized Scaffold Protein That Interacts with CELL DIVISION CYCLE48 and Is Involved in the Degradation of Lipid Droplet Proteins. Plant Cell **30**: 2137–2160

Krogh A, Larsson B, von Heijne G, Sonnhammer EL (2001) Predicting transmembrane protein topology with a hidden Markov model: application to complete genomes. J Mol Biol **305**: 567–580

Kumar D, Hazra S, Datta R, Chattopadhyay S (2016) Transcriptome analysis of Arabidopsis mutants suggests a crosstalk between ABA, ethylene and GSH against combined cold and osmotic stress. Sci Rep **6**: 36867

Kumar R, Tran L-SP, Neelakandan AK, Nguyen HT (2012) Higher Plant Cytochrome b5 Polypeptides Modulate Fatty Acid Desaturation. PLoS One **7**: e31370

Kumar R, Wallis JG, Skidmore C, Browse J (2006) A mutation in Arabidopsis cytochrome b5 reductase identified by high-throughput screening differentially affects hydroxylation and desaturation. Plant J **48**: 920–932

La Camera S, Geoffroy P, Samaha H, Ndiaye A, Rahim G, Legrand M, Heitz T (2005) A pathogen-inducible patatin-like lipid acyl hydrolase facilitates fungal and bacterial host colonization in Arabidopsis. Plant J **44**: 810–825

Leister D, Wang L, Kleine T (2017) Organellar Gene Expression and Acclimation of Plants to Environmental Stress. Front Plant Sci **8**: 387

Li F, Han X, Guan H, Xu MC, Dong YX, Gao X-Q (2022) PALD encoding a lipid droplet-associated protein is critical for the accumulation of lipid droplets and pollen longevity in Arabidopsis. New Phytol **235**: 204–219

Li Q, Zheng Q, Shen W, Cram D, Fowler DB, Wei Y, Zou J (2015) Understanding the Biochemical Basis of Temperature-Induced Lipid Pathway Adjustments in Plants. Plant Cell **27**: 86–103

Lin BL, Wang JS, Liu HC, Chen RW, Meyer Y, Barakat A, Delseny M (2001) Genomic analysis of the Hsp70 superfamily in Arabidopsis thaliana. Cell Stress Chaperones **6**: 201–208

Lin L-J, Tai SSK, Peng C-C, Tzen JTC (2002) Steroleosin, a Sterol-Binding Dehydrogenase in Seed Oil Bodies. Plant Physiol **128**: 1200–1211

Lin N-C, Martin GB (2005) An avrPto/avrPtoB mutant of Pseudomonas syringae pv. tomato DC3000 does not elicit Pto-mediated resistance and is less virulent on tomato. Mol Plant Microbe Interact **18**: 43–51

Lin Y-T, Chen L-J, Herrfurth C, Feussner I, Li H (2016) Reduced Biosynthesis of Digalactosyldiacylglycerol, a Major Chloroplast Membrane Lipid, Leads to Oxylipin Overproduction and Phloem Cap Lignification in Arabidopsis. Plant Cell **28**: 219–232

Listenberger LL, Brown DA (2007) Fluorescent Detection of Lipid Droplets and Associated Proteins. Curr Protoc Cell Biol **35**: 24.2.1-24.2.11

Maggio C, Barbante A, Ferro F, Frigerio L, Pedrazzini E (2007) Intracellular sorting of the tail-anchored protein cytochrome b5 in plants: a comparative study using different isoforms from rabbit and Arabidopsis. J Exp Bot **58**: 1365–1379

Matyash V, Liebisch G, Kurzchalia TV, Shevchenko A, Schwudke D (2008) Lipid extraction by methyl- *tert* -butyl ether for high-throughput lipidomics. J Lipid Res **49**: 1137–1146

Moellering ER, Muthan B, Benning C (2010) Freezing Tolerance in Plants Requires Lipid Remodeling at the Outer Chloroplast Membrane. Science **330**: 226–228

Mueller SP, Krause DM, Mueller MJ, Fekete A (2015) Accumulation of extra-chloroplastic triacylglycerols in Arabidopsis seedlings during heat acclimation. J Exp Bot **66**: 4517–4526

Mueller SP, Unger M, Guender L, Fekete A, Mueller MJ (2017) Phospholipid:Diacylglycerol Acyltransferase-Mediated Triacylglyerol Synthesis Augments Basal Thermotolerance. Plant Physiol **175**: 486–497

Mukherjee AK, Carp M-J, Zuchman R, Ziv T, Horwitz BA, Gepstein S (2010) Proteomics of the response of Arabidopsis thaliana to infection with Alternaria brassicicola. J Proteomics **73**: 709–720

Müller AO, Blersch KF, Gippert AL, Ischebeck T (2017) Tobacco pollen tubes – a fast and easy tool for studying lipid droplet association of plant proteins. Plant J **89**: 1055–1064

Müller AO, Ischebeck T (2018) Characterization of the enzymatic activity and physiological function of the lipid droplet-associated triacylglycerol lipase AtOBL1. New Phytol **217**: 1062–1076

Murakami Y, Tsuyama M, Kobayashi Y, Kodama H, Iba K (2000) Trienoic Fatty Acids and Plant Tolerance of High Temperature. Science **287**: 476–479

Murphy DJ (1993) Structure, function and biogenesis of storage lipid bodies and oleosins in plants. Prog Lipid Res **32**: 247–280

Nagano M, Ihara-Ohori Y, Imai H, Inada N, Fujimoto M, Tsutsumi N, Uchimiya H, Kawai-Yamada M (2009) Functional association of cell death suppressor, Arabidopsis Bax inhibitor-1, with fatty acid 2-hydroxylation through cytochrome b5. Plant J **58**: 122–134

Ng S, De Clercq I, Van Aken O, Law SR, Ivanova A, Willems P, Giraud E, Van Breusegem F, Whelan J (2014) Anterograde and Retrograde Regulation of Nuclear Genes Encoding Mitochondrial Proteins during Growth, Development, and Stress. Mol Plant **7**: 1075–1093

O'Leary B, Preston GM, Sweetlove LJ (2014) Increased β-Cyanoalanine Nitrilase Activity Improves Cyanide Tolerance and Assimilation in Arabidopsis. Mol Plant **7**: 231–243

Ono M, Isono K, Sakata Y, Taji T (2021) CATALASE2 plays a crucial role in long-term heat tolerance of Arabidopsis thaliana. Biochem Biophys Res Commun **534**: 747–751

Partridge M, Murphy DJ (2009) Roles of a membrane-bound caleosin and putative peroxygenase in biotic and abiotic stress responses in Arabidopsis. Plant Physiol Biochem **47**: 796–806

Pavicic M, Overmyer K, Rehman A ur, Jones P, Jacobson D, Himanen K (2021) Image-Based Methods to Score Fungal Pathogen Symptom Progression and Severity in Excised Arabidopsis Leaves. Plants (Basel) **10**: 158

Pieterse CMJ, Van der Does D, Zamioudis C, Leon-Reyes A, Van Wees SCM (2012) Hormonal modulation of plant immunity. Annu Rev Cell Dev Biol **28**: 489–521

Piotrowski M, Schönfelder S, Weiler EW (2001) The Arabidopsis thaliana isogene NIT4 and its orthologs in tobacco encode beta-cyano-L-alanine hydratase/nitrilase. J Biol Chem **276**: 2616–2621

Platre MP, Bayle V, Armengot L, Bareille J, Marquès-Bueno MDM, Creff A, Maneta-Peyret L, Fiche J-B, Nollmann M, Miège C, et al (2019) Developmental control of plant Rho GTPase nano-organization by the lipid phosphatidylserine. Science **364**: 57–62

Prost I, Dhondt S, Rothe G, Vicente J, Rodriguez MJ, Kift N, Carbonne F, Griffiths G, Esquerré-Tugayé M-T, Rosahl S, et al (2005) Evaluation of the antimicrobial activities of plant oxylipins supports their involvement in defense against pathogens. Plant Physiol **139**: 1902–1913

Pyc M, Cai Y, Gidda SK, Yurchenko O, Park S, Kretzschmar FK, Ischebeck T, Valerius O, Braus GH, Chapman KD, et al (2017) Arabidopsis lipid droplet-associated protein (LDAP) - interacting protein (LDIP) influences lipid droplet size and neutral lipid homeostasis in both leaves and seeds. Plant J **92**: 1182–1201

Pyc M, Gidda SK, Seay D, Esnay N, Kretzschmar FK, Cai Y, Doner NM, Greer MS, Hull JJ, Coulon D, et al (2021) LDIP cooperates with SEIPIN and LDAP to facilitate lipid droplet biogenesis in Arabidopsis. Plant Cell **33**: 3076–3103

Qi Y, Katagiri F (2012) Membrane microdomain may be a platform for immune signaling. Plant Signal Behav **7**: 454–456

Qi Y, Tsuda K, Nguyen LV, Wang X, Lin J, Murphy AS, Glazebrook J, Thordal-Christensen H, Katagiri F (2011) Physical association of Arabidopsis hypersensitive induced reaction proteins (HIRs) with the immune receptor RPS2. J Biol Chem **286**: 31297–31307

Rappsilber J, Mann M, Ishihama Y (2007) Protocol for micro-purification, enrichment, pre-fractionation and storage of peptides for proteomics using StageTips. Nat Protoc **2**: 1896–1906

Rekhter D, Lüdke D, Ding Y, Feussner K, Zienkiewicz K, Lipka V, Wiermer M, Zhang Y, Feussner I (2019) Isochorismate-derived biosynthesis of the plant stress hormone salicylic acid. Science **365**: 498–502

Roingeard P, Melo RCN (2017) Lipid droplet hijacking by intracellular pathogens. Cell Microbiol **19**: e12688

Rosenzweig R, Nillegoda NB, Mayer MP, Bukau B (2019) The Hsp70 chaperone network. Nat Rev Mol Cell Biol **20**: 665–680

Salvucci ME (2007) Association of Rubisco activase with chaperonin-60 : a possible mechanism for protecting photosynthesis during heat stress. J Exp Bot **59**: 1923–1933

Schieferle S, Tappe B, Korte P, Mueller MJ, Berger S (2021) Pathogens and Elicitors Induce Local and Systemic Changes in Triacylglycerol Metabolism in Roots and in Leaves of Arabidopsis thaliana. Biology (Basel) **10**: 920

Scholz P, Chapman KD, Mullen RT, Ischebeck T (2022) Finding new friends and revisiting old ones - how plant lipid droplets connect with other subcellular structures. New Phytol **236**: 833–838

Schuhegger R, Nafisi M, Mansourova M, Petersen BL, Olsen CE, Svatos A, Halkier BA, Glawischnig E (2006) CYP71B15 (PAD3) catalyzes the final step in camalexin biosynthesis. Plant Physiol **141**: 1248–1254

Schwanhäusser B, Busse D, Li N, Dittmar G, Schuchhardt J, Wolf J, Chen W, Selbach M (2011) Global quantification of mammalian gene expression control. Nature **473**: 337–342

Sham A, Moustafa K, Al-Ameri S, Al-Azzawi A, Iratni R, AbuQamar S (2015) Identification of Arabidopsis Candidate Genes in Response to Biotic and Abiotic Stresses Using Comparative Microarrays. PLoS One **10**: e0125666

Shevchenko A, Tomas H, Havlis J, Olsen JV, Mann M (2006) In-gel digestion for mass spectrometric characterization of proteins and proteomes. Nat Protoc **1**: 2856–2860

Shimada TL, Shimada T, Okazaki Y, Higashi Y, Saito K, Kuwata K, Oyama K, Kato M, Ueda H, Nakano A, et al (2019) HIGH STEROL ESTER 1 is a key factor in plant sterol homeostasis. Nat Plants **5**: 1154–1166

Shimada TL, Takano Y, Shimada T, Fujiwara M, Fukao Y, Mori M, Okazaki Y, Saito K, Sasaki R, Aoki K, et al (2014) Leaf oil body functions as a subcellular factory for the production of a phytoalexin in Arabidopsis. Plant Physiol **164**: 105–118

Smith MA, Jonsson L, Stymne S, Stobart K (1992) Evidence for cytochrome *b* 5 as an electron donor in ricinoleic acid biosynthesis in microsomal preparations from developing castor bean (*Ricinus communis* L.). Biochem J **287**: 141–144

Spoel SH, Koornneef A, Claessens SMC, Korzelius JP, Van Pelt JA, Mueller MJ, Buchala AJ, Métraux J-P, Brown R, Kazan K, et al (2003) NPR1 modulates cross-talk between salicylate- and jasmonate-dependent defense pathways through a novel function in the cytosol. Plant Cell **15**: 760–770

Staswick PE, Tiryaki I (2004) The oxylipin signal jasmonic acid is activated by an enzyme that conjugates it to isoleucine in Arabidopsis. Plant Cell **16**: 2117–2127

Su T, Xu J, Li Y, Lei L, Zhao L, Yang H, Feng J, Liu G, Ren D (2011) Glutathione-Indole-3-Acetonitrile Is Required for Camalexin Biosynthesis in *Arabidopsis thaliana*. Plant Cell **23**: 364–380

Sun Q, Zybailov B, Majeran W, Friso G, Olinares PDB, van Wijk KJ (2009) PPDB, the Plant Proteomics Database at Cornell. Nucleic Acids Res **37**: D969–D974

Szymanski J, Brotman Y, Willmitzer L, Cuadros-Inostroza Á (2014) Linking gene expression and membrane lipid composition of Arabidopsis. Plant Cell **26**: 915–928

Tarazona P, Feussner K, Feussner I (2015) An enhanced plant lipidomics method based on multiplexed liquid chromatography-mass spectrometry reveals additional insights into cold- and drought-induced membrane remodeling. Plant J **84**: 621–633

Taurino M, Costantini S, De Domenico S, Stefanelli F, Ruano G, Delgadillo MO, Sánchez-Serrano JJ, Sanmartín M, Santino A, Rojo E (2018) SEIPIN Proteins Mediate Lipid Droplet Biogenesis to Promote Pollen Transmission and Reduce Seed Dormancy. Plant Physiol **176**: 1531–1546

Theodoulou FL, Job K, Slocombe SP, Footitt S, Holdsworth M, Baker A, Larson TR, Graham IA (2005) Jasmonic acid levels are reduced in COMATOSE ATP-binding cassette transporter mutants. Implications for transport of jasmonate precursors into peroxisomes. Plant Physiol **137**: 835–840

Tyanova S, Temu T, Sinitcyn P, Carlson A, Hein MY, Geiger T, Mann M, Cox J (2016) The Perseus computational platform for comprehensive analysis of (prote)omics data. Nat Methods **13**: 731–740

Tzen J, Cao Y, Laurent P, Ratnayake C, Huang A (1993) Lipids, Proteins, and Structure of Seed Oil Bodies from Diverse Species. Plant Physiol **101**: 267–276

Uknes S, Winter AM, Delaney T, Vernooij B, Morse A, Friedrich L, Nye G, Potter S, Ward E, Ryals J (1993) Biological induction of systemic acquired resistance in Arabidopsis. Mol Plant Microbe Interact **6**: 692–698

Vallochi AL, Teixeira L, Oliveira K da S, Maya-Monteiro CM, Bozza PT (2018) Lipid Droplet, a Key Player in Host-Parasite Interactions. Front Immunol **9**: 1022

Vance VB, Huang AH (1987) The major protein from lipid bodies of maize. Characterization and structure based on cDNA cloning. J Biol Chem **262**: 11275–11279

Veloso J, van Kan JAL (2018) Many Shades of Grey in Botrytis-Host Plant Interactions. Trends Plant Sci **23**: 613–622

Wang T-Y, Wu J-R, Duong NKT, Lu C-A, Yeh C-H, Wu S-J (2021) HSP70-4 and farnesylated AtJ3 constitute a specific HSP70/HSP40-based chaperone machinery essential for prolonged heat stress tolerance in Arabidopsis. J Plant Physiol **261**: 153430

Widemann E, Miesch L, Lugan R, Holder E, Heinrich C, Aubert Y, Miesch M, Pinot F, Heitz T (2013) The amidohydrolases IAR3 and ILL6 contribute to jasmonoyl-isoleucine hormone turnover and generate 12-hydroxyjasmonic acid upon wounding in Arabidopsis leaves. J Biol Chem **288**: 31701–31714

Xu C, Fan J, Froehlich JE, Awai K, Benning C (2005) Mutation of the TGD1 Chloroplast Envelope Protein Affects Phosphatidate Metabolism in *Arabidopsis*. Plant Cell **17**: 3094–3110

Xu C, Fan J, Riekhof W, Froehlich JE, Benning C (2003) A permease-like protein involved in ER to thylakoid lipid transfer in Arabidopsis. EMBO J **22**: 2370–2379

Yamaguchi Y, Nakamura T, Kusano T, Sano H (2000) Three Arabidopsis genes encoding proteins with differential activities for cysteine synthase and β-cyanoalanine synthase. Plant Cell Physiol **41**: 465–476

Yang W, Dong R, Liu L, Hu Z, Li J, Wang Y, Ding X, Chu Z (2016) A novel mutant allele of SSI2 confers a better balance between disease resistance and plant growth inhibition on Arabidopsis thaliana. BMC Plant Biol **16**: 208

Yang W, Gutbrod P, Gutbrod K, Peisker H, Song X, Falz A-L, Meyer AJ, Dörmann P (2022) 2-Hydroxy-phytanoyl-CoA lyase (AtHPCL) is involved in phytol metabolism in Arabidopsis. Plant J **109**: 1290–1304

Yao J, Withers J, He SY (2013) Pseudomonas syringae infection assays in Arabidopsis. Methods Mol Biol **1011**: 63–81

Yoneda Y, Hieda M, Nagoshi E, Miyamoto Y (1999) Nucleocytoplasmic protein transport and recycling of Ran. Cell Struct Funct **24**: 425–433

Zhao Q, Leung S, Corbett AH, Meier I (2006) Identification and Characterization of the Arabidopsis Orthologs of Nuclear Transport Factor 2, the Nuclear Import Factor of Ran. Plant Physiol **140**: 869–878

Zhou N, Tootle TL, Glazebrook J (1999) Arabidopsis PAD3, a gene required for camalexin biosynthesis, encodes a putative cytochrome P450 monooxygenase. Plant Cell **11**: 2419–2428

Zhu J-K (2016) Abiotic Stress Signaling and Responses in Plants. Cell **167**: 313–324

Zipfel C, Robatzek S, Navarro L, Oakeley EJ, Jones JDG, Felix G, Boller T (2004) Bacterial disease resistance in Arabidopsis through flagellin perception. Nature **428**: 764–767
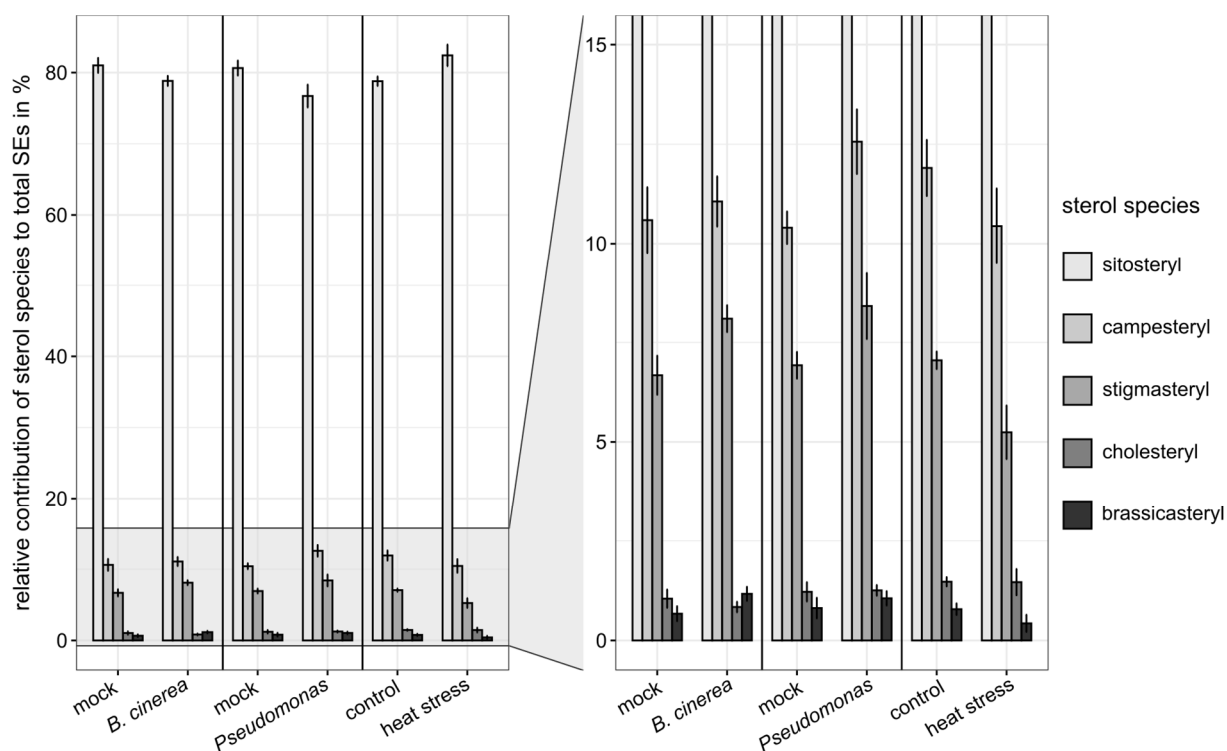
Supplemental Figure S1: Relative composition of sterol species in sterol esters of Arabidopsis leaves after different stress treatments. Sterol esters (SEs) in Arabidopsis leaves after infection with *Botrytis cinerea* (*B. cinerea*), bacterial infection with *Pto* DC3000 *ΔavrPto/ΔavrPtoB* (*Pseudomonas*) or heat stress for 24 hours at 37°C were determined. Normalised signal intensities of SEs with a common steryl moiety were combined, subsequently the relative contribution of the combined value to total SE signal intensity was calculated. Values are shown as mean ± standard deviation, n = 5 biological replicates.
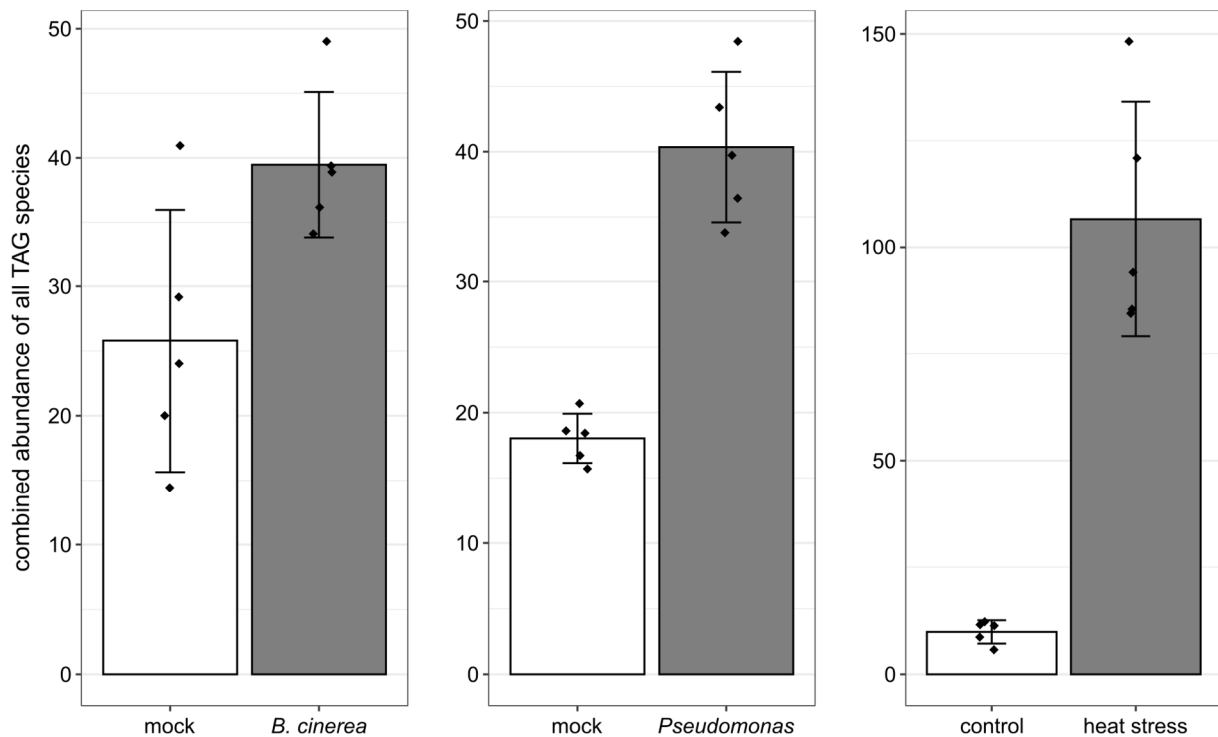
Supplemental Figure S2: Total TAG signal intensities in Col-0 leaves after different stress treatments. Arabidopsis plants were infected with *Botrytis cinerea* (*B. cinerea*), *Pto* DC3000 *ΔavrPto/ΔavrPtoB* (*Pseudomonas*) or heat stressed. Subsequently, triacylglycerol (TAGs) were analysed, their signal intensities quantified and normalised to signal intensities of the internal standard. Normalised values of all TAGs in the respective treatments were then combined together into a combined standard-corrected TAG intensity value, individual for each treatment. Values are shown as mean ± standard deviation, n = 5 biological replicates.
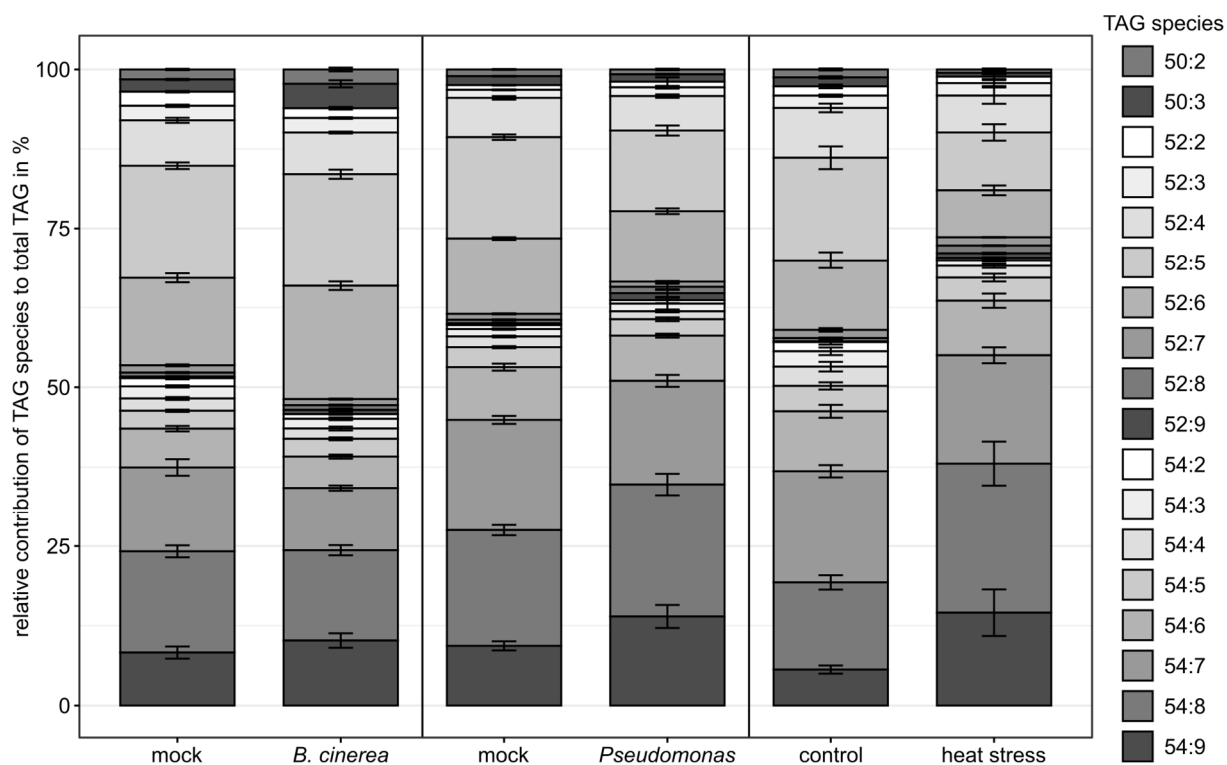
Supplemental Figure S3: Relative TAG species composition of leaves after various stress treatments. Arabidopsis Col-0 was either infected with one of the pathogens *Pto* DC3000 *ΔavrPto/ΔavrPtoB* (*Pseudomonas*) or *Botrytis cinerea* (*B. cinerea*), or heat stressed before subsequent analysis of the neutral lipid lipidome. For each treatment, signal intensities of TAG species were quantified and then normalised to the respective total TAG signal. Stacked bar plots follow TAG species composition from top to bottom as indicated in the legend, i.e. with the 50:2 TAG species at the top and the 54:9 TAG species at the bottom. Values are shown as mean ± standard deviation, n= 5 biological replicates.
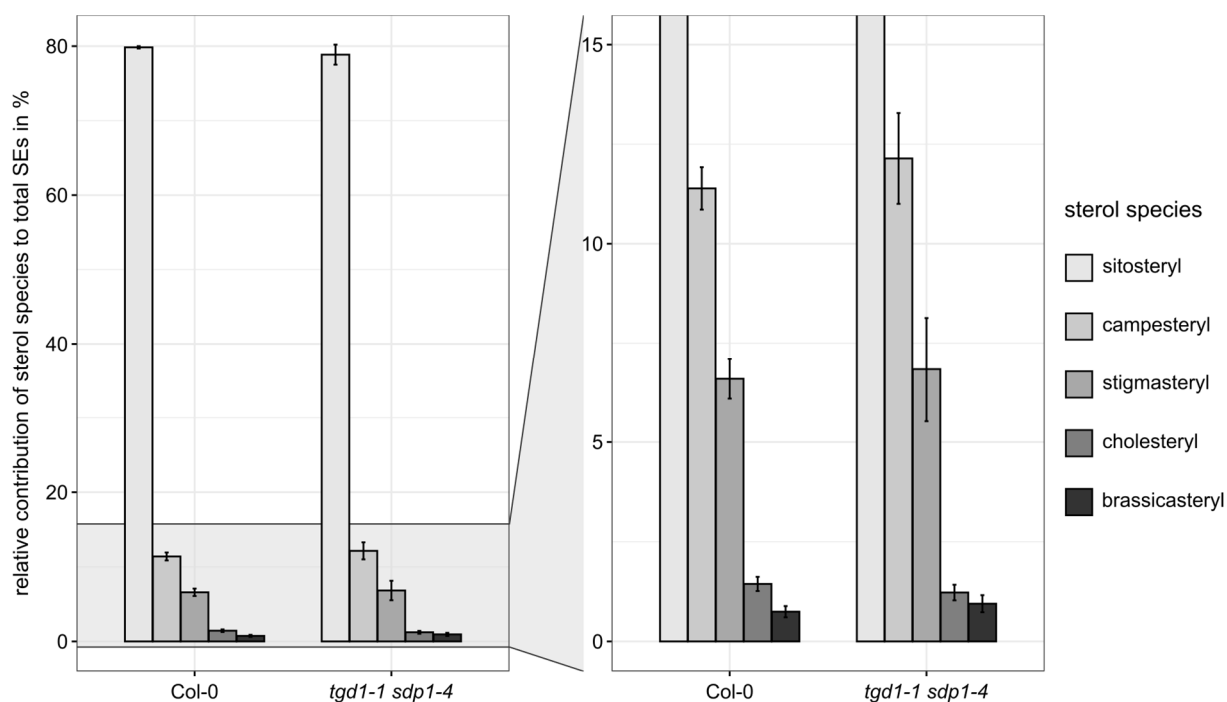
Supplemental Figure S4: Relative composition of sterol species in leaf sterol esters of Arabidopsis Col-0 and *tgd1-1 sdp1-4*. Sterol esters (SEs) in Arabidopsis leaves of Col-0 and the TAG-rich line *tgd1-1 sdp1-4* were quantified via UPLC-nanoESI-MS/MS measurements. Signals of SE species sharing the same sterol moiety were combined and their contribution to total SEs was calculated. Values are shown as mean ± standard deviation, n ≥ 4 biological replicates.
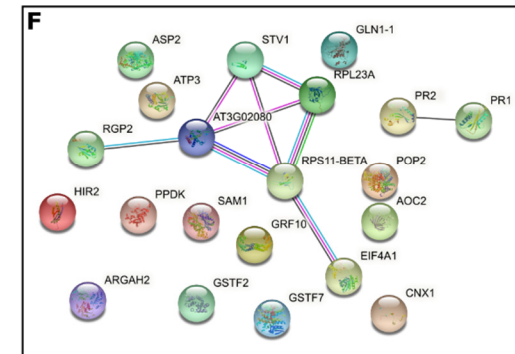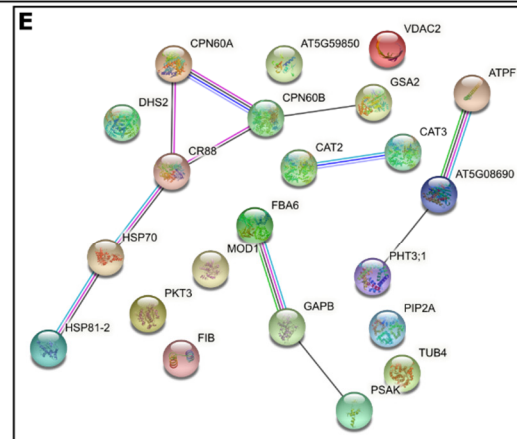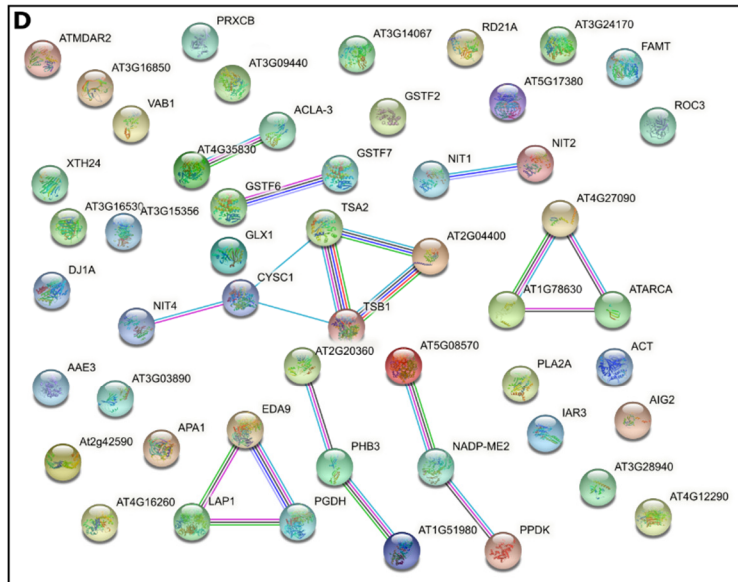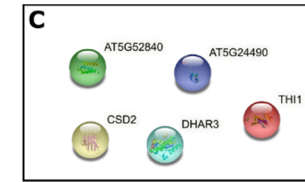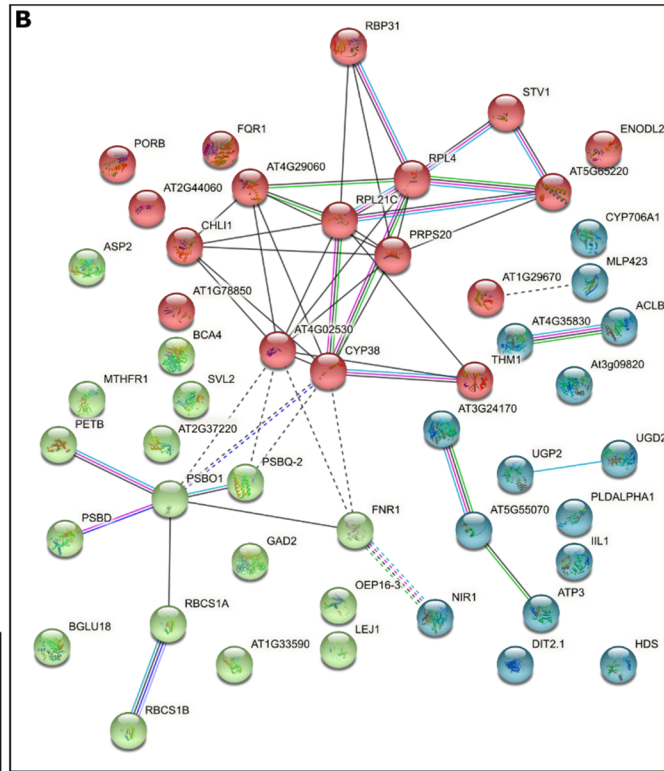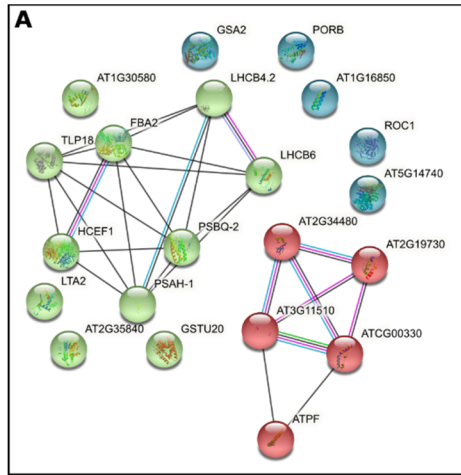
Supplemental Figure S5: STRING networks of differentially accumulating proteins in Arabidopsis Col-0 leaves after different stresses. Arabidopsis Col-0 was subjected to one of the following stress treatments: infection with *Botrytis cinerea* (A, D), heat stress for 24 hours at 37 °C (B, E) or infection with *Pseudomonas syringae* pv. *tomato* DC3000 *ΔavrPto/ΔavrPtoB* (C, F). Total protein fractions were isolated from leaves and measured by LC-MS/MS. Protein abundance in stressed plants was compared to respective mock-treated or control plants and proteins that were at least 1.5 fold depleted (A-C) or enriched (D-F) with a statistical significance of *p* < 0.05 were analysed with the STRING 11.5 webserver. Statistical significance was calculated with Student's t-test in Perseus 1.6.2.2. Proteins were clustered by STRING based on an interaction score of 0.7 or higher, including the following interaction sources: "Experiments", "Databases", "Co-expression", "Neighborhood", "Gene Fusion" and "Co-occurrence". Depleted proteins of *B. cinerea* and heat treated plants (A, B) are color-coded according to kmeans clustering of three clusters.
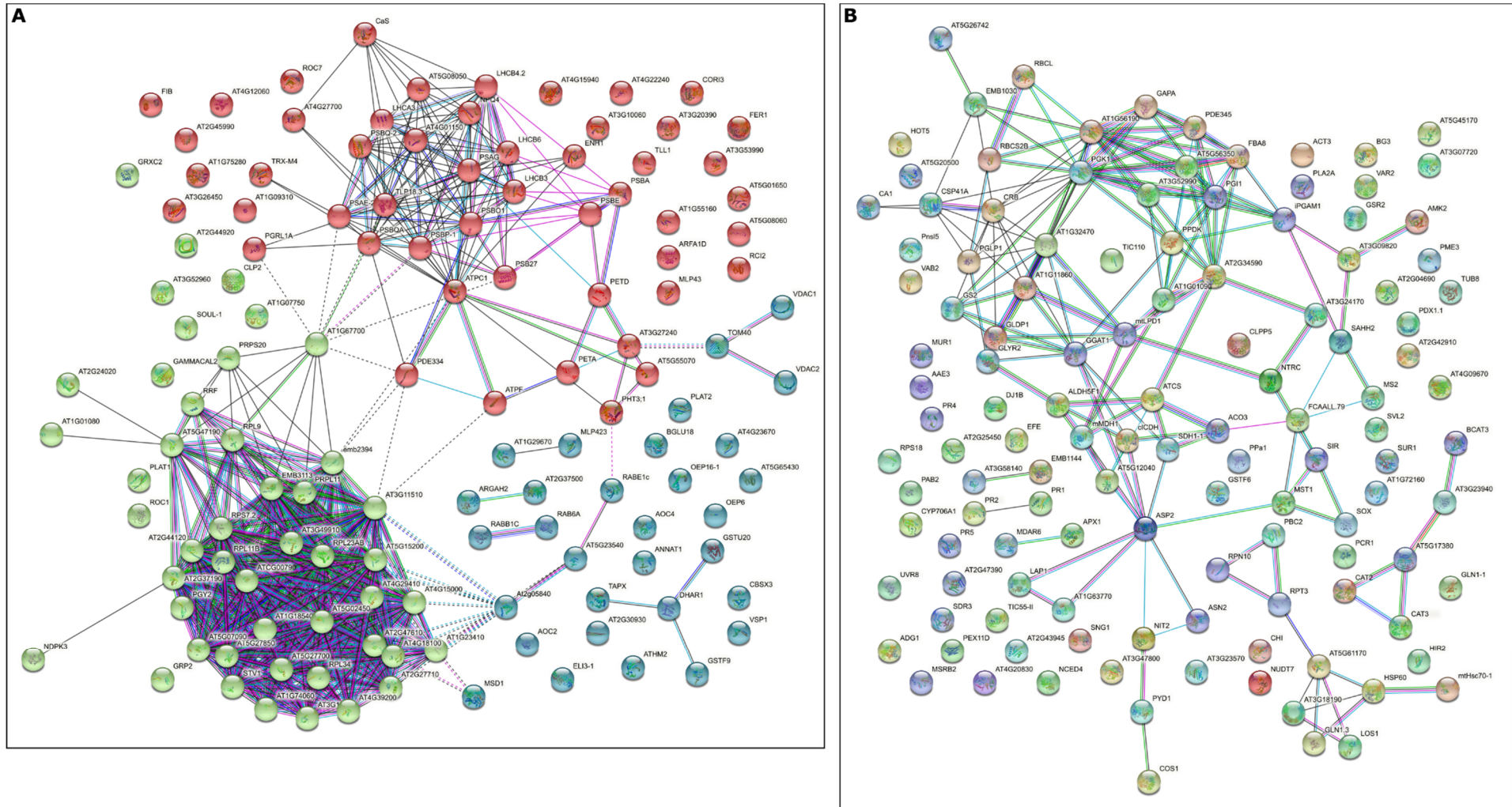
Supplemental Figure S6: STRING networks of differentially accumulating proteins in leaf total protein extracts of Arabidopsis Col-0 and *tgd1-1 sdp1-4*. The proteome of total protein extracts from non-stressed leaves of Col-0 and *tgd1-1 sdp1-4* was determined and differences in protein abundance between double mutant and wild type analysed by Student's t-test. Proteins depleted (A) or enriched (B) in the mutant with $p < 0.05$ were selected for cluster analysis with STRING 11.5. Protein interactions of high confidence (interaction score ≥ 0.7) are displayed. Interaction scores were based on the following data sources: "Experiments", "Databases", "Co-expression", "Neighborhood", "Gene Fusion" and "Co-occurrence". Depleted proteins (A) are color-coded according to kmeans clustering of three clusters.
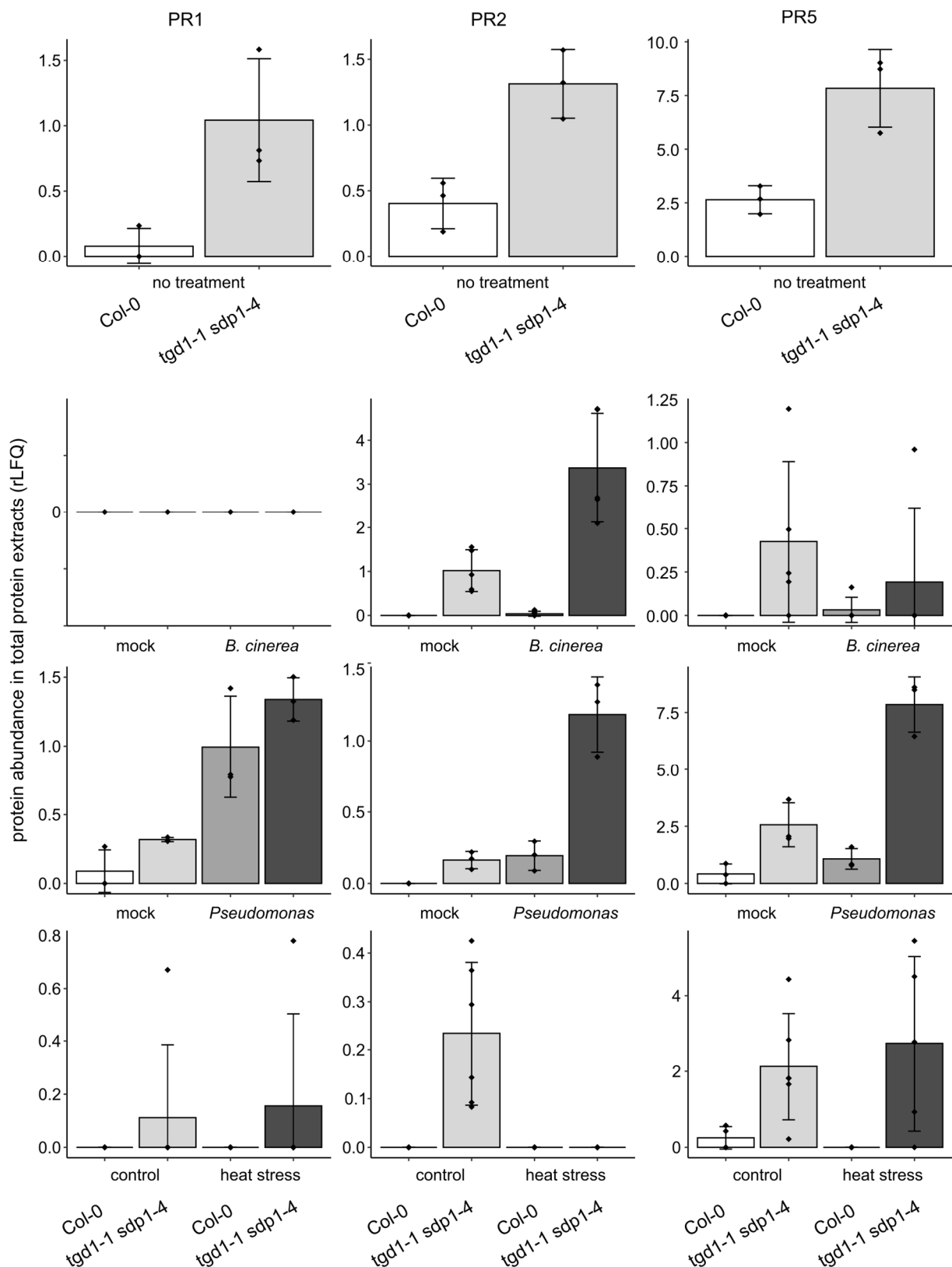
Supplemental Figure S7: Protein abundance of three pathogenesis-related proteins in Arabidopsis leaves of Col-0 and *tgd1-1 sdp1-4* after different treatments. Arabidopsis plants were harvested after infection with *Botrytis cinerea* (*B. cinerea*), *Pseudomonas syringae* pv. *tomato* DC3000 *ΔavrPto/ΔavrPtoB* (*Pseudomonas*), heat stress for 24 hours at 37 °C or no treatment at all. The proteome of total leaf protein extracts was measured and the abundance (rLFQ) of the pathogenesis-related (PR) proteins PR1, PR2 and PR5 was determined. n ≥ 3 biological replicates for each treatment.
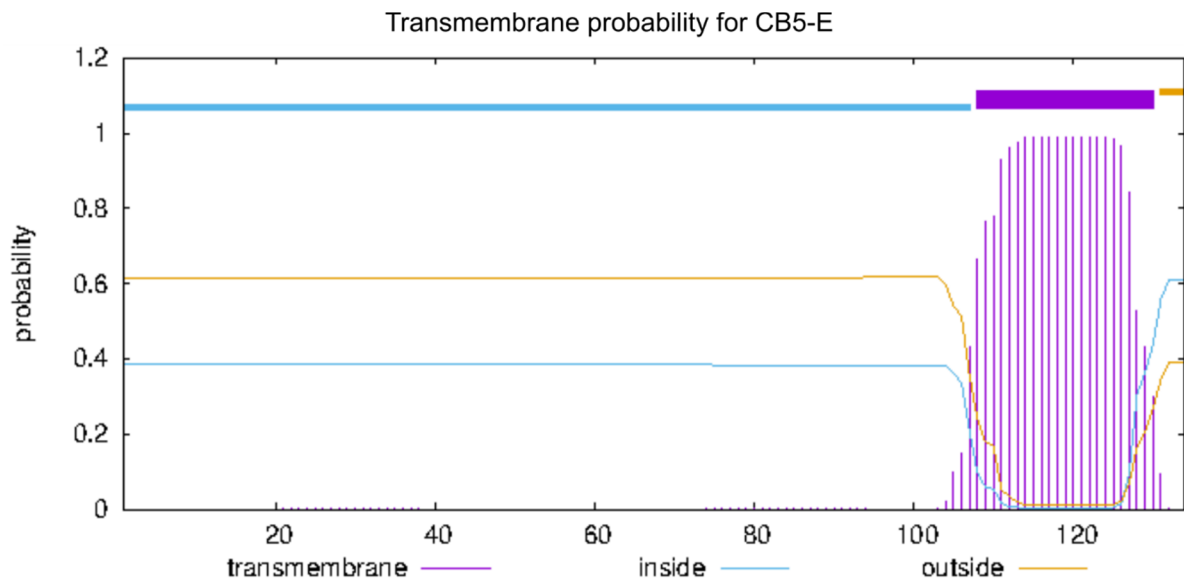
Supplemental Figure S8: Prediction of the membrane interacting region in CB5-E. The protein sequence of CB5-E with the UniProt identifier Q42342 was used to predict a putative C-terminal transmembrane region with the TMHMM 2.0 server. The prediction is based on hidden Markov models and the potential region of membrane interaction is shown in purple.
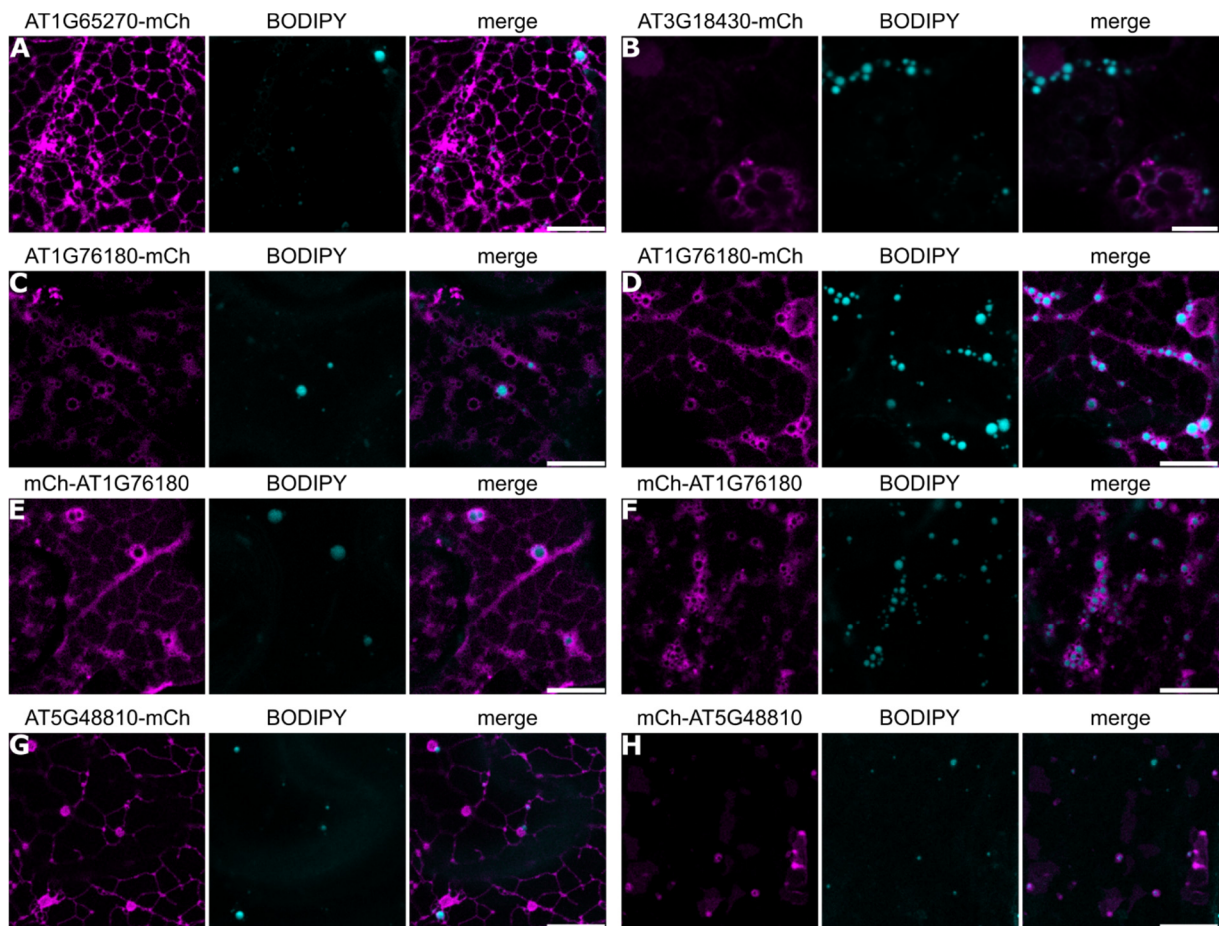
Supplemental Figure S9: Additional subcellular localisation studies of candidate proteins in *Nicotiana benthamiana* leaves. Subcellular localisation studies were carried out by transient expression in *N. benthamiana* leaves. Candidate proteins were fused to an mCherry-tag (magenta channel) and LDs were stained with BODIPY 493/503 (cyan channel). Proteins with the accession number AT1G65270 (A) and AT3G18430 (B) carried the mCherry-tag at the C-terminus of the protein, while proteins with the accession number AT1G76180 and AT5G48810 were studied with C-terminal (C,D,G) and N-terminal (E,F,H) mCherry-tag. Possible localisation of AT1G76180 to LDs was analysed with the protein expressed alone (C, E) or in co-expression experiments with the mouse enzyme DIACYLGLYCEROL ACYLTRANSFERASE 2 to induce LD-formation (D, F). Bars = 10 μm.
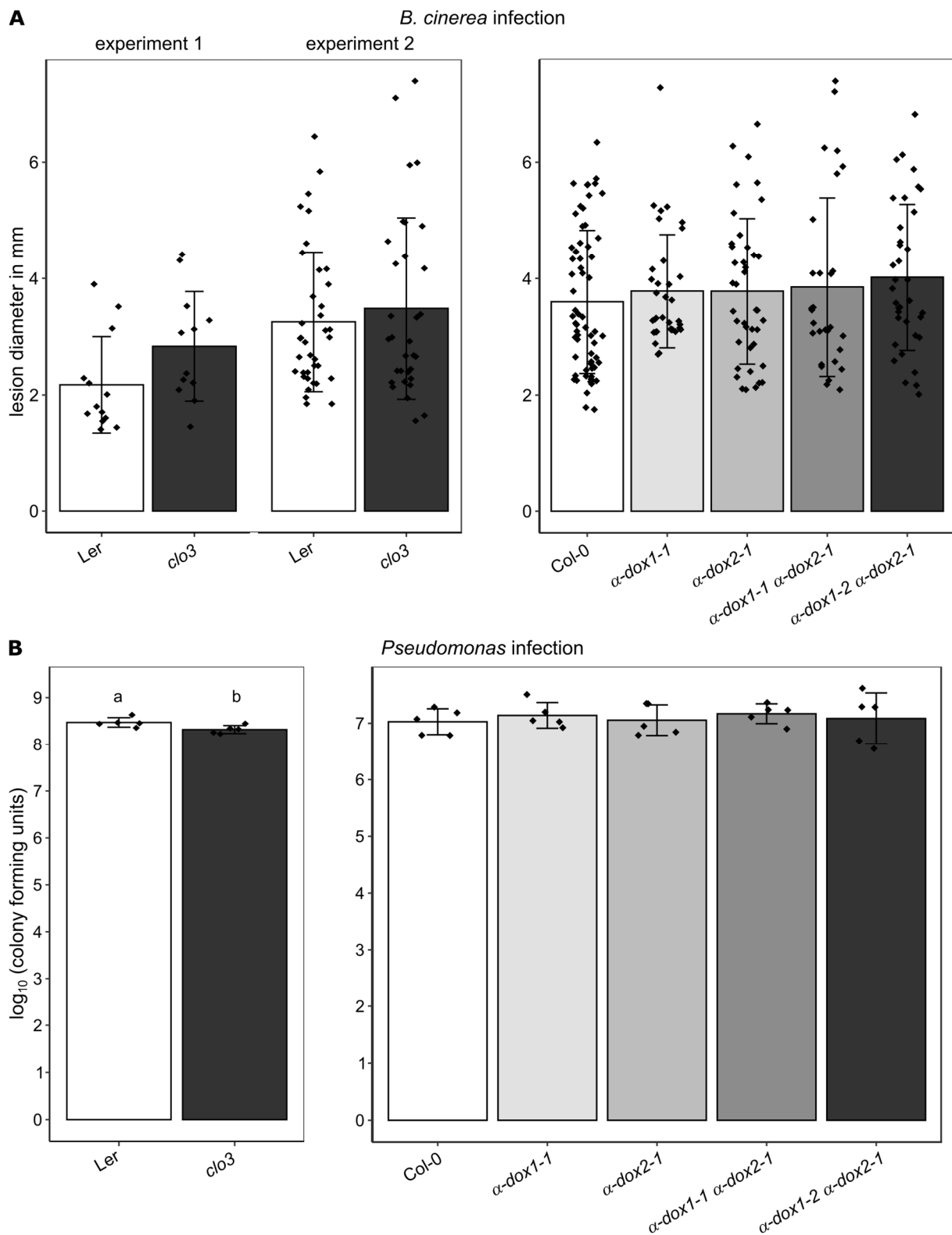
Supplemental Figure 10: Additional independent experiments testing pathogen susceptibility of T-DNA mutants of *CLO3* and *α-DOX1*. Plants were analysed by drop-inoculation of *Botrytis cinerea* (A) or spray-infection with *Pseudomonas syringae* pv. *tomato* DC3000 (B). Drop inoculation with *B. cinerea* was performed in two additional experiments for the *clo3* mutant with n ≥ 12 leaves and n ≥ 32 leaves, respectively. n ≥ 29 leaves for *B. cinerea* assays of α-dox mutants. In (B), n = 5 biological replicates for each Arabidopsis line. All results were tested for significant differences with Wilcoxon-Mann-Whitney-Test (CLO3) or Kruskal-Wallis test (α-DOX), however, a significant difference ($p > 0.05$) was only observed for *clo3* plant spray-infected with *Pseudomonas* and is indicated by different letters.

Supplemental Table S1: Metadata file for LC-MS/MS data processing with MaxQuant.	
Proteome of *Arabidopsis thaliana* leaves, see also Supplemental Dataset S5	
1. General features	
Responsible persons	Prof. Till Ischebeck[1], Dr. Oliver Valerius[2], Dr. Kerstin Schmitt[2], Prof. Gerhard H. Braus[2] 1 Institute of Plant Biology and Biotechnology (IBBP), University of Münster, Green Biotechnology, Münster 48143, Germany 2 Institute for Microbiology and Genetics and Service Unit LCMS Protein Analytics, Department for Molecular Microbiology and Genetics, University of Göttingen, Göttingen 37077, Germany

Instrument manufacturer, model	Thermo Fisher Scientific, Orbitrap Velos Pro
	    - all samples marked with V
	 Thermo Fisher Scientific, Orbitrap Q Exactive HF
	    - all samples marked with Q

Experimental Design	Analysis of total protein fraction of Arabidopsis Col-0 and *tgd1-1 sdp1-4* leaves and lipid droplet-enriched fraction of Arabidopsis *tgd1-1 sdp1-4* leaves after the following treatments: 1) no stress, 2) infection with *Botrytis cinerea* (*B. cinerea*) and mock treatment, 3) infection with *Pseudomonas syringae* pv. *tomato* DC3000 *ΔavrPto ΔavrPtoB* (*Pseudomonas*) and mock treatment, 4) heat stress for 24 hours at 37°C and control treatment
Groups	Total protein, lipid droplet-enriched fraction
Biological and technical replicates	Biological replicates: 3-6 for different treatments as indicated below Technical replicates (independent LC-MS runs): 1 for each sample, unless stated otherwise PS_V_01, 02, 03: non-stressed Arabidopsis Col-0 leaves, total protein fraction (3 biological replicates) PS_V_04, 06, 08: non-stressed Arabidopsis *tgd1-1 sdp1-4* leaves, total protein fraction (3 biological replicates) PS_V_05, 07, 09: non-stressed Arabidopsis *tgd1-1 sdp1-4* leaves, LD-enriched fraction (3 biological replicates) PS_Q_62, 71, 79: mock-treated (control to *B. cinerea*-treated) Arabidopsis Col-0 leaves, total protein fraction (3 biological replicates) PS_Q_64, 72, 75: mock-treated (control to *B. cinerea*-treated) Arabidopsis *tgd1-1 sdp1-4* leaves, total protein fraction (3 biological replicates) PS_Q_67, 70, 77: mock-treated (control to *B. cinerea*-treated) Arabidopsis *tgd1-1 sdp1-4* leaves, LD-enriched fraction (3 biological replicates) PS_Q_66, 68, 78: *B. cinerea*-treated Arabidopsis Col-0 leaves, total protein fraction (3 biological replicates) PS_Q_65, 73, 74: *B. cinerea*-treated Arabidopsis *tgd1-1 sdp1-4* leaves, total protein fraction (3 biological replicates) PS_Q_63, 69, 76: *B. cinerea*-treated Arabidopsis *tgd1-1 sdp1-4* leaves, LD-enriched fraction (3 biological replicates) PS_Q_10, 18, 27: mock-treated (control to *Pseudomonas*-treated) Arabidopsis Col-0 leaves, total protein fraction (3 biological replicates) PS_Q_14, 16, 19: mock-treated (control to *Pseudomonas*-treated) Arabidopsis *tgd1-1 sdp1-4* leaves, total protein fraction (3 biological replicates)

	PS_Q_17, 22, 25: mock-treated (control to *Pseudomonas*-treated) Arabidopsis *tgd1-1 sdp1-4* leaves, LD-enriched fraction (3 biological replicates) PS_Q_12, 21, 26: *Pseudomonas*-treated Arabidopsis Col-0 leaves, total protein fraction (3 biological replicates) PS_Q_15, 20, 24: *Pseudomonas*-treated Arabidopsis *tgd1-1 sdp1-4* leaves, total protein fraction (3 biological replicates) PS_Q_11, 13, 23: *Pseudomonas*-treated Arabidopsis *tgd1-1 sdp1-4* leaves, LD-enriched fraction (3 biological replicates) PS_V_38, 45, 51, 57: control Arabidopsis Col-0 leaves, total protein fraction (4 biological replicates) PS_V_29, 34, 43, 48, 53, 61: control Arabidopsis *tgd1-1 sdp1-4* leaves, total protein fraction (6 biological replicates) PS_V_31, 36, 41, 46, 55, 59: control Arabidopsis *tgd1-1 sdp1-4* leaves, LD-enriched fraction (6 biological replicates) PS_V_32, 37, 44, 50, 56: heat-stressed Arabidopsis Col-0 leaves, total protein fraction (5 biological replicates) PS_V_28, 39, 42, 52, 60: heat-stressed Arabidopsis *tgd1-1 sdp1-4* leaves, total protein fraction (5 biological replicates) PS_V_30, 35, 40, 49, 54, 58: heat-stressed Arabidopsis *tgd1-1 sdp1-4* leaves, LD-enriched fraction (6 biological replicates) PS_Q_174, 175, 176, 177, 178: mock-treated (control to *B. cinerea*-treated) Arabidopsis Col-0 leaves, total protein fraction (5 biological replicates) PS_Q_179, 180, 181, 182, 183: mock-treated (control to *B. cinerea*-treated) Arabidopsis *tgd1-1 sdp1-4* leaves, total protein fraction (5 biological replicates) PS_Q_189, 190, 191, 192, 193: *B. cinerea*-treated Arabidopsis Col-0 leaves, total protein fraction (5 biological replicates) PS_Q_184, 185, 186, 187, 188: *B. cinerea*-treated Arabidopsis *tgd1-1 sdp1-4* leaves, total protein fraction (5 biological replicates)
Sample amount	97
2. Electrospray Ionisation (ESI)	
Supply type (static or fed)	fed
Interface manufacturer	Thermo Fisher Scientific
Sprayer type	Nanospray Flex Ion Source
3.1 Post source component – Analyser	
	Velos Pro Hybrid: Linear ion trap – Orbitrap Q Exactive HF: Orbitrap analyser
3.2 Post source component – Activation/dissociation	
Instrument component where the activation/dissociation occurs	Velos Pro Hybrid: Velos Pro Linear ion trap Q Exactive HF: HCD cell
Gas type	Velos Pro Hybrid: Helium Q Exactive HF: Nitrogen
Activation/dissociation type	Velos Pro Hybrid: CID Q Exactive HF: HCD

4.1 Spectrum and peak list generation and annotation – Data acquisition	
Software name and version	Xcalibur 4.0
Acquisition parameters	Data-dependent Top10
Software name and version	MaxQuant 1.6.2.17
4.2 Spectrum and peak list generation and annotation – Resulting data	
Location of source and processed files	The mass spectrometry proteomics data will be deposited to the ProteomeXchange Consortium via the PRIDE partner repository
5. Description of the software and methods applied in the quantitative analysis	
Quantification software	MaxQuant 1.6.2.17
Description of the selection and/or matching method of features, together with the description of the method of the primary extracted quantification values determination for each feature and/or peptide	Upload of all .raw files into the software. Grouping of technical replicates as one Experiment ("set experiment"). Group-specific parameters: 1) Type: default 2) Digestion: default 3) Modifications: default 4) Label-free quantification: LFQ, default 5) Instrument: intensity determination: total sum, rest default 6) First search: default 7) Misc: default Global parameters 1) Sequences: updated TAIR10 peptides from 14.12.2010, rest default 2) Identification: PSM FDR=0.01, protein FDR=0.01, Match between runs ✓, rest default 3) Protein quantification: default 4) Label free quantification: iBAQ ✓ 5) Tables: default 6) Folder locations: default 7) MS/MS analyzer: FTMS recalibration ✓, rest default 8) Advanced: default
Confidence filter of features or peptides prior to quantification	Global parameters: identification: PSM FDR=0.01, protein FDR=0.01, rest default
Normalisation	All values were divided by the total iBAQ intensities or total LFQ intensities in one sample and multiplied by 1000.

Supplemental Table S2: Parameters for lipid analysis by UPLC-nanoESI-MS/MS. Neutral lipid lipidome of *Arabidopsis thaliana* leaves, see also Supplemental Datasets S1, S2. The ionisation mode depicts the polarity of the nanoESI source, while Q1 and Q3 list the structure of the respective parent and product ions.

	Solvent start condition (% B)	Flow rate (ml/min)	Ionisation mode	Q1	Q3	Declustering potential [V]	Entrance potential [V]	Collision energy [V]	Cell exit potential [V]
Glycerolipids									
Triacylglycerols	90	0.13	Positive	$[M+NH_4]^+$	$[M - RCOO]^+$	140	10	40	6
Sterol lipids									
Sterol esters	90	0.13	Positive	$[M+NH_4]^+$	$[Sterol - OH]^+$	140	10	22	6

	Primer forward (5'-3')	Primer reverse (5'-3')
Supplemental Table S3: Primers used for gene expression analysis via qPCR		
Target genes		
PR1	GTGCTCTTGTTCTTCCCTCG	GCCTGGTTGTGAACCCTTAG
PR2	GTTTCTGGAGCAGGGCTTGA	ACCTTCCTTGAGACGGAGGA
PR5	TGTGTCTCTGACCTCAACGC	TCTCACAGGCACTCTTGCAG
Reference gene		
AT3G01150	GATCTGAATGTTAAGGCTTTTAGCG	GGCTTAGATCAGGAAGTGTATAGTCTCTG

Supplemental Table S4: Primers used for Gateway cloning and sequencing

Cloning of candidates

Candidate	Vector	Primer forward (5'-3')	Primer reverse (5'-3')
LDNP	pMDC32-ChC	CTTTGTACAAAAAAGCAGGCTCATGGATCCAGCGCGGGAATG	CTTTGTACAAGAAAGCTGGGTCTTGGGAGTCAGGATCTTTACCA
CB5-E	pMDC32-ChC	CTTTGTACAAAAAAGCAGGCTCCATGTCTTCAGATCGGAAGGTTC	GGGGACCACTTTGTACAAGAAAGCTGGGTCGTCTTTCTTGGTATAGTGACGGAC
CB5-E	pMDC32-ChN	CTTTGTACAAAAAAGCAGGCTCCATGTCTTCAGATCGGAAGGTTC	CTTTGTACAAGAAAGCTGGGTCCTAGTCTTTCTTGGTATAGTGACGGAC
AT1G65270	pMDC32-ChC	CTTTGTACAAAAAAGCAGGCTCCATGGCGAAGCTCACACTTC	CTTTGTACAAGAAAGCTGGGTCTCTTCTCCTGGCAGCTGGT
AT3G18430	pMDC32-ChC	CTTTGTACAAAAAAGCAGGCTCATGGGGAATACTTCATCGATGC	CTTTGTACAAGAAAGCTGGGTCATCCACAGGAATTTCAACGTCC
AT1G76180	pMDC32-ChC	CTTTGTACAAAAAAGCAGGCTCCATGGCTGAGGAAATCAAGAATG	CTTTGTACAAGAAAGCTGGGTCTTCTTTATCTTTCTTCTCCTCCTC
AT1G76180	pMDC32-ChN	CTTTGTACAAAAAAGCAGGCTCCATGGCTGAGGAAATCAAGAATG	CTTTGTACAAGAAAGCTGGGTTTATTCTTTATCTTTCTTCTCCTCCTC
AT5G48810	pMDC32-ChC	CTTTGTACAAAAAAGCAGGCTCCATGGGCGGAGACGGAAAAGTT	CTTTGTACAAGAAAGCTGGGTCAGAAGAAGGAGCCTTGGTCT
AT5G48810	pMDC32-ChN	CTTTGTACAAAAAAGCAGGCTCCATGGGCGGAGACGGAAAAGTT	CTTTGTACAAGAAAGCTGGGTCTCAAGAAGAAGGAGCCTTGGTCT

Sequencing

Binding site	Primer forward (5'-3')	Primer reverse (5'-3')
mCherry-RP		CACCCTTGGTCACCTTCAGC
pMDC32-FP	GAGAGGACCTCGACTCTAGAGGA	
mCherry-FP	GCCTACAACGTCAACATCAAG	
pMDC32-RP		GTATTAAATGTATAATTGCGGGACTCTAATCA

6 Additional results

Supplemental datasets containing processed proteomics data are available as additionally uploaded files and are included on a data drive in the printed version of this thesis.

Author contribution:

Patricia Scholz planned and performed lipidomic analysis of steryl glycosides with the exception of LC-MS/MS measurements. She processed and analysed the raw data.

For proteomic analysis of root LDs up to data processing with MaxQuant, she planned and performed the experiments excluding LC-MS/MS measurements together with Philipp William Niemeyer. She analysed the obtained raw data.

6 Additional results

In manuscript I, Arabidopsis Col-0 and especially the mutant *tgd1-1 sdp1-4* were analysed in the context of LDs and LD proteome dynamics in leaves. However, additional results were obtained that could not be included in the manuscript but will be shown in the following. Firstly, analysis of neutral lipids in Arabidopsis leaves also comprised the examination of steryl glycoside levels in reaction to stress and in comparison between the two lines. Secondly, the *tgd1-1 sdp1-4* mutant was employed to obtain an overview of the LD proteome in Arabidopsis roots.

6.1 Steryl glycosides accumulate in leaves of the *tgd1-1 sdp1-4* mutant

We analysed the changes of TAGs and SEs in leaves of Arabidopsis Col-0 plants in reaction to different stresses and in comparison to the double mutant *tgd1-1 sdp1-4* (Figure 1 in manuscript I). In addition, we evaluated steryl glycosides (SGs), as they also derive from phytosterols by conjugation of a sugar molecule to the phytosterol's 3-hydroxy group.

In Arabidopsis leaves infected with *Botrytis cinerea*, *Pseudomonas syringae* pv. *tomato* DC3000 *ΔavrPto ΔavrPtoB*, or heat stressed at 37°C for 24 hours, SGs did not change significantly compared to respective mock or control conditions (Figure 9A, Supplemental Table S1). However, in leaves of the *tgd1-1 sdp1-4* mutant, SGs accumulated 30-fold compared to Col-0 (Figure 9B, Supplemental Table S1). The physiological reason for this accumulation is unclear, nevertheless, it is interesting to note that in this TAG-accumulating mutant sterol-derived compounds are also affected.
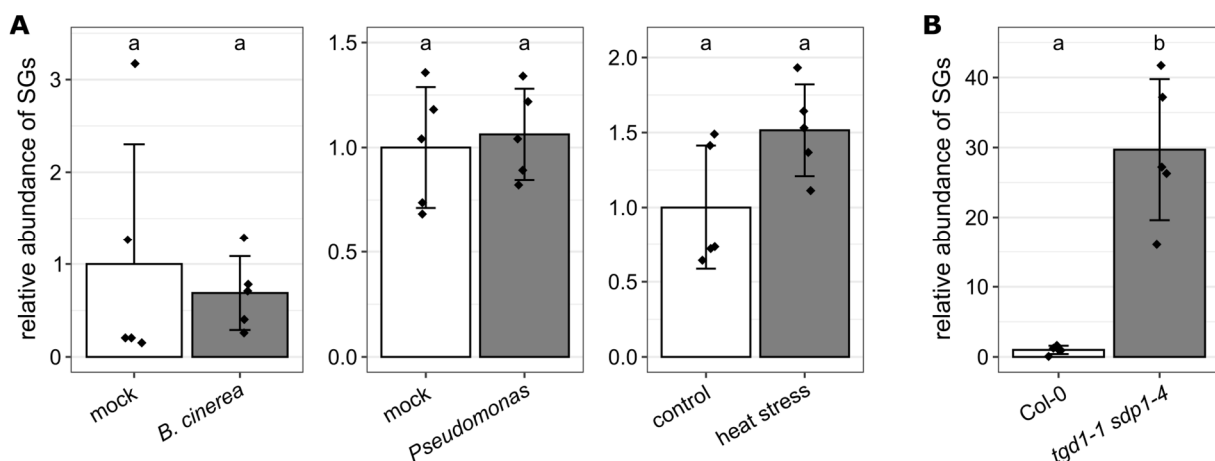
Figure 9: Changes of steryl glycosides in Arabidopsis leaves in reaction to stress and in the oil-rich mutant *tgd1-1 sdp1-4*. Arabidopsis Col-0 plants were infected with *Botrytis cinerea* (*B. cinerea*), *Pseudomonas syringae* pv. *tomato* DC3000 *ΔavrPto/ΔavrPtoB* (*Pseudomonas*) or kept for 24 hours at 37 °C (heat stress). After stress treatments, leaves were harvested and steryl glycosides (SGs) analysed via UPLC-nanoESI-MS/MS. Signal intensities were quantified and normalised to an internal standard. Values of all detected SGs were added up, and for each stress treatment the combined sum was normalised to the value of the respective control treatment (A). Furthermore, total SGs in leaves of *tgd1-1 sdp1-4* were quantified and normalised to Col-0 plants (B). Statistical comparisons were carried out using the Wilcoxon-Mann-Whitney-Test with Holm-Bonferroni correction for multiple comparisons. Different letters indicate significant differences with $p < 0.05$; n = 5 biological replicates for each treatment and line. Values are given as mean ± standard deviation.

6.2 Proteomic analysis of LDs in Arabidopsis roots

The proteome of root LDs has so far not been explored in any species, probably because LD content appears low and it is not easy to obtain sufficient material. However, the *tgd1* and *sdp1* mutation were independently observed to accumulate TAGs not only in leaves but also in roots (Xu et al., 2005; Kelly et al., 2013). In addition, cultivation of Arabidopsis in liquid culture was reported to yield high root biomass (Hétu et al., 2005). We therefore grew root cultures of *tgd1-1 sdp1-4*, enriched LDs and analysed the proteome of LD-enriched fractions in comparison to the original total cellular protein fraction. LD-enrichment and proteome analysis was carried out for five replicates (Supplemental Dataset S1).

Table 2: LD proteins detected in the LD-enriched fraction of Arabidopsis *tgd1-1 sdp1-4* roots. LDs were enriched from roots of Arabidopsis grown in axenic liquid culture, analysed via proteomics and quantified with the iBAQ algorithm. iBAQ values were then normalised to the total sum of all proteins, the normalised value in per mille is given here as riBAQ. In addition, the number of replicates in which a protein was detected is indicated with five replicates in total. * denote proteins that could not be unambiguously identified

Protein name	AGI code	riBAQ	replicates
CLO3	AT2G33380	0.20	5
CLO4	AT1G70670	2.07	5
HSD1/1 *	AT5G50700	0.10	4
HSD3	AT3G47360	0.09	4
HSD4/7 *	AT5G50690	0.45	5
LDAP1	AT1G67360	12.48	5
LDAP2	AT2G47780	0.02	4
LDAP3	AT3G05500	135.79	5
LDIP	AT5G16550	4.80	5
PUX10	AT4G10790	0.21	5
SMT1	AT5G13710	1.88	5
CAS1	AT2G07050	0.33	5
OBL1	AT3G14360	0.15	5
OBL3	AT1G45201	0.54	5
OBL4	AT1G56630	0.42	5
OBL5	AT5G42930	0.04	4
α-DOX1	AT3G01420	45.82	5
LIDL1	AT1G18460	0.08	5
LIDL2	AT1G73920	0.33	5
LIME1	AT4G33110	0.02	4
LIME2	AT4G33120	3.69	5
LDAH1	AT1G10740	0.004	1
LDAH2	AT1G23330	0.05	5
ERD7	AT2G17840	3.16	5
GPAT4	AT1G01610	0.91	5
GPAT8	AT4G00400	0.02	4
LDS1	AT1G43890	0.90	5
LDNP	AT5G04830	6.79	5
CB5E	AT5G53560	0.98	5

Several known LD proteins were found in the LD-enriched fraction of roots, 29 LD proteins in at least one replicate and 22 proteins in all five replicates of root LDs (Table 2). The detection of these LD proteins suggested a successful enrichment of LDs. Nevertheless, we wanted to analyse how proteins of different organelles are distributed into the LD fraction. To that end, we assigned subcellular localisation to proteins with unique reported localisations according to the plant proteome data base (PPDB). For each organelle, the abundance of its respective marker proteins was then added up to obtain an approximate value of the organelle protein amounts. The combined protein amounts of each organelle in the LD-enriched fraction could subsequently be normalised to the corresponding values in the proteome of total extract samples. This way, we could confirm that LD proteins are most strongly enriched, as they were 50-100 times more abundant in the LD fraction (Figure 10). Other consistently enriched organelle proteomes were found for plastoglobules, however, the highest enrichment of combined plastoglobule proteins was still less than 10-fold. All other organelles were either not consistently enriched, or depleted according to this analysis.
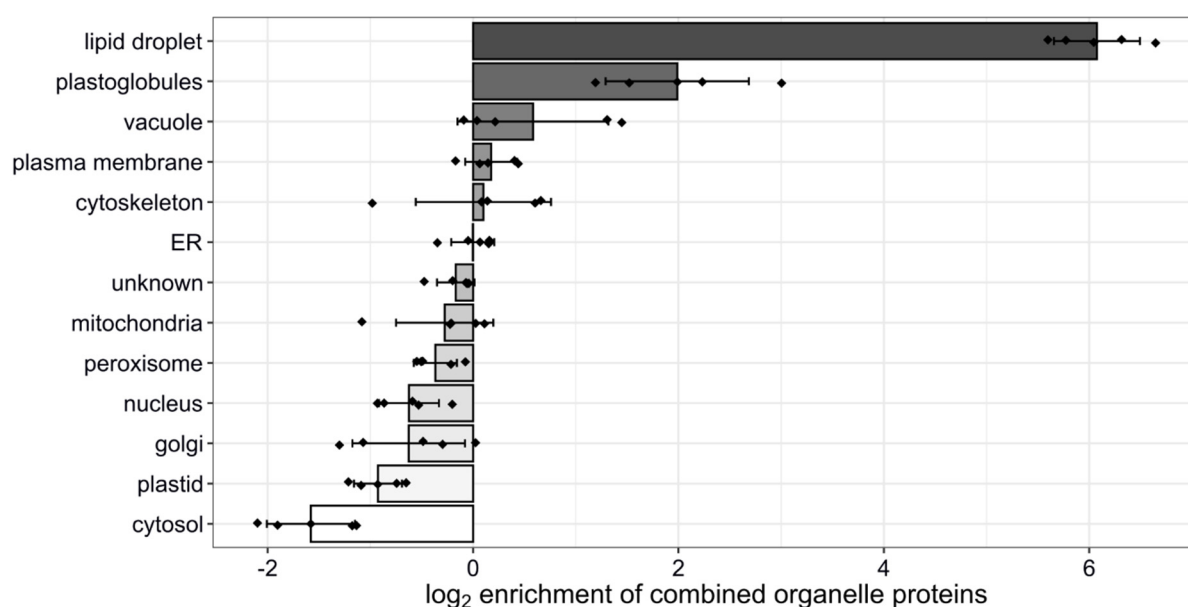
Figure 10: Enrichment of combined marker proteins of subcellular organelles. The summed abundance of marker proteins of the indicated organelles in the LD-fraction was normalised to the corresponding abundance in total extract samples. Assignment of marker proteins for all organelles was done according to the Plant Proteome Database. Log$_2$-transformed values of the enrichment are displayed. Only organelles with at least five marker proteins were considered for the analysis and all proteins that could not be assigned to a unique organelle were designated as "unknown".

6.3 Proteomics of root LDs reveal further LD protein candidates

Given the successful enrichment of known LD proteins, we looked for possible LD candidate proteins that were strongly enriched in the LD-fraction compared to the total protein fraction. To gain higher stringency in the selection of candidate proteins, we analysed only those proteins present in all five replicates of either LD-enriched fraction or total protein extract,

which resulted in a selection of 2814 proteins. For each protein, abundance in the LD-enriched fraction was divided by the abundance in the corresponding total protein extract sample and statistical significance of the enrichment was calculated by Student's t-test. Protein enrichment at LDs and the statistical significance of that enrichment was then plotted in a volcano plot (Figure 11, Supplemental Dataset S2).
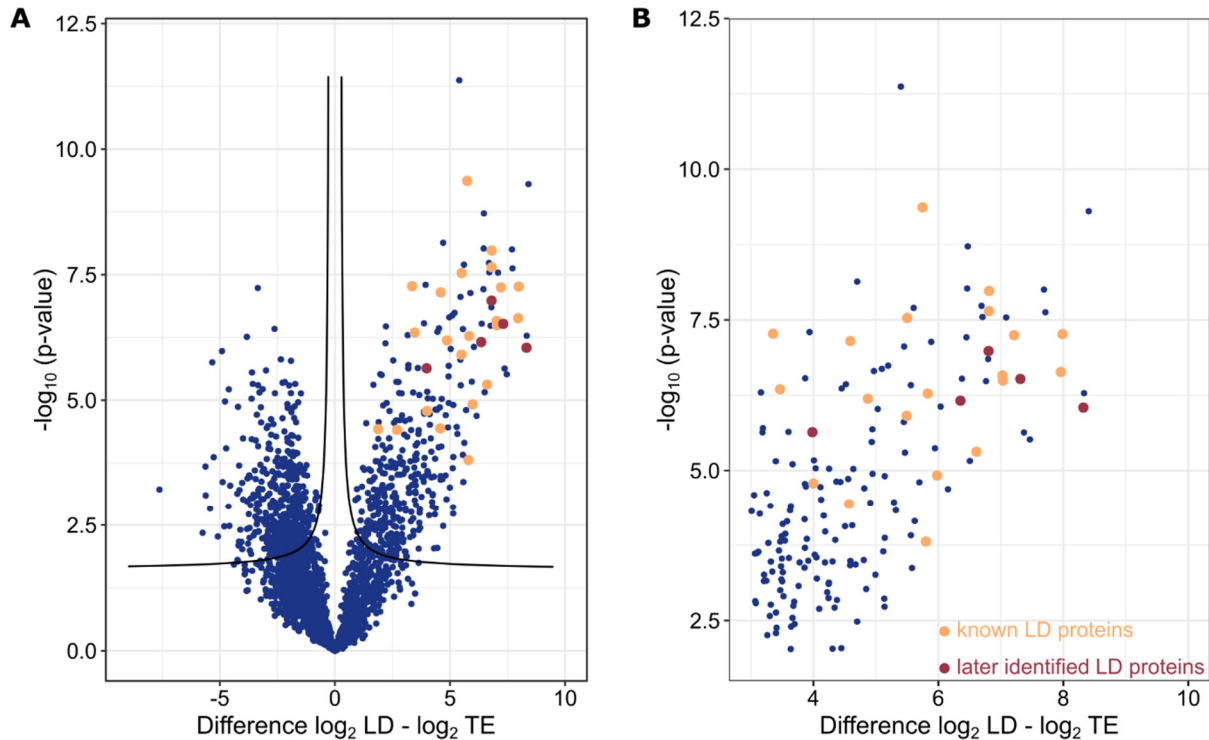
Figure 11: Analysis of Arabidopsis root proteins in the LD-enriched fraction. Protein abundance (riBAQ values) in the LD-enriched fraction was normalised to their respective abundance in total protein extracts and the significance of observed changes calculated. *P*-values were then plotted against the log$_2$-transformed ratios (A). Proteins enriched at LDs cluster in the upper right corner and a magnified section of this area is shown in (B). Previously known LD proteins are highlighted in orange and candidate proteins that were later confirmed to localise to LDs in tobacco pollen tubes are shown in dark red. Only proteins detected in all five replicates were chosen for this analysis. Black lines show a false discovery rate of 0.01.

Of the 2814 proteins analysed, 380 proteins were significantly enriched in the LD-enriched fraction (Supplemental Dataset S2). Interestingly, when analysing putative enriched GO terms of these 380 selected proteins, GO term enrichment of biological processes like 'long-chain fatty acid metabolic process', 'triterpenoid metabolic process' or 'sterol biosynthetic process' was observed. Neither GO term was enriched for the subset of proteins significantly depleted in the LD-enriched fraction of *tgd1-1 sdp1-4* roots nor for the original 2814 proteins, implicating that the respective processes could be active at LDs in roots.

Further selection of proteins significantly enriched at least 50-fold resulted in a dataset of 37 proteins, of which twelve proteins were previously described to localise to LDs. The remaining 25 proteins are interesting candidates for the identification of additional LD proteins (Supplemental Table S2). Indeed, work of other group members could confirm for four of the

listed candidate proteins that they co-localise with LDs upon transient expression in tobacco pollen tubes (unpublished work of Philipp W. Niemeyer and Janis Dabisch). Co-localisation with LDs in tobacco pollen tubes was also observed for one additional protein, ACYL-COA:LYSOPHOSPHATIDYLETHANOLAMINE ACYLTRANSFERASE 1 (LPEAT1), that had a slightly lower but still significant enrichment in the LD-enriched fraction (unpublished work of Philipp W. Niemeyer and Janis Dabisch, Table 3).

Table 3: Newly identified proteins able to localise to LDs in transiently transformed pollen tubes. Five candidate proteins could be confirmed to co-localise with LDs upon transient expression in tobacco pollen tubes. Their functional description according to TAIR, abundance in the LD-enriched fraction (riBAQ), enrichment and significance of the enrichment in the proteome of LD-fractions of roots are indicated. "n.d. in TE" denotes proteins that were not detected in total protein extract samples.

Gene symbol	AGI code	description	riBAQ	enrichment	p-value ($-\log_{10}$)
	AT1G30130	DUF1365 containing protein	0.51	n.d. in TE	6.52
LPEAT1	AT1G80950	acyl-CoA:lysophosphatidyl-ethanolamine acyltransferase	0.17	15.18	5.64
	AT4G13160	zein-binding domain containing protein	0.30	n.d. in TE	6.98
THAS1	AT5G48010	oxidosqualene cyclase	4.90	255.02	6.05
GPAT9	AT5G60620	glycerol-3-phosphate acyltransferase	0.54	77.39	6.16

Two of the new proteins found to localise to LDs have not been functionally characterised so far, so we used web tools to analyse protein structure and possible interaction with LDs. The overall domain structure was predicted by the protein family database Pfam (Mistry et al., 2021) and was dominated by a DUF1365 domain for the protein with the accession number AT1G30130 and a Zein-binding (DUF593) domain for the protein with the accession number AT4G13160, which fitted to the annotation based on TAIR. Both proteins furthermore contained disordered regions and a predicted N-terminal transmembrane region. The zein-binding domain-containing protein additionally featured a predicted coil-coil domain (Figure 12A). We also used the TMHMM web server for additional analysis of the predicted transmembrane region (Figure 12B). The TMHMM server uses hidden Markov models to predict transmembrane helices (Krogh et al., 2001). No LD protein will have a standard transmembrane helix due to the hydrophobic interior of LDs, nevertheless, the prediction identifies potential regions in the protein where interaction with the phospholipid monolayer and the hydrophobic core of LDs might occur. The TMHMM prediction corroborated the overall domain structure, by identifying putative membrane interaction regions close to the N-terminus in both proteins. These regions seem most likely to interact with the monolayer of LDs, however, in the protein with the accession number AT1G30130 an additional region between the amino acids 200-250 could be also involved in LD targeting. Further localisation studies e.g. using truncated variants will be needed to analyse the LD association of these two as of yet uncharacterised proteins.
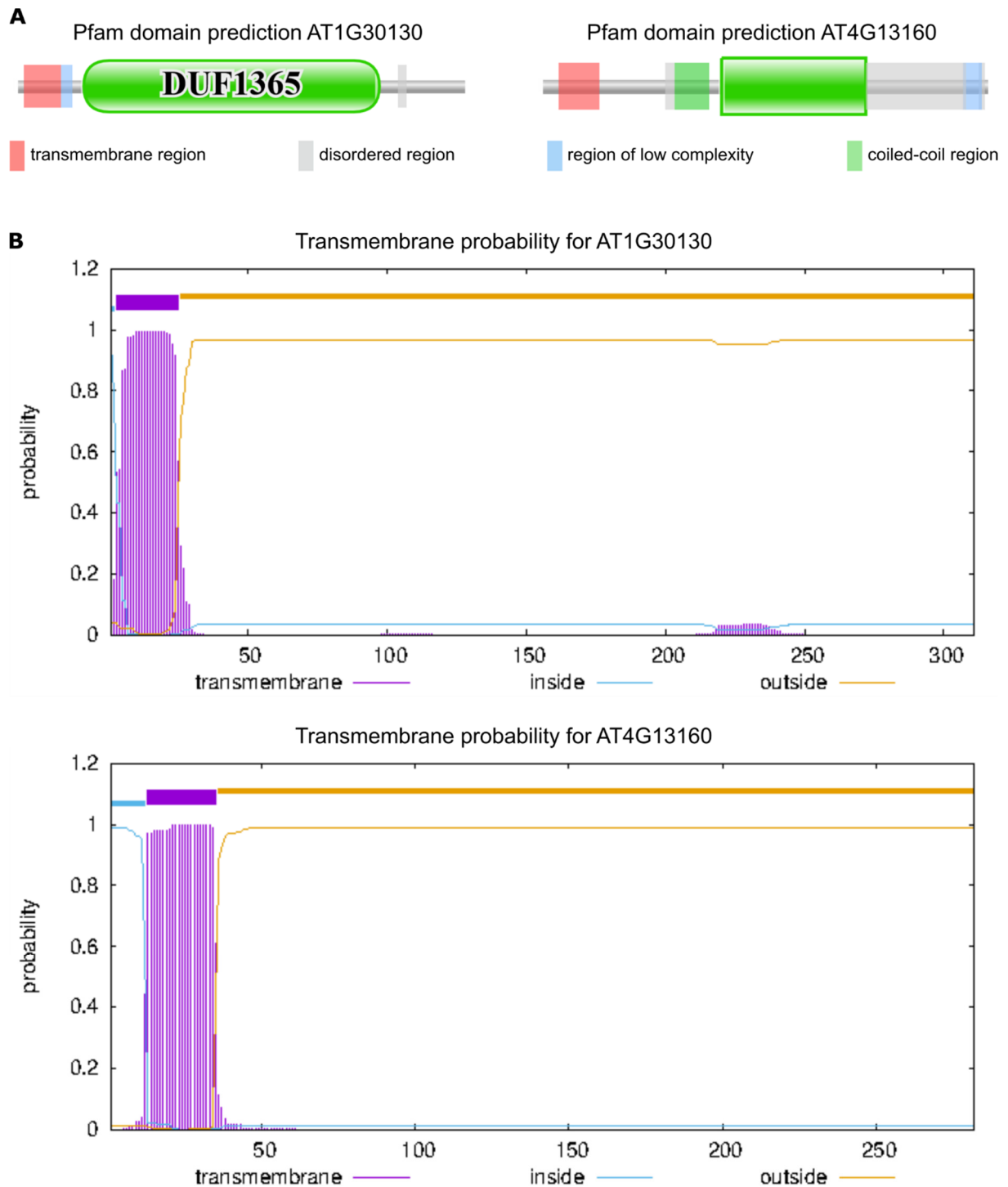
Figure 12: Predicted structural features of two LD-localising proteins with the accession numbers AT1G30130 and AT4G13160. Domain structures were predicted with the Pfam database (A) while the probability of transmembrane helices were analysed with the TMHMM – 2.0 server (B). All predictions were based on protein sequences, which are deposited in the UniProt database with the identifiers Q9C6Z4 (AT1G30130) and Q9SVR1 (AT4G13160), respectively.

Experimental procedures

Lipidomics sample preparation and measurements

Lipid extraction and measurement was carried out as described in manuscript I. The mass transitions and the isotope correction factors used for the detection of steryl glycosides are listed in Table 4.

Table 4: Mass transitions for the detection of steryl glycosides. Indicated are the fragment sizes of precursor and product ions of the detected steryl glycoside (SG)-species. In addition, the number of carbon atoms of the respective species and the resulting isotope correction factor (icf) are given.

Lipid name	Precursor ion	Product ion	Number of carbon atoms	icf
SG-sitosteryl	594.5	397.38	35	1.46
SG-campesteryl	580.5	383.37	34	1.44
SG-stigmasteryl	592.5	395.37	35	1.46
SG-isofucosteryl	592.6	395.5	35	1.46

Cultivation of axenic root cultures

Axenic cultivation of Arabidopsis plants to yield a high root biomass was adapted from Hétu et al., 2005. In brief, surface-sterilised and stratified seeds of the *tgd1-1 sdp1-4* Arabidopsis mutants were grown initially for 7 days on solid ½ MS medium (Duchefa Biochemie, Haarlem, The Netherlands) containing 1% sucrose (Carl Roth GmbH + Co. KG, Karlsruhe, Germany). Seedlings grew on sterilised steel grids, which were transferred after one week to 100 ml Erlenmeyer flasks containing 10 ml liquid ½ MS medium supplemented with 1% sucrose. Liquid cultures were grown at constant shaking (85 rpm) for 11 days with regular exchange of the medium every three days. Then, the liquid culture medium was changed to 15 ml ½ MS medium with 3% sucrose and plants were cultivated at constant shaking (85 rpm) for further 11 days with regular medium exchange. Plants were grown at 22°C with a 16 h light/ 8 h dark cycle (150 µmol photons m^{-2} s^{-1} light strength).

Isolation of total protein and LD-enriched fractions

After cultivation of axenic root cultures, plants were harvested and roots were separated from upper plant parts for LD enrichment. For one biological replicate, root pads from two independent liquid cultures were combined. Each root sample was mixed with grinding buffer (50 mM Tris-HCl pH 7.5, 10 mM KCl, 0.4 M sucrose, 200 µM proteinase inhibitor PMSF; Carl Roth GmbH + Co. KG, Karlsruhe, Germany) and ground to a homogenous suspension using sea sand as abrasive agent. Grinding buffer, mortar and pestle were precooled and all samples were kept at 0-4°C during LD-enrichment. Sand and cellular debris were removed by centrifugation for 1 minute at 100 x *g*. Of the supernatant an aliquot was taken, representing the total protein fraction, and total proteins were precipitated in 96% ethanol at -20°C. Remaining supernatant was overlayed with washing buffer (50 mM Tris-HCl pH 7.5, 10 mM KCl, 0.2 M sucrose, 200 µM proteinase inhibitor PMSF; Carl Roth GmbH + Co. KG, Karlsruhe, Germany) and centrifuged at 100,000 x *g* for 35 min using a swing-out rotor. The resulting fat pad from the top was collected and washed once in washing buffer (50 mM Tris-HCl pH 7.5,

10 mM KCl, 0.2 M sucrose, 200 µM proteinase inhibitor PMSF). After a second centrifugation at 100,000 x *g* for 35 min, LDs were collected as floating fat pad and proteins were precipitated with 96% ethanol at -20°C.

Proteomic sample preparation and LC-MS/MS analysis

After precipitation, proteins were defatted two times with 80% ethanol, dried and washed one additional time with 96% ethanol. After drying, defatted samples were dissolved in 6 M urea and 5% (w/v) SDS. Determination of protein concentration, in-gel tryptic-digest of 20 µg initial protein and peptide desalting was carried out as described previously (Shevchenko et al., 2006; Rappsilber et al., 2007; Kretzschmar et al., 2018). Subsequently, peptides were reconstituted in 20 µl sample buffer (2% acetonitrile, 0.1% formic acid) and subjected to LC-MS/MS analysis.

LC-MS/MS analysis was performed with an EASY-nLC 1200 (Thermo Fisher Scientific) coupled to an Exploris 480 mass spectrometer (Thermo Fisher Scientific). Separation of peptides was performed on 20 cm frit-less silica emitters (CoAnn Technologies, 0.75 µm inner diameter), packed in-house with reversed-phase ReproSil-Pur C18 AQ 1.9 µm resin (Dr. Maisch) and the column was constantly kept at 50 °C. Peptides were eluted in 115 min using a segmented linear gradient of 0 % to 98 % solvent B (solvent A 0 % ACN, 0.1 % formic acid; solvent B 80 % ACN, 0.1 % formic acid) at a flow-rate of 300 nL/min. Mass spectra were acquired in data-dependent acquisition mode. In case of full proteome samples, MS1 scans were acquired at an Orbitrap Resolution of 120 000 with a Scan Range (m/z) of 380-1500, a maximum injection time of 100 ms and a normalised AGC Target of 300 %. For fragmentation, only precursors with charge states 2-6 were considered. Up to 20 Dependent Scans were taken. For dynamic exclusion the exclusion duration was set to 40 sec and a mass tolerance of +/- 10 ppm was used. The Isolation Window was set to 1.6 m/z with no offset. A normalised collision energy of 30 was used. MS2 scans were taken at an Orbitrap Resolution of 15 000, with a fixed First Mass (m/z) = 120. Maximum injection time was 22 ms and the normalised AGC Target 50 %.

Computational processing of measured data and prediction of transmembrane helices in candidate proteins was carried out as described in manuscript I. GO term enrichment analysis was carried out with the PANTHER 17.0 webtool (Thomas et al., 2022) comparing a subset of proteins against all proteins predicted from the Arabidopsis genome. Standard settings were used and GO term enrichment was carried out for GO terms associated to biological processes. The subsets of proteins used for analysis were (i) all proteins identified by two peptides and detected in five replicates of either total proteins or LD-enriched fractions from Arabidopsis *tgd1-1 sdp1-4* roots, (ii) all proteins significantly enriched in the LD-enriched fractions of *tgd1-1 sdp1-4* root samples, or (iii) all proteins significantly depleted in the LD-enriched fractions of *tgd1-1 sdp1-4* root samples.

7 Discussion

This thesis focused on two different aspects of lipids in plant cells: first, on the contribution of the anionic phospholipid phosphatidic acid formed by a diacylglycerol kinase in tobacco to the signalling networks in growing pollen tubes (chapter 4). Second, on the dynamics and functions of neutral lipids and their dedicated organelles, lipid droplets (LDs), in vegetative plant tissues (chapters 5, 6). The first part on the contribution of the tobacco enzyme DIACYLGLYCEROL KINASE 5 to pollen tube growth has been published and respective results have been discussed in their scientific context in the paper presented in chaper 4. Considering this and the divergence of the topics, the following section will focus on the second part of the thesis about LDs in vegetative tissues, setting the results of leaf LDs and the root LD proteome in the wider context of LD biology.

7.1 The LD proteome of leaves and roots

7.1.1 The identified LD proteome of leaves is similar to previous data

The lipid droplet (LD) proteome of leaves has been reported so far from senescing, infected and drought-stressed Arabidopsis leaves (Brocard et al., 2017; Fernández-Santos et al., 2020; Doner et al., 2021). We wanted to obtain an overview of the LD proteome in unstressed leaves, where TAGs as core component of LDs only accumulates in very low amounts (Kelly et al., 2013). To circumvent this problem, we used the Arabidopsis double mutant *tgd1-1 sdp1-4*, which had been previously characterised to accumulate high amounts of oil in its leaves (Fan et al., 2014). We identified 16 of the LD proteins published so far and further observed LD localisation of the proteins LD-LOCALISED NTF2 FAMILY PROTEIN (LDNP) and CYTOCHROME B5 ISOFORM E (CB5-E; Table 5).

When comparing our data to previously published results from other groups, it has to be considered that LD enrichment and quantification methods differed between the experiments. Especially the datasets from Fernández-Santos et al. have to be used with caution for comparative purposes. Their protocol for LD enrichment used detergent throughout the procedure and their proteomics quantification method differed too, as protein abundance was quantified by the average number of peptides that could be assigned to the detected proteins. In contrast, in our measurements and the other two studies, MS1 intensity-based algorithms were used for protein quantification (Brocard et al., 2017; Fernández-Santos et al., 2020; Doner et al., 2021). Nevertheless, some common trends can be inferred from comparison of the relative contributions of the identified LD protein to the total LD proteome. Comparing our dataset on non-stressed leaves with the previously published studies, quantitative dominance of CALEOSIN 3 (CLO3) in the total LD proteome of Arabidopsis leaves appeared as a common feature (Brocard et al., 2017; Doner et al., 2021). The data from Fernández-Santos et al. differs quite strongly in that aspect (Table 5), however, comparison of their data on senescent leaves with the data from Brocard et al. suggests that this might rather be due to the technical differences mentioned above. *CLO3* is strongly expressed in senescent tissue and also strongly stress-induced (Partridge and Murphy, 2009; Aubert et al., 2010; Blée et al., 2014; Shimada et al., 2014; Klepikova et al., 2016), which probably accounts partially for its abundance of 60% and 90% in senescent and drought-stressed leaves, respectively (Brocard et al., 2017; Doner et al., 2021). That the amount of CLO3 in mature, non-stressed

leaves might be a bit lower is suggested from the data of the *tgd1-1 sdp1-4* mutant as presented here, however, no data on unstressed Col-0 leaves is known so far.

A striking difference was the identity of the dominant protein of the LD associated protein (LDAP) family. In proteomes of Col-0 leaves, LDAP1 was the LDAP protein of highest abundance, however, in *tgd1-1 sdp1-4*, LDAP3 dominated (Table 5). With MS1 intensity-based quantification methods, either LDAP was usually observed to be among the two most abundant LD proteins, whereby the percentage of CLO3 accounts for the largest part of the differences between datasets. LDAPs have been proposed as coat proteins for LDs in vegetative tissue, which seems a suitable explanation for their accumulation (Gidda et al., 2013, 2016; Pyc et al., 2017b). Interestingly, LDAP targeting requires the full-length proteins. The accumulated amino acid differences between LDAP1 and LDAP3 might thus induce slight changes in binding behaviour so that altered LD properties in *tgd1-1 sdp1-4* could favour binding of LDAP3. However, differences in abundance in the LD-enriched fraction suggest also variations in the total protein abundance of LDAP proteins in Col-0 or *tgd1-1 sdp1-4* leaves and the underlying cause of this variation is unclear. Gene expression of *LDAP1* and *LDAP3* differs in response to diverse stresses (Hruz et al., 2008), so overall cellular homeostasis in the mutant might mimic certain stress condition that would favour *LDAP3* expression over *LDAP1* expression and subsequently lead to altered protein levels. LDAP3 could then become the dominant protein of the LDAP family, independent of preferential targeting.

Further six LD proteins were found both in the LD proteomes of non-stressed leaves of *tgd1-1 sdp1-4* and in at least two other previously published studies on Col-0 leaf LDs (Table 5). These were α-DIOXYGENASE 1 (α-DOX1), EARLY RESPONSIVE TO DEHYDRATION 7 (ERD7), LDAP-INTERACTING PROTEIN (LDIP), LD AND STOMATA 1 (LDS1), proteins of the LD methyltransferase (LIME) family, and PLANT UBX DOMAIN-CONTAINING PROTEIN 10 (PUX10). Of those, LDIP and PUX10 have been characterised in LD homeostasis: LDIP acts as a player of LD biogenesis (Coulon et al., 2020; Pyc et al., 2021) while PUX10 interacts with the protein CELL DIVISION CYCLE 48 in protein turnover and degradation of LD proteins (Deruyffelaere et al., 2018; Kretzschmar et al., 2018). LDS1, a Rab GTPase, has also been reported very recently to be involved in LD homeostasis in stomata development (Ge et al., 2022). ERD7 and α-DOX1 on the other hand are described in stress responses. For ERD7, a yeast two-hybrid screen identified 36 potential interaction partners whose GO-Terms showed an enrichment in the category "response to stress" (Doner et al., 2021). In addition, the protein was found to accumulate upon cold stress (Barajas-Lopez et al., 2021). α-DOX1 has been reported as active enzyme that together with CLO3 produces the phytoalexine 2-hydroxyoctadecatrienoic acid (2-HOT) from the fatty acid (FA) α-linolenic acid (Shimada et al., 2014). Finally, LIME proteins are putative enzymes that were named due to homology to other methyltransferases, albeit no enzyme activity has been shown yet (Kretzschmar et al., 2020). Their physiological function is also unknown so far, however, they are consistently present as low-abundant LD proteins (Table 5), which could hint at some lipid-modifying enzyme activity.

Table 5: LD proteins detected in leaves of the Arabidopsis *tgd1-1 sdp1-4* mutant compared to previous studies with Col-0. Quantification methods differed between studies, so quantitative values are not comparable. Therefore, for each proteomics study, the respective relative amounts in the total known LD proteome are given for each protein in %. The Arabidopsis lines used for proteomic analysis and the studied treatments are indicated. Stress treatments of *tgd1-1 sdp1-4* included infection with *Botrytis cinerea* (*B. cinerea*), infection with *Pseudomonas syringae* pv. *tomato* DC3000 *ΔavrPto ΔavrPtoB* (*PstΔ*) until first symptom development and heat stress for 24 hours at 37°C. Infection treatments of Fernández-Santos et al. were performed with *Pseudomonas syringae* pv. *tomato* DC3000 *avrRpm1* (*PstR*). * denotes proteins that could not be identified unambiguously, 'hpi' means 'hours post infection'. Full protein names are listed in the following. α-DIOXYGENASE 1 (α-DOX1), CYCLOARTENOL SYNTHASE 1 (CAS1), CYTOCHROME B5 ISOFORM E (CB5-E), CALEOSIN 3 (CLO3), EARLY RESPONSIVE TO DEHYDRATION 7 (ERD7), glycerol 3-phosphate acyltransferase (GPAT), LD associated protein (LDAP), LDAP-INTERACTING PROTEIN (LDIP), LD-LOCALISED NTF2 FAMILY PROTEIN (LDNP), LD AND STOMATA 1 (LDS1), LD-ASSOCIATED LIPASE 2 (LIDL2), LD methyltransferase (LIME), oil body lipase (OBL), PLANT UBX DOMAIN-CONTAINING PROTEIN 10 (PUX10), STEROL METHYLTRANSFERASE 1 (SMT1), LD-associated hydrolase (LDAH), PHYTOALEXIN-DEFICIENT 3 (PAD3).

Study	tgd1-1 sdp1-4							Brocard et al., 2017 Col-0	Fernández-Santos et al., 2020 Col-0			Doner et al., 2021 Col-0
Protein	no treatment	mock (*B. cinerea*)	*B. cinerea*	mock (*PstΔ*)	*PstΔ*	control	heat stress	senescing leaves	senescing leaves	24 hpi *PstR*	72 hpi *PstR*	drought stress
α-DOX1	0.04		1.86		0.30	0.003		0.30		7.84	15.56	0.50
CAS1	0.45		0.07	0.65	0.15	1.54	0.59					0.15
CB5-E	2.22	3.11	3.02	1.34	5.32	1.15	0.39					0.06
CLO3	41.63	33.86	53.21	40.52	73.88	9.05	18.24	60.68	23.31	13.24	25.00	90.21
ERD7	1.46		0.49	0.03	0.06	5.38	5.23	0.29		3.43		0.51
GPAT4	0.22		0.06			2.00	0.76		25.56	15.69	12.22	
GPAT8						0.11				11.27		
LDAP1	1.07	0.89	1.92	0.40		4.17	4.23	34.71	21.05	7.35	12.22	4.71
LDAP2	0.17		0.08			0.15	0.06					
LDAP3	41.58	50.70	30.21	43.16	15.45	53.11	51.04	0.79		9.80		1.13
LDIP	4.06	2.63	2.15	2.61	0.99	6.12	7.68	1.43	6.77		4.44	0.32
LDNP	3.13	2.64	2.63	6.02	2.46	3.33	3.72					0.30
LDS1	1.80	2.56	1.25	2.36	1.06	3.54	3.21		3.92			1.92
LIDL2	0.11					0.06	0.04					
LIME1/2 *	0.43	0.47	0.70	0.61		1.96	1.35	0.08				0.15
OBL3	0.62	0.59	0.34	0.92	0.25	3.03	1.92	1.57				
PUX10	0.48	0.73	0.30	0.31		0.58	0.26	0.16	23.31	16.18	22.22	
SMT1	0.52	1.82	1.70	1.07	0.08	4.72	1.29					
LDAH1/2 *									4.90			
OBL2												0.05
PAD3										6.37	8.33	

Three proteins were found only at leaf LDs of *tgd1-1 sdp1-4*: LDAP2, LD-ASSOCIATED LIPASE 2 (LIDL2), and STEROL METHYLTRANSFERASE 1 (SMT1). However, all of these proteins have been found in the proteome of LDs in Arabidopsis Col-0 seedlings (Kretzschmar et al., 2020). Their relative quantitative contribution to the whole LD proteome is less than 1%, so it is possible that they are either not present in LDs of Col-0 or that their abundance is too low to be routinely picked up via proteomics. The increased number of LDs in the mutant would then raise their protein levels to amounts that are possible to be detected. Nevertheless, all of these proteins have been identified as *bona fide* LD proteins, so their presence in the LD-enriched fraction is caused by association to LDs and not solely by contamination (Gidda et al., 2016; Kretzschmar et al., 2018, 2020). On the other hand, three proteins were found in other proteomic data sets but not in leaves of *tgd1-1 sdp1-4*: an LD-associated hydrolase (LDAH) protein, OIL BODY LIPASE 2 (OBL2), and PHYTOALEXIN-DEFICIENT 3 (PAD3). Here again, low protein amounts are probably one reason for differences in detection, considering the small relative amounts of OBL2 and LDAH proteins in MS1 intensity-based quantification of LD proteomes from drought-stressed leaves and seedlings, respectively (Kretzschmar et al., 2020; Doner et al., 2021). Localisation of PAD3 to LDs has been reported to occur only in infected cells (Fernández-Santos et al., 2020), still we were not able to detect it even in the LD-enriched fractions of *tgd1-1 sdp1-4* leaves infected with either *Botrytis cinerea* or *Pseudomonas syringae* pv. *tomato* DC3000 *ΔavrPto ΔavrPtoB* (Table 5). Independent of the precise composition of the various leaf LD proteomes, it is notable that the detected LD proteins overall imply active cell biological and metabolic processes at leaf LDs.

7.1.2 The LD proteome of roots contains several enzymes of lipid metabolism

After the study of leaf LDs, we further investigated the LD proteome in roots (Table 2, Figure 11). For this, we used again the *tgd1-1 sdp1-4* mutant, as the respective single mutants were reported to accumulate oil also in roots (Xu et al., 2005; Kelly et al., 2013). In the LD-enriched fraction of roots, we detected 29 LD proteins that had been previously identified in other tissues (Table 2). When comparing the occurrence of LD proteins in these root samples to other tissues, it has to be considered that samples of the root LD proteome were measured on a different mass spectrometer and the difference in the number of detected LD proteins is mostly due to very low abundant LD proteins. Therefore, low-abundant LD proteins detected in roots might also be present in other tissues but escaped detection due to technical differences or different ion suppression in the complex proteome of leaves. Nevertheless, judging from the relative contribution to the LD proteome and other published datasets, the presence of some root-specific LD proteins appears likely, as shall be discussed below.

All LD proteins observed in leaves could be found in roots, however, roughly 50% of the individual protein found in LD-enriched fractions of Arabidopsis roots could not be detected in Arabidopsis leaves. Looking at whole protein families on the other hand, there were only two previously published LD protein families that were detected in roots of *tgd1-1 sdp1-4* but not in leaves of the double mutant. These protein families were the LDAH protein family and steroleosins (HSDs, derived from hydroxysteroid dehydrogenases; Table 6). Of those, LDAHs have been reported by Fernández-Santos et al. in Col-0 leaves after *Pseudomonas*-infection while they contribute only 0.3‰ to the combined abundance of all LD proteins in roots (Tables

5, 6). Their absence in the detected LD proteome of *tgd1-1 sdp1-4* leaves therefore could be without functional implications and rather be caused by technical reasons.

In contrast, no HSDs have been detected in the LD-enriched fractions from leaves so far, so their detection at root LDs could mark genuine tissue-specificity. The main steroleosin in root LDs is HSD4/7, which was quantified as 0.45‰ of all proteins in the LD-enriched fraction (Table 2). Albeit not a major contribution, this is in the range of low-abundant LD proteins described in seeds, seedlings and leaves (Suppl. Dataset S5 in manuscript I; Kretzschmar et al., 2020). Interestingly, although different HSDs have been detected in other tissues like seeds and seedlings (Baud et al., 2009; Kretzschmar et al., 2020), the detected HSDs did not include HSD4/7. Consequently, its presence at root LDs hints at a root-specific function that might revolve around modifications of plant sterols.

For the first identified HSD from sesame seeds, enzyme assays showed dehydrogenase activity on the 17 β-hydroxysteroid estradiol and the 11 β-hydroxysteroid corticosterone (Lin et al., 2002). In Arabidopsis, these enzyme activities were also reported for HSD1 (d'Andréa et al., 2007) and it has been proposed that their endogenous substrates are brassinosteroids (Chapman et al., 2012). Indeed, Arabidopsis plants overexpressing *HSD1* displayed phenotypes like taller growth, larger stems or increased number of branches that are similar to plants treated with exogenous brassinosteroids (Li et al., 2007). However, as there are no enzymatic studies on HSD4/7, it is not certain that it has similar enzymatic function to HSD1. If an analogous enzyme activity is assumed, the question arises what specific purpose the catalysed modification of sterols might fulfil in roots. It is known that the spatial distribution of brassinosteroids in roots is important for their signalling function (Vukašinović et al., 2021) and brassinosteroid-dependent signalling is crucial in differentiating between root hair cells and non-hair cells (Singh and Savaldi-Goldstein, 2015). A possible role for HSDs in roots could then be to mediate brassinosteroid activity by converting between active and less active steroid compounds (Chapman et al., 2012) and thus fine-tune brassinosteroid signalling especially between neighbouring root hair and non-hair cells. Nevertheless, brassinosteroids play a role in almost all other plant tissues as well, e.g. in the shoot apical meristem or the formation of stomata (Singh and Savaldi-Goldstein, 2015), so it remains an open question why HSDs would be needed in roots but not in other vegetative tissues. To unravel potential connections between HSDs and brassinosteroids in roots will therefore require further research on the possible enzyme activity of HSD4/7 and its root-specific function.

Besides the presence or absence of proteins at the LDs of roots or leaves, two conspicuous differences in terms of protein abundance could be observed. Firstly, the low amounts of caleosins in roots compared to leaves, where they make up around 1% and 40% of the total LD proteome, respectively (Table 6). Secondly, the high accumulation of α-DOX1 in root tissue where it is the second most abundant LD protein in our protein data set. Caleosins have been attributed stabilising functions at LDs, especially in the absence of oleosins (Jiang et al., 2009; Liu et al., 2009), however, in roots of *tgd1-1 sdp1-4* neither protein family seems to be required for this purpose. Instead, LDAPs like LDAP3 are probably the coating protein in root LDs as has been previously suggested for LDs in leaves and avocado mesocarp (Horn et al., 2013; Gidda et al., 2016; Pyc et al., 2017b). The low abundance of CLO3 is furthermore interesting in light of the high abundance of α-DOX1. As mentioned, both proteins have been

functionally described to act together in the synthesis of 2-HOT as biotic stress response in leaves (Shimada et al., 2014). However, CLO3 is hardly present in the detected proteome of roots, so α-DOX1 apparently serves an independent function. Its high accumulation might be in part an artefact of stress caused by the culture method, as gene expression of a tomato *α-DOX1* was reported to increase in roots after wounding (Tirajoh et al., 2005). Nevertheless, even under stress conditions, the strong accumulation of α-DOX1 is intriguing, considering it has been described to oxidise FAs to hydroperoxy products, however, lacks peroxidase activity that would further metabolise the instable 2-hydroperoxy FAs (Goulah et al., 2013; Shimada et al., 2014). Given the toxic potential of 2-hydroperoxy FAs (Farmer and Mueller, 2013) they likely have to be metabolised by another, as of yet unidentified peroxidase.

In addition to analysing the relative abundance of known LD proteins, we were able to identify further proteins that co-localised to LDs upon transient expression in tobacco pollen tubes. These include three enzymes of lipid metabolism, namely GLYCEROL-3-PHOSPHATE ACYLTRANSFERASE 9 (GPAT9, AT5G60620), ACYL-COA:LYSOPHOSPHATIDYLETHANOLAMINE ACYLTRANSFERASE 1 (LPEAT1, AT1G80950) and THALIANOL SYNTHASE 1 (THAS1, AT5G48010). In addition, two proteins of unknown functions, with the accession numbers AT1G30130 and AT4G13160, were identified this way. These two proteins both contain predicted transmembrane helices at their N-terminus that might convey LD-association (Figure 12), however, otherwise their functions or physiological roles remain to be explored.

More information is available about the other three proteins, of which GPAT9 and LPEAT1 are described to have acyl transferase activity (Stålberg et al., 2009; Shockey et al., 2016; Singer et al., 2016). Intriguingly, their association to LDs in pollen tubes stands in contrast to previous reports of an ER-localisation for both enzymes in tobacco BY-2 cells (Gidda et al., 2009; Jasieniecka-Gazarkiewicz et al., 2021). These differences in localisation might originate from varying abundance of LDs between the transient expression systems, so GPAT9 and LPEAT1 could be able to localise to both LDs and the ER. For THAS1, previous studies focused on its enzymatic function in triterpenoid synthesis and the impact of the produced triterpenoids on Arabidopsis roots (Fazio et al., 2004; Field and Osbourn, 2008; Bai et al., 2021). The enzyme is part of the family of oxidosqualene cyclases, which also contains another LD-localised enzyme in the form of CYCLOARTENOL SYNTHASE 1 (CAS1; Field and Osbourn, 2008; Kretzschmar et al., 2018). THAS1 was initially discovered when screening for new triterpene-synthesising enzymes and it catalyses the cyclisation of 2,3-oxidosqualene to a tricyclic compound that was subsequently named thalianol (Fazio et al., 2004). The *THAS1* gene is part of a gene cluster encoding further thalianol-modifying enzymes and the combined activity of the respective enzymes was proposed to shape the root microbiome (Field and Osbourn, 2008; Huang et al., 2019). It might be interesting to analyse the subcellular localisation of other enzymes encoded by the thalianol gene cluster and investigate if LDs act here as a source of substrates for triterpenoid metabolism.

Table 6: Comparison of LD proteins and protein families found in different tissues. To calculate respective contributions to the LD proteome of different tissues, riBAQ values of individual LD proteins were normalised to the total sum of riBAQ values of all known and detected LD proteins. For protein families, the individual relative values were then summed up to obtain the relative abundance of the whole protein family. All values are given in %. The species, tissues and Arabidopsis lines used for proteomic analysis are indicated. The data shown for *tgd1-1 sdp1-4* leaves represents the LD proteome composition in non-stressed leaves. 'hpg' means hours post germination. Protein and protein family abbreviations are as listed: LD associated protein (LDAP), LDAP INTERACTING PROTEIN (LDIP), PLANT UBX DOMAIN-CONTAINING PROTEIN 10 (PUX10), STEROL METHYLTRANSFERASE 1 (SMT1), CYCLOARTENOL SYNTHASE 1 (CAS1), oil body lipase (OBL), α-DIOXYGENASE 1 (α-DOX1), seed LD protein (SLDP), LD-associated lipase (LIDL), LD PROTEIN OF SEEDS (LDPS), LD methyltransferase (LIME), LD-associated hydrolase (LDAH), LD dehydrogenase (LDDH), EARLY RESPONSIVE TO DEHYDRATION 7 (ERD7), glycerol 3-phosphate acyltransferase (GPAT), LD AND STOMATA 1 (LDS1), LD-LOCALISED NTF2 FAMILY PROTEIN (LDNP), CYTOCHROME B5 ISOFORM E (CB5-E), POLLEN TUBE LD PROTEIN (PTLD), ACYL-COA:LYSOPHOSPHATIDYL-ETHANOLAMINE ACYLTRANSFERASE 1 (LPEAT1), THALIANOL SYNTHASE 1 (THAS1).

Study	Kretzschmar et al., 2020				Kretzschmar et al., 2018	Niemeyer et al., 2022
Protein family	*A. thaliana tgd1-1 sdp1-4*		*Arabidopsis thaliana* Col-0		*Nicotiana tabacum*	*Cyperus esculentus*
	leaves	roots	Rehydrated seeds	Seedlings 60 hpg	Pollen tube	Rehydrated tubers
oleosins			59.16	76.72	25.28	69.76
caleosins	41.63	0.99	8.30	6.21	50.64	27.13
steroleosins		0.28	32.03	10.58		1.13
α-DOX1	0.04	20.03		0.07		
CAS1	0.45	0.14	0.01	0.06	5.18	0.0004
CB5-E	2.22	0.43	0.01	0.03		0.08
ERD7	1.46	1.38				0.13
GPAT	0.22	0.64		0.01		0.01
LDAH		0.03		0.06		
LDAP	42.81	64.82	0.001	4.61	10.65	0.09
LDDH				0.09		
LDIP	4.06	2.10	0.01	0.01	0.76	0.20
LDNP	3.13	2.97	0.0006	0.04		
LDPS			0.09	0.03		
LDS1	1.80	0.39	0.02	0.03		0.003
LIDL	0.11	0.18		0.10		
LIME	0.43	1.62		0.19		
OBL	0.62	0.51	0.05	0.27	0.73	
PTLD					1.36	
PUX10	0.48	0.09	0.01	0.04	4.64	0.02
SLDP			0.32	0.64		1.40
SMT1	0.52	0.82		0.14	0.80	
LPEAT1		0.08				0.01
THAS1		2.14				
AT1G30130		0.22		0.06		
AT4G13160		0.13				

7.1.3 The seed LD proteome transitions to a distinct LD proteome in leaves and roots

In previous work, the LD proteome of Arabidopsis seeds and seedling had been established (Kretzschmar et al., 2020) to which we could compare the detected LD proteins of leaves and roots (Table 6). Additionally, the detected LD proteins in tobacco (*Nicotiana tabacum*) pollen tubes (Kretzschmar et al., 2018) and tubers of yellow nutsedge (*Cyperus esculentus*; Niemeyer et al., 2022) allowed some inferences about the comparison to these plant tissues, although species-specific differences have to be taken into consideration. The most striking difference is the complete absence of oleosins from LDs in Arabidopsis leaves and roots, while they have been detected in tobacco pollen tubes, Arabidopsis seeds and seedlings, and tubers from yellow nutsedge (Kretzschmar et al., 2018, 2020; Niemeyer et al., 2022). The absence of oleosins matches published data on their expression in Arabidopsis, which occurs mostly in desiccating tissue (Klepikova et al., 2016) and the ability to endure in a desiccated state is a common feature of all those tissues in which oleosins were found. There, oleosins were described as LD coating proteins that prevent LD fusion (Tzen et al., 1992; Shimada et al., 2008). In addition, they are observed to be degraded during seedling development (Deruyffelaere et al., 2018; Kretzschmar et al., 2018) and they are able to outcompete other proteins for LD localisation in leaves (Gidda et al., 2016). This suggests that oleosins have an LD-stabilising function, however, prevent the accessibility of LDs for other enzymes. The latter is likely to be more problematic in tissues with active lipid metabolism and membrane remodelling processes, especially during stress responses (Higashi et al., 2015; Tarazona et al., 2015). Hence, it appears that oleosins are excluded from LDs in Arabidopsis leaves and roots to allow for faster adaptations of those LDs to cellular requirements.

Judging from the measured proteome in leaves and roots, oleosins are instead replaced by LDAPs. In leaves of Arabidopsis *tgd1-1 sdp1-4*, LDAP3 dominated the known LD proteome together with CLO3 and in roots it was by far the most abundant protein (Tables 2, 5). When following the dynamics of the LD proteome from seeds to seedlings, Kretzschmar and Doner et al. observed absence of LDAP1 and LDAP3 in seeds and slowly increasing protein amounts during seedling development (Kretzschmar et al., 2020). The increase in LDAP abundance during seedling development fits to the hypothesis that LDAPs take over LD-stabilising functions in vegetative tissues. Further support comes from observations in the dandelion species *Taraxacum brevicorniculatum*: this plant accumulates rubber that is concentrated in rubber particles coated by proteins homologous to Arabidopsis LDAPs (Hillebrand et al., 2012). When these homologous proteins were depleted, rubber particles were more prone to fusions, not unlike the phenotype observed for seed LDs in Arabidopsis *ole1 ole2* and *ole1 ole3* double mutants of seed oleosins (Shimada et al., 2008; Hillebrand et al., 2012). Given their contributions to the total LD proteome in leaves and roots (Tables 2, 5), LDAP1 and LDAP3 appear as LD stabilising proteins in established vegetative tissues. LDAP2 on the other hand seems to be most important in Arabidopsis seedling development, where it increased in relative abundance (Kretzschmar et al., 2020). In contrast, it was detected only in small amounts in the LD-enriched fractions of leaves and roots, so it might have its main function during the seed-to-seedling transition (Tables 2, 5; Brocard et al., 2017; Fernández-Santos et al., 2020; Kretzschmar et al., 2020; Doner et al., 2021).

Further differences include the seed lipid droplet protein (SLDP) family and the LIPID DROPLET PROTEIN OF SEEDS (LDPS) that were absent from our datasets but present in Arabidopsis seeds and seedlings. Both had been named according to their expression profiles and for LDPS highest protein amounts were also observed in seed stages (Klepikova et al., 2016; Kretzschmar et al., 2020). SLDPs were demonstrated to be part of a membrane contact site, tethering LDs to the plasma membrane in developing seedlings (Krawczyk et al., 2022). This subcellular organisation is not necessarily observed in leaves and roots, so SLDPs as LD-organising proteins might not be required in later plant stages of Arabidopsis (Pyc et al., 2017b). Nevertheless, an orthologue of SLDP was found in the tubers of yellow nutsedge (Table 6). This is probably related to the seed-like qualities of these tubers that are desiccation-tolerant and can sprout into a new plant upon rehydration. In this context, LD-organisation might again become important so that yellow nutsedge tubers accumulate SLDP protein even though the tubers originally derive from vegetative tissue (Niemeyer et al., 2022).

In contrast, many proteins related to metabolism become important at LDs in leaves and roots. These include i.a. α-DOX1, CLO3, different lipases, the putative methyltransferases of the LIME protein family and enzymes of sterol metabolism like CAS1 and SMT1. A notable exception is the steroleosin HSD1, which steadily decreases during seedling establishment (Kretzschmar et al., 2020). However, the majority of LD protein families with demonstrated or proposed enzymatic functions showed increased proportions among the known LD proteins as seedling development progressed and reach their highest relative contribution in a vegetative tissue (Table 6). From a proteomic point of view, LDs in seeds and LDs in vegetative tissues are thus different versions of one organelle that are transformed from one to the other during seedling establishment.

7.2 Targeting and surface interaction of leaf LD proteins

7.2.1 Proteins can associate to LDs through different mechanisms

Proteins target to LDs in different ways and no targeting signal in the amino acid sequence that mediates subcellular localisation has been identified yet. Rather, two general pathways of protein targeting to the ER have been distinguished: either (i) by initial insertion into the cytosolic layer of the ER membrane and subsequent transfer onto the forming LD or (ii) by direct targeting from the cytosol (Kory et al., 2016).

Each of the two pathways for LD targeting mentioned above contains further variations of how the localisation is mediated. For example, initial insertion of oleosins into the ER takes place via the signal recognition particle-pathway while for mammalian UBX DOMAIN-CONTAINING PROTEIN 8 (UBXD8) the peroxisome-biogenesis factor proteins PEX19 and PEX3 are required (Schrul and Kopito, 2016). UBXD8 is the mammalian homolog of Arabidopsis PUX10. Therefore, a similar pathway might be required for PUX10 in plants, especially as PUX10 also shows dual localisation to LDs and the ER (Kretzschmar et al., 2018). On the other hand, targeting of LD proteins from the cytosol has been proposed to occur via amphipathic

helices, lipid anchors attached to the protein, or protein-protein interactions (Kory et al., 2016; Bersuker and Olzmann, 2017). Consequently, LD targeting cannot be estimated directly from the sequence and has to be determined experimentally for each identified LD protein.

Concerning the LD proteins identified in leaves, the targeting region is known for a few but not for all of them. Detailed truncation analyses of LDAP3 suggested that the complete protein sequence is required to mediate protein localisation (Gidda et al., 2016). However, when *LDAP3* is expressed in insect cells, it is able to localise to LDs on its own, suggesting a protein-inherent ability to localise to LDs for LDAP3 and probably all LDAPs (Pyc et al., 2021). LDIP requires an amphipathic helix for LD localisation (Pyc et al., 2017a), but when expressed in insect cells, localisation was dependent on LD-localised LDAP3 (Pyc et al., 2021). LDIP therefore appears to target to LDs via protein-protein interactions. ERD7 requires its C-terminal senescence domain for LD-targeting when localised in the overexpression system of *Nicotiana benthamiana* leaves and was otherwise described to accumulate in the cytosol (Doner et al., 2021). All of these proteins are assumed to localise to LDs from the cytosol, given their cytosolic localisation when their LD-interacting regions or interaction partners are missing.

For Arabidopsis OBL3, there is no direct microscopic evidence on its localisation region, albeit a hydrophobic region at its N-terminus appears to be involved (Eastmond, 2004; Müller and Ischebeck, 2018). AtOBL3 is part of a five-membered protein family whose members had been originally identified as homologs of the acid lipase OBL1 from castor bean (*Ricinus communis*, RcOBL1). In RcOBL1, an N-terminal hydrophobic stretch was detected at LDs after protease treatment and suggested to mediate LD targeting (Eastmond, 2004). A similar hydrophobic stretch was predicted with the TMHMM Server v. 2.0 in all Arabidopsis OBL proteins and seems likely to confer LD targeting (Müller and Ischebeck, 2018). It remains to be determined though, if targeting requires an initial localisation to the ER or occurs directly from the cytosol.

Proteins that appear to be targeted to the ER before subsequent localisation to LDs in leaves are PUX10 and the caleosin CLO3. Like oleosins, caleosins contain a proline knot motif that is required for LD localisation stabilisation (Chen et al., 1999; Chen and Tzen, 2001; Liu et al., 2009). In addition, the N-terminus of caleosins has been described to be required for LD-targeting based on recombinant protein studies of Arabidopsis CLO1 in yeast. In fractionation experiments, CLO1 was associated mainly to LDs but also to cellular membranes; truncated protein variants of CLO1 missing the first 40, 60 or 95 amino acids increasingly associated to cellular membranes at the expense of LD-association (Purkrtová et al., 2015). Based on the similarities to oleosins, AtCLO1 membrane association in yeast, and assuming a conserved localisation mechanism between different caleosins, targeting of CLO3 to LDs via initial ER-insertion seems a reasonable hypothesis. For PUX10, targeting via the ER also appears as the more likely pathway due to the observed dual localisation of tobacco NtPUX10c to both LDs and ER (Kretzschmar et al., 2018). Further analysis could pinpoint the LD-targeting region of NtPUX10c to a short stretch of about 50 amino acids combining a hydrophobic region and adjoining amino acids. As has been described above, PUX10 is the homolog of mammalian UBXD8, which contains a similar targeting region (Suzuki et al., 2012), so PUX10 might be targeted by a conserved mechanism involving peroxisome-biogenesis factor proteins. The purpose of the targeting region and the hydrophobic stretch in this case is unclear.

Of the other proteins found to localise to LDs, no confined targeting regions has been described so far, although some circumstantial evidence is known in individual cases. For example, there is a solved crystal structure for α-DOX1, where the authors distinguish two domains: a base domain and a catalytic domain. The base domain shows some similarities in terms of space orientation to the membrane-binding domain of murine CYCLOOXYGENASE 2. The domain contains eight α-helices of which three helices have amphipathic character and was consequently proposed to confer lipid binding (Goulah et al., 2013). If LD-binding is indeed provided by the amphipathic helices of the base domain, this might favour targeting from the cytosol onto the lipid monolayer of LDs rather than initial insertion into the ER cytosolic layer. Localisation studies of tobacco NtCAS1 and especially NtSMT1 in tobacco pollen tubes on the other hand showed an additional association of the proteins to reticulate structures (Kretzschmar et al., 2018). This structures could be the ER, which would speak for targeting from the ER to LDs, however, there also is the possibility of overexpression artefacts. Further studies are needed to pinpoint the targeting regions and mechanisms of known LD proteins which could in turn support the identification and characterisation of further proteins associating to LDs.

7.2.2 The surface area of leaf LDs likely contains less proteins than seed LDs

Another interesting aspect of protein targeting to LDs is the question, how much of the LD surface is actually covered by proteins. In seeds, early studies on oleosins established them as surface proteins to prevent LD fusion (Tzen et al., 1992), which would require a strong coverage of the LD surface by protein. However, the situation in leaves is less analysed. Based on experimental data from our proteomic studies of leaf LD-enriched fractions, we estimated the combined protein mass of CLO3 and LDAP3 to make up around 1 ppm of total leaf mass in the *tgd1-1 sdp1-4* mutant. Together with the published data on TAG accumulation in leaves of *tgd1-1 sdp1-4*, this enabled a rough estimate on the protein coverage of LDs in leaves of the mutant as shown below.

<u>General assumptions</u>

1) All proteins are assumed to form spheres, to allow estimation of their diameter and the surface they cover on a membrane.
2) The density of proteins was estimated as:
   ρ(protein) = 1.4 g/cm³   based on (Fischer et al., 2004)
3) The density of plant oil was estimated as:
   ρ(TAGs) = 0.91 g/cm³   based on (Sahasrabudhe et al., 2017)
4) The ratio of dry weight to fresh weight was estimated as: 0.1

<u>Estimations from published and experimental data</u>

5) The mass of both CLO3 and LDAP3 was rounded according to the TAIR database to:
   27 kDa ≈ $4.5 \cdot 10^{-20}$ g

6) Relative TAG content in leaves of *tgd1-1 sdp1-4* was taken as:

8% of leaf dry weight   based on (Fan et al., 2014).

7) Average radius of LDs in the leaves of *tgd1-1 sdp1-4* was estimated as:

r (LD) = 4 µm   based on microscopic images (Fan et al., 2014).

8) Proportion in the total leaf fresh weight of the combined proteins CLO3 and LDAP3 was approximated from experimental data of LD enrichments as:

m (total CLO3+LDAP3) = 1 ppm of leaf fresh weight

Estimation of protein coverage

9) With the proportions given above, no absolute value for total leaf fresh weight is required. The total leaf fresh weight in gram is therefore assigned to the variable 'W'.

Calculation of mass and volume of leaf TAGs using assumptions 3), 4) and 6)

$$m\ (TAGs) = \frac{dry\ weight}{fresh\ weight} \cdot relative\ TAG\ content\ in\ leaves \cdot W = 0.1 \cdot 0.08 \cdot W$$

$$m\ (TAGs) = 0.008\ W \tag{1}$$

$$V\ (TAGs) = \frac{m\ (TAGs)}{\rho\ (TAGs)} = \frac{0.008\ W}{0.91\ g/cm^3} = 0.0088 \cdot W\ cm^3 = 8.8 \cdot 10^9 \cdot W\ \mu m^3 \tag{2}$$

Calculation of volume, area and number of leaf LDs using assumption 7)

$$V\ (LD) = \frac{4}{3} \cdot \pi \cdot r\ (LD)^3 = \frac{4}{3} \cdot \pi \cdot (4\ \mu m)^3 = 268\ \mu m^3 \tag{3}$$

$$A\ (LD) = 4 \cdot \pi \cdot r\ (LD)^2 = 4 \cdot \pi \cdot (4\ \mu m)^2 = 201\ \mu m^2 \tag{4}$$

$$number\ (all\ LDs) = \frac{V\ (TAGs)}{V\ (LD)} = \frac{8.8 \cdot 10^9 \cdot W\ \mu m^3}{268\ \mu m^3} \approx 3.3 \cdot 10^7 \cdot W \tag{5}$$

Calculation of volume and number of CLO3 and LDAP3 in leaves using assumptions 1), 2), 5) and 8)

$$V\ (protein) = \frac{m\ (protein)}{\rho\ (protein)} = \frac{4.5 \cdot 10^{-20}\ g}{1.4\ g/cm^3} = 3.2 \cdot 10^{-20}\ cm^3 = 3.2 \cdot 10^{-8}\ \mu m^3 \tag{6}$$

$$r\ (protein) = \sqrt[3]{\frac{3 \cdot V\ (protein)}{4 \cdot \pi}} = \sqrt[3]{\frac{3 \cdot 3.2 \cdot 10^{-8}\ \mu m^3}{4 \cdot \pi}} = 1.97 \cdot 10^{-3}\ \mu m \tag{7}$$

$$A\ (protein) = \pi \cdot r\ (protein)^2 = \pi \cdot (1.97 \cdot 10^{-3}\ \mu m)^2 = 1.22 \cdot 10^{-5}\ \mu m^2 \tag{8}$$

$$V\ (all\ CLO3 + LDAP3) = \frac{m\ (total\ CLO3+LDAP3)}{\rho\ (protein)} = \frac{1 \cdot 10^{-6} \cdot W}{1.4\ g/cm^3} = 7.1 \cdot 10^{-7} \cdot W\ cm^3 \tag{9}$$

$$number\ (all\ CLO3 + LDAP3) = \frac{V\ (all\ CLO3+LDAP3)}{V\ (protein)} = \frac{7.1 \cdot 10^5 \cdot W\ \mu m^3}{3.2 \cdot 10^{-8}\ \mu m^3} = \approx 2.2 \cdot 10^{13} \cdot W \tag{10}$$

Calculation of total area of all LDs and all CLO3 and LDAP3 proteins using results (4), (5), (8) and (10)

$$A\ (all\ LDs) = number\ (all\ LDs)\ \cdot A\ (LD) = 3.3\ \cdot\ 10^7\ \cdot W\ \cdot\ 201\ \mu m^2$$

$$A\ (all\ LDs) \approx 6.6\ \cdot\ 10^9\ \cdot W\ \mu m^2 \qquad (11)$$

$$A\ (all\ CLO3 + LDAP3) = number\ (all\ CLO3 + LDAP3)\ \cdot A\ (protein)$$

$$A\ (all\ CLO3 + LDAP3) = 2.2\ \cdot\ 10^{13}\ \cdot W\ \cdot\ 1.22\ \cdot\ 10^{-5}\ \mu m^2 \approx 2.7\ \cdot 10^8\ \cdot\ W\ \mu m^2 \qquad (12)$$

Calculation of LD surface coverage using results (11) and (12)

$$coverage = \frac{A\ (all\ CLO3 + LDAP3)}{A\ (all\ LDs)} = \frac{2.7\ \cdot 10^8\ \cdot\ W\ \mu m^2}{6.6\ \cdot\ 10^9\ \cdot\ W\ \mu m^2} \approx 0.04 \qquad (13)$$

This rough approximation on the surface coverage comes to the conclusion that approximately 4% of the LD surface in leaves of *tgd1-1 sdp1-4* are covered with the two proteins CLO3 and LDAP3. Further proteins associate with the LDs in leaves, however, as presented above the other LD proteins make up roughly 20% of the proteome in unstressed leaves of the mutant (Table 5), so they will not substantially increase surface coverage. The value should still be interpreted with caution, as a number of the made assumptions are not met in the actual cellular situation. The proteins will not be spherical and consequently the area they cover on the surface of LDs differs. Furthermore, the calculations on the numbers of CLO3 and LDAP3 in the cell is error-prone: it depends on empirical values for the contribution of CLO3 and LDAP3 to the total leaf mass and showed considerable variations between experiments. In addition, there will be differences in the LD architectures of Arabidopsis Col-0 and *tgd1-1 sdp1-4*, considering that the mutant accumulates TAGs and its LDs in leaves are larger (Fan et al., 2014). Despite all these limitations of the approximation, it gives a hint that the surface of LDs in leaves might contain larger areas where the phospholipid monolayer is not covered with protein.

Intriguingly, a similar approximation for seeds suggests a much stronger protein coverage of the surface from seed LDs. Arabidopsis seeds were reported to contain around 7 µg TAGs and 9 µg total protein (Baud et al., 2002) and in proteomic samples of seeds, LD proteins made up roughly 6% of all proteins whereby about 60% of these LD proteins are oleosins (Kretzschmar et al., 2020). Assuming an average diameter of 0.5 µm for seed LDs and then applying the same estimations as shown above yields an estimated protein coverage of the LD surface of 100 %. Similar constraints of the approximation apply also for this number, nevertheless, it is in line with the general assumption that LDs in seeds are protected by their protein coat from fusing with each other. On the other hand, LDs in leaves appear to be stable enough during their lifecycle without the need of a completely surrounding protein coat. Also, accessibility of the LD surface e.g. for metabolic enzymes or interaction with other cellular organelles is increased. Furthermore, the association of additional proteins is easily possible without the need of first removing other proteins. Hence, LDs in leaves can respond far more dynamically to cellular changes than their counterparts in seeds.

7.3 Dynamics of the leaf LD proteome in response to environmental stress

In light of the proposed differences between LDs in seeds and leaves, we aimed not only to analyse the LD proteome of non-stressed leaves but also follow LD dynamics in Arabidopsis leaves subjected to stress. While the LD proteomes of infected and drought-stressed leaves had been described before (Fernández-Santos et al., 2020; Doner et al., 2021), they did not allow a comparison to non-stressed plants to observe LD alterations. Given that this was the first study explicitly comparing changes of the LD proteome between stress and respective control treatments, the mechanisms promoting its changes are very speculative. Changes in LD protein abundance could be the results of *de novo* synthesis, increased targeting to LDs or changes in protein degradation. In addition, different ways of targeting have to be considered: LD proteins targeting from the cytosol can more easily interact with pre-existing free LDs, whereas LD proteins originating from the ER require an LD-ER connection.

The most eye-catching alterations were the strong upregulation of α-DOX1 and CLO3 in reaction to biotic stress (Figure 8B, C in manuscript I). For CLO3, it has been reported that protein amounts increase after abiotic stress treatments like salt or cold as well as after infection with the fungal pathogen *Colletotrichum higginsianum* (Partridge and Murphy, 2009; Shimada et al., 2014). In case of α-DOX1, original identification also established protein accumulation of the homologous protein in tobacco and later studies in Arabidopsis reported enhanced gene expression after infection with *Pseudomonas* strains (Sanz et al., 1998; Hamberg et al., 1999; De León et al., 2002). Furthermore, a recent study suggests that *B. cinerea* induces the gene expression of *α-DOX1*, as the gene is target of activating histone modifications after infection (Crespo-Salvador et al., 2018). Thus it is very likely, that increased abundance of both α-DOX1 and CLO3 at LDs is attributable to *de novo* synthesis.

As the targeting mechanism of α-DOX1 to LDs is unclear, it cannot be said how the newly synthesised protein will then target to LDs. If the protein targets from the cytosol, it probably would be able to interact with the phospholipid monolayer in surface areas not covered by proteins. Localisation of α-DOX1 is likely independent from CLO3, despite its functional interaction with CLO3 in the synthesis of 2-HOT: when analysing the distribution of fluorescently-labelled proteins in infected leaves, a partially differential localisation of α-DOX1 and CLO3 was observed (Shimada et al., 2014). The different amounts of both proteins in root tissues also support the idea that they are independent from each other in their interaction with the LD surface.

CLO3 likely targets to LDs from the ER, which probably happens subsequently to its *de novo* synthesis upon stress. This requires either the formation of a membrane-continuum between the ER and pre-existing LDs, or biogenesis of new LDs onto which CLO3 can be targeted. In *Drosophila* cells, formation of ER-LD bridges to a subpopulation of LDs has been reported (Wilfling et al., 2013) and in yeast it was proposed that LDs stay connected to the ER after biogenesis (Jacquier et al., 2011). In plants, there are no reports on contact formation between ER and LDs after LD biogenesis, however, that does not exclude the possibility that LDs reattach to the ER or stay connected as mature LD. Nevertheless, it has been reported that TAG levels and LD number increase after pathogen infection (Fernández-Santos et al., 2020; Schieferle et al., 2021). Therefore, it seems more likely that infection induces LD formation and CLO3 concomitantly accumulates at the newly formed LDs.

Interestingly though, neither LDAPs nor LDIP show increases of protein abundance in the LD-enriched fraction to match CLO3 and even appeared to decrease in abundance in some treatments (Figure 8B, C in manuscript I). When the numbers of observed LDs increase after pathogen infection (Fernández-Santos et al., 2020), a concomitant increase in the proteins of the LD biogenesis machinery would have appeared plausible. However, if infection leads to increased turnover and synthesis of LDs, subcellular localisation of LDAPs and LDIP might shift towards the site of LD biogenesis at the ER. According to the currently proposed model of LD biosynthesis, LDIP initially interacts with seipins at the ER before LDAPs target to the nascent LD and then recruit LDIP to the maturing LD surface (Pyc et al., 2021). In times of higher biosynthesis activity, this would result in an increased concentration of LDAPs and LDIP at the ER, where they are less likely to be enriched in the LD fraction with our ultracentrifugation-based method of LD enrichment. Similar effects might occur in response to heat treatment, as the reported increase in number of LDs (Gidda et al., 2016) is not matched by a corresponding increase in the known LD proteome (Figure 8A in manuscript I). If LD synthesis triggered by heat stress leads to higher numbers of LDs still connected to the ER, or LDs get in contact with other cellular membranes like the plasma membrane for the purpose of membrane remodelling (Krawczyk et al., 2022; Scholz et al., 2022) they might get lost during LD enrichment as well.

The observed changes in the LD proteome thus capture most efficiently the changes in the proteome of free LDs. These are mainly driven by CLO3 and α-DOX1, albeit for α-DOX1 only in reaction to our two infection treatments and not to heat stress. Notwithstanding, the changes in proteome composition highlight LDs as dynamic organelles in leaves that form part of the cellular reaction to environmental signals.

7.4 Functions of LDs in the evolutionary context

7.4.1 LD functionality is diversified among tissues

The previous sections already hinted at differences of LDs between tissues. The context of the cell shapes LDs and in distinct tissues LDs will adapt to different requirements. In seeds, LDs have mainly a storage function and sequester neutral lipids into inert compartments so they endure the desiccated state and subsequently provide carbon skeletons and redox equivalents during seedling establishment (Baud et al., 2008; Graham, 2008). Consequently, it is most important in that phase to stabilise seed LDs, to preclude their premature degradation and to prevent LD fusion, which would impair later accessibility for hydrolysing enzymes due to decreased surface-to-volume ratios. These functions are fulfilled by oleosins that dominate the seed LD proteome (Table 6), but are degraded during seedling establishment (Tzen et al., 1992; Shimada et al., 2008; Deruyffelaere et al., 2018; Kretzschmar et al., 2018, 2020).

In roots, the functions of LDs have been hardly studied, however, the first proteome of LD-enriched fractions of root tissues from the Arabidopsis mutant *tgd1-1 sdp1-4* gives clues to possible roles of LDs (Table 2). Several of the detected LD proteins, for example the oil body lipases (OBLs), SMT1 or CAS1, have metabolic functions and other proteins have been

putatively assigned as enzymes, for example LIME1/2 (Corey et al., 1993; Diener et al., 2000; Müller, 2018; Kretzschmar et al., 2020). Proteins like HSD4/7 or THAS1 were unique for LDs in roots and could be involved in the modulation of plant hormones and the synthesis of metabolites in specialised metabolism of Arabidopsis (Fazio et al., 2004; Chapman et al., 2012). THAS1 especially seems to have a root-specific function, catalysing an initial cyclisation step to tricyclic triterpenoids that in turn could modulate plant-microbe interactions in the rhizosphere (Huang et al., 2019). After their storage function in seeds, LDs appear to become active players in cellular metabolism.

Enzymes of neutral lipid synthesis and acyl editing pathways like the glycerol-3-phosphate acyltransferases (GPATs) and LPEAT1 were also detected in the LD-enriched fraction of roots and co-localised with LDs in tobacco pollen tubes. Although at least GPAT9 takes part in the pathways leading to TAG synthesis (Shockey et al., 2016; Singer et al., 2016), the catalysed reactions have so far been assumed to occur between the leaflets of the ER (Li-Beisson et al., 2013; Jayawardhane et al., 2018; Ischebeck et al., 2020). In addition, GPAT4 and GPAT8, albeit previously described to localise to LDs (Fernández-Santos et al., 2020), are rather implicated in the synthesis of extracellular lipids for which no functional connection to LDs has been reported so far (Jayawardhane et al., 2018). One explanation could be that they are stored on the LD surface without access to substrates or in an inactive form, until they are required at the ER. Precedent for LDs as protein storage platforms comes from the animal field, where histones were reported to be stored on LDs i.a. in *Drosophila* eggs, mouse oocytes and embryos of house flies (Welte and Gould, 2017). Transient protein storage on LDs was also reported for a transcriptional regulator in adipocyte tissue and an anti-viral protein that relocalises to other compartments upon viral infection (Welte and Gould, 2017).

Finally, LDs in root hair cells might serve specialised functions in the membrane homeostasis of tip-growing cells, as has been proposed for LDs in pollen tubes. Although the contribution of LDs to pollen tube growth is not entirely clear, it has been suggested that they are used as a pool of membrane lipid precursors to enable fast synthesis of the membrane lipids needed at the tip while limiting the amount of cytotoxic intermediates (Ischebeck, 2016). As pollen tubes and root hairs have long been described to share similarities in growth and cellular organisation (Ovečka et al., 2012), LDs could play an analogous role of maintaining membrane homeostasis and providing membrane lipid precursors in root hair cells.

Like LDs in roots, LDs in leaves appear to be involved in metabolic processes, harbouring enzymes among their associated proteins (Table 5) and providing substrates e.g. for oxylipin synthesis. This might be especially important in reaction to pathogen infection, where LDs are a source of acyl chains for the concerted action of α-DOX1 and CLO3 in phytoalexine synthesis (Shimada et al., 2014). Fittingly, we also observed strong increases in their protein abundance in the LD-enriched fractions of infected Arabidopsis leaves (Figure 8C in manuscript I). In addition, another study reported that LD size distribution is altered upon treatment with fungal elicitors from *Fusarium oxysporum*. The proportion of LDs with diameters less than 0.5 µm increased at the expense of LDs with diameters larger than 1 µm (Coca and Segundo, 2010). While the functional relevance of this change was not analysed further, it could be reasoned that smaller LDs have overall increased surface-to-volume ratios that could promote LD accessibility to enzymes.

Leaf LDs in general take a role as universal stress response organelles, be it in biotic or abiotic stresses. Increased numbers of LDs in leaves are described as a common response to cold stress, heat stress, drought stress, extended darkness and *Pseudomonas* infection (Gidda et al., 2016; Fan et al., 2017; Fernández-Santos et al., 2020; Doner et al., 2021). Increased levels of its core component TAGs are also a broadly observed stress response (Vu et al., 2014; Higashi and Saito, 2019; Schieferle et al., 2021), a trend which we observed in all our treatments as well (Figure 1C in manuscript I). On the one hand, this could serve to provide lipids and energy for the cell after overcoming or adapting to the stress. On the other hand, LDs might accumulate for means of directly protecting against the stress, e.g. by sequestering toxic lipid intermediates or scavenging ROS species (Fan et al., 2017; Higashi and Saito, 2019). In the context of leaves, the latter is more strongly discussed (Ischebeck et al., 2020) especially in connection to membrane remodelling. Heat stress gives a good illustration of this as the acyl chain composition of cellular membranes is adjusted to keep membrane fluidity constant, leading to the replacement of polyunsaturated acyl chains with more saturated acyl chain species (Niu and Xiang, 2018). Concomitantly, TAG species with a high degree of desaturation, for example with three 18:3 acyl chains, accumulate. This led to the conclusion that the acyl chains of the membrane are channelled into TAGs and LDs (Higashi and Saito, 2019). During heat stress recovery, TAG levels decrease again, possibly as acyl chains are channelled back into membrane lipids (Higashi et al., 2015). Heat is the best observed example and established the idea of LDs acting as transient sink for unsuitable lipid species. Nevertheless, LDs as sink organelles have now been proposed as general feature of membrane remodelling processes, during stress response as well as during membrane turnover in senescent leaves (Troncoso-Ponce et al., 2013; Yang and Benning, 2018; Ischebeck et al., 2020). In this, organisation of LD proliferation is at least partially mediated by the coating LDAP proteins, and their gene expression is upregulated in reaction to temperature, drought and salt stress (Gidda et al., 2016; Kim et al., 2016). Given their involvement in LD biogenesis (Pyc et al., 2021), they might be important in the partitioning of the lipid intermediates into LDs during remodelling processes. All in all, LDs in leaves are nothing like inert storage organelles and play instead an important role in mediating lipid homeostasis under different environmental conditions.

7.4.2 The evolutionary past of LDs in seeds and vegetative tissue

LDs are evolutionary very conserved organelles and can be found i.a. across the green lineage (Murphy, 2012). LD-like structures have even been described in cyanobacteria (Peramuna and Summers, 2014; Gonzalez-Esquer et al., 2016; Aizouq et al., 2020), albeit these structures might be more similar to plastoglobules than to cytosolic LDs. Even with their wide distribution and despite the depicted differences of LDs in seeds and vegetative tissue of land plants, their participation in cellular processes has a common theme: stress response and stress endurance (de Vries and Ischebeck, 2020). In Arabidopsis as model for angiosperm plants, LDs are important in stress responses in leaves; LDs in seeds on the other hand are part of a desiccation-tolerant structure that enables spermatophytes to endure unfavourable conditions. In algal relatives of land plants, LDs have apparently similar functions (Herburger et al., 2015; Li-Beisson et al., 2019). Green algae of the genus *Zygnema* were reported to be able to develop into so-called "pre-akinetes" under limited resources, modified cells that are

more stress-tolerant. Importantly, these "pre-akinetes" accumulate LDs as major storage compound and show a different FA composition than young vegetative cells (Herburger et al., 2015; Pichrtová et al., 2016). The formation of these "pre-akinetes" was suggested to enable the survival of *Zygnema* in arctic habitats, allowing them to endure the unfavourable conditions of arctic winter (Pichrtová et al., 2014), in a manner similar to the seeds of spermatophytes.

Albeit seeds are a defining feature of spermatophytes, the mechanisms driving its storage accumulation and LD formation thus appear to be phylogenetically older. Consequently, distant homologs of seed LD proteins have been discovered in non-seed plants and streptophyte algae (Huang et al., 2013; de Vries and Ischebeck, 2020). Furthermore, the expression of oleosin coding genes in two algal species of the *Zygnomatophyceae* was strongly induced by drought or heat stress (Rippin et al., 2017; de Vries et al., 2020; de Vries and Ischebeck, 2020), underlining again the connection between LDs and stress. Based on these phylogenetic observations, oleosins appear as important proteins to cope with desiccation that in angiosperms have been restricted to their remaining desiccation-tolerant structures, most commonly seeds and pollen (Table 6). A connection of oleosins to desiccation-tolerance rather than to specific tissues is further strengthened by the observation of the expression of oleosin coding genes in desiccating leaves of *Oropetium thomaeum* and tubers of yellow nutsedge (VanBuren et al., 2017; Niemeyer et al., 2022). Leaves of *O. thomaeum* are able to desiccate for extended periods of drought stress before resuming cellular metabolism when they are hydrated again whereby desiccation is accompanied by LD accumulation. In hydrated states, leaves of *O. thomaeum* are, however, comparable to Arabidopsis without notable expression of oleosins genes and low numbers of LDs (VanBuren et al., 2017). Similar features were also observed in the tubers of yellow nutsedge: they are desiccation-tolerant, accumulate oil, sprout after rehydration and their LD proteome contains homologues of Arabidopsis seed LD proteins like oleosins or SLDPs (Niemeyer et al., 2022).

In addition to a phylogenetic background for LDs in long term stress endurance, the accumulation of TAGs as fast stress response also has precedent in algal relatives. In microalgae, TAG accumulation is induced by the deficiency of nutrients as well as unfavourable environmental conditions regarding i.a. light intensity, temperature or salinity (Zienkiewicz et al., 2016; Li-Beisson et al., 2019). Especially nitrogen deprivation is commonly employed to promote TAG accumulation in microalgae under laboratory conditions and has been used for example with *Chlamydomonas reinhardtii*, *Nannochloropsis oceanica* or *Nannochloropsis gaditana* (Simionato et al., 2013; Takeuchi and Benning, 2019; Zienkiewicz et al., 2020). Strikingly, in *N. gaditana* increased levels of TAG were accompanied by decreased levels of membrane glycerolipids, hinting at a role of TAGs as sink during membrane adaptations (Simionato et al., 2013). Another interesting observation related to the LD proteins in *C. reinhardtii*: no oleosin homologues were found in the LD proteome, instead a protein termed MAJOR LIPID DROPLET PROTEIN (MLDP) was identified as the dominant LD protein (Moellering and Benning, 2010). While MLDP was initially reported to have orthologs only in green algae (Moellering and Benning, 2010), more recently it was suggested that MLDP shares an evolutionary past with angiosperm LDAPs (de Vries and Ischebeck, 2020). This proposition was based on a protein of *Klebsormidium nitens* with N-terminal sequence similarities to both MLDP and LDAPs. Features of LDs in leaves, like accumulation upon stress

response, and possibly also the LDAP proteins, can thus be traced back to a common ancestor with chlorophyte algae. Altogether, Arabidopsis LDs of long term desiccation tolerance and short term lipid remodelling combine to equip different tissues with the necessary requirements for their respective interaction with environmental stressors.

8 Concluding Remarks

Lipids are one of the major biochemical compound classes and their contributions to cellular homeostasis are as important as lipids are diverse. This thesis aimed to analyse two facets of lipids in plants: (i) lipid signalling function of the anionic lipid phosphatidic acid (PA) in the plant cell model of tobacco pollen tubes and (ii) the role of the neutral lipid organelles lipid droplets (LDs) in vegetative plant tissues. For the first part we used a disturbation approach where we altered PA homeostasis in tobacco pollen tubes by transiently expressing variants of PA-producing diacylglycerol kinase enzymes. The second part employed "omics"-technologies to observe the alterations of neutral lipids and the LD proteome of Arabidopsis leaves under stress. In addition, this part of the thesis included a proteomics assessment of the LD proteome in Arabidopsis roots.

Regarding the study of PA in pollen tubes we could characterise the enzyme tobacco diacylglycerolkinase 5 (NtDGK5) and its impact on pollen tube growth. NtDGK5 was demonstrated as active PA-producing enzyme that requires a conserved ATP-binding motif for its enzymatic activity. Furthermore, its subcellular localisation could be pinpointed to the plasma membrane shortly behind the pollen tube tip of growing pollen tubes where it most likely interacts with anionic lipids of the membrane. Interfering with endogenous PA production of tobacco pollen tubes by transient overexpression of NtDGK5 or a kinase-dead variant caused obvious pollen tube growth phenotypes. The transformed pollen tubes were more likely to display a wavy growth pattern or misshaped pollen tube tips. These phenotypes were traced to altered cell wall secretion via a possible link of other signalling lipids. Altogether, we could establish NtDGK5 as additional modulator of tobacco pollen tube growth, however, several questions remain to be explored especially concerning the downstream connection of lipid signals to cell wall secretion in pollen tubes.

Following neutral lipid dynamics in stressed leaves of Arabidopsis with lipidomic measurements, we could witness a trend towards TAG hyperaccumulation as general response to infection or heat stress treatments. Interestingly, the link between stress and TAGs seemed to work both ways, as the cellular proteome of a TAG-accumulating mutant was altered in a manner resembling the reaction to pathogen infection. We used this mutant to track changes in the LD proteome of leaves following infection or heat stress. There, we could confirm that LDs are part of the cellular response to various stresses as the protein composition adapted to the applied treatments. Especially the LD protein CALEOSIN 3 stood out as an active player of LD stress response. In addition, the combined proteomic datasets of LD-enriched fractions isolated from Arabidopsis leaves allowed the identification of new putative LD-interacting proteins. Two of those could be then confirmed to associate to LDs in subcellular localisation studies using a transient expression system. Finally, in this thesis, I present the first overview of LD-associated proteins in roots. Proteomic measurements identified 29 LD proteins in LD-enriched fractions isolated from Arabidopsis roots. Later studies could also establish five new proteins to be LD-localised. Among them is the root-specific metabolic enzyme THALIANOL SYNTHASE 1 that implicates LDs as active metabolic hubs in the root tissue. Overall, this work can hopefully serve as stepping stone towards a more functional understanding of vegetative LDs and the multiple roles they play in the tissues of leaves and roots.

9 References

Abell, B.M., Holbrook, L.A., Abenes, M., Murphy, D.J., Hills, M.J., and Moloney, M.M. (1997). Role of the proline knot motif in oleosin endoplasmic reticulum topology and oil body targeting. Plant Cell **9**: 1481–1493.

Aizouq, M., Peisker, H., Gutbrod, K., Melzer, M., Hölzl, G., and Dörmann, P. (2020). Triacylglycerol and phytyl ester synthesis in Synechocystis sp. PCC6803. Proc Natl Acad Sci U S A **117**: 6216–6222.

Almeida, J., Perez-Fons, L., and Fraser, P.D. (2021). A transcriptomic, metabolomic and cellular approach to the physiological adaptation of tomato fruit to high temperature. Plant Cell Environ **44**: 2211–2229.

d'Andréa, S., Canonge, M., Beopoulos, A., Jolivet, P., Hartmann, M.A., Miquel, M., Lepiniec, L., and Chardot, T. (2007). At5g50600 encodes a member of the short-chain dehydrogenase reductase superfamily with 11beta- and 17beta-hydroxysteroid dehydrogenase activities associated with Arabidopsis thaliana seed oil bodies. Biochimie **89**: 222–229.

Angkawijaya, A.E., Nguyen, V.C., Gunawan, F., and Nakamura, Y. (2020). A Pair of Arabidopsis Diacylglycerol Kinases Essential for Gametogenesis and Endoplasmic Reticulum Phospholipid Metabolism in Leaves and Flowers. Plant Cell **32**: 2602–2620.

Antignani, V., Klocko, A.L., Bak, G., Chandrasekaran, S.D., Dunivin, T., and Nielsen, E. (2015). Recruitment of PLANT U-BOX13 and the PI4Kβ1/β2 phosphatidylinositol-4 kinases by the small GTPase RabA4B plays important roles during salicylic acid-mediated plant defense signaling in Arabidopsis. Plant Cell **27**: 243–261.

Arisz, S.A., Testerink, C., and Munnik, T. (2009). Plant PA signaling via diacylglycerol kinase. Biochim Biophys Acta **1791**: 869–875.

Aubert, Y., Vile, D., Pervent, M., Aldon, D., Ranty, B., Simonneau, T., Vavasseur, A., and Galaud, J.-P. (2010). RD20, a Stress-Inducible Caleosin, Participates in Stomatal Control, Transpiration and Drought Tolerance in Arabidopsis thaliana. Plant Cell Physiol **51**: 1975–1987.

Bai, Y., Fernández-Calvo, P., Ritter, A., Huang, A.C., Morales-Herrera, S., Bicalho, K.U., Karady, M., Pauwels, L., Buyst, D., Njo, M., Ljung, K., Martins, J.C., Vanneste, S., Beeckmann, T., Osbourn, A., Goossens, A., and Pollier, J. (2021). Modulation of Arabidopsis root growth by specialized triterpenes. New Phytol **230**: 228–243

Balla, A., Tuymetova, G., Tsiomenko, A., Várnai, P., and Balla, T. (2005). A Plasma Membrane Pool of Phosphatidylinositol 4-Phosphate Is Generated by Phosphatidylinositol 4-Kinase Type-III Alpha: Studies with the PH Domains of the Oxysterol Binding Protein and FAPP1. MBoC **16**: 1282–1295.

Banas, A., Carlsson, A.S., Huang, B., Lenman, M., Banas, W., Lee, M., Noiriel, A., Benveniste, P., Schaller, H., Bouvier-Navé, P., and Stymne, S. (2005). Cellular sterol ester synthesis in plants is performed by an enzyme (phospholipid:sterol acyltransferase) different from the yeast and mammalian acyl-CoA:sterol acyltransferases. J Biol Chem **280**: 34626–34634.

Barajas-Lopez, J. de D., Tiwari, A., Zarza, X., Shaw, M.W., Pascual, J., Punkkinen, M., Bakowska, J.C., Munnik, T., and Fujii, H. (2021). EARLY RESPONSE TO DEHYDRATION 7 Remodels Cell Membrane Lipid Composition during Cold Stress in Arabidopsis. Plant Cell Physiol **62**: 80–91.

Bartz, R., Li, W.-H., Venables, B., Zehmer, J.K., Roth, M.R., Welti, R., Anderson, R.G.W., Liu, P., and Chapman, K.D. (2007). Lipidomics reveals that adiposomes store ether lipids and mediate phospholipid traffic. J. Lipid Res. **48**: 837–847.

Bates, P.D. (2016). Understanding the control of acyl flux through the lipid metabolic network of plant oil biosynthesis. Biochim Biophys Acta **1861**: 1214–1225.

Baud, S., Dichow, N.R., Kelemen, Z., d'Andréa, S., To, A., Berger, N., Canonge, M., Kronenberger, J., Viterbo, D., Dubreucq, B., Lepiniec, L., Chardot, T., and Miquel, M. (2009). Regulation of HSD1 in Seeds of Arabidopsis thaliana. Plant Cell Physiol **50**: 1463–1478.

Baud, S., Boutin, J.-P., Miquel, M., Lepiniec, L., and Rochat, C. (2002). An integrated overview of seed development in Arabidopsis thaliana ecotype WS. Plant Physiol Biochem **40**: 151–160.

Baud, S., Dubreucq, B., Miquel, M., Rochat, C., and Lepiniec, L. (2008). Storage Reserve Accumulation in Arabidopsis: Metabolic and Developmental Control of Seed Filling. Arabidopsis Book **6**: e0113.

Baud, S. and Lepiniec, L. (2010). Physiological and developmental regulation of seed oil production. Prog Lipid Res **49**: 235–249.

Beaudoin, F., Wilkinson, B.M., Stirling, C.J., and Napier, J.A. (2000). In vivo targeting of a sunflower oil body protein in yeast secretory (sec) mutants. Plant J. **23**: 159–170.

Bersuker, K. and Olzmann, J.A. (2017). Establishing the lipid droplet proteome: Mechanisms of lipid droplet protein targeting and degradation. Biochim Biophys Acta **1862**: 1166–1177.

Bi, J., Wang, W., Liu, Z., Huang, X., Jiang, Q., Liu, G., Wang, Y., and Huang, X. (2014). Seipin Promotes Adipose Tissue Fat Storage through the ER Ca2+-ATPase SERCA. Cell Metabolism **19**: 861–871.

Bigay, J. and Antonny, B. (2012). Curvature, Lipid Packing, and Electrostatics of Membrane Organelles: Defining Cellular Territories in Determining Specificity. Dev Cell **23**: 886–895.

Blée, E., Boachon, B., Burcklen, M., Le Guédard, M., Hanano, A., Heintz, D., Ehlting, J., Herrfurth, C., Feussner, I., and Bessoule, J.-J. (2014). The Reductase Activity of the Arabidopsis Caleosin RESPONSIVE TO DESSICATION20 Mediates Gibberellin-Dependent Flowering Time, Abscisic Acid Sensitivity, and Tolerance to Oxidative Stress. Plant Physiol **166**: 109–124.

Boavida, L.C. and McCormick, S. (2007). TECHNICAL ADVANCE: Temperature as a determinant factor for increased and reproducible in vitro pollen germination in Arabidopsis thaliana: Temperature effect on Arabidopsis pollen germination. Plant J. **52**: 570–582.

Borg, M., Brownfield, L., and Twell, D. (2009). Male gametophyte development: a molecular perspective. J Exp Bot **60**: 1465–1478.

Bouvier-Navé, P., Berna, A., Noiriel, A., Compagnon, V., Carlsson, A.S., Banas, A., Stymne, S., and Schaller, H. (2009). Involvement of the *Phospholipid Sterol Acyltransferase1* in Plant Sterol Homeostasis and Leaf Senescence. Plant Physiol **152**: 107–119.

Brocard, L., Immel, F., Coulon, D., Esnay, N., Tuphile, K., Pascal, S., Claverol, S., Fouillen, L., Bessoule, J.-J., and Bréhélin, C. (2017). Proteomic Analysis of Lipid Droplets from Arabidopsis Aging Leaves Brings New Insight into Their Biogenesis and Functions. Front Plant Sci **8**: 894.

Cai, G., Parrotta, L., and Cresti, M. (2015a). Organelle trafficking, the cytoskeleton, and pollen tube growth: Organelle trafficking in pollen tubes. J Integr Plant Biol **57**: 63–78.

Cai, Y., Goodman, J.M., Pyc, M., Mullen, R.T., Dyer, J.M., and Chapman, K.D. (2015b). Arabidopsis SEIPIN Proteins Modulate Triacylglycerol Accumulation and Influence Lipid Droplet Proliferation. Plant Cell **27**: 2616–2636.

Cai, Y., McClinchie, E., Price, A., Nguyen, T.N., Gidda, S.K., Watt, S.C., Yurchenko, O., Park, S., Sturtevant, D., Mullen, R.T., Dyer, J.M., and Chapman, K.D. (2017). Mouse fat storage-inducing transmembrane protein 2 (FIT2) promotes lipid droplet accumulation in plants. Plant Biotechnol J **15**: 824–836.

Chapman, K.D., Dyer, J.M., and Mullen, R.T. (2012). Biogenesis and functions of lipid droplets in plants: Thematic Review Series: Lipid Droplet Synthesis and Metabolism: from Yeast to Man. J. Lipid Res. **53**: 215–226.

Chapman, K.D., Dyer, J.M., and Mullen, R.T. (2013). Commentary: Why don't plant leaves get fat? Plant Science **207**: 128–134.

Chapman, K.D. and Ohlrogge, J.B. (2012). Compartmentation of triacylglycerol accumulation in plants. J Biol Chem **287**: 2288–2294.

Chebli, Y., Kroeger, J., and Geitmann, A. (2013). Transport Logistics in Pollen Tubes. Mol Plant **6**: 1037–1052.

Chen, J.C.F., Tsai, C.C.Y., and Tzen, J.T.C. (1999). Cloning and Secondary Structure Analysis of Caleosin, a Unique Calcium-Binding Protein in Oil Bodies of Plant Seeds. Plant Cell Physiol **40**: 1079–1086.

Chen, J.C.F. and Tzen, J.T.C. (2001). An in vitro System to Examine the Effective Phospholipids and Structural Domain for Protein Targeting to Seed Oil Bodies. Plant Cell Physiol **42**: 1245–1252.

Chorlay, A., Monticelli, L., Veríssimo Ferreira, J., Ben M'barek, K., Ajjaji, D., Wang, S., Johnson, E., Beck, R., Omrane, M., Beller, M., Carvalho, P., and Rachid Thiam, A. (2019). Membrane Asymmetry Imposes Directionality on Lipid Droplet Emergence from the ER. Dev Cell **50**: 25-42.e7.

Choudhary, V., El Atab, O., Mizzon, G., Prinz, W.A., and Schneiter, R. (2020). Seipin and Nem1 establish discrete ER subdomains to initiate yeast lipid droplet biogenesis. J Cell Biol **219**: e201910177.

Choudhary, V., Ojha, N., Golden, A., and Prinz, W.A. (2015). A conserved family of proteins facilitates nascent lipid droplet budding from the ER. J Cell Biol **211**: 261–271.

Coca, M. and Segundo, B.S. (2010). AtCPK1 calcium-dependent protein kinase mediates pathogen resistance in Arabidopsis. Plant J. **63**: 526–540.

Colón-González, F. and Kazanietz, M.G. (2006). C1 domains exposed: from diacylglycerol binding to protein-protein interactions. Biochim Biophys Acta **1761**: 827–837.

Compiani, M. and Capriotti, E. (2013). Computational and Theoretical Methods for Protein Folding. Biochemistry **52**: 8601–8624.

Corey, E.J., Matsuda, S.P., and Bartel, B. (1993). Isolation of an Arabidopsis thaliana gene encoding cycloartenol synthase by functional expression in a yeast mutant lacking lanosterol synthase by the use of a chromatographic screen. Proc Natl Acad Sci U S A **90**: 11628–11632.

Coulon, D., Brocard, L., Tuphile, K., and Bréhélin, C. (2020). Arabidopsis LDIP protein locates at a confined area within the lipid droplet surface and favors lipid droplet formation. Biochimie **169**: 29–40.

Crespo-Salvador, Ó., Escamilla-Aguilar, M., López-Cruz, J., López-Rodas, G., and González-Bosch, C. (2018). Determination of histone epigenetic marks in Arabidopsis and tomato genes in the early response to Botrytis cinerea. Plant Cell Rep **37**: 153–166.

Cui, S., Hayashi, Y., Otomo, M., Mano, S., Oikawa, K., Hayashi, M., and Nishimura, M. (2016). Sucrose Production Mediated by Lipid Metabolism Suppresses the Physical Interaction of Peroxisomes and Oil Bodies during Germination of Arabidopsis thaliana. J Biol Chem **291**: 19734–19745.

Dahlqvist, A., Stahl, U., Lenman, M., Banas, A., Lee, M., Sandager, L., Ronne, H., and Stymne, S. (2000). Phospholipid:diacylglycerol acyltransferase: an enzyme that catalyzes the acyl-CoA-independent formation of triacylglycerol in yeast and plants. Proc Natl Acad Sci U S A **97**: 6487–6492.

De Domenico, S., Tsesmetzis, N., Di Sansebastiano, G.P., Hughes, R.K., Casey, R., and Santino, A. (2007). Subcellular localisation of Medicago truncatula 9/13-hydroperoxide lyase reveals a new localisation pattern and activation mechanism for CYP74C enzymes. BMC Plant Biol **7**: 58.

De León, I.P., Sanz, A., Hamberg, M., and Castresana, C. (2002). Involvement of the Arabidopsisα-DOX1 fatty acid dioxygenase in protection against oxidative stress and cell death. Plant J. **29**: 61–72.

Deruyffelaere, C., Purkrtova, Z., Bouchez, I., Collet, B., Cacas, J.-L., Chardot, T., Gallois, J.-L., and D'Andrea, S. (2018). PUX10 Is a CDC48A Adaptor Protein That Regulates the Extraction of Ubiquitinated Oleosins from Seed Lipid Droplets in Arabidopsis. Plant Cell **30**: 2116–2136.

Diener, A.C., Li, H., Zhou, W., Whoriskey, W.J., Nes, W.D., and Fink, G.R. (2000). Sterol methyltransferase 1 controls the level of cholesterol in plants. Plant Cell **12**: 853–870.

Doner, N.M., Seay, D., Mehling, M., Sun, S., Gidda, S.K., Schmitt, K., Braus, G.H., Ischebeck, T., Chapman, K.D., Dyer, J.M., and Mullen, R.T. (2021). Arabidopsis thaliana EARLY RESPONSIVE TO DEHYDRATION 7 Localizes to Lipid Droplets via Its Senescence Domain. Front Plant Sci **12**: 658961.

Dowd, P.E., Coursol, S., Skirpan, A.L., Kao, T., and Gilroy, S. (2006). Petunia phospholipase c1 is involved in pollen tube growth. Plant Cell **18**: 1438–1453.

Duelund, L., Jensen, G.V., Hannibal-Bach, H.K., Ejsing, C.S., Pedersen, J.S., Pakkanen, K.I., and Ipsen, J.H. (2013). Composition, structure and properties of POPC–triolein mixtures. Evidence of triglyceride domains in phospholipid bilayers. Biochim Biophys Acta **1828**: 1909–1917.

Eastmond, P.J. (2004). Cloning and characterization of the acid lipase from castor beans. J Biol Chem **279**: 45540–45545.

Eastmond, P.J. (2006). SUGAR-DEPENDENT1 Encodes a Patatin Domain Triacylglycerol Lipase That Initiates Storage Oil Breakdown in Germinating Arabidopsis Seeds. Plant Cell **18**: 665–675.

Eastmond, P.J., Quettier, A.-L., Kroon, J.T.M., Craddock, C., Adams, N., and Slabas, A.R. (2010). PHOSPHATIDIC ACID PHOSPHOHYDROLASE1 and 2 Regulate Phospholipid Synthesis at the Endoplasmic Reticulum in Arabidopsis. Plant Cell **22**: 2796–2811.

Fan, J., Yan, C., Roston, R., Shanklin, J., and Xu, C. (2014). Arabidopsis lipins, PDAT1 acyltransferase, and SDP1 triacylglycerol lipase synergistically direct fatty acids toward β-oxidation, thereby maintaining membrane lipid homeostasis. Plant Cell **26**: 4119–4134.

Fan, J., Yan, C., and Xu, C. (2013). Phospholipid:diacylglycerol acyltransferase-mediated triacylglycerol biosynthesis is crucial for protection against fatty acid-induced cell death in growing tissues of Arabidopsis. Plant J. **76**: 930–942.

Fan, J., Yu, L., and Xu, C. (2017). A Central Role for Triacylglycerol in Membrane Lipid Breakdown, Fatty Acid β-Oxidation, and Plant Survival under Extended Darkness. Plant Physiol **174**: 1517–1530.

Farmer, E.E. and Mueller, M.J. (2013). ROS-Mediated Lipid Peroxidation and RES-Activated Signaling. Annu. Rev. Plant Biol. **64**: 429–450.

Fayant, P., Girlanda, O., Chebli, Y., Aubin, C.-E., Villemure, I., and Geitmann, A. (2010). Finite Element Model of Polar Growth in Pollen Tubes. Plant Cell **22**: 2579–2593.

Fazio, G.C., Xu, R., and Matsuda, S.P.T. (2004). Genome Mining To Identify New Plant Triterpenoids. J. Am. Chem. Soc. **126**: 5678–5679.

Fei, W., Shui, G., Gaeta, B., Du, X., Kuerschner, L., Li, P., Brown, A.J., Wenk, M.R., Parton, R.G., and Yang, H. (2008). Fld1p, a functional homologue of human seipin, regulates the size of lipid droplets in yeast. J Cell Biol **180**: 473–482.

Fernández-Santos, R., Izquierdo, Y., López, A., Muñiz, L., Martínez, M., Cascón, T., Hamberg, M., and Castresana, C. (2020). Protein Profiles of Lipid Droplets during the Hypersensitive

Defense Response of Arabidopsis against Pseudomonas Infection. Plant Cell Physiol **61**: 1144–1157.

Ferrer, A., Altabella, T., Arró, M., and Boronat, A. (2017). Emerging roles for conjugated sterols in plants. Prog Lipid Res **67**: 27–37.

Feussner, I. and Kindl, H. (1992). A lipoxygenase is the main lipid body protein in cucumber and soybean cotyledons during the stage of triglyceride mobilization. FEBS Lett **298**: 223–225.

Field, B. and Osbourn, A.E. (2008). Metabolic diversification--independent assembly of operon-like gene clusters in different plants. Science **320**: 543–547.

Fischer, H., Polikarpov, I., and Craievich, A.F. (2004). Average protein density is a molecular-weight-dependent function. Protein Science **13**: 2825–2828.

Flügge, U.-I., Häusler, R.E., Ludewig, F., and Gierth, M. (2011). The role of transporters in supplying energy to plant plastids. J Exp Bot **62**: 2381–2392.

Footitt, S., Dietrich, D., Fait, A., Fernie, A.R., Holdsworth, M.J., Baker, A., and Theodoulou, F.L. (2007). The COMATOSE ATP-Binding Cassette Transporter Is Required for Full Fertility in Arabidopsis. Plant Physiol **144**: 1467–1480.

Footitt, S., Slocombe, S.P., Larner, V., Kurup, S., Wu, Y., Larson, T., Graham, I., Baker, A., and Holdsworth, M. (2002). Control of germination and lipid mobilization by COMATOSE, the Arabidopsis homologue of human ALDP. EMBO J **21**: 2912–2922.

Fulda, M., Schnurr, J., Abbadi, A., Heinz, E., and Browse, J. (2004). Peroxisomal Acyl-CoA synthetase activity is essential for seedling development in Arabidopsis thaliana. Plant Cell **16**: 394–405.

Gao, C., Luo, M., Zhao, Q., Yang, R., Cui, Y., Zeng, Y., Xia, J., and Jiang, L. (2014). A unique plant ESCRT component, FREE1, regulates multivesicular body protein sorting and plant growth. Curr Biol **24**: 2556–2563.

Garbowicz, K., Liu, Z., Alseekh, S., Tieman, D., Taylor, M., Kuhalskaya, A., Ofner, I., Zamir, D., Klee, H.J., Fernie, A.R., and Brotman, Y. (2018). Quantitative Trait Loci Analysis Identifies a Prominent Gene Involved in the Production of Fatty Acid-Derived Flavor Volatiles in Tomato. Mol Plant **11**: 1147–1165.

Ge, S., Zhang, R.-X., Wang, Y.-F., Sun, P., Chu, J., Li, J., Sun, P., Wang, J., Hetherington, A.M., and Liang, Y.-K. (2022). The Arabidopsis Rab protein RABC1 affects stomatal development by regulating lipid droplet dynamics. Plant Cell **34**: 4274–4292.

Gerth, K., Lin, F., Menzel, W., Krishnamoorthy, P., Stenzel, I., Heilmann, M., and Heilmann, I. (2017). Guilt by Association: A Phenotype-Based View of the Plant Phosphoinositide Network. Annu Rev Plant Biol **68**: 349–374.

Gidda, S.K., Shockey, J.M., Rothstein, S.J., Dyer, J.M., and Mullen, R.T. (2009). Arabidopsis thaliana GPAT8 and GPAT9 are localized to the ER and possess distinct ER retrieval signals: Functional divergence of the dilysine ER retrieval motif in plant cells. Plant Physiol Biochem **47**: 867–879.

Gidda, S.K., Watt, S., Collins-Silva, J., Kilaru, A., Arondel, V., Yurchenko, O., Horn, P.J., James, C.N., Shintani, D., Ohlrogge, J., Chapman, K.D., Mullen, R.T., and Dyer, J.M. (2013). Lipid droplet-associated proteins (LDAPs) are involved in the compartmentalization of lipophilic compounds in plant cells. Plant Signal Behav **8**: e27141.

Gidda, S.K., Park, S., Pyc, M., Yurchenko, O., Cai, Y., Wu, P., Andrews, D.W., Chapman, K.D., Dyer, J.M., and Mullen, R.T. (2016). Lipid Droplet-Associated Proteins (LDAPs) Are Required for the Dynamic Regulation of Neutral Lipid Compartmentation in Plant Cells. Plant Physiol. **170**: 2052–2071.

Gonzalez-Esquer, C.R., Smarda, J., Rippka, R., Axen, S.D., Guglielmi, G., Gugger, M., and Kerfeld, C.A. (2016). Cyanobacterial ultrastructure in light of genomic sequence data. Photosynth Res **129**: 147–157.

Goulah, C.C., Zhu, G., Koszelak-Rosenblum, M., and Malkowski, M.G. (2013). The Crystal Structure of α-Dioxygenase Provides Insight into Diversity in the Cyclooxygenase-Peroxidase Superfamily. Biochemistry **52**: 1364–1372.

Graham, I.A. (2008). Seed storage oil mobilization. Annu Rev Plant Biol **59**: 115–142.

Greer, M.S., Cai, Y., Gidda, S.K., Esnay, N., Kretzschmar, F.K., Seay, D., McClinchie, E., Ischebeck, T., Mullen, R.T., Dyer, J.M., and Chapman, K.D. (2020). SEIPIN Isoforms Interact with the Membrane-Tethering Protein VAP27-1 for Lipid Droplet Formation. Plant Cell **32**: 2932–2950.

Grillitsch, K., Connerth, M., Köfeler, H., Arrey, T.N., Rietschel, B., Wagner, B., Karas, M., and Daum, G. (2011). Lipid particles/droplets of the yeast Saccharomyces cerevisiae revisited: Lipidome meets Proteome. Biochim Biophys Acta **1811**: 1165–1176.

Hamada, S., Kishikawa, A., and Yoshida, M. (2020). Proteomic Analysis of Lipid Droplets in Sesamum indicum. Protein J **39**: 366–376.

Hamberg, M., Sanz, A., and Castresana, C. (1999). alpha-oxidation of fatty acids in higher plants. Identification of a pathogen-inducible oxygenase (piox) as an alpha-dioxygenase and biosynthesis of 2-hydroperoxylinolenic acid. J Biol Chem **274**: 24503–24513.

Hamilton, J.A., Miller, K.W., and Small, D.M. (1983). Solubilization of triolein and cholesteryl oleate in egg phosphatidylcholine vesicles. J Biol Chem **258**: 12821–12826.

Harker, M., Hellyer, A., Clayton, J.C., Duvoix, A., Lanot, A., and Safford, R. (2003). Co-ordinate regulation of sterol biosynthesis enzyme activity during accumulation of sterols in developing rape and tobacco seed. Planta **216**: 707–715.

Heilmann, I. and Ischebeck, T. (2016). Male functions and malfunctions: the impact of phosphoinositides on pollen development and pollen tube growth. Plant Reproduction **29**: 3–20.

Hemelryck, M.V., Bernal, R., Ispolatov, Y., and Dumais, J. (2018). Lily Pollen Tubes Pulse According to a Simple Spatial Oscillator. Sci Rep **8**: 12135.

Hemmerlin, A., Harwood, J.L., and Bach, T.J. (2012). A raison d'être for two distinct pathways in the early steps of plant isoprenoid biosynthesis? Prog Lipid Res **51**: 95–148.

Hepler, P.K., Rounds, C.M., and Winship, L.J. (2013). Control of Cell Wall Extensibility during Pollen Tube Growth. Mol Plant **6**: 998–1017.

Herburger, K., Lewis, L.A., and Holzinger, A. (2015). Photosynthetic efficiency, desiccation tolerance and ultrastructure in two phylogenetically distinct strains of alpine Zygnema sp. (Zygnematophyceae, Streptophyta): role of pre-akinete formation. Protoplasma **252**: 571–589.

Hernández, M.L., Lima-Cabello, E., Alché, J. de D., Martínez-Rivas, J.M., and Castro, A.J. (2020). Lipid Composition and Associated Gene Expression Patterns during Pollen Germination and Pollen Tube Growth in Olive (Olea europaea L.). Plant Cell Physiol **61**: 1348–1364.

Hernández, M.L., Whitehead, L., He, Z., Gazda, V., Gilday, A., Kozhevnikova, E., Vaistij, F.E., Larson, T.R., and Graham, I.A. (2012). A Cytosolic Acyltransferase Contributes to Triacylglycerol Synthesis in Sucrose-Rescued Arabidopsis Seed Oil Catabolism Mutants. Plant Physiol **160**: 215–225.

Hétu, M.-F., Tremblay, L.J., and Lefebvre, D.D. (2005). High root biomass production in anchored Arabidopsis plants grown in axenic sucrose supplemented liquid culture. BioTechniques **39**: 345–349.

Higashi, Y., Okazaki, Y., Myouga, F., Shinozaki, K., and Saito, K. (2015). Landscape of the lipidome and transcriptome under heat stress in Arabidopsis thaliana. Sci Rep **5**: 1–11.

Higashi, Y. and Saito, K. (2019). Lipidomic studies of membrane glycerolipids in plant leaves under heat stress. Prog Lipid Res **75**: 100990.

Hillebrand, A., Post, J.J., Wurbs, D., Wahler, D., Lenders, M., Krzyzanek, V., Prüfer, D., and Gronover, C.S. (2012). Down-Regulation of Small Rubber Particle Protein Expression Affects Integrity of Rubber Particles and Rubber Content in Taraxacum brevicorniculatum. PLoS One **7**: e41874.

Hills, M.J., Watson, M.D., and Murphy, D.J. (1993). Targeting of oleosins to the oil bodies of oilseed rape (Brassica napus L.). Planta **189**: 24–29.

Hirano, T. and Sato, M.H. (2019). Diverse Physiological Functions of FAB1 and Phosphatidylinositol 3,5-Bisphosphate in Plants. Front Plant Sci **10**: 274.

Hirano, T., Stecker, K., Munnik, T., Xu, H., and Sato, M.H. (2017). Visualization of Phosphatidylinositol 3,5-Bisphosphate Dynamics by a Tandem ML1N-Based Fluorescent Protein Probe in Arabidopsis. Plant Cell Physiol **58**: 1185–1195.

Hobbs, D.H., Lu, C., and Hills, M.J. (1999). Cloning of a cDNA encoding diacylglycerol acyltransferase from Arabidopsis thaliana and its functional expression. FEBS Lett **452**: 145–149.

Holthuis, J.C.M. and Menon, A.K. (2014). Lipid landscapes and pipelines in membrane homeostasis. Nature **510**: 48–57.

Hölzl, G. and Dörmann, P. (2019). Chloroplast Lipids and Their Biosynthesis. Annu Rev Plant Biol **70**: 51–81.

Hong, Y., Devaiah, S.P., Bahn, S.C., Thamasandra, B.N., Li, M., Welti, R., and Wang, X. (2009). Phospholipase Dε and phosphatidic acid enhance Arabidopsis nitrogen signaling and growth. Plant J **58**: 376–387.

Hong, Y., Zhao, J., Guo, L., Kim, S.-C., Deng, X., Wang, G., Zhang, G., Li, M., and Wang, X. (2016). Plant phospholipases D and C and their diverse functions in stress responses. Prog Lipid Res **62**: 55–74.

Horn, P.J., James, C.N., Gidda, S.K., Kilaru, A., Dyer, J.M., Mullen, R.T., Ohlrogge, J.B., and Chapman, K.D. (2013). Identification of a New Class of Lipid Droplet-Associated Proteins in Plants. Plant Physiol **162**: 1926–1936.

Hruz, T., Laule, O., Szabo, G., Wessendorp, F., Bleuler, S., Oertle, L., Widmayer, P., Gruissem, W., and Zimmermann, P. (2008). Genevestigator V3: A Reference Expression Database for the Meta-Analysis of Transcriptomes. Adv Bioinformatics **2008**: 420747.

Huang, A.C., Jiang, T., Liu, Y.-X., Bai, Y.-C., Reed, J., Qu, B., Goossens, A., Nützmann, H.-W., Bai, Y., and Osbourn, A. (2019). A specialized metabolic network selectively modulates Arabidopsis root microbiota. Science **364**: eaau6389.

Huang, A.H.C. (1992). Oil Bodies and Oleosins in Seeds. Annu. Rev. Plant. Physiol. Plant. Mol. Biol. **43**: 177–200.

Huang, A.H.C. (1996). Oleosins and Oil Bodies in Seeds and Other Organs. Plant Physiol. **110**: 1055–1061.

Huang, A.H.C. (2018). Plant Lipid Droplets and Their Associated Proteins: Potential for Rapid Advances. Plant Physiol **176**: 1894–1918.

Huang, C.-Y. and Huang, A.H.C. (2017). Unique Motifs and Length of Hairpin in Oleosin Target the Cytosolic Side of Endoplasmic Reticulum and Budding Lipid Droplet. Plant Physiol **174**: 2248–2260.

Huang, N.-L., Huang, M.-D., Chen, T.-L.L., and Huang, A.H.C. (2013). Oleosin of Subcellular Lipid Droplets Evolved in Green Algae. Plant Physiol **161**: 1862–1874.

Ischebeck, T. (2016). Lipids in pollen — They are different. Biochim Biophys Acta **1861**: 1315–1328.

Ischebeck, T., Krawczyk, H.E., Mullen, R.T., Dyer, J.M., and Chapman, K.D. (2020). Lipid droplets in plants and algae: Distribution, formation, turnover and function. Semin Cell Dev Biol **108**: 82–93.

Ischebeck, T., Stenzel, I., and Heilmann, I. (2008). Type B phosphatidylinositol-4-phosphate 5-kinases mediate Arabidopsis and Nicotiana tabacum pollen tube growth by regulating apical pectin secretion. Plant Cell **20**: 3312–3330.

Ischebeck, T., Vu, L.H., Jin, X., Stenzel, I., Löfke, C., and Heilmann, I. (2010). Functional Cooperativity of Enzymes of Phosphoinositide Conversion According to Synergistic Effects on Pectin Secretion in Tobacco Pollen Tubes. Mol Plant **3**: 870–881.

Jacquier, N., Choudhary, V., Mari, M., Toulmay, A., Reggiori, F., and Schneiter, R. (2011). Lipid droplets are functionally connected to the endoplasmic reticulum in *Saccharomyces cerevisiae*. J Cell Sci **124**: 2424–2437.

Jaillais, Y. and Ott, T. (2020). The Nanoscale Organization of the Plasma Membrane and Its Importance in Signaling: A Proteolipid Perspective. Plant Physiol **182**: 1682–1696.

Jasieniecka-Gazarkiewicz, K., Demski, K., Gidda, S.K., Klińska, S., Niedojadło, J., Lager, I., Carlsson, A.S., Minina, E.A., Mullen, R.T., Bozhkov, P.V., Stymne, S., and Banaś, A. (2021). Subcellular Localization of Acyl-CoA: Lysophosphatidylethanolamine Acyltransferases (LPEATs) and the Effects of Knocking-Out and Overexpression of Their Genes on Autophagy Markers Level and Life Span of A. thaliana. Int J Mol Sci **22**: 3006.

Jayawardhane, K.N., Singer, S.D., Weselake, R.J., and Chen, G. (2018). Plant sn-Glycerol-3-Phosphate Acyltransferases: Biocatalysts Involved in the Biosynthesis of Intracellular and Extracellular Lipids. Lipids **53**: 469–480.

Jiang, P.-L., Chen, J.C.F., Chiu, S.-T., and Tzen, J.T.C. (2009). Stable oil bodies sheltered by a unique caleosin in cycad megagametophytes. Plant Physiol Biochem **47**: 1009–1016.

Johnston, C., García Navarrete, L.T., Ortiz, E., Romsdahl, T.B., Guzha, A., Chapman, K.D., Grotewold, E., and Alonso, A.P. (2022). Effective Mechanisms for Improving Seed Oil Production in Pennycress (Thlaspi arvense L.) Highlighted by Integration of Comparative Metabolomics and Transcriptomics. Front Plant Sci **13**: 943585.

Jolivet, P., Boulard, C., Bellamy, A., Larré, C., Barre, M., Rogniaux, H., d'Andréa, S., Chardot, T., and Nesi, N. (2009). Protein composition of oil bodies from mature Brassica napus seeds. Proteomics **9**: 3268–3284.

Jolivet, P., Roux, E., D'Andrea, S., Davanture, M., Negroni, L., Zivy, M., and Chardot, T. (2004). Protein composition of oil bodies in Arabidopsis thaliana ecotype WS. Plant Physiol Biochem **42**: 501–509.

Kalachova, T., Škrabálková, E., Pateyron, S., Soubigou-Taconnat, L., Djafi, N., Collin, S., Sekereš, J., Burketová, L., Potocký, M., Pejchar, P., and Ruelland, E. (2022). DIACYLGLYCEROL KINASE 5 Participates in Flagellin-Induced Signaling in Arabidopsis. Plant Physiol **190**: 1978–1996.

Kang, B.-H., Nielsen, E., Preuss, M.L., Mastronarde, D., and Staehelin, L.A. (2011). Electron tomography of RabA4b- and PI-4Kβ1-labeled trans Golgi network compartments in Arabidopsis. Traffic **12**: 313–329.

Kassan, A., Herms, A., Fernández-Vidal, A., Bosch, M., Schieber, N.L., Reddy, B.J.N., Fajardo, A., Gelabert-Baldrich, M., Tebar, F., Enrich, C., Gross, S.P., Parton, R.G., and Pol, A. (2013). Acyl-CoA synthetase 3 promotes lipid droplet biogenesis in ER microdomains. J Cell Biol **203**: 985–1001.

Katan, M. and Cockcroft, S. (2020). Phosphatidylinositol(4,5)bisphosphate: diverse functions at the plasma membrane. Essays Biochem **64**: 513–531.

Katavic, V., Agrawal, G.K., Hajduch, M., Harris, S.L., and Thelen, J.J. (2006). Protein and lipid composition analysis of oil bodies from two Brassica napus cultivars. Proteomics **6**: 4586–4598.

Kelly, A.A., van Erp, H., Quettier, A.-L., Shaw, E., Menard, G., Kurup, S., and Eastmond, P.J. (2013). The sugar-dependent1 lipase limits triacylglycerol accumulation in vegetative tissues of Arabidopsis. Plant Physiol **162**: 1282–1289.

Kelly, A.A., Quettier, A.-L., Shaw, E., and Eastmond, P.J. (2011). Seed Storage Oil Mobilization Is Important But Not Essential for Germination or Seedling Establishment in Arabidopsis. Plant Physiol **157**: 866–875.

Kim, E.Y., Park, K.Y., Seo, Y.S., and Kim, W.T. (2016). Arabidopsis Small Rubber Particle Protein Homolog SRPs Play Dual Roles as Positive Factors for Tissue Growth and Development and in Drought Stress Responses. Plant Physiol **170**: 2494–2510.

Kim, S. and Swanson, J.M.J. (2020). The Surface and Hydration Properties of Lipid Droplets. Biophys J **119**: 1958–1969.

Kim, S., Swanson, J.M.J., and Voth, G.A. (2022). Computational Studies of Lipid Droplets. J Phys Chem B **126**: 2145–2154.

Klepikova, A.V., Kasianov, A.S., Gerasimov, E.S., Logacheva, M.D., and Penin, A.A. (2016). A high resolution map of the Arabidopsis thaliana developmental transcriptome based on RNA-seq profiling. Plant J **88**: 1058–1070.

Klug, Y.A., Deme, J.C., Corey, R.A., Renne, M.F., Stansfeld, P.J., Lea, S.M., and Carvalho, P. (2021). Mechanism of lipid droplet formation by the yeast Sei1/Ldb16 Seipin complex. Nat Commun **12**: 5892.

König, S., Ischebeck, T., Lerche, J., Stenzel, I., and Heilmann, I. (2008). Salt-stress-induced association of phosphatidylinositol 4,5-bisphosphate with clathrin-coated vesicles in plants. Biochem J **415**: 387–399.

König, S., Mosblech, A., and Heilmann, I. (2007). Stress-inducible and constitutive phosphoinositide pools have distinctive fatty acid patterns in Arabidopsis thaliana. FASEB J **21**: 1958–1967.

Koornneef, M. and Meinke, D. (2010). The development of Arabidopsis as a model plant. Plant J **61**: 909–921.

Kory, N., Farese, R.V., and Walther, T.C. (2016). Targeting Fat: Mechanisms of Protein Localization to Lipid Droplets. Trends Cell Biol **26**: 535–546.

Kost, B. (2008). Spatial control of Rho (Rac-Rop) signaling in tip-growing plant cells. Trends Cell Biol **18**: 119–127.

Kost, B., Lemichez, E., Spielhofer, P., Hong, Y., Tolias, K., Carpenter, C., and Chua, N.-H. (1999). Rac Homologues and Compartmentalized Phosphatidylinositol 4, 5-Bisphosphate Act in a Common Pathway to Regulate Polar Pollen Tube Growth. J Cell Biol **145**: 317–330.

Krauss, G. ed (2014). Biochemistry of Signal Transduction and Regulation (Wiley-VCH Verlag GmbH & Co. KGaA: Weinheim, Germany).

Krawczyk, H.E., Sun, S., Doner, N.M., Yan, Q., Lim, M.S.S., Scholz, P., Niemeyer, P.W., Schmitt, K., Valerius, O., Pleskot, R., Hillmer, S., Braus, G.H., Wiermer, M., Mullen, R.T., and Ischebeck, T., (2022). SEED LIPID DROPLET PROTEIN1, SEED LIPID DROPLET PROTEIN2, and LIPID DROPLET PLASMA MEMBRANE ADAPTOR mediate lipid droplet-plasma membrane tethering. Plant Cell **34**: 2424–2448.

Kretzschmar, F.K., Doner, N.M., Krawczyk, H.E., Scholz, P., Schmitt, K., Valerius, O., Braus, G.H., Mullen, R.T., and Ischebeck, T. (2020). Identification of Low-Abundance Lipid Droplet Proteins in Seeds and Seedlings. Plant Physiol. **182**: 1326–1345.

Kretzschmar, F.K., Mengel, L.A., Müller, A.O., Schmitt, K., Blersch, K.F., Valerius, O., Braus, G.H., and Ischebeck, T. (2018). PUX10 Is a Lipid Droplet-Localized Scaffold Protein That Interacts with CELL DIVISION CYCLE48 and Is Involved in the Degradation of Lipid Droplet Proteins. Plant Cell **30**: 2137–2160.

Krinke, O., Ruelland, E., Valentová, O., Vergnolle, C., Renou, J.-P., Taconnat, L., Flemr, M., Burketová, L., and Zachowski, A. (2007). Phosphatidylinositol 4-Kinase Activation Is an Early Response to Salicylic Acid in Arabidopsis Suspension Cells. Plant Physiol. **144**: 1347–1359.

Krogh, A., Larsson, B., von Heijne, G., and Sonnhammer, E.L. (2001). Predicting transmembrane protein topology with a hidden Markov model: application to complete genomes. J Mol Biol **305**: 567–580.

Kunz, H.-H., Scharnewski, M., Feussner, K., Feussner, I., Flügge, U.-I., Fulda, M., and Gierth, M. (2009). The ABC Transporter PXA1 and Peroxisomal β-Oxidation Are Vital for Metabolism in Mature Leaves of *Arabidopsis* during Extended Darkness. Plant Cell **21**: 2733–2749.

Kuroda, R., Kato, M., Tsuge, T., and Aoyama, T. (2021). Arabidopsis phosphatidylinositol 4-phosphate 5-kinase genes PIP5K7, PIP5K8, and PIP5K9 are redundantly involved in root growth adaptation to osmotic stress. Plant J **106**: 913–927.

Kusano, H., Testerink, C., Vermeer, J.E.M., Tsuge, T., Shimada, H., Oka, A., Munnik, T., and Aoyama, T. (2008). The Arabidopsis Phosphatidylinositol Phosphate 5-Kinase PIP5K3 is a key regulator of root hair tip growth. Plant Cell **20**: 367–380.

Laibach, N., Schmidl, S., Müller, B., Bergmann, M., Prüfer, D., and Schulze Gronover, C. (2018). Small rubber particle proteins from Taraxacum brevicorniculatum promote stress tolerance and influence the size and distribution of lipid droplets and artificial poly(cis-1,4-isoprene) bodies. Plant J **93**: 1045–1061.

Lara, J.A., Burciaga-Monge, A., Chávez, A., Revés, M., Lavilla, R., Arró, M., Boronat, A., Altabella, T., and Ferrer, A. (2018). Identification and Characterization of Sterol Acyltransferases Responsible for Steryl Ester Biosynthesis in Tomato. Front Plant Sci **9**: 588.

Lee, E., Vanneste, S., Pérez-Sancho, J., Benitez-Fuente, F., Strelau, M., Macho, A.P., Botella, M.A., Friml, J., and Rosado, A. (2019). Ionic stress enhances ER–PM connectivity via phosphoinositide-associated SYT1 contact site expansion in Arabidopsis. Proc Natl Acad Sci U S A **116**: 1420–1429.

Leprince, O., Pellizzaro, A., Berriri, S., and Buitink, J. (2017). Late seed maturation: drying without dying. J Exp Bot **68**: 827–841.

Li, F., Asami, T., Wu, X., Tsang, E.W.T., and Cutler, A.J. (2007). A Putative Hydroxysteroid Dehydrogenase Involved in Regulating Plant Growth and Development. Plant Physiol **145**: 87–97.

Li, F., Han, X., Guan, H., Xu, M.C., Dong, Y.X., and Gao, X.-Q. (2022). PALD encoding a lipid droplet-associated protein is critical for the accumulation of lipid droplets and pollen longevity in Arabidopsis. New Phytol **235**: 204–219.

Li, W., Song, T., Wallrad, L., Kudla, J., Wang, X., and Zhang, W. (2019). Tissue-specific accumulation of pH-sensing phosphatidic acid determines plant stress tolerance. Nat Plants **5**: 1012–1021.

Liao, P., Hemmerlin, A., Bach, T.J., and Chye, M.-L. (2016). The potential of the mevalonate pathway for enhanced isoprenoid production. Biotechnology Advances **34**: 697–713.

Li-Beisson, Y. Y., Shorrosh, B., Beisson, F., Andersson, M.X., Arondel, V., Bates, P.D., Baud, S., Bird, D., Debono, A., Durrett, T.P., Franke, R.B., Graham, I. A., Katayama, K., Kelly, A.A., Larson, T., Markham, J.E., Miquel, M., Molina, I., Nishida, I., Rowland, O., Samuels, L., Schmid, K.M., Wada, H., Welti, R., Xu, C., Zallot, R., and Ohlrogge, J. (2013). Acyl-lipid metabolism. Arabidopsis Book **11**: e0161.

Li-Beisson, Y., Thelen, J.J., Fedosejevs, E., and Harwood, J.L. (2019). The lipid biochemistry of eukaryotic algae. Prog Lipid Res **74**: 31–68.

Lin, D.-L., Yao, H.-Y., Jia, L.-H., Tan, J.-F., Xu, Z.-H., Zheng, W.-M., and Xue, H.-W. (2020). Phospholipase D-derived phosphatidic acid promotes root hair development under phosphorus deficiency by suppressing vacuolar degradation of PIN-FORMED2. New Phytol **226**: 142–155.

Lin, F., Krishnamoorthy, P., Schubert, V., Hause, G., Heilmann, M., and Heilmann, I. (2019). A dual role for cell plate-associated PI4Kβ in endocytosis and phragmoplast dynamics during plant somatic cytokinesis. EMBO J **38**.

Lin, L.-J., Tai, S.S.K., Peng, C.-C., and Tzen, J.T.C. (2002). Steroleosin, a Sterol-Binding Dehydrogenase in Seed Oil Bodies. Plant Physiol **128**: 1200–1211.

Lin, W. and Oliver, D.J. (2008). Role of triacylglycerols in leaves. Plant Science **175**: 233–237.

Listenberger, L.L., Han, X., Lewis, S.E., Cases, S., Farese, R.V., Ory, D.S., and Schaffer, J.E. (2003). Triglyceride accumulation protects against fatty acid-induced lipotoxicity. Proc Natl Acad Sci U S A **100**: 3077–3082.

Liu, F., Hu, W., Li, F., Marshall, R.S., Zarza, X., Munnik, T., and Vierstra, R.D. (2020). AUTOPHAGY-RELATED14 and Its Associated Phosphatidylinositol 3-Kinase Complex Promote Autophagy in Arabidopsis. Plant Cell **32**: 3939–3960.

Liu, H., Wang, C., Chen, F., and Shen, S. (2015). Proteomic analysis of oil bodies in mature Jatropha curcas seeds with different lipid content. J Proteomics **113**: 403–414.

Liu, T., Chyan, C., Li, F., and Tzen, J.T.C. (2009). Stability of Artificial Oil Bodies Constituted with Recombinant Caleosins. J Agric Food Chem **57**: 2308–2313.

Löfke, C., Ischebeck, T., König, S., Freitag, S., and Heilmann, I. (2008). Alternative metabolic fates of phosphatidylinositol produced by phosphatidylinositol synthase isoforms in *Arabidopsis thaliana*. Biochem J **413**: 115–124.

Lundquist, P.K., Shivaiah, K.-K., and Espinoza-Corral, R. (2020). Lipid droplets throughout the evolutionary tree. Prog Lipid Res **78**: 101029.

Lupette, J., Jaussaud, A., Seddiki, K., Morabito, C., Brugière, S., Schaller, H., Kuntz, M., Putaux, J.-L., Jouneau, P.-H., Rébeillé, F., Falconet, D., Couté, Y., Jouhet, J., Tardif, M., Salvaing, J., and Maréchal, E. (2019). The architecture of lipid droplets in the diatom Phaeodactylum tricornutum. Algal Research **38**: 101415.

Luttgeharm, K.D., Kimberlin, A.N., and Cahoon, E.B. (2016). Plant Sphingolipid Metabolism and Function. Subcell Biochem **86**: 249–286.

Marković, V. and Jaillais, Y. (2022). Phosphatidylinositol 4-phosphate: a key determinant of plasma membrane identity and function in plants. New Phytol **235**: 867–874.

Marshall, R.S. and Vierstra, R.D. (2018). Autophagy: The Master of Bulk and Selective Recycling. Annu. Rev. Plant Biol. **69**: 173–208.

McLachlan, D.H., Lan, J., Geilfus, C.-M., Dodd, A.N., Larson, T., Baker, A., Hõrak, H., Kollist, H., He, Z., Graham, I., Mickelbart, M.V., and Hetherington, A.M. (2016). The Breakdown of Stored Triacylglycerols Is Required during Light-Induced Stomatal Opening. Curr Biol **26**: 707–712.

Mellema, S., Eichenberger, W., Rawyler, A., Suter, M., Tadege, M., and Kuhlemeier, C. (2002). The ethanolic fermentation pathway supports respiration and lipid biosynthesis in tobacco pollen. Plant J **30**: 329–336.

Mistry, J., Chuguransky, S., Williams, L., Qureshi, M., Salazar, G.A., Sonnhammer, E.L.L., Tosatto, S.C.E., Paladin, L., Raj, S., Richardson, L.J., Finn, R.D., and Bateman, A. (2021). Pfam: The protein families database in 2021. Nucleic Acids Res **49**: D412–D419.

Moellering, E.R. and Benning, C. (2010). RNA Interference Silencing of a Major Lipid Droplet Protein Affects Lipid Droplet Size in Chlamydomonas reinhardtii. Eukaryot Cell **9**: 97–106.

Moellering, E.R., Muthan, B., and Benning, C. (2010). Freezing Tolerance in Plants Requires Lipid Remodeling at the Outer Chloroplast Membrane. Science **330**: 226–228.

Mueller, S.P., Krause, D.M., Mueller, M.J., and Fekete, A. (2015). Accumulation of extra-chloroplastic triacylglycerols in Arabidopsis seedlings during heat acclimation. J Exp Bot **66**: 4517–4526.

Mueller-Roeber, B. and Pical, C. (2002). Inositol phospholipid metabolism in Arabidopsis. Characterized and putative isoforms of inositol phospholipid kinase and phosphoinositide-specific phospholipase C. Plant Physiol **130**: 22–46.

Müller, A. (2018). Acid lipases in the degradation of lipid droplets. University of Göttingen

Müller, A.O., Blersch, K.F., Gippert, A.L., and Ischebeck, T. (2017). Tobacco pollen tubes – a fast and easy tool for studying lipid droplet association of plant proteins. Plant J **89**: 1055–1064.

Müller, A.O. and Ischebeck, T. (2018). Characterization of the enzymatic activity and physiological function of the lipid droplet-associated triacylglycerol lipase AtOBL1. New Phytol **217**: 1062–1076.

Munnik, T. and Testerink, C. (2009). Plant phospholipid signaling: "in a nutshell." J Lipid Res **50 Suppl**: S260-265.

Murphy, D.J. (2001). The biogenesis and functions of lipid bodies in animals, plants and microorganisms. Prog Lipid Res **40**: 325–438.

Murphy, D.J. (2012). The dynamic roles of intracellular lipid droplets: from archaea to mammals. Protoplasma **249**: 541–585.

Nettebrock, N.T. and Bohnert, M. (2020). Born this way – Biogenesis of lipid droplets from specialized ER subdomains. Biochim Biophys Acta **1865**: 158448.

Niemeyer, P.W., Irisarri, I., Scholz, P., Schmitt, K., Valerius, O., Braus, G.H., Herrfurth, C., Feussner, I., Sharma, S., Carlsson, A.S., de Vries, J., Hofvander, P., and Ischebeck, T. (2022). A seed-like proteome in oil-rich tubers. Plant J **112**: 518–534.

Niu, Y. and Xiang, Y. (2018). An Overview of Biomembrane Functions in Plant Responses to High-Temperature Stress. Front Plant Sci **9**: 915.

Noack, L.C., Bayle, V., Armengot, L., Rozier, F., Mamode-Cassim, A., Stevens, F.D., Caillaud, M.-C., Munnik, T., Mongrand, S., Pleskot, R., and Jaillais, Y. (2022). A nanodomain-anchored scaffolding complex is required for the function and localization of phosphatidylinositol 4-kinase alpha in plants. Plant Cell **34**: 302–332.

Noack, L.C. and Jaillais, Y. (2020). Functions of Anionic Lipids in Plants. Annu Rev Plant Biol **71**: 71–102.

Ohlrogge, J. and Browse, J. (1995). Lipid biosynthesis. Plant Cell **7**: 957–970.

Olarte, M.-J., Kim, S., Sharp, M.E., Swanson, J.M.J., Farese, R.V., and Walther, T.C. (2020). Determinants of Endoplasmic Reticulum-to-Lipid Droplet Protein Targeting. Dev Cell **54**: 471–487.

Olzmann, J.A. and Carvalho, P. (2019). Dynamics and functions of lipid droplets. Nat Rev Mol Cell Biol **20**: 137–155.

Ovečka, M., Illés, P., Lichtscheidl, I., Derksen, J., and Šamaj, J. (2012). Endocytosis and Vesicular Recycling in Root Hairs and Pollen Tubes. In Endocytosis in Plants, J. Šamaj, ed (Springer Berlin Heidelberg: Berlin, Heidelberg), pp. 81–106.

Pace, C.N., Shirley, B.A., McNutt, M., and Gajiwala, K. (1996). Forces contributing to the conformational stability of proteins. FASEB J **10**: 75–83.

Packter, N.M. and Stumpf, P.K. (1975). Fat metabolism in higher plants: Production of short- and medium-chain acyl-acyl carrier protein by spinach stroma preparations treated with cerulenin. Biochim Biophys Acta **409**: 274–282.

Partridge, M. and Murphy, D.J. (2009). Roles of a membrane-bound caleosin and putative peroxygenase in biotic and abiotic stress responses in Arabidopsis. Plant Physiol Biochem **47**: 796–806.

Pejchar, P., Sekereš, J., Novotný, O., Žárský, V., and Potocký, M. (2020). Functional analysis of phospholipase Dδ family in tobacco pollen tubes. Plant J **103**: 212–226.

Peramuna, A. and Summers, M.L. (2014). Composition and occurrence of lipid droplets in the cyanobacterium Nostoc punctiforme. Arch Microbiol **196**: 881–890.

Pical, C., Westergren, T., Dove, S.K., Larsson, C., and Sommarin, M. (1999). Salinity and Hyperosmotic Stress Induce Rapid Increases in Phosphatidylinositol 4,5-Bisphosphate, Diacylglycerol Pyrophosphate, and Phosphatidylcholine in Arabidopsis thaliana Cells. J Biol Chem **274**: 38232–38240.

Pichrtová, M., Arc, E., Stöggl, W., Kranner, I., Hájek, T., Hackl, H., and Holzinger, A. (2016). Formation of lipid bodies and changes in fatty acid composition upon pre-akinete formation in Arctic and Antarctic Zygnema (Zygnematophyceae, Streptophyta) strains. FEMS Microbiol Ecol **92**: fiw096.

Pichrtová, M., Hájek, T., and Elster, J. (2014). Osmotic stress and recovery in field populations of *Zygnema* sp. (*Zygnematophyceae* , *Streptophyta*) on Svalbard (High Arctic) subjected to natural desiccation. FEMS Microbiol Ecol **89**: 270–280.

Piffanelli, P., Ross, J.H.E., and Murphy, D.J. (1998). Biogenesis and function of the lipidic structures of pollen grains. Sex Plant Reprod **11**: 65–80.

Piffanelli, P., Ross, J.H.E., and Murphy, D.J. (1997). Intra- and extracellular lipid composition and associated gene expression patterns during pollen development in Brassica napus. Plant J **11**: 549–562.

Pinfield-Wells, H., Rylott, E.L., Gilday, A.D., Graham, S., Job, K., Larson, T.R., and Graham, I.A. (2005). Sucrose rescues seedling establishment but not germination of Arabidopsis mutants disrupted in peroxisomal fatty acid catabolism. Plant J **43**: 861–872.

Platre, M.P., Noack, L.C., Doumane, M., Bayle, V., Simon, M.L.A., Maneta-Peyret, L., Fouillen, L., Stanislas, T., Armengot, L., Pejchar, P., Caillaud, M.-C., Potocký, M., Čopič, A., Moreau, P.,

and Jaillais, Y. (2018). A Combinatorial Lipid Code Shapes the Electrostatic Landscape of Plant Endomembranes. Dev Cell **45**: 465–480.

Platre, M.P., Bayle, V., Armengot, L., Bareille, J., Marquès-Bueno, M.D.M., Creff, A., Maneta-Peyret, L., Fiche, J.-B., Nollmann, M., Miège, C., Moreau, P., Martinière, A., and Jaillais, Y. (2019). Developmental control of plant Rho GTPase nano-organization by the lipid phosphatidylserine. Science **364**: 57–62.

Pleskot, R., Li, J., Žárský, V., Potocký, M., and Staiger, C.J. (2013). Regulation of cytoskeletal dynamics by phospholipase D and phosphatidic acid. Trends Plant Sci **18**: 496–504.

Pleskot, R., Pejchar, P., Bezvoda, R., Lichtscheidl, I., Wolters-Arts, M., Marc, J., Žárský, V., and Potocký, M. (2012). Turnover of Phosphatidic Acid through Distinct Signaling Pathways Affects Multiple Aspects of Pollen Tube Growth in Tobacco. Front Plant Sci **3**: 54.

Pleskot, R., Potocký, M., Pejchar, P., Linek, J., Bezvoda, R., Martinec, J., Valentová, O., Novotná, Z., and Žárský, V. (2010). Mutual regulation of plant phospholipase D and the actin cytoskeleton: Reciprocal regulation of plant PLD and actin. Plant J **62**: 494–507.

Pokotylo, I., Kolesnikov, Y., Kravets, V., Zachowski, A., and Ruelland, E. (2014). Plant phosphoinositide-dependent phospholipases C: Variations around a canonical theme. Biochimie **96**: 144–157.

Pokotylo, I., Kravets, V., Martinec, J., and Ruelland, E. (2018). The phosphatidic acid paradox: Too many actions for one molecule class? Lessons from plants. Prog Lipid Res **71**: 43–53.

Pokotylo, I., Pejchar, P., Potocký, M., Kocourková, D., Krčková, Z., Ruelland, E., Kravets, V., and Martinec, J. (2013). The plant non-specific phospholipase C gene family. Novel competitors in lipid signalling. Prog Lipid Res **52**: 62–79.

Potocký, M., Eliás, M., Profotová, B., Novotná, Z., Valentová, O., and Zárský, V. (2003). Phosphatidic acid produced by phospholipase D is required for tobacco pollen tube growth. Planta **217**: 122–130.

Potocký, M., Pleskot, R., Pejchar, P., Vitale, N., Kost, B., and Žárský, V. (2014). Live-cell imaging of phosphatidic acid dynamics in pollen tubes visualized by Spo20p-derived biosensor. New Phytol **203**: 483–494.

Pourcher, M., Santambrogio, M., Thazar, N., Thierry, A.-M., Fobis-Loisy, I., Miège, C., Jaillais, Y., and Gaude, T. (2010). Analyses of SORTING NEXINs Reveal Distinct Retromer-Subcomplex Functions in Development and Protein Sorting in Arabidopsis thaliana. Plant Cell **22**: 3980–3991.

Prasanna, X., Salo, V.T., Li, S., Ven, K., Vihinen, H., Jokitalo, E., Vattulainen, I., and Ikonen, E. (2021). Seipin traps triacylglycerols to facilitate their nanoscale clustering in the endoplasmic reticulum membrane. PLoS Biol **19**: e3000998.

Preuss, M.L., Schmitz, A.J., Thole, J.M., Bonner, H.K.S., Otegui, M.S., and Nielsen, E. (2006). A role for the RabA4b effector protein PI-4Kbeta1 in polarized expansion of root hair cells in Arabidopsis thaliana. J. Cell Biol. **172**: 991–998.

Prévost, C., Sharp, M.E., Kory, N., Lin, Q., Voth, G.A., Farese, R.V., and Walther, T.C. (2018). Mechanism and Determinants of Amphipathic Helix-Containing Protein Targeting to Lipid Droplets. Dev Cell **44**: 73-86.e4.

Purkrtová, Z., Chardot, T., and Froissard, M. (2015). N-terminus of seed caleosins is essential for lipid droplet sorting but not for lipid accumulation. Archives of Biochemistry and Biophysics **579**: 47–54.

Pyc, M., Gidda, S.K., Seay, D., Esnay, N., Kretzschmar, F.K., Cai, Y., Doner, N.M., Greer, M.S., Hull, J.J., Coulon, D., Bréhélin, C., Yurchenko, O., de Vries, J., Valerius, O., Braus, G.H., Ischebeck, T., Chapman, K.D., Dyer, J.M., and Mullen, R.T. (2021). LDIP cooperates with SEIPIN and LDAP to facilitate lipid droplet biogenesis in Arabidopsis. Plant Cell **33**: 3076–3103.

Pyc, M., Cai, Y., Gidda, S.K., Yurchenko, O., Park, S., Kretzschmar, F.K., Ischebeck, T., Valerius, O., Braus, G.H., Chapman, K.D., Dyer, J.M., and Mullen, R.T. (2017a). Arabidopsis lipid droplet-associated protein (LDAP) - interacting protein (LDIP) influences lipid droplet size and neutral lipid homeostasis in both leaves and seeds. Plant J **92**: 1182–1201.

Pyc, M., Cai, Y., Greer, M.S., Yurchenko, O., Chapman, K.D., Dyer, J.M., and Mullen, R.T. (2017b). Turning Over a New Leaf in Lipid Droplet Biology. Trends Plant Sci **22**: 596–609.

Qu, R., Wang, S.M., Lin, Y.H., Vance, V.B., and Huang, A.H. (1986). Characteristics and biosynthesis of membrane proteins of lipid bodies in the scutella of maize (Zea mays L.). Biochem J **235**: 57–65.

Qu, R.D. and Huang, A.H. (1990). Oleosin KD 18 on the surface of oil bodies in maize. Genomic and cDNA sequences and the deduced protein structure. J Biol Chem **265**: 2238–2243.

Rahman, F., Hassan, M., Rosli, R., Almousally, I., Hanano, A., and Murphy, D.J. (2018). Evolutionary and genomic analysis of the caleosin/peroxygenase (CLO/PXG) gene/protein families in the Viridiplantae. PLoS One **13**: e0196669.

Rappsilber, J., Mann, M., and Ishihama, Y. (2007). Protocol for micro-purification, enrichment, pre-fractionation and storage of peptides for proteomics using StageTips. Nat Protoc **2**: 1896–1906.

Read, S.M., Clarke, A.E., and Bacic, A. (1993). Stimulation of growth of culturedNicotiana tabacum W 38 pollen tubes by poly(ethylene glycol) and Cu(II) salts. Protoplasma **177**: 1–14.

Renne, M.F., Corey, R.A., Ferreira, J.V., Stansfeld, P.J., and Carvalho, P. (2022). Seipin concentrates distinct neutral lipids via interactions with their acyl chain carboxyl esters. J Cell Biol **221**: e202112068.

Rippin, M., Becker, B., and Holzinger, A. (2017). Enhanced Desiccation Tolerance in Mature Cultures of the Streptophytic Green Alga Zygnema circumcarinatum Revealed by Transcriptomics. Plant Cell Physiol **58**: 2067–2084.

Rosado, A. and Bayer, E.M. (2021). Geometry and cellular function of organelle membrane interfaces. Plant Physiol **185**: 650–662.

Rotsch, A.H., Kopka, J., Feussner, I., and Ischebeck, T. (2017). Central metabolite and sterol profiling divides tobacco male gametophyte development and pollen tube growth into eight metabolic phases. Plant J **92**: 129–146.

Rowe, E.R., Mimmack, M.L., Barbosa, A.D., Haider, A., Isaac, I., Ouberai, M.M., Thiam, A.R., Patel, S., Saudek, V., Siniossoglou, S., and Savage, D.B. (2016). Conserved Amphipathic Helices Mediate Lipid Droplet Targeting of Perilipins 1-3. J Biol Chem **291**: 6664–6678.

Ruggiano, A., Mora, G., Buxó, L., and Carvalho, P. (2016). Spatial control of lipid droplet proteins by the ERAD ubiquitin ligase Doa10. EMBO J **35**: 1644–1655.

Ruiz-Lopez, N., Pérez-Sancho, J., del Valle, A.E., Haslam, R.P., Vanneste, S., Catalá, R., Perea-Resa, C., Damme, D.V., García-Hernández, S., Albert, A., Vallarino, J., Lin, J., Friml, J., Macho, A.P., Salinas, J., Rosado, A., Napier, J.A., Amorim-Silva, V., and Botella, M. A. (2021). Synaptotagmins at the endoplasmic reticulum–plasma membrane contact sites maintain diacylglycerol homeostasis during abiotic stress. Plant Cell **33**: 2431–2453.

Sahasrabudhe, S.N., Rodriguez-Martinez, V., O'Meara, Meghan., and Farkas, B.E. (2017). Density, viscosity, and surface tension of five vegetable oils at elevated temperatures: Measurement and modeling. International Journal of Food Properties **20**: 1965–1981.

Sanz, A., Moreno, J.I., and Castresana, C. (1998). PIOX, a new pathogen-induced oxygenase with homology to animal cyclooxygenase. Plant Cell **10**: 1523–1537.

Sašek, V., Janda, M., Delage, E., Puyaubert, J., Guivarch, A., López Maseda, E., Dobrev, P. I., Caius, J., Bóka, K., Valentová, O., Burketová, L., Zachowski, A., and Ruelland, E (2014). Constitutive salicylic acid accumulation in pi4kIIIβ1β2 Arabidopsis plants stunts rosette but not root growth. New Phytol **203**: 805–816.

Scheible, N. and McCubbin, A. (2019). Signaling in Pollen Tube Growth: Beyond the Tip of the Polarity Iceberg. Plants (Basel) **8**: E156.

Schieferle, S., Tappe, B., Korte, P., Mueller, M.J., and Berger, S. (2021). Pathogens and Elicitors Induce Local and Systemic Changes in Triacylglycerol Metabolism in Roots and in Leaves of Arabidopsis thaliana. Biology (Basel) **10**: 920.

Scholz, P., Chapman, K.D., Mullen, R.T., and Ischebeck, T. (2022). Finding new friends and revisiting old ones - how plant lipid droplets connect with other subcellular structures. New Phytol **236**: 833–838.

Schrul, B. and Kopito, R.R. (2016). Peroxin-Dependent Targeting of a Lipid Droplet-Destined Membrane Protein to ER-subdomains. Nat Cell Biol **18**: 740–751.

Schuhmacher, M., Grasskamp, A.T., Barahtjan, P., Wagner, N., Lombardot, B., Schuhmacher, J.S., Sala, P., Lohmann, A., Henry, I., Shevchenko, A., Coskun, Ü., Walter, A.M., and Nadler, A. (2020). Live-cell lipid biochemistry reveals a role of diacylglycerol side-chain composition for cellular lipid dynamics and protein affinities. Proc Natl Acad Sci U S A **117**: 7729–7738.

Sekereš, J., Pejchar, P., Šantrůček, J., Vukašinović, N., Žárský, V., and Potocký, M. (2017). Analysis of Exocyst Subunit EXO70 Family Reveals Distinct Membrane Polar Domains in Tobacco Pollen Tubes. Plant Physiol **173**: 1659–1675.

Selinski, J. and Scheibe, R. (2014). Pollen tube growth: where does the energy come from? Plant Signal Behav **9**: e977200.

Shevchenko, A., Tomas, H., Havlis, J., Olsen, J.V., and Mann, M. (2006). In-gel digestion for mass spectrometric characterization of proteins and proteomes. Nat Protoc **1**: 2856–2860.

Shimada, T.L., Shimada, T., Okazaki, Y., Higashi, Y., Saito, K., Kuwata, K., Oyama, K., Kato, M., Ueda, H., Nakano, A., Ueda, T., Takano, Y., and Hara-Nishimura, I. (2019). HIGH STEROL ESTER 1 is a key factor in plant sterol homeostasis. Nat Plants **5**: 1154–1166.

Shimada, T.L., Shimada, T., Takahashi, H., Fukao, Y., and Hara-Nishimura, I. (2008). A novel role for oleosins in freezing tolerance of oilseeds in Arabidopsis thaliana. Plant J **55**: 798–809.

Shimada, T.L., Takano, Y., Shimada, T., Fujiwara, M., Fukao, Y., Mori, M., Okazaki, Y., Saito, K., Sasaki, R., Aoki, K., and Hara-Nishimura, I. (2014). Leaf oil body functions as a subcellular factory for the production of a phytoalexin in Arabidopsis. Plant Physiol **164**: 105–118.

Shiva, S., Samarakoon, T., Lowe, K.A., Roach, C., Vu, H.S., Colter, M., Porras, H., Hwang, C., Roth, M.R., Tamura, P., Li, M., Schrick, K., Shah, J., Wang, X., Wang, H., and Welti, R. (2020). Leaf Lipid Alterations in Response to Heat Stress of Arabidopsis thaliana. Plants (Basel) **9**: 845.

Shockey, J., Regmi, A., Cotton, K., Adhikari, N., Browse, J., and Bates, P.D. (2016). Identification of Arabidopsis *GPAT9* (At5g60620) as an Essential Gene Involved in Triacylglycerol Biosynthesis. Plant Physiol **170**: 163–179.

Siegler, H., Valerius, O., Ischebeck, T., Popko, J., Tourasse, N.J., Vallon, O., Khozin-Goldberg, I., Braus, G.H., and Feussner, I. (2017). Analysis of the lipid body proteome of the oleaginous alga Lobosphaera incisa. BMC Plant Biol **17**: 98.

Simionato, D., Block, M.A., La Rocca, N., Jouhet, J., Maréchal, E., Finazzi, G., and Morosinotto, T. (2013). The Response of Nannochloropsis gaditana to Nitrogen Starvation Includes De Novo Biosynthesis of Triacylglycerols, a Decrease of Chloroplast Galactolipids, and Reorganization of the Photosynthetic Apparatus. Eukaryot Cell **12**: 665–676.

Simon, M.L.A., Platre, M.P., Assil, S., van Wijk, R., Chen, W.Y., Chory, J., Dreux, M., Munnik, T., and Jaillais, Y. (2014). A multi-colour/multi-affinity marker set to visualize phosphoinositide dynamics in Arabidopsis. Plant J **77**: 322–337.

Simon, M.L.A., Platre, M.P., Marquès-Bueno, M.M., Armengot, L., Stanislas, T., Bayle, V., Caillaud, M.-C., and Jaillais, Y. (2016). A PtdIns(4)P-driven electrostatic field controls cell membrane identity and signalling in plants. Nature Plants **2**: 1–10.

Singer, S.D., Chen, G., Mietkiewska, E., Tomasi, P., Jayawardhane, K., Dyer, J.M., and Weselake, R.J. (2016). Arabidopsis GPAT9 contributes to synthesis of intracellular glycerolipids but not surface lipids. J Exp Bot **67**: 4627–4638.

Singh, A.P. and Savaldi-Goldstein, S. (2015). Growth control: brassinosteroid activity gets context. J Exp Bot **66**: 1123–1132.

Sousa, E., Kost, B., and Malhó, R. (2008). Arabidopsis phosphatidylinositol-4-monophosphate 5-kinase 4 regulates pollen tube growth and polarity by modulating membrane recycling. Plant Cell **20**: 3050–3064.

Stålberg, K., Ståhl, U., Stymne, S., and Ohlrogge, J. (2009). Characterization of two Arabidopsis thaliana acyltransferases with preference for lysophosphatidylethanolamine. BMC Plant Biology **9**: 60.

Stenzel, I., Ischebeck, T., König, S., Hołubowska, A., Sporysz, M., Hause, B., and Heilmann, I. (2008). The type B phosphatidylinositol-4-phosphate 5-kinase 3 is essential for root hair formation in Arabidopsis thaliana. Plant Cell **20**: 124–141.

Stephan, O.O.H. (2017). Actin fringes of polar cell growth. J Exp Bot **68**: 3303–3320.

Strasser, R. (2018). Protein Quality Control in the Endoplasmic Reticulum of Plants. Annu Rev Plant Biol **69**: 147–172.

Sui, X., Arlt, H., Brock, K.P., Lai, Z.W., DiMaio, F., Marks, D.S., Liao, M., Farese, R.V., and Walther, T.C. (2018). Cryo-electron microscopy structure of the lipid droplet-formation protein seipin. J Cell Biol **217**: 4080–4091.

Suzuki, M., Otsuka, T., Ohsaki, Y., Cheng, J., Taniguchi, T., Hashimoto, H., Taniguchi, H., and Fujimoto, T. (2012). Derlin-1 and UBXD8 are engaged in dislocation and degradation of lipidated ApoB-100 at lipid droplets. Mol Biol Cell **23**: 800–810.

Synek, L., Pleskot, R., Sekereš, J., Serrano, N., Vukašinović, N., Ortmannová, J., Klejchová, M., Pejchar, P., Batystová, K., Gutkowska, M., Janková-Drdová, E., Marković, V., Pečenková, T., Šantrůček, J., Žárský, V., and Potocký, M. (2021). Plasma membrane phospholipid signature recruits the plant exocyst complex via the EXO70A1 subunit. Proc Natl Acad Sci U S A **118**: e2105287118.

Szumlanski, A.L. and Nielsen, E. (2009). The Rab GTPase RabA4d regulates pollen tube tip growth in Arabidopsis thaliana. Plant Cell **21**: 526–544.

Szymanski, K.M., Binns, D., Bartz, R., Grishin, N.V., Li, W.-P., Agarwal, A.K., Garg, A., Anderson, R.G.W., and Goodman, J.M. (2007). The lipodystrophy protein seipin is found at endoplasmic reticulum lipid droplet junctions and is important for droplet morphology. Proc Natl Acad Sci U S A **104**: 20890–20895.

Takáč, T., Pechan, T., Šamajová, O., and Šamaj, J. (2013). Vesicular Trafficking and Stress Response Coupled to PI3K Inhibition by LY294002 as Revealed by Proteomic and Cell Biological Analysis. J Proteome Res **12**: 4435–4448.

Takatsuka, C., Inoue, Y., Matsuoka, K., and Moriyasu, Y. (2004). 3-Methyladenine Inhibits Autophagy in Tobacco Culture Cells under Sucrose Starvation Conditions. Plant Cell Physiol **45**: 265–274.

Takeuchi, T. and Benning, C. (2019). Nitrogen-dependent coordination of cell cycle, quiescence and TAG accumulation in Chlamydomonas. Biotechnol Biofuels **12**: 292.

Tarazona, P., Feussner, K., and Feussner, I. (2015). An enhanced plant lipidomics method based on multiplexed liquid chromatography-mass spectrometry reveals additional insights into cold- and drought-induced membrane remodeling. Plant J **84**: 621–633.

Taurino, M., Costantini, S., De Domenico, S., Stefanelli, F., Ruano, G., Delgadillo, M.O., Sánchez-Serrano, J.J., Sanmartín, M., Santino, A., and Rojo, E. (2018). SEIPIN Proteins Mediate Lipid Droplet Biogenesis to Promote Pollen Transmission and Reduce Seed Dormancy. Plant Physiol **176**: 1531–1546.

Testerink, C. and Munnik, T. (2011). Molecular, cellular, and physiological responses to phosphatidic acid formation in plants. J Exp Bot **62**: 2349–2361.

Thakur, A. and Bhatla, S.C. (2016). Proteomic analysis of oil body membrane proteins accompanying the onset of desiccation phase during sunflower seed development. Plant Signal Behav **10**: e1030100.

Thazar-Poulot, N., Miquel, M., Fobis-Loisy, I., and Gaude, T. (2015). Peroxisome extensions deliver the Arabidopsis SDP1 lipase to oil bodies. Proc Natl Acad Sci U S A **112**: 4158–4163.

Thiam, A.R. and Forêt, L. (2016). The physics of lipid droplet nucleation, growth and budding. Biochim Biophys Acta **1861**: 715–722.

Thomas, P.D., Ebert, D., Muruganujan, A., Mushayahama, T., Albou, L.-P., and Mi, H. (2022). PANTHER: Making genome-scale phylogenetics accessible to all. Protein Science **31**: 8–22.

Tirajoh, A., Aung, T.S.T., McKay, A.B., and Plant, A.L. (2005). Stress-responsive α-dioxygenase expression in tomato roots. J Exp Bot **56**: 713–723.

Tnani, H., López, I., Jouenne, T., and Vicient, C.M. (2011). Protein composition analysis of oil bodies from maize embryos during germination. J Plant Physiol **168**: 510–513.

Troncoso-Ponce, M.A., Cao, X., Yang, Z., and Ohlrogge, J.B. (2013). Lipid turnover during senescence. Plant Sci **205–206**: 13–19.

Tzen, J., Cao, Y., Laurent, P., Ratnayake, C., and Huang, A. (1993). Lipids, Proteins, and Structure of Seed Oil Bodies from Diverse Species. Plant Physiol **101**: 267–276.

Tzen, J.T., Lie, G.C., and Huang, A.H. (1992). Characterization of the charged components and their topology on the surface of plant seed oil bodies. J Biol Chem **267**: 15626–15634.

Valitova, J.N., Sulkarnayeva, A.G., and Minibayeva, F.V. (2016). Plant sterols: Diversity, biosynthesis, and physiological functions. Biochemistry (Mosc) **81**: 819–834.

Van Leeuwen, W., Vermeer, J.E.M., Gadella Jr, T.W.J., and Munnik, T. (2007). Visualization of phosphatidylinositol 4,5-bisphosphate in the plasma membrane of suspension-cultured tobacco BY-2 cells and whole Arabidopsis seedlings. Plant J **52**: 1014–1026.

VanBuren, R., Wai, C.M., Zhang, Q., Song, X., Edger, P.P., Bryant, D., Michael, T.P., Mockler, T.C., and Bartels, D. (2017). Seed desiccation mechanisms co-opted for vegetative desiccation in the resurrection grass Oropetium thomaeum. Plant Cell Environ **40**: 2292–2306.

Vaz Dias, F., Serrazina, S., Vitorino, M., Marchese, D., Heilmann, I., Godinho, M., Rodrigues, M., and Malhó, R. (2019). A role for diacylglycerol kinase 4 in signalling crosstalk during Arabidopsis pollen tube growth. New Phytol **222**: 1434–1446.

Veerabagu, M., Rinne, P.L.H., Skaugen, M., Paul, L.K., and van der Schoot, C. (2021). Lipid Body Dynamics in Shoot Meristems: Production, Enlargement, and Putative Organellar Interactions and Plasmodesmal Targeting. Front Plant Sci **12**: 674031.

Vermeer, J.E.M., van Leeuwen, W., Tobeña-Santamaria, R., Laxalt, A.M., Jones, D.R., Divecha, N., Gadella, T.W.J., and Munnik, T. (2006). Visualization of PtdIns3P dynamics in living plant cells: PtdIns3P dynamics in plant cells. Plant J **47**: 687–700.

de Vries, J., de Vries, S., Curtis, B.A., Zhou, H., Penny, S., Feussner, K., Pinto, D.M., Steinert, M., Cohen, A.M., von Schwartzenberg, K., and Archibald, J.M. (2020). Heat stress response in the closest algal relatives of land plants reveals conserved stress signaling circuits. Plant J **103**: 1025–1048.

de Vries, J. and Ischebeck, T. (2020). Ties between Stress and Lipid Droplets Pre-date Seeds. Trends Plant Sci **25**: 1203–1214.

Vu, H.S., Shiva, S., Roth, M.R., Tamura, P., Zheng, L., Li, M., Sarowar, S., Honey, S., McEllhiney, D., Hinkes, P., Seib, L., Williams, T.D., Gadbury, G., Wang, X., Shah, J., and Welti, R. (2014). Lipid changes after leaf wounding in Arabidopsis thaliana: expanded lipidomic data form the basis for lipid co-occurrence analysis. Plant J **80**: 728–743.

Vukašinović, N., Wang, Y., Vanhoutte, I., Fendrych, M., Guo, B., Kvasnica, M., Jiroutová, P., Oklestkova, J., Strnad, M., and Russinova, E. (2021). Local brassinosteroid biosynthesis enables optimal root growth. Nat Plants **7**: 619–632.

Walther, T.C., Chung, J., and Farese, R.V. (2017). Lipid Droplet Biogenesis. Annu Rev Cell Dev Biol **33**: 491–510.

Wang, H. and Jiang, L. (2011). Transient expression and analysis of fluorescent reporter proteins in plant pollen tubes. Nat Protoc **6**: 419–426.

Wasternack, C. and Feussner, I. (2018). The Oxylipin Pathways: Biochemistry and Function. Annu Rev Plant Biol **69**: 363–386.

Waterworth, W.M., Bray, C.M., and West, C.E. (2019). Seeds and the Art of Genome Maintenance. Front Plant Sci **10**: 706.

Weixel, K.M., Blumental-Perry, A., Watkins, S.C., Aridor, M., and Weisz, O.A. (2005). Distinct Golgi populations of phosphatidylinositol 4-phosphate regulated by phosphatidylinositol 4-kinases. J Biol Chem **280**: 10501–10508.

Welte, M.A. and Gould, A.P. (2017). Lipid droplet functions beyond energy storage. Biochim Biophys Acta **1862**: 1260–1272.

Whitley, P., Hinz, S., and Doughty, J. (2009). Arabidopsis FAB1/PIKfyve proteins are essential for development of viable pollen. Plant Physiol **151**: 1812–1822.

Wilfling, F., Wang, H., Haas, J.T., Krahmer, N., Gould, T.J., Uchida, A., Cheng, J.-X., Graham, M., Christiano, R., Fröhlich, F., Liu, X., Buhman, K. K., Coleman, R. A., Bewersdorf, J., Farese, R.V., and Walther, T.C. (2013). Triacylglycerol Synthesis Enzymes Mediate Lipid Droplet Growth by Relocalizing from the ER to Lipid Droplets. Dev Cell **24**: 384–399.

Winship, L.J., Rounds, C., and Hepler, P.K. (2016). Perturbation Analysis of Calcium, Alkalinity and Secretion during Growth of Lily Pollen Tubes. Plants (Basel) **6**: E3.

Xu, C., Fan, J., Froehlich, J.E., Awai, K., and Benning, C. (2005). Mutation of the TGD1 Chloroplast Envelope Protein Affects Phosphatidate Metabolism in *Arabidopsis*. Plant Cell **17**: 3094–3110.

Yan, R., Qian, H., Lukmantara, I., Gao, M., Du, X., Yan, N., and Yang, H. (2018). Human SEIPIN Binds Anionic Phospholipids. Dev Cell **47**: 248-256.e4.

Yang, Y. and Benning, C. (2018). Functions of triacylglycerols during plant development and stress. Curr Opin Biotechnol **49**: 191–198.

Zaaboul, F., Raza, H., Chen, C., and Liu, Y. (2018). Characterization of Peanut Oil Bodies Integral Proteins, Lipids, and Their Associated Phytochemicals. J Food Sci **83**: 93–100.

Zárský, V., Kulich, I., Fendrych, M., and Pečenková, T. (2013). Exocyst complexes multiple functions in plant cells secretory pathways. Curr Opin Plant Biol **16**: 726–733.

Zhang, M., Fan, J., Taylor, D.C., and Ohlrogge, J.B. (2009). DGAT1 and PDAT1 Acyltransferases Have Overlapping Functions in Arabidopsis Triacylglycerol Biosynthesis and Are Essential for Normal Pollen and Seed Development. Plant Cell **21**: 3885–3901.

Zhi, Y., Taylor, M.C., Campbell, P.M., Warden, A.C., Shrestha, P., El Tahchy, A., Rolland, V., Vanhercke, T., Petrie, J.R., White, R.G., Chen, W., Singh, S.P., and Liu, Q. (2017). Comparative Lipidomics and Proteomics of Lipid Droplets in the Mesocarp and Seed Tissues of Chinese Tallow (Triadica sebifera). Front Plant Sci **8**: 1339.

Zhou, X.-R., Shrestha, P., Yin, F., Petrie, J.R., and Singh, S.P. (2013a). AtDGAT2 is a functional acyl-CoA:diacylglycerol acyltransferase and displays different acyl-CoA substrate preferences than AtDGAT1. FEBS Letters **587**: 2371–2376.

Zhou, Y., Peisker, H., Weth, A., Baumgartner, W., Dörmann, P., and Frentzen, M. (2013b). Extraplastidial cytidinediphosphate diacylglycerol synthase activity is required for vegetative development in Arabidopsis thaliana. Plant J **75**: 867–879.

Zienkiewicz, A., Zienkiewicz, K., Poliner, E., Pulman, J.A., Du, Z.-Y., Stefano, G., Tsai, C.-H., Horn, P., Feussner, I., Farre, E.M., Childs, K.L., Brandizzi, F., and Benning, C. (2020). The Microalga *Nannochloropsis* during Transition from Quiescence to Autotrophy in Response to Nitrogen Availability. Plant Physiol **182**: 819–839.

Zienkiewicz, A., Zienkiewicz, K., Rejón, J.D., Rodríguez-García, M.I., and Castro, A.J. (2013). New insights into the early steps of oil body mobilization during pollen germination. J Exp Bot **64**: 293–302.

Zienkiewicz, K., Du, Z.-Y., Ma, W., Vollheyde, K., and Benning, C. (2016). Stress-induced neutral lipid biosynthesis in microalgae — Molecular, cellular and physiological insights. Biochim Biophys Acta **1861**: 1269–1281.

Zipfel, C., Robatzek, S., Navarro, L., Oakeley, E.J., Jones, J.D.G., Felix, G., and Boller, T. (2004). Bacterial disease resistance in Arabidopsis through flagellin perception. Nature **428**: 764–767.

Zolman, B.K., Silva, I.D., and Bartel, B. (2001). The Arabidopsis pxa1 Mutant Is Defective in an ATP-Binding Cassette Transporter-Like Protein Required for Peroxisomal Fatty Acid β-Oxidation. Plant Physiol **127**: 1266–1278.

Zoni, V., Khaddaj, R., Lukmantara, I., Shinoda, W., Yang, H., Schneiter, R., and Vanni, S. (2021). Seipin accumulates and traps diacylglycerols and triglycerides in its ring-like structure. Proc Natl Acad Sci U S A **118**: e2017205118.

Zou, J., Wei, Y., Jako, C., Kumar, A., Selvaraj, G., and Taylor, D.C. (1999). The Arabidopsis thaliana TAG1 mutant has a mutation in a diacylglycerol acyltransferase gene. Plant J **19**: 645–653.

10 Supplemental Data

Supplemental Table S1: Steryl glycosides in Arabidopsis leaves – normalised icf-corrected peak areas.
Arabidopsis Col-0 were subjected to either of the following stress treatments: infection with *Botrytis cinerea*, infection with *Pseudomonas syringae* pv. *tomato* DC3000 *ΔavrPto ΔavrPtoB* (*Pseudomonas*) or heat stress for 24 hours at 37°C. Each stress was accompanied by a respective mock or control treatment. After the stress, leaves were harvested and neutral lipids were extracted and measured by UPLC-NanoESI-MS/MS. In addition, neutral lipids of non-stressed leaves from Arabidopsis *tgd1-1 sdp1-4* were analysed in comparison to the Col-0. Signal intensities of steryl glycosides were integrated, corrected for C13-isotope distribution and normalised to the internal standard tripentadecanoin and sample mass. The steryl species is indicated. SG, steryl glycoside.

Botrytis cinerea										
	Mock - replicates					*Botrytis cinerea* - replicates				
SG-Sitosteryl	1.86	1.88	1.67	1.02	1.16	2.06	1.78	1.49	1.31	1.09
SG-Campesteryl	0.44	0.31	0.30	0.24	0.21	0.44	0.40	0.38	0.29	0.29
SG-Stigmasteryl	0.29	0.18	0.14	0.09	0.10	0.20	0.20	0.17	0.14	0.20
SG-Isofucosteryl	0.34	0.18	0.14	0.12	0.12	0.19	0.25	0.20	0.18	0.20

Pseudomonas										
	Mock - replicates					*Pseudomonas* - replicates				
SG-Sitosteryl	15.74	5.69	0.81	0.78	0.63	5.40	2.93	2.31	1.50	1.00
SG-Campesteryl	3.04	1.45	0.22	0.20	0.18	1.43	0.87	0.72	0.43	0.33
SG-Stigmasteryl	2.62	1.23	0.26	0.27	0.17	1.48	1.07	1.16	0.56	0.32
SG-Isofucosteryl	2.90	1.34	0.29	0.32	0.18	1.55	1.11	1.24	0.60	0.34

Heat stress										
	Control - replicates					Heat stress - replicates				
SG-Sitosteryl	0.53	0.22	0.27	0.56	0.27	0.55	0.66	0.59	0.43	0.42
SG-Campesteryl	0.11	0.06	0.05	0.11	0.06	0.13	0.16	0.11	0.13	0.07
SG-Stigmasteryl	0.06	0.03	0.04	0.05	0.03	0.06	0.11	0.08	0.09	0.05
SG-Isofucosteryl	0.05	0.03	0.03	0.07	0.03	0.06	0.09	0.09	0.07	0.05

No treatment										
	Col-0 - replicates					*tgd1-1 sdp1-4* - replicates				
SG-Sitosteryl	0.21	0.28	0.16	0.18	0.01	4.29	4.14	6.72	5.74	2.23
SG-Campesteryl	0.03	0.06	0.03	0.03	0.00	0.89	0.99	1.29	1.24	0.67
SG-Stigmasteryl	0.02	0.02	0.01	0.02	0.00	0.57	0.51	0.88	0.88	0.41
SG-Isofucosteryl	0.02	0.03	0.02	0.03	0.00	0.65	0.55	0.93	0.89	0.47

Supplemental Table S2: Candidate proteins for LD localisation in roots. LDs of Arabidopsis roots were enriched and the proteome of the LD-enriched fractions and their original total cellular protein fractions was measured by LC-MS/MS. Raw data was analysed and quantified with the iBAQ algorithm. iBAQ values were then normalised as per mille of the total sum of all proteins (riBAQ). riBAQ values of LD-enriched and total protein fractions were log2-transformed and missing values were imputed from a normal distribution to enable statistical comparison. Protein enrichment values were calculated as ratio between riBAQ-values of LD-enriched fractions to riBAQ values of total protein extracts viz as difference of their respective log2-transformed values. P-values were calculated by Student's t-test and p-values below a false discovery rate of 0.01 were taken as significant. Candidate proteins were then selected with the following criteria: (i) enrichment in the LD-enriched fraction of at least 50-fold whereby (ii) the enrichment had to be significant. Leaving out already known LD protein, this resulted in the 25 candidate proteins listed below. Their AGI code and, if present, their gene symbol is given in addition to their respective enrichment values and their average abundance in LD-enriched fractions. In addition, the *p*-values of the enrichment are indicated. "n.d. in TE" denotes proteins that were not detected in total protein extract samples.

AGI code	Gene symbol	enrichment	riBAQ (LD)	-log$_{10}$ (p-value)
AT1G11755	LEW1	152.63	0.26	4.69
AT1G17430		n.d. in TE	0.43	7.63
AT1G25520	PML4	n.d. in TE	0.20	7.14
AT1G30130		n.d. in TE	0.51	6.52
AT1G44170	ALDH4	90.64	6.55	8.72
AT1G72175		n.d. in TE	0.15	4.80
AT1G78800		n.d. in TE	1.00	8.00
AT3G11430	GPAT5	n.d. in TE	0.32	7.21
AT3G23175		n.d. in TE	0.25	7.73
AT3G63520	CCD1	83.91	1.13	8.02
AT4G00550	DGD2	143.42	0.79	7.54
AT4G13160		n.d. in TE	0.30	6.98
AT4G27760	FEY3	132.49	0.91	5.52
AT4G33180		n.d. in TE	0.19	5.37
AT4G33360	FLDH	74.94	3.51	5.16
AT4G38540		96.68	2.97	6.85
AT5G01220	SQD2	101.80	3.71	6.48
AT5G04070		n.d. in TE	0.19	6.52
AT5G10050		1974.13	1.23	9.30
AT5G15860	PCME	179.83	1.08	5.63
AT5G48010	THAS1	255.02	4.90	6.05
AT5G49900		99.24	0.91	7.55
AT5G59960		283.33	1.13	6.28
AT5G60620	GPAT9	77.39	0.54	6.16
AT5G64440	FAAH	61.60	1.53	6.06

The following datasets can be found as individually uploaded file or on the data drive appended to this thesis:

Supplemental Dataset S1: Proteins found in Arabidopsis roots of the *tgd1-1 sdp1-4* mutant - normalised riBAQ and rLFQ values.

Supplemental Dataset S2: Comparison of proteins in LD-enriched fractions to total protein fractions isolated from Arabidopsis *tgd1-1 sdp1-4* roots.

11 Further contributions

Further contribution were made in another study on plant lipid droplets and in collaborations for which metabolites were analysed. Author contributions are listed below and title pages of respective papers are given in the following pages.

SEED LIPID DROPLET PROTEIN1, SEED LIPID DROPLET PROTEIN2, and LIPID DROPLET PLASMA MEMBRANE ADAPTOR mediate lipid droplet–plasma membrane tethering

Krawczyk, H.E., Sun, S., Doner, N.M., Yan, Q., Lim, M.S.S., **Scholz, P.**, Niemeyer, P.W., Schmitt, K., Valerius, O., Pleskot, R., Hillmer, S., Braus, G.H., Wiermer, M., Mullen, R.T., Ischebeck, T.

The article was published online the journal The Plant Cell in March 2022. The article including supplemental material can be found under the following DOI:

https://doi.org/10.1093/plcell/koac095

Author contribution:

Patricia Scholz performed cDNA synthesis and transcript analysis of *SLDP* and *LIPA* genes by qPCR as shown in supplemental figures S3, S4 and S17. She processed and analysed the data and wrote corresponding parts of the manuscript.
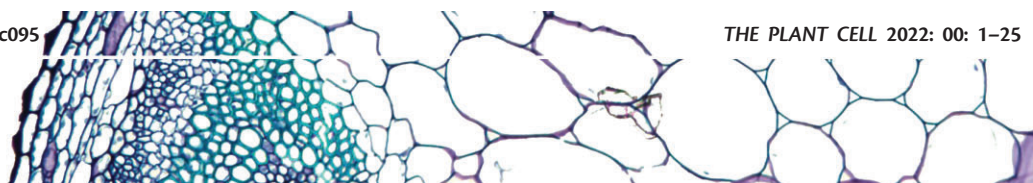
Research Article

SEED LIPID DROPLET PROTEIN1, SEED LIPID DROPLET PROTEIN2, and LIPID DROPLET PLASMA MEMBRANE ADAPTOR mediate lipid droplet–plasma membrane tethering

Hannah Elisa Krawczyk [iD],[1] Siqi Sun [iD],[1] Nathan M. Doner [iD],[2] Qiqi Yan [iD],[3]
Magdiel Sheng Satha Lim [iD],[1] Patricia Scholz [iD],[1] Philipp William Niemeyer [iD],[1]
Kerstin Schmitt [iD],[4,5] Oliver Valerius [iD],[4,5] Roman Pleskot [iD],[6] Stefan Hillmer [iD],[7]
Gerhard H. Braus [iD],[4,5] Marcel Wiermer [iD],[3,5] Robert T. Mullen [iD][2] and Till Ischebeck [iD][1,5,8,*,†]

1 Albrecht-von-Haller-Institute for Plant Sciences and Göttingen Center for Molecular Biosciences (GZMB), Department of Plant Biochemistry, University of Göttingen, Göttingen, Germany
2 Department of Molecular and Cellular Biology, University of Guelph, Guelph, ON N1G 2W1, Canada
3 Albrecht-von-Haller-Institute for Plant Sciences and Göttingen Center for Molecular Biosciences (GZMB), Molecular Biology of Plant-Microbe Interactions Research Group, University of Göttingen, Göttingen, Germany
4 Institute for Microbiology and Genetics and Göttingen Center for Molecular Biosciences (GZMB) and Service Unit LCMS Protein Analytics, Department for Molecular Microbiology and Genetics, University of Göttingen, Göttingen, Germany
5 Göttingen Center for Molecular Biosciences (GZMB), University of Göttingen, Göttingen, Germany
6 Institute of Experimental Botany of the Czech Academy of Sciences, Prague, Czech Republic
7 Electron Microscopy Core Facility, Heidelberg University, Heidelberg, Germany
8 Institute of Plant Biology and Biotechnology (IBBP), Green Biotechnology, University of Münster, Münster, Germany

*Author for correspondence: till.ischebeck@uni-muenster.de
†Senior author.
H.E.K., R.P., G.H.B., M.W., R.T.M., and T.I. designed the work. H.E.K., S.S., N.M.D., Q.Y., M.S.S.L., P.S., P.W.N., K.S., O.V., R.P., S.H., and T.I. performed research. H.E.K., S.S., N.M.D., Q.Y., M.S.S.L., P.S., P.W.N., K.S., O.V., R.P., S.H., G.H.B., M.W., R.T.M., and T.I. analyzed data. H.E.K., N.M.D., R.P., R.T.M., and T.I. wrote the manuscript. All authors critically read and revised the manuscript and approved the final version.
The author responsible for distribution of materials integral to the findings presented in this article in accordance with the policy described in the Instructions for Authors (https://academic.oup.com/plcell) is: Till Ischebeck (till.ischebeck@uni-muenster.de).

Abstract

Membrane contact sites (MCSs) are interorganellar connections that allow for the direct exchange of molecules, such as lipids or Ca^{2+} between organelles, but can also serve to tether organelles at specific locations within cells. Here, we identified and characterized three proteins of *Arabidopsis thaliana* that form a lipid droplet (LD)–plasma membrane (PM) tethering complex in plant cells, namely LD-localized SEED LD PROTEIN (SLDP) 1 and SLDP2 and PM-localized LD-PLASMA MEMBRANE ADAPTOR (LIPA). Using proteomics and different protein–protein interaction assays, we show that both SLDPs associate with LIPA. Disruption of either *SLDP1* and *SLDP2* expression, or that of *LIPA*, leads to an aberrant clustering of LDs in Arabidopsis seedlings. Ectopic co-expression of one of the *SLDPs* with *LIPA* is sufficient to reconstitute LD–PM tethering in *Nicotiana tabacum* pollen tubes, a cell type characterized by dynamically moving LDs in the cytosolic

Open Access

IN A NUTSHELL

Background: Germinating seeds are not yet able to produce energy from sunlight. Therefore, the energy and carbon required for seedling establishment has to be provided from other sources such as oil. Seeds accumulate oil inside organelles called lipid droplets. Besides oil storage, lipid droplets might have additional functions during seedling establishment especially under unfavorable environmental conditions. Unfortunately, research on lipid droplets is hampered by the fact that only few proteins associated to lipid droplets are described in detail. Recently, we discovered several lipid droplet–localized proteins of unknown functions. One such protein is SEED LIPID DROPLET PROTEIN (SLDP).

Question: We set out to investigate SLDP, to understand its cellular function and its role in seedling establishment.

Findings: We determined that SLDP is important for spatial organization of lipid droplets during seedling establishment in the model plant *Arabidopsis thaliana*. Normally, lipid droplets line the inner side of the plasma membrane that surrounds cells. The loss of SLDP, however, causes lipid droplets to form clusters within the cells. Furthermore, SLDP interacts with another protein, LIPID DROPLET PLASMA MEMBRANE ANCHOR (LIPA), a protein that is anchored to the plasma membrane. Through their interaction, the proteins form a bridge, called membrane contact site, and thereby anchor lipid droplets to the plasma membrane.

Next steps: Although the effect of a loss of SLDP or LIPA on the cellular level is striking, no effect on the level of the whole plant was observed. Next steps will therefore aim at understanding the relevance of a contact site between the plasma membrane and lipid droplets on the level of the cell and the whole organism, especially under unfavorable environmental conditions.

streaming. Furthermore, confocal laser scanning microscopy revealed both SLDP2.1 and LIPA to be enriched at LD–PM contact sites in seedlings. These and other results suggest that SLDP and LIPA interact to form a tethering complex that anchors a subset of LDs to the PM during post-germinative seedling growth in Arabidopsis.

Introduction

As knowledge on organelle-specific functions and their proteomes has expanded in recent years, there has been ever mounting interest in interorganelle interactions that are in part facilitated by membrane contact sites (MCSs; Prinz et al., 2020). MCSs foster physical interactions and the exchange of molecules between organelles without the need of membrane fusion events. The transient connections are established through tethering proteins, connecting the membranes of interacting organelles and allowing for direct exchange of lipids, cellular signals (e.g. Ca^{2+}, reactive oxygen species [ROS], etc.) and/or other molecules (Baillie et al., 2020; Prinz et al., 2020; Rossini et al., 2020).

MCSs can form between nearly all organelles (Eisenberg-Bord et al., 2016; Valm et al., 2017; Shai et al., 2018; Baillie et al., 2020). The endoplasmic reticulum (ER) and peroxisomes, for example, are organelles with well-described interactomes (Shai et al., 2016; Zang et al., 2020). Also, several multiorganelle MCSs have been described, including the three-way connection between mitochondria, ER, and lipid droplets (LDs) that promotes *de novo* lipogenesis in human adipocytes (Freyre et al., 2019).

Although ER-derived LDs can engage in various MCSs, the LD interactome is less well described than that of other organelles (Bohnert, 2020). LDs consist of a lipophilic core of neutral lipids, such as triacylglycerols (TAGs) and sterol esters, surrounded by a phospholipid monolayer and a variety of surface-associated "coat" proteins. Long believed to be an inert storage organelle, it is now widely accepted that LDs actively participate in a wide range of cellular processes involving lipids and their derivatives (Thiam and Beller, 2017; Welte and Gould, 2017; Ischebeck et al., 2020). As such, rather than just housing storage lipids, LDs are now considered to be dynamic hubs for lipid homeostasis and specialized metabolism (Schaffer, 2003). Furthermore, LDs can serve as a sink for reducing cytosolic free fatty acids (Fan et al., 2017; Olzmann and Carvalho, 2019; de Vries and Ischebeck, 2020) and ROS (Muliyil et al., 2020), and also sequester potentially harmful proteins (Geltinger et al., 2020) or histone complexes at the LD surface (Johnson et al., 2018).

Given the established role(s) of MCSs in the nonvesicular transport of lipids (Cockcroft and Raghu, 2018), it is not surprising that LDs form contacts with many other organelles (Gao and Goodman, 2015; Schuldiner and Bohnert, 2017; Valm et al., 2017; Bohnert, 2020; Rakotonirina-Ricquebourg et al., 2022). The majority of these described LD MCSs, however, were found in mammalian or yeast cells. Knowledge in plants is so far still limited to LD–ER and LD–peroxisome MCSs, which are involved in storage lipid accumulation (Cai et al., 2015; Greer et al., 2020; Pyc *et al.*, 2021) and

Cell wall-localized BETA-XYLOSIDASE4 contributes to immunity of Arabidopsis against *Botrytis cinerea*

Guzha, A., McGee, R., **Scholz, P.**, Hartken, D., Lüdke, D., Bauer, K., Wenig, M., Zienkiewicz, K., Herrfurth, C., Feussner, I., Vlot, A.C., Wiermer, M., Haughn, G., Ischebeck, T.

The article was published online in the journal Plant Physiology in April 2022. Article and supplementary materials can be found under the following link:

https://doi.org/10.1093/plphys/kiac165
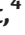
Author contribution:

Patricia Scholz helped to adjust the method for GC-MS-based monosaccharide analysis of mucilage and leaves. She performed monosaccharide analysis of leaves depicted in figures S3A and S8. She performed statistical analysis of monosaccharide composition in leaves.

Research Article

Cell wall-localized BETA-XYLOSIDASE4 contributes to immunity of Arabidopsis against *Botrytis cinerea*

Athanas Guzha [ID] ,[1,†] Robert McGee [ID] ,[2] Patricia Scholz [ID] ,[1] Denise Hartken,[3] Daniel Lüdke [ID] ,[3,‡]
Kornelia Bauer [ID] ,[4] Marion Wenig [ID] ,[4] Krzysztof Zienkiewicz [ID] ,[1,5,6] Cornelia Herrfurth [ID] ,[1,5]
Ivo Feussner [ID] ,[1,5] A. Corina Vlot,[4] Marcel Wiermer [ID] ,[3,7] George Haughn [ID] [2] and Till Ischebeck [ID] [1,8,§,*]

1   Department of Plant Biochemistry, Albrecht-von-Haller-Institute for Plant Sciences and Goettingen Center for Molecular Biosciences (GZMB), University of Goettingen, Justus-von-Liebig Weg 11, D-37077 Goettingen, Germany
2   Department of Botany, University of British Columbia, Vancouver, British Columbia, Canada V6T 1Z4
3   Molecular Biology of Plant-Microbe Interactions Research Group, Albrecht-von-Haller-Institute for Plant Sciences and Goettingen Center for Molecular Biosciences (GZMB), University of Goettingen, Justus-von-Liebig Weg 11, D-37077 Goettingen Germany
4   Helmholtz Zentrum Muenchen, Institute of Biochemical Plant Pathology, Ingolstaedter Landstrasse 1, 85764 Neuherberg, Germany
5   Service Unit for Metabolomics and Lipidomics, Goettingen Center for Molecular Biosciences (GZMB), University of Goettingen, D-37077 Goettingen, Germany
6   UMK Centre for Modern Interdisciplinary Technologies, Nicolaus Copernicus University, 87-100 Toruń, Poland
7   Freie Universität Berlin, Institute of Biology, Dahlem Centre of Plant Sciences, Biochemistry of Plant-Microbe Interactions, Königin-Luise-Str. 12-16, 14195 Berlin, Germany
8   Institute of Plant Biology and Biotechnology (IBBP), Green Biotechnology, University of Münster, Schlossplatz 8, D-48143 Münster, Germany

*Author for correspondence: till.ischebeck@uni-muenster.de
†Present address: Department of Biological Sciences, BioDiscovery Institute, University of North Texas, Denton, Texas 76203, USA.
‡Present address: The Sainsbury Laboratory, University of East Anglia, Norwich Research Park, NR4 7UH Norwich, UK.
§Senior author

A.G., A.C.V., G.H., M.Wiermer, I.F., and T.I. designed the research. A.G., R.M., D.H., P.S., C.H., K.B., M.Wenig, D.L., and K.Z. performed the experiments. M.Wiermer, A.C.V., I.F., G.H., and T.I. analyzed the data. A.G. and T.I. wrote the manuscript with contributions from the other authors.

The author responsible for distribution of materials integral to the findings presented in this article in accordance with the policy described in the Instructions for Authors (https://academic.oup.com/plphys/pages/general-instructions) is: Till Ischebeck (till.ischebeck@uni-muenster.de).

Abstract

Plant cell walls constitute physical barriers that restrict access of microbial pathogens to the contents of plant cells. The primary cell wall of multicellular plants predominantly consists of cellulose, hemicellulose, and pectin, and its composition can change upon stress. *BETA-XYLOSIDASE4* (*BXL4*) belongs to a seven-member gene family in Arabidopsis (*Arabidopsis thaliana*), one of which encodes a protein (BXL1) involved in cell wall remodeling. We assayed the influence of BXL4 on plant immunity and investigated the subcellular localization and enzymatic activity of BXL4, making use of mutant and overexpression lines. BXL4 localized to the apoplast and was induced upon infection with the necrotrophic fungal pathogen *Botrytis cinerea* in a jasmonoyl isoleucine-dependent manner. The *bxl4* mutants showed a reduced resistance to *B. cinerea*, while resistance was increased in conditional overexpression lines. Ectopic expression of *BXL4* in Arabidopsis seed coat epidermal cells rescued a *bxl1* mutant phenotype, suggesting that, like BXL1, BXL4 has both xylosidase and arabinosidase activity. We conclude that BXL4 is a xylosidase/arabinosidase that is secreted to the apoplast and its expression is upregulated under pathogen attack, contributing to immunity against *B. cinerea*, possibly by removal of arabinose and xylose side-chains of polysaccharides in the primary cell wall.

Open Access

Sustained Control of Pyruvate Carboxylase by the Essential Second Messenger Cyclic di-AMP in *Bacillus subtilis*

Krüger, L., Herzberg, C., Wicke, D., **Scholz, P.**, Schmitt, K., Turdiev, A., Lee, V.T., Ischebeck, T., Stülke, J.
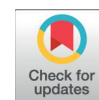
The article was published online in the journal mBio in February 2022. The article and supplemental data can be found under the following link:

https://doi.org/10.1128/mbio.03602-21

Author contribution:

Patricia Scholz extracted and measured oxaloacetate, aspartate and threonine from bacterial samples as displayed in figure 4.

Sustained Control of Pyruvate Carboxylase by the Essential Second Messenger Cyclic di-AMP in *Bacillus subtilis*

Larissa Krüger,[a] Christina Herzberg,[a] Dennis Wicke,[a] Patricia Scholz,[b] Kerstin Schmitt,[c] Asan Turdiev,[d] Vincent T. Lee,[d] Till Ischebeck,[b]
Jörg Stülke[a]

[a]Department of General Microbiology, Institute for Microbiology & Genetics, GZMB, Georg-August-University Göttingen, Göttingen, Germany
[b]Department of Plant Biochemistry, GZMB, Georg-August-University Göttingen, Göttingen, Germany
[c]Department of Molecular Microbiology and Genetics, Service Unit LCMS Protein Analytics, Institute for Microbiology & Genetics, GZMB, Georg-August-University Göttingen, Göttingen, Germany
[d]Department of Cell Biology and Molecular Genetics, University of Maryland, College Park, Maryland, USA

ABSTRACT In *Bacillus subtilis* and other Gram-positive bacteria, cyclic di-AMP is an essential second messenger that signals potassium availability by binding to a variety of proteins. In some bacteria, c-di-AMP also binds to the pyruvate carboxylase to inhibit its activity. We have discovered that in *B. subtilis* the c-di-AMP target protein DarB, rather than c-di-AMP itself, specifically binds to pyruvate carboxylase both *in vivo* and *in vitro*. This interaction stimulates the activity of the enzyme, as demonstrated by *in vitro* enzyme assays and *in vivo* metabolite determinations. Both the interaction and the activation of enzyme activity require apo-DarB and are inhibited by c-di-AMP. Under conditions of potassium starvation and corresponding low c-di-AMP levels, the demand for citric acid cycle intermediates is increased. Apo-DarB helps to replenish the cycle by activating both pyruvate carboxylase gene expression and enzymatic activity via triggering the stringent response as a result of its interaction with the (p)ppGpp synthetase Rel and by direct interaction with the enzyme, respectively.

IMPORTANCE If bacteria experience a starvation for potassium, by far the most abundant metal ion in every living cell, they have to activate high-affinity potassium transporters, switch off growth activities such as translation and transcription of many genes or replication, and redirect the metabolism in a way that the most essential functions of potassium can be taken over by metabolites. Importantly, potassium starvation triggers a need for glutamate-derived amino acids. In many bacteria, the responses to changing potassium availability are orchestrated by a nucleotide second messenger, cyclic di-AMP. c-di-AMP binds to factors involved directly in potassium homeostasis and to dedicated signal transduction proteins. Here, we demonstrate that in the Gram-positive model organism *Bacillus subtilis*, the c-di-AMP receptor protein DarB can bind to and, thus, activate pyruvate carboxylase, the enzyme responsible for replenishing the citric acid cycle. This interaction takes place under conditions of potassium starvation if DarB is present in the apo form and the cells are in need of glutamate. Thus, DarB links potassium availability to the control of central metabolism.

KEYWORDS *Bacillus subtilis*, cyclic di-AMP, TCA cycle, protein-protein interaction, pyruvate carboxylase, c-di-AMP, second messenger

In most organisms, the tricarboxylic acid (TCA) cycle is the central hub in metabolism. The cycle provides the cells with reducing power for respiration and to fuel anabolic reactions, and it generates precursors for important anabolic reactions, such as 2-oxoglutarate and oxaloacetate, for the biosynthesis of glutamate and aspartate and the derived amino acids, respectively. Accordingly, at least a partial TCA cycle is present in most organisms, with the notable

Characterization of glyphosate-resistant *Burkholderia anthina* and *Burkholderia cenocepacia* isolates from a commercial Roundup® solution

Hertel, R., Schöne, K., Mittelstädt, C., Meißner, J., Zschoche, N., Collignon, M., Kohler, C., Friedrich, I., Schneider, D., Hoppert, M., Kuhn, R., Schwedt, I., **Scholz, P.**, Poehlein, A., Martienssen, M., Ischebeck, T., Daniel, R., Commichau, F.M.

The article was published online in Environmental Microbiology Reports in November 2021. The full article including supplemental data can be found online using the following DOI:

https://doi.org/10.1111/1758-2229.13022

Author contribution:

Patricia Scholz extracted glyphosate from culture medium samples and measured glyphosate abundance depicted in figure 2C. She processed and analysed the data.

Highlight

Characterization of glyphosate-resistant *Burkholderia anthina* and *Burkholderia cenocepacia* isolates from a commercial Roundup® solution

Robert Hertel,[1] Kerstin Schöne,[1] Carolin Mittelstädt,[1]
Janek Meißner,[2] Nick Zschoche,[1] Madeline Collignon,[1]
Christian Kohler,[3] Ines Friedrich,[4] Dominik Schneider,[4]
Michael Hoppert,[2] Ramona Kuhn,[5] Inge Schwedt,[1]
Patricia Scholz,[6] Anja Poehlein, [ID][4]
Marion Martienssen,[5] Till Ischebeck,[6] Rolf Daniel [ID][4]
and Fabian M. Commichau [ID][1]*

[1]*FG Synthetic Microbiology, Institute for Biotechnology, BTU Cottbus-Senftenberg, Senftenberg, 01968, Germany.*
[2]*Department of General Microbiology, Institute for Microbiology and Genetics, University of Goettingen, Göttingen, 37077, Germany.*
[3]*Friedrich Loeffler Institute of Medical Microbiology, University Medicine Greifswald, Greifswald, Germany.*
[4]*Department of Genomic and Applied Microbiology, Institute for Microbiology and Genetics, University of Goettingen, Göttingen, 37077, Germany.*
[5]*Chair of Biotechnology of Water Treatment, Institute of Environmental Technology, BTU Cottbus-Senftenberg, Cottbus, 03046, Germany.*
[6]*Department of Plant Biochemistry, Albrecht-von-Haller-Institute for Plant Sciences and Göttingen Center of Molecular Biosciences (GZMB), University of Goettingen, Göttingen, 37077, Germany.*

Summary

Roundup® is the brand name for herbicide solutions containing glyphosate, which specifically inhibits the 5-enolpyruvyl-shikimate-3-phosphate (EPSP) synthase of the shikimate pathway. The inhibition of the EPSP synthase causes plant death because EPSP is required for biosynthesis of aromatic amino acids. Glyphosate also inhibits the growth of archaea, bacteria, Apicomplexa, algae and fungi possessing an EPSP synthase. Here, we have characterized two glyphosate-resistant bacteria from a Roundup solution. Taxonomic classification revealed that the isolates 1CH1 and 2CH1 are *Burkholderia anthina* and *Burkholderia cenocepacia* strains respectively. Both isolates cannot utilize glyphosate as a source of phosphorus and synthesize glyphosate-sensitive EPSP synthase variants. *Burkholderia*. *anthina* 1CH1 and *B*. *cenocepacia* 2CH1 tolerate high levels of glyphosate because the herbicide is not taken up by the bacteria. Previously, it has been observed that the exposure of soil bacteria to herbicides like glyphosate promotes the development of antibiotic resistances. Antibiotic sensitivity testing revealed that the only the *B*. *cenocepacia* 2CH1 isolate showed increased resistance to a variety of antibiotics. Thus, the adaptation of *B*. *anthina* 1CH1 and *B*. *cenocepacia* 2CH1 to glyphosate did not generally increase the antibiotic resistance of both bacteria. However, our study confirms the genomic adaptability of bacteria belonging to the genus *Burkholderia*.

Introduction

Roundup is the brand name for a solution containing the systemic broad-spectrum herbicide glyphosate [*N*-(phosphonomethyl(glycine)] (Franz, 1979; Duke and Powles, 2008). Glyphosate specifically inhibits the 5-enolpyruvyl-shikimate-3-phosphate (EPSP) synthase of the shikimate pathway (Steinrücken and Amrhein, 1980). The EPSP synthase converts phosphoenolpyruvate (PEP) and shikimate-3-phosphate to EPSP, which is an essential precursor for *de novo* synthesis of phenylalanine, tyrosine and tryptophan (Steinrücken and Amrhein, 1980; Herrmann and Weaver, 1999). The glyphosate-dependent inactivation of the EPSP synthase results in the depletion of the cellular levels of the three amino acids and thus in plant death (Gresshoff, 1979; Fischer *et al*., 1986; Wicke *et al*., 2019). Glyphosate targets the PEP binding site of the EPSP synthase, thereby acting as a competitive

Neuronal cholesterol synthesis is essential for repair of chronically demyelinated lesions in mice

Berghoff, S.A., Spieth, L., Sun, T., Hosang, L., Depp, C., Sasmita, A.O., Vasileva, M.H., **Scholz, P.**, Zhao, Y., Krueger-Burg, D., Wichert, S., Brown, E.R., Michail, K., Nave, K.A., Bonn, S., Odoardi, F., Rossner, M., Ischebeck, T., Edgar, J.M., Saher, G.

The article was published online in the journal Cell Reports in October 2021. The full text with supplementary data can be found online:

https://doi.org/10.1016/j.celrep.2021.109889

Author contribution:

Patricia Scholz extracted and measured sterols from neurons and tissues samples as shown in figures 2F and S2A. She processed and analysed the data.

Cell Reports

Report

Neuronal cholesterol synthesis is essential for repair of chronically demyelinated lesions in mice

Stefan A. Berghoff,[1,10,*] Lena Spieth,[1,10] Ting Sun,[1,2,10] Leon Hosang,[3] Constanze Depp,[1] Andrew O. Sasmita,[1] Martina H. Vasileva,[1] Patricia Scholz,[4] Yu Zhao,[2] Dilja Krueger-Burg,[5] Sven Wichert,[6] Euan R. Brown,[7] Kyriakos Michail,[7] Klaus-Armin Nave,[1] Stefan Bonn,[2] Francesca Odoardi,[3] Moritz Rossner,[6] Till Ischebeck,[4,8] Julia M. Edgar,[1,9] and Gesine Saher[1,11,*]

[1]Department of Neurogenetics, Max Planck Institute of Experimental Medicine, Göttingen, Germany
[2]Institute for Medical Systems Biology, Center for Molecular Neurobiology Hamburg, Hamburg, Germany
[3]Institute for Neuroimmunology and Multiple Sclerosis Research, University Medical Center Göttingen, Göttingen, Germany
[4]Department of Plant Biochemistry, Albrecht-von-Haller-Institute for Plant Sciences and Göttingen Center for Molecular Biosciences (GZMB), University of Göttingen, Göttingen, Germany
[5]Department of Molecular Neurobiology, Max Planck Institute of Experimental Medicine, Göttingen, Germany
[6]Department of Psychiatry and Psychotherapy, University Hospital, LMU Munich, Munich, Germany
[7]School of Engineering and Physical Sciences, Institute of Biological Chemistry, Biophysics and Bioengineering, James Naysmith Building, Heriot Watt University, Edinburgh, UK
[8]Service Unit for Metabolomics and Lipidomics, Göttingen Center for Molecular Biosciences (GZMB), University of Göttingen, Göttingen, Germany
[9]Axo-glial Group, Institute of Infection, Immunity and Inflammation, College of Medical Veterinary and Life Sciences, University of Glasgow, Glasgow, UK
[10]These authors contributed equally
[11]Lead contact
*Correspondence: berghoff@em.mpg.de (S.A.B.), saher@em.mpg.de (G.S.)
https://doi.org/10.1016/j.celrep.2021.109889

SUMMARY

Astrocyte-derived cholesterol supports brain cells under physiological conditions. However, in demyelinating lesions, astrocytes downregulate cholesterol synthesis, and the cholesterol that is essential for remyelination has to originate from other cellular sources. Here, we show that repair following acute versus chronic demyelination involves distinct processes. In particular, in chronic myelin disease, when recycling of lipids is often defective, *de novo* neuronal cholesterol synthesis is critical for regeneration. By gene expression profiling, genetic loss-of-function experiments, and comprehensive phenotyping, we provide evidence that neurons increase cholesterol synthesis in chronic myelin disease models and in patients with multiple sclerosis (MS). In mouse models, neuronal cholesterol facilitates remyelination specifically by triggering oligodendrocyte precursor cell proliferation. Our data contribute to the understanding of disease progression and have implications for therapeutic strategies in patients with MS.

INTRODUCTION

During normal brain development, cholesterol is produced locally by *de novo* synthesis involving all CNS cells (Berghoff et al., 2021; Camargo et al., 2012; Fünfschilling et al., 2012). Neuronal cholesterol is essential during neurogenesis (Fünfschilling et al., 2012), but the highest rates of cholesterol synthesis in the brain are achieved by oligodendrocytes during post-natal myelination (Dietschy, 2009). The resulting cholesterol-rich myelin enwraps, shields, and insulates axons to enable rapid conduction of neuronal impulses. In the adult brain, cholesterol synthesis is attenuated to low steady-state levels (Dietschy and Turley, 2004).

Destruction of lipid-rich myelin in demyelinating diseases such as multiple sclerosis (MS) likely impairs neuronal function

by disrupting the axon-myelin unit (Stassart et al., 2018). Remyelination is considered crucial for limiting axon damage and slowing progressive clinical disability. Statin-mediated inhibition of the cholesterol synthesis pathway impairs remyelination (Miron et al., 2009). Previously, we showed that following an acute demyelinating episode, oligodendrocytes import cholesterol for new myelin membranes from damaged myelin that has been recycled by phagocytic microglia (Berghoff et al., 2021). In contrast, oligodendroglial cholesterol synthesis contributes to remyelination following chronic demyelination (Berghoff et al., 2021; Voskuhl et al., 2019). Notably, astrocytes reduce expression of cholesterol synthesis genes following demyelination (Berghoff et al., 2021; Itoh et al., 2018). As in the healthy brain, astrocytes support neurons

Microglia facilitate repair of demyelinated lesions via post-squalene sterol synthesis

Berghoff, S.A., Spieth, L., Sun, T., Hosang, L., Schlaphoff, L., Depp, C., Düking, T., Winchenbach, J., Neuber, J., Ewers, D., **Scholz, P.**, van der Meer, F., Cantuti-Castelvetri, L., Sasmita, A.O., Meschkat, M., Ruhwedel, T., Möbius, W., Sankowski, R., Prinz, M., Huitinga, I., Sereda, M.W., Odoardi, F., Ischebeck, T., Simons, M., Stadelmann-Nessler, C., Edgar, J.M., Nave, K.-A. and Saher, G.

The article was published online in the journal Nature Neuroscience in December 2020. The full article including supplementary data can be found under the following DOI:

Author contribution:

Patricia Scholz performed sterol extraction and sterol analysis by GC-MS of animal and cell culture samples presented in figures 4f, 4g, 5b, 5d and 5e. She processed and analysed the data.

Check for updates

Microglia facilitate repair of demyelinated lesions via post-squalene sterol synthesis

Stefan A. Berghoff[1], Lena Spieth [1], Ting Sun[1,2], Leon Hosang[3], Lennart Schlaphoff [1], Constanze Depp [1], Tim Düking[1], Jan Winchenbach[1], Jonathan Neuber[1], David Ewers [1,4,5], Patricia Scholz [6], Franziska van der Meer[7], Ludovico Cantuti-Castelvetri [8], Andrew O. Sasmita [1], Martin Meschkat[1], Torben Ruhwedel [1], Wiebke Möbius [1], Roman Sankowski [9], Marco Prinz [9,10,11], Inge Huitinga [12], Michael W. Sereda[1,4,5], Francesca Odoardi[3], Till Ischebeck[6,13], Mikael Simons[8], Christine Stadelmann-Nessler[7], Julia M. Edgar[1,14], Klaus-Armin Nave [1]✉ and Gesine Saher [1]✉

The repair of inflamed, demyelinated lesions as in multiple sclerosis (MS) necessitates the clearance of cholesterol-rich myelin debris by microglia/macrophages and the switch from a pro-inflammatory to an anti-inflammatory lesion environment. Subsequently, oligodendrocytes increase cholesterol levels as a prerequisite for synthesizing new myelin membranes. We hypothesized that lesion resolution is regulated by the fate of cholesterol from damaged myelin and oligodendroglial sterol synthesis. By integrating gene expression profiling, genetics and comprehensive phenotyping, we found that, paradoxically, sterol synthesis in myelin-phagocytosing microglia/macrophages determines the repair of acutely demyelinated lesions. Rather than producing cholesterol, microglia/macrophages synthesized desmosterol, the immediate cholesterol precursor. Desmosterol activated liver X receptor (LXR) signaling to resolve inflammation, creating a permissive environment for oligodendrocyte differentiation. Moreover, LXR target gene products facilitated the efflux of lipid and cholesterol from lipid-laden microglia/macrophages to support remyelination by oligodendrocytes. Consequently, pharmacological stimulation of sterol synthesis boosted the repair of demyelinated lesions, suggesting novel therapeutic strategies for myelin repair in MS.

Approximately 70% of brain cholesterol in adults is associated with myelin[1], a lipid-rich membrane stack that insulates axons. During brain development, oligodendrocytes synthesize most of the cholesterol for myelin membrane expansion, and, correspondingly, oligodendroglial cholesterol synthesis is rate limiting for myelination[2]. In the adult brain, all cell types contribute to CNS cholesterol homeostasis, which is independent of peripheral sources[1]. Cholesterol synthesis is counterbalanced by LXR-mediated release of cellular cholesterol[3]. As mammals cannot degrade cholesterol, it is either excreted from the brain or locally recycled.

Functional repair of demyelinated lesions in individuals with MS, an inflammatory demyelinating disease of the CNS[4,5], is inevitably linked to local cholesterol metabolism. Myelin degenerates and releases myelin-associated cholesterol, which decreases local sterol synthesis by feedback inhibition[6–9]. To phagocytose and clear myelin debris, microglia/macrophages adopt a pro-inflammatory signature[10]. In MS, chronic neuroinflammation also involves T lymphocytes and can cause permanent brain damage. As immunomodulatory treatments of MS ameliorate neuroinflammation but cannot rescue neurological disabilities[4,5], novel treatment strategies should also support remyelination.

Spontaneous repair of demyelinated lesions occurs in animal models, and likely also in the early stages of MS, but necessitates the transition to a regenerative environment[4]. Oligodendrocytes can then synthesize myelin membranes for functional repair[11,12]. In atherosclerosis, a lipid-driven inflammatory disease of the vasculature, LXR signaling is critically involved in the resolution of inflammation[13]. However, whether LXR signaling links local sterol metabolism to inflammation in demyelinated CNS lesions and which cell types mediate endogenous repair remain poorly understood.

In this study, we investigated cell-type-specific sterol synthesis in the microenvironment of demyelinated lesions and its role in inflammation and remyelination. We made the surprising observation that sterol synthesis in microglia/macrophages was essential for repair after acute demyelination. The LXR ligand desmosterol, not cholesterol, orchestrated the resolution of inflammation and facilitated lipid recycling for remyelination. Our findings highlight

[1]Department of Neurogenetics, Max Planck Institute of Experimental Medicine, Göttingen, Germany. [2]Institute for Medical Systems Biology, Center for Molecular Neurobiology Hamburg, Hamburg, Germany. [3]Institute for Neuroimmunology and Multiple Sclerosis Research, University Medical Center Göttingen, Göttingen, Germany. [4]Department of Clinical Neurophysiology, University Medical Centre Göttingen, Göttingen, Germany. [5]Department of Neurology, University Medical Centre, Göttingen, Germany. [6]Department of Plant Biochemistry, Albrecht-von-Haller-Institute for Plant Sciences and Göttingen Center for Molecular Biosciences (GZMB), University of Göttingen, Göttingen, Germany. [7]Institute for Neuropathology, University Medical Centre Göttingen, Göttingen, Germany. [8]Institute of Neuronal Cell Biology, Technical University Munich, German Center for Neurodegenerative Diseases, Munich Cluster of Systems Neurology (SyNergy), Munich, Germany. [9]Institute of Neuropathology, Medical Faculty, University of Freiburg, Freiburg, Germany. [10]Signalling Research Centres BIOSS and CIBSS, University of Freiburg, Freiburg, Germany. [11]Center for Basics in NeuroModulation (NeuroModul Basics), Faculty of Medicine, University of Freiburg, Freiburg, Germany. [12]Neuroimmunology Research Group, Netherlands Institute for Neuroscience, an institute of the Royal Netherlands Academy of Arts and Sciences, Amsterdam, the Netherlands. [13]Service Unit for Metabolomics and Lipidomics, Göttingen Center for Molecular Biosciences (GZMB), University of Göttingen, Göttingen, Germany. [14]Applied Neurobiology Group, Institute of Infection, Immunity and Inflammation, College of Medical, Veterinary and Life Sciences, University of Glasgow, Glasgow, UK. ✉e-mail: nave@em.mpg.de; saher@em.mpg.de

Acknowledgements

"No man is an island" and no dissertation is the work of one person alone. I count myself lucky to have had so much support during my PhD time and I would like to thank from the bottom of my heart all those who have accompanied me on my journey so far.

First and foremost, I would like to thank Prof. Dr. Till Ischebeck for all the assistance over the years. Till, you encouraged and challenged me to follow my interests and passions in science and always supported me to become a better scientist. I am more grateful than words can express for the support on and off work, for the advice on science and career paths, for the freedom you gave me, and for the backing I have always received. It has been a wild ride, with ups and downs, frustrations and stellar moments, but I've always considered myself lucky to be a part of your group.

A big thank you goes to the other members of my TAC, for their advice, ideas and support in scientific discussions. I am grateful to Prof. Dr. Marcel Wiermer for the help with all the plant pathogen assays, which I could not do justice to on these pages. I am also thankful to Prof. George Haughn, who was a wonderful host in Vancouver and whose scientific achievements are an immense inspiration.

I want to thank Prof. Dr. Ivo Feußner, who welcomed me in his amazing department and supported me through the years. Thank you to Prof. Dr. Gerhard Braus for agreeing to be my 2nd referee but also for the access to his proteomics platform, which I have used extensively. Thank you also to Prof. Dr. Ivo Feußner and Prof. Dr. Andrea Polle for being part of my examination board.

Thank you also to Prof. Simone Techert, my mentor helps me to dream ahead and think of the future and the possible roads opening up for me.

I am extremely happy to have been part of the AG Ischebeck for such a long time and I am indebted to all its present and former members. Anna, Franzi, Athanas and Elisa, you were the best that could have happened to me in my master time and you set the example I tried to follow during my PhD. Philipp, Siqi, Magdiel and Janis, you are their worthy successors who make LD-related and not LD-related life much easier. Kathi and Lea, you are the best postdocs this group ever had 😊 and I cannot express how much your support carried me through the final stages of my PhD. Thank you all for being there when I need you, for hiking trips and apple plucking, for scientific discussion and other advice, for being the great people that you are and for making the whole group such a joyful place to be. Thank you also to my student helpers Jannis, Denis, Annabel and Fabienne who supported me with skilled hands and clever heads.

I have to thank departments of people, including all the members of the AG Biochemie der Pflanze and the AG de Vries in Göttingen. Special thanks to Benedikt and Alisa where I could always drop in for discussions about whatever topic and who could be relied on to have helpful suggestions and spark (scientific) ideas. Furthermore, thanks must go to Dr. Ellen Hornung for lab advice, cake and lunch alimentation, Dr. Kirstin Feußner and Dr. Cornelia Herrfurth for metabolomic and lipidomic support, Dr. Amélie Kelly as voice of reason in anything related to plant genetics and for her other advice, Dr. Tegan Haslam for her open ear, clever mind and

supportive spirit that made scientific discussion a lot of fun, Sabine Freitag for saving me from doing very stupid things to my samples, Susanne Mester for preventing me from killing my plants, Heike Lott for advice and support in all bureaucratic challenges and Tarek Morsi and Malte Bürsing for being the saviours in any technical or IT-related problems. I am also happy to have met previous PhD students of the department, especially Jasmin and Kathi who were just as important as the Ischebeck group members in the "first floor PhD community".

I am grateful to all students of the IRTG PRoTECT, with Steven as our fearless leader. You all formed a very supportive group and Vancouver would have been much less fun without you guys! In addition, thank you to Judith Wassiltschenko, Anja Vogelpohl and Janina Feierabend for their support in the IRTG and especially to Judith for her open ear and advice on everything and anything.

Science is a collaborative effort and I am happy to have worked with many amazing scientists in the past years. I am lucky to have such great proteomics support from Dr. Oliver Valerius and Dr. Kerstin Schmitt who measured endless samples for me and could be relied on to give helpful advice to all my questions.

Similarly, I count myself lucky to have researched with such amazing scientists as Prof. Kent Chapman, Prof. Robert Mullen and Nathan Doner. Thank you for the helpful discussions and suggestions, for sharing your projects and ideas and for your enthusiasm that helped me enjoy my own projects.

Dr. Martin Potocký, Dr. Přemysl Pejchar and Dr. Roman Pleskot and all their group members made my time(s) in Prague unforgettable in a positive way. I enjoyed your scientific and non-scientific discussions, the political comments, the jokes and the working atmosphere so much that even in my PhD I had to come back to you. Thank you for everything you taught me about Fiji, R and Czech politics, your appreciation and your belief in me.

Outside of the lab I have been lucky enough to become friends with Marjorie Ladd Parada. I can't believe that our time together stretches now more than eight years, it feels like just yesterday that you visited me and my family in Leipzig and Dresden. A mexican and a german scientist becoming friends in the UK and meet on Easter in Czechia is a great story and I cherish our friendship as special and precious. And it is always good to discuss books, life and everything with a new Terry Pratchett convert 😊.

Außerdem möchte ich der Gemeinschaft der Biologieolympiade danken, die mich immer wieder für Biologie und die Wissenschaft allgemein begeistert. Danke an Alex, Annabel, Arne, Christina, Clara, Jan, Lucia und so viele andere, die mir zur Seite standen und stehen.

Katrin Wenzel und Thomas Fritz eröffnen mir bei jedem Treffen neue Horizonte und ihre Neugier über meine Forschung lässt mich selbst immer wieder Neues entdecken. Ich betrauere bis heute den Verlust, der uns zusammengeführt hat, doch ich möchte keine Minute meiner Zeit mit euch missen.

Ein Leben ohne Trapez ist möglich aber sinnlos – und ohne die fabelhafte Akrobatengruppe in Göttingen hätte diese Doktorarbeit wohl nie das Licht der Welt gesehen. Allen Akrobat*innen sei es gedankt, dass sie mir ein- bis fünfmal in der Woche in ihrer Gemeinschaft das Fliegen ermöglichen. Besonderer Dank an Ken, Jessi, Paulina und Helge, die mich mit Rat und Tat dabei